جامعة بني وليد

مجلة جامعة بني وليد للعلوم الإنسانية والتطبيقية

E-ISSN: 3005-3900

العدد التاسع والعشرون
سبتمبر 2023

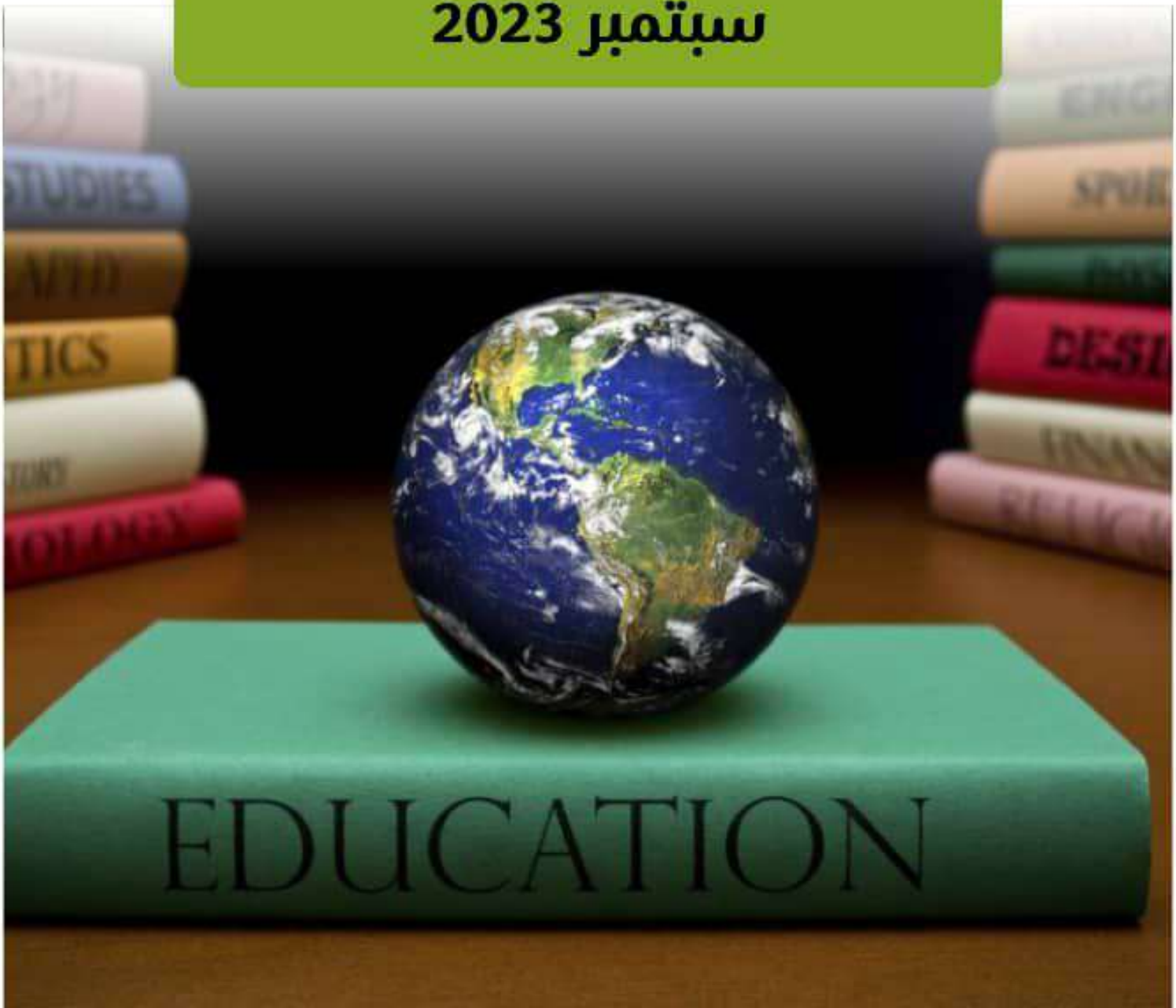

Papers Index فهرس الورقات البحثية

المؤتمر الدولي الثاني للعلوم والهندسة
2nd International Conference on Science and Engineering
ICSE 2023
Faculty of Engineering - University of Bani Waleed
Bani Waleed, Libya

Paper Code: ICSE-006

EVALUATION OF AGING AND MOISTURE DAMAGE POTENTIAL OF WARM MIX ASPHALT INCORPORATING A SYNTHETIC WAX ADDITIVE

Bashir M. Aburawi
Civil Engineering Department, College of Engineering / AL-Margeb University, Libya
*Crosspnding author: Aburawi2018@Gmail.com

Abstract: This paper presents the effects of a warm mix additive on the moisture damage of warm mix asphalt (WMA). Asphalt mixtures were made using different WMA contents (0, 2 and 3%) at different compaction temperatures. Aging properties were studied from the effects of artificial long-term aging on resilient modulus (M_R) and indirect tensile strength (ITS) of WMAs. Moisture damage was investigated in term of tensile strength ratio (TSR) of unaged and aged specimens conditioned in one and three cycles of freezing and thawing. The results showed that the aging significant affected the M_R and ITS of WMA. The additive content increased with air voids but in contrary with the bulk density. Hence, the use of higher additive content can be more beneficial in terms of resilient modulus. Decreasing compaction temperature could significantly decrease the ITS while the TSR of WMA reduced as compaction temperature decreased. From moisture damage tests, the TSR of aged samples was found to be lower than that of unaged samples.

Keywords: WMA, Moisture Damage, Aging, Resilient Modulus, Wax Additive

Introduction

During the construction of transportation amenities and infrastructures, the emission of greenhouse gases into the atmosphere is among the prominent causes of pollution. One of the latest technologies developed in the field of highway engineering, Warm Mix Asphalt (WMA) technology, has numerous benefits that are not connected to greenhouse gas emissions [1-4]. The technology of WMA is also environmentally friendly because it produces asphalt at considerably lower temperatures than Hot Mix Asphalt (HMA). The WMA technology achieved temperature reduction by using additives, which can be classified as chemical additives, organic additives and water-containing foaming additives or processes [5-7]. The basic purpose of adding additives is to strengthen mix workability by reducing the viscosity of the bitumen. Thus, this produces lesser emissions and creates improved working conditions [8-10]. The preservation and protection of both natural and workspace environments are the main objectives in the field of road engineering Worldwide there is an ever-increasing use of new environmentally friendly materials and

 ISBN 978-9959-9703-2-9

techniques. One of these innovative processes includes WMA [7,11-13]. Such asphalt mixtures, compared to traditional HMA, can be mixed and compacted at lower mixing and compaction temperatures thereby reducing CO_2 and fume emissions and promoting low energy consumption and operative benefits [4-16]. It was reported that the mixing temperatures of WMA ranged from 100°C to 140°C compared to the mixing temperatures of 150°C to 180°C for conventional HMA [17-21]. In this paper, the effects of a new friendly environmental material named RH-WMA on the basic properties of asphalt mixtures were investigated.

RH-WMA is a relatively new warm mix additive that was designed to reduce the viscosity of the asphalt binder at elevated temperatures. The ability of WMA additives to decrease the binder viscosity leads to lower production temperatures of asphalt mixtures.

Lowering viscosity allows the aggregate to be coated completely by the binder at lower mixing temperatures [11,18-19]. Lower mixing and compaction temperatures can result in incomplete drying of the aggregate. The resulting water trapped in the coated aggregate may cause moisture damage. Hence, the stripping potential of this product needs to be investigated. On the other hand, aging plays a key role in the long-term performance of asphalt mixtures especially when it acts in combination with moisture damage. Therefore, the stiffness properties of the mixture before and after aging conditioning can provide good information about the performance of WMA [20-24]. Thus, this paper compares the volumetric and mechanical properties of WMA containing warn mix additives to traditional mixtures.

Materials and Method

A virgin PG64 asphalt binder used in the mixtures was obtained from Shell Bitumen Company, Singapore. Malaysia was used as the control binder; the physical and rheological properties are shown in Table 1. A wax-based WMA additive called RH-WMA developed in China was used as the warm mix additive [25]. RH-WMA was added into the base binder at 2% and 3% by the total mass of the asphalt binder as recommended by the producer. RH-WMA was blended with the binder at 145°C using an electrical propeller mixer for 30 minutes to ensure uniformity and homogeneity of the binder blend.

Granite as a source of mineral aggregates used in the preparation of all the mixtures was supplied by Kuad Quarry Sdn. Bhd., Penang. Malaysia was used for producing AC14 mixtures based on local specifications.

 ISBN 978-9959-9703-2-9

Table 1: Properties of PG64 binder

Aging condition	Test Properties	Value
Original binder	Viscosity at 135°C (Pa.s)	0.425
	Softening point (°C)	43
	Penetration (0.1 mm)	81
	Ductility (cm)	>100
	Flash point (°C)	331
	G*/sin δ at 64°C (Pa)	1486
Short-term aged binder	G*/sin δ at 64°C (Pa)	2830

This aggregate was washed, dried, and sieved according to the proposed aggregate gradation. Table 2 show the engineering properties of the aggregate used.

Table 2: Engineering properties of aggregates used [26]

Property	Test result	Test method
Coarse aggregates bulk density	2.62	AASHTO T85
Absorption (%)	0.40	AASHTO T85
Fine aggregates bulk specific gravity	2.57	AASHTO T84
Flat and elongated (%)	23.3	BS 812-105
Los Angeles abrasion value (%)	23.86	AASHTO T96
Aggregate crushing value (%)	19.25	BS 812-110

Different types of fillers have different effects on the performance of asphalt mixtures [27]. This paper was made to prepare asphalt mixtures using a non-conventional filler named Pavement Modifier (PMD) which is locally available in Malaysia. Thus, the secondary aim of this investigation is to examine the effect of this filler as an anti-stripping agent on the performance of asphalt mixtures. PMD is a grayish-black powder mineral filler and it is used as an anti-stripping agent. The addition of approximately 5% of PMD by aggregate weight acts as mineral filler in asphalt mixtures. Fig. 1 shows the RH-WMA and PMD filler used in this paper.

RH-WMA PMD

Fig. 1: The warm mix additive and filler used

For the production of fully binder-coated aggregates in the laboratory, the HMA construction temperature was selected at 160°C for the PG64 binder, while the WMA construction temperatures were selected based on laboratory experiences. Table 3 shows the mixing and compaction temperatures of mixtures. RH-WMA mixtures were workable enough to be compacted at selected lower compaction temperatures.

Table 3: Construction temperatures of HMA and WMA

RH-WMA (%)	Mixture Type	Construction temperatures (°C)	
		Mixing	Compaction
0	HMA	160	150
2	WMA	130, 115, 100	125, 110, 95

ISBN 978-9959-9703-2-9

3	130, 115, 100	125, 110, 95

For more ease of reference, mixtures were designated according to their mixture type (W for WMA and H for HMA), binder type (64 for PG64 binder), compaction temperatures (125°C, 115°C and 95°C) and RH-WMA content (2% and 3%). Hence, W2RH64C125 denotes the WMAs prepared using a PG64 binder containing 2% RH-WMA, compacted at 125°C.

The volumetric properties of fabricated mixtures were determined based on the bulk-specific gravity, air voids and voids in mineral aggregates. The resilient modulus test and indirect tensile strength test were selected to determine the stiffness properties of the mixture before and after aging conditioning.

The water sensitivity of asphalt mixtures was determined using TSR. Three test specimen sets were prepared and separated. All specimens were compacted to an air void content of 7 ± 1% using a gyratory compactor. The first set of specimens (dry) was left at room temperature for one day and then conditioned at 15°C before the TSR test. The second set of specimens (wet) was left at room temperature for one day and then subjected to one cycle of freeze-thaw. The third set of specimens (wet) was left in the room for 1 day and then subjected to three cycles of freezing-thaw. Indirect tensile strength (ITS) test was conducted on the samples to evaluate the moisture sensitivity of HMAs and WMAs.

Tests were conducted at 15°C using a loading rate of 50 mm/min until failure. A low temperature of 15°C was used because the asphalt mixture becomes brittle under low temperatures and therefore disintegrates easily when subjected to external loads. Thus, the low-temperature condition ensures that asphalt mixtures achieve near-elastic properties [28]. A higher TSR is generally believed to indicate improved resistance to moisture-induced damage. Moisture conditioning was performed in the laboratory to evaluate the effects of accelerated water conditioning through a freeze-thaw cycle on compacted asphalt mixtures. The conditioning of all the compacted samples was performed according to ASTM D4867 (2006) procedures with the only modification of using distilled water with the addition of Na2CO3 at 6.62 gm concentration instead of distilled water. Water with Na_2CO_3 was used to increase the pH value to enhance the stripping rate/damage inside the asphalt samples. The samples were immersed in the solution and vacuumed for 15 min to achieve saturation levels between 55% and 80% as shown in Fig. 2a. These samples were later exposed to freezing conditions at -18±3°C for 16 hours as shown in Fig. 2b and thawing condition at 60°C for 24 hours as one cycle according to ASTM D4867 (2006) as

 ISBN 978-9959-9703-2-9

shown in Fig. 2c. Three sets of samples including unconditioned, conditioned in one freeze–thaw cycle, and conditioned in three freeze–thaw cycles were separated.

(a)

(b)

(c)

Fig. 2: Moisture conditioning (a) Vacuum saturation (b) freezing cycle (c) Thawing cycle

Test Results and Discussions

Several studies have been carried out evaluating the properties of WMA. It has been found that warm mix additives work in different ways either in reducing the viscosity of the binder or improving the workability of the mix at lower temperatures [29]. This section investigates the effects of compaction temperatures on the volumetric properties of WMA containing different amounts of RH-WMA additive. With lower compaction temperatures, WMAs might result in several problems, such as inadequate volumetric properties like higher air voids and lower VFA. Akisetty et al [30] showed that the warm mix processes were effective in improving the volumetric properties of rubberized mixes at a certain range of compaction temperatures.

Fig. 3a shows the relationship between the compaction temperature and bulk-specific gravity of the asphalt concrete mixtures. It is observed that the bulk specific gravity increases with the increase of compaction temperature. This is true for all mixtures containing different RH-WMA content. The increase in temperature decreases the viscosity of the mixture and in turn, facilitates easy compaction.

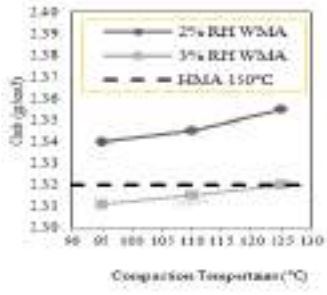

(a)

 ISBN 978-9959-9703-2-9

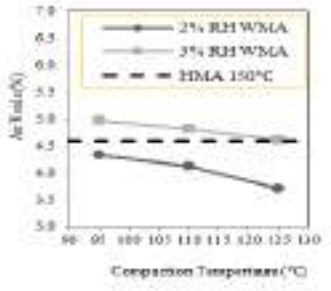

(b)

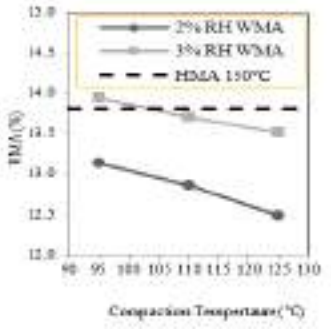

(c)

Fig. 3: Relationship between compaction temperature and (a) bulk specific gravity, (b) air voids, (c) voids in mineral aggregates

The relationship between compaction temperature and air voids is shown in Fig. 3b.

Fig. 3b clearly shows that the percent air void decreases with increasing compaction temperature. This is also true for all mixes containing different RH-WMA content. The decrease in percent air void with the increase in compaction temperature is due to the lubricating effect of asphalt concrete keeping the viscosity of the binder suitable for compaction.

Fig. 3c shows the relationship between compaction temperature and % VMA. It is noticed that the percent (VMA) decreases with the increase of compaction temperature. The increase in the compaction temperature increases the lubricating effect of the binder due to a decrease in viscosity. This increases its workability and therefore improves the compaction process which in turn decreases the percent air voids and percent voids in mineral aggregates.

Resilient modulus (M_R) is used in mechanistic pavement design. It is used as one of the inputs in multi-layered elastic methods and finite elements to evaluate structural pavement response under traffic loading. The resilient behavior of the mixture depends on the binder type, test temperature, aggregate gradation and aging condition.

The relationship between resilient modulus and RH-WMA content for un-aged and aged asphalt mixtures at different compaction and test temperatures are shown in Fig. 4. Results show that compaction temperature, RH-WMA content, and test temperature affect the resilient modulus of asphalt samples. Since higher compaction temperatures have a stiffening effect on the asphalt binder rheology, the resilient modulus of samples fabricated at higher compaction temperatures is greater than those fabricated at lower compaction temperatures. Also, the resilient modulus of samples increases due to aging but reduces

 ISBN 978-9959-9703-2-9

when the test temperature increases. Generally, the resilient modulus of WMA samples is lower than the corresponding values of HMA.

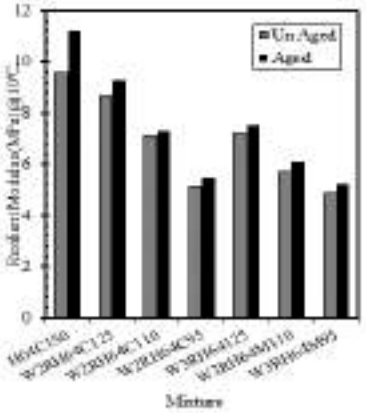

(a)

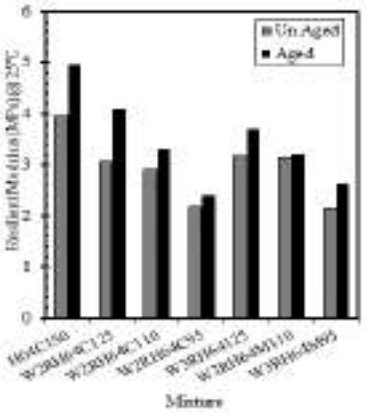

(b)

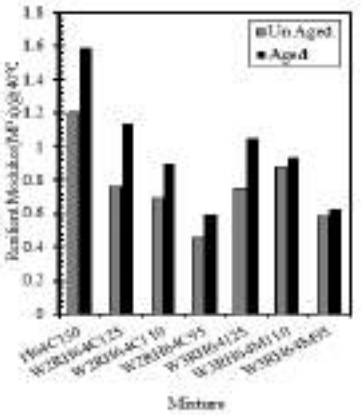

(c)

Fig. 4: Resilient modulus results tested at (a)10°C, (b) at 25°C, (c) at 40°C

ITS test results of un-aged and aged asphalt mixtures are presented in Fig. 5. It can be observed from the figure that HMA mixture has a higher value of ITS than WMA mixture at test temperature of 15°C.

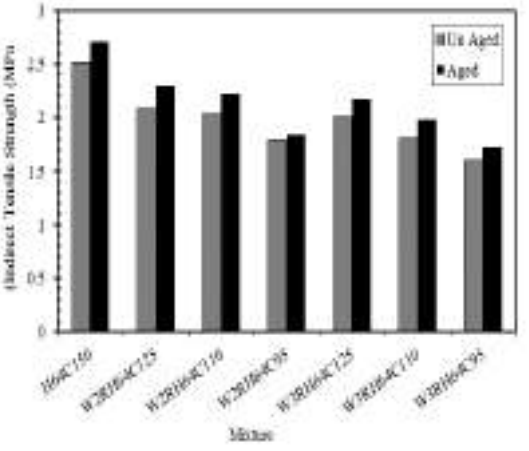

Fig. 5: Indirect Tensile Strength at 15°C

The influence of RH-WMA content, compaction temperature and aging condition on the ITS

 ISBN 978-9959-9703-2-9

are presented in Fig. 6. The results show that there is an insignificant difference in the ITS of WMA samples prepared by employing different RH-WMA content and compacted. The RH-WMA content had limited impact on the ITS of un-aged and aged samples. On the other hand, the ITS of WMA increases with mixing temperatures, regardless of RH-WMA content and aging condition. This is because higher mixing temperatures lead to more aging and stiffen the binder. In addition, the density of the mixture increases as the mixing temperature increases. It also shows that ITS decreases as RH-WMA content increases irrespective of mixing temperature. For all mixtures, the aging of HMA and WMA increases the ITS of the asphalt mixtures.

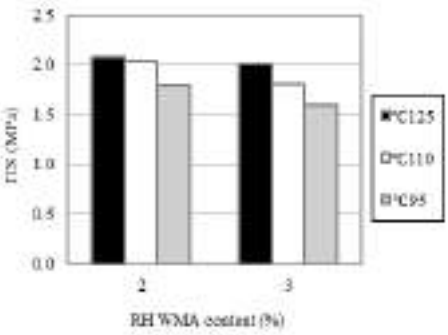

Unaged Mixtures

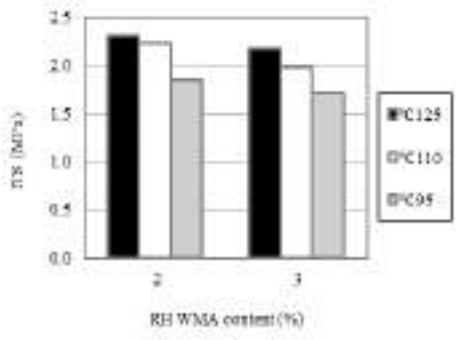

Aged Mixtures

Fig. 6: Relationship between ITS and RH-WMA content for unaged and aged mixtures

Indirect tensile strength (ITS) of asphalt mixtures indicates their overall strength and their resistance to cracking. ITS results of samples at different moisture conditioning are shown in Fig. 7. From the figures, HMA has higher dry and wet ITS than WMA regardless of RH-WMA content and aging condition.

The ITS of WMA compacted at 125°C was comparable to those of HMA (150°C) these ITS of HMAs were higher than the ITS of WMA mixtures compacted at 110°C. This finding indicates that reducing the production temperature of WMA may lead to an increased tendency toward moisture sensitivity. This condition can be partly attributed to the reduced asphalt binder aging. Similar results were obtained for dry and wet ITS. However, a trend is evident in the effect of temperature reduction. In addition, comparing the ITS results shows that as compaction temperature

 ISBN 978-9959-9703-2-9

decreases, the ITS value decreases for both specimens containing 2% and 3%. However, low compaction temperature causes high binder viscosity and results in inadequate compaction [31].

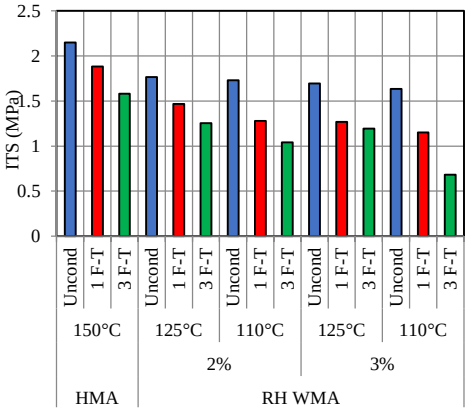

(a) Unaged asphalt mixtures

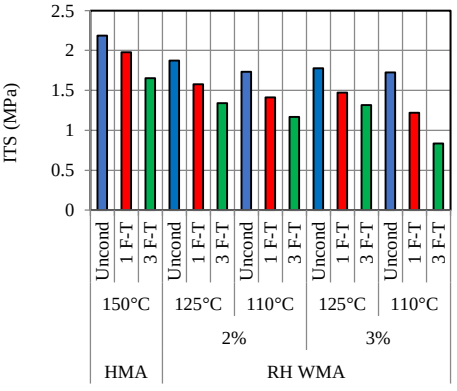

(b) Aged asphalt mixtures

Fig. 7: ITS at different moisture conditioning

Tensile strength ratio (TSR) is commonly used as one of the indicators of moisture damage potential for asphalt mixtures. TSR of unaged and aged HMA and WMA conditioned by one and three cycles of freeze-thaw are presented in Fig. 8. From the figures, the TSR of aged samples is higher than that of unaged samples. It means that selected laboratory aging conditions could not accelerate moisture damage of samples. For instance, the TSR of aged WMA compacted at 125˚C containing 3% of additive after one cycle of freeze-thaw is higher than 80%, while the corresponding value for unaged samples is lower than 80%. As expected, the effects of three freeze-thaw for reducing TSR is higher than that of one freeze-thaw. This is because of severe moisture damage in three cycles of freeze-thaw as compared to one cycle of freeze-thaw. The TSR of HMA is higher than that of WMA. It means that lower compaction temperatures increase the potential for moisture damage. In most cases, 3% of additive showed lower TSR as compared to 2% additive regardless of compaction temperature and number of moisture conditioning.

ISBN 978-9959-9703-2-9

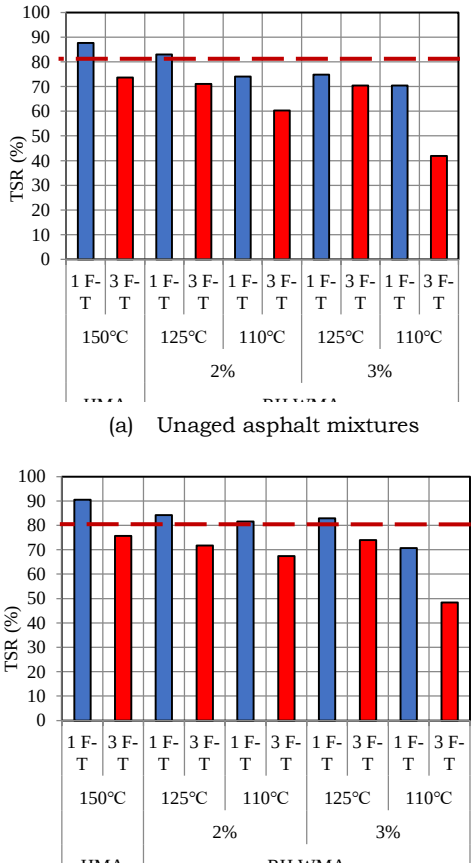

(a) Unaged asphalt mixtures

(b) Aged asphalt mixtures

Fig. 8: TSR at conditioned by one and three cycles of freeze-thaw

Conclusions

The research work investigated the mechanical and volumetric properties of WMA, in order to evaluate its potential and limits as compared to traditional HMA. The investigation was conducted by analyzing HMA and two WMA's made with two contents of RH-WMA additive. Based on the findings of the experimental test results, the following conclusions were drawn:

HMA mixtures significantly had higher dry and wet ITS than other mixtures. The test results revealed that reducing the production temperature of WMA may result in increased susceptibility to moisture-induced damage, whereas increasing the wax additive content (2, 3% of the weight of the asphalt binder) negatively affects WMA performance.

The test results indicated that long-term aging improved the moisture resistance of WMA mixtures regardless of WMA additives. The decrease in compaction temperature significantly reduced the ITS.

With respect to water sensitivity results, the addition of a higher amount of synthetic wax did not increase the potential for moisture damage. Moreover, lower mixing temperatures resulted in a decrease in the tensile strength ratio of the mixtures.

Acknowledgment

The authors would like to acknowledge the School of Civil Engineering, Universiti Sains Malaysia. Many thanks are also due to the technicians of the Highway Engineering Laboratory at the Universiti Sains Malaysia for their kind assistance and providing support to conduct this paper.

References

[1] Abdullah, M. E., Zamhari, K. A., Hainin, M. R., Oluwasola, E. A., Yusoff, N. I. M., & Hassan, N. A. (2016). High temperature characteristics of warm mix asphalt mixtures

 ISBN 978-9959-9703-2-9

with nanoclay and chemical warm mix asphalt modified binders. Journal of Cleaner Production, 122, 326-334.

[2] Kok, B. V., & Yilmaz, M. (2009). The effects of using lime and styrene–butadiene–styrene on moisture sensitivity resistance of hot mix asphalt.Construction and building materials, 23(5), 1999-2006.

[3] Abdullah, M. E., Zamhari, K. A., Hainin, M. R., Oluwasola, E. A., Hassan, N. A., & Yusoff, N. I. M. (2016). Engineering properties of asphalt binders containing nanoclay and chemical warm-mix asphalt additives. Construction and Building Materials, 112, 232-240.

[4] Rubio, M. C., Martínez, G., Baena, L., & Moreno, F. (2012). Warm mix asphalt: an overview. Journal of Cleaner Production, 24, 76-84.

[5] Capitão, S. D., Picado-Santos, L. G., & Martinho, F. (2012). Pavement engineering materials: Review on the use of warm-mix asphalt. Construction and Building Materials, 36, 1016-1024.

[6] Vaitkus, A., Vorobjovas, V., & Ziliut, L. (2009). The research on the use of warm mix asphalt for asphalt pavement structures. Road Department, Vilnius Gediminas Technical University, Vilnius, Lithuania.

[7] Oliveira, J. R., Silva, H. M., Abreu, L. P., & Fernandes, S. R. (2013). Use of a warm mix asphalt additive to reduce the production temperatures and to improve the performance of asphalt rubber mixtures. Journal of Cleaner Production, 41, 15-22.

[8] Mo, L., Li, X., Fang, X., Huurman, M., & Wu, S. (2012). Laboratory investigation of compaction characteristics and performance of warm mix asphalt containing chemical additives. Construction and Building Materials,37, 239-247.

[9] Xiao, F., Jordan, J., & Amirkhanian, S. (2009). Laboratory investigation of moisture damage in warm-mix asphalt containing moist aggregate.Transportation Research Record: Journal of the Transportation Research Board, (2126), 115-124.

[10] Del Carmen Rubio, M., Moreno, F., Martínez-Echevarría, M. J., Martínez, G., & Vázquez, J. M. (2013). Comparative analysis of emissions from the manufacture and use of hot and half-warm mix asphalt. Journal of Cleaner Production, 41, 1-6.

[11] Cardone F., P.V., Virgili A., Barbati S (2009). An evaluation of use of synthetic waxes in warm mix asphalt. in 7th International RILEM Symposium on advanced testing and characterization of bituminous materials, Rhodes.

[12] Sufian, Z., Aziz, N. A., Matori, M. Y., Hussain, M. Z., Hainin, M. R., & Oluwasola, E. A. (2014). Influence of active filler, curing time and moisture content on the strength properties of emulsion and foamed bitumen stabilized mix. Jurnal Teknologi, 70(4).

[13] Vidal, R., Moliner, E., Martínez, G., & Rubio, M. C. (2013). Life cycle assessment of hot mix asphalt and zeolite-based warm mix asphalt with reclaimed asphalt pavement. Resources, Conservation and Recycling, 74, 101-114.

[14] Hamzah, M.O., A. Jamshidi, and Z. Shahadan, Evaluation of the potential of Sasobit® to reduce required heat energy and CO 2 emission in the asphalt industry. Journal of Cleaner Production, 2010. 18(18): p. 1859-1865.

[15] Shu, X., Huang, B., Shrum, E. D., & Jia, X. (2012). Laboratory evaluation of moisture susceptibility of foamed warm mix asphalt containing high percentages of RAP. Construction and Building Materials, 35, 125-130.

[16] Akisetty, C. K., Lee, S. J., & Amirkhanian, S. N. (2009). High temperature properties of rubberized binders containing warm asphalt additives.Construction and Building Materials, 23(1), 565-573.

[17] Mo. Liantong, L.X., Fang. Xing, Huurman. M, Wu, Shaopeng, Laboratory investigation of compaction characteristics and performance of warm mix asphalt containing chemical additives. Construction and Building Materials, 2012. 37: p. 239-247.

[18] Bennert, T., Reinke, Gerald., Mogawer, Walaa., Mooney, Karissa, Assessment of workability and compactability of warm-mix asphalt. Transportation Research Record: Journal of the Transportation Research Board, 2010(2180): p. 36-47.

[19] Akisetty, C., Xiao, F., Gandhi, T., & Amirkhanian, S. (2011). Estimating correlations between rheological and engineering properties of rubberized asphalt concrete mixtures containing warm mix asphalt additive.Construction and Building

 ISBN 978-9959-9703-2-9

Materials, 25(2), 950-956.

[20] Ameri, M., Hesami, S., & Goli, H. (2013). Laboratory evaluation of warm mix asphalt mixtures containing electric arc furnace (EAF) steel slag. Construction and Building materials, 49, 611-617.

[21] Kristjánsdóttir, Ó., Muench, S., Michael, L., & Burke, G. (2007). Assessing potential for warm-mix asphalt technology adoption. Transportation Research Record: Journal of the Transportation Research Board, (2040), 91-99.

[22] Xiao, F., Zhao, W., Gandhi, T., & Amirkhanian, S. N. (2010). Influence of antistripping additives on moisture susceptibility of warm mix asphalt mixtures. Journal of Materials in Civil Engineering, 22(10), 1047-1055.

[23] Oluwasola, E. A., Hainin, M. R., & Aziz, M. M. A. (2015). Evaluation of rutting potential and skid resistance of hot mix asphalt incorporating electric arc furnace steel slag and copper mine tailing. Indian Journal of Engineering & Materials Sciences, 22, 550-558.

[24] Oluwasola, E. A., Hainin, M. R., Aziz, M. M. A., Singh, S., & Singh, L. M. (2015). Effect of Aging on the Resilient Modulus of Stone Mastic Asphalt Incorporating Electric Arc Furnace Steel Slag and Copper Mine Tailings. InInCIEC 2014 (pp. 1199-1208). Springer Singapore.

[25] Wang, H., Dang, Zhengxia., You, Zhanping., Cao, Dongwei (2012). Effect of warm mixture asphalt (WMA) additives on high failure temperature properties for crumb rubber modified (CRM) binders. Construction and Building Materials, 35: p. 281-288.

[26] Hamzah, M.O., B. Golchin, and C.T. Tye (2013). Determination of the optimum binder content of warm mix asphalt incorporating Rediset using response surface method. Construction and Building Materials, 47: p. 1328-1336.

[27] Rahman, M. and M. Sobhan (2013). Use of Non-Conventional Fillers on Asphalt-Concrete Mixture. International Journal of Innovation and Applied Studies, 3(4): p. 1101-1109.

[28] Hamzah, M.O.K., Muhammad Rafiq. Quadri, Sayed Abulhasan. Valentin, Jan, (2014). Quantification of moisture sensitivity of warm mix asphalt using image analysis technique. Journal of Cleaner Production, 68: p. 200-208.

[29] Al-Shalout, I., R. Stas, and O. Miro (2007). Effects of Moisture, Compaction Temperature and Gradation Types on Durability of Asphalt Concrete Mixtures1.

[30] Akisetty, C.K., S.-J. Lee, and S.N. Amirkhanian (2009). Effects of compaction temperature on volumetric properties of rubberized mixes containing warm-mix additives. Journal of Materials in Civil Engineering, 21(8): p. 409-415.

[31] Aman, M.Y. and M.O. Hamzah (2014). Effects of Anti-Stripping Additives on Moisture Sensitivity of Warm Porous Asphalt Mixtures. International Journal of Construction Technology and Management, 1(1): p. 1-7.

 ISBN 978-9959-9703-2-9

المؤتمر الدولي الثاني للعلوم والهندسة
2nd International Conference on Science and Engineering
ICSE 2023
Faculty of Engineering - University of Bani Waleed
Bani Waleed, Libya

Paper Code: ICSE-008

INFLUENCE OF WASTE POLYSTYRENE FOAM ON THE ENGINEERING PROPERTIES OF CONCRETE MADE FROM LOCAL MATERIALS

Nurdeen M. Altwair[a] , Heba M. Elghwari[a]
[a]Department of Civil Engineering, Faculty of Engineering/ El-Mergib University, Libya
*Crosspnding author: nmaltwair@elmergib.edu.ly

Abstract: One of the waste materials currently used in the manufacture of lightweight concrete is polystyrene. However, the effects of this material on most concrete properties have not been studied in Libya. In this paper, experimental data for plain concrete were obtained by replacing natural sand with waste polystyrene foam (WPSF) in volume ratios of 0%, 10%, 20%, and 30%. The properties of concrete, such as slump, air content, density, water absorption, compressive strength, flexural strength, free shrinkage, and UPV, were determined experimentally. The findings indicate that as the amount of WPSF in the concrete mix increases, the slump, density, compressive strength, and flexural strength as well as the elastic modulus and UPV of the plain concrete decrease. Conversely, an increase in the replacement level of natural sand by WPSF leads to an increase in air content, water absorption, and free shrinkage. Even though the incorporation of WPSF did not enhance most of the established engineering properties of concrete, the results obtained still fall within the acceptable limits for concrete use in all engineering applications. As such, this type of concrete may be suitable for construction applications that require less thermal and acoustic insulation.

Keywords: Plain concrete, Engineering properties, Waste polystyrene foam, Natural sand

Introduction

One of the biggest consumers of raw materials nowadays is the building industry. There must be a significant decrease in the consumption of raw resources if we are to have a sustainable future. For this reason, it is crucial to consider waste reduction and material recycling both during the construction of new structures and during the recycling of demolition materials [1–5].

A very common type of plastic used for packaging is polystyrene. In the case of land filling, it is fundamentally non-biodegradable and takes hundreds of years to degrade, whereas other disposal or treatment options have harmful environmental effects. Polystyrene is made up of 98% air and only 2% polystyrene as a result of expandable polystyrene foam processing, and its base material is styrene monomer [6]. Polystyrene foam represents 0.1% of total municipal solid waste [7]. This material is known to have qualities like sound absorption, high thermal conductivity, and light weight, which

 ISBN 978-9959-9703-2-9

make it an excellent additive to concrete [8]. Recycling and reusing waste materials is seen as the most environmentally friendly solution to the disposal issue. The waste product polystyrene (PS) is one example. A thermoplastic material called polystyrene has the potential to make lightweight concrete by replacing the conventional aggregate in concrete [9]. Low-density concretes needed for building applications can be made with polystyrene aggregate, and it can also be used for other specialized purposes like sub-base material for roads, railway track beds, the construction of floating marine structures and sea fences, energy absorption for the defense of buried military structures, and fenders on offshore oil platforms. Additionally, polystyrene aggregate concrete was shown to be fire-resistant, making it an excellent material for thermal insulation in building construction [10]. The effects of adding different types and dosages of polystyrene foam, both commercial and recycled, on the physical and mechanical properties of Portland cement mortars have been studied previously. These investigations have found that with a high amount of polystyrene foam, it is possible to produce mortars with mechanical properties suitable for use in masonry, rendering, and plaster mortars [11].

The objective of this paper is to determine the slump, water absorption, air content, density, flexural strength, modulus of elasticity, free shrinkage, and compressive strength of plain concrete containing polystyrene foam waste (WPEF) as a partial replacement for fine aggregate in relation to the percentage of polystyrene waste incorporated. In addition, the scope of the study is to compare the mechanical properties of plain concrete with polystyrene foam waste and observe which percentage of replacement is most appropriate in construction applications.

1. Materials and methods

2.1 Materials

The cement used in this investigation was ordinary Portland cement (OPC), complying with the standard LSS-340-09 [12]. Tab water was used, which was obtained from one of the water desalination plants in the city of Al-Khums. According to standard BSI 812-1995 [13], natural sand with a maximum size of 1.2 mm was used as a fine aggregate, and it was collected from Zlitan quarry. The sand has a 2.85 fineness modulus, a 2.6 specific gravity, and a 0.83% water absorption. The coarse aggregate (crushed sedimentary aggregate) of different maximum sizes, viz., 19 mm and 14 mm, was complying with the standard BSI 812-1995 [13], obtained from the quarries of the Al-Alous region located on the outskirts of the city of Al-Khums. The coarse aggregate (gravel) has a specific gravity of 2.75, water absorption of 0.47 % and a bulk density of 1542 kg/m^3. Table 1 shows the gradation of fine and coarse aggregates used in this study. Waste polystyrene foam (WPSF) used in this study was

 ISBN 978-9959-9703-2-9

supplied from landfills located in the city of Al-Khums. WPSF had a loss of ignition of 100% and water absorption by immersion after 28 days of between 1.5% and 3% volume. Ground WPSF was obtained by mechanical grinding and sieving after crushing (Fig. 1). 100% of the ground WPSF particles passed through a 2.36 mm sieve, and the specific gravity was 0.025.

Table 1: The gradation of used aggregate.

Sieve size	Cumulative passing (%)	
	Natural sand	Coarse aggregate
19 mm	100	100
14 mm	100	56.45
10 mm	100	36.73
5 mm	100	1.01
2.36 mm	100	0
1.18 mm	97.12	0
0.6 mm	86.45	0
0.3 mm	62.14	0
0.15 mm	2.92	0
0.075 mm	0.74	0

Fig. 1: Photograph showing the aspect of WPSF.

1.2 Mix proportions

In order to produce structural WPTP concrete, natural sand was replaced with WPTP by 10%, 20%, and 30% by volume. The details of mixture proportions are illustrated in Table 2. The standard mixture was one of four concrete mixtures that were developed..

Table 2: Mixture proportion.

 ISBN 978-9959-9703-2-9

Mix ID	Cement (Kg/m^3)	Water (Kg/m^3)	Sand (Kg/m^3)	Gravel (Kg/m^3)	WPSF volume (%)
M-0	330	198	725	1088	0
M-10	330	198	718	1088	10
M-20	330	198	711	1088	20
M-30	330	198	704	1088	30

All the materials were mixed together by adding about half of water while mixing goes on for 1 minute. The remaining water was added to the mixture and continued mixing it for 3 minutes [14]. Fresh concrete tests, i.e., air content and slump tests, were carried out immediately after the completion of the mixing. According to each test for hardened concrete, the concrete mixes were cast into molds, and after the specimens hardened, they were cured at ambient temperature and tested on a specific day.

3.3 Test procedure

According to ASTM C185-15 [15], the air content of fresh concrete mix was investigated. This test was conducted on fresh concrete containing different contents of WPSF to determine the percentage of air voids. The concrete slump test is to determine the workability or consistency of the WPSF concrete mix. The slump test is the most simple workability test for concrete because it provides an immediate result. In this study, the slump test is carried out as per procedures mentioned in ASTM C143 /C143M [16].

The density test was accomplished at the age of 28 days, following BS 1881-114 [17] and ASTM C642-13 [18]. The specimen, after 28 curing days, was taken out for measuring its (bulk) density. The mass of the specimen was weighed, and the dimensions of the specimen were also measured to calculate the volume, The mass density was then calculated by the mass weight divided by the volume. For the water absorption test, the absorption of water by concrete specimens was determined by measuring the increase in mass resulting from the absorption of water. The water absorption values are the average of three specimens with a size of 100×100 ×100 mm^3. After the curing period, specimens were dried in an oven at a temperature of 80 °C until a constant weight was attained. This is because WPSF is extremely sensitive to thermal degradation when subjected to relatively high temperatures. These were then immersed in water, and the weight gain was measured at regular intervals until a constant weight was reached. The water absorption is given by [19]:

 ISBN 978-9959-9703-2-9

$$\text{Water Absorption (\%)} = \left(\frac{W_s - W_d}{W_d}\right) \times 100 \quad \ldots..(1)$$

Where $\mathbf{W_s}$ and $\mathbf{W_d}$ are the saturated and dry weight of specimens, respectively.

The compressive strength of mix proportions with different WPSF volumes was evaluated according to BS 1881-116:1983 [20], with a loading rate of 70 kN/min, by using cubic specimens of size 100×100 ×100 mm^3 at ages corresponding to 7 and 28 days after water curing (Fig. 2). The flexural strength is determined by conducting the test method of ASTM C78/C78M [21] (third-point loading or 4-point bending test). Prisms with sizes of 100 mm × 100 mm × 400 mm were tested (Fig. 2).

Fig. 2: Compression and flexural test specimen.

The flexural strength at 7 and 28 days was determined by using a four-point loading test. The specimens rest on two supports, and half of the load is applied at each of the third of the span length. The specimen was loaded at a constant rate of 2.3 KN/min until the failure.

The modulus of elasticity of the studied WPSF concrete mixtures was found according to the standard ACI 318-08 [22], which gives the following expression for the modulus of elasticity of normal weight concrete:

$$E_c = 4700\sqrt{f_c} \quad \ldots\ldots\ldots\ldots\ldots\ldots\ldots\ldots\ldots(2)$$

where;

$\boldsymbol{E_c}$ = static modulus of elasticity.

$\boldsymbol{f_c}$ = compressive strength.

The free shrinkage of WPSF specimens was tested according to ASTM C157/C157M-08 Stranded [23]. The size of the specimen was 100 mm ×100 mm ×400 mm (Fig, 3a).

 ISBN 978-9959-9703-2-9

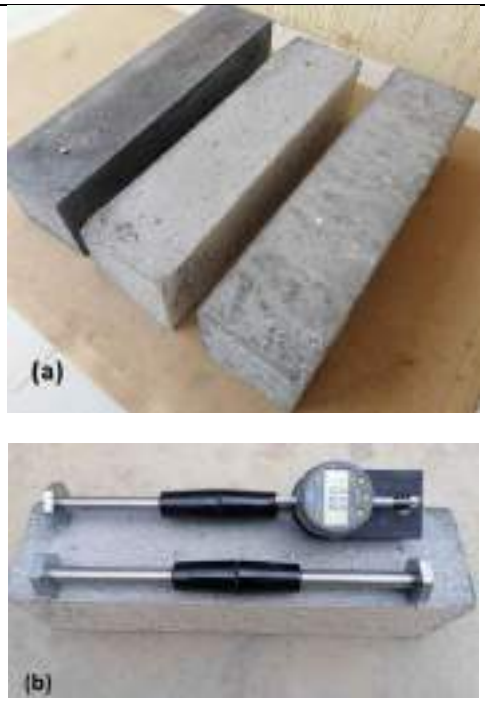

Fig. 3: (a) Free shrinkage specimens **(b)** Digital strain gauge.

To measure shrinkage strains along the length of the specimens, two pairs of stainless steel discs of gauge length (L_0) 25 mm were fixed at both ends of the specimens, so that there is a pair of every two opposite surfaces. A digital strain gauge with a precision of 10^{-3} mm was used (Fig. 3b). The specimens were dried at room temperature for 56 days. Subsequent shrinkage readings were taken after 3, 5, 10, 15, 20, 30, 40 and 56 days. The initial length was recorded as (L_1) and the subsequent length (L) was measured periodically. The free shrinkage is expressed by the following:

$$\text{Free shrinkage } (\varepsilon_f) = \left(\frac{L_1 - L}{L_0}\right) \times 100 \quad \ldots\ldots\ldots (3)$$

In order to evaluate the effect of WPSF on the acoustic characteristics of plain concrete, such as sound transmission, an ultrasonic pulse velocity test was approved. At age of 7 and 28 days, the average ultrasonic pulse velocity was calculated. This test was conducted in accordance with ASTM C597-09 Standard [24].

4. Results and discussion

 ISBN 978-9959-9703-2-9

4.1 Slump and air content

The slump of concrete specimens containing different percentages of WPSF is presented in Fig. 4. In general, mixes produced with WPSF experienced a slump. The results indicate a sharp reduction in slump at a percentage of sand replacement between 10% and 30%. With a replacement level of 10%, 20%, and 30%, the concrete mix slump values were about 65 mm, 60 mm, and 52 mm, respectively; i.e., when the content is increased from 10% to 30%, the slump is reduced by 45% to 67 %, meaning the slump is decreased as the content of WPSF is increased. The reason may be due to the large size of polystyrene foam grains compared to sand grains. As well as increasing the absorption of water in mixtures containing WPSF. However, the results obtained in this test are consistent with a previous study conducted by Kin and Ariffin [25].

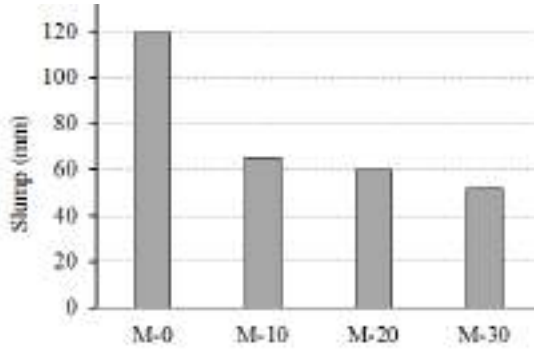

Fig. 4: Effect of percentage (%) replacement of WPSF on concrete slump.

The air content of concretes containing 0, 10, 20, and 30% WPSF is presented in Fig. 5.

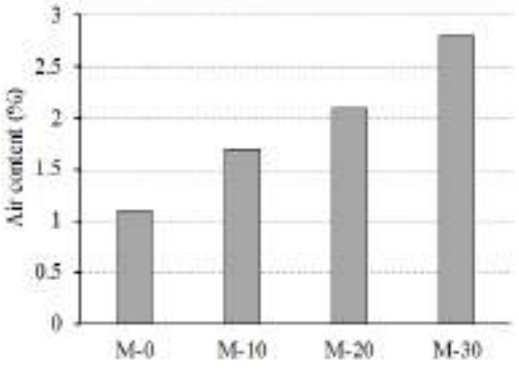

Fig. 5: Effect of percentage (%) replacement of WPSF on air content of concrete.

 ISBN 978-9959-9703-2-9

The results show that the incorporation of WPSF caused an increase in the air content of concrete, depending on the level of replacement with sand. The air content of the WPSF concretes decreased by 53%, 120%, and 164% at replacement level 10%, 20%, and 30%, respectively.

Such a result allows for justifying the decrease in density in the hardened stage. This behavior may be explained by the fact that the WPSF increases total porosity by affecting the air content of mixtures and may contribute significantly to the formation of air voids in the fresh concrete containing the WPSF, resulting in lower density and thermal conductivity. In addition, the surface and inside of WPSF particles caught molecules of air that entered the fresh concrete, leading to an increase in air content [26]. However, the effect of incorporating different levels of WPSF on the mechanical properties of fresh concrete, such as slump and air content, is almost identical to that of those containing rubber residue [26].

4.2 Water absorption and density

Figure 6 illustrates the water absorption of concrete containing varying amounts of WPSF. It can be observed that the concrete with a higher volume of WPSF, showed higher water absorption. The percentage of increase was about 54%, 91%, and 154% when the percentage of sand replacement was 10%, 20%, and 30%, respectively. The water absorption mainly increased as a result of the combination of the highly porous interfacial transition zone between the WPSF and cement paste of the mixture [27]. Due to the difference in the surface of the WPST grains compared to the sand grains, when mixed with water, the volumetric paste content is increased. In addition, the surface area surrounding the grains decreases with the increase in the amount of WPSF, leading to a reduction in the amount of cement paste surrounding the grains. When decreasing the amount of paste, the voids or pores in the concrete increase, and so does the water absorption [19].

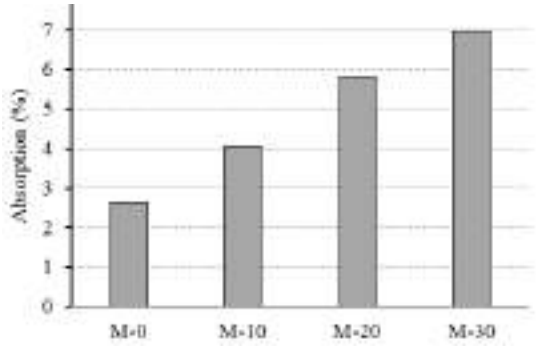

 ISBN 978-9959-9703-2-9

Fig. 6: Effect of percentage (%) replacement of WPSF on water absorption content of concrete.

The inclusion of WPSF to the concrete reduces its density almost by the same percent as its addition, as shown in Fig. 7. The inclusion of WPSF to concrete by 10% causes a reduction of 7% in its density. While this reduction in weight becomes almost 11% when the WPSF content is 30%.

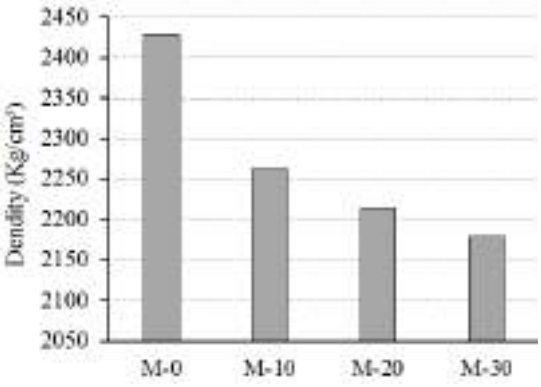

Fig. 7: Variation of concrete density with WPSF content.

The decrease in the density of concrete with the increase in WPSF content can be attributed to the weight of the WPSF, which is about 98% air [28]. Thus, there will be a decrease in density due to the increase in air content in the concrete. There is another reason related to the first, which is that the density of WPSF is much lower than that of natural sand. When more sand is replaced by WPSF, the density of concrete is lower. The results obtained in this study show similar results to those obtained by Herki and Khatib [27] and Askar et al. [28]. According to their study, as the replacement level of expanded polystyrene aggregate increased, the density of the concrete reduced. This is due to the fact that aggregate made of expanded polystyrene has a far lower density than aggregate made of natural materials.

4.3 Compressive strength and modulus of elasticity

The compressive strength and modulus of elasticity for concrete containing varying amounts of WPSF at the ages of 7 and 28 days of curing are shown in Figures 8 and 9. The relationship between compressive strength and modulus of elasticity of concrete is generally direct, meaning that as compressive strength increases, modulus of elasticity also tends to increase. This relationship is based on the fact that both properties are influenced by the same underlying factors, such as the density,

 ISBN 978-9959-9703-2-9

porosity, and composition of the concrete. Therefore, the discussion of the results related to compressive strength corresponds to what will be mentioned in the results of the modulus of elastic. At both ages (7 and 28 days), the results show that the incorporation of WPSF caused a reduction in the compressive strength of concrete depending on the level of replacement with natural sand. The mixes containing 10%, 20%, and 30% WPSF have shown a decrease in compressive strength at 7 days of approximately 8%, 18% and 23%, respectively, in relation to the reference mortar. After 28 days of curing, the percentage reduction is almost 11%, 15%, and 25%, respectively.

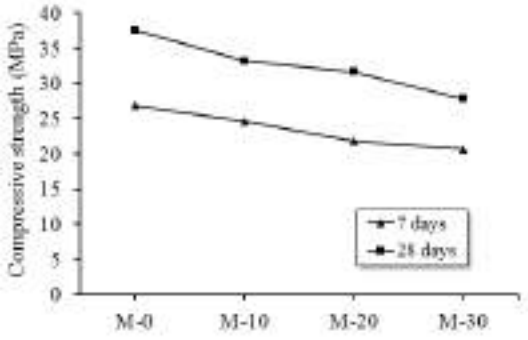

Fig. 8: Compressive strength of concrete at 7 and 28 days.

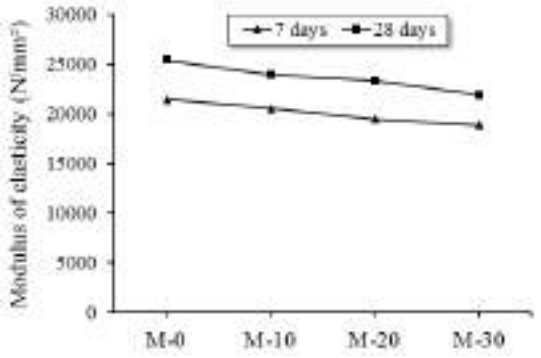

Fig. 9: Modulus of elasticity of concrete at 7 and 28 days.

This reduction may be associated with the increase in air content in the fresh state and because WPSF has a low density. Another reason for the decrease in compressive strength as well as modulus of elasticity is the replacement of natural sand with WPSF and the resulting increase in the surface area of fine particles of WPSF, which can lead to weakening of the interfacial zone between the WPSF

 ISBN 978-9959-9703-2-9

and the cement paste [7]. The WPSF fills in the gaps left by the absence of natural sand. In addition, the compressive strength of polystyrene is lower than that of natural sand [29]. This will lead to a decrease in the compressive strength by increasing the WPSF. However, despite the decrease in compressive strength at 28 days for the mixture containing a 30% percentage of natural sand replacement, this mixture is still very suitable for construction applications.

4.4 Flexural strength

The flexural strength of concrete with different percentages of WPSF as sand replacement at the ages of 7 and 28 days is shown in Figure 10.

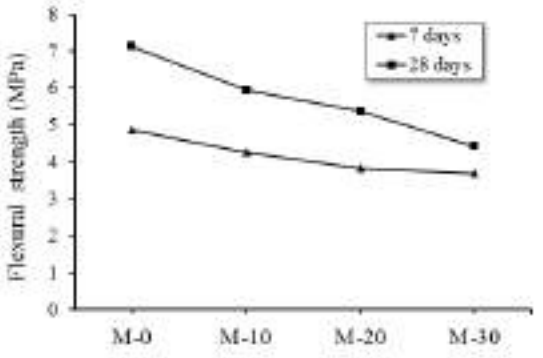

Fig. 10: Flexural strength of concrete at 7 and 28 days.

The results showed that WPSF had a remarkable influence on the flexural strength of plain concrete. Comparing with the control concrete, the results of the flexural strength test of WPSF concrete follow the same trend as the compressive strength test results: as the amount of WPSF in the mixture increases, the flexural strength decreases.

The reason for the decrease in flexural strength with an increase in the amount of WPSF is the same as explained in the discussion of the results of the compressive strength test. However, these results agree with a previous study conducted by Salahaldeen and Al-Hadithi [29] on the flexural strength of concrete made with expanded polystyrene.

4.5 Free shrinkage

Figure 11 shows the development of the free shrinkage strains with the measurement time for concrete containing varying amounts of WPSF. Therefore, one objective of the current study was to provide a clearer understanding of the free shrinkage of WPSF concrete by monitoring it over a period of time (i.e., 56 days). The majority of free shrinkage, as determined by the findings of the current study, took

 ISBN 978-9959-9703-2-9

place in the first 30 days. Beyond that time, the free shrinking rate decreased until the 56-day monitoring period's completion. It can be observed that high WPSF replacement levels in concrete make it less resistant to shrinkage. This could be explained by the presence of fine aggregates that may restrain the amount of shrinkage of the cement paste, and this effect gradually fades with increasing the amount of WPSF in the concrete mixes [30]. The low stiffness and compressibility of polystyrene particles, which provide very little restraint to the shrinkage of paste [31]. As was previously noted, WPSF is a compressible material with a high porosity, which indicates more water can wick through its pores (up to 7%), decreasing its mechanical and durability properties [27]. Generally, polystyrene is a lightweight material that has a low density and is highly porous. When polystyrene beads are mixed with concrete, they create voids within the material that can trap air and moisture. As the concrete cures and dries, the trapped air and moisture can escape, leaving behind small voids in the material. These voids can cause the concrete to shrink and contract, leading to cracking and other forms of damage [27]. Similar findings were reported by Herki and Khatib [27] and Tang and Nadeem [30].

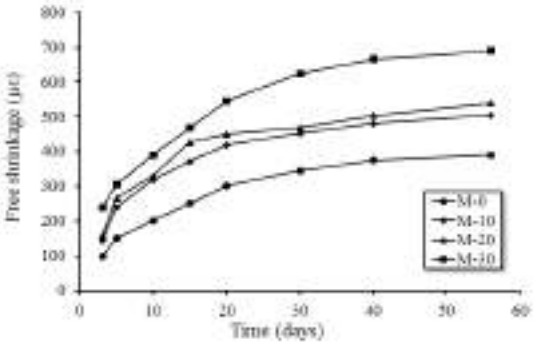

Fig. 11: Free shrinkage of concrete containing varying amounts of WPSF at different times.

4.6 Ultrasonic pulse velocity (UPV)

The UPV values of concrete containing varying amounts of WPSF at 7 and 28 days are presented in Figure 12. At both ages (i.e., 7 and 28 days), it can be observed that the higher the percentage of WPSF replacement accompanied the decrease in the UPV.

 ISBN 978-9959-9703-2-9

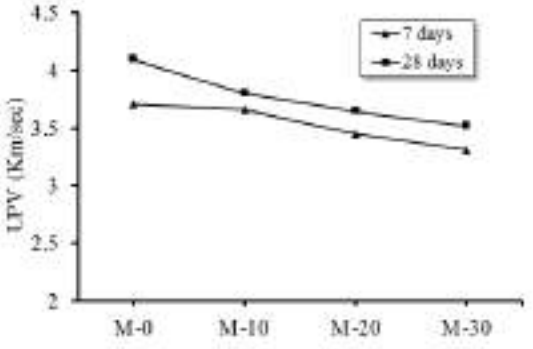

Fig. 12: UPV of concretes containing varying amounts of SPS at 7 and 28 days.

The trend is similar to that of concrete compressive and flexural strengths in that an increase in WPSF in concrete leads to a decrease in UPV. The UPV values of the concretes containing 30% WPSF at 7 and 28 days of age decreased by 10% and 14%, respectively, compared to the control mixture. The ultrasonic pulse velocity of a material is determined by its density. When WPSF is incorporated into concrete, it reduces the overall density of the concrete, which in turn decreases the UPV that can pass through it. Overall, adding WPSF to concrete can improve its acoustic and thermal properties, making it more effective at absorbing sound and temperature. This can have a range of structural applications.

5 Conclusions

The following are the conclusions of this study:

- The incorporation of WPSF caused a sharp reduction in the slump of the concrete at replacement levels between 10% and 30%.
- The air content of the WPSF concrete increased with the level of replacement, resulting in a lower density.
- The concrete with a higher volume of WPSF showed higher water absorption. The inclusion of WPSF in concrete reduces its density.
- The incorporation of WPSF caused a reduction in the compressive strength and modulus of elasticity of the concrete depending on the level of replacement with natural sand. After 28 days of curing, the mixture containing a 30% percentage of sand replacement still had suitable compressive strength for construction applications.
- The flexural strength of WPSF concrete decreased as the amount of WPSF in the mixture increased.

 ISBN 978-9959-9703-2-9

- High WPSF replacement levels in concrete made it less resistant to free shrinkage, with the majority of free shrinkage taking place in the first 30 days.

Increasing the WPSF content in concrete led to a higher UPV, which contributes to improving thermal and acoustic insulation.

Overall, the study suggests that the use of WPSF in concrete can have both positive and negative effects on various properties of concrete. The results should be considered when designing concrete mixtures, and further research is needed to better understand the potential of WPSF as a sustainable construction material.

References

[1] Altwair, N., M. & Sryh, L., S., (2020), Effect of Sawdust on The Mechanical Properties of Mortar Using Local Materials, Third Conference for Engineering Sciences and Technology, 1-3 December 2020 /Alkhoms –Libya. DOI: http://dspace.elmergib.edu.ly/xmlui/handle/123456789/208.

[2] Akcaozoglu, S. & Atis, C.D., (2011), Effect of Granulated Blast Furnace Slag and Fly Ash Addition on the Strength Properties of Lightweight Mortars Containing Waste PET Aggregates. Constr Build Mater, **25**, 4052–8. DOL: https://doi.org/10.1016/j.conbuildmat.2011.04.042

[3] Kockal, N.U & Ozturan, T., (2011), Strength and Elastic Properties of Structural Lightweight Concretes. Mater Des ,**32**, 2396–403. DOL: https://doi.org/10.1016/j.matdes.2010.12.053

[4] Altwair, N.M., Megat Johari, M.A., and Saiyid Hashim, S.F., (2012), Flexural Performance of Green Engineered Cementitious Composites Containing High Volume of Palm Oil Fuel Ash, Const. Build. Mater., **37**, 518–525. DOI: https://doi.org/10.1016/j.conbuildmat.2012.08.003.

[5] Altwair, N.M., Johari, M.A.M., and Hashim, S.F.S., (2013), Influence of Treated Palm Oil Fuel Ash on Compressive Properties and Chloride Resistance of Engineered Cementitious Composites. Mater. Structu., **47,** 667–682. doi:10.1617/s11527-013-0087-4.

[6] Pczieczek, A., Schackow, A., Effting, C., Dias, T. F. & Gomes, I., (2018), Properties of Mortars Containing Tire Rubber Waste and Expanded Polystyrene (EPS), Urb. Enviro. Eng., **11**, 219-225. DOI: 10.4090/juee.2017.v11n2.219225

[7] Ferrándiz-Mas, V. & García-Alcocel, E., (2013), Durability of Expanded Polystyrene Mortars, Constr. Build. Mater., **46**, 175-182. DOI: https://doi.org/10.1016/j.conbuildmat.2013.04.029

[8] Ubi, S. E., Ewa, D. E., Bessong, A. R. & Nyah, K. D, (2022), Effects of Incorporating Expanded Polystyrene in Concrete Construction., Buil. Constr. Plan. Res., **10**, 79-101. DOL: 10.4236/jbcpr.2022.103004.

[9] Herki, B. A. & Khatib, J. M., (2013), Lightweight Concrete Incorporating Waste Expanded Polystyrene, Adv. Mate. Res., **787**, 131-137. DOI: https://doi.org/10.4028/www.scientific.net/AMR.787.131.

[10] Babu, K.G., Babu, D.S. & Wee, T.H., (2006), Effect of Polystyrene Aggregate Size on Strength and Moisture Migration Characteristics of Lightweight Concrete. Cem. Conc. Comp., **28**, 520-527.DOI: https://doi.org/10.1016/j.cemconcomp.2006.02 .018

[11] Ferrándiz-Mas V & García-Alcocel E., (2012), Physical and Mechanical Characterization of Portland Cement Mortars Made with Expanded Polystyrene Particles Addition, Mater. Constr, **62**, 547–66. DOI: 10.3989/mc.2012.04611.

[12] LSS 340-09, Libyan Standard Specifications in Portland Cement, Libyan National Center for Standardization and Metrology, 2009.

[13] BSI 812-95, Methods of Sampling and Testing of Mineral Aggregates, Sands, Fillers, Part 1, British Standard Institution (BSI), London, 1995.

 ISBN 978-9959-9703-2-9

[14] Mazizah, E. M., Robert T., Razak, A., Kifli, A. Z. & Nisa A., (2022), Compressive Strength of Concrete Containing Expanded Polystyrene Styrofoam (EPS) Concrete and Partial Cement Replacement of Fly Ash and Silica Fume, Mechan. Eng., **11**, 301-317. DOI: https://doi.org/10.1177/2633366X2091.

[15] ASTM C185 – 15, Standard Test Method for Air Content of Hydraulic Cement Mortar, ASTM International: West Conshohocken, PA, USA, 2015.

[16] ASTM C143/C143M-00. Standard Test Method for Slump of Hydraulic-Cement Concrete, ASTM International: West Conshohocken, PA, USA, 2000.

[17] BS 1881-114, testing concrete - Methods for Determination of Density of Hardened Concrete, British Standard, Part 114, British Standard Institution (BSI), London, 1983.

[18] ASTM C642, Standard Test Method for Density, Absorption, and Voids in Hardened Concrete, ASTM International: West Conshohocken, PA, USA, 2013.

[19] Bengin M. A. H., (2017), Absorption Characteristics of Lightweight Concrete Containing Densified Polystyrene, Civi. Eng. J., **3**, 594-609. DOI: 10.28991/cej-2017-00000115

[20] BS 1881-116, Testing concrete. Method for Determination of Compressive Strength of Concrete Cubes, Fillers, Part 1, British Standard Institution (BSI), London, 1983.

[21] ASTM C78/C78M – 16, Standard Test Method for Flexural Strength of Concrete (Using Simple Beam with Third- Point Loading) ASTM International: West Conshohocken, PA, USA, 2016.

[22] ACI 318-08, (2008), Building Code Requirements for Structural Concrete and Commentary. American Concrete Institute.

[23] ASTM C157/C157M-08 Standard Test Method for Length Change of Hardened Hydraulic-Cement Mortar and Concrete, ASTM International, West Conshohocken, PA, USA, 2008.

[24] ASTM C597–09, Standard Test Method for Pulse Velocity Through Concrete, ASTM International, West Conshohocken, PA, USA, 2009.

[25] Kin, L. W. & Ariffin, M. A. M., (2016), Strength Properties of Expanded Polystyrene Concrete and Cold Formed Steel Wall Frame Composite, Mater. Scie., **11**, 126-173. DOI: 10.36108/laujoces/9102/20(0121

[26] Roman C. , Tomáš T. , Fládr, J. & Petr B., (2017), Mechanical properties and durability of crumb rubber concrete, Mater. Sci. Eng.g, **236**, 1-7. DOI: 10.1088/1757-899X/236/1/012093

[27] Herki, B. A. & Khatib, j., (2016), Valorisation of Waste Expanded Polystyrene in Concrete Using a Novel Recycling Technique, Europe. J. Environ. Civi. Eng., 1-19. DOI: doi.org/10.1080/19648189.2016.1170729

[28] Askar, L. K., Albarwary, I. H. & Askar, M. K., (2019), Use of Expanded Polystyrene (Eps) Beads in Silica-Fume Concrete, J. Univ. Duhok, **22**, 30-38. DOI: https://doi.org/10.26682/sjuod.2019.22.1.5

[29] Salahaldeen, A. S., & Al-Hadithi, A. I., (2022), The Effect of Adding Expanded Polystyrene Beads (EPS) on the Hardened Properties of Concrete, Eng. Tech. Appl. Sci. Rese., **12**, 9692-9696. DOI: https://doi.org/10.48084/etasr.5278

[30] Tang, W.C., Lo, Y. & Nadeem, A., (2008), Mechanical and Drying Shrinkage Properties of Structural-graded Polystyrene Aggregate Concrete, Cem. Conc. Comp., **30**, 403–409. DOI: https://doi.org/10.1016/j.cemconcomp.2008.01.002

[31] Elsalah, J., Al-Sahli, Y., Akish, A., Saad, O., & Hakemi, A., (2013). The Influence of Recycled Expanded Polystyrene (EPS) on Concrete Properties: Influence on Flexural Strength, Water Absorption and Shrinkage, AIP Conference Proceedings, **1569**, 181–185. DOI: https://doi.org/10.1063/1.4849254

 ISBN 978-9959-9703-2-9

المؤتمر الدولي الثاني للعلوم والهندسة
2nd International Conference on Science and Engineering
ICSE 2023
Faculty of Engineering - University of Bani Waleed
Bani Waleed, Libya

Paper Code: ICSE-022

THE BEHAVIOUR OF DIFFERENCE LOCATIONS OPENING SHAPES IN DEEP BEAM

First Author ,Ashraf M.L.Milad Second Author Nori.S.A.Ateig
Third Author Juhaynah .S.Alshukri
Department of civil Engineerin , College of Engineering /Bain Waleed-University, Libya
*Crosspnding author: nuriwerfali@gmail.com

Abstract: The aim of this study is to examine the deep beam opening behavior of lightweight reinforced concrete (LWC) beams with or without web openings, analyzed by ansys19 software. The analysis included five samples of different shapes, deep solid beam, deep beam containing two square holes with sides length of 80 mm and the horizontal spacing between the two holes is 220 mm, deep beam containing two holes Square with side lengths of 80 mm and the maximum distance between the two holes is 420 mm, a deep beam contains two round holes with a diameter of 80 mm and the distance between the two holes is 220 mm, a deep beam contains two round holes with a diameter of 80 mm and the distance between the two holes is 420 mm. Each sample was subjected to one point load. The effect of distances between the gaps on the behavior of the sample was analyzed and compared. The results indicated that the distances between the gaps affect the The behavior of the deep beam, where it was found that the deep beams with gaps spaced from the edges of the beams are the closest behavior to the deep beams without gaps, except that the results showed that the difference is not significant, but it is noteworthy and noteworthy and must be taken care of.

Keywords:

Introduction

Lightweight foam concrete is a new type of lightweight concrete, with the advantages of ordinary concrete, aerated concrete and self-compressing concrete, as through it the natural aggregate is partially replaced by polystyrene foam, and this leads to reducing the weight of the concrete unit as well as maintaining the required strength. This reduces the dead load by 15 to 20%, reduces the size of columns, bases and other bearing elements, and reduces the total cost. Deep beams are members that are loaded on one side and supported on the opposite face so that stress supports can develop between the loads and the supports, and have either clear spans (Ln), at, equal to, or less than four times the depth of the total member (H). Or that the areas of concentrated loads (a) be within twice the depth of the member (d) from the support face. In some facilities, deep beams with

 ISBN 978-9959-9703-2-9

different openings and shapes are required, and this affects the behavior of the deep beams and the basic services of the deep beams. In such cases, it is important to know the behavior of these beams and their ultimate strength. There are many previous studies that studied the behavior of deep beams that contain and do not contain gaps, and also studied the behavior of the sample in the presence of gaps of different shapes and distances including that: Amr H. Zaher, Wael Montaser and Mohamed Ramadan studied the shear behavior of simple, continuous beams of light concrete with openings. The testing program included seven simple deep beams of light concrete, and the most important variables studied Simple beam test is the size of the holes, the location of the holes, the design pressure resistance of the concrete and the percentage of accidental reinforcement for the bunch. The results showed that when the side openings are present at the beam height equal to 02% to 22%, respectively, of the total height of the beam, this leads to a decrease in the final shear strength of the simple deep beams by about 15% to 62% compared to the deep beam that has no side openings [1].

(Nishitha Nair, Kavitha PE), University of Kerala, India, studied the effect of loads on seven different samples of deep beams (Deep beam without hole , deep beam with a circular hole one at centre , deep beam with a rectangular hole one at centre , deep beam with one circular hole one at side, deep beam with one square hole one at side, Deep beam with circular hole at two sides and Deep beam with rectangular hole at two sides) with ansys 14. It was found that the maximum tolerance was in the deep beam without hole, and the lowest tolerance was in the deep beam with rectangular hole at two sides [2]. (Hawraz Karim M. Amin, V.C .Agarwal and Omar Q. Aziz) studied the effect of different volumes and locations of holes in deep hollow beams. By comparing the numerical results shown, deep beam models without gaps were studied and were created by (An-sys + CivilFEM) to study the effect of openings compared to a beam without openings but with the same size to show the effect of creating openings in the actual beam with variable sizes of gaps. Shear causes a sharp decrease in final shear by about (53.6%) and when opening is located in the reinforced area supports an average decrease in stress (23.93%) but between the mid-range a small effect, as the average decrease in stress (8%), when creating square openings with dimensions (0.45 h x 0.45 h), the average decrease in shear stress was approximately (45.78%) and dimensions (0.30 h x 0.30 h).Less effect where the average reduction in shear stress is (11.55%) [3].

 ISBN 978-9959-9703-2-9

Khattab Salim Abdel-Razzaq, Haider Ali and Mays Mohamed Abdel-Karim studied the effect of different forms of gaps in deep beams. The study was carried out on thirteen deep beams under the effect of point load with rectangular, square, circular, horizontal and vertical openings. Choose two holes per beam, one in each cut-out. Creating square, circular, horizontal, and vertical rectangular openings reduced the final capacity by about 20.5%, 18.3%, 24.7%, and 31.7%, respectively, compared to the reference solid beam. In general, the opening size was found to be inversely proportional to the maximum capacity of the deep beam and the mid-section deviation because the reduction of the opening size resulted in less interruption in the compressive support connecting the loading and support points [4].

EXPERIMTAL PROGRAM

The pilot study consisted of five simply supported reinforced concrete girders with mesh and no openings, and made of lightweight concrete. The packages were tested under the influence of a single concentrated payload by applying them to ANSYS19 software. All tested samples have the same geometry and the main upper and lower longitudinal reinforcement. The research sample was taken from the study (Amr Hassan Zahir, Wael Montaser and Muhammad Ramadan) entitled (An experimental study of the behavior of lightweight reinforced concrete deep beams with mesh holes)[1].

Conclusion

A conclusion must include advantages, limitations, and applications and don't repeat the abstract, delete and type).

Geometry of the Deep Beam:

The geometry of the full size beam is 1100mm x 400mm x 80mm. The beam is supported simply by providing a plate support on both sides. Single point loads are applied at the center of the beam. The concrete grade was 28.9 MPa and yield strength 550 MPa.

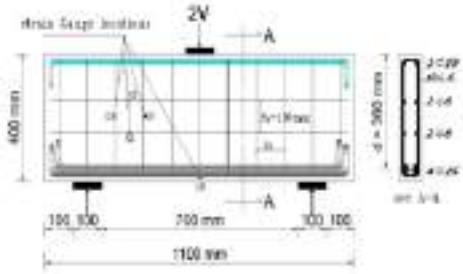

Figure (1): Reinforcement detail

Test Specimens

Table (1) shows samples of deep beams for treatment by research, its dimensions and the dimensions of the gaps in it.

Table (1): Typical dimensions of tested beams

Name	shape of specimen

ISBN 978-9959-9703-2-9

BWOH	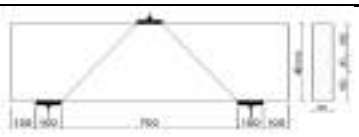
BSHmS	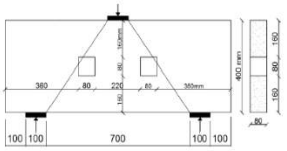
BSHeS	
BCmHS	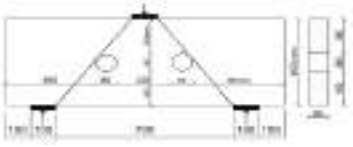
BCeHS	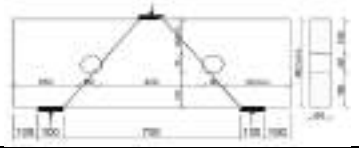

Beam components	Selected from ANSYS library	Element characteristics
Reinforced Concrete Structural Solid	SOLID65	8-node Brick Element (3 Translation DOF per node).
1-Reinforcing bars (main, horizontal and vertical stirrups).	LINK180	2-node Discrete Element (3 Translation DOF per node).
Layered Structural Solid	SOLID186	20-node Brick Element (3 Translation DOF per node).

Elements used for Modeling:

Table (2): shows the characteristics and identifications of the selected ANSYS finite element type representative of the main components for all beams.

Table (2): Characteristics and identifications of the selected ANSYS finite element types representative of the main components for all beams. (12)

RESULTS:

Evolutions of Crack and Load Capacity for RC.

Deep Beam:

The appearance of cracks begins when the samples are exposed to excessive loads or to more than they can bear, as when increasing loads more the samples reach the final breaking point and that varies from one sample to another due to the difference in the shapes of gaps, their dimensions and the distance between them.

First crack:

 ISBN 978-9959-9703-2-9

The five samples were subjected to an Aries point, and as the load increased, primary cracks appeared in the samples. It turned out that the BSHmS sample was the one that showed cracks first among the four hollow samples, so it started to crack when subjected to a load of 60 kN, while it was the last one that showed the first cracks among the four experimental samples. The cracks started when subjected to a load of 70 kN. The result is closer to the BWOH reference, the sample starting to flex under a load of 92 kN. The following figure shows all the results of five samples from the first part:

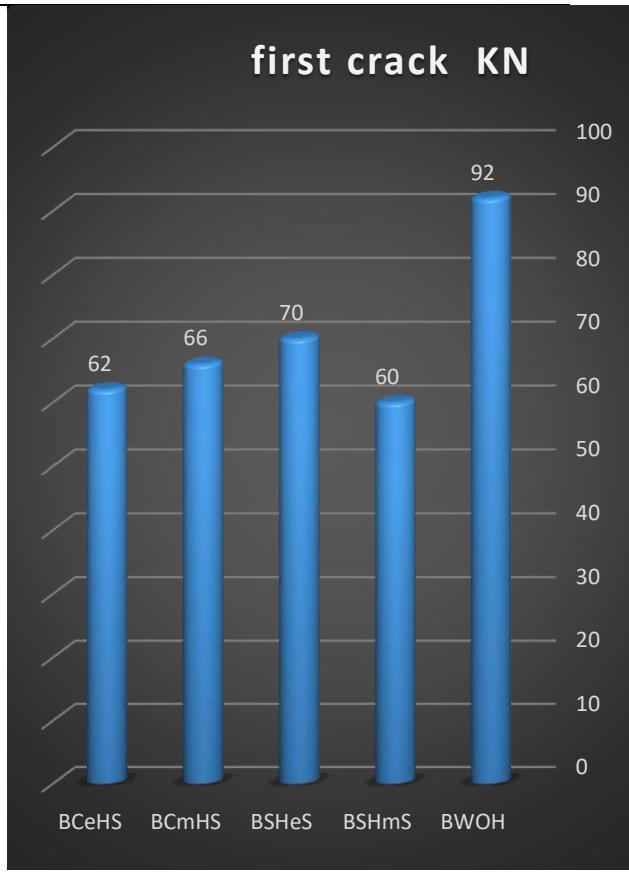

Figure (2): First Crack

final load:

The samples reached collapse mode when subjected to excessive loads.

In the BWOH reference sample, which collapsed at an exposure load of 213 kN, the BCmHS sample was closest to the reference sample, and collapsed at a load of 205.25 kN, which means that it requires behavior very close to 96% steel. The BSHeS sample was the

 ISBN 978-9959-9703-2-9

furthest in behavior compared to the BWOH reference sample, and it collapsed at a load of 197 kN, this indicates that it possesses 92% of the strength reference sample. The following figure (3) shows all the results of the five samples in terms of final load:

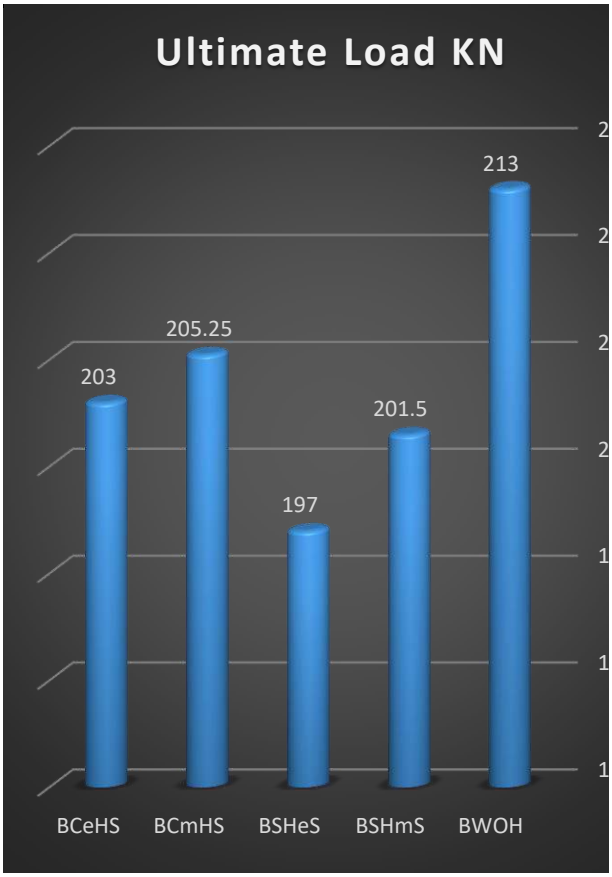

Figure (3): Ultimate load

Cracking Pattern and Mode of Failure:

The ANSYS program crack pattern records a crack pattern at each load step evolution of crack pattern developing for each beam at last loading step. ANSYS program display circles at locations of cracking or crushing in concrete elements. Cracking is shown with a circle outline in the plane of the crack, and crushing is shown with an octahedron outline the first crack at an integration point is shown with a red circle outline, second crack with green outline, and third crack with a blue outline (ANSYS manual version 10.0).

Table (3): shows the evolution of cracks in the five experimental samples.

 ISBN 978-9959-9703-2-9

Name	Cracks develop in the sample
BWOH	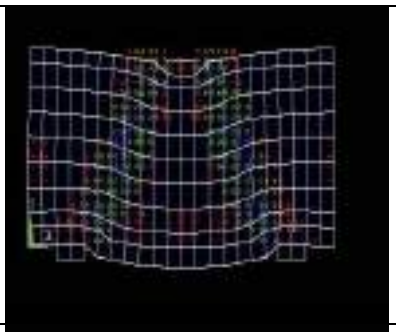
BSHmS	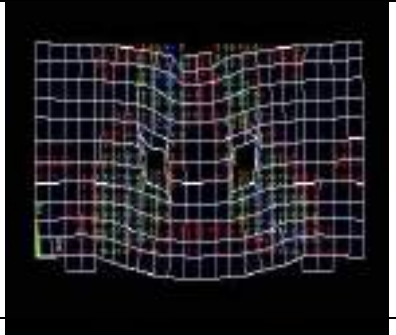
BSHeS	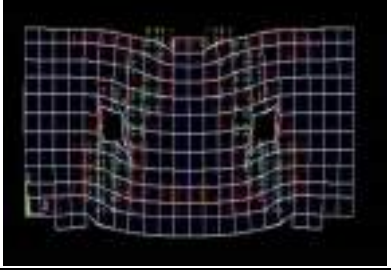
BCmHS	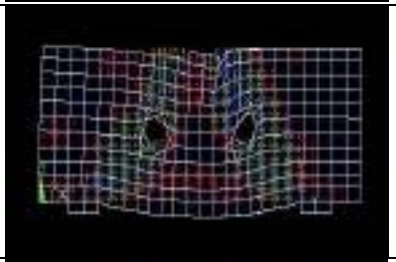
BCeHS	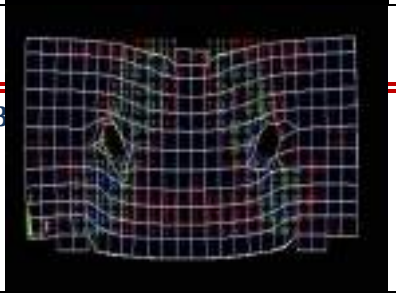

Load Deflection Curve:

The following figure shows the deflection results for the five samples as a result of exposure to different loads:

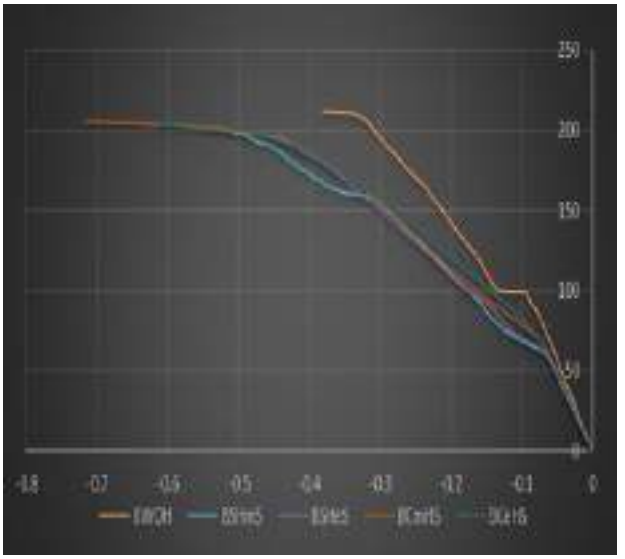

Figure (4): Comparison of load-deflection curve for specimens with different web opining type.

CONCLUSION:

ISBN 978-9959-9703-2-9

1- Behavior of deep hollow beams With different distances between the gaps gaps.

2- It contains a cavity containing damage containing chemicals containing the closest.

3 - the ray that contains part of this form of the shape that contains the shape of the saviors.

4- Deep beams that contain two square gaps with a distance of 220 mm between them.

5- The closer the gaps are to the end of the deep beam, the more danger will be posed to the behavior of the sample.

6- Deep beams with a circular cavity and the gaps between them are 220 mm The most flexible of the five samples.

7- Deep beams with a square cavity and a distance of 420 mm is the least flexible among the five samples.

Recommendations:

1- Testing the behavior of the deep beam with one gap, but with different positions.

2- Testing the behavior of the deep beam with two gaps of the same shape and size and with different distances, not just two.

3- Testing the behavior of the deep beam, so that its dimensions are in meters or centimeters, so that there is more room for spacing between the gaps.

4- Testing the behavior of the deep beams that contain gaps, so as to change the location of the gaps in the vertical form, not the horizontal one.

References :

1-Amr H. Zaher , Wael Montaser & Mohamed Ramadan. Experimental Study of Behavior of Reinforced Light-Weight Concrete Deep Beams with Web Openings , 2017.

2-Nishitha Nair, Kavitha P.E ,M.Tech Student, Civil Department EFFECT OF OPENINGS IN DEEP BEAMS USING STRUT AND TIE MODEL METHOD , 2015.

3-Hawraz Karim M. Amin, V.C. Agarwal, Omar Q. Aziz . Effect of Opening Size and Location on the Shear Strength Behavior of R.C Deep Beams without Web Reinforcement , 2013 .

4-Khattab Saleem Abdul-Razzaq , Hayder I. Ali and Mais M. Abdul-Kareem . A New Strengthening Technique for Deep Beam Openings Using Steel Plates , 2017.

5-R. Khaldoun and A. Khaled, “Minimum transvers reinforcement in 65 Mpa concrete beams, “ACI Structural Journal, vol. 101, pp.872-878, 2004.

6-Campione, Giuseppe and Minafò, Giovanni. Behaviour of concrete deep beams with openings and low shear span-to-depth ratio. Italy : Università di Palermo, 2012.

7-Haider M. Alsaeq .Effects of Opening Shape and Location on the Structural Strength of R.C. Deep Beams with Openings , 2013 .

8-Bashir, A, et al., et al. Identification of Shear Cracks in Reinforced Beams Using Finite

 ISBN 978-9959-9703-2-9

Element Method. s.l. : Pakistan Journal of Science, 2014.

9-KANCHANADEVI, A and UMARANI, C. Non-Linear Finite Element Analysis for Assessment of Bridges. s.l. : International Journal of Earth Science and Engineering, 2015.

10-YANG, SIOW SIN. EFFECT OF OPENING WITH VARIOUS SIZE AND LOCATION ON RC DEEP BEAM. s.l. : Faculty of Civil Engineering and Earth Resources UNIVERSITI MALAYSIA PAHANG, 2015.

11- Er. Sheelu Mariam Punnoose , Er. Afia.S , Hameed EXPERIMENTAL STUDY OF STRENGTHENING OF RC DEEP BEAM WITH WEB OPENING , 2016 .

12-Building Code Requirements for Structural Concrete (ACI 318-11).

13-k, Kong f and r, Sharp g. Taylor & Francis book. [book auth.] Kong F K. Strength of reinforced concrete deep beams. New York.

 ISBN 978-9959-9703-2-9

المؤتمر الدولي الثاني للعلوم والهندسة
2nd International Conference on Science and Engineering
ICSE 2023
Faculty of Engineering - University of Bani Waleed
Bani Waleed, Libya

Paper Code: ICSE-035

THE EFFECT OF REPLACING FRESH WATER WITH SALT WATER AND SEA WATER IN CONCRETE

Abdulrahman Abdulsalam Bin Zayd
Civil Engineering, Higher Institute of Engineering Technology/Zliten, Libya
abdo.zaid1979@yahoo.com

Abstract: This study aim to verify the possibility of using salt water and sea water instead of fresh water for concrete in mixing and treatment. Comparing its results with the pressure resistance test of a previous study, where this study relied on two previous studies, the first one, which I was involved in, depended on determining the place underground water wells and the highest salinity water. But in second study, which I have conducted, the water of the highest salinity wells was used in the first study in addition to the use of fresh water and sea water. Concrete cubes for all this water were prepared and immersed in fresh water. This study is the same as the second one mentioned above, however, the difference between them is the use of sea water in immersion of concrete cubes.
The results showed that the used underground water had a resistance in 7 days between (22.66-26.66)Mpa, while the result in 28 days were between (28.06- 34.13)Mpa. For fresh water submerged in sea water in 7 days were 25.06 Mpa, and in 28 days were 31.16 Mpa, while sea water in 7 days were 22.1 Mpa and in 28 days 28.93 Mpa.

Keywords: (treatment, sea water, fresh water, underground, resistance test)

Introduction

Libya is located on the northern coast of Africa. It is considered among the poorest Arab countries in water resources, due to its location within arid and semi-arid areas [1,2]. The main and important resource in Libya is underground water, and it represent 95% of human consumption for various purposes [3]. About 85% of underground water available is consumed in agriculture and 11.5% for urban purposes while the industrial consumption represents 3.5% [4]. The Libya coast on the Mediterranean Sea is about 1980 km [4].

The increase in population led to an increase in demand for water in all fields, and the lack of infrastructure encourages the citizens to dig wells and break the restrictions on drilling wells [5]. All of which caused the deterioration of underground water, especially in coastal areas [6,7]. Water resources are one of the most important elements of development that control the continuity of sustainable development. It is impossible to plan for

 ISBN 978-9959-9703-2-9

continuous development without managing and planning the most important resources for its establishment and preservation for future generations.

Mr. A. C. Govalkar and Mr. D. S. Lalal is study showed good and satisfactory results of use of sea water in mixing and treatment of concrete [8]. Also, another study by Mr. Rita Irmawaty showed that sea water can be used in mixing and treatment [9].

1-1 Objective

Libya is considered one of the poorest countries for fresh water resources and it depends on groundwater as the main resource. Because of its geographical site along the seashore, the idea of this study rose by providing an alternative to preserve fresh water and groundwater. The main objective is to use sea water, groundwater and fresh water in mixing concrete and curing it with sea water. The impact of each of them on compressive resistance of concrete during 7 and 28 days and comparing the obtained results with a previous study results of freshwater treatment.

1-2 Background of study

In this study, the compressive resistance of concrete was determined by carrying out compression tests in 7 and 28days. The concrete cubes were prepared using a prescribed concrete mix ratio of 1:3.31:1.68 and the water cement ratio was taken as 0.6. The concrete was produced using salt water, fresh water and sea water.

A total of 60 numbers of 150 x150x150mm concrete cubes were cast. The mixing of concrete was carried out manually by hand. After twenty-four hours the cubes were cast, the hardened concrete cubes were de-molded, and the cubes were submerged carefully in the curing tank filled with water sea. At each specified period of days, the cubes were crushed to determine the compressive resistance of the concretes.

1-3 Literature Review

Studies carried out by researchers related to this area are highlighted and the gaps required to be filled by this project work our pointed out.

1- Similarly, Akinkurolere O.O et al (2007), in their paper titled “The Influence of salt water on the compressive strength of concrete” presented the result and findings of an experimental research on the influence of salt water from Lagos Lagoon, in Nigeria on the compressive strength of concrete. In the research, 132 concrete cubes of mould size 150x150x150mm were casted with fresh water (66 cubes) and salt water (66 cubes) in the ratio of 1:2:4 by weight of concrete and water-cement ratio of 0.6. They were cured in fresh water and seawater respectively. The concrete cubes were tested for compressive strength for 7, 14, 21 and 28 days respectively. The compressive strength of concrete is shown to

 ISBN 978-9959-9703-2-9

increased by the presence of salt or ocean salt in the mixing and curing water. The rate of strength gain is also affected when the concrete is cast with fresh water and cured with salt water.

2- Felah M Wegian (2010) observed that the compressive strength and consequently the other related strengths of concrete were shown to increase for specimens mixed and cured in sea water at early ages up to 14 days, while a definite decrease in the respective strengths was observed for ages more than 28 days and up to 90 days. The reduction in strength increases with an increase in exposure time, which may be due to salt crystallization formation affecting the strength gain.

3- M.I Retno Susilorini et al (2005) conducted experimental and analytical method. Through experimental method they investigated the compressive strength of concrete cylinders, with 7 days and 14 days with seawater curing and plain water curing. After 7 days and 14 days of curing, the concrete cylinders were tested by compressive testing machine. This research concludes that both experimentally and analytically, the compressive strength of 7 days and 14 days old concrete specimens cured by seawater are higher than those cured by plain water.

4- E.M. Mbadike et al (2011) investigated the effect of sea water in the concrete production and reported that the strength reduction is about 8%.

5- Md. Moinul Islam, Md. Saiful Islam(2012) reported that, when the concrete specimens made with sea water and cured with sea water compared to concrete made with plain water and cured with plain water the loss of compressive strength of concrete is 10%.

2- MATERIALS USED AND METHODS

All the materials used in this study are from Zliten.

2-1 Cement

The used cement is from Al-Burj Contracting Company.

2-2 Coarse aggregate and fine aggregate

They were prepared in quantities sufficient to conduct the previous study [10] and the current study. The tests were conducted in the Faculty of Engineering laboratories at the Alasmarya University. It included the tests of granular gradient of coarse and fine aggregates and the results that are shown in figures (1) and (2) respectively satisfy the American specifications [11]. Los Angeles test, the percentage of absorption and specific weight of coarse aggregate results are shown in table (1). The specific test of sand is shown in table (2). All the states tests are within the mentioned specifications.

 ISBN 978-9959-9703-2-9

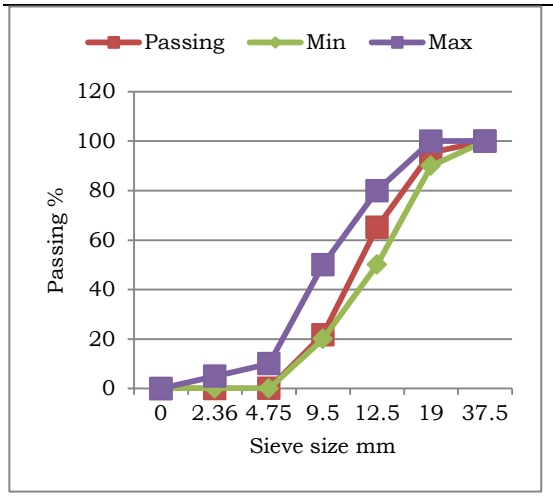

Fig. 1: The granular gradient of coarse aggregate [10]

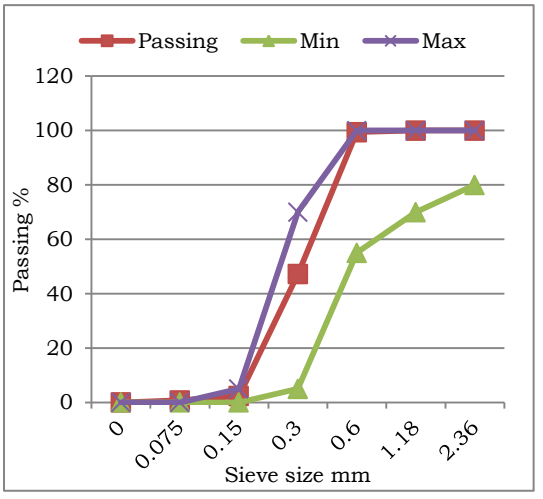

Fig. 2: The granular gradient of sand [10]

Table 1: Properties of aggregate observed in laboratory test [10].

No	Description	Test Result	Range Specification	ASTM
1	specific gravity test	2.667	2.5 – 2.75	C127[11]
2	water absorption %	2.15	Max = 2.5%	C127[11]
3	Los Angeles Abrasion test %	26.9	Max = 40%	C131[12]

Table 2: Physical properties of fine aggregate.

Description	Test Result	Range Specification	ASTM
specific gravity test	2.63	2.5 – 2.75	C128[13]
water absorption %	0.94	Max = 2.5%	C128[13]

2-3 Water used in mixing

2-3-1 Concrete mixing

The high salinity underground water from three wells taken from previous study which I involved – was used to mix the concrete. Table (3) shows the results of wells water tests [7]. Also, sulfate test and fresh water test were carried on the results are shown in table (4). All these tests were conducted in the Environmental Sanitary Office laboratory in Zliten. Sea water was used to flood the concrete cubes.

ISBN 978-9959-9703-2-9

Table 3: The amount of salt and chloride in wells water [7].

No. Of well	Name of well	TDS mg/L	CL mg/L	PH	SO_4 mg/L
W_1	Gwellat	2388	1503	7.4	1414
W_2	Ka'am Al	3114	890	7.4	1860
W_3	Shaheed Hamza	6131	2475	7.1	870

Table 4: Fresh water test

No. Of well	Name of well	TDS mg/L	CL mg/L	PH	SO_4 mg/L
W_4	Fresh Water	62	40	7.53	22

2-3-2 Immersion water

After completion of the preparation of thirty concrete cubes for underground water for the three wells, as well as fresh water and sea water, they were immersed in sea water.

2-3-3 Mixing process

In Higher Institute of Engineering Technology. The components of concrete had been mixed manually because there were some problems in mechanical mixing. Figure (3) shows the components of the mixture and the mixing process. The mixing ratio of the components was (1:3.31:1.68:0.6), which expresses cement, coarse aggregate, sand, water respectively [10].

Fig. 3: The components of the mixture

4- Results and discussion

4-1 Concrete compressive strength

After mixing the concrete components manually, preparing the cubes and immersing them in sea water, and conducting a cracking test for concrete cubes after 7 and 28 days in Faculty of Engineering laboratory, the obtained results were recorded in tables (5, 6). Also, the results were compared with the results of the previous study [10] which are shown in figure (4).

Table 5: Results of weights and compressive

ISBN 978-9959-9703-2-9

resistance of concrete cubes in 7 days.

SSample Well	Sample symbol	Sample No.	Weight (g)	Concrete Resistance (Mpa)	AV
Gwellat Well	W1	1	8007	26	26.6
		2	8271	26	
		3	7993	28	
Ka'am Well	W2	1	8302	21.3	25.2
		2	8024	29.8	
		3	8013	24.5	
Al Shaheed Hamza Well	W3	1	7879	25.3	22.66
		2	7983	22.3	
		3	8401	20.4	
Fresh water	W4	1	8246	25	25.06
		2	7892	28	
		3	7979	22.2	
Sea water	W5	1	8435	17	22.1
		2	8015	232.3	
		3	8178	26	

Table 6: Results of weights and compressive resistance of concrete cubes in 28 days.

Sample Well	Sample symbol	Sample No.	Weight (g)	Concrete Resistance (Mpa)	AV
Gwellat Well	W1	1	7960	28	28.06
		2	8269	29.9	
		3	8337	26.3	
Ka'am Well	W2	1	8119	29.1	28.9
		2	8218	30.1	
		3	8107	27.5	
Al Shaheed Hamza Well	W3	1	7839	28.8	34.13
		2	8118	33.1	
		3	8189	40.5	
Fresh water	W4	1	8044	34	31.16
		2	7977	29.2	
		3	7989	30.3	
Sea water	W5	1	8130	26.5	28.93
		2	8326	34.8	
		3	8025	25.8	

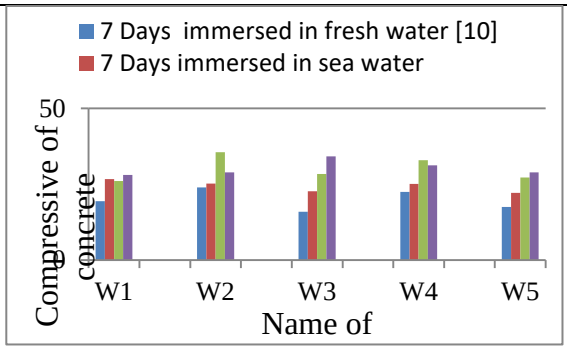

Fig. 4: A comparison of the compression resistance results of concrete cubes immersed in sea water and fresh water.

(w_1, w_2, w_3 are three salty wells water respectively and w_4, w_5 are fresh and sea water respectively).

Figure (4) shows the results of the concrete compression resistance for cubes immersed in fresh water [10] and for cubes immersed in sea water. From the results It can be concluded that sea water can be used in mixing and curing of concrete, as it gave satisfactory results up to 28 days. The results also showed that the average compression resistance of concrete immersed in sea water exceeded 25 Mpa.

From the results, it can be concluded that:

4-2 Salt:

ISBN 978-9959-9703-2-9

From figure (4), it can be noticed that the higher the concentration of dissolved salts in wells water, the higher the compressive resistance of concrete after 28 days, and it gave the greatest resistance to the highest salinity at W_3, in concrete to 7 days, which gave the maximum resistance to the lowest salinity at W_1, and figure (5) explains the relationship between the soluble salt of the water used in the study and the compressive resistance of concrete.

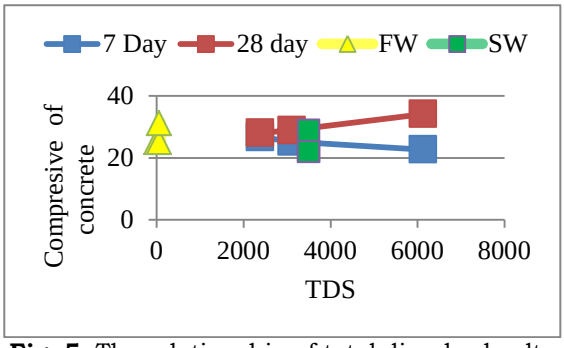

Fig. 5: The relationship of total dissolved salts to the compressive resistance of concrete

4-3 Chlorides:

The results indicated a fluctuation in the compressive resistance of the concrete in 7, 28 days. Figure (6) shows the relationship between the compressive resistance of concrete and the sulfates present in the water. Where it has been noticed from the figure that the compressive resistance of both fresh water and sea water ranges between higher and lower concrete resistance to underground water.

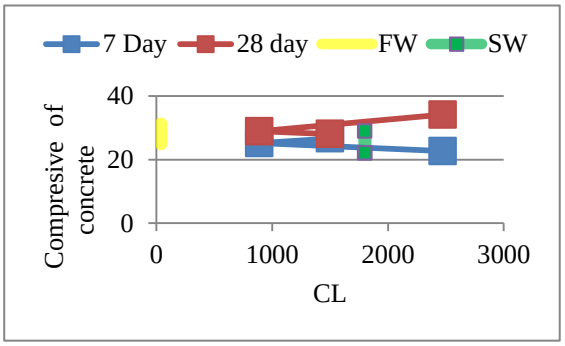

Fig. 6: The relationship of chlorides to the compressive resistance of concrete

4-4 PH:

The results of wells water in 7 days indicate that the relationship between PH and compressive resistance of concrete is a direct relationship, unlike in 28 days, the relationship is considered inverse. Figure (7) shows the relationship between compressive resistance of concrete and the PH of water used in concrete.

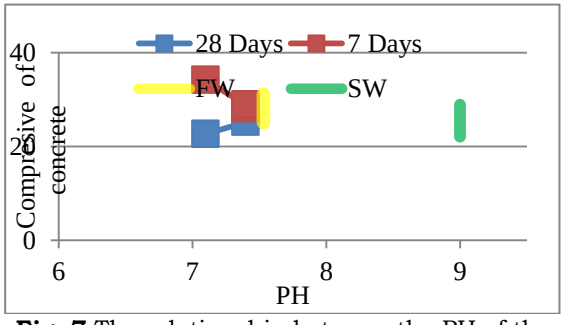

Fig. 7 The relationship between the PH of the used water and the compressive resistance of

ISBN 978-9959-9703-2-9

concrete

4-5 Sulfates:

The results showed a fluctuation in the compressive resistance of concrete between rise and fall in 7, 28 days, where it can be noted that in 28 days the maximum strength of concrete is the lowest concentration of sulfate, while fresh water and sea water pressure resistance varies between the results of concrete strength for wells water. Figure (8) indicates the relationship between the compressive resistance of concrete and the concentration of sulfate in water.

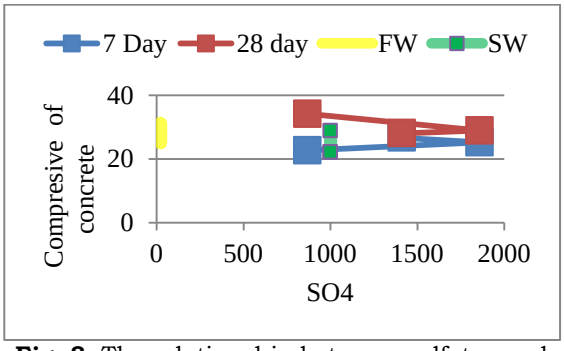

Fig. 8: The relationship between sulfates and the compressive resistance of concrete

5- Recommendations:

According to the results and the fact of limited underground water in Libya, the following recommendations can be considered:

1- Conducting tests on concrete: tensile, bending and corrosion tests in the short and long term.

2- Benefiting from sea water and using it instead of the man-made –river water or underground water.

3- The use of recycled or treated water from sewage in the fields of industry and conducting the necessary tests, while preserving human health and the environment.

الملخص بالعربي:

تأثير استبدال المياه العذبة بالمياه المالحة ومياه البحر

قسم التقنيات المدنية ، المعهد العالي للتقنيات الهندسية ، زليتن
*ترسل المقترحات علي snclibya@bwu.edu.ly

الملخص

تهدف هذه الدراسة في التحقق من إمكانية استخدام المياه المالحة ومياه البحر بدلا من المياه العذبة للخرسانة في الخلط والمعالجة ، ومقارنة نتائجها باختبار مقاومة الضغط لدراسة سابقة، حيث اعتمدت هذه الدراسة علي دراستين سابقتين ، الأولي: اعتمدت علي تحديد أماكن الآبار للمياه الجوفية والأعلى ملوحة، وكنت احد البحاث بها، أما الدراسة الثانية فتم استخدام مياه الآبار الأعلى ملوحة في الدراسة الأولي

 ISBN 978-9959-9703-2-9

بالإضافة إلي استخدام المياه العذبة ومياه البحر وإعداد مكعبات خرسانية لكل هذه المياه وغمرها بالماء العذب، وكنت الباحث بالدراسة، بينما هذه الدراسة فهي نفس الدراسة الثانية والفارق بينها هو استخدام مياه البحر في غمر المكعبات الخرسانية.

وأظهرت النتائج في خلط أنواع المياه وغمرها بمياه البحر، أن المياه الجوفية المستخدمة تراوحت مقاومتها في 7 أيام بين (22.66-26.66) ميجا باسكال، بينما أعطت النتائج في 28 يوم (28.06- 34.13) ميجا باسكال، والمياه العذبة المغمورة بمياه البحر أعطت في 7 و 28 يوم 25.06 و 31.16 ميجا باسكال علي التوالي، بينما مياه البحر أعطت في 7 و 28 يوم 22.1 و 28.93 ميجا باسكال علي التوالي.

الكلمات المفتاحية: المعالجة، مياه البحر، المياه العذبة، مياه الآبار، اختبار المقاومة.

References

[1] عمران علي احمد امشهر، سالم فرج مفتاح عطاف(2021). "تقييم وتصنيف نوعية مياه الآبار بمنطقة وادي زمزم ومدي صلاحيتها لإغراض الشرب والري". مجلة جامعة سبها للعلوم البحتة والتطبيقية. مجلد 20 العدد (4) 2021 . صفحة 143- 148.

[2] مصباح الصادق عبدالعزيز، ناصر مولود عبدالسلام. (2020). "تقييم الوضع المائي في المنطقة الممتدة من ساحل البحر بمدينة صبراته إلى منطقة عفار". Alexandria Journal of Agricultural Sciences, 65(1), page 15.

[3] حنان صالح فرج، نعيمة خليفة الغرياني، سالم محمد الرشراش. (2019). "دراسة هيدروجيوكيميائية للمياه الجوفية لمنطقة غدامس، درج، سينون شمال غرب ليبيا". المجلة الليبية للعلوم الزراعية، مجلد 24 العدد (2) السنة 2019، ص 1.

[4] م خالد عبدالسلام الفويرس، أ مفتاح فرج العماري .(2012). " الوضع المائي في ليبيا مشكلة العجز والحلول المقترحة". Libyan Agriculture Research Center Journal international . 3(S). 2012. Pp 1303.

[5] المادة رقم (9) لسنة 2003،بالقانون الليبي بشان رفع القيود المفروضة علي حفر ابار المياه المنصوص عليها القانون رقم (3) لسنة 1982.

[6] جمعة علي الميان، موسي خليل سعيد. (2019). " تقييم تداخل مياه البحر لساحل منطقة زليتن- ليبيا ". مجلة العلوم الإنسانية والتطبيقية جامعة الأسمرية. العدد 23 يونيو 2019. صفحة 338-339.

[7] إسماعيل حمودة، محمد خوجة، عبدالرحمن بن زيد.(2021). " التغير في الأملاح الذائبة والكلورايد للمياه الجوفية في عدة مناطق بمدينة زليتن". الجامعة الإسلامية- كلية الهندسة – زليتن (14-16 ديسمبر 2021-CEST الأسمرية المؤتمر الرابع للعلوم الهندسية والتقنية. صفحة 241.

[4] Govalkar, M. A., & Lal, M. D.(2020)., A Review on Effect of Saline Water And Fresh Water on Concrete., Wutan Huatan Jisuan Jishu. Volume XVI . JUNE/2020., Pp 439. ISSN:1001-1749

[5] Irmawaty, R., & Tjaronge, M. W. (2014)., Effect of seawater as mixing water on the mechanical properties of mortar and concrete., In ConCERN (Conference for Civil Engineering Research Networks) (Vol. 2014, pp. 61).

[6] Abdulrahman Bin Zayd. (2022)., Effect of Water Salinity on Concrete Strength., BANI WALEED UNIVERSITY JOURNAL OF SCIENCES & HUMANITIES. Twenty-six issue. Volume 2-December 2022.

[7] American Society for Testing and Materials ASTM C 136: Standard test method for sieve analysis of fine and coarse aggregates.

[8] American Society for Testing and Materials ASTM C 127: Standard Test Method for specific gravity and the absorption of coarse aggregate.

[9] American Society for Testing and Materials ASTM C 131: Standard Test Method for Resistance to Degradation of Small-Size Coarse Aggregate by Abrasion and Impact in the Los Angeles Machine.

[10] American Society for Testing and Materials ASTM C 128: Standard Test Method for Relative Density (Specific Gravity) and Absorption of Fine Aggregate.

[11] Akinkurolere, O. O, Jiang, C and Shobola O. M., (2007), The Influence of Salt water on the compressive strength of concrete., Journal of

 ISBN 978-9959-9703-2-9

Engineering and Applied Sciences., 2(2) Pp 414-415.

[12] Falah M. Wegian., (2010), Effects of sea water for mixing and curing on structural concrete studies., The IES Journal Part A: Civil & structural Engineering., Vol. 3, No. 4 Pp237-242. DOI: 10.1080/19373260.2010.521048.

[13] M. I. Reton Susilorini. Kristina Retno Dewi W, Tri Wibowo., (2005), The Performance of realy-age concrete with sea water curing., Journal of Coastal Department., Vol. 8, No. 2, Pp 85-95.

[14] Mbadike, E. M., & Elinwa, A. U. (2011)., Effect of salt water in the production of concrete., Nigerian Journal of Technology., 30(2), Pp 105-110.

Islam, M. M., Islam, M. S., Al-Amin, M., & Islam, M. M. (2012)., Suitability of sea water on curing and compressive strength of structural concrete., Journal of Civil Engineering (IEB)., 40(1), 37-45.

 ISBN 978-9959-9703-2-9

Paper Code: ICSE-038

PHYSICO-MECHANICAL AND SULFATE RESISTANCE EVALUATION OF CONCRETE MADE WITH GROUND GRANULATED BLAST-FURNACE SLAG

S. Attelisi[a], M. Albgoul[a], M. Ebailila[a], A. Abdulla[b]
[a] Department of Civil Engineering/Faculty of Engineering/Bani Waleed University, Libya
[b] Department of Civil Engineering/ College of Technical Sciences Bani Waleed, Libya
*Crosspnding author: mansour.ebailila@yahh.co.uk

Abstract: In recent years, with the aim of restricting the formation of ettringite and reducing the environmental impact associated with cement manufacturing, the incorporation of ground granulated blast-furnace slag (GGBS) as a partial replacement of cement has become a common tendency, due to its efficiency in enhancing the physico-mechanical properties of concrete. This research study reports the experimental results on the properties of concrete containing GGBS at different partial cement substitution levels (0, 50, and 75%). A total of three concrete mixes were manufactured using a water/cement ratio (w/c) of 0.55 and binder: sand: aggregate proportion of 1: 2: 3. Thereafter, a physico-mechanical evaluation including slump test, compactability degree test, unconfined compression strength (UCS) test, tensile splitting strength (TSS) test and sulfate attack, were performed to assess the concrete performance. The experimental results suggested that, although the use of GGBS as a partial cement replacement slightly affects the mechanical performance at the early curing age, its usage improves the consistency and yielded a higher residual mechanical performance after immersion in sulfate solution, particularly at higher substitution level (75%).

Keywords: (Ettringite, magnesium sulfate, mechanical strength, sodium sulfate, sulfate attack)

Introduction

Global warming is one of the substantial concerns for human civilization's future, imposing the necessity for the development of eco-friendly and sustainable construction strategies [1]. Generally, concrete is considered a widely versatile construction substance, probably due to its cost efficiency, its ability to be moulded into various shapes, and raw material availability [2]. Concrete is also rated as the second most utilized material globally, behind water [3], with an estimated usage of 30 million tons annually [1]. It is typically composed of binder, aggregates, sand, and water, of which Portland cement is the traditional binder used for binding the matrix. However, there have been some negative environmental and sustainability issues associated with the manufacturing of Portland

 ISBN 978-9959-9703-2-9

cement. These included; 1) the use of a huge amount of natural raw materials especially limestone and clay (2.8 tons of raw materials per one ton of cement) [4]; 2) the enormous energy consumption (5000 MJ per one ton) [5]; and 3) the higher carbon dioxide gas emissions emitted to the atmosphere (one ton of CO_2 per one ton of cement), which represents 5 % of anthropic emissions in the world [6].

Apart from the environmental consequences, the development of concrete using Portland cement also show limited efficiency in the presence of sulfate, causing serious problematic issues including concrete crack, expansion, spalling, and deterioration, due to the formation of gypsum and ettringite [7]. Ettringite is a hydrous calcium aluminate sulfate mineral that forms due to the reaction between the hydrated compounds (from cement hydration), sulfate (from cement or penetrated to concrete from an external source), and water [8]. This mineral has a higher water absorption capability [9,10], attracting water, growing in pore voids as a needle-shaped crystal, causing cracks, expansion and thus, softening the concrete matrix. Therefore, the use of industrial and agricultural by-products (pozzolans) such as rice husk ash-RHA (agricultural by-product), ground granulated blast-furnace slag-GGBS (an industrial by-product of steel manufacturing), and pulverized fly ash-PFA (a by-product of the coal-fired electric power station), has been encouraged [11]. This is due to the potential of these supplementary cementitious materials in enhancing the physico-mechanical properties of concrete through their pozzolanic reactions and filler effect, along with their beneficial impacts on preserving the environment [12].

GGBS, which is a latent hydraulic material produced as a by-product of the steel industry, is one of the superior cementitious materials, as this is an effective way of enhancing the sulfate resistance of concrete. In the literature, Yan et al., 2019 [7], for example, used GGBS as a partial replacement (0, 25, 50, and 75%) of cement, and reported that 50% replacement yielded a beneficial sulfate resistance under the standard curing, while 75% was the optimum amount for steam-cured specimens immersed in 5% sodium sulfate solution. Hadisadok et al., 2012 [13] investigated the effect of separate 5% sodium and 5% magnesium sulfate on concrete and suggested the use of more than 30% of low reactivity GGBS as a partial cement replacement for better sulfate resistance. El-Hachem et al., 2012 [14] concluded that mortar with lower water/cement (w/c) ratio is superior in sulfate resistance because it induces better permeability. Zhang et al., 2013 [15] studied

 ISBN 978-9959-9703-2-9

the effect of a mixed solution of different sodium sulfate and chloride concentration, and concluded that the expansion of concrete was directly and adversely proportional to the sulfate and chloride concentration, respectively,

Given the above-mentioned literature, it is obvious that designing a concrete mix containing GGBS to restrict the sulfate attack, is possible. However, the relevant literature in terms of the effect of a binary solution of magnesium and sodium sulfate on the mechanical performance of concrete is still vague and insignificant. Therefore, an attempt has been made in this study to explore the effect of the binary solution of magnesium and sodium sulfate on the performance of concrete made with different proportions (0, 50 and 75%) of GGBS.

Methodology

1- Materials

The raw materials used in this research study included Portland cement (PC), ground granulated blast-furnace slag (GGBS), coarse aggregate (CA), fine aggregate (FA), deionized water, and binary sulfate solution. **Table 1** and **Table 2** summarize the oxide compositions and some physical characteristics for PC and GGBS, whereas **Fig.1** and **Fig.2** plot, respectively, the particle size distribution of the raw materials, and the thermogravimetric-TG and derivative thermogravimetric-DTG analysis for PC and GGBS.

Table 1: Oxide compositions of PC and GGBS.

Oxides	PC	GGBS
CaO	61.49	37.99
MgO	3.54	8.78
SiO_2	18.84	35.54
Al_2O_3	4.77	11.46
Na_2O	0.02	0.37
P_2O_5	0.1	0.02
Fe_2O_3	2.87	0.42
Mn_2O_3	0.05	0.43
K_2O	0.57	0.43
TiO_2	0.26	0.7
V_2O_5	0.06	0.04
BaO	0.05	0.09
SO_3	3.12	1.54
Loss on ignition	4.3	2

Table 2: Physical properties of PC and GGBS.

Oxides	PC	GGBS
Insoluble residue	0.5	0.3
Bulk density (kg/m^3)	1400	1200
Specific gravity (Mg/m^3)	3.15	2.9
Glass content	-	90
Blaine fineness (m^2/kg)	365	450
Alkalinity value (pH)	13.41	10.4
Colour	Grey	Off-white
Physical form	Powder	Powder

ISBN 978-9959-9703-2-9

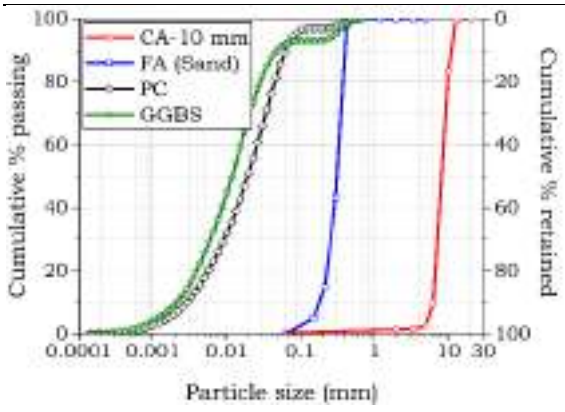

Fig. 1: Particle size distribution of the raw materials.

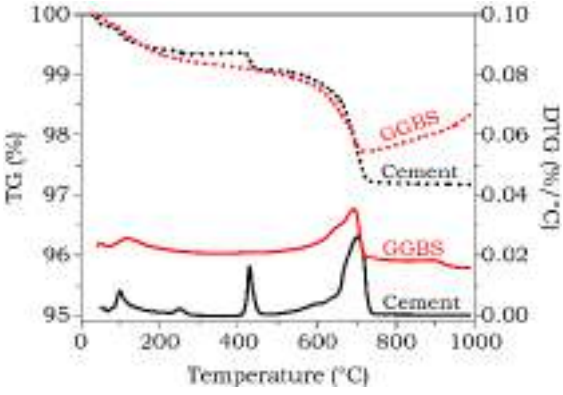

Fig. 2: TG (dotted lines) and DTG (solid lines) curves for PC and GGBS.

The PC used was a commercial Portland cement (CEM-I 42.5 N) in the form of grey fine powder. It was manufactured in compliance with the requirements of BS EN 197-1:2011 [16] and obtained from large cement UK by a local contractor. The TG/DTG analysis of the un-hydrated CEM-I PC indicated a negligible mass loss of 2.8%, as the temperature increases up to 1000 ℃, which is represented in the DTG curve by three endothermic peaks. The first peak located in the range of 50-150 ℃ is due to the dehydration of gypsum, whereas the second peak at 400-450 ℃, and the third peak at 650-750 ℃, are due to the dihydroxylation of portlandite (calcium hydroxide) and the decomposition of calcite, respectively.

The GGBS utilized was a latent hydraulic pozzolan complied with BS EN 15167-1:2006 [17], and obtained from Civil and Marine Slag Cement Ltd, LIanwern, Newport, UK, by a local contractor. The TG curve (see **Fig. 2**) indicated that, as the temperature increases to 1000 ℃, the mass was reduced by 2.26%, which is represented in the DTG by a single peak at 550-700 ℃, owing to the calcite decomposition.

The coarse aggregate (CA) was a limestone in the grade of 10 mm, while fine aggregate (FA) is natural river sand from Bristol Channel. Both aggregates complied with BS EN 12620:2002+A1 [18] and were obtained from a local quarry through a local supplier.

The binary sulfate solution used was prepared by dissolving a total amount of 750g of an equal quantity of magnesium sulfate ($MgSO_4$)

 ISBN 978-9959-9703-2-9

and sodium sulfate ($NaSO_4$) in 20 liters. Both magnesium and sodium sulfate were obtained from Fisher Scientific Ltd, UK, through a local supplier. As for the relatively higher sulfate concentration, it was adopted to accelerate the effect of sulfate on concrete, thus, the ease of identifying the benefit of GGBS in concrete.

2- Mix design and specimen preparation

The concrete mix compositions assessed under this study were designed using, 1) a fixed binder: sand: aggregate proportion of 1:2:3, 2) a w/c ratio of 0.55, and 3) three various binder combinations. These binders (see **Table 3**) were made of; 1) 100% of PC (as a control mix); 2) 50PC-50GGBS (M2), representing an intermediate cement replacement; and 3) 25PC-75GGBS (M3), representing a high cement replacement. The purpose was to obtain an eco-friendly concrete mix design, with a high sulfate resistance performance.

Table 3: Mix compositions of PC-based and GGBS-based concrete mixes.

Mix Design	PC	GGBS	W	FA	CA
M1 (100PC)	6	-	3.3	12	18
M2(50PC-50GGBS)	3	3	3.3	12	18
M3(25PC-75GGBS)	1.5	4.5	3.3	12	18

A total of 18 cubes (100 mm × 100 mm × 100 mm) and 6 cylinders (200 mm in height and 100 mm in diameter) were prepared in line with BS EN 206:2013+A2:2021 [19], BS EN 12350-1:2019 [20], and BS EN 12390-1:2021 [21], for all the concrete mixes. For each mix, the dry ingredients (PC, GGBS, CA and FA) were initially mixed in a mixer for 3 minutes, before the water was introduced and the mixing continued for further 3 minutes. Afterwards, the consistency of fresh concrete was measured, in accordance with the relevant standard. The semi-paste mixture was then poured into the pre-oiled moulds and vibrated for 1 minute to remove air voids. Thereafter, the concrete-filled moulds were stored at 20±2 ℃ to be de-moulded after 24 hours, preparing for the curing. Finally, 9 cubes and 3 cylinders were cured in a water tank at 20±2 ℃, while the remaining specimens were cured in a sulfate solution, until the date of testing.

3- Testing method

The designed concrete mixes were evaluated in terms of consistency (slump and compactability degree), mechanical properties (UCS and TSS), and sulfate resistance (variation in UCS and TSS). The slump and compactability degree tests were carried out in accordance with BS EN 12350-2:2019 [22] and BS EN 12350-4:2019 [23], respectively. The UCS test was conducted on three water-cured specimens per mix composition at each of the prescribed curing periods (7, 28 and 56 days), in line with BS EN 12350-3 2019 [24]. The TSS test was performed in accordance with BS EN 12350-6: 2009 [25] on three cylinders per mix

 ISBN 978-9959-9703-2-9

composition at the end of 28 days of moist curing. As for the sulfate resistance, it was measured in terms of the variation in UCS and TSS of sulfate-cured specimens, relative to their water-cured counterparts.

Results and discussion

1- Consistency of fresh concrete

Fig. 3 presents the consistency results of concrete batches obtained from the slump test and compactability degree test.

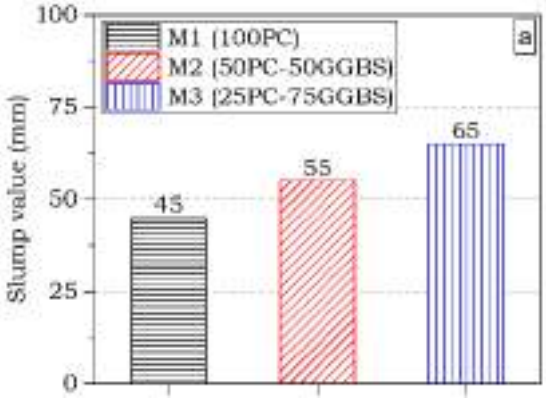

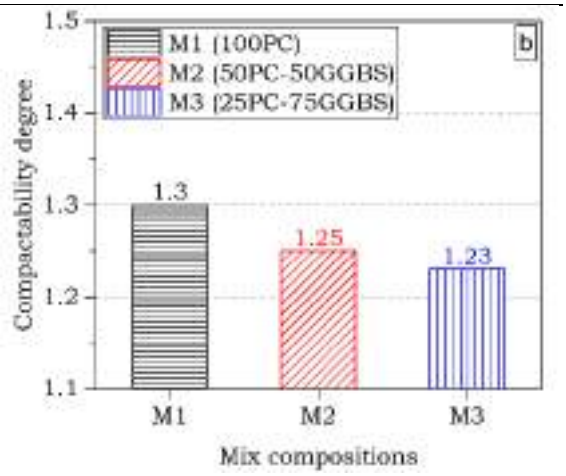

Fig 3: Consistency of fresh concrete; **a)** slump values, and **b)** compactability degree.

The results revealed a gradual increase in the slump value, as the quantity of GGBS increased, where the control concrete mix (M1; 100PC) exhibited the lowest slump (45 mm), relative to that of 55 and 65 mm for M2 (50PC-50GGBS) and M3 (25PC-75GGBS), respectively. This trend, however, was in reverse order in the case of the compactability degree (see **Fig. 3b**), proving the accuracy of the laboratory experiments. The improvement in the consistency due to GGBS is an indicator of reducing the water demand and improving the pumpability. In addition, the consistency was in line with the observation of several studies [26–30]. This enhancement is probably attributed to the smoothness of the GGBS, the poorer early hydration, the lower calcium oxide

 ISBN 978-9959-9703-2-9

of the GGBS, and the lower water absorption capability of the GGBS-based system, compared to the cement-based system [26–30].

2- Strength development in water

2.1-UCS of concretes cured in water

Fig. 4 presents the unconfined compression strength development of all the formulated concretes over a prolonged ambient curing period of up to 56 days.

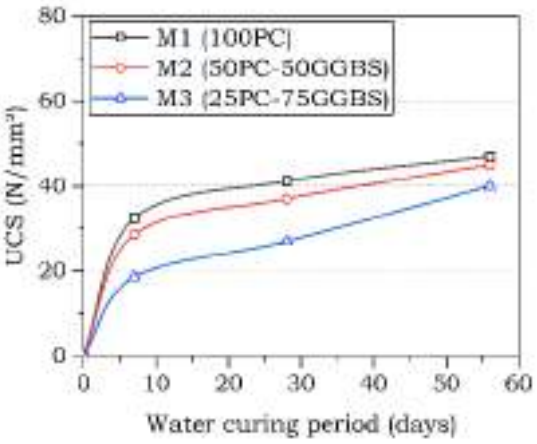

Fig 4: Unconfined compression strength development of water-cured concrete.

Generally, a steady increase in the UCS was observed for all the concretes cured in water, demonstrating the formation of new hydrates, and confirming that the strength of cubes followed the general trend of UCS development. This strength development is owing to the initial hydration of cement components with water to produce hydrated products (calcium silicate hydrate; CSH and calcium aluminate hydrate; CAH), which are responsible for the densification of the concrete system [2].

The effect of the use of GGBS observed in M2 and M3 showed that there was a steady decrease in the UCS value at all the curing ages, as the quantity of GGBS increases. However, such a strength reduction was more pronounced at the early curing age (7 and 28 days) and was also in agreement with the consensus among engineering researchers [30]. The strength reduction associated with the incorporation of GGBS at the early age (7 and 28 days) is due to; 1) the lower calcium oxide within the GGBS-based system; 2) the slow hydration reactivity of GGBS, as the GGBS is a latent hydraulic binder providing minimal hydration; and 3) the delay of the hydration reaction resulting in the retardation of the setting time of GGBS-based concrete, relative to PC-based concrete [31]. As for the strength enhancement of GGBS-based concrete at the later curing age (56 days) is probably due to the higher alumina oxide and silicon oxide released from the dissolution of GGBS. These dissolved products lead to the formation of further hydrated products (pozzolanic products). The additional hydrates fill the pore spaces, thereby densifying and interlocking the system, and inducing a more

 ISBN 978-9959-9703-2-9

compacted concrete structure, all of which induces a UCS improvement [31,32].

2.2- TSS of concretes cured in water

The tensile splitting strength (TSS) is an essential parameter for indicating the behavior of the formulated concrete mixes to crack development, shear failure, steel anchorage and other applications in hardened concrete. **Fig. 5** shows the variation in the TSS of all the formulated concrete mixes at the end of 28 days of an ambient curing period in water.

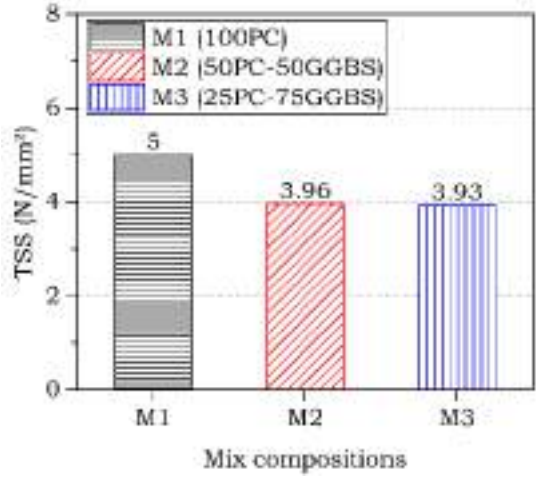

Fig. 5: 28-day-TSS of hardened concretes.

Like the UCS, the result showed that the 28-day-TSS of concrete mixes was adversely affected by the inclusion of GGBS. This was evident from the **Fig.5**, as the TSS was reduced from 5 N/mm^2 (for M1: 100PC) to 3.96 N/mm^2 (for M2: 50PC-50GGBS) and then to 3.93 N/mm^2 (M3: 25PC-75GGBS), when 50% and 75% of the cement content was replaced with GGBS, respectively. A similar decreasing trend in TSS was reported by other researchers [33–38], who attribute the TSS reduction to the inadequate interfacial transition zone bond between the cement matrix and the aggregates at the early curing age. Mo et al., [36] also pointed out that the incorporation of GGBS as a higher cement replacement level (60%) yielded a poorer adhesion with steel fibers, reducing the beneficial impact of steel fibers on the tensile splitting strength of oil palm shell concrete containing GGBS.

3- Strength development in sulfate solution

3.1-UCS of concretes cured in sulfate

The UCS development of all the formulated concretes cured in a hybrid sulfate solution of sodium sulfate and magnesium sulfate over a prolonged curing period of up to 56 days, is depicted in **Fig. 6**, along with their water-cured counterparts for comparison.

 ISBN 978-9959-9703-2-9

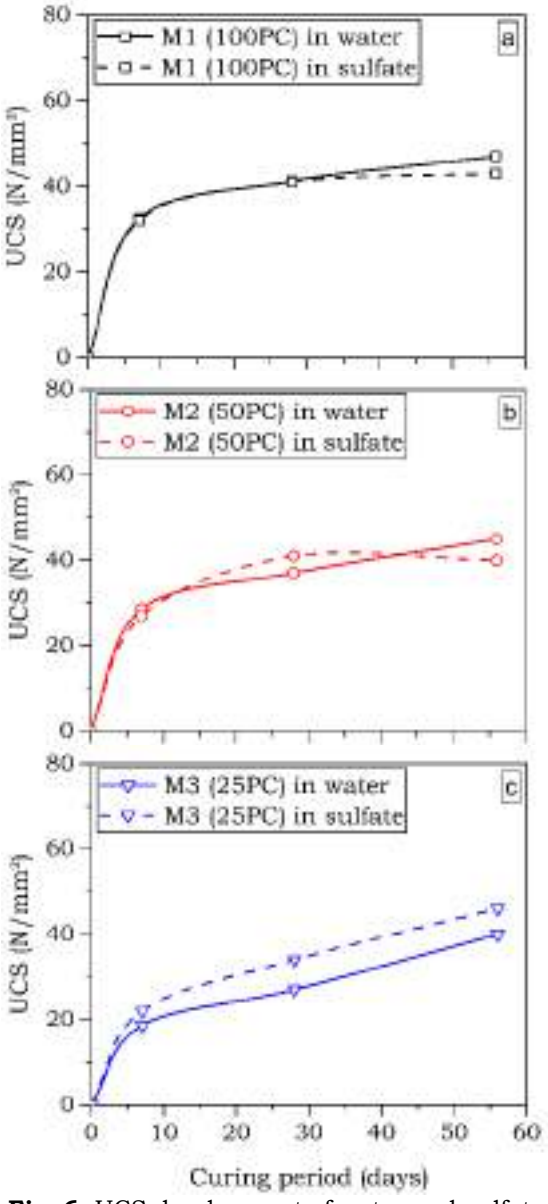

Fig. 6: UCS development of water and sulfate-cured concrete specimens.

In general, the observation indicated that the effect of binary sulfate solution on the UCS performance is proportional to both the curing period and the binder composition. In the case of the control mix (M1: 100PC), the result revealed a strength reduction in the range of 1 to 5 N/mm^2, and such a reduction was more noticeable at 56-days curing in sulfate, where the UCS was reduced from 47.5 to 43 N/mm^2. This deteriorative strength could be credited to the interaction between the sulfate and hydrated products of cement, which forms a series of topochemical interactions [39], mainly gypsum and then ettringite, of which the growth of the latter leads to cracks and expansion of the host matrix [40-41]. Briefly, in the presence of sulfate in concrete, the first reaction that takes place is the formation of gypsum. This typically occurred as a result of three main reactions; mainly due to; 1) the reaction between the calcium ions released from the cement hydration and the sulfate ions released through the ionic dissociation of magnesium and sodium sulfate [42]; 2) the reaction between the sulfate and the formed calcium silicate hydrate (CSH) [39,43]; and 3) the reaction between the portlandite (calcium hydroxide) formed during the cement hydration and the penetrated sulfate [39].

Whatever the origin of gypsum formation, these formed minerals have been associated

 ISBN 978-9959-9703-2-9

with softening (strength reduction) of the concrete and maximizing the volume of hardened concrete structure [44,45]. Additionally, the formed gypsum minerals can react with non-hydrated and hydrated calcium aluminate compounds (such as hydrated calcium aluminate; C_4AH_{13}, mono-sulfate; $C_4A\bar{S}H_{12\text{-}18}$, hydro-garnet; C_3AH_6, and non-hydrated tricalcium aluminate; C_3A) to form an additional secondary ettringite ($C_6A\bar{S}H_{32}$). The non-hydrated tricalcium aluminate and mono-sulfate can also react with sodium sulfate to form additional ettringite [43]. This formed mineral (ettringite) is a hydrous calcium aluminate sulfate mineral, growing typically as needle or rod-shaped crystals in the pore spaces of the concrete, and having higher water absorption capability. These highly hydrated crystalline minerals (ettringite) have a higher specific surface area with unbalanced surface charges, so they inflict bipolar water molecules attraction [9,10], and hence, the orientation of water molecules to mitigate their surface energy. This, therefore, builds up a water layer around the surface of ettringite, which in turn densifies the concrete pores.

Once the volume of the ettringite exceeds the volume of concrete pores, the further continuous growth of ettringite then generates internal stress, expressing a gap between the ettringite crystals and hydrated gel [14,45,46]. This is typically followed by the appearance of cracks and expansion of the host concrete matrix once the generated stress exceeds the tensile strength. Subsequently, a concrete UCS deterioration cooccurred [43,47], which was also in support of why the UCS of M1: 100PC cured in sulfate reduced relative to their water-cured counterparts.

Conversely, a slight strength gain was recorded for the UCS of M2: 50PC-50GGBS at the end of 28 days, where the mix experienced a higher UCS value of 42 N/mm^2 in sulfate, relative to its water-cured counterpart of 38 N/mm^2. This, however, was not the case for the M3: 25PC-75GGBS, as the strength observation exhibited a strength gain in the range of 4-to-8 N/mm^2 at all the curing ages. The strength gain associated with the incorporation of GGBS is possibly attributed to the lower quantity of portlandite produced during the cement hydration, the lower Al_2O_3 of the GGBS and the reduction of non-hydrated tricalcium aluminate (C_3A) of the binder, all of which reduce the formation of ettringite. Therefore, the concrete pores were probably enough for the nucleation and growth of the ettringite in the case of M2 up to 28 days, before such a growth exerts pressure on the surrounding hydrated gels, thus, causing cracks and a strength reduction at the end of 56 days. This

 ISBN 978-9959-9703-2-9

explanation is also in line with the observation of M3: 25PC-75GGBS due to the further reduction in the quantity of portlandite, the quantity of non-hydrated tricalcium aluminate, and the quantity of Al_2O_3, all of which induce a small amount of ettringite, which was also in line with the X-ray diffraction pattern of several publications [7].

3.1-TSS of concretes cured in sulfate

The representative TSS values of all the concrete cylinders cured in a binary sulfate solution of sodium and magnesium sulfate over a curing period of 28 days are illustrated in **Fig.7**, alongside their water-cured counterparts as references.

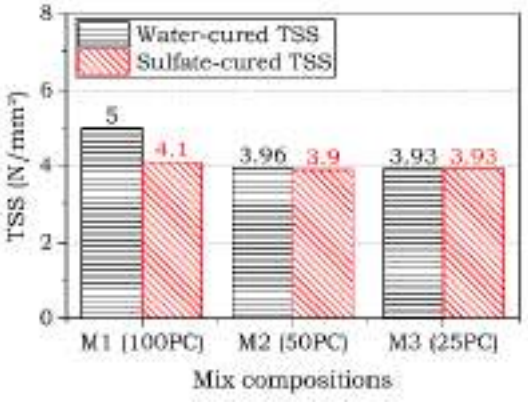

Fig.7: 28-day-TSS of concrete specimens cured in water and sulfate.

Like the case of UCS, the TSS observation indicated that the effect of sulfate on concrete is proportional to GGBS content in the mix. The control mix (M1), which was fabricated using cement only, suffered considerably from sulfate, where the 28-day-TSS value was reduced from 5 N/mm^2 to 4.1 N/mm^2, accounting for a 0.9 N/mm^2 reduction in the TSS due to exposure to sulfate attack. On the contrary, only a TSS reduction of 0.1 and 0 N/mm^2 was monitored when 50% and 75% cement substitution percentage with GGBS was utilized, respectively. This, therefore, suggests the beneficial impact of GGBS on the residual TSS of concrete after exposure to sulfate attack, particularly at a higher cement substitution level (75%). This improvement in TSS can be credited to the lower quantity of portlandite, the lower Al_2O_3, and the reduction of non-hydrated tricalcium aluminate (C_3A) of the GGBS-based concrete matrix, all of which reduce the ettringite, thus eliminating the crack formation and concrete deterioration.

Conclusion

The main conclusions can be drawn as follows:

The use of GGBS as a partial cement substation experienced an increase in the consistency of concrete due to the poorer early hydration, the lower calcium oxide, and the lower water absorption of the GGBS-based system.

Under the water curing condition, the UCS results of concrete revealed a reduction in the

 ISBN 978-9959-9703-2-9

UCS as the GGBS content increases, at the early curing ages (7 and 28 days), due to the reduction in calcium oxide and the delay of the hydration. However, such a UCS reduction was compensated at 56 days, particularly for M2 (50PC-50GGBS), due to the formation of further hydrated products, which densifies the structure and thus improves the UCS.

The exposure of PC-based concrete to a sulfate solution of magnesium and sodium sulfate induces a reduction in the UCS and TSS at all the curing ages, due to the growth of ettringite.

The use of GGBS as a cement substitution yielded a superior sulfate resistance, as the retained UCS and TSS of GGBS-based concrete after the immersion in sulfate solution, was higher than the strength of PC-based concrete. This superiority is attributed to the lower portlandite content, the lower Al_2O_3, and the reduced non-hydrated tricalcium aluminate (C_3A), which restricts the ettringite formation.

The limitations to this research study, which could have an impact on the authenticity of the experimentation outcomes, are the use of a single concentration of hybrid sulfate solution of magnesium sulfate and sodium sulfate, and the use of single grade of GGBS. Hence, a research studies considering the effect of different sulfate combinations and different GGBS grads, are advised for future work to overcome this deficiency.

Overall, the feasibility of developing a sustainable concrete capable of restricting sulfate attack by using GGBS as a partial cement substitution, has been confirmed in this research study. This finding may have some bearing on the current practices, and relevant to all the civil engineers who are involved in concrete technology, as this document will serve as an invaluable resource of in-depth and up-to-date information on the use of GGBS as a partial replacement of cement. The application of this type of concrete is also anticipated to alleviate the soci-economic and environmental concerns associated with the manufacturing of Portland cement, as it will reduce the total carbon dioxide emissions and the intensive energy consumption associated with concrete.

Arabic section:

العنوان: تقييم الخصائص الفيزيائية والميكانيكية ومقاومة الكبريتات للخرسانة المصنعة من حبيبات خبث الافران العالية الحبيبية.

المؤلفون: شيماء التليسي، ملاك الباقول، منصور إبعيليلة، عبد الدايم عبد الله،

الكلمات المفتاحية: (إترينجيت، كبريتات المغنيسيوم، القوة الميكانيكية، كبريتات الصوديوم، هجوم الكبريتات)

الملخص: في السنوات الاخيرة، وبهدف الحد من تكوين الايترينجيت وتقليل التأثير البيئي المرتبط بالإسمنت، أصبح دمج خبث الافران العالية الحبيبية كبديل جزئي للإسمنت اتجاها شائعا، نظرا لكفاءته في تعزيز الخواص الفيزيائية والميكانيكية للخرسانة. توضح هده الدراسة البحثية النتائج التجريبية على خواص الخرسانة

 ISBN 978-9959-9703-2-9

المحتوية على نسب مختلفة من خبث الافران العالية الحبيبية (0، 50، و75 %). تم تصميم ثلاث خلطات خرسانية باستخدام نسبة الماء الى الاسمنت (0.55) ونسبة تصميم الخلطة 1: 2: 3 (كماده رابطة: رمل: ركام). بعد ذلك، قد تم اجراء تقييم فيزيائي وميكانيكي بما في ذلك اختبار الركود، اختبار درجة الانضغاطية، اختبار مقاومة الضغط، اختبار قوة الانقسام (الشد)، وهجوم الكبريتات، ودالك لتقييم أداء الخرسانة. اشارت النتائج المعملية الى انه على الرغم من ان استخدام خبث الافران العالية الحبيبية كبديل جزئي للإسمنت يؤثر على الخصائص الميكانيكية في سن المعالجة المبكرة، الا ان استخدامه يحسن تشغيلية الخرسانة وينتج عنه أداء ميكانيكي اعلى بعد الغمر في محلول الكبريتات، وخاصتا عند مستوى إحلال عالي.

References

[1] Abdalla, T.A., Koteng, D.O., Shitote, S.M., and Matallah, M., (2022), Mechanical and durability properties of concrete incorporating silica fume and a high volume of sugarcane bagasse ash., Results in Engineering., **16**, 100666. DOI: 10.1016/j.rineng.2022.100666.

[2] Adeleke, B.O., Kinuthia, J.M., Oti, J., and Ebailila, M., (2023), Physico-mechanical evaluation of geopolymer concrete activated by sodium hydroxide and silica fume-synthesised sodium silicate solution., Materials., **16**(6), 2400. DOI: 10.3390/ma16062400.

[3] Nukah, P.D., Abbey, S.J., Booth, C.A., and Oti, J., (2022), Evaluation of the structural performance of low carbon concrete., Sustainability., **14**(24), 16765. DOI: 10.3390/su142416765.

[4] Samad, S., Shah, A., and Limbachiya, M.C., (2017), Strength development characteristics of concrete produced with blended cement using ground granulated blast furnace slag (GGBS) under various curing conditions., Sadhana - Academy Proceedings in Engineering Sciences., **42**, 1203-121342. DOI: 10.1007/s12046-017-0667-z.

[5] Oti, J.E., Kinuthia, J.M., and Bai, J., (2009), Compressive strength and microstructural analysis of unfired clay masonry bricks., Engineering Geology., **109**(3-4), 230-240. DOI: 10.1016/j.enggeo.2009.08.010.

[6] Dave, N., Misra, A.K., Srivastava, A., and Kaushik, S.K., (2016), Experimental analysis of strength and durability properties of quaternary cement binder and mortar., Construction and Building Materials., **107**, 117-124. DOI: 10.1016/j.conbuildmat.2015.12.195.

[7] Yan, X., Jiang, L., Guo, M., Chen, Y., Song, Z., and Bian, R., (2019), Evaluation of sulfate resistance of slag contained concrete under steam curing., Construction and Building Materials., **195**, 231-237. DOI: 10.1016/j.conbuildmat.2018.11.073.

[8] Ogawa, S., Nozaki, T., Yamada, K., Hirao, H., and Hooton, R.D., (2012), Improvement on sulfate resistance of blended cement with high alumina slag., Cement and Concrete Research, **42**(2), 244-251. DOI: 10.1016/j.cemconres.2011.09.008.

[9] Ebailila, M., Kinuthia, J., Oti, J., and Al-Waked, Q., (2022), Sulfate soil stabilisation with binary blends of lime–silica fume and lime–ground granulated blast furnace slag., Transportation Geotechnics., **37**, 100888. DOI: 10.1016/j.trgeo.2022.100888.

[10] Ebailila, M., Kinuthia, J., and Oti, J., (2022), Suppression of Sulfate-Induced Expansion with Lime–Silica Fume Blends., Materials., **15**, 2821. DOI: 10.3390/ma15082821.

[11] Mehta, A., and Ashish, D.K., (2020), Silica fume and waste glass in cement concrete production: A review., Journal of Building Engineering., **29**, 100888. DOI: 10.1016/j.jobe.2019.100888.

[12] Johari, M.M., Brooks, J.J., Kabir, S., and Rivard, P., (2011), Influence of supplementary cementitious materials on engineering properties of high strength concrete., Construction and Building Materials., **25**, 2639-2648. DOI: 10.1016/j.conbuildmat.2010.12.013.

[13] Hadjsadok, A., Kenai, S., Courard, L., Michel, F., and Khatib, J., (2012), Durability of mortar and concretes containing slag with low hydraulic activity., Cement and Concrete Composites, **34**(5), 671-677. DOI: 10.1016/j.cemconcomp.2012.02.011.

[14] El-Hachem, R., Rozière, E., Grondin, F., and Loukili, A., (2012), Multi-criteria analysis of the mechanism of degradation of Portland cement based mortars exposed to external sulphate attack., Cement and Concrete

 ISBN 978-9959-9703-2-9

Research., **42**(10), 1327-1335. DOI: 10.1016/j.cemconres.2012.06.005.

[15] Zhang, M., Chen, J., Lv, Y., Wang, D., and Ye, J., (2013), Study on the expansion of concrete under attack of sulfate and sulfate–chloride ions., Construction and Building Materials, **39**, 26-32. DOI: 10.1016/j.conbuildmat.2012.05.003.

[16] BS EN 197-1:2011, Cement — Part 1: Composition, specifications and conformity criteria for common cements, BSI Standards Limited, London, UK, 2011. https://doi.org/10.3403/30205527.

[17] BS EN 15167-1:2006, Ground granulated blastfurnace slag for use in concrete, mortar and grout—Part 1: definitions, specifications and conformity criteria, BSI Standards Limited, London, UK, 2006. https://doi.org/10.3403/30130594.

[18] BS EN 12620:2002+A1:2008, Aggregates for concrete, BSI Standards Limited, London, UK, 2008. https://doi.org/10.3403/02661981.

[19] BS EN 206:2013+A2:2021, Concrete — Specification, performance, production and conformity., BSI Standards Limited, London, UK, 2021. https://doi.org/10.3403/30257890.

[20] BS EN 12350-1:2019, Testing fresh concrete—Part 1: Sampling and common apparatus, BSI Standards Limited, London, UK, 2019. https://doi.org/10.3403/30360061.

[21] BS EN 12390-1: 2021, Testing hardened concrete—Part 1: Shape, dimensions and other requirements for specimens and moulds, BSI Standards Limited, London, UK, 2021. https://doi.org/10.3403/30397529U.

[22] BS EN 12350-2: 2019, Testing fresh concrete — Part 2: Slump test, BSI Standards Limited, London, UK, 2019. https://doi.org/10.3403/30360058.

[23] BS EN 12350-4: 2019, Testing fresh concrete — Part 4: Degree of compactability, BSI Standards Limited, London, UK, 2019. https://doi.org/10.3403/30360064.

[24] BS EN 12390-3:2019, Testing hardened concrete — Part 3: Compressive strength of test specimens, BSI Standards Limited, London, UK, 2019. https://doi.org/10.3403/30360070.

[25] BS EN 12390-6:2009, Testing hardened concrete — Part 6: Tensile splitting strength of test specimens, BSI Standards Limited, London, UK, 2009. https://doi.org/10.3403/30200045.

[26] Gu, P., Beaudoin, J.J., Zhang, M.H., and Malhotra, V.M., (2000), Performance of reinforcing steel in concrete containing silica fume and blast-furnace slag ponded with sodium chloride solution., ACI Materials Journal., **97**(3), 254-262. DOI: 10.14359/4620.

[27] Park, C.K., Noh, M.H., and Park, T.H., (2005), Rheological properties of cementitious materials containing mineral admixtures., Cement and concrete research., **35**(5), 842-849. DOI: 10.1016/J.CEMCONRES.2004.11.002.

[28] Teng, S., Lim, T.Y.D., and Divsholi, B.S., (2013), Durability and mechanical properties of high strength concrete incorporating ultra fine ground granulated blast-furnace slag., Construction and Building Materials., **40**, 875-881. DOI: 10.1016/J.CONBUILDMAT.2012.11.052.

[29] Bostancı, Ş.C., Limbachiya, M., and Kew, H., (2016), Portland slag and composites cement concretes: engineering and durability properties., Journal of Cleaner Production., **112**, 542-552. DOI: 10.1016/J.JCLEPRO.2015.08.070.

[30] Özbay, E., Erdemir, M. and Durmuş, H.İ., 2016), Utilization and efficiency of ground granulated blast furnace slag on concrete properties–A review., Construction and Building Materials., **105**, 423-434. DOI: 10.1016/J.CONBUILDMAT.2015.12.153.

[31] Mo, K.H., Ling, T.C., Alengaram, U.J., Yap, S.P., and Yuen, C.W., (2017), Overview of supplementary cementitious materials usage in lightweight aggregate concrete., Construction and Building Materials., **139**, 403-418. DOI: 10.1016/J.CONBUILDMAT.2017.02.081.

[32] Gholampour, A., and Ozbakkaloglu, T., (2017), Performance of sustainable concretes containing very high volume Class-F fly ash and ground granulated blast furnace slag., Journal of Cleaner Production., **162**, 1407-1417. DOI: 10.1016/J.JCLEPRO.2017.06.087.

[33] Türkmen, İ., and Fındık, S.B., (2013), Several properties of mineral admixtured lightweight

 ISBN 978-9959-9703-2-9

mortars at elevated temperatures., Fire and materials, **37**(5), 337-349. DOI: 10.1002/FAM.1030.

[34] Mo, K.H., Alengaram, U.J., Jumaat, M.Z., and Yap, S.P., (2015), Feasibility study of high volume slag as cement replacement for sustainable structural lightweight oil palm shell concrete., Journal of cleaner production., **91**, 297-304. DOI: 10.1016/J.JCLEPRO.2014.12.021.

[35] Mo, K.H., Alengaram, U.J., and Jumaat, M.Z., (2015), Utilization of ground granulated blast furnace slag as partial cement replacement in lightweight oil palm shell concrete., Materials and structures., **48**, 2545-2556. DOI: 10.1617/S11527-014-0336-1/METRICS.

[36] Mo, K.H., Chin, T.S., Alengaram, U.J., and Jumaat, M.Z., (2016), Material and structural properties of waste-oil palm shell concrete incorporating ground granulated blast-furnace slag reinforced with low-volume steel fibres., Journal of Cleaner Production., **133**, 414-426. DOI: 10.1016/J.JCLEPRO.2016.05.162.

[37] Sekar, S.K., (2016), Mechanical and fracture characteristics of Eco-friendly concrete produced using coconut shell, ground granulated blast furnace slag and manufactured sand., Construction and Building Materials., **103**, 1-7. DOI: 10.1016/J.CONBUILDMAT.2015.11.035.

[38] Jayaprithika, A., and Sekar, S.K., (2016), Stress-strain characteristics and flexural behaviour of reinforced Eco-friendly coconut shell concrete., Construction and Building Materials., **117**, 244-250. DOI: 10.1016/J.CONBUILDMAT.2016.05.016.

[39] Cefis, N., and Comi, C., (2017), Chemo-mechanical modelling of the external sulfate attack in concrete. Cement and Concrete Research, **93**, 57-70. DOI: 10.1016/J.CEMCONRES.2016.12.003.

[40] Ebailila, M., Kinuthia, J., and Oti, J., (2022), Role of Gypsum Content on the Long-Term Performance of Lime-Stabilised Soil., Materials., **15**(15), 5099. DOI: 10.3390/ma15155099.

[41] M. Ebailila, Sulfate soil stabilisation with silica fume-based binders, Doctoral Thesis, University of South Wales, England, UK, 2022.

[42] Sun, D., Wu, K., Shi, H., Miramini, S., and Zhang, L., (2019), Deformation behaviour of concrete materials under the sulfate attack., Construction and Building Materials., **210**, 232-241. DOI: 10.1016/J.CONBUILDMAT.2019.03.050.

[43] Sarkar, S., Mahadevan, S., Meeussen, J.C.L., Van der Sloot, H., and Kosson, D.S., (2010), Numerical simulation of cementitious materials degradation under external sulfate attack., Cement and Concrete Composites., **32**(3), 241-252. DOI: 10.1016/J.CEMCONCOMP.2009.12.005.

[44] Santhanam, M., Cohen, M.D., and Olek, J., (2003), Effects of gypsum formation on the performance of cement mortars during external sulfate attack., Cement and concrete research., **33**(3), 325-332. DOI: 10.1016/S0008-8846(02)00955-9.

[45] Rahman, M.M., and Bassuoni, M.T., (2014), Thaumasite sulfate attack on concrete: Mechanisms, influential factors and mitigation., Construction and Building Materials., **73**, 652-662. DOI: 10.1016/J.CONBUILDMAT.2014.09.034.

[46] Tian, B., and Cohen, M.D., (2000), Does gypsum formation during sulfate attack on concrete lead to expansion?., Cement and concrete research., **30**(1), 117-123. DOI: 10.1016/S0008-8846(99)00211-2.

[47] Sun, C., Chen, J., Zhu, J., Zhang, M., and Ye, J., (2013), A new diffusion model of sulfate ions in concrete., Construction and Building Materials., **39**, 39-45. DOI: 10.1016/J.CONBUILDMAT.2012.05.022.

 ISBN 978-9959-9703-2-9

المؤتمر الدولي الثاني للعلوم والهندسة
2nd International Conference on Science and Engineering
ICSE 2023
Faculty of Engineering - University of Bani Waleed
Bani Waleed, Libya

Paper Code: ICSE-044

A COMPARATIVE STUDY ON SOIL STABILISATION WITH CALCIUM AND MAGNESIUM-BASED BINDERS

M. Ebailila[a], J. Kinuthia[b], J. Oti[b], A. Muhmed[c],
[a] Department of Civil Engineering/Faculty of Engineering/ Bani Waleed University, Libya
[b] Faculty of Computing, Engineering and Science/University of South Wales, UK
[c] Department of Civil Engineering/Faculty of Engineering/Tobruk University, Libya
*Crosspnding author: mansour.ebailila@yahh.co.uk

Abstract: Soil stabilisation using cementitious materials is a promising technique for improving the mechanical characteristics and suppressing the swelling of expansive and sulfate soil. This study compares the viability of two calcium-based stabilisers (Portland cement-C and lime-L) and one MgO-based stabiliser (magnesium oxide-M) in soil stabilisation. A set of specimens produced by use of two soil materials (pure kaolin soil and artificially gypsum-dosed kaolin) at a constant stabiliser content of 10 wt%, were examined in terms of the unconfined compressive strength (UCS), swelling and derivative thermogravimetric (DTG) analysis. Accordingly, the results revealed that Portland cement (10%C) experienced a superior UCS of 1830 kN/m^2 and expansion of 0.44% in the absence of sulfate, whereas magnesium oxide (10%M) outperformed both Portland cement and lime in the suppression of swelling of the artificial sulfate soil, where it induced an expansion magnitude of 1%, relative to that of 15% and 24% for 10%C and 10%L, respectively. However, the 10%M yielded a lower UCS (927 kN/m^2) relative to that of 2030 kN/m^2 for 10%C and 1995 kN/m^2 for 10%L in the presence of sulfate. The superiority of 10%C in the absence of sulfate is due to its higher Si^{+4} and Al^{+3} ions, which provide the needed oxides for the nucleation of the hydrates that interlock the system. As for the dominance of 10%M in the suppression of expansion of sulfate kaolin, it can be assigned to the restriction of the nucleation and growth of ettringite crystals owing to the unavailability of calcium ions.

Keywords: (Ettringite, Portland cement, lime, magnesium oxide, linear expansion, swelling)

Introduction

Expansive soil materials, which are distributed worldwide, is normally characterized as problematic soil due to its sensitivity to change under moisture fluctuation [1], thus inducing shrink-swell behaviour [2]. This reversible shrink-swell behaviour represents a challenging task and threatens sustainability [3], by inducing differential settlement, crack formation, and overlying structure collapse [4]. Therefore, the construction of engineering structures such as pavements and highway embarkments on such soil can be destructive [5], due to its unpredictable behaviour.

To suppress the reversible shrink-swell

 ISBN 978-9959-9703-2-9

behaviour of the expansive soil, engineers traditionally tend to treat the available soil with cementitious materials such as calcium-based stabiliser (Portland cement and lime) due to their efficiencies in enhancing the physicomechanical properties such as the reduction of plasticity, swelling and permeability, as well as increase of shear strength, UCS, bearing capacity and durability resistance [5-8]. However, there have been some environmental concerns related to the manufacturing of calcium-based stabilisers such as the higher energy consumption (5000 MJ/t for cement and 4000 MJ/t for lime) associated with their production, with a carbon dioxide emission of 1000 and 800 kg/ton, respectively [6]. Calcium-based stabilisers also exhibit a limited efficiency in the treatment of sulfate-bearing soils due to the formation of ettringite (see equation 1) from the interaction between calcium, alumina (from soil), sulfate (from soil or groundwater), and water [7].

$$6Ca^{2+} + 2Al(OH)_4^- + 4OH^- + 3(SO_4)^{2-} + 26H_2O \rightarrow Ca_6[Al(OH)_6]_2 \cdot (SO_4)_3 \cdot 26H_2O \quad \text{.....(1)}$$

Correspondingly, engineering researchers have investigated several techniques including double application of lime, pre-compaction mellowing, pre-treatment with barium compounds, use of sulfate resistance cement and use of agricultural and industrial by-products, to improve the properties of expansive soil and preserve the economy [8].

Recently, reactive magnesia (MgO) is gaining great attention, particularly in sulfate-bearing soils. This is probably due to its higher surface area, its higher reactivity [9], lower manufacturing temperature (700-1000℃) [10-11], and lesser energy needs (2400 MJ/t) [12], although it induces a higher carbon dioxide emissions of 1.4 ton per ton [13], relative to 0.95 tons of CO_2 for cement and 0.8 ton of CO_2 for lime [9,14]. Of course, these carbon dioxide emissions are not promising and may form the refusal of its applications. Nevertheless, Liska and Al-Tabbaa [13] conducted a research study on MgO and reported that MgO can reach a 71% carbonation, suggesting the reduction of CO_2 from 1400 to 420 kg/tone.

Concerning the research studies on the effect of magnesium oxide (M), Seco et al., (2011) [15] carried out a comparative study between magnesium oxide and other pozzolans (including coal bottom ash, rice husk ash, steel fly ash and lime among others) in the stabilisation of expansive soil. The results revealed a superior swelling performance in the case of magnesium oxide at a binder dosage of 2%, while lime induced a lower swelling magnitude at a binder content of 4%. Li et al., (2019) [11] investigated the efficiency of lime, Portland cement, and magnesium oxide on the

 ISBN 978-9959-9703-2-9

stabilisation/solidification of heavy metals-contaminated soils and concluded that no single binder can be effective for all the heavy metals, thus the choice of binder is a site-specific problem. Li et al., (2020) [16] compare MgO-activated ground granulated blast-furnace slag (MgO-GGBS) with cement on the swelling suppression of sulfate soil and observed a better swelling behaviour and superior residual strength after soaking in water for the case of MgO-activated GGBS, which was in line with [9,12,17-24]. So far, however, there is a lack of comparative studies between quicklime, Portland cement and magnesium oxide on the stabilisation of both non-sulfate and sulfate-bearing soil.

To this end, the key aim of this research was to determine the optimum binder (among Portland cement, lime, and magnesium oxide) in terms of both UCS and expansion kaolin soil in the presence and absence of gypsum.

Methodology

1- Materials

The raw materials used in this study included kaolin soil (K), gypsum (G), Portland cement (PC), lime (L) and magnesium oxide (M). **Table 1** and **Table 2** outline the oxide and physical characteristics of the raw materials, respectively, whereas **Fig.1** plots the results of sieve analysis for the raw materials.

Table 1: Oxide compositions of kaolin, Portland cement, lime, and magnesium oxide.

Oxides	K	C	L	M
CaO	0.01	61.5	71.6	-
MgO	0.21	3.54	0.58	>98
SiO_2	47.3	18.8	0.67	-
Al_2O_3	35.9	4.77	0.07	-
Na_2O	0.07	0.02	0.02	-
P_2O_5	0.01	0.1	0.03	-
Fe_2O_3	0.7	2.87	0.05	-
Mn_2O_3	0.02	0.05	0.02	-
K_2O	1.79	0.57	0.01	-
TiO_2	0.02	0.26	0.01	-
V_2O_5	0.01	0.06	0.02	-
BaO	0.07	0.05	0.01	-
SO_3	0.01	3.12	0.19	-
LOI	0.1	4.3	27.4	-

Table 2: Some physical characteristics of kaolin, Portland cement, lime, magnesium oxide.

Properties	K	C	L	M
Bulk density (kg/m^3)	-	1400	480	-
Specific gravity (Mg/m^3)	2.14	3.15	2.82	3.58
pH Value	5.37	13.41	12.62	11.90
Colour	White	Grey	White	White

ISBN 978-9959-9703-2-9

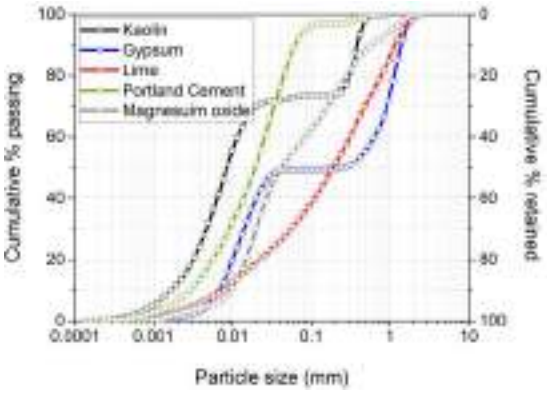

Fig.1: Sieve analysis results of kaolin, gypsum, lime, Portland cement and magnesium oxide.

The kaolin (K) used was an industrial kaolin soil, sourced from Potterycrafts Ltd, Stoke-on-Trent, UK. It has a liquid limit, plastic limit, and plasticity index of 56.7%, 33.3%, and 23.4%, respectively. Therefore, the kaolin was characterized as a medium-graded sandy SILT.

The gypsum (G) used was a calcium sulfate dihydrate and has a physical form of white powder; it was obtained from Fisher Scientific Ltd, Loughborough, Leicestershire, UK. The gypsum was used to prepare an artificial gypsum-bearing soil, based on the premise of being the most typical source of sulfate type encountered in natural sulfate-bearing soils.

The cement (C) used was a commercially available CEM-I Portland cement having grey colour; it was produced in line with BS EN 197-1: 2011 [25], and supplied by Large Cement, UK. The utilization of this type of cement in this study can be credited to its traditional recognition in the treatment of clay soils.

The lime (L) used was in the form of off-white quicklime with a relative density of 3.31: it was sourced from Tarmac Cement and Lime Company, Derbyshire, Derby, UK. The choice of adopting quicklime in this study is attributed to its relatively higher calcium content, facilitating the faster drying of moisture content within soil and in turn enables the best degree of soil stabilisation [26-29].

The magnesium oxide (M) used was a commercial reactive magnesia having a physical form white powder; it was obtained from Fisher Scientific Ltd, Loughborough, Leicestershire, UK.

2- Mix proportions

The mix configurations (see **Table 3**) evaluated in the laboratory experimentations involved using; 1) two soil materials including pure kaolin soil and gypseous kaolin soil); 2) three different binders (Portland cement, lime, and magnesium oxide); and 3) fixed moisture content of 31%.

Table 3: Mix compositions of designed soil mixes stabilised with different binders.

Design code	Target soil materials (%)	
	K	G
K0G-10%L	100	0
K0G-10%C	100	0

ISBN 978-9959-9703-2-9

K0G-10%M		100	0
K9G-10%L		91	9
K9G-10%C		91	9
K9G-10%M		91	9

Design code	MC	Binder in % by target soil material		
		L	C	M
K0G-10%L	31	10		
K0G-10%C	31		10	
K0G-10%M	31			10
K9G-10%L	31	10		
K9G-10%C	31		10	
K9G-10%M	31			10

For clarity, the mix design code comprised of kaolin (K), gypsum (G) and the binder (C for Portland cement, L for lime or M for magnesium oxide), of which G, C, L and M proceeded by a number, representing the solid amount. The gypsum content displayed in the design code denotes the gypsum percentage by the total mass of gypseous kaolin, while the stabilizer amount represents the stabilizer dosage by the total mass of dry soil materials.

The gypseous kaolin was prepared by blending kaolin soil with 9 wt% of gypsum in a dry form. The choice of adopting pure kaolin and gypseous-bearing kaolin soil was due to; 1) the homogeneity of kaolin soil, as it simplifies the understanding of the interactions; 2) the relatively higher alumina content of kaolin, as it enables the nucleation of relatively higher ettringite quantity; 3) the gypsum is the commonly encountered source of sulfate in natural sulfate soil; and 4) the gypsum content of 9%, was the worst sulfate concentration for ettringite nucleation [6,8,14,30]. The purpose of using three binders was to select the optimum binder in the presence and absence of sulfate. As for the adoption of 31 % moisture content, which was equal to 1.1 of the corresponding standard proctor optimum condition, it was because the soil is always compacted wet of moisture to actualize the best durability performance [6,8,14,30]. In addition, it was not found necessary to establish the optimum moisture content (OMC) for each system due to the time-consuming nature of proctor test and the impracticability of establishing the OMC for each mix [30].

3- Specimen preparation

A total of 11 stabilized samples were produced for each mix. Two of these samples were used for simulating the swelling behaviour, whereas nine samples were used for evaluating the UCS after 7, 28 and 90 days of moist curing. For each specimen, adequate quantity of dry materials, as per the mix composition outlined in **Table 3**, capable of manufacturing stabilised sample with dimensions of 50 mm in diameter and 100 mm in height, were blended in dry form using a mixer for 3 minutes. Hereafter, the moisture content was added, and the mixing was continued for further three minutes to ensure the homogeneity of the

 ISBN 978-9959-9703-2-9

mixture. Consequently, the semi-paste was accommodated into a steel mould and compacted by use of a jack in aid of a steel frame as detailed in [6]. At the end of three minutes for specimen stability, the stabilized sample was extruded by use of a plunger, wrapped in a cling film, and stored in a plastic container at 20 ± 2, allowing for moist curing.

4- Testing method

4.1- UCS

The UCS test was conducted, in line with BS EN ISO 17892-7: 2018 [31], on three samples per mix after each of the prescribed moist curing periods (7, 28 and 90 days). Three specimens were axially compressed using a Hounsfield Testing Machine (see **Fig.2**) at a displacement ratio of two mm per minute. The average of the UCS of three specimens was calculated and used as the representative UCS.

Fig.2: The 10kN capacity Hounsfield compression machine.

4.2- Swelling

The swelling behaviour (linear expansion) was conducted on two samples per mix composition, in accordance with BS EN 13286-49: 2004 [32], using Perspex cells (see **Fig.3**), as commonly adopted in the literature [6, 8, 14, 33–35].

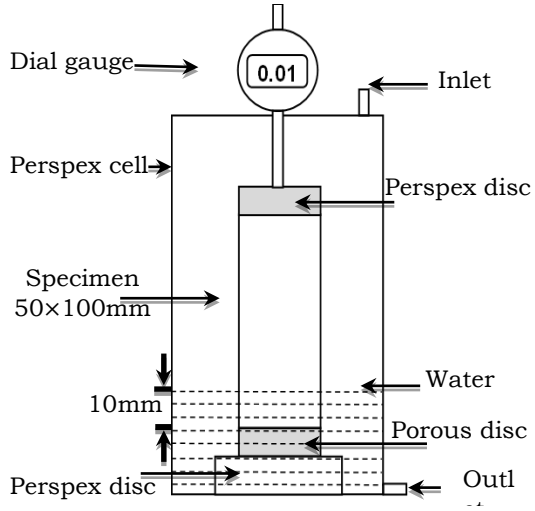

Fig.3: The Perspex cell set-up used for the vertical displacement (swelling) measurement.

Immediately, after seven days of moist curing, about ten mm of the upper and bottom part of the stabilized samples were unwrapped and accommodated separately in the Perspex cell as shown in **Fig.4**.

ISBN 978-9959-9703-2-9

Fig.4: Linear expansion specimens under expansion measurement.

Afterwards, the dial gauge was adjusted to zero, and the water was added through the inlet until the bottom ten mm part of the samples was soaked in water, allowing for expansion. This water height was used for the reason that it was adopted in several publications [33–35]. Subsequently, the dial gauge reading was monitored periodically, and the ratio (%) of dial gauge reading (mm) to the original height (100 mm) of the specimens was calculated randomly through a prolonged water soaking period of 200 days. Finally, the mean vertical movement (linear expansion value) of the two stabilized samples was then calculated and represented as the linear expansion (swelling) magnitude of the mix.

4.3- Derivative thermogravimetric analysis

The derivative thermogravimetric (DTG) analysis was carried out from 20±5 ℃ up to 1000 ℃. The analysis was run at a heating ratio of 20 ℃/min and under an argon environment using a TGA55 kit shown in **Fig.5**. The specimen used for the analysis was taken from the fractured 7-day UCS specimens and after being dried with the aid of silica gel in a desiccator at a temperature of 40 ℃, in order to prevent hydration.

Fig.5: Thermogravimetric (TG) and derivative thermogravimetric (DTG) analyser used in this study (TGA55).

Results and discussion

1- UCS performance

Fig.6 illustrates the UCS evolution over a moist curing period of up to 90 days for pure and gypseous kaolin soil stabilized with 10%C, 10%L, and 10%M.

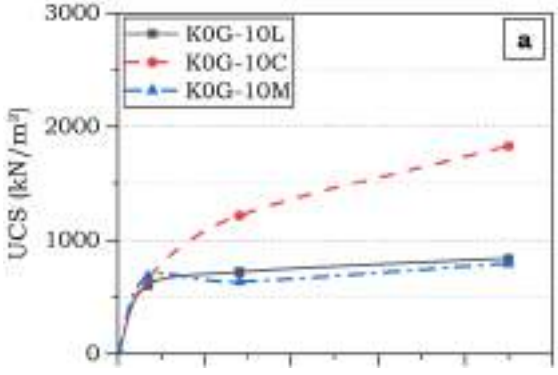

 ISBN 978-9959-9703-2-9

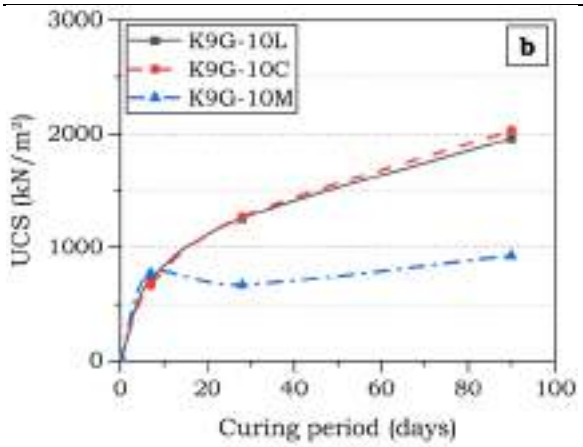

Fig.6: The UCS development of **a)** kaolin and **b)** gypseous kaolin specimens, made with lime, Portland cement and magnesium oxide.

In general, there was a gradually increasing strength trend over 90 days of moist curing, suggesting the continuous development of hydrates, and indicating that the samples followed the typical UCS trend of soil stabilization [6,8,14,33–35]. The display of strength development in a 10%C-based system is commonly assigned to cement hydration, which forms hydrates such as calcium silicate hydrate (C-S-H) and calcium aluminate hydrate (C-A-H). These hydrates crystalline with time and interlock the soil system [36]. As for the 10%L and 10%M-based systems, the UCS development is because of the cation exchange, flocculation, and agglomeration of soil particles) as well as the pozzolanic reactions [6,7,37]. These reactions, therefore, form a stiff matrix and increase the robustness against loading, thus increasing the strength performance [30].

In the non-attendance of gypsum, the result revealed that the stabiliser domination with respect to the highest UCS was in the order of 10%C>10%L>10%M, where the 90-day UCS was 1830, 839 and 793 kN/m^2, respectively. This, therefore, suggests the superiority of 10%C on the expense of 10%L and 10%M in the stabilization of non-sulfate soil. The possible explanation for the cement superiority is the higher amount of Si^{+4} and Al^{+3} ions of the cement-based system [38], which provide the needed oxides for the nucleation and growth of hydrated products that are responsible for strength evolution [39]. The presence of unconsumed portlandite in L-based and brucite in M-based system, as detected in the DTG curves (detailed later), is also a contributing factor to the superiority of cement, as these two minerals coat the soil particles, postponing the dissolution of soil minerals [40], delaying the pozzolanic reactions, and reducing the cohesion of the system [41]. In addition, the nucleation of ettringite in C-based system due to the reaction between gypsum, tricalcium aluminate and water is another contributing factor for the superiority of cement. The strength enhancement induced by the formation of ettringite occurs through; 1) the porosity reduction owing to the ettringite

 ISBN 978-9959-9703-2-9

growth which fill the voids; 2) the dewatering of the system owing to higher water absorption of the ettringite; and 3) the interlocking of the system owing to the growth of ettringite crystals surrounding the soil particles [6,30,42,43]. As for the better UCS induced by lime relative to magnesium oxide, this could be assigned to the lower reactivity of the magnesium oxide which is known to be a contributor to the performance of the magnesium oxide-based system [8].

In the presence of gypsum (sulfate), the UCS observations revealed that across all the formulations, the UCS of gypseous kaolin also outperformed their counterparts of pure kaolin at all the curing ages, and such superior performance, was more pronounced in specimens stabilized with calcium-based stabilizer (L and C). In this context, the stabilizer domination was in the sequential order of 10%C>10%L>10%M, where 10%C experienced the highest 90-day UCS of 2030 kN/m^2, relative to that of 1995 kN/m^2 for 10%L and 927 kN/m^2 for 10%M. With further in-depth, however, it can be inferred that the positive effect of sulfate was not consistent across all the formations, where lime-based specimens experienced the greatest UCS gain of 1156 kN/m^2, representing a strength gain ratio of about 140% relative to its stabilized none-sulfate counterpart, whereas 10%C- and 10%M-based specimens yielded a UCS gain of 200 and 130 kN/m^2, accounting for a strength gain ratio of about 11% and 16% relative to their stabilized none-sulfate counterparts, respectively. To the best experience of the authors, the strength gain induced by the presence of sulfate in specimens stabilized with calcium-based stabilizer is because of the variation in the quantity of formed ettringite, which depends on the amount of lime, sulfate, alumina, and water of the system [14]. As for the slight strength gain of M-based specimen in the presence of sulfate, this could be accredited to the proper particle distribution and the introduction of calcium ions (from gypsum), of which the latter is expected to induce fabric modification due to cation exchange [8].

2- Linear expansion

Fig.7 displays the average linear expansion plots over a prolonged water soaking period of 200 days for kaolin samples stabilised with a single binder of 10%C, 10%L and 10%M. Like the case of UCS, the specimen stabilized with cement (K9G-10%C) exhibited the best (lowest) expansion magnitude of 0.44%, followed by K0G-10%M and K0G-10%L with an expansion magnitude of 0.66% and 4%, respectively. The reduction induced by C, L or M is already described in previous publications as a result of two reaction mechanisms; 1) fabric

 ISBN 978-9959-9703-2-9

modification due to cation exchange, and flocculation and agglomeration of soil particles; and 2) the nucleation and growth of hydrates such as C-S-H, C-A-H, and M-S-H due to the pozzolanic reactions between the soil and the cementitious materials [7,8,14,44–48].

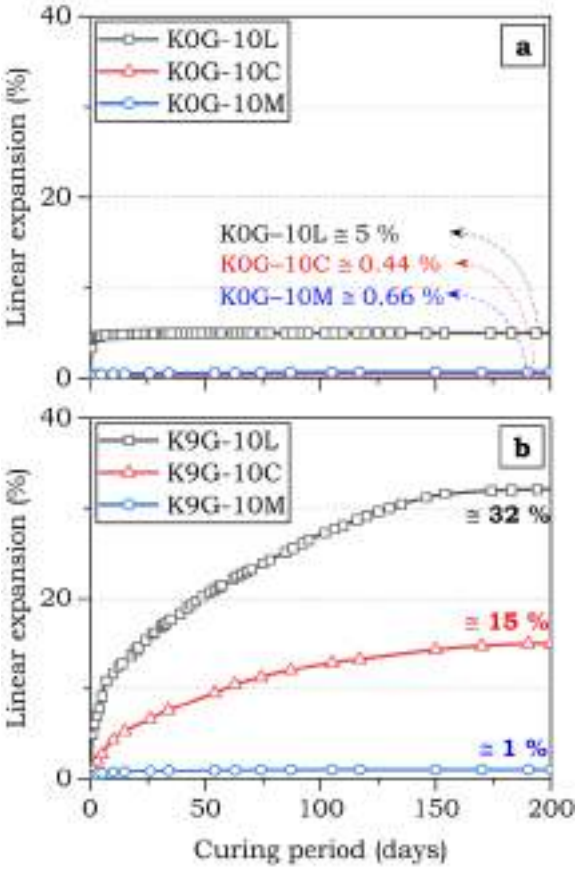

Fig.7: Linear expansion plots of **a)** pure kaolin and **b)** gypseous kaolin specimens, made with cement, lime and magnesium oxide.

The superiority of 10%C on the expanse of 10%L and 10%M in the restriction of expansion is possibly due to the faster hydration process, as it induces higher earlier UCS. The higher strength prevents the reorientation of soil particles and the enlargement of inter-particle pore spacing, of which the latter induces a reduced sorptivity [49]. As for the dominance of 10%M over 10%L, this can be assigned to the fineness of MgO, and the degree of saturation of the stabilized matrix [8]. The extreme fineness of MgO enables homogeneity of MgO distribution and eases the ion migration within the system. This improvement in ion distribution facilitates a proper fabric modification, thus reducing the repulsion force between soil particles and eventually minimizing the water adsorption of soil particles [8,14]. The higher saturation level of K9G-10%M, which is anticipated to be higher than the K9G-10%L because of the exothermic reaction of CaO, is also deemed to be a contributor to the superiority of 10%M over 10%L. This is because the higher saturation degree improves the water pore interconnection within the system [26], thus a homogenous and accelerated ion migration has occurred, and thereby lesser capillary forces are exerted through the rise of water within the stabilized samples.

In the presence of gypsum, the stabilizer domination order, however, was changed, where 10%M yielded the lowest expansion of

 ISBN 978-9959-9703-2-9

1%, relative to that of 15% and 24% experienced by gypseous specimen stabilised with cement (K9G-10%C) and lime (K9G-10%L), respectively. With further in-depth, however, it can be inferred that the negative effect of sulfate was not consistent across all the formations, where lime-based specimens experienced the greatest swelling gain of 27%, representing a swelling gain ratio of about 140% relative to its stabilized none-sulfate counterpart, whereas 10%C- and 10%M-based specimens yielded a swelling gain of 14.5% and 0.4%, respectively. The difference in the swelling trend can be credited to the concentration of ettringite crystals grown during the reaction [30], which was reinforced by the DTG curve (discussed later). These produced minerals grow in pores as a needle or rod-shaped crystals and have a high-water absorption capability [6]. On the continuous growth of ettringite crystalles, internal stress is generated once these minerals intersected with each other or with soil particles, causing cracks and expansion of the stabilized system, and such an expansion is proportional to the amount of ettringite formed.

3- Derivative thermogravimetric analysis

The 7-day derivative thermogravimetric (DTG) of pure kaolin and gypseous kaolin samples made with 10%L, 10%C and 10%M are plotted in **Fig.8**, alongside demonstrative notes for the causativeness of the key peaks.

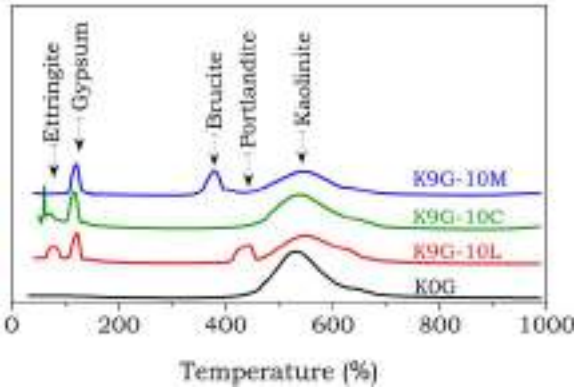

Fig.8: The 7-days DTG curves of pure kaolin and gypseous kaolin samples, made with 10% of cement, lime and magnesium oxide.

On the 7 days of moist curing, the pure kaolin specimen revealed the presence of a major endothermic peak at a temperature of 400-700℃ due to the decomposition of kaolinite minerals [37]. On the use of 10%L, 10%C, and 10%M for the stabilization of gypseous kaolin (K9G-10%L), the DTG analysis exhibited four additional peaks; 1) the first peak at 50-100℃ owing to the dehydration of ettringite [6]; 2) the second peak at a temperature range of 100-200℃ due to the dehydration of moisture content of gypsum crystallization [30]; 3) the third peak at 350-450℃ due to the decomposition of brucite [8]; and 4) the fourth peak at 400-500℃ due to the decomposition of portlandite [6]. By comparing the height of ettringite peaks, it was apparent that the ettringite mineral was only

 ISBN 978-9959-9703-2-9

formed in gypseous kaolin specimens stabilized with a calcium-based stabilizer, and such a mineral was more pronounced in the case of K9G-10%L. This was also confirmed by the higher gypsum peak, both of which are in support of why K9G-10%L yielded a superior UCS gain in the presence of sulfate. Apart from ettringite and gypsum peaks, portlandite and brucite peaks were also detected in K9G-10%L and K9G-10%M, respectively, indicating the incomplete consumption of lime and magnesium oxide through the fabric modification, which in turn indicates the surplus of both binders. This surplus binder content is not favorable, as it prevents the dissolution of soil, delays the pozzolanic reactions, and reduces the cohesion of the system. Therefore, this is in partial support of why lime and magnesium oxide yielded a lower UCS relative to cement, particularly in the absence of sulfate.

Conclusions

The main conclusions of the experimental investigations of this research can be illustrated as follows:

Stabilisation of pure kaolin using Portland cement yielded the highest UCS and lowest linear expansion, relative to both lime and magnesium oxide. This is due to the higher concentration of Si^{+4} and Al^{+3} ions of Portland cement, which provide the needed oxides for the nucleation and growth of hydrates that are main responsible for the interlocking of the system.

The presence of sulfate (gypsum) in kaolin soil stabilised with calcium-based binders (Lime and Portland cement) yielded an increase in the UCS and linear expansion due to the formation of ettringite, and such an increase was more pronounced in samples stabilized with quicklime.

The utilisation of MgO in the stabilisation of gypsum-dosed kaolin soil experienced the lowest unconfined compressive strength and the lowest linear expansion magnitude due to the restriction of ettringite.

The limitations of the current research study that may have an influence on the generalisation of the experimentation results of this research study, are the use of artificial gypsum-dosed soil, the use of a constant moisture level, and the use of a single source of sulfate (gypsum). Therefore, to enable the generalisation of the outcomes emerged from the laboratory experimentations conducted on the semi-processed industrial soil, research studies concerning the use of different natural soils, different sources of sulfate, and different moisture contents are recommended for future work to overcome this deficiency.

Overall, the use of MgO or cement experienced superior effectiveness in the inhibition of

 ISBN 978-9959-9703-2-9

swelling of non-sulfate kaolin, whereas only the MgO demonstrated an accepted swelling in the existence of gypsum. This finding may have some bearing on the current practices, and relevant to all the engineers involved in soil stabilisation and suppression of ettringite-induced expansion, as this document will serve as a helpful resource of in-depth information on soil stabilisation.

Arabic section:

العنوان: دراسة تقارن تثبيت التربة بواسطة المواد اللاصقة المستندة على الكالسيوم والمغنيسيوم.

المؤلفون: منصور إبعيليلة، جون كينوتيا، جونتان أوتي، أسماء محمد.

الكلمات المفتاحية: (إترينجيت، الاسمنت البورتلاندي، الحجر الجيري، أكسيد المغنيسيوم، التمدد الخطي، الانتفاخ)

الملخص: يعد تثبيت التربة باستخدام المواد الاسمنتية تقنية واعدة لتحسين الخصائص الميكانيكية وقمع سلوك الانتفاخ والانكماش للتربة المنتفخة والكبريتية. تقارن هده الدراسة جدوى اثنين من المثبتات القائمة على الكالسيوم ومثبت قائم على المغنيسيوم في تثبيت التربة. تم تصنيع مجموعة من العينات المختبرية باستخدام مادتين من مواد التربة المستهدفة (الكيولين النقي والكيولين الممزوج بالجبس) ومحتوى رابط ثابت (10%) ومن تم قد تم تقييم هده العينات من ناحية مقاومة الضغط والتوسع الخطي (الانتفاخ) والتحليل الحراري الوزني. وفقا لدلك، أظهرت النتائج أن الاسمنت البورتلاندي أظهر أداء متفوق من ناحية قوة الضغط والتمدد الخطي في غياب الكبريتات، بينما تفوق أكسيد المغنيسيوم على كل من الاسمنت البورتلاندي والحجر الجيري في قمع التمدد الخطي في وجود الكبريتات، على الرغم من أنه أسفر عن مقاومة ضغط ضعيفة بالمقارنة بالأسمنت والحجر الجيري. تفوق الاسمنت في غياب الكبريتات يرجع سببه الى ارتفاع كمية السيليكا والألومينا التي توفر الاكاسيد اللازمة لتكوين هيدرات سيليكات الكالسيوم وهيدرات ألومينات الكالسيوم التي تلعب دورا حيوا في ربط النظام. أما بالنسبة لتفوق أكسيد المغنيسيوم على الاسمنت والحجر الجيري في تثبيت الانتفاخ للتربة الكبريتية فيرجع دلك لتقييد تكون الإترينجيت.

References

[1] Al-Atroush, M.E., and Sebaey, T.A., (2021), Stabilization of expansive soil using hydrophobic polyurethane foam: A review., Transportation Geotechnics., **27**, 100494. DOI: 10.1016/j.trgeo.2020.100494.

[2] Ikeagwuani, C.C., and Nwonu, D.C., (2019), Emerging trends in expansive soil stabilisation: A review., Journal of rock mechanics and geotechnical engineering., **11**(2), 423-440. DOI: 10.1016/j.jrmge.2018.08.013.

[3] Kalkan, E., (2011), Impact of wetting–drying cycles on swelling behavior of clayey soils modified by silica fume., Applied clay science., **52**(4), 345-352. DOI: 10.1016/j.clay.2011.03.014.

[4] Jha, A.K., and Sivapullaiah, P.V., (2016), Volume change behavior of lime treated gypseous soil—influence of mineralogy and microstructure., Applied Clay Science., **119**, pp.202-212. DOI: 10.1016/j.clay.2015.09.017.

[5] Cheshomi, A., Eshaghi, A., and Hassanpour, J., (2017), Effect of lime and fly ash on swelling percentage and Atterberg limits of sulfate-bearing clay., Applied Clay Science., **135**, 190-198. DOI: 10.1016/j.clay.2016.09.019.

[6] Ebailila, M., Kinuthia, J., and Oti, J., (2022), Suppression of Sulfate-Induced Expansion with Lime–Silica Fume Blends., Materials., **15**(8), 2821. DOI: 10.3390/ma15082821.

[7] Seco, A., Miqueleiz, L., Prieto, E., Marcelino, S., García, B., and Urmeneta, P., (2017), Sulfate soils stabilization with magnesium-based binders., Applied Clay Science., **135**, 457-464. DOI: 10.1016/j.clay.2016.10.033.

[8] M. Ebailila, Sulfate soil stabilisation with silica fume-based binders, Doctoral Thesis, University of South Wales, England, UK, 2022.

[9] Yi, Y., Liska, M., and Al-Tabbaa, A., (2014), Properties of two model soils stabilized with different blends and contents of GGBS, MgO, lime, and PC., Journal of Materials in Civil

 ISBN 978-9959-9703-2-9

Engineering., **26**(2), 267-274. DOI: 10.1061/(ASCE)MT.1943-5533.0000806.

[10] Jin, F., and Al-Tabbaa, A., (2014), Evaluation of novel reactive MgO activated slag binder for the immobilisation of lead and zinc., Chemosphere., **117**, 285-294. DOI: 10.1016/j.chemosphere.2014.07.027.

[11] Li, W., Ni, P., and Yi, Y., (2019), Comparison of reactive magnesia, quick lime, and ordinary Portland cement for stabilization/solidification of heavy metal-contaminated soils., Science of the Total Environment., **671**, 741-753. DOI: 10.1016/j.scitotenv.2019.03.270.

[12] Yi, Y., Zheng, X., Liu, S. and Al-Tabbaa, A., (2015), Comparison of reactive magnesia-and carbide slag-activated ground granulated blastfurnace slag and Portland cement for stabilisation of a natural soil., Applied Clay Science., **111**, 21-26. DOI: 10.1016/j.clay.2015.03.023.

[13] Liska, M., and Al-Tabbaa, A., (2009), November. Ultra-green construction: reactive magnesia masonry products., In Proceedings of the Institution of Civil Engineers-Waste and Resource Management., **162**, 185-196. DOI: 10.1680/warm.2009.162.4.185.

[14] Ebailila, M., Kinuthia, J., Oti, J., and Al-Waked, Q., (2022), Sulfate soil stabilisation with binary blends of lime–silica fume and lime–ground granulated blast furnace slag., Transportation Geotechnics., **37**, 100888. DOI: 10.1016/j.trgeo.2022.100888.

[15] Seco, A., Ramírez, F., Miqueleiz, L., and García, B., (2011), Stabilization of expansive soils for use in construction., Applied Clay Science., **51**(3), 348-352. DOI: 10.1016/j.clay.2010.12.027.

[16] Li, W., Yi, Y., and Puppala, A.J., (2020), Suppressing ettringite-induced swelling of gypseous soil by using magnesia-activated ground granulated blast-furnace slag., Journal of Geotechnical and Geoenvironmental Engineering., **146**(7), 06020008. DOI: 10.1061/(asce)gt.1943-5606.0002292.

[17] Yi, Y., Gu, L., Liu, S., and Jin, F., (2016), Magnesia reactivity on activating efficacy for ground granulated blastfurnace slag for soft clay stabilisation. Applied Clay Science., **126**, 57-62. DOI: 10.1016/j.clay.2016.02.033.

[18] Yi, Y., Li, C., Liu, S., and Al-Tabbaa, A., (2014), Resistance of MgO–GGBS and CS–GGBS stabilised marine soft clays to sodium sulfate attack., Géotechnique., **64**(8), 673-679. DOI: 10.1680/geot.14.t.012.

[19] Yi, Y., Liska, M., Unluer, C., and Al-Tabbaa, A., (2013), Carbonating magnesia for soil stabilization., Canadian Geotechnical Journal., **50**(8), 899-905. DOI: 10.1139/cgj-2012-0364.

[20] Yi, Y., Liska, M., Jin, F., and Al-tabbaa, A., (2016), Mechanism of reactive magnesia-GGBS soil stabilisation., Canadian Geotechnical Journal., **55**, 773–782. DOI: 10.1139/cgj-2015-0183.

[21] Yi, Y., Gu, L., and Liu, S., (2015), Microstructural and mechanical properties of marine soft clay stabilized by lime-activated ground granulated blastfurnace slag., Applied Clay Science., **103**, 71-76. DOI: 10.1016/j.clay.2014.11.005.

[22] Yi, Y., Liska, M., and Al-Tabbaa, A., (2012) Initial investigation into the use of GGBS-MgO in soil stabilisation., In Grouting and Deep Mixing 2012., 444-453.

[23] Goodarzi, A.R., and Movahedrad, M., (2017), Stabilization/solidification of zinc-contaminated kaolin clay using ground granulated blast-furnace slag and different types of activators., Applied Geochemistry., **81**, 155-165. DOI: 10.1016/j.apgeochem.2017.04.014.

[24] Gu, K., Jin, F., Al-Tabbaa, A., Shi, B., Liu, C., and Gao, L., (2015), Incorporation of reactive magnesia and quicklime in sustainable binders for soil stabilisation., Engineering Geology., **195**, 53-62. DOI: 10.1016/j.enggeo.2015.05.025.

[25] BS EN 197-1:2011, Cement — Part 1: Composition, specifications and conformity criteria for common cements, BSI Standards Limited, London, UK, 2011. https://doi.org/10.3403/30205527.

[26] Beetham, P., Dijkstra, T., Dixon, N., Fleming, P., Hutchison, R., and Bateman, J., (2015), Lime stabilisation for earthworks: a UK perspective., Proceedings of the Institution of Civil Engineers-Ground Improvement., **168**(2), 81-95. DOI: 10.1680/grim.13.00030.

[27] Boardman, D.I., Glendinning, S., and Rogers, C.D.F., (2001), Development of stabilisation and solidification in lime–clay mixes., Geotechnique., **51**(6), 533-543. DOI:

 ISBN 978-9959-9703-2-9

10.1680/geot.2001.51.6.533.

[28] Obuzor, G.N., Kinuthia, J.M., and Robinson, R.B., (2011), Enhancing the durability of flooded low-capacity soils by utilizing lime-activated ground granulated blastfurnace slag (GGBS)., Engineering Geology., **123**(3), 179-186. DOI: 10.1016/j.enggeo.2011.07.009.

[29] Afrin, H., (2017), A review on different types soil stabilization techniques., International Journal of Transportation Engineering and Technology., **3**(2), 19-24. DOI: 10.11648/j.ijtet.20170302.12.

[30] Ebailila, M., Kinuthia, J., and Oti, J., (2022), Role of Gypsum Content on the Long-Term Performance of Lime-Stabilised Soil., Materials., **15**(15), 5099. DOI: 10.3390/ma15155099.

[31] BS EN ISO 17892-7: 2018, Geotechnical investigation and testing-Laboratory testing of soil — Part 7: Unconfined compression test, BSI Standards Limited, London, UK, 2018.

[32] BS EN 13286-49: 2004, Unbound and hydraulically bound mixtures — Part 49: Accelerated swelling test for soil treated by lime and/or hydraulic binder, BSI Standards Limited, London, UK, 2004.

[33] Obuzor, G.N., Kinuthia, J.M., and Robinson, R.B., (2011), Utilisation of lime activated GGBS to reduce the deleterious effect of flooding on stabilised road structural materials: A laboratory simulation., Engineering geology., **122**(3-4), 334-338. DOI: 10.1016/j.enggeo.2011.06.010.

[34] Oti, J.E., Kinuthia, J.M., and Robinson, R.B., (2014), The development of unfired clay building material using Brick Dust Waste and Mercia mudstone clay., Applied clay science., **102**, 148-154. DOI: 10.1016/j.clay.2014.09.031.

[35] Kinuthia, J.M., and Nidzam, R.M., (2011), Towards zero industrial waste: Utilisation of brick dust waste in sustainable construction., Waste Management., **31**(8), 1867-1878. DOI: 10.1016/j.wasman.2011.03.020.

[36] Behnood, A., (2018), Soil and clay stabilization with calcium-and non-calcium-based additives: A state-of-the-art review of challenges, approaches and techniques., Transportation Geotechnics., **17**, 14-32. DOI: 10.1016/j.trgeo.2018.08.002.

[37] Al-Mukhtar, M., Lasledj, A., and Alcover, J.F., (2014), Lime consumption of different clayey soils., Applied Clay Science., **95**, 133-145. DOI: 10.1016/j.clay.2014.03.024.

[38] Sharma, L.K., Sirdesai, N.N., Sharma, K.M., and Singh, T.N., (2018), Experimental study to examine the independent roles of lime and cement on the stabilization of a mountain soil: A comparative study., Applied Clay Science., **152**, 183-195. DOI: 10.1016/j.clay.2017.11.012.

[39] Degirmenci, N., Okucu, A., and Turabi, A., (2007), Application of phosphogypsum in soil stabilization., Building and environment., **42**(9), 3393-3398. DOI: 10.1016/j.buildenv.2006.08.010.

[40] Konan, K.L., Peyratout, C., Smith, A., Bonnet, J.P., Rossignol, S., and Oyetola, S., (2009), Comparison of surface properties between kaolin and metakaolin in concentrated lime solutions., Journal of colloid and interface science., **339**(1), 103-109. DOI: 10.1016/j.jcis.2009.07.019.

[41] Choobbasti, A.J., and Kutanaei, S.S., (2017), Microstructure characteristics of cement-stabilized sandy soil using nanosilica., Journal of Rock Mechanics and Geotechnical Engineering., **9**(5), 981-988. DOI: 10.1016/j.jrmge.2017.03.015.

[42] Puppala, A.J., Talluri, N., and Chittoori, B.C., (2014), Calcium-based stabiliser treatment of sulfate-bearing soils., Proceedings of the Institution of Civil Engineers-Ground Improvement., **167**(3), 162-172. DOI: 10.1680/grim.13.00008.

[43] Jha, A.K., and Sivapullaiah, P.V., (2014), Role of gypsum on microstructure and strength of soil., Environmental Geotechnics., **3**(2), 78-89. DOI: 10.1680/envgeo.13.00084.

[44] Aldaood, A., Bouasker, M. and Al-Mukhtar, M., (2016), Effect of water during freeze–thaw cycles on the performance and durability of lime-treated gypseous soil., Cold Regions Science and Technology., **123**, 155-163. DOI: 10.1016/j.coldregions.2015.12.008.

[45] Aldaood, A., Bouasker, M., and Al-Mukhtar, M., (2021), Mechanical behavior of gypseous soil treated with lime., Geotechnical and Geological Engineering, **39**, 719-733. DOI: 10.1007/s10706-020-01517-w.

[46] Aldaood, A., Bouasker, M., and Al-Mukhtar, M., (2014), Free swell potential of lime-treated gypseous soil., Applied Clay Science., **102**, 93-103. DOI: 10.1016/j.clay.2014.10.015.

 ISBN 978-9959-9703-2-9

[47] Aldaood, A., Bouasker, M., and Al-Mukhtar, M., (2014), Geotechnical properties of lime-treated gypseous soils., Applied Clay Science., **88**, 39-48. DOI: 10.1016/j.clay.2013.12.015.

[48] Yi, Y., Zheng, X., Liu, S., and Al-Tabbaa, A., (2015), Comparison of reactive magnesia-and carbide slag-activated ground granulated blastfurnace slag and Portland cement for stabilisation of a natural soil., Applied Clay Science., **111**, 21-26. DOI: 10.1016/j.clay.2015.03.023.

[49] Hossain, K.M.A., Lachemi, M., and Easa, S., (2007), Stabilized soils for construction applications incorporating natural resources of Papua New Guinea., Resources, Conservation and Recycling., **51**(4), 711-731. DOI: 10.1016/j.resconrec.2006.12.003.

 ISBN 978-9959-9703-2-9

المؤتمر الدولي الثاني للعلوم والهندسة
2nd International Conference on Science and Engineering
ICSE 2023
Faculty of Engineering - University of Bani Waleed
Bani Waleed, Libya

Paper Code: ICSE-043

THE ROLE OF MOISTURE CONTENT, MIXING METHOD AND SAMPLE SIZE ON THE SWELLING OF SULFATE SOIL STABILISED WITH LIME-SILICA FUME BLEND

N. Alsharaa[a], N. Saleh[a], M. Ebailila[a], A. Muhmed[b],
[a] Department of Civil Engineering/Faculty of Engineering/Bani Waleed University, Libya
[b] Department of Civil Engineering/Faculty of Engineering/Tobruk University, Libya
*Crosspnding author: mansour.ebailila@yahh.co.uk

Abstract: Chemical soil stabilisation, a conventional soil treatment technique, is a function of several variables including the mineralogical compositions of soil, the oxide contents of the stabiliser, the sulfate concentration of soil, and the water content used for compaction, among other variables. This paper reports an experimental study investigating the impact of variation in the moisture compaction content, mixing method and specimen size on sulfate soil stabilisation with the co-addition of lime (L) and silica fume (S). A series of artificially gypsum-dosed kaolin specimens were prepared using a binder composition of 3L-7S, two different moisture contents (31 and 33%), two different mixing methods (dry mixing method-DM and slurry mixing method-SM) and two different specimen dimensions; one with 100 mm in height and one with 19 mm in height. Thereafter, a set of physico-mechanical engineering tests including the unconfined compressive strength (UCS) test, linear expansion test and swelling potential test were conducted to examine their physical and mechanical behaviour. The finding of this study indicated that the use of SM instead of DM induced a compromise on both the expansion and UCS performance due to the clumping and the heterogeneity of the formed hydrates. As for the moisture content variation, the result showed that the higher moisture content of 33% yielded a better expansion and lower UCS performance due to the enlargement of voids which reduces the robustness against loading and facilitates the accommodation of ettringite.

Keywords: (Ettringite, soil stabilisation, calcium-based stabiliser, compressive strength, expansion)

Introduction

Soils specifically those comprised mainly of clay minerals, in their natural state, are typically characterised as weak and low-grade construction materials with a reversible shrink-swell behaviour [1], as their properties are influenced by the variation of moisture content [2]. Hence, the construction of engineering structures on such soil is a challenging task and can be harmful [3], facilitating crack formation, differential settlement, and sudden failure due to their changing behaviour [4], thus inducing economic concerns. For example, the annual damage cost associated with the reversible

 ISBN 978-9959-9703-2-9

shrink-swell behaviour of expansive soil exceeds £400 million in the UK [5], and 15 billion in the USA [6]. However, replacement of the sub-grade layer with high-bearing capacity soil is considered costly and time-consuming [7]. For this reason, engineers tend to stabilise and improve the physico-mechanical properties of the local soil materials by using cementitious materials including calcium-based binders such as lime (quicklime or hydrated lime) and Portland cement, of which lime is the most preferred binder [8], due to its effectiveness in the stabilisation of soil, and its lesser price related to Portland cement.

The use of lime in soil improves the physico-mechanical properties through two key reaction mechanisms: short-term reactions (including cation exchange and flocculation and agglomeration of soil particles), and long-term reactions (pozzolanic reactions) [9]. Upon the addition of hydrated lime to the soil in the presence of moisture, the hydrated lime first dissolves into calcium ions (Ca^{2+}) and hydroxide ions (OH). The Ca^{2+} ions fix to the outer surface of soil particles, substituting the exchangeable cations through replaceability order of $Na^{+}<K^{+}<Mg^{++}<Ca^{++}$, in which higher valence cations substitute those lower valence cations [10]. This cations substitution balances the electronic charge of soil particles, induces flocculation of soil particles [11], and promotes different particle arrangements [12]. Besides, the hydroxide ions (OH) cause a significant increase in the alkalinity value up to (pH=12.4), thus creating a corrosive alkaline environment, which in turn aids the aluminate and silicate sheets of soil particles to release silica and alumina ions. This, thereafter, initiates the pozzolanic interactions between the Ca^{2+} from the binder, silica and alumina from soil, and water, thereby, forming hydrates such as calcium silicate hydrate (C-S-H), and calcium aluminate hydrate (C-A-H). These hydrates interlock and improve the physico-mechanical properties of the soil-lime mixture. However, in the presence of sulfate, an alteration in the reaction mechanism occurs due to the formation of ettringite from the reaction between calcium, alumina, sulfate, and water [13]. This mineral is an issue in sulfate soil stabilisation, as it induces a massive expansion [14]. Apart from that, lime production requires enormous energy (4000 MJ per tonne) [15], with corresponding carbon dioxide emissions of 800 kilograms per tonne released to the atmosphere [14]. Therefore, the use of industrial by-products (pozzolans) such as silica fume, has been recently encouraged due to its pozzolanic reactivity and its superior efficiency in the restriction of the swelling of gypsum-bearing soils [14, 16-26].

In the literature, Ghorbani et al., 2015 [17]

 ISBN 978-9959-9703-2-9

observed a significant swelling reduction by using a binary blend of lime-silica fume (L-S) as a stabiliser for gypsum-based sandy soil with a gypsum content of 25%. Ebailila et al., [14] examine the viability of L-S blends at different binder contents on the suppression of artificial gypseous kaolin and concluded that a 3L-7S is the optimal bended combination for restricting the nucleation of ettringite in kaolin soil made with the gypsum concentration of 9%. Recently, Ebailila et al., 2022 [26] compares the efficiency of 3L-7S with that of a binary binder containing 3% lime and 7% ground granulated blast-furnace slag (3L-7GGBS) on the expansion of gypseous kaolin. This study concluded that both blended binders (3L-7GGBS and 3L-7S) are effective in sulfate soil stabilisation, of which 3L-7GGBS was the optimum for the UCS while the 3L-7S was the best for the expansion.

Given the description above, it can be stated that the use of L-S in sulfate soil stabilisation is beneficial. However, studies concerning the effect of moisture content, mixing method and sample size variation on sulfate soil treated with the co-addition of Lime and silica fume, are still insufficient. Therefore, complementary to the existing knowledge, this study aimed at examining the co-effect of L-S on gypseous kaolin specimens made with different mixing methods, different moisture contents and different specimen sizes, to propose the optimum mixing and optimum moisture compaction condition. To do so, a set of samples mixed using different moisture contents (31% and 33%) and different mixing methods and produced with different dimensions, were evaluated in terms of the UCS, linear expansion and swelling potential.

Methodology

1- Materials

The raw materials used in this research included one target soil material (artificial gypseous kaolin soil-K9G made from Kaolin-K and gypsum-G), two cementitious materials (lime-L and silica fume-S) and tap water. **Table 1** and **Table 2** show the oxide and physical properties of the raw materials, respectively, whereas **Fig. 1** and **Fig. 2** present the x-ray diffraction of kaolin and the sieve analysis results of the raw materials, respectively.

Table 1: Oxide characteristics of the raw materials.

Oxides	K	L	S
CaO	<0.01	71.56	0.2
MgO	0.21	0.58	0.1
SiO_2	47.32	0.67	98.4
Al_2O_3	35.96	0.07	0.2
Na_2O	0.07	<0.02	-
P_2O_5	0.12	0.03	0.03
Fe_2O_3	0.69	0.05	0.01
Mn_2O_3	0.02	0.02	-
K_2O	1.8	<0.01	0.2
TiO_2	0.02	<0.01	-
V_2O_5	<0.01	0.02	-
BaO	0.07	<0.01	-
SO_3	0.01	0.19	0.1
LOI	0.1	27.4	0.5

ISBN 978-9959-9703-2-9

Table 2: Physical properties of the raw materials used in this study.

Properties	K	L	S
Bulk density (kg/m^3)	-	480	300
Particle density (Mg/m^3)	2.1	2.82	3.15
pH Value	5.37	12.62	7
Colour	White	White	White

The K9G was prepared by mixing industrial kaolin soil (K) with 9%, by the dry weight, of gypsum (G) in a mixer for about 3 minutes, as commonly adopted for sulfate soil stabilisation-based research [13,14]. The K used was in the texture form of white powder and was sourced from Potterycrafts Ltd., Stoke-on-Trent, UK. The XRD analysis revealed that K is composed of kaolinite minerals and quartz, while the sieve analysis indicated that K composes of 12% clay, 60% silt and 28% sand. The characterisation tests indicated that the K has a liquid limit (LL), plastic limit (PL) and plasticity index (PI) of 56.7%, 33.3% and 23.4%, respectively, so the K is classified as a medium-graded sandy SILT.

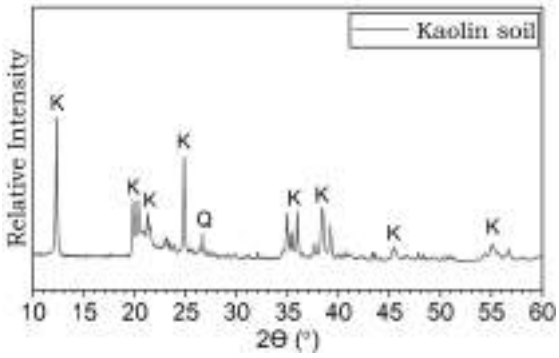

Fig.1: The XRD pattern of kaolin soil

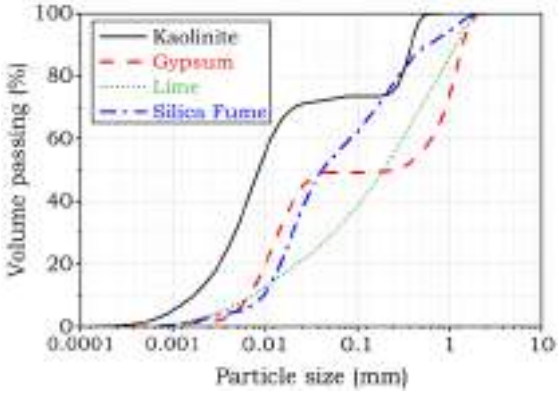

Fig.2: Sieve analysis curve for the raw materials.

The G used was a calcium sulfate dihydrate with a white powder form; it was acquired from Fisher Scientific Ltd, Loughborough, Leicestershire, UK. The L used was quicklime with an off-white powder form and calcium oxide percentage of 71%; it was sourced from Tarmac Cement and Lime Company, Buxton Lime and Powders, Derby, UK. As for the S, it was a commercially reactive micro-silica with a light grey powder form and silicon dioxide

 ISBN 978-9959-9703-2-9

concentration of 98.4%; it was sourced from Tarmac Cement and Lime Company, Buxton Lime and Powders, Derbyshire, Derby, UK.

2- Mix design

To evaluate the independent role of the variation in the moisture compaction content, mixing method and specimen dimensions on sulfate soil stabilisation with the co-addition of lime and silica fume binder, the methodology of this research study involved using; 1) one target soil material (artificial gypseous kaolin-K9G); 2) a constant blended binder content (10% by the weight of the target soil material); 3) a constant blended binder composition (lime-silica fume) of 3L-7S; 4) two different moisture compactions contents; 5) two different mixing methods; and 6) two different specimens.

The blended binder composition was made of 30% lime and 70% silica fume, in line with the previous study [14]. The moisture compaction contents adopted were 31% and 33%, corresponding to 1.1 and 1.2, respectively, of the corresponding standard proctor optimum compaction condition. This was selected; 1) to ensure the soil material is compacted wet of OMC, as it is the typical condition for soil compaction in practice to actualise the best durability behaviour [13,14], and 2) to determine the optimum moisture compaction condition for the sulfate soil. The two mixing methods selected were mainly the dry mixing method (denoted as DM) and the slurry mixing method (denoted as SM), which differ in terms of the order of the mixing procedure. For the case of dry mixing method (DM), all the dry raw materials were firstly mixed in a dry form for about 3 minutes before the predetermined moisture content was steadily introduced and the mixing was restarted for additional three minutes, preparing for the compaction process. However, in the case of slurry mixing method (SM), firstly, the binder and water were mixed for three minutes, before the artificial gypseous soil was poured and the mixing was continued for further three minutes, preparing for the compaction process. Therefore, in total, the detailed mix proportions of the sulfate-bearing kaolin soils stabilised with the co-addition of lime and silica fume at a constant binder content examined in the experimentations can be summarised in **Table 3**.

As for the two different specimens, they were fabricated in a cylindrical form with different dimensions. The first one (referred to as a jack-compacted specimen) was cast using a prefabricated mould with internal diameter of 50 mm and internal height of 100 mm and compacted using a manual jack. This kind of specimen was used to evaluate the linear expansion behaviour using Perspex cells in line with [13,14] and the UCS performance at the

 ISBN 978-9959-9703-2-9

end of 7, 28 and 90 days of moist curing. The second specimen (referred to as a ring-shaped specimen) was compacted using similar procedure to that of proctor compaction test and extruded manually in a miniaturized cylinder with a diameter of 76.2 mm and height of 19 mm, corresponding to the initial dimensions of the ring of the standard one-dimensional odometer apparatus. This was used to evaluate the swelling potential of the control mix (K9G–3L7S–1.1MC–DM) using a standard one-dimensional odometer.

Table 3: Mix compositions of artificially gypseous kaolin specimens treated with lime-silica fume blend at a constant stabiliser content of 10% by the total weight of the soil materials.

Elaborated abbreviation	Mix compositions (%)				
	Target material		Binder		MC
	K	G	L	S	
K9G-3L7S-1.1MC-DM	91	9	3	7	31
K9G-3L7S-1.1MC-SM	91	9	3	7	31
K9G-3L7S-1.2MC-DM	91	9	3	7	33

Explanation
This was considered a control mix
An SM was used, as against to DM for the control
A 1.2 MC was used, as against 1.1MC for the control

3- Specimens preparation

3.1- Jack-compacted specimen

A total of 11 jack-compacted cylinders with an outer diameter of 50 mm and height of 100 mm were fabricated for each of the mix compositions outlined in **Table 3**. Two of these specimens were employed for measuring the linear expansion, while the nine specimens were utilised for evaluating the UCS after 7, 28 and 90 days of moist curing. For each specimen, after mixing the raw ingredients as per the selected mix design outlined in **Table 3**, the semi-paste mixture was placed into the mould and compacted by means of a jack wherein a compression force was applied in aid of a steel frame as photographed elsewhere [14]. Hereafter, the samples were kept in the mould for about three minutes, permitting the stability of samples. Consequently, the specimens were extruded using a plunger, and wrapped individually in several runs of cling film to reduce moisture evaporation and carbonation, as well as regulate humidity, in line with [13,14]. Eventually, the compacted samples were further kept in a sealed plastic container and stored in the laboratory at 20∓2℃, allowing for moist curing until the date of testing.

3.2- One-dimensional odometer specimen

Two ring-shaped specimens were prepared in this study for the control mix to evaluate the swelling potential and form a relationship

 ISBN 978-9959-9703-2-9

between the linear expansion and the standardised swelling methods (ASTM D4546). For each specimen, all the dry raw materials, as per the mix composition outlined in **Table 3**, were firstly mixed in a dry form for three minutes, before the moisture was included and the mixing was continued for extra three minutes. Thereafter, the semi-paste was poured into the proctor compaction mould (with height of 116 mm and diameter of 102 mm) in three layers, of which each layer was compressed by the application of 25 using a 2.5 kg rammer. Subsequently, the ring-shaped sample was extruded by pushing the ring of the oedometer device into the compacted mixture, wrapped and stored under a similar condition to that of jack-compacted specimens for 7 days of moist curing.

4- Testing method

4.1- UCS

The UCS test was conducted on three specimens per mix composition at the end of 7, 28 and 90 days of moist curing. The test was operated in accordance with [27], using a Hounsfield compression machine equipped with a self-levelling device to guarantee a uniaxial load application. The load application was performed at a continuous compressed strain ratio of two mm per minute, and the average value of the three specimens was adopted as the presentative UCS.

4.2- Linear expansion

The linear expansion was conducted, in line with DS EN 13286-49: 2004 [28], on two jack-compacted specimens per mix over a 200-days water soaking period, using Perspex cells, as commonly adopted for soil stabilisation-based research [8,14,26,29-31]. Immediately after seven days of curing, the 10 mm-top and 10 mm-bottom part of the samples were unwrapped and accommodated individually into the Perspex cell as presented in **Fig. 3**. Afterwards, the dial gauge was adjusted to zero and the water was introduced through the upper inlet until the 10 mm-bottom of the samples was immersed in water, allowing for swelling as shown in **Fig.4**. The gauge reading was then recorded daily for 28 days, and then random reading was recorded for the remaining period. Ultimately, the ratio of the dial gauge reading (mm) to the original height (100 mm) of the specimens was calculated, and the mean of the two swelled samples was adopted as the representative linear expansion.

 ISBN 978-9959-9703-2-9

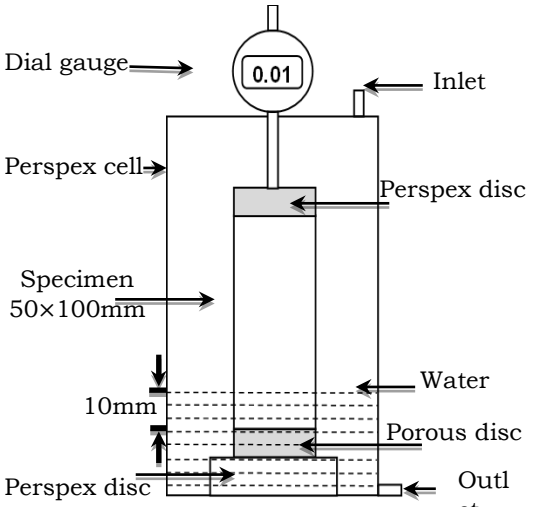

Fig.3: The Perspex cell set-up used for expansion (swelling) measurement.

Fig.4: Linear expansion specimens under expansion measurement.

The swelling potential test was performed on two ring-shaped specimens for the control mix after 7 days of moist curing. The test was operated using the standard one-dimensional odometer equipment, according to ASTM D4546. After calibration with an initial pressure of 2.75 kPa (cap load) and adjusting the dial gauge to zero, the water was introduced until the specimens were completely submerged in water as schematically shown in **Fig. 5**. Thereafter, the specimens were allowed to swell for a prolonged soaking period of 100 days, and the dial gauge reading was monitored regularly till no vertical displacement was recorded. Finally, the ratio of the dial gauge reading (mm) to the original height (19 mm) of the specimen was calculated for both specimens, and the mean value in percentage was used as the presentative swelling potential (%).

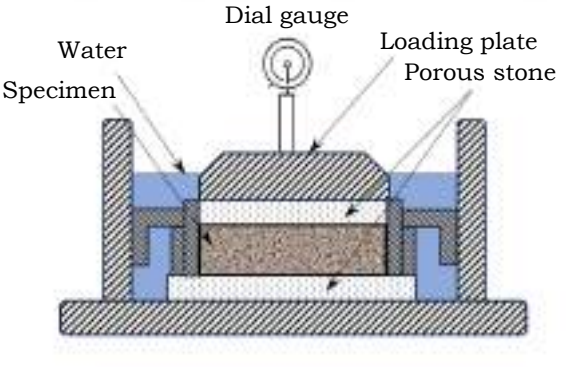

4.3- Swelling potential

ISBN 978-9959-9703-2-9

Fig.5: The schematic diagram of swelling potential specimen in the standard one-dimensional odometer apparatus.

Results and discussion

1- UCS

Fig.6 shows the influence of change in moisture content and mixing method on the UCS evolution of the artificially gypseous kaolin (K9G) samples treated with lime-silica fume blend of 3L-7S. In this perspective, the UCS revealed a progressively increasing trend as the curing age increases, confirming the classical UCS development trend of soil stabilisation. This development trend is normally assigned to the cation exchange and flocculation-agglomeration of soil particles (short-term interaction) and the pozzolanic reactions (long-term interaction) between the soil and binder, which eventually form hydrates such as calcium silicate hydrate (C-S-H) and calcium aluminate hydrate (C-A-H). These hydrates, whose kinetics is dependent on the mineralogy of the soil and the available quantities of the concerned oxides within the binder, crystalline with time, fill the pore space [10] and interlock the soil system. This consequently forms a stiff soil matrix and enhances the mechanical performance such as the shear resistance and the UCS performance [32].

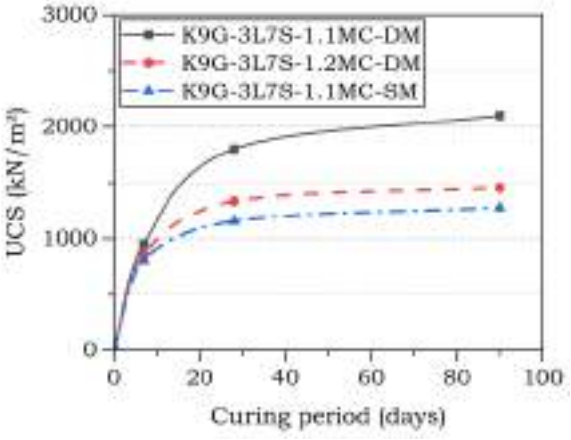

Fig.6: The UCS of K9G-3L7S specimens mixed at different mixing methods and moisture contents.

On increasing the moisture compaction content from 31% (K9G-3L7S-1.1MC-DM) to 33% (K9G-3L7S-1.2MC-DM), the stabilised specimens exhibited a compromise on the UCS. This compromise on UCS was further increased corresponding to the change of mixing method from DM (K9G-3L7S-1.1MC-DM) to SM (K9G-3L7S-1.1MC-SM). This, therefore, implies that the increase in moisture content and the use of the SM are not favourable for a higher degree of soil stabilisation. The reduction in UCS induced by the moisture content increase is probably owing to that the increase in moisture induces a lower inter-particle friction and a relatively poorer interlocking, both of which induce larger inter-particle void spaces [33]. Thereby, this void enlargement negatively affects the

 ISBN 978-9959-9703-2-9

interlocking of the soil matrix by increasing the porosity, thus, minimising the robustness against loading [34,35]. In addition, the nucleation and growth of a higher quantity of ettringite, is also a contributing factor for the reduction in UCS [36,37], as the nucleation of a higher ettringite quantity induces resistance in compaction and facilitates the formation of extensive cracks within the system, both of which induce an increase in porosity and thereby induce a compromise on the UCS. As for the reduction in the UCS corresponding to the change of mixing method from DM to SM, it is supposed to be caused by the clumping of the cementitious ingredients (lime and silica fume) during the mixing and the poorer distribution of the hydrates, both of which induce poorer interlocking, and lowered UCS.

2- Volume change behaviour.

2.1-Effect of variation of water content and mixing method.

The effect of water compaction content and mixing procedure on the expansion of gypseous kaolin treated with a lime-silica fume blend of 3L-7S, is presented in **Fig. 7**.

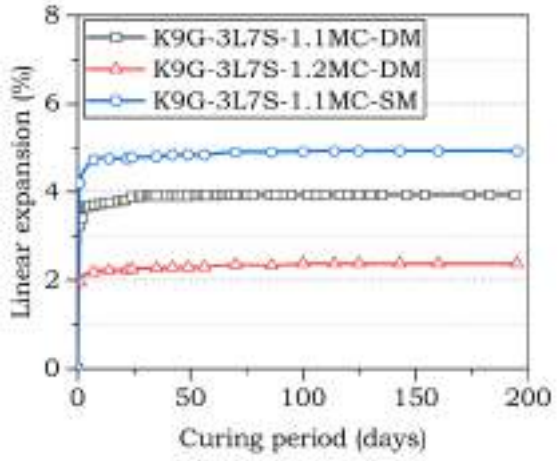

Fig.7: The linear expansion plots of K9G-3L7S specimen mixed at different mixing methods and moisture contents.

Accordingly, the utilisation of higher water compaction content (1.2MC as against 1.1MC) shows a beneficial impact on the expansion behaviour, where the total expansion of K9G-3L7S was reduced from 4% to 2.3%, as the moisture content increased from 31% (1.1MC) to 33% (1.2MC), respectively. Conversely, the utilisation of SM (slurry mixing) instead of DM (dry mixing) negatively affects the expansion trend, where the total expansion magnitude was increased from 4% for the case of DM to about 5% for the SM, representing about 23% increase in the expansion. Therefore, it can be stated that using higher water compaction content is beneficial in terms of the expansion, while the use of the SM is not recommended. The possible rationale for the reduction in

 ISBN 978-9959-9703-2-9

expansion induced by the higher moisture content could be the increase in the inter-particle void pores [33]. At higher water level (33%), the stabilised samples would not be at the maximum dry density, thus a higher volume of voids would be available for the nucleation and the growth of ettringite, and thereby a lesser swelling magnitude would be induced [38]. As for the increase in the expansion induced by the slurry mixing method, it is expected to be due to the poorer interlocking as a result of the clumping of the cementitious ingredients during the mixing process and the poorer distribution of pozzolanic hydrates within the stabilised system.

2.2- Effect of specimen size and testing approach.

The swelling potential trend measured using the standard one-dimensional odometer test for the gypsum-dosed kaolin specimen stabilised with 3L7S is plotted in **Fig.8**, in comparison with its expansion counterpart measured using Perspex cell.

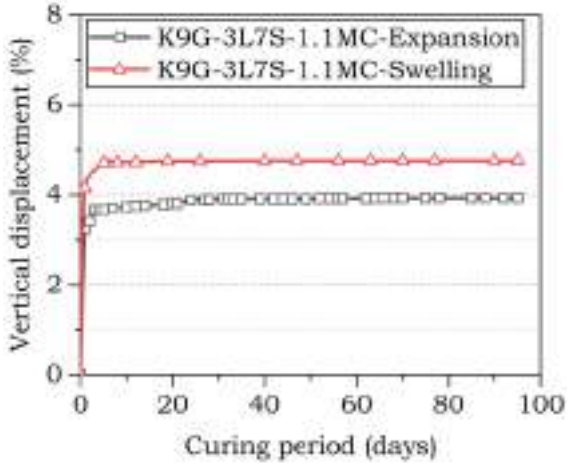

Fig.8: The linear expansion and swelling potential plots of K9G-3L7S mixed using the dry mixing method and compacted at 1.1MC.

As expected, the mix composition of K9G-3L7S-1.1MC-DM exhibited a higher swelling potential of 4.7%, relative to that of 3.9% expansion obtained using Perspex cell. This increase in swelling potential can be attributed partly to the densification degree of the specimen, and partly to the specimen confinement matter during the test. As discussed earlier, the one-dimensional odometer specimen was compressed on the matter of proctor test in which 25 blows were applied using a 2.5 kg rammer, as against that of the linear expansion specimens which were compacted using a simple hydraulic jack. This implies that the samples used for the swelling potential are likely to be compressed at a higher dry density, thus the volume of voids is lower than those of the linear expansion

 ISBN 978-9959-9703-2-9

specimen, thereby lesser space is available for accommodating the ettringite and in turn a higher swelling potential would be induced. As for specimen confinement condition, the perimeter of the odometer specimens was confined by the ring, thus the displacement (swelling) of the specimens occurred only in the vertical direction, thereby a higher swelling potential was recorded. On the contrary, the perimeter of the linear expansion specimens was unconfined, thus the expansion occurs in both the vertical direction and perimeter direction. Eventually, it can be inferred that the volume change of gypseous kaolin treated with lime and silica fume is also a function of compaction degree and sample confinement matter during the experimentation analysis.

Conclusions

The role of moisture compaction content, mixing method and specimen size on the UCS performance and swelling behaviour of sulfate soil stabilisation with the co-addition of lime (L) and silica fume (S) has been examined in this research study. Accordingly, the following specific conclusions can be outlined:

The utilisation of a moisture compaction content of 1.2 of the corresponding standard Proctor optimum compaction condition yielded a compromise on the UCS, relative to that of 1.1 MC, although such a relatively higher moisture content reduces the ultimate expansion magnitude. This is attributed to the lower inter-particle friction and the enlargement of voids within the system, both of which reduce the robustness against loading and facilitate the accommodation of ettringite.

The slurry mixing method, in which the binder was initially mixed with water and then the soil was incorporated, yielded a compromise on both the UCS and linear expansion due to the clumping of the binding constituents and the poorer distribution of the hydrates formed from the binder hydration. Hence, slurry mixing is not suggested for a better soil stabilisation.

The volume change of gypseous soil samples treated with a binary blend of 3L-7S is a function of densification degree and testing approach, where the comparison between swelling potential measured using a one-dimensional odometer test and linear expansion test indicated a higher swelling potential magnitude due to the higher degree of specimen densification and the confinement of specimen's perimeter under the testing.

Arabic section:

العنوان: دور المحتوى الرطوبي، طريقة الخلط وحجم العينة في انتفاخ التربة الكبريتية المثبتة بمزيج من الحجر الجيري ودخان السيليكا.

المؤلفون: ندى الشرع، ندى صالح، منصور إبعيليلة، أسماء محمد،

الكلمات المفتاحية: (إترينجيت، تثبيت التربة، مثبت قائم على الكالسيوم، قوة الضغط، الانتفاخ)

الملخص: يعتمد التثبيت الكيميائي للتربة، وهو تقنية تقليدية لمعالجة التربة، على عدة

 ISBN 978-9959-9703-2-9

متغيرات منها تركيب التربة، تركيب المادة الرابطة، محتوى الكبريتات، والمحتوى الرطوبي من بين متغيرات أخرى. يقدم هذا البحث دراسة معملية تدرس التأثير المستقل لكل من المحتوى الرطوبي، طريقة الخلط وحجم العينة على أداء تثبيت التربة الكبريتية بمزيج تنائي من الحجر الجيري ودخان السيليكا. تم تحضير مجموعة من عينات الكيولين الممزوجة بكبريتات الكالسيوم باستخدام مثبت تنائي (3% من الحجر الجيري و7% من دخان السيليكا)، محتوين رطوبة مختلفين (31% و33%)، طريقتين مختلفتين للخلط (طريقة الخلط الجاف وطريقة الملاط) وحجمي عينتين مختلفين (واحده بقطر 50 مم وارتفاع 100 مم وأخرى بقطر 76.2 مم وارتفاع 19 مم). بعد دالك، قد تم اجراء العديد من الاختبارات الفيزيائية والميكانيكية بما في دالك قوة الضغط غير المحصورة، التوسع الخطي واختبار الانتفاخ لتقييم أدائهما. اشارت نتائج هده الدراسة الى أن استخدام طريقة خلط الملاط بدلا من طريقة الخلط الجافة تسبب في مساومة على كل من التمدد وقوة الضغط بسبب تكتل المواد الرابطة خلال عملية الخلط وبالتالي عدم توزيع الهيدرات المنتجة من التفاعل في الخليط. اما بالنسبة لتباين المحتوى الرطوبي، فان المحتوى الرطوبي الأعلى (33%) قد أسفر عن تمدد أفضل (أي اقل) وقوة ضغط اقل نتيجتا لتضخم حجم الفراغات مما يقلل من المتانة ضد التحميل ويوفر مساحة لاستيعاب الإترينجيت.

References

[1] Al-Atroush, M.E., and Sebaey, T.A., (2021), Stabilization of expansive soil using hydrophobic polyurethane foam: A review., Transportation Geotechnics., **27**, 100494. DOI: 10.1016/j.trgeo.2020.100494.

[2] Ikeagwuani, C.C., and Nwonu, D.C., (2019), Emerging trends in expansive soil stabilisation: A review., Journal of rock mechanics and geotechnical engineering., **11**(2), 423-440. DOI: 10.1016/j.jrmge.2018.08.013.

[3] Cheshomi, A., Eshaghi, A., and Hassanpour, J., (2017), Effect of lime and fly ash on swelling percentage and Atterberg limits of sulfate-bearing clay., Applied Clay Science., **135**, 190-198. DOI: 10.1016/j.clay.2016.09.019.

[4] Jha, A.K., and Sivapullaiah, P.V., (2016), Volume change behavior of lime treated gypseous soil—influence of mineralogy and microstructure., Applied Clay Science., **119**, pp.202-212. DOI: 10.1016/j.clay.2015.09.017.

[5] Jones, L.D., and Terrington, R., (2011), Modelling volume change potential in the London Clay., Geological Society of London., **44**, 109–122. DOI: 10.1144/1470-9236/08-112.

[6] Igwe, O., and Umbugadu, A.A., (2020), Characterization of structural failures founded on soils in Panyam and some parts of Mangu, Central Nigeria., Geoenvironmental Disasters., **7**, 1-26. DOI: 10.1186/s40677-020-0141-9.

[7] Nazari, Z., Tabarsa, A., and Latifi, N., (2021), Effect of compaction delay on the strength and consolidation properties of cement-stabilized subgrade soil., Transportation Geotechnics., **27**, 100495. DOI: 10.1016/j.trgeo.2020.100495.

[8] M. Ebailila, Sulfate soil stabilisation with silica fume-based binders, Doctoral Thesis, University of South Wales, England, UK, 2022.

[9] H. Ali, M. Mohamed, Ali, H., and Mohamed, M., (2017), The effects of compaction delay and environmental temperature on the mechanical and hydraulic properties of lime-stabilized extremely high plastic clays., Applied Clay Science., **150**, 333-341. DOI: 10.1016/j.clay.2017.09.019.

[10] Behnood, A., (2018), Soil and clay stabilization with calcium-and non-calcium-based additives: A state-of-the-art review of challenges, approaches and techniques., Transportation Geotechnics., **17**, 14-32. DOI: 10.1016/j.trgeo.2018.08.002.

[11] Vitale, E., Deneele, D., Russo, G., and Ouvrard, G., (2016), Short-term effects on physical properties of lime treated kaolin., Applied Clay Science., **132**, 223-231. DOI: 10.1016/j.clay.2016.04.025.

[12] Nidzam, R.M., and Kinuthia, J.M., (2010), Sustainable soil stabilisation with blastfurnace slag–a review., Proceedings of the Institution of Civil Engineers-

 ISBN 978-9959-9703-2-9

Construction Materials., **163**(3), 157-165. DOI: 10.1680/coma.2010.163.3.157.

[13] Ebailila, M., Kinuthia, J., and Oti, J., (2022), Role of Gypsum Content on the Long-Term Performance of Lime-Stabilised Soil., Materials., **15**(15), 5099. DOI: 10.3390/ma15155099.

[14] Ebailila, M., Kinuthia, J., and Oti, J., (2022), Suppression of Sulfate-Induced Expansion with Lime–Silica Fume Blends., Materials., **15**(8), 2821. DOI: 10.3390/ma15082821.

[15] Oti, J.E., Kinuthia, J.M., and Bai, J., (2009), Compressive strength and microstructural analysis of unfired clay masonry bricks. Engineering Geology., **109**(3-4), 230-240. DOI: 10.1016/j.enggeo.2009.08.010.

[16] Wang, L., Roy, A., Seals, R.K., and Metcalf, J.B., (2003), Stabilization of sulfate-containing soil by cementitious mixtures mechanical properties., Transportation Research Record., **1837**(1), 12-19. DOI: 10.3141/1837-02

[17] Ghorbani, A., Hasanzadehshooiili, H., Karimi, M., Daghigh, Y., and Medzvieckas, J., (2015), Stabilization of problematic silty sands using microsilica and lime., The Baltic Journal of Road and Bridge Engineering, **10(**1), 61-70. DOI: 10.3846/bjrbe.2015.08.

[18] Goodarzi, A.R., Akbari, H.R., and Salimi, M., (2016), Enhanced stabilization of highly expansive clays by mixing cement and silica fume., Applied Clay Science., **132**, 675-684. DOI: 10.1016/j.clay.2016.08.023.

[19] Mousavi, S.E., (2018), Utilization of silica fume to maximize the filler and pozzolanic effects of stabilized soil with cement., Geotechnical and Geological Engineering., **36**(1), 77-87. DOI: 10.1007/s10706-017-0305-x.

[20] Singh, P., Dash, H.K., and Samantaray, S., (2020), Effect of silica fume on engineering properties of expansive soil., Materials Today: Proceedings., **33**, 5035-5040. DOI: 10.1016/j.matpr.2020.02.839.

[21] Tiwari, N., Satyam, N., and Singh, K., (2020), Effect of curing on micro-physical performance of polypropylene fiber reinforced and silica fume stabilized expansive soil under freezing thawing cycles., Scientific Reports., **10**(1), 1-16. DOI: 10.1038/s41598-020-64658-1.

[22] Türköz, M., Umu, S.U., and Öztürk, O., (2021), Effect of silica fume as a waste material for sustainable environment on the stabilization and dynamic behavior of dispersive soil., Sustainability., **13**(8), 4321. DOI: 10.3390/su13084321.

[23] Murthi, P., Saravanan, R., and Poongodi, K., (2021) Studies on the impact of polypropylene and silica fume blended combination on the material behaviour of black cotton soil., Materials Today: Proceedings., **39**, 621-626. DOI: 10.1016/j.matpr.2020.09.004.

[24] Ghavami, S., Naseri, H., Jahanbakhsh, H., and Nejad, F.M., (2021), The impacts of nano-SiO2 and silica fume on cement kiln dust treated soil as a sustainable cement-free stabilizer., Construction and Building Materials., **285**, 122918. DOI: 10.1016/j.conbuildmat.2021.122918.

[25] Saygili, A., and Dayan, M., (2019) Freeze-thaw behavior of lime stabilized clay reinforced with silica fume and synthetic fibers., Cold Regions Science and Technology., **161**, 107-114. DOI: 10.1016/j.coldregions.2019.03.010.

[26] Ebailila, M., Kinuthia, J., Oti, J., and Al-Waked, Q., (2022), Sulfate soil stabilisation with binary blends of lime–silica fume and lime–ground granulated blast furnace slag., Transportation Geotechnics., **37**, 100888. DOI: 10.1016/j.trgeo.2022.100888.

[27] BS EN ISO 17892-7: 2018, Geotechnical investigation and testing-Laboratory testing of soil — Part 7: Unconfined compression test, BSI Standards Limited, London, UK, 2018.

[28] BS EN 13286-49: 2004, Unbound and hydraulically bound mixtures — Part 49: Accelerated swelling test for soil treated by lime and/or hydraulic binder, BSI Standards Limited, London, UK, 2004.

[29] Obuzor, G.N., Kinuthia, J.M., and Robinson, R.B., (2011), Utilisation of lime activated GGBS to reduce the deleterious effect of flooding on stabilised road structural materials: A laboratory simulation., Engineering geology., **122**(3-4), 334-338. DOI: 10.1016/j.enggeo.2011.06.010.

[30] Oti, J.E., Kinuthia, J.M., and Robinson, R.B., (2014), The development of unfired clay building material using Brick Dust Waste and Mercia mudstone clay., Applied clay science., **102**, 148-154. DOI: 10.1016/j.clay.2014.09.031.

 ISBN 978-9959-9703-2-9

[31] Kinuthia, J.M., and Nidzam, R.M., (2011), Towards zero industrial waste: Utilisation of brick dust waste in sustainable construction., Waste Management., **31**(8), 1867-1878. DOI: 10.1016/j.wasman.2011.03.020.

[32] Beetham, P., Dijkstra, T., Dixon, N., Fleming, P., Hutchison, R., and Bateman, J., (2015), Lime stabilisation for earthworks: a UK perspective., Proceedings of the Institution of Civil Engineers-Ground Improvement., **168**(2), 81-95. DOI: 10.1680/grim.13.00030.

[33] Obuzor, G.N., Kinuthia, J.M., and Robinson, R.B., (2012), Soil stabilisation with lime-activated-GGBS—A mitigation to flooding effects on road structural layers/embankments constructed on floodplains., Engineering Geology., **151**, 112-119. DOI: 10.1016/j.enggeo.2012.09.010.

[34] Horpibulsuk, S., Miura, N., and Nagaraj, T.S., (2003), Assessment of strength development in cement-admixed high water content clays with Abrams' law as a basis., Geotechnique., **53**(4), 439-444. DOI: 10.1680/geot.2003.53.4.439.

[35] Ho, L.S., Nakarai, K., Ogawa, Y., Sasaki, T., and Morioka, M., (2017), Strength development of cement-treated soils: effects of water content, carbonation, and pozzolanic reaction under drying curing condition., Construction and Building Materials., **134**, 703-712. DOI: 10.1016/j.conbuildmat.2016.12.065.

[36] Rahmat, M.N. and Ismail, N., (2011), Sustainable stabilisation of the Lower Oxford Clay by non-traditional binder., Applied Clay Science, **52**(3), 199-208. DOI: 10.1016/j.clay.2011.02.011.

[37] Wild, S., Abdi, M.R., and Leng-Ward, G., (1993), Sulphate expansion of lime-stabilized kaolinite: II. Reaction products and expansion., Clay minerals., **28**(4), 569-583. DOI: 10.1180/claymin.1993.028.4.07.

[38] Wild, S., Kinuthia, J.M., Jones, G.I., and Higgins, D.D., (1999), Suppression of swelling associated with ettringite formation in lime stabilized sulphate bearing clay soils by partial substitution of lime with ground granulated blastfurnace slag (GGBS)., Engineering geology., **51**(4), 257-277. DOI: 10.1016/S0013-7952(98)00069-6.

 ISBN 978-9959-9703-2-9

المؤتمر الدولي الثاني للعلوم والهندسة
2nd International Conference on Science and Engineering
ICSE 2023
Faculty of Engineering - University of Bani Waleed
Bani Waleed, Libya

Paper Code: ICSE-040

A COMPARATIVE STUDY ON THE LONG-TERM MICROSTRUCTURE OF SOIL STABILISATION WITH CALCIUM AND MAGNESIUM-BASED BINDERS

M Ebailila[a], J. Kinuthia[b], J. Oti[b], S. Attelisi[a],
[a] Department of Civil Engineering/Faculty of Engineering/Bani Waleed University, Libya
[a] Faculty of Computing, Engineering and Science/University of South Wales, UK
*Crosspnding author: mansour.ebailila@yahh.co.uk

Abstract: Analytical and microstructure investigations such as x-ray diffraction (XRD), derivative thermogravimetric (DTG), and scanning electron microscopy (SEM) among others, are typically used by researchers to detect and quantify the amount of formed minerals including ettringite minerals in gypseous soil treated with lime or cement. However, the detection of ettringite crystals is sometimes difficult, suggesting that the appearance of ettringite under the microstructure analysis is also dependent on the curing and experimental procedure. Therefore, a series of soil mixtures designed by use of two different soils (pure kaolin soil and artificial gypseous kaolin soil) and stabilised with 10 wt% of lime-L, cement-C and MgO-M, were investigated using multi-scale investigations including XRD, DTG and SEM. Accordingly, the result revealed that, under 90-days of moist curing, the key minerals detected in gypseous kaolin stabilised with calcium-based stabiliser are kaolinite, calcium silicate hydrate, portlandite, and ettringite, whereas only kaolinite, gypsum, brucite and magnesium silicate hydrate were detected in gypseous kaolin stabilised with magnesium oxide. However, under 200-days of water soaking period, no trace of gypsum, ettringite and portlandite were detected in the XRD of 10L- and 10C-based specimens, accompanied by the indication of new minerals (hemihydrate, anhydrite, calcite, and aragonite), suggesting the carbonation of ettringite during the soaking in water.

Keywords: (Ettringite, sulfate, ettringite carbonation, lime, Portland cement, magnesium oxide)

Introduction

Stabilisation of expansive soils with hydraulic stabilisers (Portland cement, lime, and magnesium oxide) has been a promising treatment technique for improving the physico-mechanical characteristics and reducing the swell-shrink attitude of expansive soil under moisture fluctuations [1]. The cement-induced improvement is typically assigned to the cement hydration; a basic reaction involved the dissolution of C_3S, C_3A, C_2S, and C_4AF, with the formation, by precipitation, of calcium silicate hydrate (C-S-H), calcium aluminate hydrate (C-A-H) and calcium hydroxide (CH, also called portlandite) [2]. These hydrates crystalline with time, binding/interlocking the host soil mixture and improving plasticity

 ISBN 978-9959-9703-2-9

index [3], shear strength [4], compressive strength [5], robustness against freezing and thawing [5-6], and the swelling behaviour of the soil [7], As for the improvement induced by lime and magnesium oxide, this essentially occurs due to two basic sets of reaction mechanisms: one being shorth-term reactions (cation exchange and flocculation of soil particles) while the second is a long-term reaction (pozzolanic reaction). Upon the addition of quicklime (calcium oxide) and magnesium oxide to the soil in the existence of moisture, the quicklime initially hydrated to calcium hydroxide and then dissolved releasing calcium ions and hydroxyl ions [8], in line with equations 1-to-2. As for the magnesium oxide, it gets protonated by H+ ions and then the magnesium oxide precipitates [9], in line with equations 3-to-6.

$$CaO+H_2O \rightarrow Ca(OH)_2+\uparrow heat \ldots\ldots\ldots\ldots(1)$$

$$Ca(OH)_2 \rightarrow Ca^{2+} + 2OH^- \ldots\ldots\ldots\ldots\ldots\ldots(2)$$

$$MgO + H_2O \rightarrow MgOH^+_{(surface)} + OH^-_{(aqueous)} \ldots(3)$$

$$MgOH^+_{(surface)} + OH^-_{(aqueous)} \rightarrow MgOH^+ \cdot OH^- \ldots\ldots(4)$$

$$MgOH^+ \cdot OH^-_{(surface)} \rightarrow Mg^{2+} + 2OH^-_{(aqueous)} \ldots\ldots(5)$$

$$Mg^{2+} + 2OH^-_{(aqueous)} \rightarrow Mg(OH)_{2\,(solid)} \ldots\ldots\ldots(6)$$

These reactions, therefore, cause the cation exchange on the soil particles, and such a replacement in cations occurs in the order of $Na^+ < K^+ < Mg^{++} < Ca^{++}$, in which higher valence cations replace those of lower valence cations [8]. This ions substitution balances the electronic charge of the soil particles, induces flocculation-agglomeration of soil particles [10], and promotes different soil particle arrangements [11]. Besides, the hydroxide ions (OH) cause a significant increase in the alkalinity (pH) value (>10), aiding the octahedral and tetrahedral sheets of soil particles to release silica and alumina ions [12]. Thereafter, this initiates the pozzolanic reactions, forming hydrates such as CSH, and CAH in the case of lime [10], and magnesium silicate hydrate (MSH) in the case of magnesium oxide [13-16], all of which enable the interlocking of the system and improving the physico-mechanical chractaristics of the soil. Portlandite (calcium hydroxide) and brucite may also remain from the interaction between the binder and soil if a surplus binder content was provided. This surplus binder coats the particles, delaying the dissolution of soil particles and the pozzolanic reaction, as well as reducing the cohesion of the soil matrix [17-18].

In the attendance of gypsum, however, the calcium-based stabiliser reaction mechanisms are altered due to the nucleation of highly hydrated mineral in the form of needles- and rod-shaped crystals in line with equation 7, known as ettringite [19], owing to the interaction between calcium, alumina, and

 ISBN 978-9959-9703-2-9

sulfate in the existence of water.

$$6Ca^{2+} + 2Al(OH)_4^- + 4OH^- + 3(SO_4)^{2-} + 26H_2O \rightarrow Ca_6[Al(OH)_6]_2 \cdot (SO_4)_3 \cdot 26H_2O \quad \text{.....(7)}$$

The ettringite is a problematic issue from a soil stabilisation point of view, as it has a higher water absorption, thus facilitating the volume increase of the host matrix [20]. The ettringite also occurs in a complex mechanism and of dependence on the mineralogy of soil, binder composition, moisture content, temperature and so on. Therefore, researchers use multi-scale analytical investigations such as XRD, DTG, and SEM analysis among others, to quantify the amount of formed ettringite within the stabilised soil mixture for deeper understanding of the reaction mechanisms.

In this context, Puppala et al., (2005) [21], conducted a laboratory investigation using both XRD and SEM and reported that calcium oxide produces both crystalline ettringite and calcite, of which the latter seems to act as a seeding or templating material promoting the formation of calcite over the formation of ettringite. Aldaood et al., (2014) [22], detected the ettringite reflections in the XRD of UCS kaolin samples treated with 3% of lime and containing gypsum content of ≥ 5%, of which the intensity of ettringite reflections was increased as the curing period and temperature increase.

However, in some cases, the detection of ettringite crystals is difficult particularly in the case of the XRD pattern after completion of the expansion, suggesting the appearance of ettringite under the microstructure analysis is also dependent on the curing and experimental procedure. For example, Jha and Sivapullaiah (2015) [23], reported no trace of ettringite crystalline in the XRD of gypsum-dosed soil samples dosed with lime and containing sulfate content of up to 6%, although the specimens represent a continues increasing swelling (heaving) trend indicating the formation needles-like ettringite. So, despite the extensive existing research studies, there are still outstanding questions about the appearance of ettringite minerals in stabilised sulfate soils under the microstructure analysis.

In this context, this research study was carried out using a variety of analytical and microstructural investigations including XRD, DTG, and SEM, with a view to identifying the possible rationale for the detection and the absence of ettringite under these tests.

Methodology

1- Materials

The raw ingredients utilized during the laboratory experimentations included kaolin soil (K), gypsum (G), Portland cement (C), lime (L), magnesium oxide (M), and deionized water. **Table 1** and **Table 2** outline the main oxide

 ISBN 978-9959-9703-2-9

charactaristics and physical charactaristics of the raw materials, respectively, whereas **Fig.1** and **Fig.2** plot the sieve analysis curves and the DTG curves curves of the raw ingredients.

Table 1: Oxide properties of raw ingredients.

Oxides	K	C	L	M
CaO	0.01	61.5	71.6	-
MgO	0.21	3.54	0.58	>98
SiO_2	47.3	18.8	0.67	-
Al_2O_3	35.9	4.77	0.07	-
Na_2O	0.07	0.02	0.02	-
P_2O_5	0.12	0.1	0.03	-
Fe_2O_3	0.69	2.87	0.05	-
Mn_2O_3	0.02	0.05	0.02	-
K_2O	1.8	0.57	0.01	-
TiO_2	0.02	0.26	0.01	-
V_2O_5	0.01	0.06	0.02	-
BaO	0.07	0.05	0.01	-
SO_3	0.01	3.12	0.19	-
LOI	0.1	4.3	27.4	-

Table 2: Physical charactaristics of kaolin, Portland cement, lime, and magnesium oxide.

Properties	K	C	L	M
Density (kg/m^3)	-	1400	480	-
Particle density(Mg/m^3)	2.14	3.15	2.8	3.58
pH Value	5.37	13.41	12.6	11.90
Colour	White	Grey	White	White

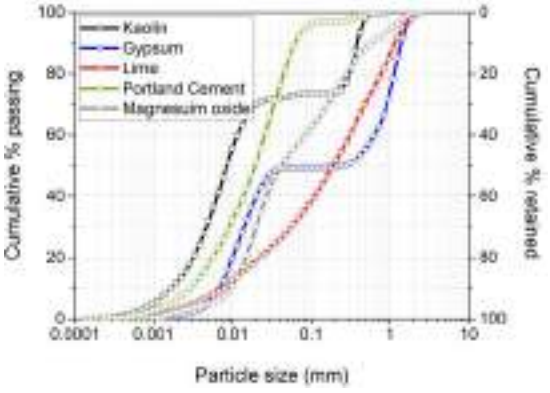

Fig.1: Sieve analysis curves of kaolin, gypsum, lime, Portland cement and magnesium oxide.

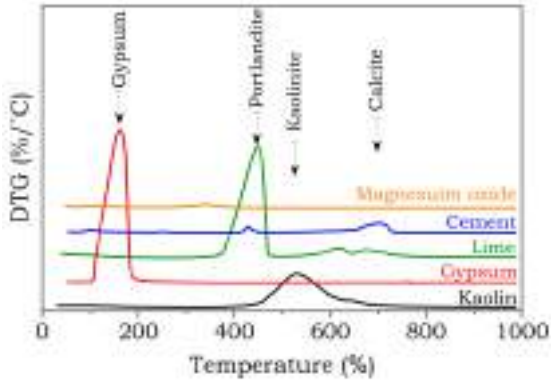

Fig.2: Derivative thermogravimetric (DTG) of raw materials.

The kaolin (K) used was a semi-processed kaolin soil with a liquid limit, plastic limit, and plasticity index of 56.7%, 33.3%, and 23.4%, respectively; it was sourced from Potterycrafts Ltd, Stoke-on-Trent, UK. The DTG curve (see **Fig.2**) revealed a major endothermic peak at 400-700°C because of the decomposition of

ISBN 978-9959-9703-2-9

kaolinite minerals [24].

The gypsum (G) utilised was a calcium sulfate dihydrate with a white form; it was obtained from Fisher Scientific Ltd, Loughborough, Leicestershire, UK. The DTG curve (see **Fig.2**) revealed a major endothermic peak at a temperature range of 100-200℃ because of the dehydration of the moisture of gypsum [25], confirming the purity of the product.

The cement (C) utilised was a commercially available CEM-I Portland cement with a grey powder texture; it was produced in line with BS EN 197-1: 2011 [26], and supplied by Large Cement, UK. The DTG curve (see **Fig.2**) revealed two major endothermic peaks; the first peak at a temperature of 400-500℃ due to the dehydroxylation of portlandite; and the second peak at 650-750℃ due to the decomposition of calcite [27].

The lime (L) utilised was a quicklime with an off-white texture: it was sourced from Tarmac Cement and Lime Company, Derby, UK. The DTG (see **Fig.2**) revealed two main endothermic peaks; sharp peak at a temperature of 350-500℃ because of the decomposition of quicklime and weaker peak at a temperature of 550-750℃ owing to the de-carbonation of calcite [25].

The magnesium oxide (M) used was a commercial reactive magnesia with a white powder texture; it was gotten from Fisher Scientific Ltd, Leicestershire, UK. The DTG curve (see **Fig.2**) revealed a straight flat line without any endothermic peaks.

2- Mix proportions

The mixes (see **Table 3**) evaluated during the experimentations were designed using; 1) two soil materials (industrial kaolin and gypseous kaolin soil); 2) three different binders (Portland cement, lime, and magnesium oxide); and 3) fixed moisture content of 31%. For clarity, the mix design code contains kaolin (K), gypsum (G) and the binder (C for Portland cement, L for lime or M for magnesium oxide), of which G, C, L and M proceeded by a number, representing the solid amount. The G content shown in the designation code denotes the gypsum percentage by the total mass of the artificially gypseous kaolin, whereas the stabiliser amount represents the sabiliser dosage by the total mass of the dry soil. The purpose of designing these mix compositions was to investigate the microstructure of soil stabilization using L, C, and M in the presence and absence of sulfate. As for the adoption of 31 % moisture content (MC), which was equal to 1.1 of the corresponding standard proctor optimum condition, it was because the soil is always compacted wet of moisture to accommodate any moisture losses. In addition, it was not found necessary to establish the optimum moisture content (OMC) for each

 ISBN 978-9959-9703-2-9

system due to the time-consuming nature of proctor test and the impracticability of establishing the OMC for each mix [25].

Table 3: Mix compositions of kaolin specimens made with L, C and M at a constant stabiliser content of 10 % by the total weight of the soil.

Design code	Target soil materials (%)	
	K	G
K0G-10L	100	0
K0G-10C	100	0
K0G-10M	100	0
K9G-10L	91	9
K9G-10C	91	9
K9G-10M	91	9

Design code	MC	Binder in % by target soil material		
		L	C	M
K0G-10L	31	10		
K0G-10C	31		10	
K0G-10M	31			10
K9G-10L	31	10		
K9G-10C	31		10	
K9G-10M	31			10

3- Specimen preparation

A total of two stabilized pure kaolin specimens and six stabilized gypseous specimens were fabricated for each mix; 1) two samples were cured in a sealed plastice container for a period of 7-days of moist curing and then used for the DTG analysis; 2) two samples were cured in a sealed plastic container for a period of 90-days of moist curing and then used for the XRD analysis; and 3) two samples were cured in a sealed plastic container for 7 days before being soaked in water for a period 200-days and then tested using XRD and SEM analysis. For each specimen, enough dry ingredients for fabricating a sample with a diameter of 50 mm and height of 100 mm, were mixed using a mixer for 3 minutes. Hereafter, the predetermined moisture content was added, and the mixing was restarted and continued for exra three minutes. Consequently, the mixture was filled into a steel mould and compacted using a jack in aid of a steel frame as detailed elsewhere [20]. Therefore, the specimens were extruded using a plunger, covered with a cling film, and stored in a plastic container, allowing for moist curing until the testing date. At the end of 7 days, the upper and bottom 10mm-part of two specimens were unwrapped and soaked in water for 200 days using a similar procedure used elsewhere [20], for swelling.

4- Testing method

The analytical and microstructure tests

 ISBN 978-9959-9703-2-9

adopted in this research study included DTG, XRD and SEM analysis. Prior to testing, the specimens were fractured and dried in a desiccator at 40 ◦C, milled, sieved through a 0.074 mm sieve, and stored in a plastice bottle at 20∓2 ◦C, preparing for the tests. Thereafter, the DTG analysis was carried out at 7 days of moist curing. The DTG analysis was run from 20∓2 up to 1000 ℃, at a flow heating ratio of 20 ℃/min and under an argon environment using a TGA55 kit. The XRD was operated using an STOE powder diffraction system at 90 days of moist curing and after 200 days of soaking in water. The XRD analysis was run at a wavelength (λ) of 1.540598 Å, a step size of 0.015°, and an angle scan in the range of 10 to 84. The microstructure analysis was inspected at 200 days of soaking in water, using JSM-7900F scanning electron microscopy (SEM) at an accelerating voltage of 5 kV and magnifications up to 30000x.

Results and discussion

1- Derivative thermogravimetric (DTG).

The DTG curves of pure kaolin samples (K0G) and gypseous kaolin samples (K9G) stabilised with 10L, 10C and 10M at 7-days of moist curing period, are shown in **Fig. 3**.

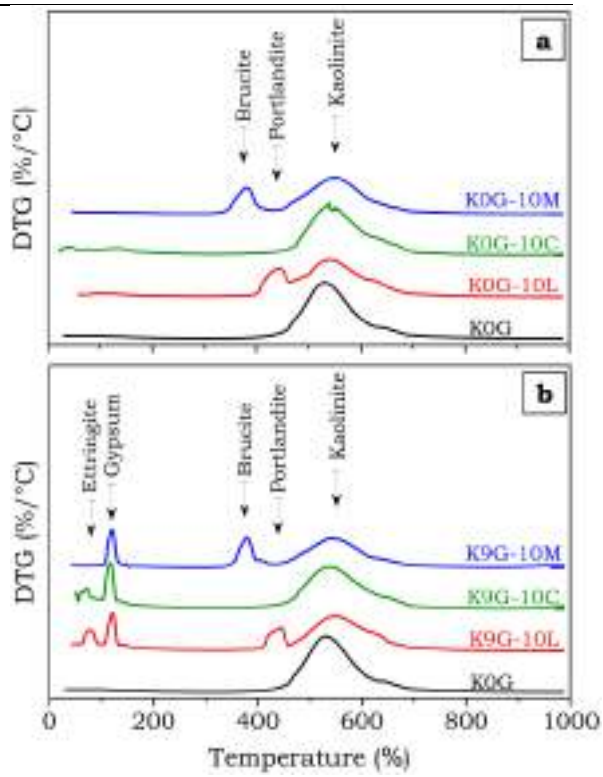

Fig.3: The DTG curves of **a)** kaolin samples and **b)** gypseous kaolin samples, made with 10L, 10C and 10M after 7 days of moist curing.

In the absence of sulfate (K0G), the specimen revealed the presence of a major endothermic peak at 400-700℃ pertained to the decomposition of kaolinite [24]. On the use of 10L, 10C, and 10M for stabilisation of pure kaolin (K9G-10L), the DTG analysis exhibited two additional peaks; 1) the first at 350-450℃ owing to the decomposition of brucite [28]; and 2) the second peak at 400-500℃ due to the

 ISBN 978-9959-9703-2-9

decomposition of portlandite [20]. The presence of brucite and portlandite is an indication of the incomplete consumption of binder through the cation exchange, flocculation, and agglomeration of soil particles [28]. However, in the presence of sulfate (K9G), the DTG analysis exhibited two further peaks; 1) the first peak at 50-100℃ due to the dehydration of ettringite minerals [20]; and 2) the second peak at a temperature range of 100-200℃ due to the dehydration of gypsum [25]. By comparing the height of ettringite peaks, it was apparent that the ettringite mineral was only formed in gypseous kaolin specimens stabilized with a calcium-based stabilizer, and such a mineral was more pronounced in the case of K9G-10L. This was confirmed by the higher gypsum peak, both of which are in support of why calcium-based stabilizers normally yield a superior UCS through soil stabilisation in the presence of sulfate. Apart from ettringite and gypsum peaks, portlandite and brucite peaks were also detected in K9G-10L and K9G-10M, respectively, indicating the incomplete consumption of lime and magnesium oxide used through the fabric modification, which in turn indicates the surplus of both binders. This surplus binder content is not favourable, as it restricts the dissolution of soil particles, delays the pozzolanic reactions, and reduces the cohesion of the system [20]. Therefore, this is in partial support of why 10L induces lower UCS performance in previous study [20].

3- XRD analysis

Fig.4 presents the comparative XRD pattrens of kaolin samples treated with 10L, 10C and 10M after 90 days of moist curing, denoted as M, and after 200 days of water soaking, denoted as S).

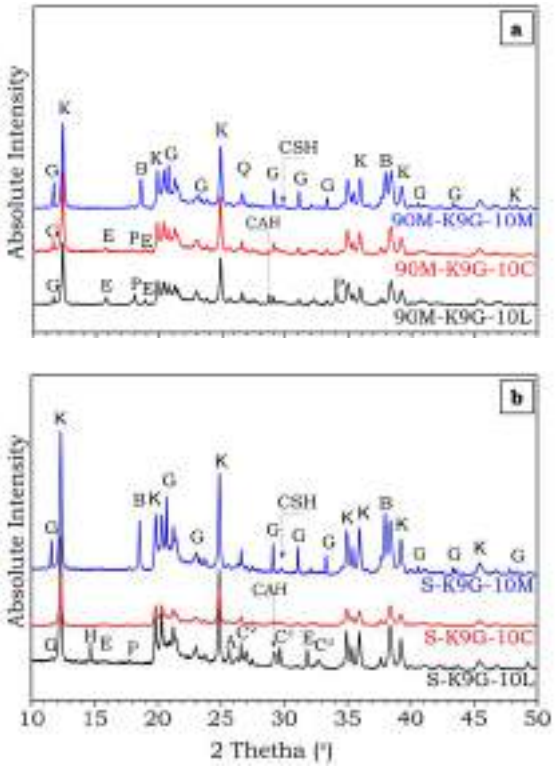

Fig.4: The XRD pattrens of gypseous kaolin treated with 10L, 10C, and 10M at **a)** 90 days of moist curing and **b)** 200-days of water soaking.

After 90-days of moist curing, the primary minerals identified in the XRD patterns were

ISBN 978-9959-9703-2-9

kaolinite-K, gypsum-G, quartz-Q, ettringite-E, portlandite-P, brucite-B, CSH, and CAH. The peak of quartz at 2θ = 26.6° appeared to be stable in all the XRD pattrens, whereas the portlandite at 2θ = 18.08° was appeared in the 10L-based and 10C-based specimens, with a sharper intensity in the case of the 10L-based specimen, the appreance of which indicates the surplus supply of lime and the incomplete consumption of lime. Similarly, the ettringite peaks at 2θ = 15.7° and 18.8° were only detected in 10L-based and 10C-based specimens with a sharper intensity in the case of 10L-based specimens. This was coupled with a reversal order for the gypsum peaks 2θ = 11.7°, 20.7°, 23.4°, 29.1°, 31.1° and 48.2°, where the gypsum peaks appeared sharper in the 10M-based system, relatively low in the 10L-based specimen, and almost disappeared in the 10L-based specimen, the appearance of which suggests the partial gypsum consumption through the formation and growth of ettringite in the case of 10L and 10C. In contrast, the brucite peak at 2θ = 26.6° was only detected in the 10M-based specimen, which also suggests the surplus supply of magnesium oxide within the system. As for the hydrated products, the CAH at 2θ = 28.6° was detected only in 10L-based specimen, whereas the CSH 2θ = 29.2° was detected with a hardly visible peak in all the x-ray diffractograms, the appearance of which is most likely because of the overlapping with other minerals. However, during the water soaking, the x-ray diffractograms of gypseous kaolin specimens exhibited considerable micro-structural changes. In this context, a hardly visible trace of portlandite in 10L-based specimens and no trace of portlandite in the 10C-based pattren were detected. This demonstrates the importance of both moisture content and the curing age in the complete consumption of lime. Traces of gypsum peaks in 10L-based and 10C-based diffractograms also disappeared. This disappearance is probably attributed to the presence of water molecules due to the change of curing from moist curing to soaking in water, which eases the solubilization of gypsum and become a source of ions source at the formation sites of the ettringite. As for the ettringite peaks, the x-ray diffractograms exhibited a reduction in the trace of ettringite peaks at 2θ = 15.7° and 18.8° to the background, although it appeared at 2θ =32°. The disappearance of ettringite is possibly due to the carbonation of ettringite under water soaking condition. This justification was also reinforced by the appearance of new minerals such as hemihydrate (bassanite)-H at 2θ =14.6° [29-30], in line with [31], and anhydrite-A at 2θ =25.6°, as well as some calcium carbonates

ISBN 978-9959-9703-2-9

in the form of calcite (C^1) at 2θ =29.2°, and aragonite (C^2) at 2θ =27 and 32.7°. This is also in support of why the ettringite peaks under the XRD were not detected by [21] and [23].

4- SEM analysis

Fig.5 shows the morphology of gypseous kaolin samples made with 10L, 10C, and 10M at 200 days of water soaking. Accordingly, the SEM images exhibited the presence of plate-like kaolinite minerals, needle-like structures, and some small globular-like particles. In the absence of EDS, the only change that can be visualized is the difference in terms of the morphology of hydrats and ettringite minerals. The globular-like particles of the hydrates in the 10L-based system possessed a clumped cluster form with no defined shapes, whereas such hydrates appeared in a well-distributed form in the case of the 10C-based and 10M-based systems. This difference can be assigned to the fineness of both cement and magnesium oxide and the richness of cement with the main oxides needed for the formation of hydrates, both of which promote the distribution of the binder within the system, and thus, facilitates the formation of less clumped hydrates on the edge of soil particles. As for the ettringite, the SEM images revealed the formation of massive ettringite in the case of the 10C-based system with a thicker diameter, relative to that of small and thinner morphology for needles-like prisms formed in the 10L-based system.

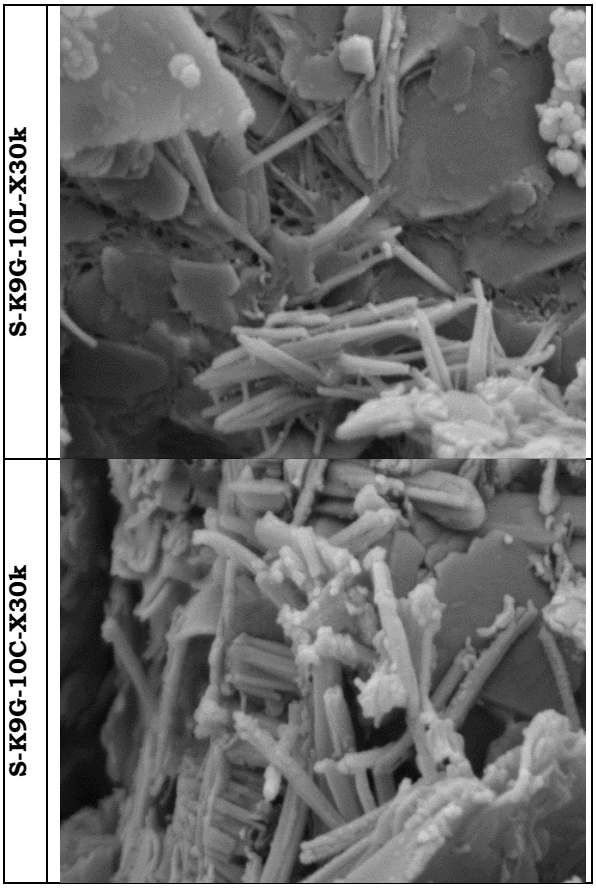

 ISBN 978-9959-9703-2-9

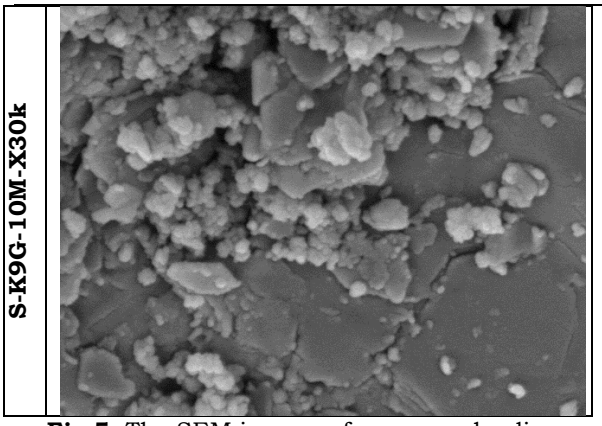

Fig.5: The SEM images of gypseous kaolin samples made with 10L, 10C, and 10M at 200 days of soaking in water.

In theory, the ettrgnite minerals should not be as massive as that of 10L-based cement since cement promotes less calcium hydroxide during hydration [28]. However, because of the faster cement hydration and hardening, and the subsequent restriction of cracks at early curing age, which all tighter inhibit the possibility of carbonation of ettringite within the system, the microstructure morphology obtained here in this study is logical. The thinner ettringite crystals in the 10L-based specimen are also in support of the ettringite carbonation detected in the XRD diffractogram of K9G-10L.

Conclusions

The main conclusions of the analytical and microstructure investigations of this research study are outlined as follows:

The DTG and XRD analysis revealed the existence of portlandite, CSH and CAH in pure kaolin specimen stabilised with 10L and 10C, whereas only brucite was detected in the DTG of pure kaolin specimen stabilised with 10M, the presence of which indicates the surplus supply of the binder.

In the presence of sulfate, all the analytical tests exhibited the nucleation of ettringite in samples treated with L and C, and such minerals seemed to be carbonated under water soaking, forming new minerals such as hemihydrate, anhydrite, calcite, and aragonite.

The main advantage of this research study is the conduction of comprehensive analytical and microstructure tests on sulfate soil stabilised with different binders, facilitating the exploration of a scientific rationale for the absance of ettringite traces in the XRD of gypseous soil treated with L and C, which in turn fills the knowledge gap.

The limitations of this research that could have an influence on the authenticity of the outcomes of the experimentations are the utilisation of an artificially gypseous soil, one source of sulfate (gypsum), and a fixed binder content of 10%. Hence, research studies simulating different sources of sulfate such as magnesium sulfate and sodium sulfate, as well as different binder contents, are recommended to overcome this deficiency.

 ISBN 978-9959-9703-2-9

Overall, it can be inferred that the utilization of Portland cement, lime, and magnesium oxide as a soil stabiliser in the absence of sulfate, is a promising technique. However, only magnesium oxide was effective in the presence of sulfate due to the restriction of ettringite.

Arabic section:

العنوان: دراسة تقارن البنية المجهرية طويلة المدى لتثبيت التربة بواسطة مواد رابطة قائمة على الكالسيوم والمغنيسيوم.

المؤلفون: منصور إبعيليلة، جون كينوتيا، جونتان اوتي، شيماء التليسي،

الكلمات المفتاحية: (إترينجيت، كبريتات، كربونات الإترينجيت، كبريتات الجير، الاسمنت البورتلاندي، أكسيد المغنيسيوم)

الملخص: عادةً ما يستخدم الباحثون التحقيقات المجهرية مثل حيود الأشعة السينية، ومشتقات قياس الوزن الحراري، والفحص المجهري الإلكتروني من بين اختبارات أخرى، لاكتشاف وقياس كمية المعادن المتكونة بما في ذلك الإترينجيت في تربة الكبريتات المثبتة باستخدام مثبت قائم على الكالسيوم. ومع ذلك، فإن اكتشاف بلورات الإترينجيت يكون صعبًا في بعض الأحيان، مما يشير إلى أن ظهور الإترينجيت تحت تحليل البنية المجهرية يعتمد أيضًا على طريقة المعالجة والتجربة. لذلك، تم فحص سلسلة من مخاليط التربة المصممة باستخدام مادتين من مواد التربة المستهدفة (الكيولين النقي والكيولين المصطنع بالجبس) والمثبتة بنسبة 10٪ من الوزن بالجير والأسمنت البورتلاندي وأكسيد المغنيسيوم، باستخدام تحقيقات متعددة المقاييس بما في ذلك حيود الأشعة السينية، قياس الوزن الحراري المشتق، والمجهر الإلكتروني الماسح. وفقًا لذلك، أظهرت النتائج أنه في ظل المعالجة الرطبة لمدة 90 يومًا، فإن المعادن الرئيسية المكتشفة في الكيولين الجبسي المتثبت باستخدام مثبت أساسه الكالسيوم هي الكيولين، هيدرات سيليكات الكالسيوم، البورتلانديت، والإترينجيت، في حين أن الكيولين فقط والجبس والبروسيت وسيليكات المغنيسيوم هيدرات تم الكشف عنها في الكيولين الجبسي المثبت بأكسيد المغنيسيوم. ومع ذلك، بعد 200 يوم من فترة النقع في الماء، لم يتم الكشف عن أي أثر للجبس، الإيترينجيت والبورتلانديت في حيود الأشعة السينية للعينات القائمة على الجير والأسمنت، مصحوبة بإشارة إلى معادن جديدة (نصفي، أنهيدريت، كالسيت، وأراجونيت)، مما يشير إلى كربنة الإيترينجيت أثناء النقع في الماء.

Abbreviations and Acronyms

XRD: x-ray diffraction, DTG: derivative thermogravimetric,
SEM: scanning electron microscopy,
K: kaolin,
G: gypsum,
L: lime,
C: Portland cment,
M: magnesium oxide,
C_3S: Tricacluim silicate,
C_3A: Tricacluim aluminate,
C_2S: Diacalcuim silicate,
C_4AF: Tetracacluim aluminoferrite,
90M: 90 days of moist curing,
S: Soakiing in water for 200 days,
CSH: calcium silicate hydrate,
MSH: magnesium silicate hydrate,
CAH: calcium aluminate hydrate
CH: calcium hydroxide,
Na^+: sodium
K^+: potassium
Mg^{++}: magnesium
Ca^{++}: clacuim
B: brucite,

 ISBN 978-9959-9703-2-9

P: portalandite,

E: ettrnigte,

C^1: calcite,

C^2: aragonite,

A: anhydrite,

H: hemihydrate,

Acknowledgement

The authors would like to acknowledge the Advanced Materials Testing Centre (AMTsC), within the School of Engineering at the University of South Wales, for the continuous support during the implementation of the laboratory experimentations.

References

[1] Al-Atroush, M.E., and Sebaey, T.A., (2021), Stabilization of expansive soil using hydrophobic polyurethane foam: A review., Transportation Geotechnics., **27**, 100494. DOI: 10.1016/j.trgeo.2020.100494.

[2] Millán-Corrales, G., González-López, J.R., Palomo, A., and Fernandez-Jiménez, A., (2020), Replacing fly ash with limestone dust in hybrid cements., Construction and Building Materials., **243**, 118169. DOI: 10.1016/j.conbuildmat.2020.118169.

[3] Nigam, S.K., Sinha, A.K., and Madan, S.K., (2023), Characterisation of stabilised red mud waste material for road infrastructure., Materials Today: Proceedings. DOI: 10.1016/j.matpr.2023.06.229.

[4] Salehi, M., Bayat, M., Saadat, M., and Nasri, M., (2023), Prediction of unconfined compressive strength and California bearing capacity of cement-or lime-pozzolan-stabilised soil admixed with crushed stone waste., Geomechanics and Geoengineering., **18**(4), 272-283. DOI: 10.1080/17486025.2022.2040606.

[5] Chenarboni, H.A., Lajevardi, S.H., MolaAbasi, H., and Zeighami, E., (2021), The effect of zeolite and cement stabilization on the mechanical behavior of expansive soils., Construction and Building Materials., **272**, p.121630. DOI: 10.1016/j.conbuildmat.2020.121630.

[6] Orazi, M., Orazi, U.S., Romeo, E., Van Rompaey, G., and Tebaldi, G., (2023), Mechanical recovery of lime-stabilised clays subjected to freeze–thaw damage., Road Materials and Pavement Design., 24(8), pp.2104-2112. DOI: 10.1080/14680629.2022.2117070.

[7] Saleem, A., ur Rehman, Z., Qamar, S., Katubi, K.M., Khan, A.H., Akhtar, M.N., Qamar, N., Alrowaili, Z.A., Saeed, U., Ullah, S., and Assiri, M.A., (2023), Investigations of graphene oxides and cement on strength performance of soil., Journal of Building Engineering., **73**, 106857. DOI: 10.1016/j.jobe.2023.106857.

[8] Jeremiah, J.J., Abbey, S.J., Booth, C.A., and Kashyap, A., (2023), Behaviour and Microstructural Characteristics of Lime-GGBS-Treated Kaolin Clay Contaminated with Gypsum., Materials, **16**(2), 874. DOI: 10.3390/ma16020874.

[9] Park, S., Ma, J., Yun, T.S., Jeon, S., Byeun, Y., Kang, D., and Jang, J., (2020), Pore-scale swelling mechanism of magnesium oxide granules during hydration., Construction and Building Materials., **251**, 119101. DOI: 10.1016/j.conbuildmat.2020.119101.

[10] Vitale, E., Deneele, D., Russo, G., and Ouvrard, G., (2016), Short-term effects on physical properties of lime treated kaolin., Applied Clay Science., **132**, 223-231. DOI: 10.1016/j.clay.2016.04.025.

[11] Pallanza, A., To, P., and Matheson, M., (2023), Lime stabilised road batters: A laboratory simulation of site flood conditions using a customised erosion apparatus and sample digitisation., Transportation Geotechnics., **40**, 100975. DOI: 10.1016/j.trgeo.2023.100975.

[12] Kinuthia, J.M., and Nidzam, R.M., (2011), Towards zero industrial waste: Utilisation of brick dust waste in sustainable construction., Waste Management., **31**(8), 1867-1878. DOI: 10.1016/j.wasman.2011.03.020.

[13] Seco, A., Del Castillo, J.M., Espuelas, S., Marcelino, S., and García, B., (2022), Sulphate soil stabilisation with magnesium

 ISBN 978-9959-9703-2-9

binders for road subgrade construction., International Journal of Pavement Engineering., **23**(6), 1840-1850. DOI: 10.1080/10298436.2020.1825711.

[14] Xu, B., and Yi, Y., (2022), Stabilisation/solidification of lead-contaminated soil by using ladle furnace slag and carbon dioxide., Soils and Foundations, 62(5), 101205. DOI: 10.1016/j.sandf.2022.101205.

[15] Seco, A., Miqueleiz, L., Prieto, E., Marcelino, S., García, B., and Urmeneta, P., (2017), Sulfate soils stabilization with magnesium-based binders., Applied Clay Science., **135**, 457-464. DOI: 10.1016/j.clay.2016.10.033.

[16] Li, W., Yi, Y., and Puppala, A.J., (2020), Suppressing ettringite-induced swelling of gypseous soil by using magnesia-activated ground granulated blast-furnace slag., Journal of Geotechnical and Geoenvironmental Engineering., **146**(7), 06020008. DOI: 10.1061/(asce)gt.1943-5606.0002292.

[17] Chemeda, Y.C., Deneele, D. and Ouvrard, G., (2018), Short-term lime solution-kaolinite interfacial chemistry and its effect on long-term pozzolanic activity., Applied Clay Science., **161**, 419-426. DOI: 10.1016/j.clay.2018.05.005.

[18] Choobbasti, A.J., and Kutanaei, S.S., (2017), Microstructure characteristics of cement-stabilized sandy soil using nanosilica., Journal of Rock Mechanics and Geotechnical Engineering., **9**(5), 981-988. DOI: 10.1016/j.jrmge.2017.03.015.

[19] Kinuthia, J.M. and Wild, S., (2001), Effects of some metal sulfates on the strength and swelling properties of lime-stabilised kaolinite., International Journal of Pavement Engineering., **2**(2), 103-120. DOI: 10.1080/10298430108901720.

[20] Ebailila, M., Kinuthia, J., and Oti, J., (2022), Suppression of Sulfate-Induced Expansion with Lime–Silica Fume Blends., Materials., **15**(8), 2821. DOI: 10.3390/ma15082821.

[21] Puppala, A.J., Intharasombat, N., and Vempati, R.K., (2005), Experimental studies on ettringite-induced heaving in soils., Journal of Geotechnical and Geoenvironmental Engineering., **131**(3), 325-337. DOI: 10.1061/ASCE1090-02412005131:3325.

[22] Aldaood, A., Bouasker, M., and Al-Mukhtar, M., (2014), Free swell potential of lime-treated gypseous soil., Applied Clay Science., **102**, 93-103. DOI: 10.1016/j.clay.2014.10.015.

[23] Jha, A.K., and Sivapullaiah, P.V., (2016), Volume change behavior of lime treated gypseous soil—influence of mineralogy and microstructure., Applied Clay Science., **119**, pp.202-212. DOI: 10.1016/j.clay.2015.09.017.

[24] Al-Mukhtar, M., Lasledj, A., and Alcover, J.F., (2014), Lime consumption of different clayey soils., Applied Clay Science., **95**, 133-145. DOI: 10.1016/j.clay.2014.03.024.

[25] Ebailila, M., Kinuthia, J., and Oti, J., (2022), Role of Gypsum Content on the Long-Term Performance of Lime-Stabilised Soil., Materials., **15**(15), 5099. DOI: 10.3390/ma15155099.

[26] BS EN 197-1:2011, Cement — Part 1: Composition, specifications and conformity criteria for common cements, BSI Standards Limited, London, UK, 2011. https://doi.org/10.3403/30205527.

[27] Adeleke, B.O., Kinuthia, J.M., Oti, J., and Ebailila, M., (2023), Physico-mechanical evaluation of geopolymer concrete activated by sodium hydroxide and silica fume-synthesised sodium silicate solution., Materials., **16**(6), 2400. DOI: 10.3390/ma16062400.

[28] M. Ebailila, Sulfate soil stabilisation with silica fume-based binders, Doctoral Thesis, University of South Wales, England, UK, 2022.

[29] Vakili, M.V., Chegenizadeh, A., Nikraz, H., and Keramatikerman, M., (2016), Investigation on shear strength of stabilised clay using cement, sodium silicate and slag., Applied Clay Science., **124**, 243-251. DOI: 10.1016/j.clay.2016.02.019.

[30] Ahmed, A., (2015), Compressive strength and microstructure of soft clay soil stabilized with recycled bassanite., Applied clay science., **104**, 27-35. DOI: 10.1016/j.clay.2014.11.031.

[31] Aldaood, A., Bouasker, M. and Al-Mukhtar, M., (2014), Impact of wetting–drying cycles on the microstructure and mechanical properties of lime-stabilized gypseous soils., Engineering Geology., **174**, 11-21. DOI: 10.1016/j.enggeo.2014.03.002.

 ISBN 978-9959-9703-2-9

 ISBN 978-9959-9703-2-9

المؤتمر الدولي الثاني للعلوم والهندسة
2nd International Conference on Science and Engineering
ICSE 2023
Faculty of Engineering - University of Bani Waleed
Bani Waleed, Libya

Paper Code: ICSE-045

REVIEW THE DEVELOPMENT OF GEOPOLYMER TECHNOLOGY TO ENHANCE THE PERFORMANCE OF RIGID PAVEMENT

Foad Mohamed Elkut[a],
[a]Department of Civil Engineering, Faculty of Engineering, Elmergib University, Al-komes, Libya,
*Corresponding author: foad.elkut@yahoo.com

Abstract: Geopolymer cement is a sustainable material that serves as a viable alternative to ordinary Portland cement (OPC) in the construction of transportation infrastructure and buildings. The chemical activator, curing process, and sources of geopolymer materials are essential factors that significantly impact the strength, durability properties, and microstructure of the resulting geopolymer matrices. In contemporary construction practices, concrete is a widely used material that can be expensive to produce with adverse effects on the environment. In order to decrease the reliance on OPC, a novel form of concrete known as geopolymer concrete (GPC) has been developed. This review aims to present the development of geopolymer technology to enhance the strength and durability of rigid pavement. It is imperative for pavement engineers to comprehend and tackle the challenges associated with geopolymer construction methodologies, encompassing placement, curing, and pavement efficacy. Based on the literature survey, it can be concluded that geopolymer concrete is a viable substitute for OPC concrete (PCC) due to its superior physical, mechanical, and durability characteristics. Various types of GPC demonstrated satisfactory performance in terms of drying shrinkage and thermal expansion compared to PCC. Geopolymer concrete exhibits high resistance against acid, sulfate, and salt attacks. The utilization of geopolymer cement in the construction of rigid pavement has been identified as a potential solution to address concerns related to global warming and enhance the durability of such infrastructure.

Keywords: Rigid pavement, Geopolymer concrete, Performance, Global warming, Durability

Introduction

Geopolymer is a novel construction material which can be an alternative binder to Portland cement. Geopolymer materials represent an innovative technology that is generating considerable interest in the construction industry, particularly in light of the ongoing emphasis on sustainability. It relies on minimally processed natural materials or industrial byproducts to significantly reduce its carbon footprint, while also being very resistant to the durability issues that can plague conventional concrete [1]. A source material that is high in silica and alumina reacts with alkaline liquids to produce geopolymer concrete. The soluble alkali metals that are used to make the alkaline liquids are

 ISBN 978-9959-9703-2-9

typically sodium- or potassium-based. As shown in the figure 1, all alkali-activated materials are created by reacting an aluminosilicate material, which is typically provided in powder form as an industrial byproduct, with an alkaline activator, which is typically in the form of a concentrated aqueous solution of alkali hydroxide, silicate, carbonate, or sulfate [2]. Natural minerals such as kaolinite, clays, alternatively, by-product materials such as fly ash, silica fume, slag and red mud could be used as source materials [3].

Fig. 1: The Process of Geopolymer Cement

Geopolymer-based concrete using fly ash has a high potential for the construction industry to replace OPC based concrete with comparable structural properties as shown in Figure 2 [4].

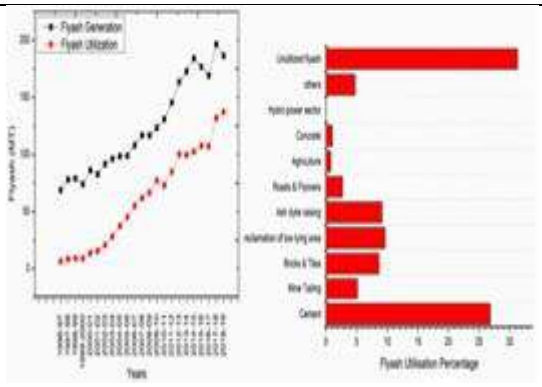

Fig. 2: Fly Ash Generation and Utilisation, as reported in reference [4]

Nowadays, the application of nano materials has received numerous attentions to enhance the Geopolymer concrete properties [5]. The choice of the source materials for making geopolymers depends on factors such as availability, cost, and type of application [6]. The construction of concrete pavements must be improved to ensure effective transportation, reduce cost, and promote environmental sustainability, considering the effects of weather, fuel use, cost of repairs and paving lifetime. Because the initial cost of rigid pavement is higher than that of flexible pavement; the latter has been preferred to date, even though the maintenance cost of rigid pavement is lower [7]. This paper aims to review individual studies conducted by researchers that have put their efforts into showing the properties of Geopolymer concrete materials, which will help us understand their

 ISBN 978-9959-9703-2-9

behaviour as high-quality rigid pavement concrete and promote environmental sustainability.

Geopolymer Concrete

Geopolymer concrete is a type of concrete that is formed by using inorganic aluminosilicate materials. The use of cement has been found to have a negative impact on the environment and deplete natural resources. The production process of Ordinary Portland Cement (OPC) necessitates substantial fuel consumption for combustion and the breakdown of limestone, leading to notable CO_2 emissions. Cement manufacturing facilities emit approximately 1.5 billion tons of carbon dioxide into the atmosphere on an annual basis. Geopolymer concrete has been introduced to reduce this problem. Geopolymer concrete is an inorganic polymer concrete that can be produced at ambient temperature by utilizing industrial waste or by-products as source materials to create a solid binder. It serves a comparable purpose to OPC.

As illustrated in Figure 3, binders such as fly-ash and ground granulated blast furnace slag (GGBS) are utilized, along with alkali activators such as sodium hydroxide and sodium silicate, to enhance the binding characteristics of the concrete [8-9]. Geopolymer binder may be used in applications to totally or partially replace OPC for environmental and technological reasons. A previous study found that geopolymers had no adverse alkali-aggregate interaction, high early strength, low shrinkage, sulphate, corrosion, acid, and fire, and resistance to freeze-thaw and corrosion [10].

Fig. 3: The Manufacturing Geopolymer Concrete [9].

Properties of Geopolymer Concrete

– Non-toxic and bleed free.

– Sets at room temperature.

– Light in weight.

– Higher compressive strength

– Higher resistance to heat and all inorganic solvents. Moreover, GPC source materials provide promising ways to convert waste into resources, thereby contributing to and producing low carbon footprint concrete. The obstinate characteristics of GPC are mentioned in Figure 4 [11].

 ISBN 978-9959-9703-2-9

Fig. 4. Desirable Properties of Geopolymer Matrix [11]

In comparison to regular Portland cement concrete, geopolymer concrete has a very high compressive strength. The early strength of geopolymer concrete was quite high [12].

Under ideal mix design conditions, geopolymer concrete's compressive strength and mechanical characteristics outperform OPC concrete's [13]. The geopolymer is an environmentally benign and sustainable alternative to conventional Portland Cement (OPC)-based concrete because it has the advantages of rapid strength growth, elimination of water curing, good mechanical and durability properties. Portland cement manufacture results in the emission of air pollutants, which causes environmental pollution in the construction sector. It lowers CO2 emissions by 80–90% [14]. Water is a crucial component throughout the geopolymerization process since it helps the initial paste work better but is excluded from the final geopolymer structure. Water does not significantly influence the primary chemical processes of polymerization, in contrast to hydration reactions in ordinary concrete. The mechanical and chemical characteristics of geopolymer concrete are significantly impacted by its excretion during heat treatment and subsequent drying. According to M. S. Eisa (2021), employing geopolymer concrete (GPC) based on metakaolin is more efficient at implementing stiff pavement slabs than Portland cement concrete (PCC) and performs better in terms of drying shrinkage than geopolymer concrete based on slag or fly ash [15]. Several geopolymer pastes (GPPs) compressive strength is mostly influenced by the type of binder, as depicted in Figure. 5 [11]. According to Farooq, F. (2021), as the concentration of GGBFS rises, so will the compressive strength of the sodium silicate (NS), sodium hydroxide (NH), and sodium hydroxide plus sodium silicate solution (NHNS) series [16]. According to researchers who studied the mechanical properties of GPC based on recycled concrete aggregate (RCA) with 50% and 100% RCA content, the compressive strength of GPC increases by more than 10% from 7 to 28 days [17]. According to Palomo et al.'s findings, different FA samples that have been cured at 85 °C for 1 day create materials with compressive strengths ranging from 35 to 40 MPa [18].

 ISBN 978-9959-9703-2-9

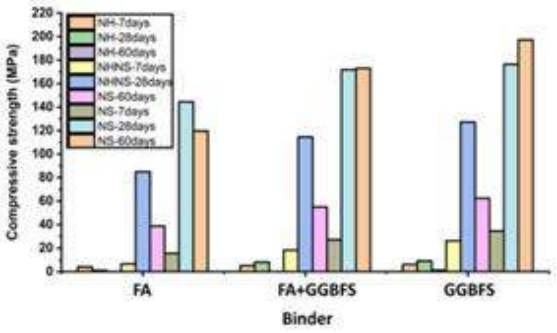

Fig. 5. Effect of Waste Material with Activator on Compressive Strength [11]**.**

Rigid pavements

As a crucial component of the transportation infrastructure, pavement is crucial to contemporary society. Concrete constructed of Portland cement, either plain, reinforced, or prestressed, is used to create rigid pavements. According to Figure 6 [19], the rigid pavement is made up of three layers: the base course, the subgrade, and the cement concrete slab. A solid base or subbase course layer placed beneath the cement concrete slab greatly extends the pavement's life and, as a result, is ultimately more cost-effective. The elastic theory is used to construct rigid pavements and analyze stresses [20]. A rigid pavement tends to spread the load across a somewhat broader area of soil due to its rigidity and high tensile strength, and the majority of the structural capacity is provided by the slab itself. The rigid pavements are used for heavier loads and can be constructed over relatively poor subgrade [21].

Fig. 6: Geopolymer Concrete [19].

Advantage of Rigid Pavements: [22,23]

- Because rigid pavements have a service life of up to 30 years and do not get deteriorated in wet weather, routine and periodic maintenance expenses are very cheap because only joint repair is needed.
- Rigid pavements have a lower life cycle cost than flexible pavements.
- In especially for the construction of highways passing through weak soils and carrying strong traffic loads, rigid pavements require less total thickness less than flexible pavements.
- Good night visibility even under wet weather conditions.

Rigid Pavement Types

To control the forces acting on concrete pavement, various pavement types require a variety of joints and reinforcement. Four types of rigid pavements can be distinguished:

•Jointed plain concrete pavement (JPCP),

•Jointed reinforced concrete pavement (JRCP),

 ISBN 978-9959-9703-2-9

•Continuous reinforced concrete pavement (CRCP), and
•Pre-stressed concrete pavement (PCP).

Continuously Reinforced Concrete Pavement (CRCP)

Both longitudinal and transverse steel is included in CRCP. Except at construction joints, the CRCP lacks transverse joints. The standard reinforcing steel configuration for CRCP is shown in Figure 7 [24]. The longitudinal steel's purpose is to control temperature and moisture-related changes in concrete volume as well as to maintain transverse fissures well sealed, not to reinforce the concrete slab. The transverse steel's purpose is to maintain the integrity of longitudinal joints and cracks. Concrete stresses in the concrete slab due to traffic loading are decreased if the steel performs its intended purpose and prevents fractures from enlarging [25].

Fig. 7: Continuously Reinforced Concrete Pavement [21]

Concrete Pavement Contraction Design (CPCD)

Transverse joints on CPCD are spaced regularly. The concrete's temperature-related contraction and expansion are managed by the transverse joints. To transfer load, smooth dowel bars are employed at the transverse joints. The transverse joints are separated by 15 feet. Random longitudinal cracking is managed using longitudinal joints. Tie bars are used to secure longitudinal joints. Figure 8 depicts the usual CPCD arrangement [26].

Fig. 8: Concrete Pavement Contraction [26]

The majority of joint failures in concrete pavement are brought on by joint failures rather than slab breakdowns. Cohesive and adhesive failures, in general, and faulting, pumping, blowups, spalling, corner breaks, and mid-panel cracking, in particular, are among the failures. A suitable frequency for maintenance, or joint resealing, can be established since finite element analysis has been used to study the mechanisms of sealant damage [27].

Rigid Pavement Failures

 ISBN 978-9959-9703-2-9

Fatigue cracking has been regarded as the primary requirement for rigid pavement design. The ratio of flexural tensile stress to the concrete modulus of rupture determines the maximum number of load repetitions that can occur before fatigue cracking starts. Pumping has recently been recognized as a crucial failure criterion. Pumping is the downward movement of the slab under heavy wheel loads that results in the ejection of soil slurry through the joints and fractures of cement concrete pavement. Faulting, spalling, and degradation are additional forms of discomfort on rigid pavements [28].

Conclusion

The studies undertaken in the area of applying geopolymer technology to transform raw materials or different wastes into green and sustainable materials, as well as in the direction of sustainable urban development, are briefly discussed in this review article using the life cycle assessment technique. Research shows that the geopolymer production method combines processed natural minerals, wastes, and industrial by-products to manufacture bonding agents, unlike Portland cement. Contrarily, Geopolymer Concrete is extensively used in the building sector due to its superior performance and environmental benefits. Due to their application in bridge construction, high-rise structures, and rigid-paved highways, geopolymer materials can be utilised as eco-friendly and sustainable building materials in future cities.

Acknowledgment

I would like to express my gratitude to Elmergib University's Department of Civil Engineering, Faculty of Engineering, and all of its staff for their kind welcome, assistance in achieving my goals, and role as my home.

References

[1] Almutairi, A. L., Tayeh, B. A., Adesina, A., and Zeyad, A. M. (2021). Potential applications of geopolymer concrete in construction: A review. Case Studies in Construction Materials, 15, e00733.

[2] Provis, J. L. (2014). Geopolymers and other alkali activated materials: why, how, and what? Materials and structures, 47, 11-25.

[3] Muthuramalingam, P., and Dharmar, B. (2022). Synthesis of Slag-Ash-Phosphate Based Geopolymer Concrete in the Production of Sustainable Concrete Under Ambient Curing Conditions. Iranian Journal of Science and Technology, Transactions of Civil Engineering, 46(6), 4243-4254.

[4] Verma, M., Dev, N., Rahman, I., Nigam, M., and Mallick, J. (2022). Geopolymer concrete: a material for sustainable development in Indian construction industries. Crystals, 12(4), 514.

[5] Shamsaei, E., de Souza, F. B., Yao, X., Benhelal, E., and Duan, W. (2018). Graphene-based nanosheets for stronger and more durable concrete: A review. Construction and Building Materials, 183, 642-660.

[6] Lahoti, M., Tan, K. H., and Yang, E. H. (2019). A critical review of geopolymer

 ISBN 978-9959-9703-2-9

properties for structural fire-resistance applications. Construction and Building Materials, 221, 514-526.

[7] Shakor, P., Hasan, S., Awuzie, B. O., Singh, A. K., Rauniyar, A., and Karakouzian, M. (2023). Evaluating the potential of geopolymer concrete as a sustainable alternative for thin white-topping pavement. Frontiers in Materials, 10, 1181474.

[8] Rao, A. K., and Kumar, D. R. (2020). Comparative study on the behaviour of GPC using silica fume and fly ash with GGBS exposed to elevated temperature and ambient curing conditions. Materials Today: Proceedings, 27, 1833-1837.

[9] Zhuang, X. Y., Chen, L., Komarneni, S., Yang, H. M., and Wang, H. (2016). Fly ash-based geopolymer: clean production, properties and applications. Journal of cleaner production, 125, 253-267.

[10] Schutte, C. (2018). Value added utilisation possibilities of coal combustion products in South Africa (Doctoral dissertation, North-West University).

[11] Farooq, F., Jin, X., Javed, M. F., Aslam, F., and Alyousef, R. (2021). Geopolymer concrete as sustainable material: A state of the art review. Construction and Building Materials, 306, 124762.

[12] Al Bakri, A. M., Kamarudin, H., Binhussain, , and Zarina, Y. (2015). Comparison of Geopolymer Fly Ash and OPC to the Strength of Concrete. All content following this paper was uploaded by Mohd Mustafa Al Bakri Abdullah on, 8.

[13] Hadi, M. N., Zhang, H., and Parkinson, S. (2019). Optimum mix design of geopolymer pastes and concretes cured in ambient condition based on compressive strength, setting time and workability. Journal of Building engineering, 23, 301-313.

[14] Gargav, A., and Chauhan, J. S. (2016). Role of geopolymer concrete for the construction of rigid pavement. IJEDR, 4(3), 473-476.

[15] Eisa, M. S., Basiouny, M. E., and Fahmy, E. A. (2021). Effect of metakaolin-based geopolymer concrete on the length of rigid pavement slabs. Innovative Infrastructure Solutions, 6, 1-9.

[16] Talakokula, V., and Bhalla, S. (2016). Non-destructive strength evaluation of fly ash based geopolymer concrete using piezo sensors. Procedia Engineering, 145, 1029-1035.

[17] Shi, X. S., Wang, Q. Y., Zhao, X. L., and Collins, F. (2012). Discussion on properties and microstructure of geopolymer concrete containing fly ash and recycled aggregate. In Advanced Materials Research (Vol. 450, pp. 1577-1583). Trans Tech Publications Ltd.

[18] Palomo, A., Grutzeck, M. W., & Blanco, M. T. (1999). Alkali-activated fly ashes: A cement for the future. Cement and concrete research, 29(8), 1323-1329.

[19] Delatte, N. J. (2014). Concrete pavement design, construction, and performance. Crc Press.

[20] Rambabu, D., Sharma, S. K., and Abdul Akbar, M. (2022). A review on suitability of using geopolymer concrete for rigid pavement. Innovative Infrastructure Solutions, 7(5), 286.

[21] Dewangan, Arvind and Gupta, D.P. (2012). The study of rigid and flexible pavement in transportation engineering with special reference to N.H.-1. Engg. and Tech. in India, 3(1,2): 55-58.

[22] Mohod, M. V., and Kadam, K. N. (2016). A comparative study on rigid and flexible pavement: A review. IOSR Journal of Mechanical and Civil Engineering (IOSR-JMCE), 13(3), 84-88.

[23] Patil, R. R.,and Katare, V. D. (2023). Application of fiber reinforced cement composites in rigid pavements: A review. Materials Today: Proceedings.

[24] Aryan, K., Gupta, A. K., and Tiwari, M. (2018). Analysis and Design of Rigid Pavement on Collapsible and Expansive Soils.

 ISBN 978-9959-9703-2-9

IJRAR- International Journal of Research and Analytical Reviews, Volume 5 I Issue 2.

[25] Katre, L., and Harinkhede, B. (2021). Continuously Reinforced Concrete Pavement: A Review. Int. J. Eng. Res. Technol, 10, 300-304.

[26] Roesler, J. R., Hiller, J. E., and Brand, A. S. (2016). Continuously Reinforced Concrete Pavement Manual, Guidelines for Design, Construction, Maintenance,and rehabilitation, USA.Federal Highway. (FHWA-HIF-16-026).

[27] Kim, J., and Zollinger, D. G. (2021). Portland cement concrete pavement joint sealant practices and performance (No. NCHRP Project 20-05, Topic 51-09).

[28] Pandey, V. K., and Srivastava, S. (2022). Failure of rigid pavement at different locations of Hussain Ganj–Hathgaon–Alipur section of MDR no. 81-C (Vol. 2413, No. 1, p. 030020). AIP Publishing LLC.

 ISBN 978-9959-9703-2-9

المؤتمر الدولي الثاني للعلوم والهندسة
2nd International Conference on Science and Engineering
ICSE 2023
Faculty of Engineering - University of Bani Waleed
Bani Waleed, Libya

Paper Code: ICSE-049

EFFECT OF REDUCING THE AMOUNT OF COARSE AGGREGATE ON SOME PROPERTIES OF SELF-COMPACTING CONCRETE

A . Emhemmed
Department of Civil Engineering/Faculty of Engineering/University of Bani Waleed, Libya
Crosspnding author: alborhanbani@gmail.com

Abstract: In recent years, self compacting concrete (SCC) has become widely used especially in crowded reinforced concrete structures with difficult casting conditions. For such applications, fresh concrete must possess high fluidity and good cohesion. One of the most important projects in which this type of concrete was used is the foundation system for Khalifa tower in Dubai, which is the most important high-rise building in the world. The content of coarse aggregate has a significant impact on the properties of the required concrete. Some studies have suggested that the total volume of coarse aggregate be within 50% of the solid concrete volume.
In this research, six mixtures were studied with different combinations of water-cement ratio and coarse aggregate quantity. Slump test (flow test), (J-RING test) and concrete strength determination test were performed to determine the effect of reducing the amount of coarse aggregate in the mixture on some fresh and hardened properties of self compacting concrete (SCC).
The results showed that reducing the amount of coarse aggregate used in concrete requires increasing the amount of water required for mixing to achieve the required flow of self-tamping concrete, which leads to a decrease in the strength of concrete, and that the best ratio of coarse aggregate to the total aggregate is 65%, as it provides the highest resistance to concrete and achieves flow required, and using a percentage higher than that leads to not achieving the required flow and crossing completely.

Keywords: (SCC , flow test , J-RING test, ratio of coarse aggregate)

Introduction

High Performance Concrete (HPC) is concrete that is characterized by containing the best quality of materials with distinct proportions and properties to produce high performance concrete, which has become important in engineering and architectural applications, and the components of this type of concrete are chosen carefully according to standard specifications, What is known as chemical additives (superplasticizers) are added to the main components of concrete.
Self-compacting concrete is one of the types of high-performance concrete, and it is the product of technological progress in the field of concrete additives, where both the addition of viscosity improvement and the additives to reduce mixing water (superplasticizer) are the two basic elements required for its production, and Self-compacting concrete is used as the primary building material for all applications in many global markets, It is the concrete that has a high degree of fluidity and flow and has a high resistance to granular separation and can be cast successfully in narrow and crowded sectors with reinforcing steel without the use of any external compaction method.

 ISBN 978-9959-9703-2-9

Okamura [6] indicated that SCC can flow at any angle and pass through the spaces between the reinforcing steel without vibration. The most important characteristic of SCC over conventional concrete is : fast flow, high resistance to separation and does not require vibration. Okamura and Ozawa [7] also indicated in SCC that the total coarse content is not limited but pozzolans and superplasticizers can also be used to prevent segregation and increase flow. Yurugi et al. [9] reported that the aggregate coarse content has a significant effect on the packing capacity of concrete and Okamura [6] suggested that the total volume of coarse aggregate be within 50% of the solid volume of concrete.

Materials used and experimental mixtures :

The purpose of the experimental mixtures is to determine the appropriate quantities of materials included in the mixtures so that the required results are given, which is obtaining self-compacting concrete in which the technical conditions are met, the most important of which is that the slump diameter (flow) is not less than 650 mm and not more than 800 mm without the occurrence of granular separation. These mixtures were according to the following principles:

The total content of cement binders = 450 kg / m3, which is made up of ordinary Portland cement (Zliten Factory).

1. The amount of coarse aggregate is variable, starting with a large amount and then gradually being reduced.
2. The largest nominal size of coarse aggregate is 14 mm.
3. The dosage of the super-plasticizer is 0.8 liters per 100 kg of cement.
4. The ratio of water to cement is variable according to the needs of each mixture.
5. The superplasticizer is injected into the concrete during mixing after adding 70% of the water.

Our aim is to test the mixtures and whether they meet the technical conditions and properties of the self-compacting concrete or not. Fast and sequential to avoid possible errors and obtain the most accurate possible results of this study.

The first experimental mixture was carried out using superplasticizer RHEOBUILD 561E and its quantity, where 0.8 liters / 100 kg of cement was used, and the ratio of coarse aggregate to total aggregate was 45%, and the ratio of water to cement was 48%. One that is similar to normal concrete, but without the occurrence of granular separation or exudation, and through this result it became clear to us that the reason for this could be one of the following possibilities:

1. The ratio of water to cement is low and must be increased to obtain the required flowability of concrete, especially since there is no granular separation or exudation.
2. The amount of super-plasticizer used is high and should be reduced.

Accordingly, we first reduced the amount of superplasticizer used in several attempts, but the result did not change much, so we had the only option is to increase the ratio of water to cement, although it will affect the resistance of concrete. The flow of self-compacting concrete is as shown in Figure (1). In the same way, the ratio of water to cement was determined for other mixtures, with an increase in the ratio of coarse aggregate to total aggregate.

 ISBN 978-9959-9703-2-9

Figure (1) shape of the flow of concrete with a coarse aggregate percentage of 55%.

Thus, the final mixtures which will be used in this study, have been determined. The following table No. (1) shows the ratios of water to cement required for all mixtures that will be used in this study.

Table 1: Water cement ratio and ratio of coarse aggregate required for all mixtures

Mix. No.	1	2	3
Ratio Of Coarse Aggregate	70%	65%	60%
w/cm	50.17%	50.47%	50.67%
Mix. No.	4	5	6
Ratio Of Coarse Aggregate	55%	50%	45%
w/cm	50.84%	53.03%	54.88%

After the experimental mixtures program was completed, through which the necessary quantity of all materials included in the mixtures was determined, the final laboratory mixtures program was started, which will be the focus of research in this study.

1. Mixture No. (1), in which the ratio of coarse aggregate to total aggregate is 70%, and the ratio of water to cement is (50.17). Simple granular separation due to the accumulation of coarse aggregate and its complete immersion in the cement mortar.
2. Mixture No. (2), in which the ratio of coarse aggregate to total aggregate is 65%, and the percentage of water to cement is (50.47). It is a medium operational mixture compared to the rest of the mixtures, and it is better than the first mixture. Coarse aggregate and its complete immersion in the cement mortar.
3. Mixture No. (3), in which the ratio of coarse aggregate to total aggregate is 60%, and the ratio of water to cement is (50.67).
4. Mixture No. (4), in which the ratio of coarse aggregate to total aggregate is 55%, and the ratio of water to cement is (50.84), and it is a mixture of good to very good performance compared to the rest of the mixtures, and the flow diameter condition is met without the occurrence of clear granular separation
5. Mixture No. (5), in which the ratio of coarse aggregate to total aggregate is 50%, and the ratio of water to cement is (53.03), and it is a very good operational mixture compared to the rest of the mixtures.
6. Mixture No. (6), in which the ratio of coarse aggregate to total aggregate is 45%, and the ratio of water to cement is (54.88).

Table 2: Mix proportions of concrete

Mix. No.	Ratio OF Coarse Aggregate %	w/cm %	Water)Kg/m3(	Cement)Kg/m3(	Aggregate)Kg/m3(		superplasticizer Litter/ 100 Kg Cement
					Fine	Coarse	
1	70	50.17	225.8	450	509.76	1190.24	0.8
2	65	50.47	227.1	450	593.22	1101.47	0.8

ISBN 978-9959-9703-2-9

3	60	50.67	228	450	676.19	1014.28	0.8
4	55	50.84	228.8	450	758.92	927.75	0.8
5	50	53.03	238.6	450	829.05	829.05	0.8
6	45	54.88	246.9	450	897.82	734.72	0.8

Tests of concrete mixtures in their solid state:
The compressive strength test was carried out according to the specifications [4] for different concrete mixtures.

Results :
Several tests were carried out for the final mixtures in the plastic state (fresh) immediately after the mixing process was completed, which is the slump test to measure the flow diameter (Ds) and the (J-RING) test to measure the ability of concrete crossing through narrow spaces by the flow diameter (Dj). In both tests, the rates of granular separation and exudation of concrete were observed and evaluated.

The following table No. (3) shows the results of the tests in the soft case as follows:

Table 3: Test results of fresh concrete

Test results	Mix. No. and Ratio Of Coarse Aggregate)					
	1 70 %	2 %65	3 %60	4 %55	55 %50	6 %45
Diameter of flow (Ds) mm	660	695	690	690	700	700
Diameter of flow (Dj) mm	630	685	680	680	690	690
(Dj-Ds) mm	30	10	10	10	10	10

Limits	10 mm					
1-(Dj/Ds) %	4.55	1.44	1.45	1.45	1.43	1.43

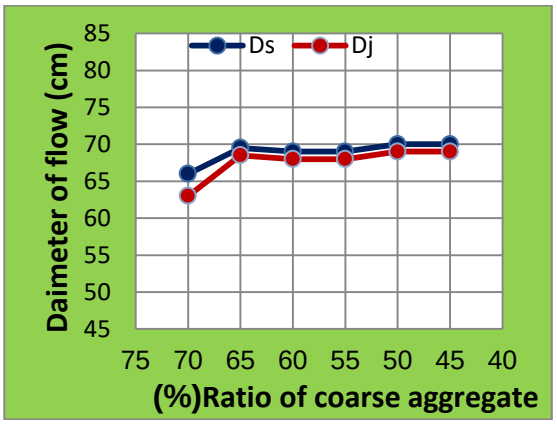

Fig 2 : The Relation between Ratio Of Coarse Aggregate and Diameter of flow

Table 4: Test results of of concrete Compressive strength

Mix. No. and Ratio Of Coarse Aggregate	Compressive strength		
	3 days	7 days	28 days
(70%) 1	16	28.44	40.95
(65%) 2	15.56	29.33	41.84
(60%) 3	15.56	25.78	35.44
(55%) 4	13.78	25.78	33.47
(50%) 5	12.44	24.44	31.43
(45%) 6	11.56	20	29.21

ISBN 978-9959-9703-2-9

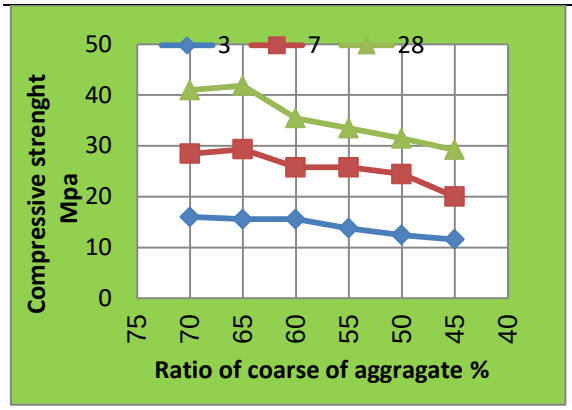

Fig 3 : The Relation between Ratio Of Coarse Aggregate and Compressive strength

The table No. (4) shows the results of the tests in the hard condition, which is the strength of concrete after 3 days, 7 days, and 28 days for each mixture.

For further clarification of these results, it was presented in a graph in Figure (2), which summarizes the relationship between the proportion of coarse aggregate in the concrete mixture and the diameter of its flow in the absence of obstacles and in the case of the presence of obstacles.

From figure (2), we notice the following:

1. The lower the percentage of coarse aggregate in the mixture, the greater the flow diameter Ds, and there is no noticeable change, and therefore the relationship is positive in all cases, and this also applies to the flow diameter Dj.
2. The flow diameter Ds in all cases is higher than 650 mm, and therefore all mixtures fulfill the condition of the flow diameter in the absence of obstacles.
3. The difference between the diameter of flow, Ds and Dj, decreases as the percentage of coarse aggregate decreases in all cases, and this expresses that the crossing property improves as the percentage of coarse aggregate decreases.
4. The difference between the diameter of flow, Ds and Dj, fulfills the condition stipulated in the specifications in all mixtures, except for the mixture that contains 70% coarse aggregate, as it is the only one in which the crossing property is not achieved, and therefore this mixture does not meet all the technical conditions of self-compacting concrete.

For further clarification of the results presented in Table (4), they are presented in a graph in Figure (3), which summarizes the relationship between the proportion of coarse aggregate in the concrete mix and the strength of the concrete.

Through Figure No. (3) we note that the lower the percentage of coarse aggregate in the mixture, the lower the concrete strength, due to the mixtures needing a larger amount of water to achieve the flow diameter condition, which in turn led to a significant decrease in its resistance.

Conclusion and recommendations

The aim of this research was to study the effect of reducing the amount of coarse aggregate used in concrete on the properties of self-compacting concrete.

Conclusion : After completing the implementation of the practical program in this study and discussing the obtained results, this can be summarized as follows:

1. The decrease in the amount of coarse aggregate used in concrete requires an increase in the amount of water required for mixing, that is, an increase in the proportion of water to the cement used to achieve the required flow of self-compacting concrete.
2. When using the super-plasticizer (R561) and using the ratio of coarse aggregate to total aggregate in concrete more than 65%, the extruded concrete did not fully fulfill the conditions of flow and passage, although it did not notice the presence of granular separation or exudation of the

 ISBN 978-9959-9703-2-9

concrete when testing the diameter of its flow without the presence of obstacles.

3. The strength of concrete is inversely proportional to the decrease in the proportion of coarse aggregate in concrete.

4. When using the super-plasticizer (R561), the best ratio of coarse aggregate to total aggregate is 65%, as it provides the highest resistance to concrete and has the properties of self-compacting concrete.

5. The use of superplasticizer (R561) provides high workability of concrete, but at the same time produces concrete with less strength compared to some other plasticizers.

Recommendations :

Based on the results obtained in this study, we recommend the following :

1. In the event that what is required is the production of self-compacting concrete with high performance and the sufficiency of concrete resistance is not high, the best is to use the plasticizer (R561).

2. It should be noted that decreasing the ratio of coarse aggregate to total aggregate in the mixture gives the concrete a better performance, but weakens its resistance.

3. When a coarse aggregate percentage greater than 65% is used, care must be taken because this may cause granular separation of the concrete in the event that there are obstacles such as reinforcing steel or narrow places through which the concrete passes.

4. Focusing on coarse aggregate ratios greater than 65% in other studies to try to improve their properties by replacing part of the used coarse aggregate with another material such as greenilia, for example, or improving the quality of the used sand by mixing it with another material that reduces or increases the coefficient of fineness of the sand, or by using other superplasticizer. It contributes to increasing the workability of concrete or replacing part of the cement with another soft material, and this is all in order to benefit from the high resistance feature that results from the use of these proportions of aggregate in concrete.

Arabic section:

العنوان: تأثير التخفيض في كمية الركام الخشن على بعض خواص الخرسانة ذاتية الدمك .

المؤلفون : عبدالرحمن امحمد

المفتاحية الكلمات: (SCC، اختبار J-RING، اختبار التدفق ، نسبة الركام الخشن الملدنات الفائقة ،)

الملخص: (SCC في السنوات الأخيرة ، اصبحت الخرسانة ذاتية الدمك ذات استخدامًا واسعًا خاصة في الهياكل الخرسانية المسلحة المزدحمة ذات ظروف الصب الصعبة. فلمثل هذه التطبيقات ، يجب أن تمتلك الخرسانة الطازجة سيولة عالية وتماسكًا جيدًا. ومن اهم المشاريع التي تم فيها استخدام هذا النوع من الخرسانة هو نظام الأساسات لبرج خليفة بدبي وهو اهم مبني شاهق في العالم ، محتوى الركام الخشن له تأثير كبير على خصائص الخرسانة المطلوبة وقد اقترحت بعض الدراسات ان يكون الحجم الإجمالي للركام الخشن ضمن 50٪ من الحجم الصلب للخرسانة. في هذا البحث تم دراسة ست خلطات مع توليفات مختلفة من نسبة الماء الى الأسمنت وكمية الركام الخشن . وتم إجراء اختبار الهبوط واختبار) واختبار تحديد مقاومة الخرسانة لتحديد تأثير التخفيض في J-RING (كمية الركام الخشن بالخلطة على بعض خواص للخرسانة ذاتية الدمك). أظهرت النتائج أن التخفيض في كمية الركام الخشن SCC(المستعمل في الخرسانة يستوجب زيادة كمية الماء اللازم للخلط لتحقيق التدفق المطلوب للخرسانة ذاتية الدمك مما يؤدي ذلك الى الانخفاض في مقاومة الخرسانة ، وأن أفضل نسبة للركام الخشن إلى الركام الكلى هي 65% حيث توفر أعلى مقاومة للخرسانة وتحقق التدفق المطلوب ، وان استعمال نسبة اعلى من ذلك يؤدي الى عدم تحقيق التدفق والعبور المطلوبين بشكل كامل.

Reference :

[1] American Concrete Institute , " ACI 237-07: Self-Consolidating Concrete", 2007.

[2] European Research Project "Guidelines for Testing Fresh Self-Compacting Concrete" , Sep.

 ISBN 978-9959-9703-2-9

2005 .
[3] EFNARC, "Specification and Guidelines for Self-Compacting Concrete" , February 2002 .
[4] British Standard Institution, "BS 1881: Testing Concrete, Part 116: Method for determination of compressive strength of concrete cubes", London, 1983.
[5] Japan Society of Civil Engineering, Recommendations for Construction of Self-Compacting Concrete, JSCE (1998).
[6] Okamura, H., "Self-Compacting High-PerformanceConcrete," Concrete International, Vol. 19, No. 7, pp.50-54 (1998).
[7] Okamura, H. and Ozawa, K., "Mix-design for Self-Compacting Concrete", Concrete library of JSCE, Vol.25, pp. 107-120 (1995).
[8] Yurugi, M., Sakata, N., Iwai, M. and Sakai, G., "Mix Proportion for Highly Workable Concrete," Proceedings, Concrete 2000, Dundee, pp. 579-589 (1989).

 ISBN 978-9959-9703-2-9

المؤتمر الدولي الثاني للعلوم والهندسة
2nd International Conference on Science and Engineering
ICSE 2023
Faculty of Engineering - University of Bani Waleed
Bani Waleed, Libya

Paper Code: ICSE-052

PERFORMANCE EVALUATION OF ECO-FRIENDLY MORTAR MADE WITH NATURAL AND ARTIFICIAL POZZOLANS; RED CLAY AND GLASS POWDER

S. Almakhzoum[a], R. Alwerfally[a], M. Alseed[a], A. Alfirjani[a], M. Ebailila[a],
[a] Department of Civil Engineering, Faculty of Engineering/Bani Waleed University, Libya
* aimanwerflla@gmail.com

Abstract: To reduce the environmental impact associated with Portland cement (PC) manufacturing, the use of supplementary cementitious (pozzolanic materials) materials in the development of cement-based materials such as concrete and mortar, has gained great attention in recent years. For this reason, this research study investigates the effect of using two types of pozzolanic material (natural and industrial pozzolan), represented by red clay (RC) and glass powder (GP), as a partial substitution for Portland cement in the preparation of cement-based mortar. The methodology of this study involved the design of seven mortar mix compositions and evaluating them in terms of workability and unconfined compression strength (UCS). Accordingly, the results showed that the addition of glass powder as a cement substitution yielded a gradual workability improvement, whereas the incorporation of red clay as a cement substitution induces a gradual workability reduction. In contrast, the unconfined compression strength revealed that the optimum glass powder content for strength performance was 5%, whereas no strength improvement was observed in this study using red clay, thus indicating the superiority of glass powder in enhancing the mechanical properties of mortar. Therefore, the outcome of this study suggests the possibility of improving both the fresh and hardened mortar properties using glass powder, as a partial replacement for cement.

Keywords: (Mortar, pozzolanic materials, red clay, glass powder)

Introduction

Global warming is one of the considerable concerns for the future of human civilization, indicating the importance of developing sustainable engineering construction strategies [1]. Commonly, cement-based materials such as concrete and mortar are characterized as widely versatile construction materials, probably due to their ability to be moulded into different forms, and raw material availability, along with their cost efficiency [2]. Cement-based materials are also rated as the second most utilized material worldwide, following water [3], with an estimated concrete usage of 30 million tons yearly [1]. In addition, Mortar is typically composed of binder, fine aggregates (sand), and water, of which Portland cement is the conventional binder used for binding the mortar matrix. However, there are some

 ISBN 978-9959-9703-2-9

negative issues associated with Portland cement manufacturing including; 1) the consumption of huge quantities of natural raw materials such as limestone and clay (2.8 tons of raw materials per ton of Portland cement) [4]; 2) the enormous energy consumption (5000 MJ per one ton) [5]; and 3) the higher carbon dioxide emissions released to the atmosphere (a ton of CO_2 per ton of Portland cement)[6]. Apart from that, the use of cement in concrete technology also shows limited proficiency in the attendance of sulphate, inducing problematic issues such as crack formation, expansion, and deterioration, due to the nucleation and growth of gypsum and ettringite [7]. Ettringite is a hydrous calcium aluminate sulfate crystalline, which forms due to the reaction between the hydrated compounds (from cement hydration), and sulfate (from cement or the surrounding soil and seawater), in the presence of water [8]. This mineral has a higher water absorption capacity [9,10], adsorbing water, thus its volume increases significantly, thereby causing cracks, expansion and softening of the cement-based material. Consequently, the utilization of supplementary cementitious materials such as industrial pozzolanic materials and waste materials (including rice husk ash, ground granulated blast-furnace slag, glass powder, natural clay soil and pulverized fly ash), as a part of Portland cement in cement-based materials (mortar and concrete) has been encouraged [11]. This is because of their efficiency in enhancing the performance of cement-based products through their pozzolanic reactions, along with their positive effects on minimizing the environmental impacts of cement manufacturing [12].

In the literature, Yan et al., 2019 [7], utilized GGBS as a partial replacement (0, 25, 50, and 75%) of Portland cement, and reported that 75% was the optimum replacement amount in terms of the sulfate resistance of concrete immersed in 5% sodium sulfate. Cercel et al., (2021) [13] investigated the physicomechanical properties of mortar made by activation of both ground granulated blast-furnace slag and glass powder with a binary combination of sodium carbonate and quicklime and concluded that the produced mortars are a viable replacement for the traditional Portland cement. Hwang and Cortes, (20121) [14] studied the effect of co-utilization of fly ash and glass powder as a partial substation of Portland cement and reported the enhancement of the ratio and unconfined compressive strength development of mortar and previous concrete, thus suggesting the feasibility of producing a sustainable and green infrastructure pervious concrete by the co-utilization of fly ash and glass powder as a part of Portland cement. Nahi

 ISBN 978-9959-9703-2-9

et al., (2020) [14] examine the incorporation of powdered soda lime glass powder as a 0, 10, 25, 35, and 60% replacement of Portland cement in mortar, and reported a reduction in the flowability of the mortar when more than 25% cement replacement was introduced.

Given the above-mentioned literature, it is obvious that the use of pozzolanic materials in cement-based materials is encouraged, to improve the physico-mechanical properties and reduce the environmental concerns of cement manufacturing. Therefore, this study aimed to explore the effect of using red clay and glass powder as a partial replacement (0, 5, 10, 15%) of cement in mortar, of which the former was activated by 3 wt% of quicklime to accelerate the dissolution of clay particles and the release of silica and alumina within the system. To this end, seven mortar mixes were designed and evaluated in terms of workability and compressive strength. Accordingly, the results suggested the feasibility of developing a sustainable mortar using glass powder.

Methodology

1- Materials

The raw materials used in this study included: 1) four cementitious materials (Portland cement-PC, quicklime-L, glass powder-GP, red clay-RC); 2) one fine aggregate (Sand-S); and 3) water. **Table 1** shows the oxide compositions of the Portland cement, lime, red clay, and glass powder, whereas **Table 2** and **Table 3** represent some physical properties.

Table 4: Oxide compositions of Portland cement, lime, glass powder and red clay.

Oxides	PC	L	RC	GP
SiO_2	20.13	0.67	71.84	72
Al_2O_3	4.49	0.07	12.71	3.52
Fe_2O_3	4.26	0.05	3.51	1.77
CaO	63.24	71.6	0.39	10.59
MgO	2.42	0.58	0.95	1.56
Na_2O	0.02	0.02	0.54	10.46
P_2O_5	0.1	0.03	-	-
Mn_2O_3	0.05	0.02	-	-
K_2O	0.57	0.01	-	0.89
TiO_2	0.26	0.01	-	-
V_2O_5	0.06	0.02	-	-
BaO	0.05	0.01	-	-
SO_3	1.12	0.19	-	-
LOI	4.3	27.4	19.9	-

Table 5: Physical properties of Portland cement (PC) and Lime (L), red clay (RC) and glass powder (GP).

Oxides	PC	Lime	RC	GP
Density (kg/m^3)	1400	-	-	1200
Specific gravity (Mg/m^3)	3.15	2.82	-	2.5
Fineness (m^2/kg)	365	750	-	-
pH	13.41	12	7	-
Colour	Grey	white	Brown	white
Form	Powder	powder	Powder	powder

The PC used was a commercially available Portland cement (CEM-II) in the form of grey fine powder. It was manufactured in compliance with the Libyan standard specifications No. 340 of 2009 and obtained from the Arab Union Cement Company in Zliten, Libya, through a local supplier. The characterization tests conducted on the as-received product indicated that the PC has a softness of 3575, initial setting time of 135

ISBN 978-9959-9703-2-9

minutes, final setting time of 225 minutes, 3-days compressive strength of 22.3 N/mm^2 and 7 days- unconfined compressive strength of 49.3 N/mm^2. The red clay (RC) was a natural clay with oxide compositions as outlined previously in **Table 1**, with a liquid limit of 56%, plastic limit of 33% and plasticity index of 23%. It was collected from the valley of Souf al-Jeen in the city of Bani Waleed, Libya.

The glass powder (GP) was prepared by grinding various types of glass bottles in the laboratory, after being dried and washed. The grounded powder was then sieved through a 0.063 mm sieve size and the particles passing the prescribed sieve, which has oxide compositions as outlined in **Table 1**, were used. The fine aggregate used in the experimentations was natural sand with particle size distribution results as shown in **Fig. 1** and some physical properties as outlined in **Table 3**. The sand was brought from Zliten through a local quarry and supplied by a local contractor. The water used in this study was potable water with chemical compositions as outlined in **Table 4,** which was obtained through a commercial service by a local company. By comparing the oxide compositions with those outlined in Libyan specifications No. 294, it was observed that the water used was suitable for use.

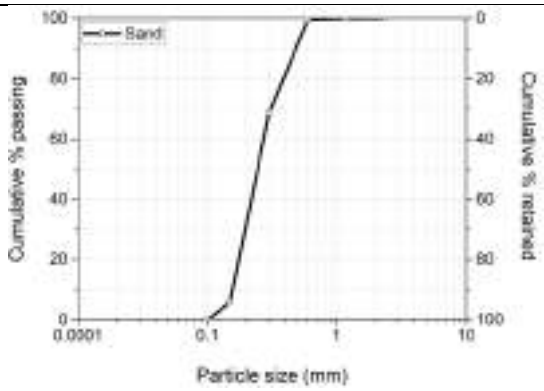

Fig. 1: Particle size distribution of sand.

Table 6: Some properties of sand

Physical properties	Sand
Specific Weight	2.58
Density	1736
Absorption Rate %	1.25
Fine Material Content %	0.15
Chloride Content %	0.75
Colour	White
Sulfate Content %	0.165

Table 7: Chemical compositions of water.

Chemical compositions	Quantity (mg/litter)
CO_3	57.97
HCO_3	104.12
CI	216.29
Na	120.62
Mg	5.43
Ca	3.32
K	62.18
$CaCO_3$	30.84
Dissolved solids	698.0
Conductivity	1.21
pH	9

2- Mix design

The mortar mix compositions assessed through the laboratory experimentations were

ISBN 978-9959-9703-2-9

designed using, 1) a fixed binder: sand proportion of 1:3;

2) a constant water/cement ratio of 0.55, and 3) seven various binder combinations. These binders (see **Table 5**) were made of; 1) 100% of PC (as a control mix); 2) M2-5%GP, representing 5% cement replacement with glass powder; 3) M3-10%GP, representing 10% cement replacement with glass powder; 4) M4-15%GP, representing 15% cement replacement with glass powder; 5) M5-5%RC, representing 5% cement replacement with red clay; 6) M6-10%RC, representing 10% cement replacement with red clay; and 7) M7-15%RC, representing 15% cement replacement with red clay. However, it should be noted that 3% of the total amount of red clay was a quicklime to enhance the dissolution of clay particles. As for the purpose of designing such mixes, this was to obtain an eco-friendly mortar, with equivalent characteristics to the control mix.

Table 8: Proportions of Binder combination.

Mix Design	PC	GP	RC
M1 (100 % PC)	100	-	-
M2 (5 % GP)	95	5	-
M3 (10 % GP)	90	10	-
M4 (15 % GP)	85	15	-
M5 (5 % RC)	95	-	5
M6 (10 % RC)	90	-	10
M7 (15 % RC)	85	-	15

3- Sample preparation and testing

A total of six cubical specimens with dimensions of 50 mm × 50 mm × 50 mm were prepared for each mix composition, in accordance with [17-21]. For each mix, the dry ingredients (PC, L, RC and GP) were firstly mixed in a mixer for 3 minutes, before the water was introduced and the mixing continued for further 3 minutes. Subsequently, the consistency of fresh mortar was measured by slump test, in accordance with BS EN 12350-2:2019 [20]. The semi-paste mixture was afterwards poured into the pre-oiled moulds and vibrated for 1 minute to remove air voids. Afterwards, the mortar-filled moulds were stored at 20±5 ℃ to be de-moulded after 24 hours, preparing for the curing. Finally, six cubes were cured in a water tank at 20±5 ℃, preparing for the unconfined compressive strength test at 7 and 28 days of moist curing. Finally, the unconfined compressive strength was conducted using a compressive machine at a load speed ratio of 1.4 kN/sec, in accordance with BS EN 12350-3 2019 [21].

Results and discussions

1- Slump test

The slump value of mortars made with glass powder and red clay is presented in **Fig.2**, alongside the slump value of Portland cement-based mortar as a benchmark.

ISBN 978-9959-9703-2-9

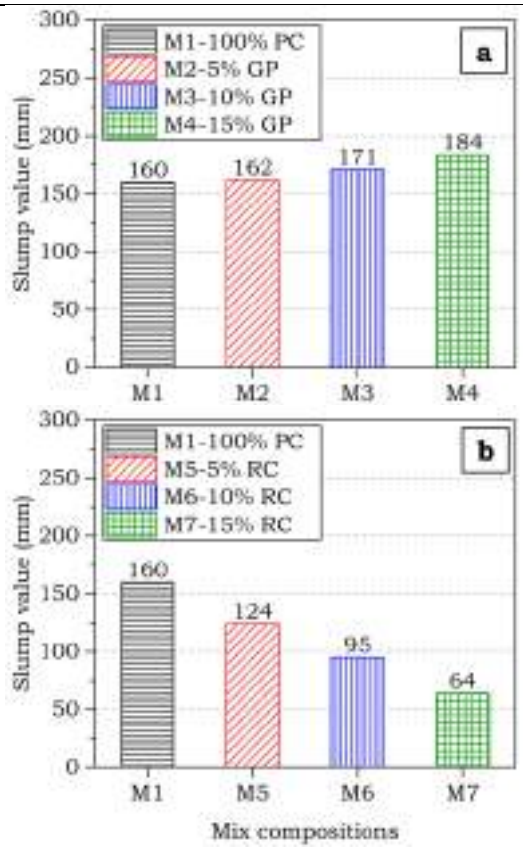

Fig. 2: Slump values of mortars made with; **a)** glass powder, and **b)** red clay.

As seen in **Fig.2**, the observations revealed a gradual increase in the slump value, as the quantity of glass powder increased, where the control mortar mix (M1-100%PC) displayed the lowest slump value of 160 mm, relative to that of 162 mm, 171 mm, and 184 mm for the case of M2-5%GP, M3-10%GP and M4-15%GP, respectively. This trend, however, was in reverse order in the case of cement substitution with red clay (see **Fig. 2b**), where the slump value was reduced gradually from 160 mm to 124 mm, 95 mm, and 64 mm for the mortar mix composition of M5-5%RC, M6-10%RC and M7-15%RC, respectively. The increase in slump value in the case of using glass powder as a partial cement substitution, therefore, suggests the possibility of reducing the water demand and improvement of the pumpability of the mortar, whereas the reduction in slump in the case of red clay indicates the needs for using lubricants such as superplasticizer if higher workable mortar is required.

The gradual enhancement in the slump value induced by using glass powder as a replacement for cement, which was in line with the outcomes of the slump value of concrete made with glass powder reported in [22], can be attributed to the glassy (smoothness) of glass powder surface, the lower water absorption capability of glass powder relative to Portland cement, and the coarser texture of glass powder, all of which ease the slumping of the mortar mixture. As for the gradual reduction induced by the application of lime-activated red clay is probably because of several reasons: 1) the high-water absorption capability of clay due to its negatively charged particle surface; 2) the substantial heat induced by the extremely high exothermic

 ISBN 978-9959-9703-2-9

hydration reaction of quicklime which causes the evaporation of water; and 3) the fineness of the clay particles [22-27].

2- Unconfined compressive strength (UCS)

The unconfined compressive strength (UCS) development of mortar fabricated using different glass powder and red clay contents as a partial replacement of Portland cement is plotted in **Fig. 3**, alongside the UCS of the Portland cement-based mortar (M1) as a benchmark.

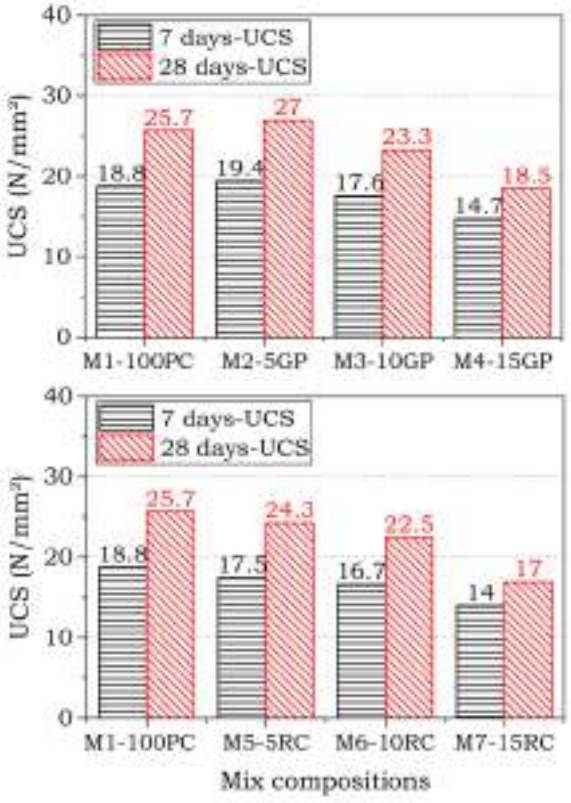

Fig. 3: The UCS evolution of mortars made with; **a)** glass powder, and **b)** red clay, at 7 and 28 days of curing age.

Generally, there was a steady increasing development in the UCS as the curing age increases from 7 to 28 days for all the mortars cured in water. This, therefore, demonstrates the formation of new hydrates and confirms that the strength of cubical mortars followed the general trend of UCS evolution of cement-based materials. This strength development is owing to the initial hydration of cement components with water to produce hydrated products such as calcium silicate hydrate (CSH) and calcium aluminate hydrate (CAH), which are responsible for the densification of the concrete system and the interlocking of the mixture [2].

The effect of the incorporation of glass powder observed in M2, M3 and M4 showed that the unconfined compressive strength was increased as the quantity of glass powder increases to 10%, beyond which further increase induces a compromise on the UCS. As an instance, the 28 days-UCS was increased from 25.7 N/mm^2 for M1-100%PC to 27 N/mm^2 for M2-5%GP, and then reduced to 23.3 N/mm^2 for M3-10%GP, and 18.5 N/mm^2 for M4-15%GP, indicating that 5% cement replacement with glass powder is the optimum substitution level in terms of the UCS. This

ISBN 978-9959-9703-2-9

unconfined compressive strength trend was also in agreement with the unconfined compressive strength trend of another researcher [22], who reported that 5% and 10% cement substitution is the optimum replacement level for concrete grade 33MPa and 45MPa, respectively.

The improvement of unconfined compressive strength induced by the incorporation of glass powder at a 5% cement replacement level, is probably due to the reaction between the glass powder and the calcium hydroxide produced during the hydration of Portland cement, which facilitates the formation of further calcium silicate hydrate (C-S-H). These hydrates crystalline with time, densifying the mortar matrix, reducing the porosity, and inducing better bonding, all of which enhance the UCS performance. As for the reduction in UCS induced by the higher replacement level, this can be credited to the reduction in the quantity of cement, which induces a compromise on the needed oxides for the formation of calcium silicate hydrate (C-S-H) and calcium aluminate hydrate (C-A-H).

On the application of red clay soil as a part of Portland cement, however, the observation revealed a gradual compromise on the unconfined compressive strength as the quantity of red clay soil was increased. In this context, the 28 days-UCS was reduced from 25.7 N/mm^2 for M1-100%PC to 24.3 N/mm^2 for M5-5%RC, 22.5 N/mm^2 for M6-10%RC, and 17 N/mm^2 for M7-15%RC, indicating the negative impact of red clay on the strength development of mortar. This strength trend was not in line with the observation of the finding reported in [22], where the strength was increased corresponding to the addition of calcined clay, the difference of which can be assigned to the reactivity and the calcination of the clay used. For this reason, research studies considering the effect of heating the red clay at elevated temperatures are encouraged for future work, to select the appropriate calcination temperature for this particular clay (red clay) and to enhance the application of red clay as a partial replacement of cement.

Conclusions

The feasibility of developing an eco-friendly mortar by using both glass powder and red clay as a partial Portland cement substitution has been investigated under this study in terms of the workability and the unconfined compressive strength, and the main conclusions emerged from the results of the experimentations can be drawn as follows:

The utilization of glass powder as a partial replacement of Portland cement in mortar mixture improves the workability (slump value)

 ISBN 978-9959-9703-2-9

as the cement substitution level increases, due to its glassy surface (smoothness), its lower water absorption capability, and the coarser texture of the glass powder, relative to that of the Portland cement.

The incorporation of red clay soil as a cement substitution in mortar reduces the workability of mortar, due to the high-water absorption capability and the fineness of the clay particles.

The unconfined compressive strength of mortar increases as the quantity of glass powder increases up to a 10% cement substitution level, beyond which the strength exhibited a gradual reduction. The enhanced strength at a 5% cement replacement level is due to the pozzolanic reaction between the glass powder and the calcium hydroxide, enabling the formation of further calcium silicate hydrate, thus densifying the matrix, and inducing better interlocking. As for the reduction in UCS beyond 5% replacement, this could be due to the reduction in the cement content, which induces a compromise on the needed oxides for the formation of hydrates responsible for strength development.

The application of red clay in mortar as a cement substitution yielded a gradual compromise on the unconfined compressive strength, as the amount of red clay increased. This is probably due to the lower reactivity of the clay used.

The limitations of this study, which can have an impact on the authenticity of the experimentation findings are the use of clay without calcination, which is anticipated the main reason for the reduction of strength. Therefore, studies considering the heating of clay at elevated temperatures and investigating the effect of calcination temperature on the ability of clay with respect to the mechanical performance of mortar are recommended for future work. In the process of heating, the silica content of the clay is improved and became more active, which in turn induces an enhanced mechanical property of the mortar matrix.

Arabic section:

العنوان: تقييم أداء الملاط الصديق للبيئة المصنوع من البوزولان الطبيعي والاصطناعي؛ الطين الأحمر ومسحوق الزجاج.

المؤلفون: شهد المخزوم، رؤى الورفلي، موده الصيد، ايمن الفرجاني، منصور إبعيليلة

الكلمات المفتاحية: (الملاط، المواد البوزولانية، الطين الاحمر، مسحوق الزجاج)

الملخص: بهدف الحد من التأثير البيئي المرتبط بتصنيع الأسمنت البورتلاندي، اكتسب استخدام المواد الإسمنتية التكميلية (المواد البوزولانية) في تطوير المواد القائمة على الأسمنت مثل الخرسانة والملاط، اهتمامًا كبيرًا في السنوات الأخيرة. لهذا السبب، تبحث هذه الدراسة في تأثير استخدام نوعين من المواد البوزولانية (البوزولان الطبيعي والصناعي)، ممثلة بالطين ومسحوق الزجاج، كبديل جزئي للأسمنت البورتلاندي في تحضير الملاط الأسمنتي. تضمنت منهجية هذه الدراسة البحثية تصميم سبع تركيبات

 ISBN 978-9959-9703-2-9

من خليط الملاط وتقييمها من حيث قابلية التشغيل وقوة الضغط غير المحصورة. وفقًا لذلك، أوضحت النتائج أن إضافة مسحوق الزجاج كبديل للأسمنت أدى إلى تحسن تدريجي في قابلية التشغيل، في حين أن دمج الطين الأحمر كبديل للأسمنت يؤدي إلى انخفاض تدريجي في قابلية التشغيل. في المقابل، أظهرت مقاومة الضغط غير المحصورة أن محتوى مسحوق الزجاج الأمثل لأداء القوة كان 5٪، بينما لم يلاحظ أي تحسن في القوة في هذه الدراسة باستخدام الطين الأحمر، مما يشير إلى تفوق مسحوق الزجاج في تعزيز الخواص الميكانيكية للملاط. لذلك، تشير نتائج هذه الدراسة إلى إمكانية تحسين خصائص الملاط الطازج والمصلب باستخدام مسحوق الزجاج، كبديل جزئي للأسمنت.

References

[1] Abdalla, T.A., Koteng, D.O., Shitote, S.M., and Matallah, M., (2022), Mechanical and durability properties of concrete incorporating silica fume and a high volume of sugarcane bagasse ash., Results in Engineering., **16**, 100666. DOI: 10.1016/j.rineng.2022.100666.

[2] Adeleke, B.O., Kinuthia, J.M., Oti, J., and Ebailila, M., (2023), Physico-mechanical evaluation of geopolymer concrete activated by sodium hydroxide and silica fume-synthesised sodium silicate solution., Materials., **16**(6), 2400. DOI: 10.3390/ma16062400.

[3] Nukah, P.D., Abbey, S.J., Booth, C.A., and Oti, J., (2022), Evaluation of the structural performance of low carbon concrete., Sustainability., **14**(24), 16765. DOI: 10.3390/su142416765.

[4] Samad, S., Shah, A., and Limbachiya, M.C., (2017), Strength development characteristics of concrete produced with blended cement using ground granulated blast furnace slag (GGBS) under various curing conditions., Sadhana - Academy Proceedings in Engineering Sciences., **42**, 1203-121342. DOI: 10.1007/s12046-017-0667-z.

[5] Oti, J.E., Kinuthia, J.M., and Bai, J., (2009), Compressive strength and microstructural analysis of unfired clay masonry bricks., Engineering Geology., **109**(3-4), 230-240. DOI: 10.1016/j.enggeo.2009.08.010.

[6] Dave, N., Misra, A.K., Srivastava, A., and Kaushik, S.K., (2016), Experimental analysis of strength and durability properties of quaternary cement binder and mortar., Construction and Building Materials., **107**, 117-124. DOI: 10.1016/j.conbuildmat.2015.12.195.

[7] Yan, X., Jiang, L., Guo, M., Chen, Y., Song, Z., and Bian, R., (2019), Evaluation of sulfate resistance of slag contained concrete under steam curing., Construction and Building Materials., **195**, 231-237. DOI: 10.1016/j.conbuildmat.2018.11.073.

[8] Ogawa, S., Nozaki, T., Yamada, K., Hirao, H., and Hooton, R.D., (2012), Improvement on sulfate resistance of blended cement with high alumina slag., Cement and Concrete Research, **42**(2), 244-251. DOI: 10.1016/j.cemconres.2011.09.008.

[9] Ebailila, M., Kinuthia, J., Oti, J., and Al-Waked, Q., (2022), Sulfate soil stabilisation with binary blends of lime–silica fume and lime–ground granulated blast furnace slag., Transportation Geotechnics., **37**, 100888. DOI: 10.1016/j.trgeo.2022.100888.

[10] Ebailila, M., Kinuthia, J., and Oti, J., (2022), Suppression of Sulfate-Induced Expansion with Lime–Silica Fume Blends., Materials., **15**, 2821. DOI: 10.3390/ma15082821.

[11] Mehta, A., and Ashish, D.K., (2020), Silica fume and waste glass in cement concrete production: A review., Journal of Building Engineering., **29**, 100888. DOI: 10.1016/j.jobe.2019.100888.

[12] Johari, M.M., Brooks, J.J., Kabir, S., and Rivard, P., (2011), Influence of supplementary cementitious materials on engineering properties of high strength concrete., Construction and Building Materials., **25**, 2639-2648. DOI: 10.1016/j.conbuildmat.2010.12.013.

[13] Cercel, J., Adesina, A. and Das, S., (2021), Performance of eco-friendly mortars made with alkali-activated slag and glass powder as a binder., Construction and Building Materials, **270**, 121457.

[14] Hwang, S.S. and Cortes, C.M.M., 2021. Properties of mortar and pervious concrete with co-utilization of coal fly ash and waste glass powder as partial cement replacements. Construction and Building Materials, **270**, 121415.

 ISBN 978-9959-9703-2-9

[15] Nahi, S., Leklou, N., Khelidj, A., Oudjit, M.N. and Zenati, A., (2020), Properties of cement pastes and mortars containing recycled green glass powder. Construction and Building Materials., **262**, 120875.

[16] BS EN 12620:2002+A1:2008, Aggregates for concrete, BSI Standards Limited, London, UK, 2008. https://doi.org/10.3403/02661981.

[17] BS EN 206:2013+A2:2021, Concrete — Specification, performance, production and conformity., BSI Standards Limited, London, UK, 2021. https://doi.org/10.3403/30257890.

[18] BS EN 12350-1:2019, Testing fresh concrete—Part 1: Sampling and common apparatus, BSI Standards Limited, London, UK, 2019. https://doi.org/10.3403/30360061.

[19] BS EN 12390-1: 2021, Testing hardened concrete—Part 1: Shape, dimensions and other requirements for specimens and moulds, BSI Standards Limited, London, UK, 2021. https://doi.org/10.3403/30397529U.

[20] BS EN 12350-2: 2019, Testing fresh concrete — Part 2: Slump test, BSI Standards Limited, London, UK, 2019. https://doi.org/10.3403/30360058.

[21] BS EN 12390-3:2019, Testing hardened concrete — Part 3: Compressive strength of test specimens, BSI Standards Limited, London, UK, 2019. https://doi.org/10.3403/30360070.

[22] Aliabdo, A.A., Abd Elmoaty, M. and Aboshama, A.Y., 2016. Utilization of waste glass powder in the production of cement and concrete. Construction and Building Materials, 124, pp.866-877.

[23] Ebailila, M., Kinuthia, J., and Oti, J., (2022), Role of Gypsum Content on the Long-Term Performance of Lime-Stabilised Soil., Materials., **15**(15), 5099. DOI: 10.3390/ma15155099.

[24] M. Ebailila, Sulfate soil stabilisation with silica fume-based binders, Doctoral Thesis, University of South Wales, England, UK, 2022.

[25] Dawood, E.T., Mohammed, W.T. and Plank, J., 2022. Performance of sustainable mortar using calcined clay, fly ash, limestone powder and reinforced with hybrid fibers. Case Studies in Construction Materials, 16, p.e00849.

[26] Nair, N., Haneefa, K.M., Santhanam, M. and Gettu, R., 2020. A study on fresh properties of limestone calcined clay blended cementitious systems. Construction and Building Materials, 254, p.119326.

[27] Sposito, R., Beuntner, N. and Thienel, K.C., 2020. Characteristics of components in calcined clays and their influence on the efficiency of superplasticizers. Cement and Concrete Composites, 110, p.103594.

 ISBN 978-9959-9703-2-9

المؤتمر الدولي الثاني للعلوم والهندسة
2nd International Conference on Science and Engineering
ICSE 2023
Faculty of Engineering - University of Bani Waleed
Bani Waleed, Libya

Paper Code: ICSE-060

STUDY THE EFFECT OF SOURCE OF PORTLAND CEMENT IN COMPRESSIVE STRENGTH (COPERESION STUDY)

Naji amhimmid salih, Malak ALbagol
Civil Engineering Department-Faculty of Engineering – Bani- Walid University
Najisalah320@gmail.com

Abstract: As it is known, ordinary Portland cement is the basic material in the concrete industry, and the quality of cement is very important in producing concrete according to the required specifications, given the desire among citizens and companies to use certain types of cement in addition to the discrepancy in prices, and this indicates doubts about the quality and specifications of some types of manufactured cement Locally or imported, and in order to give confidence to the consumer, we had to conduct a comparative study between cement manufactured locally in the factories of (Al-Ittihad Al-Arabi - Souk Alkhamis - Almargab) and imported from (Turkey-Tunisia), as these types are the most consumed, especially in the western region of the country. The aim of this The study is to verify the extent of the effect of cement production sources on the compressive strength property of concrete, which is the most important property, whereby a concrete mixture was designed to achieve pressure resistance (25Mpa) and the use of the same proportions for the components of the concrete mixture (coarse aggregate - sand, water) from the same source and the only variable for each mixture is Cement has been tested for slump and (6 cubes) for each mixture are prepared. (3 cubes) are tested to determine the compressive strength after (7 days), and (3 cubes) to determine the compressive strength after 28 days. It turns out that the variation in the pressure resistance after (28 days) is simple. Between each of the cements of the Arab Union, Souk Al-Khamis, Turkish Falcon and Tunisian Kairouan Cement, while Al-Margab Cement and Tunisian Central Mountain Cement did not achieve the target of the mixture.

Keywords:

Introduction

The civilizational development that the world is witnessing, which includes the development of construction works of various kinds, and Libya is among the countries that have witnessed urban development at various levels for decades, and it consumes very large quantities of cement and the construction of many factories in various regions of the country. However, very large quantities are imported from countries Many of them, including Tunisia, Egypt, Turkey, and others. Whereas, concrete is the basic material used in most constructions, and cement is the material that possesses cohesive properties (cohesive) and

 ISBN 978-9959-9703-2-9

adhesion (adhesive) in the presence of water, which makes it able to bind the components of concrete to each other and its cohesion with reinforcing steel and turn it into a complete unit Cement has the property of setting and hardening due to chemical reactions in the presence of water, so it is known as hydraulic cement[1]. The raw materials used in the Portland cement industry consist mainly of limestone (Cao), silica (Sio2) and alumina AL2O3) and iron oxide (Fe2O3). These compounds interact inside the furnace until a chemical equilibrium state is reached. This reaction results in clinker. The clinker contains four main compounds, namely: **1.** Tri-calcium silicate C3S **2**. Di-calcium silicate ((C2S) **3**. Tri-calcium aluminate (C3A) **4.** Calcium iron aluminate (C4AF) [2] Due to the different proportions of oxides in raw materials according to the composition and environmental conditions surrounding these materials, and since factories use raw materials The raw material is from different sources according to its location. Therefore, the quality and specifications of this important material depend on the quality of the raw materials.

practical program:

To achieve the objective of this study, a practical program was prepared that included the preparation of a standardized concrete mix design according to the proportions mentioned in Table (3). Six cubes were prepared from each mixture, i.e. for each type Cement to determine the strength of concrete was tested after a 7 days and after 28 days, and the results were as shown in Table (4) and we measure the slump for each mix and the results shown in the table (5).

Materials used:

Cement:

Considering the aim of the study is to compare the compressive strength of concrete using different sources of, Portland cement type (42.5) was chosen according to Libyan Standard Specifications No. (340/2009) from the following sources:

Tabel.1: Sources 0f cement

[No	Sources of cement	Name of cement
1	Zlitn	Union Arab company (Cement borag factory)
2	SOUK ALKAMES	Souk alkames
3	KOMES	Almirgab (Cement almirgab factory)
4	TURKY	Falcon cement
5	TUNIS	Kairouan
6	TUNIS	Jabal oust

Coarse and fine aggregate:

Coarse aggregate from a quarry in Bani Walid and fine aggregate from Zliten quarries were used. The granular gradient test of coarse and fine aggregate was carried out using the laboratory equipment of the Bani Walid College of Engineering. The results were as shown in Figure No. (1) and (2) according to American specifications [3] .

ISBN 978-9959-9703-2-9

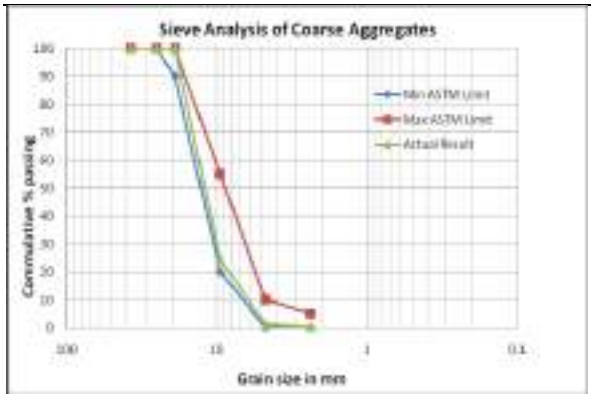

Figure.1: the granular gradient of coarse aggregate

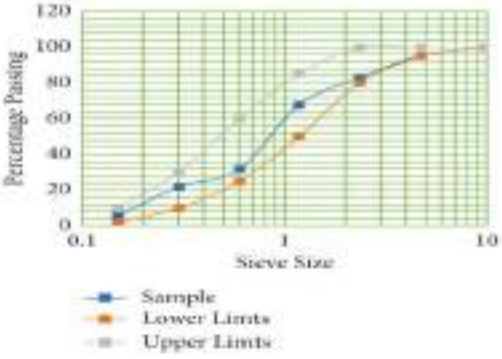

Figure.2: the granular gradient of fine aggregate

water:

The water of the Great Man-Made River was used, and the results of the chemical analysis were as shown in Table No. (2)

Chemical composition	T.D.S	CL	SO4	CaCo3	PH
Result	1031 mg/L	354.53 mg/L	532 mg/L	425 mg/L	8

Mix design:

To investigate the compressive strength of concrete by using different sources of cement, a concrete mix was designed to achieve compressive strength (25Mpa) with uniform proportions. The only variable in it is cement according to Table No. (3).

Table .3: Mix design component

Mix component	Cement (kg)	Course aggregate (Kg)	Fine aggregate (Kg)	Water (litter)	Water cement ratio W/C
	323	1139	741	200	0.62

Laboratory tests:

Concrete mixtures have been prepared for various cement sources, using equipment in the laboratory of the College of Engineering, Bani Walid (balance - mechanical mixer - slump test device - cubes - pressure testing machine). **6** cubes were prepared from each mixture. **3** cubes are tested after **7** days and **3** cubes After **28** days, with a total number of **36** cubes, bearing in mind that all cubes have been processed according to the specifications' recommendation, and the results were according to Table No. (4), and as Figure No(2). shows the test results after **7** days, and Figure No. (4) shows the test results after **28** days.

Table .4: Compressive strength of concrete

No	Name of cement	Compressive strength after (7 days) (Mpa)	Compressive strength after(28 days) (Mpa)
1	Union Arab company	18.5	27.93
2	SOUK ALKAMES	17.67	28
3	ALMERGAB	14.27	21.7
4	FALCON CEMENT	20.5	29.36
5	KAIROUAN	22.36	27.4
6	JBEl OUST	19	24.63

Table .5: Slump test

No	Name of cement	Slump(cm)
1	Union Arab company	12
2	SOUK ALKAMES	18
3	ALMERGAB	10

ISBN 978-9959-9703-2-9

4	FALCON CEMENT	15
5	KAIROUAN	20
6	JBE OUST	8

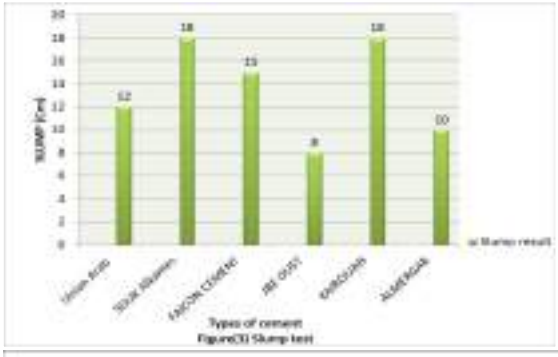

Figure(3) Slump test

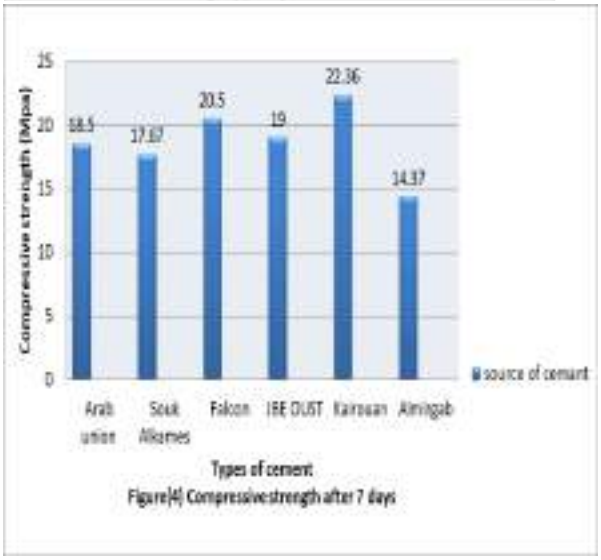

Figure(4) Compressive strength after 7 days

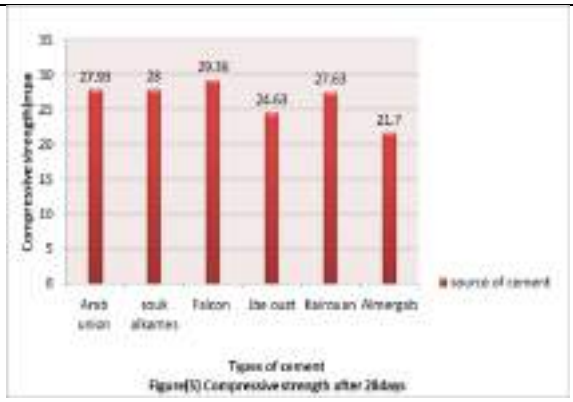

Figure(5) Compressive strength after 28days

Analysis of the results:

By looking at Table No. (5) and Figure No. (3), which show the slump test values for the various mixtures, where it was found that the highest slump value for the mixtures was the cement of Souk Al-Khamis and Al-Qairouan, and this indicates that these two types of cement show high operational performance of concrete, while Jabal Al-Wasat cement showed the lowest slump value This indicates that the performance of the concrete is low. As for Al-Ittihad Al-Arabi cement, Souq Al-Khamis and Falcon cement showed a moderate decline, this indicates that the performance of using these two types of cement is good.

By looking at the table of tests for pressure resistance No. (4) and Figure No. (4) which shows the average results of the cube test after 7 days, it is clear that the slight discrepancy between each of the cements (Al-Ittihad Al-Arabi - Kairouan and - Souk Al-Khamis and Jabal Al-Wasat - and Falcon) in achieving a rate of 70% from designed value in this age of mixture, and this indicates that the cement specifications are good, while Al-Margab cement showed pressure resistance of 57%only from designed value in this age of mixture.

By looking at the test table No. (4) for pressure resistance and Figure No. (5) which shows the results of the tests after 28 days, it is clear that the slight discrepancy between each of the cements (Arab Union - Suq Al-Khamis - Falcon

ISBN 978-9959-9703-2-9

Cement - Kairouan Cement) where the value of the compressive strength exceeded the design value and this It also indicates the quality and specifications of these types and their conformity with the Libyan specifications, while Al-Margab cement and Jabal Al-Wasat showed a value less than the design pressure resistance value.

Conclusion and recommendations:

Referring to the laboratory results that were reached in this research to test the pressure resistance of the manufactured concrete from the mentioned sources, we can draw the following conclusions:

1. The Tunisian Jabal oust Cement showed a low workability.
2. Souk El Khamis Cement and Tunisian Kairouan Cement showed high workability.
3. Union Arab Cement, Souq Al-Khamis, and Turkish Falcon Cement showed good workability.
4. According to the results obtained from the pressure resistance tests after 28 days, it was found that the cements of (Al Ittihad Al Arabi - Souk Al Khamis - Turkish Falcon Cement - Tunisian Kairouan Cement) exceeded the design value of the pressure resistance, and this indicates the quality of these sources and their conformity with the Libyan standard specifications.
5. According to the results obtained from the pressure resistance tests after 28 days, it was found that the cements of (Al-Margab and the Tunisian Central Mountain Cement) did not achieve the design value for the pressure resistance.
6. Recommends the need for periodic control by the competent authorities on the specifications of raw materials and on all materials used in the cement industry, in addition to the necessity of periodic inspection of the factory and ensuring the calibration of devices and machines for locally manufactured cement.
7. The need to comply with the approved Libyan specifications for all types of cement supplied from abroad, with inspection of these factories prior to supply.

References:

1. Technology of concrete. Mohamed Hamoud Mhana, Civil engineering department, Anbar university.
2. Sixth National conference on building materials and structural engineering. Garyan libya2016.
3. American standard and specification for raw materials 2015.
4. Huynh, T., Ngo, S., Hwang, C. Performance of concrete made with different coarse aggregate particle sizes under sulfate solution. International Journal of Materials Science and Engineering. 2017.
5. Nasir Kabir. Characteristics of Different Type of Coarse Aggregate on Properties of High Performance Concrete . International Journal of Materials Science and Engineering. 2019.
6. S. K., Song, Y. C., and Won, J.-P. (2011). “Enhanced durabilityperformance of face slab concrete in Concrete-Faced Rock-filledDam using fly ash and PVA fibr.
7. Ghana: A Key to Understand the Behavior of Cement. Advances in Materials Science and Engineering, 2015.

 ISBN 978-9959-9703-2-9

المؤتمر الدولي الثاني للعلوم والهندسة
2nd International Conference on Science and Engineering
ICSE 2023
Faculty of Engineering - University of Bani Waleed
Bani Waleed, Libya

Paper Code: ICSE-011

VISUAL BASIC PLATFORM TO EVALUATE LIBYANA ALMADAR PERFORMNACE

Fathi Masouda, Departement of Communications Engineering, College of Electronic Technology BaniWaled, Libya
*Crosspnding author: fshuggaf@gmail.com

Abstract: Cellular system is widely used in most countries, where the main adopted scheme is frequency reuse, as the same bandwidth is utilized by each group of cells (cluster). The clusters are repeated among significant geographical area which leads to interference between the cells of the same frequency, furthermore, the cells of high population suffers from high probability of blocking PoB, where the user can not access the network, in addition to the number of users outside the coverage area.
The aim of this paper is to build Visual Basic application to measure the above mentioned parameters. Visual Basic platform has been successfully built and operated, where simulation experiment is performed on BaniWalid city. the application could be used in improving the performance of existing wireless networks such as Libyana and Almadar.

Keywords: Cellular System, Bandwidth, SIR, Probability of blocking, Coverage, Visual Basic

Introduction

Cellular theory suggests dividing the geographical area into many groups of cells (clusters). [1] [2] [3]

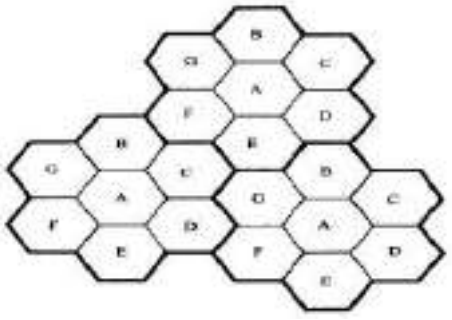

Figure 1: Cellular System Geographical Diagram

According to Frequency Reuse rule, each cluster is given the same frequency bandwidth, which is shared among three, four or seven cells, therefore interference occurs between co-channels, for example, between the cells in Figure1 with letter G, or any cells having the same letters, Co-cells, that results an interference at user's mobile . [1] [2] [3]
Signal-to- Interference Ratio, SIR, is the ratio of signal of cell where the user exits to remote co-cell [10] [11] [12]:

$$SIR = \frac{1}{\sum_{i=1}^{i_0} (\frac{d}{dk_i})^n} \quad \text{.....(1)}$$

 ISBN 978-9959-9703-2-9

where:
d is the distance from the mobile station to serving base station. dk is the distance from mobile station to interfering base stations.
i_0 is the number of co-channel interfering cells.
Path loss parameter defines the amount of loss that the signal encounters in its path from transmitter to receiver, its value from 2 to 3 [4] [5] [6]

Probability of Blocking P_n, the probability that the user finds the network busy, can be calculated by the following formula [9] [8] [7]:

$$A = \lambda.h \ldots\ldots\ldots\ldots\ldots\ldots (2)$$

$$P_n = \frac{A^n / n!}{\sum_{m=1}^{n} A^m / m!} \ldots\ldots\ldots\ldots\ldots\ldots (3)$$

λ is the call arrival rate, number of calls per unit of time, h, is the average holding time (duration of the call), A is the traffic, n is the number of channels per cell (Capacity).
Number of users who are out of coverage is determined by calculating the customers who receives less than a lowest nominated threshold power (sensitivity). [1] [2] [3]

Visual Basic

Visual Basic is programming language for designing applications that run under Microsoft's

Windows operating systems. The language is useful for both beginners and specialists, beginning programmers, who deal with the direct visual projects of building simple applications that include texts, lists and various menus; and specialist programmers, who aim to build sophisticated Windows-based projects with lowest possible cost. [13].

The purpose of the paper

The purpose of the paper is to build VB application in order to measure SIR in equation 1, POB in equation 3, and number of users out of coverage.

Proposed Application

Figure 2: Main Page

Figure2 shows the area where the application is tested, the picture illustrates a populated region in Bani Walid city, underneath the picture, group of command buttons, text boxes, where data are to be entered, labels, and menus that are explained as follows:

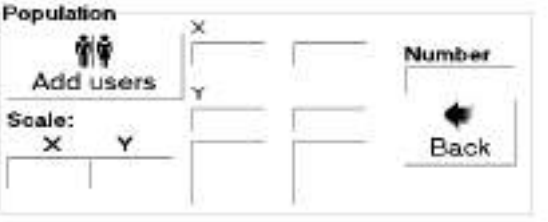

Figure3: Population Management.

Add Users button is used to distribute the users of the cellular network among dedicated area, this area is limited by X and Y coordinates and Scales. The distribution is performed randomly, required number of

 ISBN 978-9959-9703-2-9

people is written in the text box which labelled by (Number). Two list menus present the location of each user; Back button is used to clear the population in the case of mistaken distribution.

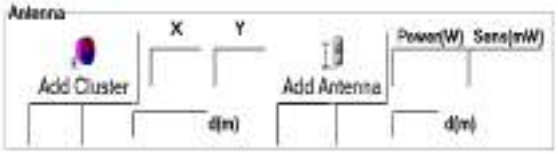

Figure4: Antenna Parameters.

Add cluster button starts the establishment of group of antennas (Cluster), which usually contains three, four or seven antennas. The frequency Bandwidth is divided equally among the antennas; therefore, each antenna has its own group of channels. Before pressing Add Cluster or Add antenna, X Y location of the antenna should be entered, as well as the transmitting power and Mobile sensitivity, these parameters determine the area of coverage.

Figure5: DATA IMPORT/EXPORT.

Bring/Save Buttons are used to save and import data such as Antennas locations and number of users and their locations, after completing the distributions and antenna localization, the work can be saved and imported in another session.

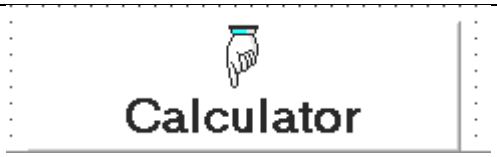

(a)

(b)

(c)

(d)

ISBN 978-9959-9703-2-9

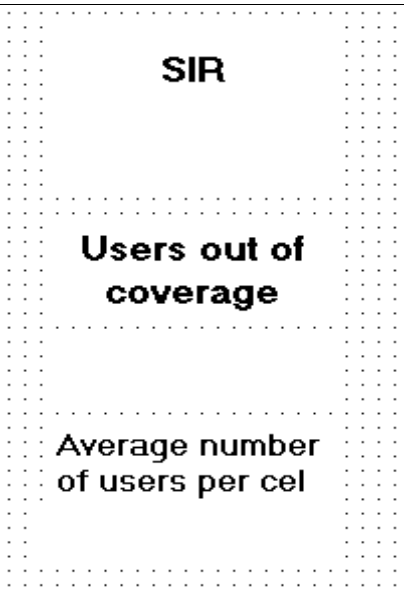

(e)

Figure6: (A) BUTTON TO SHOW RESULTS PAGE.(b) Results Page . (c) Path loss text box. (d) Traffic Management tools. (e) Users distribution Measurement.

Clicking Calculator button shows the results page, path loss text box (c) is used to type the value of the path loss parameter which is indicated in equation 1.

Request Rate is the number of calls per minute, Holding Time is the call period, and Capacity is the number of channels in each cell, these values are to be entered in the mentioned text boxes respectively before clicking Calculate button.

P(blocking) is the probability that the user finds the network busy, i.e all the channels are occupied, this command is used after filling the above boxes.

SIR button is pressed to determine the Signal to Interference Ratio, SIR, which is the ratio of the signal from nearest antenna to the signal from another antenna having the same frequency Band Width, co-cell.

Users out of coverage calculates the number of users that receive weak signal, lower than their mobiles' sensitivity.

Results

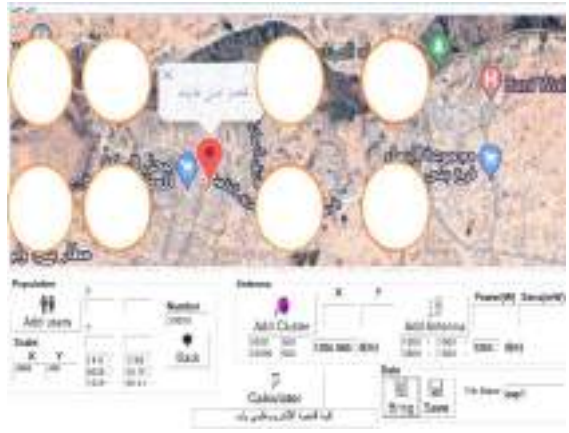

(a)

(b)

ISBN 978-9959-9703-2-9

Figure7: (A) USER DISTRIBUTION RESULTS.(b) Traffic Results

Two clusters have been proposed, each cluster contains four antennas, the population is considered to be 30000 users distributed randomly among the area (20 Km x 2 Km), and Request Rate is assumed to be one call every five minute, with average duration of 12 seconds.

SIR is found to be about 137.4, and 8038 users are out of coverage, with 2745.25 users per cell.

Probability of Blocking is 7%, i.e. the user finds the network busy at seven calls out of hundred calls.

Conclusion

Robust Visual Basic application has been built in order to measure the performance of cellular systems; the application could be used as a tool to enhance the performance of existing wireless network such as Libyana and Almadar.

Many practical conclusions are accomplished from this study, the most major conclusion is that antenna location distribution plays primary role in changing the performance parameters, which means that the service can be improved by low cost action (moving the antenna location).

Transmit power has an obvious outcome on SIR, and the number of (out of coverage users). While number of channels and users per cell affect the probability of blocking.

The application has many options such as changing the picture and working with different areas, which gives appropriate flexibility and reliability in order to evaluate and improve various cellular networks.

Arabic section:

شبكات الهاتف الخلوي تعاني من قصور في أداءها لأسباب كثيرة من أهمها النمو السكاني والتمدد الجغرافي الذي يحدث بعد فترة من بداية إنشائها الأمر الذي يتسبب في خروج العديد من المشتركين من التغطية خصوصا في مناطق الدواخل بالإضافة إلى الضغط الذي يحدث على الشبكة نتيجة زيادة عدد المشتركين في المناطق المزدحمة وعدم تمكن العديد منهم من الوصول للشبكة نظرا لإنشغال خطوطها باستمرار. في هذا المشروع تم تصميم وتنفيذ مشروع فيجوال بيسك يعرض خريطة أي منطقة والمحطات الخلوية الموجودة بها وقياس البراميترات ذات العلاقة بالأداء واقتراح مواقع جديدة لهوائيات إضافية أوتغيير مواضع الهوائيات الحالية أو تغيير خصائص الهوائيات من أجل الحصول على أداء أفضل.

Abbreviations and Acronyms

CS: Cellular System, BW: Bandwidth, SIR: Signal to Noise Ratio, PoB: Probability of Blocking, VB: Visual Basic.

Acknowledgment

ISBN 978-9959-9703-2-9

The author wish to thank CETB staff for their help and support.

References

[1] Alexander Kukushkin "Introduction to Mobile NetworkEngineering: GSM, 3G-WCDMA, LTE and the Road to 5G,"

[2] Joseph Hoy, "Forensic Radio Survey Techniques for Cell Site Analysis," John Wiley & Sons, Ltd, First Edition, © 2015.

[3] Asrar U. H. Sheikh, "Wireless Communications: Theory and Techniques," Springer, First Edition, © 2004.

[4] Jochen H. Schiller, "Mobile Communications," Second Edition, © 2003.

[5] Theodore S. Rappaport, "Communications principles and practice-Prentice," Hall PTR, Second Edition, © 2002.

[6] By V. H. MAC DONALD(Manuscript received July 17, "Advanced Mobile Phone Service: The Cellular Concep," © 1978.

[7] KavehPahlavan & Prashant Krishnamurthy, "Principles of Wireless Networks," Hall PTR, First Edition, © 2002

[8] Michel DaoudYacoub, "WIRELESS TECHNOLOGY Protocols, Standards, and Technique," CRC Press, First Edition, © 2002.

[9] C. Y. Lee (Wiley (1993), "Mobile communications design fundamentals," John Wiley & Sons, Ltd, Second Edition, © 1993..

[10] Mischa Schwartz, "Mobile Wireless Communications," Cambridge University Press, First Edition, © 2005.

[11] Ajay R Mishra, "ADVANCEDCELLULAR NETWORK PLANNING AND OPTIMISATION," John Wiley & Sons, Ltd, First Edition, © 2007.

[12] Simon Haykin, "Communication system," John Wiley & Sons, Ltd, Fourth Edition, © 2001

[13] BYRON S. GOTTFRIED, "SCHAUM'S OUTLINE OFTHEORY AND PROBLEMS OF PROGRAMMING
WITH VISUAL BASIC," SCHAUM'S OUTLINE SERIES MCGRAW-HILL, INC.

 ISBN 978-9959-9703-2-9

المؤتمر الدولي الثاني للعلوم والهندسة
2nd International Conference on Science and Engineering
ICSE 2023
Faculty of Engineering - University of Bani Waleed
Bani Waleed, Libya

Paper Code: ICSE-025

COMPRESSION OF MEDICAL IMAGES BASED ON 2D-DISCRETE COSINE TRANSFORM AND VECTOR QUANTIZATION ALGORITHMS

Azuwam Ali Alhadi
Department of Communication Engineering, College of Electronic Technology, Bani-Walid, Libya
alzwam.alialhady@gmail.com

Abstract: In this paper, two types of Medical images which were collected from CT scan and Ultrasound system in order to reduce the number of bits needed to represent a medical image with preservation of image quality. Medical imaging has a great impact on diagnosis of diseases and preparation to surgery. On the other hand, the storage and transmission is an important issue due to massive size of medical image data. For example, each slice of CT images is 512 by 512, and the data set consists of 200 to 400 images leading to 150 MB of data in average .An efficient compression of the medical data can solve the storage and transmission problem. Medical images are compressed using proposed algorithm that includes two techniques which are discrete cosine transform DCT and Vector Quantization VQ. The paper started from collecting Medical images, and developing compression algorithms by DCT-QV using MATLAB and evaluate the performance of these techniques by measuring the difference between the original image and compressed images using Peak Signal to Noise Ratio PSNR, mean square error MSE, compression ratio CR, and bit per pixel BPP and. Experimental results show that proposed algorithm produces a high quality for compressed images with acceptable compression rate in terms quantization level is more than 30%.

Keywords: (PSNR, JPEG, DCT, Compression Ratio, CT)

Introduction

With the improvement of medical imaging facilities, a growing amount of data is brought out in the modern image processing, and it leads to an increasingly heavy burden for data storage and transmission. Image compression is a technique of reducing the redundancies in image and represents it in shorter manner, which can allow more cost-effective utilization of network bandwidth and storage capacity. Therefore, the medical image compression plays an important role in many applications. In the past decades, numerous and diverse image compression methods have been proposed to compress the digital images [1]. Digital image are generally characterized by three types of redundancies: spatial redundancy, coding redundancy and psych visual redundancy. The compression algorithms exploit these redundancies to compress image. Spatial redundancy

 ISBN 978-9959-9703-2-9

represents a fact that grey value of one pixel may be partially calculated by values of other pixels. The coding redundancy also called statistical redundancy refers to the use of variable length code to match the statistics of the original image. Psych visual redundancy is based on the human perception of the image information. Removing psych visual redundancy introduces distortion in uncompressed images, so this step is skipped during lossless image compression. Image compression can be classified as lossy and lossless. In lossy compression scheme, there is loss of information. And encoding is achieved with an acceptable degree of deterioration in the reconstructed image, with a high compression ratio, such as JPEG, JPEG2000. But lossless scheme is reversible and this represents an image signed with the smallest possible number of bits without loss of any information, and the compression ratio achieved is low JPEG2000. Applications like satellite image compression, medical image compression where any loss in data may lead to incorrect prediction or diagnosis, lossless compression methods are used. Lossy compression methods are used for compressing general purpose digital images where minor loss of data is no hindrance. Here we proposed compression method based on a frequency transform that is able to compress Medical image which is DCT-VQ. This transform contains unique features which allow for the creation of an efficient image compression. The main edge of image transformation using DCT-VQ is the elimination of redundancy between neighbour pixels. Efficiency or performance of the transformation scheme can be directly measured by its ability to array input data into as few coefficients as possible [1, 2].

Transform Coding

In transform coding, a reversible linear transform is used to map the image into a set of transform coefficients, which are then quantized and coded. The decoder is just reverse of the encoder. A typical transform coding system has four steps which are Decomposition of image into sub-images, forward transformation, quantization, and coding. An N x N image is subdivided into sub images of size n x n (mostly 8 x 8), which are then transformed; so as to collect as much information into a smaller number of transform coefficients. The quantization then quantizes the coefficients that contain the least information. The encoding process ends with the coding of the transformed coefficients. The most famous transform coding systems are Discrete Cosine Transform (DCT) .Transform Coding are preferred over all the transform coding techniques as it involves less number

 ISBN 978-9959-9703-2-9

of calculations. The standard presently accepted, created by the Joint Photographic Experts Group (JPEG) for lossy compression of images uses DCT as the transformation

JPEG Image Compression

Joint Photographic Expert Group (JPEG) image compression is an accepted technology. JPEG is a modern lossy/loss-less compression technique for colour or grey scale static images. In a case where there are neighbouring similar coloured pixels, this compression works well on continuous tone images. JPEG utilizes many parameters to in order to enable the users to manipulate the amount of information lost (and in this way likewise the compression ratio) over a very wide range.

DCT Computation

DCT is a computationally intensive algorithm which takes several electronic applications. DCT is a mathematical transformation that converts the data in the space or time domains to the frequency domain providing a close version of the signals with fast transmission, memory saves and many more. This algorithm is known to be exactly efficient due to its regularity and simple ability. Several DCT coefficients which are located in the frequency domain is a converted version of a DCT-2D pixel values a spatial image in the region. The image data inside the storage is distributed into some blocks MCU (minimum code units) before compression. Each block comprises of 8x8 pixels [2]. Some of the compression processes plus DCT-2D inside it will be carried out on every block. Each pixel value in the 2-D matrix is a value in the range of 0 to 255 for the intensity or luminance values and the range of -128 to + 127 for the chrominance values. Before DCT is computed, all the values are moved to the range of -128 to +127. The average of every (64) values in the matrix is [DC] coefficient and the value are in the transformed matrix location F[0,0] while the remaining values(63) are known as the AC coefficients which contains a frequency coefficient associated with them. Furthermore, spatial frequency coefficients increment as it move amongst left and right (on a level plane) or between start to finish (vertically). Low spatial frequencies are grouped in the left top corner. Moreover, DC coefficient and the lower spatial frequency coefficients and the DC coefficient are responded to by the human eye. Besides, the eye will not detect the frequencies if a higher frequency coefficient magnitude reaches a certain low threshold.

The two dimensional DCT can be expressed as the following equation which is F (u,v) .

$$\frac{4}{N^2}\alpha(u)\alpha(v)\sum_{x=0}^{N-1}\sum_{y=0}^{N-1}f(u,v).\cos\left(\frac{(2x+1)u\pi}{2N}\right).\cos\left(\frac{(2y+1)u\pi}{2N}\right) \quad (1)$$

 ISBN 978-9959-9703-2-9

The two dimensional inverse DCT is given by *f(x,y)*

$$\sum_{u=0}^{N-1}\sum_{v=0}^{N-1}\alpha(u)\alpha(v)\,F(u,v).\cos\left(\frac{(2x+1)u\pi}{2N}\right).\cos\left(\frac{(2y+1)u\pi}{2N}\right) \quad (2)$$

Where:

*F(u,v)*and *F*: coefficient values in the transform domain.

*f(x,y)*and *f*: coefficient values in the spatial domain.

x,y: spatial coordinates in the pixel domain.

u,v: coordinates in the transform domain.

$$\alpha(u),\alpha(v)=\begin{cases}1/\sqrt{2} & \text{for } u,v=0\\ 1 & \text{for } u,v=1,2,\ldots,N-1\end{cases} \quad (3)$$

Equation (1) shows that the two dimensional DCT is derived by multiplying the horizontal one dimensional basis function with the vertical one dimensional basis function. Both one and two dimensional DCT works in similar approach [3].

Vector Quantization

Quantization is the manner by which visual data are carefully disposed without a major lack in the visible effect. Quantization helps to decrease the number of bits that is used to represent an integer value for the purpose of reducing the precision of the integer. Every component of the DCT is divided by different quantization coefficient also gathered together to an entire whole integer value step in the JPEG compression algorithm to evacuate a lot of data, this however lessens the entropy of the info streams of data. Quantization helps the compression process because of it lossy compression technique. Each nonzero AC coefficient in the intermediate symbol sequence is denoted by combining with the "run - length" (succeeding number) of zero-valued AC coefficients that go before it in the zigzag sequence [2]. Image compression contains standard quantization matrices that changes in every stage and quality that allows the user to determine on the level of quality that ranges between 1 to 100, where the lowest image quality is 1 and maximum compression 100 gives the finest quality and lowest compression. Due to this reason, quality/compression ratio can be designed according to purpose or requirement. From fig.1. It is good to note that quantization matrix that has a quality level 50 can produce a very good compression and tremendous decompressed image quality.

 ISBN 978-9959-9703-2-9

$$Q50 = \begin{bmatrix} 16 & 11 & 10 & 16 & 24 & 40 & 51 & 61 \\ 12 & 12 & 14 & 19 & 26 & 58 & 60 & 55 \\ 14 & 13 & 16 & 24 & 40 & 57 & 69 & 56 \\ 14 & 17 & 22 & 29 & 51 & 87 & 80 & 62 \\ 18 & 22 & 37 & 56 & 68 & 109 & 103 & 77 \\ 24 & 35 & 55 & 64 & 81 & 104 & 113 & 92 \\ 49 & 64 & 78 & 87 & 103 & 121 & 120 & 101 \\ 72 & 92 & 95 & 98 & 112 & 100 & 103 & 99 \end{bmatrix}$$

Fig. 1:Quantization Matrix

Zigzag Scan

The sequential zeros that occurs within each and every block are exploited with zigzag pattern. It normally start increasing from low-frequency to high frequency terms and the quantization will probably remove high frequency term in the quantization stage. This process will generally produce a more compressed output by positioning entropy for more order. The lower frequency components depict the steady luminance variations and are essential to the human visual system than the high frequency changes since human eye cannot note changes in higher frequency components. More zeros are expected to run after the quantization process where the important coefficients in the order of 8x8 blocks can be expected towards the end of the 8x8 block to enable more compression in the entropy [4]. Figure.2 displays the zigzag pattern. Data of 64 addresses that are organized in a zigzag pattern.

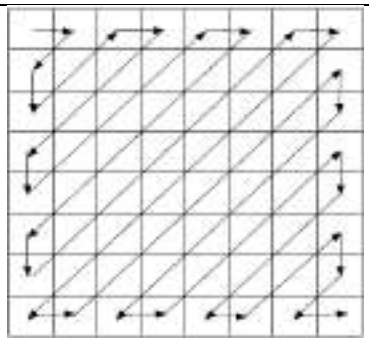

Fig. 2: Zigzag-sequence

Run Length Encoding RLE

RLE is used to encode the zero values contained in the AC coefficients by retaining the omitted value and this are the number of zeros and the next non-zero component.

Experimental Procedures

The Compression algorithm for medical image compression based on the DCT-VQ implemented using MATLAB is given in the following steps as the figure

1. Load the original image into MATLAB.
2. split the image into 8x8 blocks of pixels.
3. Process a DCT on every pixel block from left to right, Top to bottom
4. Then quantize each block of DCT coefficients using weighting functions in order to optimize for the human eye.
5. Differentiate the DC and AC coefficient.

 ISBN 978-9959-9703-2-9

6. Encode the resulting AC coefficients (image data) of Zig-Zag Scan using a RLE Encoding

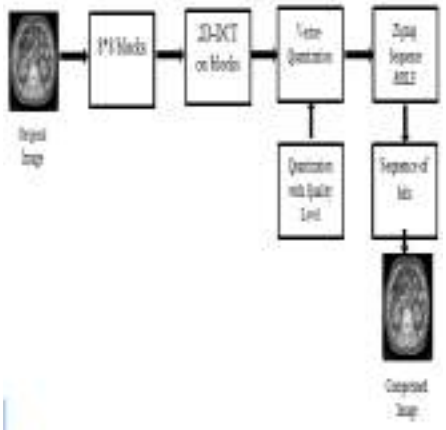

Fig. 3: The proposed algorithm of medical image compression

Implementation of Algorithm

Firstly the proposed algorithm is modelled and verified using MATLAB code as shown in the figure 4. Compression and reconstruction is performed and the performance is measured using several standard measurements for compression algorithm such as PSNR, MSE, CR, and BBP which are introduced in next topic.

Fig. 4: Implementation proposed algorithm on MATLAB environment

Image Quality Assessment Methods

Objectively, four most significant similarity measures are employed to compare the image that reconstructed after the process of compression algorithm with the actual image. It starts with the measure of PSNR and the next step is the measure of MSE whiles the third step and fourth step are the BBP and compression rate.

1. **Peak Signal to Noise Ratio**

PSNR measures the estimates of the quality of reconstructed image compared with the original image and is a standard Way to measure image fidelity. The PSNR can be evaluated as:

$$PSNR = 20log_{10}\frac{255}{RMSE} \quad (4)$$

2. **Mean Square Error**

The MSE is the cumulative squared error

 ISBN 978-9959-9703-2-9

between the compressed and the original image. This metric is applied as:

$$MSE = \frac{1}{NM}\sum_{i=1}^{N}.\sum_{j=1}^{M}\left(I_o(i,j) - I_{rec}(i,j)\right)^2 \quad (5)$$

$I_{original}$is the original image before the compression process and $I_{reconstructed}$ is the image after applying DCT algorithms and MxN is size of image , A lower value of MSE signifies lesser error in the reconstructed image.

3. Compression measures

The basic measure of the performance of a compression algorithm is the compression ratio *(Cr)* and is defined by equation.

$$\text{Cr} = \frac{\text{original data size}}{\text{reconstrucated data size}} \quad (6)$$

The higher the value of the compression rate will be worst image quality and vice versa.

4. Bit Per Pixel

The image quality is represented by the number of bits per pixel in the compressed image *(BBP)* which is defined as the total number of bits in the compressed image divided by the number of pixels. Moreover, bit per pixel BPP Can be calculated as 8 bit divided by compression ratio

$$\text{BBP} = \frac{\text{bits in the compressed image}}{\text{number of pixel}} \quad (7)$$

Results and Discussion

In this analysis, the proposed compression algorithm is conducted on CT scan and ultrasound images with different quality levels. These quality levels are from 10 to 90 scales. PSNR, MSE, CR, and BBP are used to evaluate the differenc between the original image and reconstructed image. In this paper , medical image compression quality was performed with five quality levels. These quality levels indicate that perfect reconstructed images is related with high quality level. However, inferior image quality came with low quality level due to colour depth is reduced and the detail of sections of the image are removed. Figure 5&8 illustrate the original image of CT scan and Ultrasound images with reconstructed images with different quality respectivly. Table 1&2 show that, if quality level is high the error measurements for reconstructed images were excellent and if quality level is low , image quality was inferior. The best value for PSNR at quality level 90. This parameter indicates that reconstructed image had no perceptual difference from the original. On the other hand, as shown in table 1&2 when quality level is decreased the error measurements start getting worse until a point is reached where it is easy to note perceptual difference from the original image. Table 1&2 illustrate that there is inverse relationship between PSNR and MSE because higher value of PSNR is good because it means that the ratio of signal to noise is higher. Here, the signal is the

 ISBN 978-9959-9703-2-9

original image, and the noise is the error in reconstruction. If compression scheme have a lower MSE and a high PSNR, you can recognize that it is a better. Figures 7&10 illustrate that there are proportional relationship between bit per pixel and PSNR. Because of bit per pixel indicates how much data can be recorded for each pixel. A high number of bits per pixel records more subtle gradations in colour so images are more accuracy and closer to original images. There are inverse relationship between bit per pixel and MSE, and proportional relationship between bit per pixel and PSNR. Because of bit per pixel indicates how much data can be recorded for each pixel.


(a) Original Image (b) Quality level 10


(c) Quality level 30 (d) Quality level 50


(e) Quality level 70 (f) Quality level 90

Fig. 5 : Original & Reconstructed CT Scan images with different Quality levels

Table 1: The Proposed Algorithm compression of CT Scan Image

CT scan Images				
Q	**PSNR**	**MSE**	**CR**	**BPP**
10	32.08	40.25	3.73	2.14
30	38.08	9.7	2.05	3.88
50	40.77	5.44	1.74	4.57
70	43.26	3.06	1.54	5.07
90	48.6	1.02	1.42	5.60

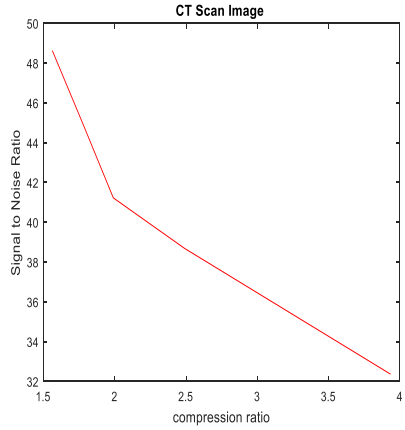

Fig. 6: The relationship between CR & SNR of CT scan

 ISBN 978-9959-9703-2-9

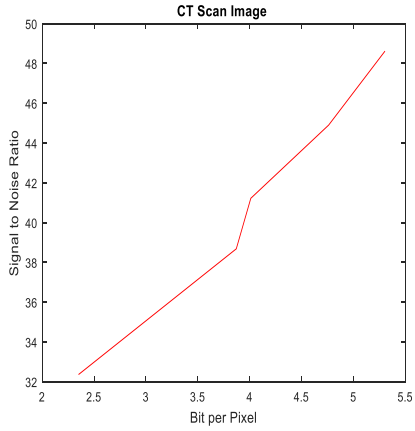

Fig. 7: The relationship between BPP &SNR of CT scan Scan Image

a)Original Image

(b) Quality level 10

(c) Quality level 30

(d) Quality level 50

(e) Quality level 70

(f) Quality level 90

Fig. 8: original & reconstructed Ultrasound Images with different quality level

Table 2: The Proposed Algorithm compression of Ultrasound Image

Ultrasound Images				
Q	**PSNR**	**MSE**	**CR**	**BPP**
10	32.7	34.7	3.77	2.11
30	38.5	9.17	1.97	4.04
50	41.08	5.06	1.73	4.62
70	43.59	2.84	1.59	5.01
90	48. 8	0.86	1.4	5.70

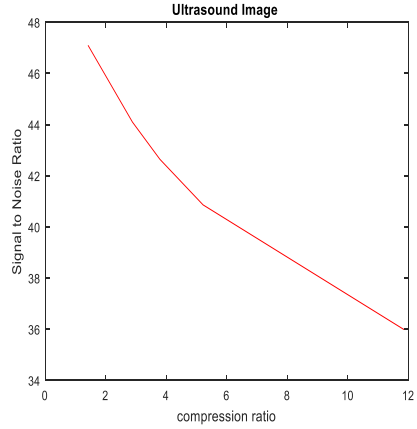

Fig. 9: The relationship between CR & SNR of Ultrasound Scan Image

ISBN 978-9959-9703-2-9

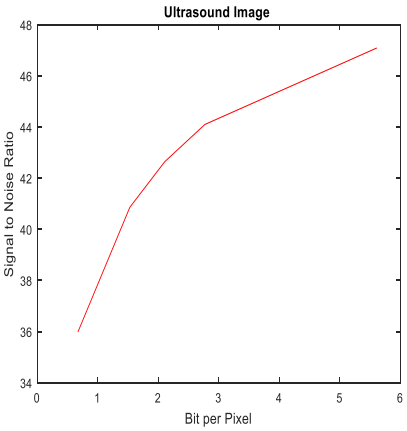

Fig. 10: The relationship between BBP & SNR of Ultrasound Scan Image

Conclusions

A successful algorithm has been applied for compressing of medical images. This paper was successfully compressed medical images using DCT and VQ techniques. These techniques were applied on two medical images as CT scan, and Ultrasound images. Compression of medical images was performed with five different quality levels. The performance of compression process was successfully using the proposed techniques namely as MSE, PSNR, BBP, and CR. From the experimental and mathematical results it can be deduced that the proposed algorithm produces a high PSNR with different quality levels.

References

[15] Mohta, J. (2015). Image Compression and Gamma Correction using DCT. T International Conference on Futuristic Trend in Computational Analysis and Knowledge Management (ABLAZE- 2015, 1(1).

[16] Kusuma, E. D., & Widodo, T. S. (2010). FPGA Implementation of Pipelined 2D-DCT and Quantization Architecture for JPEG Image Compression. IEEE.

[17] Trang, & Bihn, D. N. (2010). A High-Accuracy and High-Speed 2-D 8x8 Discrete Cosine Transform Design. Proceedings of ICGCRCICT, 1, 135–138.

[18] Jain, N., & Mishra, B. (2015). DCT and CORDIC on a Novel Configurable Hardware. 2015 IEEE Asia Pacific Conference on Postgraduate Research in Microelectronics and Electronics (PrimeAsia) DCT, 51–56.

[19] Wang, Y. L., Liao, C. Te, Su, A. W. Y., & Lai, S. H. (2010). Fingerprint compression: An adaptive and fast DCT-based approach. Proceedings - International Conference on Image Processing,ICIP,3109–3112.

[20] Zheng, W., & Liu, Y. (2011). Research in a fast DCT algorithm based on JPEG. 2011 International Conference on Consumer Electronics, Communications and Networks, CECNet2011-Proceedings,551–553.

[21] An, S., & Wang, C. (2009). A computation structure for 2-D DCT watermarking. Midwest Symposium on Circuits and Systems, (1), 577–580. https://doi.org/10.1109/MWSCAS.2009.5236026

[22] Li, Z., Sun, X., Du, C., & Ding, Q. (2013). JPEG algorithm analysis and application in image compression encryption of digital chaos. Proceedings - 3rd International Conference on Instrumentation and Measurement, Computer, Communication and Control, IMCCC 2013, 185–189.

 ISBN 978-9959-9703-2-9

المؤتمر الدولي الثاني للعلوم والهندسة
2nd International Conference on Science and Engineering
ICSE 2023
Faculty of Engineering - University of Bani Waleed
Bani Waleed, Libya

Paper Code: ICSE-028

DESIGN AND SIMULATION OF UHF RFID READER ANTENNA BASED ON GENERAL PURPOSE APPLICATIONS

Mohamed S. Alshulle[a], Maram A. Gomaa[b] and Jihan A Albendag[c]
[a]Military Industries Organization, Bani-walid, Libya.
[b]College of Science and Technology, Bani Walid, Libya.
[c]College of Science and Technology, Bani Walid, Libya.
*dr.engineeralshole@gmail.com

Abstract: The fast expansion of global manufacturing and commerce has led to an increasing need for the automated and univocal identification of goods everywhere in the globe. In this regard, radio frequency identification (RFID) technology has been developing as a suitable and more advanced substitute for barcodes. RFID technology is already being used in a wide range of everyday applications, and the on-metal tagging solutions that are currently available are thicker and significantly more expensive than conventional RFID tags. Additionally, it is currently difficult to create miniature RFID tags with uniform (or nearly uniform) reading patterns that would enable identification of small objects regardless of their orientation. As opposed to that,, The design of RFID tags with optimum reading distance is an intriguing study topic within the context of RFID technology since some applications demand maximizing the reading distance, even at the price of the tag dimensions.
The primary goal of this paper is to design a UHF RFID reader antenna for emerging identification and sensor applications. To better select the best antenna based on the application and design it, the antenna theory required for a reader designed for a particular application is investigated. By exploring antenna size reduction and optimization strategies, which leads to the creation of computer-aided simulations, , a brand-new UHF RFID reader with low cost and tiny size and high gain and directivity was invented. Despite being tiny, this antenna was nevertheless able to deliver an excellent free space read range performance. Analysis and measurement findings were explained, and HFSS was used to introduce antenna analysis.

Keywords: (Radio Frequency Identification (RFID) technology, Voltage Standing Wave Ratio (VSWR), Return Loss (S))

Introduction

RFID is a technology that is more reliable than a bar code and offers wireless identification and tracking capabilities. A reader is primarily a radio frequency (RF) transmitter and receiver, managed by a microprocessor or digital signal processor, and is now more frequently referred to as an RFID interrogator. Where an RFID tag receives electricity from it, an RFID reader emits electromagnetic signals. The circuits inside the microchip are subsequently powered by this energy. The chip modifies the waves and then transmits the

 ISBN 978-9959-9703-2-9

modified wave back to the reader. Where the reader can see the tag, this technique is known as backscattering. Antennas (for reader and tag) play a crucial part in RFID systems. The chip may broadcast the identification-related data thanks to the antenna. Since the tag antenna can be placed anywhere on the target, the reader antenna should have circular polarization characteristics. The system developer's main concerns have been shrinking the size of the UHF RFID reader antenna and increasing its gain.

Microstrip antennas are often used in telecommunications due to their many benefits, including their tiny weight, low volume, affordable production, and ability to operate at two or three frequencies simultaneously. Microstrip antennas, however, have a variety of drawbacks. These microstrip patch antenna's narrow bandwidth is a severe drawback [1], but by reshaping the antenna as a bow tie, it may be used as a great example of a frequency-independent antenna. And the primary reason for selecting this antenna is to include a new communication technology that is improved and effective for sophisticated applications.

1. This article describes the construction of a single band Bow-Tie Octagonal antenna for wireless communications and RFID readers that will resonant on the UHF RFID band of 860 to 960Mhz. HFSS simulation software is used to do the theoretical simulations. **Design of Bow-Tie antenna for UHF RFID Reader Application**

Antennas play a crucial role in radio transmission systems. The selection of an antenna is dependent on the requirements of the application, such as frequency, gain, price, coverage, weight, etc. Bow tie antennas are renowned for their beneficial qualities and multiband capabilities. An antenna's properties (such as its impedance, polarization, radiation pattern, etc.) will vary if its dimensions change even if it was constructed with ideal conductors and dielectrics. will not vary as long as the operating wavelength is altered by the same amount. As a result, if an antenna's shape is only dictated by angles, its performance would be independent of frequency since it would be scale-invariant [2]. A great illustration of a frequency-independent antenna is the bow tie. And the primary reason for selecting this antenna is to include a new communication technology that is improved and effective for sophisticated applications.

An antenna is built into the mobile UHF RFID device, also known as a hand-held RFID reader. The antenna needs to be significantly smaller than the typical reader antenna for these applications. With a 2-4 dBi antenna gain, the read range of handheld RFID scanners is really three to five meters. Applications requiring portable RFID readers have employed a variety of antenna designs. For the RFID reader in [2], two corner truncated stacked patches are employed. In this study, a straightforward modified bow-tie antenna is suggested for use with handheld, all-purpose RFID readers. The antenna is made up of two arms, a stepped transformer, and a bow-tie antenna..

2. Bow-Tie antenna dimensions calculation

The Bow-Tie antenna's [4] construction is straightforward since the antenna structure is entirely determined by its angle and length L1, Figure 1. The Bow-Tie antenna's length and degree of inclination both affect its impedance

 ISBN 978-9959-9703-2-9

and operational bandwidth.

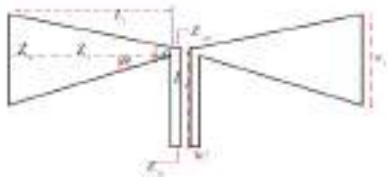

Fig. 1: Conventional Bow-Tie antenna geometry.

Following formula/equations are used in the Bowtie Antenna Calculator.
Wavelength $\lambda = c/f$
Length in mm: $L=0.375x\lambda.= 125.$
Width in mm: $w=0.25x\lambda=83.3.$

3. Optimization of antenna design workflow

This study starts by modeling and optimizing a traditional printed bowtie antenna supplied by a coaxial wire. The intended parameters, however, cannot be met since the greatest size of the substrate is less than a fourth of the working wavelength. Then, significant low values of VSWR at the operational frequency are acquired by introducing and modifying adjustments to the antenna's shape, and an omnidirectional gain is achieved. The gain of a conventional printed bowtie antenna is maintained since the introduced alterations do not impair the antenna's radiating pattern. The overall process for the antenna design is as follows.

1. Create a Traditional Bow-Tie antenna as indicated in Figure (2) without using a typical ground plane.

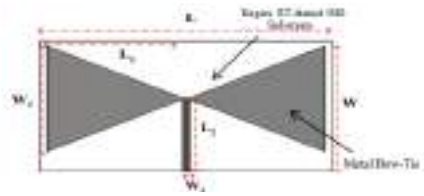

Fig. 2. Traditional Bow-Tie antenna.

2. Improve the standard bowtie antenna.
3. Add rounded arms to the traditional bowtie antenna, as illustrated in Figure 3, to lower the size by 40%.

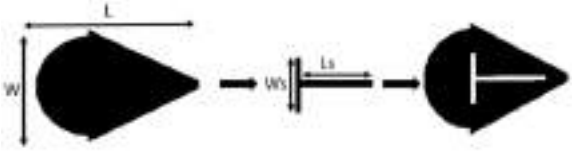

Fig. 3. Rounded Bow-Tie antenna.

Table1. Traditional Bow-Tie antenna parameters at 900 MHz.

L	W	Ls	Ws
54.2	39.4	28	20

4. Add a T slot to the radiating arms of the conventional bowtie antenna, as illustrated in Figure (4), as the initial alteration.

Fig. 4. Proposed Bow-Tie reader antenna geometry.

5. Modify the settings of the two modifications introduced to boost the performance of the antenna and meet its requirements. The performance and handling requirements of the antenna.

Utilizing the Ansys HFSS software, all computational models were created. Figure (5) displays the final dimensions following simulation and optimization.

ISBN 978-9959-9703-2-9

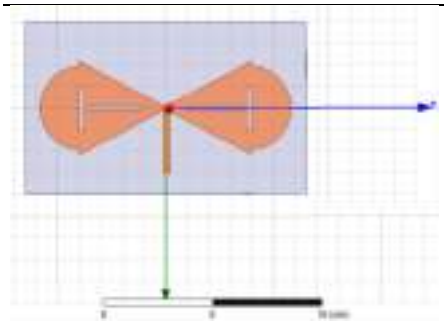

Fig. 5. View of Bow-Tie reader antenna, dimensions (mm).

In HFSS, the published structure is implemented. To acquire the scattering parameters, the required simulations are run. The collected findings lined up with the data those had been published, completing the antenna validation.

3.2 Simulated Results

For designing, simulation is employed, which is quite common for designing antennas. Antenna gain, total directivity, return loss, VSWR, current distribution, and radiation patterns are only a few of the simulated graphs that are created and displayed in the images. Using electromagnetic full wave simulation (HFSS), this has been verified.

a- Antenna Return Loss

Figure (6) displays the 2x1 microstrip antenna array's simulated reflection coefficient.It is clear that the reported antenna has a bandwidth that ranges from 838 MHz to 1 GHz and can operate in the band (under -10 dB) at centered 900 MHz (-20.98 dB). Therefore, it is evident that this working spectrum complies with UHF RFID's design specifications.

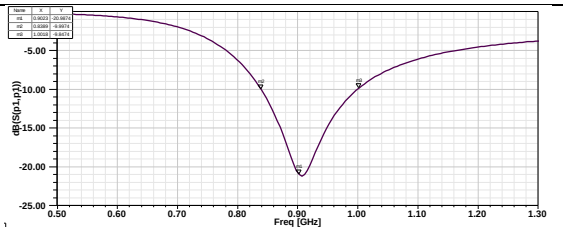

Fig. 6. Simulation results of the Bow-Tie reader antenna.

b- Voltage Standing Wave Ratio (VSWR)

Figure (7) depicts the UHF RFID antenna's VSWR. At 900 MHz, we recorded 1.18 dB with excellent values, indicating good received signals.

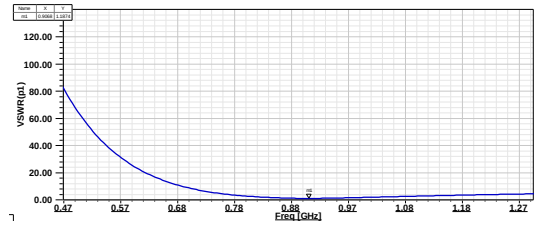

Fig. 7. VSWR of the Bow-Tie reader antenna.

c- Radiation Pattern in 3D

Figure (8) displays the radiation patterns for the UHF RFID design reader antenna array.

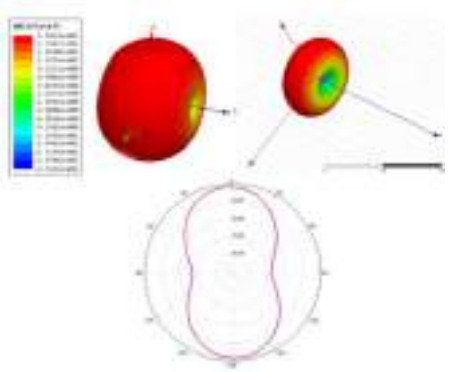

Fig. 8. 2D and 3D radiation pattern of the Bow-Tie reader antenna.

ISBN 978-9959-9703-2-9

Since the antennas are patch type, they exhibit directional radiation patterns in the phi=0 deg (x-y plane) and phi=90 deg (y-z plane) planes. There is a directional pattern on the antenna.

c- Gain and Directivity

The intended antenna radiates with a gain of 2.21dB and a directivity of 2.22dB in the broadside direction. Figure (9) below shows 3D far field plots for gain and direction. The gain and directivity of the antenna are good.

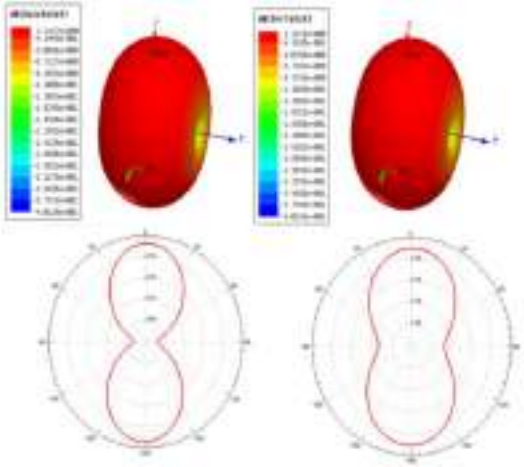

Fig. 9. 2D and 3D of Gain and directivity of the Bow-Tie reader antenna.

f- Current Distribution on the antenna

The field distribution between the patch and the ground plane is referred to as the current distribution, and it is utilized as a gauge for the radiation from microstrip patches. The 900 MHz current distribution pattern is seen in Figure (10). At this frequency, the maximum current in the proposed antenna is 40 (A/m). The red arrows depict the strongest current distribution in the antenna patch.

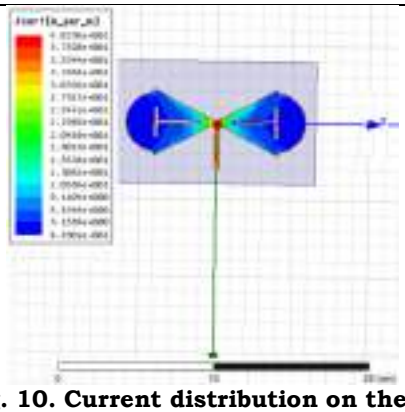

Fig. 10. Current distribution on the Bow-Tie reader antenna.

4. Conclusion

The following observations are reached in light of the simulation findings presented in this article. This study provided an illustration of the UHF RFID band RFID reader antenna design method. Despite the recent surge in popularity of RFID technologies, there is still a sizable gap in the appropriate design of tags depending on particular applications or uses, such as inventories, apparel, medications, etc. Optimal reader performance parameters, such as read range, antenna radiation, gain, and antenna efficiency, among others, are the major challenge that antenna designers must solve.

This study offers a systematized RFID reader antenna design process to close this gap. Because Bow-Tie antenna have been a fast expanding area of study due to its light weight, compact size, and simplicity of manufacture, a small reader antenna for UHF-RFID applications has been described. In this study, a Bow-Tie antenna that increases gain and directivity is constructed, and the effects of adding T-shape slots for a UHF RFID reader are explored. For the UHF band, the return loss was less than 10 dB (-20.9 dB). The value of the radiation pattern changes to be directional once the slot is added, with a gain of 2.21 dB and a dircativity of 2.22 dB. also

ISBN 978-9959-9703-2-9

When compared to conventional antennas, the projected size decrease is roughly 40It can be readily and cheaply manufactured. By using a substrate material with a low dielectric constant, the antenna is small and thin. These qualities are notably helpful for RFID applications and the mobility of wireless communication equipment throughout the world.

References

[23] T. Beijing, "A Design of Phased Array Antenna Based on the Vivaldi Antenna," pp. 334–337, 2010.

[24] M. Tegegn, "Design and Analysis of a 28 GHz Microstrip Patch Antenna for 5G Communication Systems", International Research Journal of Engineering and Technology (IRJET) e Volume: 08 Issue: 02 | Feb 2021.

[25] G.J.Foschini, "Layered space-time architecture for wireless communication in a fading environment when using multi element antennas",BLTJ, Autumn, 1996.

[26] Primer "Wi-Fi: Overview of the 802.11 Physical Layer and Transmitter Measurements", Copyright © 2013,

[27] P. Ngocle, "Antenna selection for energy effivent MIMO OFDM wirless systems ", university of wollonogong thesis collection, 2015.

C. A. Balanis "Antenna Theory Analysis and Design", John Wiley & sons, inc., Publication, 3rd Edition, ISBN: 0-471-66782, 2005.

 ISBN 978-9959-9703-2-9

المؤتمر الدولي الثاني للعلوم والهندسة
2nd International Conference on Science and Engineering
ICSE 2023
Faculty of Engineering - University of Bani Waleed
Bani Waleed, Libya

Paper Code: ICSE-029

METAMATERIAL BASED HIGH ISOLATED FOUR PORT MIMO ANTENNA FOR 5G SMARTPHONE APPLICATIONS

Mohamed S. Alshullea, Areej. M. Ahmeidb and Hana. R. Matouqc
aMilitary Industries Organization, Bani-walid, Libya.
*dr.engineeralshole@gmail.com

Abstract: The growth of mobile communications has considerably expanded the number of linked devices. Lack of efficient and small antenna components is one of the most frequent causes of this. The demand for more effective and efficient mobile terminals has substantially risen as a result of the growing number of linked devices and the requirement for high-speed wireless communication. A conventional Multiple Input Multiple Output MIMO antenna system only functions as an antenna array if the coupling between the components is high. However, it is well recognized that this technology has a flaw, and that flaw is the coupling between the various components of the system. In the event that there is a strong connection between the radiating elements, a MIMO antenna system just functions as an antenna array. Because of this, To take use of MIMO technology's advantages, there needs be a significant decoupling between the radiating parts. This paper's major goal is to research and construct printed multi-port MIMO antenna designs with integrated decoupling strategies for 5G smartphones. The excellent electromagnetic characteristics of these materials have drawn a considerable deal of interest in recent years. These substances are man-made structures that display traits not seen in nature. By regularly merging artificial structures, a metamaterial may be created. Additionally possessing lending qualities, metamaterials are known to enhance antenna gain and high isolation coupling when put next to them.
The findings from simulation and measurement are well-coordinated. The suggested structure would work with mm-wave 5G applications in the 28 GHz frequency region. Additionally, the operational frequency band's max gain is 9.14 dB. Metrics of MIMO performance such the Envelope Correlation Coefficient (ECC), Mean Effective Gain (MEG), and Channel Capacity Loss (CCL), Analysis of the suggested structure's diversity gain (DG) The final design incorporated a size/performance trade-off in favor of shrinking the structure's size to enable its application in smaller size devices. and the outcomes show that the design is suitable as a possible competitor for MIMO 5G Smartphone applications. Using Ansoft HFSS, the suggested antennas' simulation was performed.

Keywords: (Multiple Input Multiple Output (MIMO), Voltage Standing Wave Ratio (VSWR), Return Loss (S))

Introduction

RFID technology offers wireless communication. The shift from 4G to 5G technology is now taking place in the realm of mobile communication technology. Users' needs for better wireless communication services are being driven by the fast increase of mobile data. Information must be accessible promptly and quickly, transmission efficiency

 ISBN 978-9959-9703-2-9

must be increased, and system security must be improved. As a result, 4G is gradually beginning to fall short of the increased communication requirements, and its flaws are becoming more apparent. From 2020, When 5G reached the commercial stage, it indicated that it was progressively taking over as the standard mobile communication technology. Its frequency range includes the mm-Wave band (24.25-54.6 GHz) and sub-6 GHz (450 MHz-6 GHz). High-speed data transfer and dependable connectivity with minimal latency are the key characteristics of 5G [1]. Furthermore, the 5G user's positive Quality of Experience (QoE) are necessitates superior antenna diversity and increased channel capacity.

Diversity systems with two receivers were created as a solution to multipath effects' signal fading, and thus marked the beginning of the development of MIMO. Studies already conducted [4,5] have demonstrated that, in comparison to simple input simple output (SISO) systems with a straightforward layout as illustrated in Figure (1), MIMO systems include several extra pathways, and by reducing multipath impact, latency, and packet loss, the communication modes may be improved. Additionally, Shannon's theorem states that the signal-to-noise ratio (SNR) and channel bandwidth affect the channel capacity. Additionally, because to the multi-port architecture, MIMO systems have shown the ability to double data throughput with a fixed bandwidth and transmission power [2]. As a result, researching MIMO systems is crucial to creating 5G communication systems.

Fig. 1. Block diagram of MIMO wireless system.

One of the greatest electromagnetic revolutions of the 20th century has been predicted by the emergence of metamaterials. Human-made composite materials known as metamaterials enable the customization of electromagnetic and acoustic wave propagation through media. The geometrical arrangement of its constituent parts, sometimes referred to as "meta-atoms," controls a significant portion of the mechanical or electrical response of these artificial structures, much like crystals and protein chains. The most remarkable feature of met materials is their ability to be created with unusual properties that are rarely seen in nature [2], such as artificial magnetism (magnetism without naturally magnetic materials), negative-refractive indices from positive-index materials, and invisibility cloaking (or "invisible" materials that do not interact with light).

As a result, the design difficulties and characteristics for obtaining high channel capacity with minimal complexity pique the interest of the researchers and serve as a motivator for the study and design of multiport MIMO antennas using met-materials for high data rate 5G applications.

This study describes a compact four antenna system for wireless multi-port MIMO applications. Each of the six antennas in the proposed MIMO antenna works at 28 GHz. Each antenna element is created using a single composite right/left unit cell. A novel strategy relies on current cancellation between the antennas to reduce mutual coupling without the use of extra structures. The suggested antenna has been evaluated for its high

 ISBN 978-9959-9703-2-9

isolation, compact size, low cost, and characteristic evaluations of the prototype antenna array's return loss (RL), bandwidth, isolation, VSWR, and radiation pattern.

1. Metamaterials

Because the wave vector, electric-field, and magnetic-field vectors constitute an LH system, metamaterials are often referred to as DNG or LH media. This name was originally used by Veselagoin 1968 [3]. Veselago noted that LH metamaterials (LHMs) exhibit certain unusual features, including the inverse Snell effect, an inverse Doppler shift, and backward-directed Cherenkov radiation in his groundbreaking study [3]. LHMs also have simultaneous negative permittivity and permeability. However, because there weren't any resources that could be used to make his idea until 1999. essential features of In the next subsections, LHMs are described and contrasted with those of conventional materials.

Metamaterials (MTMs) are substances that have been designed to generate electromagnetic characteristics that are rare or challenging to get in nature. Due to their assurance that they will provide permittivity ε, permeability μ and index of refraction, The potential use of metamaterials in several electromagnetic applications has sparked widespread attention. owing to their special electromagnetic characteristics, which include zero propagation constant at non-zero frequency, anti-parallel phase and group velocities, and so on.

The idea that materials with simultaneously negative permittivity and permeability are technically possible and have a negative index of refraction was put up by Russian scientist Victor Georgievich Veselago in the 1960s. These media were given the label "left-handed" by Veselago because they produce a left-handed triplet rather than the right-handed triplet that is produced by traditional right-handed media (RHM) [3].

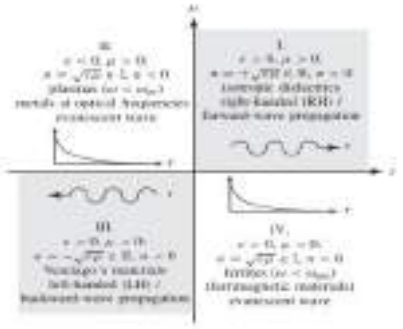

Fig. 2. The possible combinations of permittivity and permeability, [32].

The characteristics of the materials involved affect how a system reacts to the presence of an electromagnetic field. By describing these materials' macroscopic qualities like permittivity and permeability, these properties are characterized. using permeability and permittivity.

2. Design of a CRLH Unit-Cell (Interdigital) Antenna

We take into consideration the unit cell depicted in Figure (3.4) in order to extract the parameters L_R C_R L_L and C_L in the CRLH implementation of Figure (3).Figure (3) (a) depicts the equivalent circuit of this unit cell, which is made up of a series connection between the interdigital capacitor and the shorted stub inductor, while Figure (4) (b) depicts an additional T-network that will be utilized for extraction. The interdigital capacitor's and the stub inductor's scattering parameters are first calculated independently using either measurement or full-wave modeling. To do this, a brief piece of microstrip TL must be inserted at each end of the component to guarantee the extinction of the higher-order modes caused by the discontinuity in the transition from the coaxial connection to the microstrip. because phase is

 ISBN 978-9959-9703-2-9

connected to the most significant characteristics of MTMs. [4].

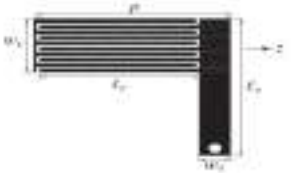

Fig. 3. Unit cell of the microstrip CRLH TL.

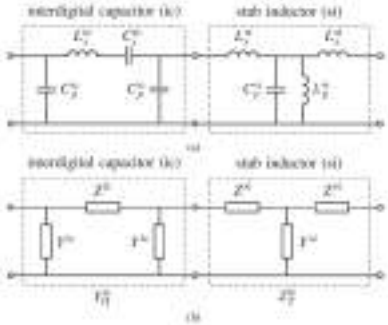

Fig. 4. Circuit models for the parameters extraction of the unit cell. (a) Equivalent circuit. (b) Auxiliary equivalent π and T networks.

the calculations for the ZOR antenna design's original unit cell model. The arrangement was changed several times to get the desired outcome, as illustrated in Figures (5) and (6).

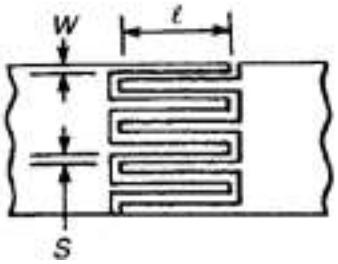

Fig. 5. Layout of the Interdigital Capacitor [34].

To calculate the Interdigital Capacitor values, we use the below equation [5].

$$C(pF) = \frac{\varepsilon_e 10^{-3} K(k)}{18\pi K'(k)} (N-1)l \quad (1)$$

where:

K(k): is the complete elliptic integral of the first kind

K: Complementary Function of K

$k = \tan^2(\frac{a\pi}{4b})$

$a = W/2$

$b = (w+s)/2$

$K' = \sqrt{1-K^2}$

$$\varepsilon_e = \begin{cases} \frac{\varepsilon_r+1}{2} + \frac{\varepsilon_r-1}{2}\left[\frac{1}{\sqrt{1+\frac{12h}{W}}} + 0.04\left(1-\frac{W}{h}\right)^2\right] & \text{for } \frac{W}{h} < 1 \\ \frac{\varepsilon_r+1}{2} + \frac{\varepsilon_r-1}{2}\left(\frac{1}{\sqrt{1+\frac{12h}{W}}}\right) & \text{for } \frac{W}{h} > 1 \end{cases} \quad (2)$$

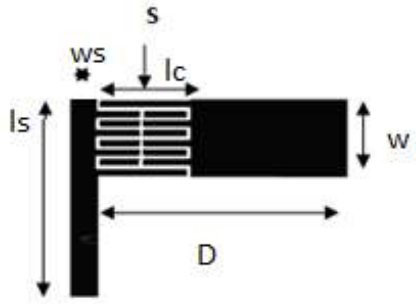

Fig. 6. Proposed unit cell of the microstrip CRLH TL.

1. Choose center frequency, fo, which represents broadside radiation. (fo=28 GHz)
2. Calculate width required to obtain Zo, set w to this value. (w=5.0 mm).
3. Set stub width, ws, to 20% of w. (ws=1.0 mm).
4. Set stub length (ls=li- w) to w; the electrical length of the stub has to be less than ʎ /2.
5. Set the number of fingers, N, to 6 or 10. Then determine required wc and S=2wc/3. N=6 chosen.

$$w_c \simeq \frac{w}{\frac{5N}{3} - \frac{2}{3}} \simeq 0.39mm$$

ISBN 978-9959-9703-2-9

$$S = 0.26\text{mm}$$

6. Calculate length of interdigital finger.

$$l_c \simeq \frac{\lambda_g}{8} \simeq \frac{c_0}{8f_0\sqrt{\varepsilon_r}} \simeq 8.15\text{mm}$$

After optimization, the geometric parameters are carefully modified. Antenna's actual dimensions are 2.45 mm x 8.21 mm. The final dimensions are displayed in Figure (7) following simulation and optimization using HFFS Software.

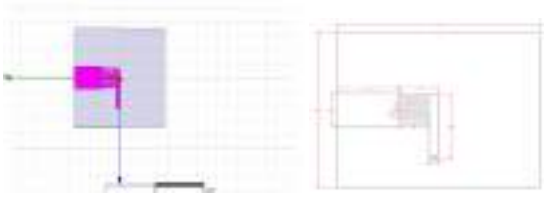

Fig. 7. Geometry Structure of proposed CRLH Antenna in (mm).

The outcomes for the solitary antenna. To verify the simulated outcomes produced by the HFSS software.

a- Antenna Return Loss

The suggested 28 GHz antenna's return loss in dB is illustrated in Figure (8). The simulated return loss (reflection coefficient) of the CRLH antenna demonstrates that it can operate (under -10 dB) with a 28 GHz center frequency and a -17.8999 dB bandwidth (FBW16.79%). This indicates that the antenna uses the 5G band.

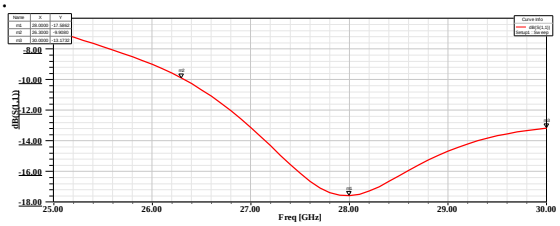

Fig. 8. The reflection coefficient of CRLH antenna.

b- Voltage Standing Wave Ratio VSWR

Figure (9) displays the planned single antenna's VSWR. At 28 GHz, we found 1.3 dB with excellent values, indicating good received signals.

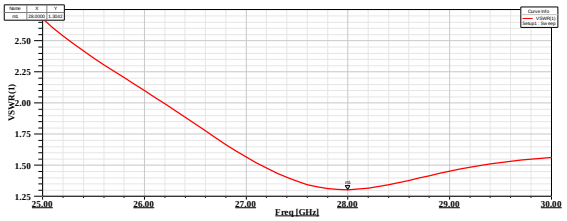

Fig. 9. VSWR of 28 GHz CRLH single antenna.

c- Radiation Pattern

The proposed antenna's simulated 2D and 3D, xz-plane and yz-plane radiation patterns are shown in Figure 10 for the 28 GHz frequency. The developed antenna exhibits good broadside radiation patterns in the xz-plane and yz-plane, as illustrated in Figure (10). The intended antenna emits energy in a focused beam.

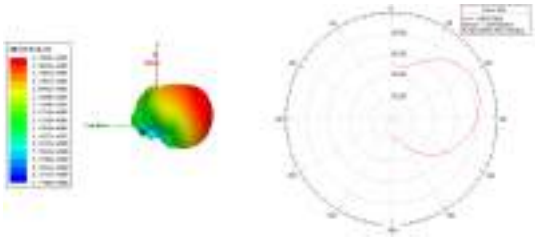

Fig. 10. 2D and 3D radiation pattern of the proposed 28 GHz CRLH antenna .

d- Gain and Directivity

With a gain of 9.149 dB and a directivity of 9.259 dB, the proposed antenna emits a directed beam of radiation. Figure(11) below shows 3D far field plots for gain and directivity. Because of the antenna's strong gain and directivity, its efficiency is 98.8%.

ISBN 978-9959-9703-2-9

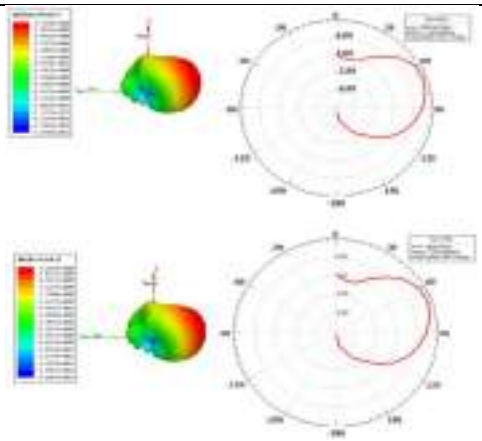

Fig. 11. Gain and directivity of 28 GH the antenna.

f- Current Distribution on the CRLH single antenna

The field distribution between the patch and the ground plane is referred to as the current distribution, and it is utilized as a gauge for the radiation from microstrip patches. The red arrows in Figure (12), which depicts the current distribution pattern at 28 GHz, indicate the strongest current spread in the antenna patch.

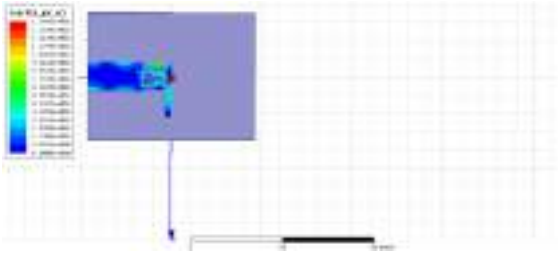

Fig. 12. Current distribution of the CRLH antenna.

From the CRLH single antenna findings (proposed antenna), it can be shown that the antenna performs well at 28 GHz, has a high gain and a directed beam, and is less in size than a typical microstrip antenna—by more than 40%.The multi-port MIMO antenna design for 5G smartphones works well and is suited for this size.

4. Design of a Metamaterial Multi Port MIMO Antenna (28 GHz)

Figure (13), which depicts the suggested MIMO antenna's construction. By emphasizing the arrangement of components in an orthogonally symmetric way with various inter-element spacings, the four-port MIMO design development is primarily accomplished. The dimensions of the MIMO antenna are 37371.6 mm3 for a 0 mm edge-to-edge separation (d) between the components. Each MIMO antenna component on the opposing sides of substrate, They make up a structural block and are generally used in 6.5-inch smartphones. They are positioned at one of the four corners of the RT-Duroid 5880 dielectric substrate (loss angle tangent: 0.02, relative permittivity: 2.2). Because the feed line (orange) and ground (blue) are made by printing copper on the front and back of the substrate, it is sometimes referred to as a printed circuit board (PCB). We included an interdigital to lower the mutual coupling and return loss. It should be emphasized that every antenna component is symmetrical in every way. Contrary to the structure used in earlier investigations, which had a CRLH metamaterial TL etched on the dielectric substrate's front surface, the feeding technique results in a dual-polarized radiation characteristic. The prototype of the suggested antenna is simulated and optimized using HFFS Software to validate this simulation. Each antenna component is made to function in the 28 GHz range. One of the most promising bands for 5G communication is this one. Modern Smartphone devices may make advantage of the MIMO antenna that is being suggested.

An antenna's final performance is optimized by carefully adjusting the geometric characteristics. Antenna's physical dimensions are 76x169x1.6 mm3. Figures (13), and Figure (14), which display the final dimensions

 ISBN 978-9959-9703-2-9

following simulation and optimization using HFFS Software.

Fig. 13. Layout of the multi port MIMO antenna of CRLH MIMO antenna.

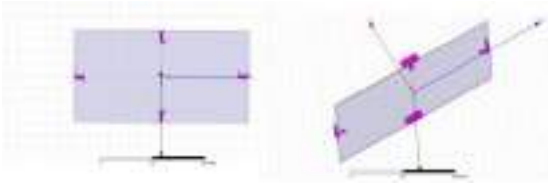

Fig. 14. Geometry structure of proposed MIMO antennas.

In HFSS, the published structure is implemented. To acquire the scattering parameters, the required simulations are run. The collected findings lined up with the data that had been published, completing the antenna validation. The outcomes for the solitary antenna. in order to verify the computer-simulated outcomes produced by HFSS software.

a- Antenna Return Loss (reflection coefficient) and mutual coupling

Figure (15) shows that the return loss values for S11, S22, S33, and S44 have reached the target value of less than -10 dB, which is centered at 28 GHz with -12.76, -12.5, -12.4, and -12.33 dB, bandwidth that ranges from 2.05 GHz to 2.2 GHz, indicating that the antenna is operating at 5G band.

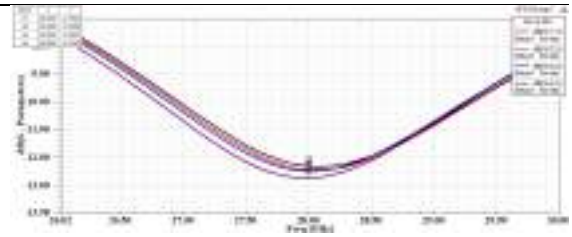

Fig. 15. The Reflection coefficient (S11S22, S33, and S44) of the 4-Port 28 GHz MIMO antenna.

However, the corresponding observed isolation parameter values for S12, S13, S14 and S41, S42, S43,... etc ranged from -44.5 dB to 51 dB at the 28 GHz resonance frequency, as shown in Figure (16). The minimum isolation between the ports in the simulated frequency range is more than -51 dB. The manufacturing mistake and port/cable coupling losses that caused the difference in these data indicate that high isolation was achieved.

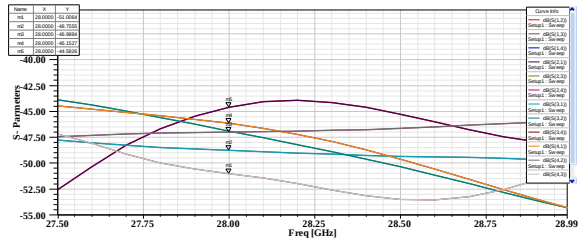

Fig. 16. The Mutual Coupling (S12, S13, and S14) and (S41, S42, and S43) (S21, S23, and S24) and (S31, S32, and S34) of 4-Port 28 GHz MIMO antenna.

b- Voltage Standing Wave Ratio (VSWR)

The measured isolation parameters VSWR-1, VSWR-2, VSWR-3, and VSWR-4 at 28 GHz resonant frequency match to the values of 1.59, 1.62, 1.62, and 1.63 in Figure (17), which depicts the VSWR for 4G-LTE MIMO antenna. This indicates well received signals

ISBN 978-9959-9703-2-9

when the values are good.

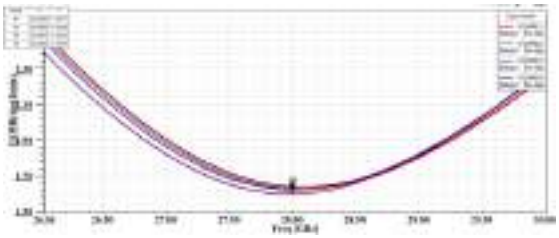

Fig. 17. VSWR (1,2,3,4) of the Proposed MIMO Antenna.

c- Radiation Pattern Gain and Directivity of the Proposed MIMO Antenna

Antenna 1 is terminated with 50 impedances, while the other three elements are produced with far-field patterns in an anechoic room. Due to the proposed antenna's symmetry, port 1 is measured because other ports produce the same patterns when activated. Figure (18) depicts the radiation patterns for the proposed MIMO antenna for the 5G frequency. Since the antennas are patch type, the radiation patterns in the phi=0 deg (x-y plane) and phi=90 deg (y-z plane) planes are directional as would be expected.

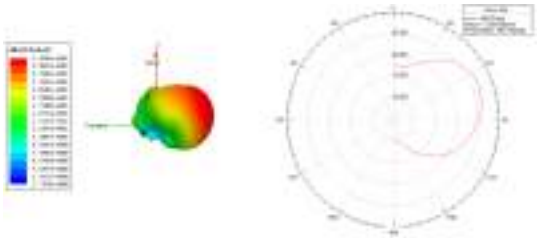

Fig. 18. 2D and3D Radiation Pattern of the Proposed MIMO Antenna.

For Ant.1, Ant.2, Ant.3, Ant.4, the suggested design shows a simulated peak gain value of 9.149 dB and the directivity of 9.259 dB. The antenna efficiency is around 81%. Figure (19) below shows the 2D and 3D far field plots for the planned antenna's gain and directivity. The antenna's gain and directivity are also good.

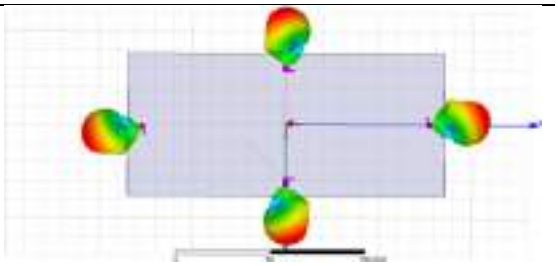

Fig. 19. Gain and Directivity of the proposed 28 GHz MIMO antenna .

d- Current Distribution and E-field on the proposed MIMO Antenna

Investigating the surface current density allowed for a deeper analysis of the reported MIMO antenna system's radiating process. Investigating the antenna components that affect radiation characteristics and clarifying the degree of connection between various MIMO antennas were the main goals of this study. When port 1 is enabled at 28 GHz, the surface current distribution is shown in Figure (20). The feed line and the margins of the slot-shaped antenna are where the current is most heavily concentrated. Additionally, the ground's rectangular holes show a noticeable current dispersion. The metamaterial in radiation behavior is established by this. Additionally, as seen in Figure 20, the metamaterial makes the concentration of the coupling current between MIMO antennas minimal.

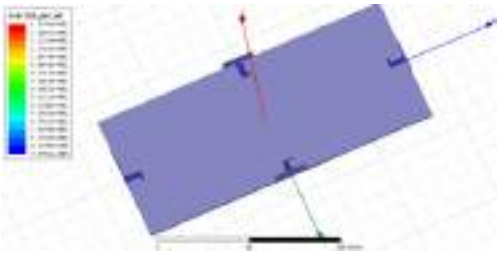

Fig. 20. Current distribution on the proposed 28 GHz MIMO Antenna.

ISBN 978-9959-9703-2-9

5.MIMO Performance Parameters The parameters, which have been studied to analyze the performance of MIMO antennas include.

1- Envelope Correlation Coefficient 'ρ' (ECC)

The degree of coupling between various antenna components in a MIMO system is measured using the envelope correlation coefficient (). The performance of the decoupling increases with decreasing envelope correlation coefficient value. Ideally, it is 0, but in reality it is less than 0.5. Higher isolation results from a lower ECC value, which improves diversity performance. In [5], formula expresses the S parameters based on the suggested four-port MIMO antenna's calculated ECC of 0.3.

2- Total active reflection coefficient (TARC)

One of the diversity parameters used to verify the accuracy of the observed S parameters is the TARC. Random signals and their phase angles for adjacent and diagonal ports are involved. Additionally, for specific phase angles between ports, it confirms the true behavior of the isolation parameters S12, S13, and S14. Efficiency and bandwidth will be impacted when all antenna components are used in MIMO at once. Therefore, the TARC is a reliable tool for determining the MIMO system's performance over S parameters. When the first port is kept constant while the input signals of the other three ports are stimulated with phase variations between 0 and 180, TARC is monitored. According to calculations, TARC is 27 dB for 28 GHz. This guarantees steady TARC and shows little mutual coupling between the ports.

3- Diversity Gain (DG)

For the MIMO arrangement, diversity gain illustrates "the loss in transmission power when diversity schemes are performed on the module." included in source [5]. According to calculations, the DG is around 9.2 dB across the band, which guarantees that the antenna will perform well in terms of diversity.

4- Channel Capacity Loss (CLL)

The number of radiators in a MIMO system enhances the channel capacity without increasing bandwidth or transmitted power levels. However, interference between the components reduces capacity. CCL can only go as fast as 0.4 bits/s/Hz. CCL was added to the list of MIMO performance characteristics, giving information on the system's channel capacity losses due to the correlation effect. Equations from [5] are used to quantitatively compute the CCL. Calculation shows that the obtained CCL for the proposed MIMO antenna is less than the realistic requirement of 0.4 bit/s/Hz over the entire 28 GHz operating spectrum, ensuring the proposed system's high throughput.

6. Conclusion

This work introduces a unit cell antenna based on metamaterials methods. First, a discussion and design for a single antenna have been made. It has been claimed that good optimization, good matching, and a typical radiation pattern across the antenna MIMO. The findings support a good compromise between the radiation pattern and reflection coefficient that generated a frequency range with good matching properties starting at around 28 GHz. The minimum value of VSWR is around 1.3 at 28 GHz, and the bandwidth ranges from 26.3 GHz to 31 GHz (FBW16.79%). The reflection coefficient S11 is -17.8999 dB. The suggested MIMO antenna has a directedness of 9.25 dB and a gain of 9.14 dB, indicating strong reception signal and a directional beam radiation pattern. The

 ISBN 978-9959-9703-2-9

suggested antenna's benefits include compactness (8x3x1.6 mm3 in dimension, a size decrease of about 60%). Additionally, it is pretty obvious that the suggested antenna operating band complies with the 5G standard operating frequency design criteria.

The primary goal of the study is to propose and analyze a 4-port MIMO antenna for 5G smartphone designs with good isolation. The suggested shaped construction produced high isolation performance. Four antennas make up the construction of the proposed MIMO antenna. Each of the four corners of the RT-Duroid 5880 dielectric substrate (relative permittivity=2.2, antenna elements on opposing sides form a structural block) is occupied by an antenna element. loss angle tangent is 0.02). The substrate has a 1.6 mm and is commonly utilized in the Infinix 8 Smartphone. the gain is 9.25 dB, the directivity is 9.14 dB, and the reflection coefficient S11 is -12.76 dB, which indicates a good reception signal and directed radiation pattern for each port. Metamaterials are used to enhance gain and directivity. The advantages of the suggested antenna include compactness, which results in a size reduction of about 60%. Additionally, the developed antenna provides improved values for the observed isolation parameters S12, S13, and S14 between the two ports at operating frequencies, ranging from -44.5 dB to 51 dB at 5.06 GHz resonant frequency. Without the use of any additional structure such as DGS or parasitic elements, the orientation of the interdigital capacitor has reduced the mutual coupling between two antennas, demonstrating the effectiveness of metamaterials in reducing the electric field distributed between antennas. The concentration of the coupling current between MIMO antennas is negligible as a result of the metamaterials' structural design. Additionally, the proposed system's high throughput is guaranteed by the MIMO performance metrics, which include the envelope correlation coefficient (ECC) of 0.3, diversity gain (DG) of 0.92 dB, total active reflection coefficient (TARC) of -27, and channel capacity loss (CCL) of less than 0.4 bit/s/Hz. The suggested antennas are simple and inexpensively fabricatable. Utilizing a substrate material with a low dielectric constant, the suggested antenna is small and thin. All simulations in this study have been carried out using the electromagnetic program Ansoft HFSS, making it clearly evident that these properties of the proposed antenna operating at 28 GHz band fulfill the design criteria of 5G standard operating frequency.

References

[1] E, Ezhilarasan. And M. Dinakaran,“A Review on Mobile Technologies: 3G, 4G and 5G,”, 2nd International Conference on Recent Trends and Challenges in Computational Models, India, February 2017Primer “Wi-Fi: Overview of the 802.11 Physical Layer and Transmitter Measurements", Copyright © 2013,

[2] M. Jensen,“A history of MIMO wireless communications,”. In Proceedings of the 2016 IEEE International Symposium on Antennas and Propagation, July 2016.

[3] V. Viktor, “The electrodynamics of substances with simultaneously negative values of and μ.”, Soviet Physics, 2016.

[4] M. Alibakhshikenar, “A Comprehensive Survey of “Metamaterial Transmission-Line Based Antennas: Design, Challenges, and Applications”, IEEE ACCESS.2020.

[5] C. Caloz and T. Itoh, “Electromagnetic Metamaterials: Transmission Line Theory and Microwave Applications”. New York: Wiley, 2004.

 ISBN 978-9959-9703-2-9

المؤتمر الدولي الثاني للعلوم والهندسة
2nd International Conference on Science and Engineering
ICSE 2023
Faculty of Engineering - University of Bani Waleed
Bani Waleed, Libya

Paper Code: ICSE-031

DESIGN AND IMPLEMENTATION OF 2X1MICROSTRIP PATCH ANTENNA ARRAY FOR WITH PARASITIC ELEMENT STRUCTURE ISOLATION FOR 4G APPLICATIONS

Lubna. A. Attelisi[a], Mohamed, S, Alshulle[b], and Belqees. M. Hanad[c]
[a]College of Electronic Technology, Bani-walid, Libya.
[b]Military Industries Organization, Bani-walid, Libya.
[c]College of Electronic Technology, Bani-walid, Libya.
*dr.engineeralshole@gmail.com

Abstract: For 4G-LTE applications, this study presents an integrated design with an array antenna system. With cut rectangular shape and a slightly sloped ground, a two-shared radiator for 2.1 GHz is presented. A 2-element slot is included in each port of the suggested design. Two antenna system components are housed on a single, inexpensive FR4 substrate that is fed by a 50 microstrip. In order to construct tiny antennas for communications, it is essential to provide enough antenna isolation. The findings show that the antenna has a better than 10 dB return loss at 2.1 GHz. The cancellation of current between any two antennas is a novel method for reducing mutual coupling. The suggested antenna achieves greater isolation than -26.7 dB between a pair of inputs. Additionally, the suggested antenna has a compact size reduction of around 60% compared to traditional patch antennas operating at the same frequency. This is due to the tiny spacing between antenna pieces.

Keywords: (Fourth generation (4G), Voltage Standing Wave Ratio (VSWR), Return Loss (S))

Introduction

Typically, each element offers modest values of directivity (gain) and has a rather broad radiation pattern. To address the needs of long distance communication, it is often required to construct antennas with particularly directional properties (quite high gains). Only by expanding the antenna's electrical size would this be possible. Increasing the size of individual pieces frequently results in more directive properties. Forming an assembly of radiating elements in an electrical and geometrical structure is another technique to increase the antenna's size without necessarily increasing the size of the individual elements. An array is the name given to this novel multi-element antenna. An array's elements are

 ISBN 978-9959-9703-2-9

frequently the same. Although it is not required, doing so is frequently more practical, easier, and convenient. An array's constituent components, such as its wires and apertures, can take on any shape. The vector sum of the fields emitted by the individual elements yields the array's total field. The fields from the array's elements must interact constructively (add) in the appropriate directions and destructively (cancel each other) in the empty space in order to produce extremely directed patterns. In theory, this is possible, but in reality, it can only be approximated.

An antenna array is made up of a number of antenna components that are spatially dispersed according to a common fixed point at predetermined places. It is possible to electronically scan the main beam and/or place nulls in any direction by adjusting the phase and amplitude of the exciting currents in each of the antenna elements. The arrangement of the antenna components is flexible, with linear, circular, and planar arrays being the most popular geometries. When using a linear array, The array's elements' centers are arranged in a straight line. It is referred to be a uniformly spaced linear array if there is identical distance between each element of the array. A circular array is one whose elements' centers are located on a circle. The centers of the array elements of a planar array all lie on the same plane. The planar array includes both the circular array and the linear array as special examples. The radiation patterns of the individual elements, their orientations and relative locations in space, and the amplitude and phase of the feeding currents all affect the radiation pattern of an array [1].

The three definitions that appear in literary works the most are presented. The classification of various types of adaptive antenna systems in Figure 1 is the sole distinction between them.

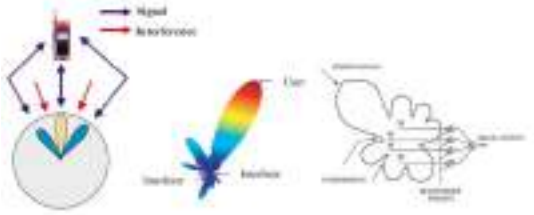

Fig. 1: Adaptive antenna array definition a- Adaptive array. b- Adaptive array coverage c- Different adaptive array concepts.

By integrating the impacts of multipath propagation or by effectively using the various data streams from various antennas, adaptive antenna systems can enhance connection quality. The advantages of adaptive antennas are best summed up as follows [2].

1. Increased range/coverage.
2. Increased Capacity.
3. Lower power requirements and/or cost reduction.
4. Improved link quality/reliability.
5. Increased spectral efficiency.
6. Security.
7. Reduction of handoff .
8. Spatial information.

In this study, a 2x1 array antenna for wireless applications (4G-LTE applications) is provided. The two elements have modest sizes and very

 ISBN 978-9959-9703-2-9

low mutual coupling, and each one is mounted on a FR4 substrate with a dielectric constant of 4.4. The antenna has 2.1 GHz bandwidth coverage. The electromagnetic full wave simulations HFSS have been used to validate the designed outcomes.

7. Basic single patch Microstrip antenna for 2.1 GHz band (G-LTT applications)

The relative permittivity (also known as the dielectric constant) of the substrate, substrate height (h), and operating frequency (also known as the resonance frequency) are the three key factors for the operation of a microstrip patch antenna.Following evaluation of these three factors, length, width, patch input impedance, and fed dimensions are measured. Then, the antenna's performance, including its radiation pattern, S parameter, efficiency, and gain, is discovered.

Utilizing HFFS software, the 4G-LTE microstrip patch antennas were created. The antenna's shape was decided to be a square patch antenna with the dimensions W L and FR4 substrate with a dielectric constant of 4.4, and its height is equivalent to 1.6 mm. The antenna is intended to function at 2.1 GHz. Using a microstrip transmission line is the feeding method. The microstrip calculation website made it really easy and useful to determine the dimensions of the microstrip feed line for matching.

Figure (2) depicts the antenna, whose dimensions were determined using the microstrip antenna transmission line analysis model (3). Figure (2) displays the final dimensions following simulation using HFFS Software.

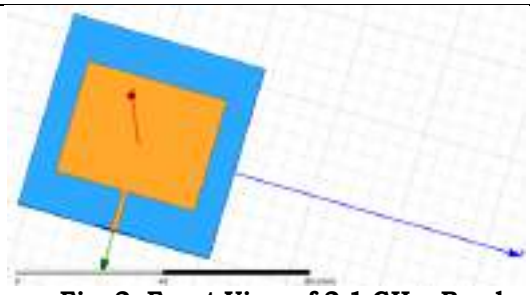

Fig. 2: Front View of 2.1 GHz -Band Microstrip Antenna, Dimensions in (mm).

The 2.1 GHz microstrip antenna's design parameter parameters are shown in Table (1) below.

Table 1: Design Parameter Specifications of the 2.1 GHz Microstrip Antenna

Parameter	Value
Operating frequency	2.1 GHz
Dielectric Constant	4.4 (FR4)
Height of the substrate	1.6 mm
Width of the patch (W)	42.46mm
length of the patch (L)	32.93mm
Width of the ground (Wg)	100mm
length of the ground (Lg)	95mm
Z_0	50
Feeding method	Microstrip Line

In HFSS, the published structure is implemented. To acquire the scattering parameters, the required simulations are run. The collected findings lined up with the data that had been published, completing the antenna validation.

2.1 Simulation results

For designing, simulation is employed, which is quite common for designing antennas. Several simulated graphs, including those for antenna gain, return loss, VSWR, total directivity, and current distribution (mapped 2D and 3D view), are produced and displayed

 ISBN 978-9959-9703-2-9

in the figures. Using electromagnetic full wave simulation (HFSS), this has been verified.

A- Antenna Return Loss

The operating band is cantered at 2.1 GHz (under -10 dB) with -12 dB, making it obvious that this operating band satisfies the design criteria of the 4 G-LTE standard operating frequency. Figure 3 shows the return loss in dB for 2.1 GHz microstrip antenna.

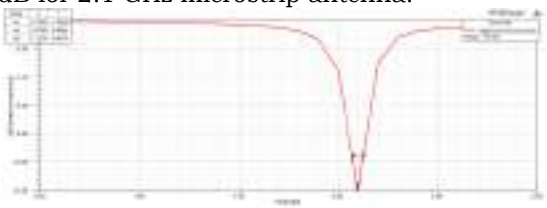

Fig. 3: Microstrip antenna return loss at 2.1 GHz

B- Voltage Standing Wave Ratio VSWR

Figure (4) displays a microstrip antenna's good values for the VSWR (dimensionless), which was 1.67 at 2.1 GHz.

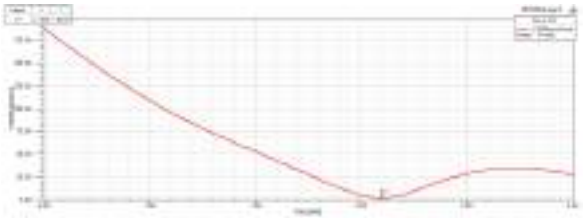

Fig. 4: Microstrip antenna VSWR at 2.1 GHz.

Microstrip patch antennas were the ideal choice for communication systems engineers based on performance and benefits such as low weight, low profile, and cheap cost from planned and simulated findings. However, it has a few shortcomings, including low gain, poor efficiency, and a small (3-6%) core frequency bandwidth, which is insufficient for the majority of modern wireless communication systems. Being able to reduce the size of different wireless equipment, including antennas as a crucial component of wireless communication systems, is one of the primary problems in antenna design for contemporary wireless communication systems. However, developing the radiation qualities throughout the whole frequency range presents greater difficulties and is important to get good results.

A typical definition of antenna gain is the ratio of the power generated by the antenna from a distant source on the beam axis to the power generated by an idealized lossless isotropic antenna that is equally sensitive to signals coming from all directions. Decibels are typically used to indicate this ratio. Due to the influence of substrate thickness and relative dielectric constant on antenna gain, microstrip antennas are infamous for having low gain. Thickness is inversely related to gain and directivity. Many techniques, including Left Handed Material (LHM) and array antenna, are employed to increase antenna gain [6].

To offer more thorough information on the antenna design and optimization, the proposed antenna is changed to explore the influence on gain. Parametric analyses of the proposed antenna are also presented. The variables under investigation include slot addition and antenna size reduction. to more clearly grasp how the settings affect the antenna's performance.

8. Optimization of conventional microstrip antenna for 4G-LTE applications

The simulated antenna model displayed in the preceding section had a reasonable return loss and VSWR over the whole antenna band, but the band was tiny and the radiation pattern was weak. This section makes a novel design suggestion to increase the performance of a standard microstrip patch antenna by increasing bandwidth and radiation pattern. This slotted microstrip patch antenna is brand-new. Modern design elements including slotted patches, microstrip line feeding, and patch structures are used. The combined

 ISBN 978-9959-9703-2-9

impact of using these methods with the suggested patch results in a low profile, high gain, and decreased size. Utilizing HFSS software, theoretical simulations are carried out.

Figure (5) depicts the proposed antenna's configuration. The antenna's r = 4.4 low-cost FR4 substrate served as the design foundation. It was fed by a microstrip-line, which can be readily integrated on the same substrate. The single patch's dimensions were constructed with a rectangular patch's shaped slot on it; these measurements are: W = 14.7 mm, L = 12 mm, a = 4 mm, b = 10 mm, and c = 3x2 mm. A 11.5 mm x 3.11 mm microstrip line is used to obtain the feed. The proposed antenna has a ground plane that measures 20.3 mm by 17.4 mm and is hung 1.6 mm above it. The size of the patch antenna is being reduced by around 50%. The suggested can be simply made at a very minimal cost.

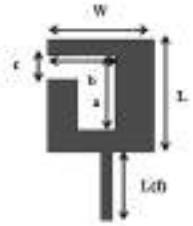

Fig. 5: Optimization of conventional microstrip antenna.

The simulated antenna model using HFSS software is shown in Figure (6).

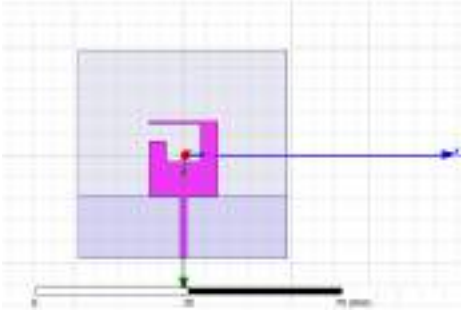

Fig. 6: Geometry of Proposed microstrip antenna at 2.1 GHz in (mm).

The right choice of loading left-handed components was made when designing the suggested antenna. Using electromagnetic full wave simulation (HFSS), this has been verified. Figure (7) displays the proposed antenna's simulated reflection coefficient. The described antenna can obviously function in the 2.1 GHz frequency. The bandwidth ranges from 1.94 GHz to 2.23 GHz (FBW 13.8%), and the operational band is cantered at 2.1 GHz (under -10 dB) with -18.49 dB. Therefore, it is evident that this operating band complies with the 4 G-LTE standard operating frequency's design criteria..

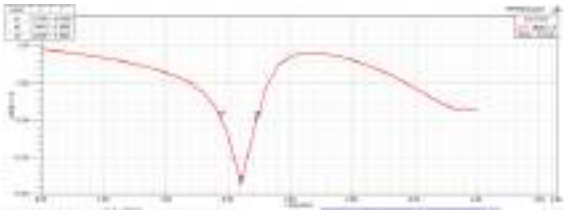

Fig. 7: The return loss of the proposed microstrip antenna at 2.1 GHz.

The construction known as a single element microstrip patch antenna is often made for low power applications. Additionally, it is restricted by its low gain, constrained bandwidth, and lossy directive. The most popular way to boost the bandwidth, directivity, and gain for applications that call for high gain and high directivity in small and conformal devices is to use multi-element devices, often known as arrays. Because of its straightforward production and adaptability with MMIC (Microwave Monolithic Integrated Circuits) technology, a microstrip patch antenna array is employed. Microstrip patch antenna's cost is one of the main considerations when selecting an array element. because it is inexpensive and widely accessible. The goal of this work is to create a microstrip antenna with a high

 ISBN 978-9959-9703-2-9

directional gain for use in the 2.1 GHz band. Initially, we configured our antenna as a single-element microstrip patch, but after analyzing the results for antenna characteristics, operation frequency, radiation patterns, reflected loss, efficiency, and antenna gain, we changed it to a 4-pot array antenna with two elements per port. This produced better results than the original single-element antenna because the gain and directivity of the rectangular microstrip shape increase as the number of elements increases. The design and analysis of 4x1 linear antenna arrays to improve directivity, gain, efficiency, and radiation patterns are covered in the following section.

9. Microstrip Antenna Array (2x1) Design for 4G-LTE Application

Making tiny, inexpensive, high gain, compact antennas is one of the problems in antenna design. The microstrip antenna has several benefits over traditional microwave antennas, which have led to its widespread application. Numerous benefits of microstrip antenna arrays, including their low profile, light weight, and low price, make them popular. Microstrip antennas have poor power handling capacity, low efficiency, and low gain. This section proposes and uses a high gain antenna array with 2x1 components activated using probe-feeding for 4G-LTE and WLAN applications.

The suggested array's architecture is based on a traditional antenna that operates in the 2.1 GHz cantered 4G-LTE and WLAN frequency spectrum. A rectangular patch with a microstrip feed line was employed, and its dimensions are depicted in Figure(8).

There are two components to the array computation. The patch calculation comes first, followed by the 50-, 70-, and 100-transmission lines.

The following equation may be used to calculate the Impedance for a Quarter-Wave Transformer by substituting Z0 for 50 and R_{in} for 100. The characteristic impedance of a transformer is shown in equation [4] as follows.

$$Z_o = \sqrt{R_{in} Z_o} \quad (1)$$

For an antenna array system that makes use of a power-splitting network, such as a parallel or corporate feed system, the employment of a 3-port power divider is particularly crucial. The corporate feed is just a device that maintains equal route lengths between input and output ports while dividing power amongst n output ports with a specific distribution. Here, a 2x1 antenna array power divider circuit was employed. Due to impedance matching, power dividers may be used with microstrip lines of various resistances. Two-antenna arrays should have a 50 ohm input impedance since single microstrip patch antenna has that. For impedance matching, the maximum power theorem is used. Figure (8) below shows the 2x1 antenna array's power divider. Table (2) contains the dimensional parameters for the planned power divider.

Table (2). Dimensional Parameters of Designed Fed Network.

Connection	Parameters Value (Ω)	Dimensions Value (mm)
(1)	50	transmission line 13.85x3.11
(2)	100	transmission line 1.7x11.73
(3)	70	transmission line 9x0.49

ISBN 978-9959-9703-2-9

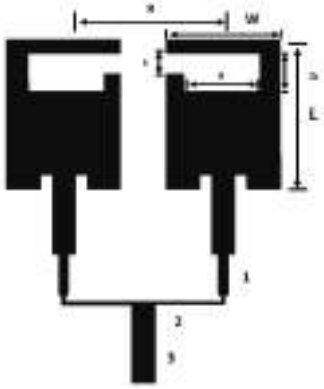

Fig. 8: Proposed 2x1 array geometry microstrip antenna.

The parasitic element in this array antenna is an element of a certain size and form that is put between other elements (nonphysically linked) or attached to the ground plane [16]. In order to lessen the reciprocal coupling between the elements, a parasitic element with a non-physical connection is employed in this research. The antennas are not really linked to parasitic components. By generating an opposing coupling field, these devices are utilized between the antennas to terminate some of the coupled fields, hence reducing the overall coupling on the target antenna. They might be floating, shorted stubs, or resonator-type devices. Additionally, parasitic components are created to regulate the coupling, isolation range, and bandwidthThis parasitic element will produce opposing coupling fields on both of its sides in order to weaken the original field and minimize coupling overall [5]. The stub enhances antenna matching, and the slot inside it reduces radiation from the environment and enhances ground plane isolation strips are used to construct a stop band to reduce interference in the WLAN spectrum. An element with a certain shape and size that is connected to other components in an unphysical way or that is connected to the ground plane as a resonator is known as a parasitic element. To lessen the reciprocal coupling between the elements, a parasitic element with a non-physical connection is employed. In order to weaken the initial field, this parasitic element will produce an opposing coupling field on both sides of itlowering the total coupling in the process. It is suggested to use a parasitic element with a new spatial form, as shown in Figure (9).

Fig. 9: Geometric Shape of the proposed parasitic element.

The parasitic stub is 40mm × 5mm in size and is situated in the center of the substrate 6.5 mm from each patch's border. There are two parasitic components, each measuring 2mm x 4mm.

Figure (10), which depicts the final dimensions following simulation and optimization using HFFS Software, shows these dimensions.

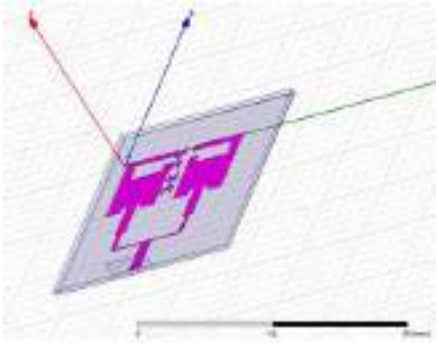

Fig. 10:View of Microstrip Antenna Array 2x1, Dimensions in (mm).

In HFSS, the published structure is implemented. To acquire the scattering parameters, the required simulations are run. The collected findings lined up with the data that had been published, completing the antenna validation.

4.1 Simulated Results

Antenna gain, total directivity, return loss, VSWR, current distribution, and radiation patterns are only a few of the simulated graphs

 ISBN 978-9959-9703-2-9

that are created and displayed in the images. Using electromagnetic full wave simulation (HFSS), this has been verified.

a- Antenna Return Loss

Figure (11) displays the microstrip antenna array's 2x1 simulated reflection coefficient. The reported antenna's operational band is clearly under -10 dB at cantered 2.1 GHz (-17.58 dB), and its bandwidth spans 2.056 GHz to 2.14 GHz (FBW 4.28%). Therefore, it is abundantly obvious that this operating band satisfies the 4G-LTE standard operating frequency design criteria.

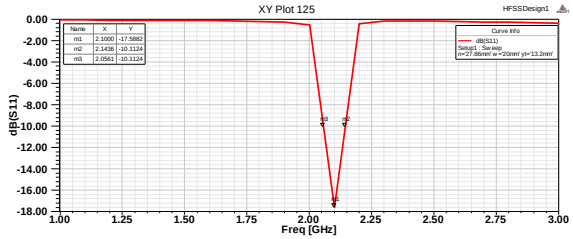

Fig. 11: Return Loss of the Microstrip Antenna Array 2x1.

b- Radiation Pattern in 3D

Figure (12) depicts the radiation patterns for the 2x1 microstrip patch antenna array designed for 4G-LTE. Since the antennas are patch type, they exhibit directional radiation patterns in the phi=0 deg (x-y plane) and phi=90 deg (y-z plane) planes. There is a directional pattern on the antenna.

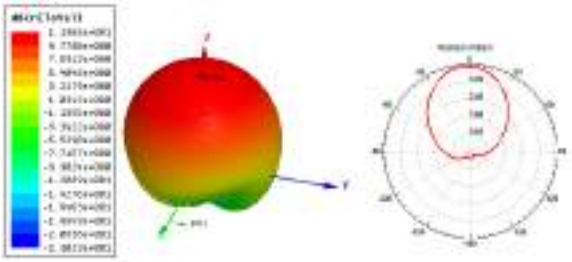

Fig. 12: 3D Radiation pattern of the 2x1microstrip antenna array.

c- Gain and Directivity

The intended antenna radiates with a gain of 4.91 dB and a directivity of 6.32 dB in the broadside direction. Figure (13), which shows 3D far field plots of gain and direction, is shown below. High directivity and gain characterize the antenna.

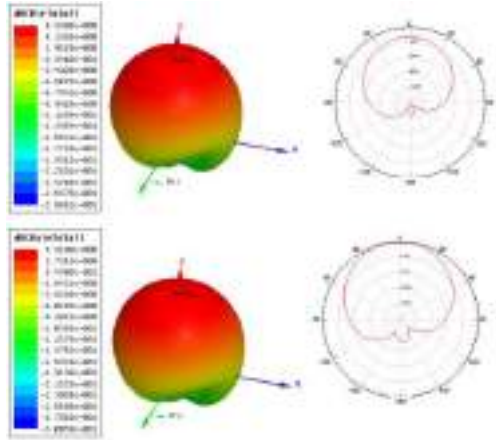

Fig. 13: Gain and Directivity of the microstrip antenna array 2x1.

d- Voltage Standing Wave Ratio (VSWR)

The VSWR for a 4G-LTE microstrip antenna array is shown in Figure (14). At 2.1 GHz, we had 1.3 with excellent values, indicating good received signals.

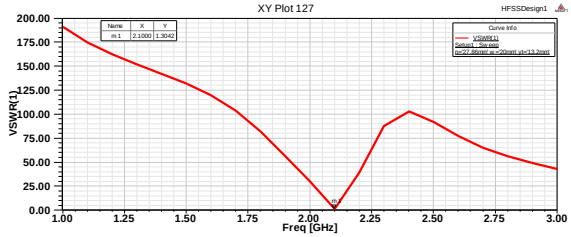

Fig. 14: VSWR of the Microstrip Antenna Array 2x1.

e- Current Distribution on the Antenna.

The field distribution between the patch and the ground plane is referred to as the current distribution, and it is employed as a measure of the radiation from microstrip patches. According to Figure (15), the highest current

ISBN 978-9959-9703-2-9

distribution is 155(A/m) at 2.1 GHz.

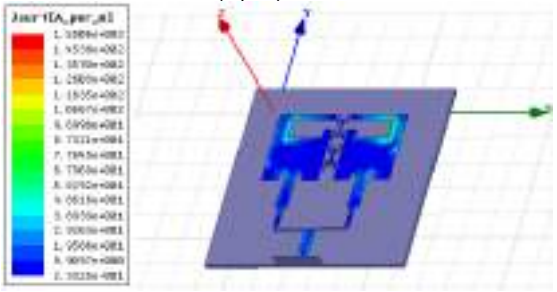

Fig. 15: Current distribution for microstrip antenna array.

4.2 Mutual Coupling Reduction of an Antenna using Parasitic Element Technique

The antennas are not really linked to parasitic components. By generating an opposing coupling field, these devices are utilized between the antennas to terminate some of the coupled fields, hence reducing the overall coupling on the target antenna. They may be floating, shorted stubs, or resonator-type devices [16].

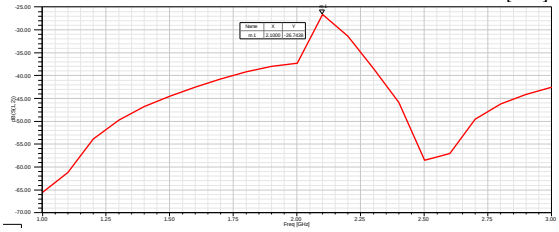

Fig. 16: The Return Loss and Mutual Coupling (S11-S12) of the microstrip antenna array with parasitic at 2.1 GHz.

Additionally, parasitic components are made to regulate coupling, isolation range, and bandwidth. Based on the simulation presented in figure (16), the values of isolation with parasitic components are -22.22 dB. Because of the tiny size of the antenna, this approach is effective for isolation and is ideal for small devices like mobile phones.

The present 2.1 GHz dispersion pattern is seen in Figure 17. At 2.1 GHz, the patch antenna's maximum current is 22.8 (A/m), and the E-field is 52.9 (kv/m), as illustrated in Figure (16). The surface current distribution and E-field distribution with parasitic elements are clearly terminated at the parasitic stub, indicating that the parasitic element approach is effective at lowering the electric field spread between antennas.

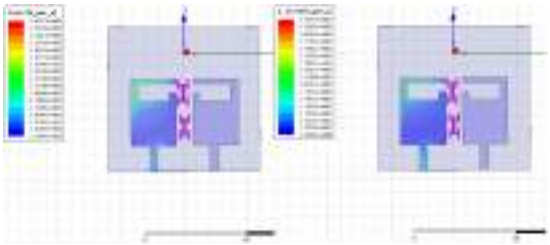

Fig. 17: Current Distribution and E-field on the array antenna at 2.1 GHz with parasitic element.

10. Conclusion

In this article, a 2x1 array antenna for 4G-LTE and other wireless communication technologies is presented. As a radiating element, a low profile antenna with microstrip has been employed. A band operation was successfully simulated in order to accomplish. The suggested design offers a two-element system for one port and is low profile, small, simple, and only requires one substrate. The 2.1 GHz band is covered by the integrated antenna system. The findings show that a suitable balance between the reflection coefficient and radiation pattern led to a frequency range with acceptable matching properties starting at about 2.1 GHz. A high isolation two-antenna system has been suggested and researched. Through the application of the suggested shaped structure and parasitic network element, satisfactory isolation performance was attained. This indicates a strong receiving signal and a directed radiation pattern because the return

 ISBN 978-9959-9703-2-9

loss S11 is -18.49 dB. The suggested antenna's features include compactness (just 110 x 93 mm in dimension, a size decrease of about 50%). Additionally, at the working frequencies, the developed antenna offers greater coupling isolation between any two ports than 26.7 dB. Additionally, there is a 4.91 dB gain and a 6.32 dB directivity. A promising contender for 4G-LTE wireless communication equipment, the given antenna is also very small, inexpensive, conformal, and easy to construct. It exhibits excellent radiation properties across its working frequency spectrum.

References

[6] S. Ali. "Design and Development of Fractioal Microstrip Antenna Array for Applications", Thapar university, 2016.

[7] G. Meida. "Multiband Microstrip Patch Antenna for 4G (LTE)". Mohamed Khider Biskra University, 24 June 2018.

[8] C. A. Balanis "Antenna theory analysis and design". John Wiley & sons. inc.. Publication. 3rd Edition, ISBN: 0-471-66782, 2005.

[9] S. Weigand. G. Huff. K. Pan. and J. Bernhard. "Analysis and Design of Broad-band Single Layer Rectangular U- Slot Microstrip Patch Antennas". IEEE Trans. Antennas and Propag.,vol. 51, No.3, pp. 457-468, March, 2003.

M. A. Abdalla1 ,. " Small size high isolation CRLH meta- material closely spaced MIMO antenna"., 30th national radio science conference (NRSC 2013).

 ISBN 978-9959-9703-2-9

المؤتمر الدولي الثاني للعلوم والهندسة
2nd International Conference on Science and Engineering
ICSE 2023
Faculty of Engineering - University of Bani Waleed
Bani Waleed, Libya

Paper Code: ICSE-032

AN ADAPTIVE EIGEN-VALUE BASED DIAGONAL LOADING TECHNIQUE TO IMPROVE WIDEBAND DIRECTION OF ARRIVAL ESTIMATION (DOA) ACCURACY FOR SMART ANTENNA SYSTEM

Taqwa. A. Muhammad[a] , Mohamed S. Alshullea[b]
[b]Military Industries Organization, Bani-walid, Libya.
*dr.engineeralshole@gmail.com

Abstract: The need for mobile communications is continually expanding, which drives up the demand for greater coverage, more capacity, and enhanced transmission quality. As a result, the radio spectrum needs to be used more effectively. The sort of antenna array that is adaptive Smart antenna systems hold out hope for a viable remedy to the issues with current wireless systems while attaining dependable and robust high-speed high-data-rate transmission. Smart antenna systems are capable of effectively exploiting the radio spectrum. Radars may effectively employ direction of arrival estimation (DOA) algorithms and interference cancellation to rebuild the original received signals and aid in the position determination of those signals. military surveillance, sonars, seismic exploration, and communications systems. Wideband signals are more challenging since they require more data and computer power to solve the same problem. Both fixed diagonal loading and diagonal loading based on Eigenvalues employ fixed diagonal loading factors that are independent of direction inaccuracy. The approaches, known as FDL and EDL, estimate the loading factor by adequately adapting already-presented narrowband beamforming techniques, and they demand perfect knowledge of the steering vector error, just like narrowband techniques do.
Wideband DOA estimation techniques like Incoherent Subspace Processing (ISSM) and Coherent Signal Subspace Processing (CSSM) with Eigen-value Based Diagonal Loading Technique are presented in this study to improve wideband DOA accuracy. A uniform linear array antenna was used to test the mathematical adjustment for various correlated and uncorrelated wideband signals entering at various incoming angles. with knowledge of or an estimate of the incoming signal direction. This document will be processed entirely on a computer using MATLAB.

Keywords: Coherent Signal Subspace Processing (CSSM), Incoherent Subspace Processing (ISSM)

Introduction

The development of adaptive antenna arrays is based on digital signal processing techniques. In order to improve reception in the direction of signals that are of interest while reducing interference in the direction of signals that are of no interest, the adaptive antenna array system gains the ability to find and track signals from both users and interference sources. The performance of an adaptive antenna array system is significantly influenced by the efficiency of digital signal processing techniques. Several DOA estimation approaches are used in adaptive antenna arrays to locate the target signal. The number

 ISBN 978-9959-9703-2-9

of plane wave occurrences and their angles on the antenna array are calculated using the DOA algorithms [1].

Wideband sources can also be located using array processing techniques. As was previously indicated, compared to the center frequency, the frequency bandwidth for wideband transmissions is rather big. Compared to narrowband signals, which had an indefinite length and just one frequency, wideband signals had a bounded duration. These presumptions can be loosened to accommodate signals with narrow bandwidths compared to carrier frequencies and lengthy durations compared to array sizes. Wideband signals are more challenging since they require more data and computer power to solve the same problem. While the phase delays of the narrowband signals may be used to estimate the time delays, wideband signals require further signal processing before the detection and estimation issues can be resolved using the current techniques.

11. Wideband Processing Beamformer

Based on time-domain processing and frequency-domain processing, there are two primary methods for wideband beamforming [2]. These methods can create beam patterns that are frequency-invariant over a wide range of signal bandwidths. However, for signals with large bandwidths, the frequency-domain approach offers computational benefit compared to the time-domain method [2]. Figure (1) depicts the structural layout of a beamformer for frequency-domain processing. The fast Fourier transform (FFT) is used in this beamformer to convert wideband signals from each element into frequency domain, and a narrowband processor processes each frequency bin. the time-domain technique has a computational benefit [2].

Figure (1) depicts a beamformer's structural layout for frequency-domain processing. In this beamformer, the fast Fourier transform (FFT) is used to convert wideband signals from each element into frequency domain, and a narrowband processor processes each frequency bin. Additionally, the frequency-domain beamformer's employment results in inexpensive hardware costs because it does not call for a high A/D conversion sample rate. In contrast to the frequency-domain approach, which only needs a sampling rate equal to the Nyquist frequency, the time domain method often requires five to ten times the Nyquist rate in order to provide accurate beamforming. When a large number of antenna components are employed particularly in high-frequency bands, the cost associated with high sampling rates will be more noticeable. However, the data storage needs and computing effort (for example, for FFT, inverse FFT) are higher for frequency-domain beamformers.

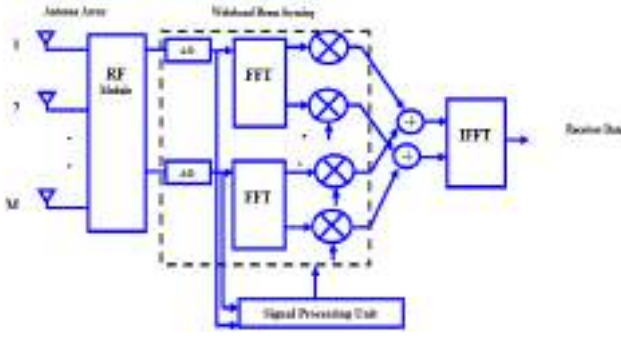

Fig. (1). Frequency-Domain Processing Beamformer.

The FFT is used in the FDFIB to convert wideband time-domain signals to frequency domain, and each frequency bin is subsequently weighted by a suitably set complex factor. A FDFIB's structure is seen in Figure (1). Any antenna array can be used in conjunction with the FDFIB. Additionally, the beam pattern's frequency-invariant property is only dependent on the phases of the beamforming weights. Since the amplitudes of the beamforming weights may be changed, the FDFIB has an advantage in manipulating beam shape.

 ISBN 978-9959-9703-2-9

12. Incoherent Frequency Combining Methods

These techniques are wideband adaptive DOAs. The typical method for processing wideband signals involves taking a spectrum sample of the incoming signals from each sensor to create an array of narrowband signals. The narrowband signals at each frequency are treated independently in the so-called incoherent signal-subspace processing approach, and the outcomes from all frequency bins are then merged to provide the final result. However, when the sources are coupled and the SNR is low, the performance of this technique suffers. The subspace fitting methods, specifically MUSIC [3], are among the techniques for incoherent wideband DOA estimation that are now accessible.

3.1 Wideband MUSIC Beamformer

The observation space is often divided into signal and noise subspaces using subspace decomposition techniques. Through the decomposition of the array correlation matrix into its Eigen-structure form, the signal and noise subspaces are estimated in the first stage of these methods. The phrase "signal subspace" refers to the region of space that is covered by the covariance matrix eigenvectors that correspond to the dominating eigenvalues. The fact that signals' Eigen-values are greater than those of noise is used by the detection techniques. The approach for calculating the specific frequencies of many time-harmonic signals, known as MUSIC (Multiple Signal Classification) [3], is one of the most widely used techniques. By performing the Fourier transform of the aforementioned equation, one may derive the vector X(t)'s representation in the frequency domain.

$$X(\omega,\theta) = A(\omega,\theta)S(\omega) + N(\omega) \quad (1)$$

Where,

$X(\omega,\theta) = [X_1(\omega,\theta), X_2(\omega,\theta), \ldots\ldots X_M(\omega,\theta)]^T$ is the M vector of array output.

$S(\omega,\theta) = [S_1(\theta), S_2(\theta), \ldots\ldots S_d(\theta)]^T$ Is the d vector of source signals.

$N(\omega) = [N_1(\omega), N_2(\omega), \ldots\ldots N_M(\omega)]^T$ is the N vector of noise.

The array steering vector takes into account the far-field and assumes that the arrays are similar. A(ω,θ) can be written as $A(\omega,\theta) = [a(\omega,\theta_1), \ldots\ldots\ldots\ldots a(\omega,\theta_D)]$.

Fig. (2). Basic Principle of Incoherent Method.

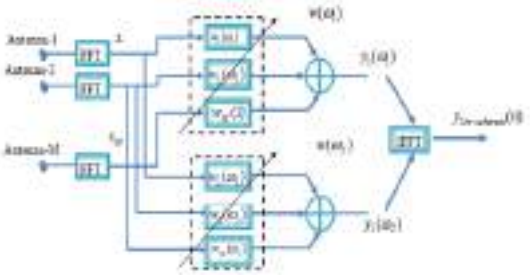

Fig. (3). Block Diagram of the Incoherent Wideband Adaptive Beamformer.

The output covariance matrix is used in all traditional beamforming methods to identify the source's direction of arrival. The output power at each of the sensors can be seen using the covariance matrix, and the matrix may simply be changed to achieve improvements at all of the sensors. [3] provides the symmetric covariance matrix of X in Eq. 2.

$$R_{XX}(\omega,\theta) = E[X.X^H] = \frac{1}{M}\sum_{n=1}^{M} X(\omega,\theta)X(\omega,\theta)^H \quad (2)$$

Where, E[·] is the expectation operator and $[.]^H$ denotes complex conjugate transpose.

 ISBN 978-9959-9703-2-9

$$R_{XX}(\omega,\theta) == \frac{1}{M}\sum_{n=1}^{M}(A(\omega,\theta)S(\omega)+N(\omega)). \quad (3)$$

$$(A(\omega,\theta)S(\omega)+N(\omega))^{H}$$

The Eq. 3.11 is further calculated as Hence the Covariance matrix is given by.

$$R_{XX}(\omega,\theta) = A(\omega,\theta)R_{ss}A^{H}(\omega,\theta)+\sigma^{2}I \quad (4)$$

Where I is the M x M identity matrix. σ2 is the noise variance in each channel if the noise is white, $\sigma^2 I$ is the MxM covariance matrix of the noises. R_{ss} is the d x d Auto-covariance matrix of input signal. For MUSIC to be applicable the input signals are assumed to be uncorrelated, so the covariance matrix R_{ss} will be a diagonal matrix having full rank d [4].

$$R_{ss} = diag\{P_1,.....P_d\} \quad (5)$$

Where $P_d = dE\left[\left|S_d(\omega)\right|^2\right]$ is the spectral power density of the d^{th} signal. R_{ss} will be positive-definite if and only if the d signal vectors are linearly independent. Under these assumptions, $\mathrm{A}(\omega,\theta).\mathrm{R}_{ss}.\mathrm{A}(\omega,\theta)^{\mathrm{H}}$ is a positive semi definite M x M matrix of rank d with $\mathrm{rank}\,(\mathrm{A}(\omega,\theta).\mathrm{R}_{ss}.\mathrm{A}(\omega,\theta)^{\mathrm{H}}) = span[a(\theta_1),.....a(\theta_D)] < M$

Let $\lambda_1 \geq \lambda_2 \geq ..... \geq \lambda_M$ denote the Eigen-values of R_{xx} and $\eta_1 \geq \eta_2 \geq ..... \geq \eta_M$ denote the Eigen-values of matrix $\mathrm{A}(\omega,\theta).\mathrm{R}_{ss}.\mathrm{A}(\omega,\theta)^{\mathrm{H}}$ respectively. From Eq. (5) we can easily see the following relation.

$$\lambda_i = \eta_i + \sigma^2 I \quad (6)$$

Since the rank of R_{SS} is d and the number of sources d is smaller than the number of arrays M, the matrix $\mathrm{A}(\omega,\theta).\mathrm{R}_{ss}.\mathrm{A}(\omega,\theta)^{\mathrm{H}}$ is singular, i.e.

$$\mathrm{A}(\omega,\theta).\mathrm{R}_{ss}.\mathrm{A}(\omega,\theta)^{\mathrm{H}} = 0 \quad (6)$$

Eq. 3.15 implies that the d columns of $\mathrm{A}(\omega,\theta).\mathrm{R}_{ss}.\mathrm{A}(\omega,\theta)^{\mathrm{H}}$ span a D-dimensional subspace of M-dimensional complex space. This subspace is referred as Signal Subspace. The smallest (M-d) Eigen-values of $\mathrm{A}(\omega,\theta).\mathrm{R}_{ss}.\mathrm{A}(\omega,\theta)^{\mathrm{H}}$ are zero [4], i.e.

$$\eta_{D+1} = ... = \eta_M = 0 \quad (7)$$

Finding the D distinct elements of A(ω ,θ) that cross the subspace will yield the DOA for the no-noise. But if we take into account the matrix's inclusion of a noise component $\mathrm{A}(\omega,\theta).\mathrm{R}_{ss}.\mathrm{A}(\omega,\theta)^{\mathrm{H}}$ Given that the eigenvectors of the MxM matrix R_{XXx} are all linearly independent, the Eigen-value decomposition (EVD) can be carried out as follows:

$$R_{xx} = \begin{bmatrix}E & Q & E^H\end{bmatrix}\begin{pmatrix}E_S & E_R\end{pmatrix}\begin{bmatrix}Q_S & 0\\ 0 & Q_R\end{bmatrix} = \begin{bmatrix}E_S^H\\ E_R^H\end{bmatrix} \quad (8)$$

$$= E_S.Q_S.E_S^H + E_R.Q_R.E_R^H$$

$$R_{xx} = \sum_{i=1}^{M}\lambda_i e_i e_i^H = \sum_{i=1}^{D}(\eta_i+\sigma^2)_i e_i e_i^H + \sum_{i=D+1}^{M}\sigma^2{}_i e_i e_i^H \quad (9)$$

Because is a Hermitian matrix R_{XX} of full rank, each of the matrix's eigenvectors e_i is mutually orthogonal to one another, i.e.

$$e_i^H e_j = \delta_{ij} \qquad where \qquad \delta_{ij} = \begin{cases}1 & i = j\\ 0 & i \neq j\end{cases}$$

Because λ_i denotes the Eigen-value and e_i denotes the eigenvector of matrix R_{xx}, the implies

$$R_{xx}e_i = \sigma^2 e_i \qquad i = D+1,.....M \quad (10)$$

or

$$(R_{xx} - \sigma^2 I)e_i = 0 \qquad i = D+1,.....M \quad (11)$$

Hence Eq (6) can be rewritten as.

$$\mathrm{A}(\omega,\theta).\mathrm{R}_{ss}.\mathrm{A}(\omega,\theta)^{\mathrm{H}} e_i = 0 \qquad i = D+1,.....M \quad (12)$$

Since covariance matrix R_{XX} is real, positive, full rank diagonal matrix, it follows that

$$.\mathrm{A}(\omega,\theta)^{\mathrm{H}} e_i = 0 \qquad i = D+1,.....M \quad (13)$$

According to the equation above, the steering

ISBN 978-9959-9703-2-9

vector's $[a(\omega,\theta_1),.....a(\omega,\theta_D)]$subspace is the orthogonal complement of the subspace spanned by the eigenvectors. $\{e_{D+1},e_{D+2},.....,e_M\}$ This is shown as The eigenvectors of the covariance matrix, as was previously noted, are orthogonal to each other, so E_S and E_R are orthogonal complement. This can be expressed as

$span[e_{D+1},e_{D+2},.....,e_M]\perp span[a(\omega,\theta_1),.....a(\omega,\theta_D)]$

As mentioned above that the eigenvectors of the covariance matrix R_{XX} are orthogonal to each other, so E_S and E_R are orthogonal complement. This can be expressed as

$$E_S=[e\ ,,.....,e_D]^T\perp E_n[e_{D+},,.....,e_M] \quad (14)$$

As a result, we can observe that the columns of E_S span the M-dimensional complex space's d-dimensional signal subspace similarly to the column vectors of matrix A(ω ,θ) ,that is.

$span[e_1,e_2,.....,e_D]^T=span[a(\omega,\theta_1),.....a(\omega,\theta_D)]$

the subspace covered by the d greatest eigenvalues of R_{xx} the D eigenvectors, has the name "signal subspace." The subspace covered by the M-d eigenvectors of R_{xx} the M-D lowest Eigen-values is known as the noise space. The orthogonal complement of the signal subspace and the noise subspace is one another. Finding steering vectors on the array manifold that have zero paperion in the noise subspace allows one to identify the direction of arrival. These steering vectors must be orthogonal to the noise subspace. The real direction of arrival is the direction that the best steering vector steers in. The DOAs are calculated by the MUSIC algorithm as the peaks of the MUSIC spectrum as [4].

$$P_{music}(\omega,\theta)=\frac{1}{a^H(\omega,\theta)E_nE_n^Ha(\omega,\theta)} \quad (15)$$

The second stage is transforming a real Time domain signal to a complex Frequency domain since the approach acts in the Frequency domain. This is accomplished for each data block using FFT.

$$X(\omega_k,\theta)=A(\omega_k,\theta)S(\omega_k)+N(\omega_k) \quad (16)$$

$$P_{music}(\omega,\theta)=\frac{a^H(\omega,\theta)a(\omega,\theta}{a^H(\omega,\theta)E_nE_n^Ha(\omega,\theta)} \quad (17)$$

All beam-patterns or pseudo spectrum are incoherently averaged in this final stage, as illustrated in Fig. (3), to produce the resulting spectrum.

$$P_{Incoherent-music}(\omega_k,\theta)=\sum_{k=1}^{M}\frac{1}{a^H(\omega_k,\theta)E_nE_n^Ha(\omega_k,\theta)} \quad (18)$$

The orthogonality of and Un will decrease it to the minimum, which will grow, as can be seen from the denominator.

$P_{Incoherent-music}(\omega_k,\theta)$. Thus, the highest peaks of the MUSIC spectrum are corresponding to the DOAs of the d signals impinging on the array.

3.2 Simulation Results

To assess the performance of the MUSIC method, a computer program is created using MATLAB. With arrival angles of [-20° 0° 20°] and uncorrelated, respectively, the array is lighted. When compared to the white Gaussian noise in the background, the three sources are considered to have identical power, which is 0 dB. There are 128 pictures captured. then used to identify the DOA estimate on the MUSIC Beamformer. The outcomes shown in Figure (5) demonstrate that, when incident signals are expected to be uncorrelated, the MUSIC Beamformer can accurately determine the direction of arrival. Figure (5) displays the spatial spectral function produced by the multipath version of the signal at -20°, which is the situation in another scenario.

ISBN 978-9959-9703-2-9

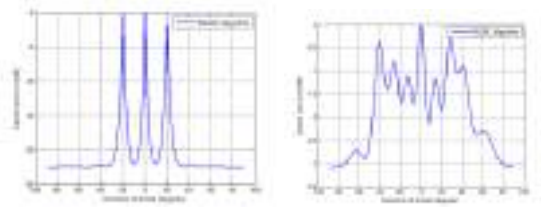

(a) (b)

Fig. (5). Spatial Spectrum of MUSIC Estimations for a- Un-Coherent Sources b-Coherent Sources.

As can be seen, the MUSIC algorithm is unable to determine the corresponding DOA of either of the linked signals at -20° and -20° since the direction of both signals could not be determined with sufficient accuracy. When it comes to identifying linked input signals, MUSIC fails. Figure (6b) shows that the response of the music is not sharp at the peaks as opposed to being sharp in the case of an input signal that is uncorrelated. The source covariance matrix does not meet the complete rank constraint required by the MUSIC for Eigen decomposition $E_n(\omega_i)$, which leads to this issue. Any narrowband approach may be used to calculate the degrees of freedom (DOAs) at each frequency where is the noise subspace at frequency (ω_i) rather than MUSIC.

The incoherent method's conclusions and operation are straightforward, but it is susceptible to inaccurate wideband DOA estimations. Utilizing the narrowband into Line DOA computed using the Coherent Signal Subspace Method (CSSM) for each narrowband signal's Covariance matrix of the focus to the reference frequency. Wideband signal information may be used more effectively, and DOA estimation performance is superior than CSSM algorithm's low signal-to-noise ratio. The DOA estimated starting value [5], high signal to noise, and the ISSM method's performance below it make the CSSM algorithm susceptible.

4. Coherent Frequency Combining

Wideband non-adaptive DOAs are the coherent technique. introduced the CSSM in this section. The first approach for estimating wideband DOA is based on splitting the frequency band into non-overlapping narrowbands and estimating narrowband DOA in each band. To get the final DOA estimate, the DOA estimates for the various bands are then added together. However, this method cannot handle coherent signal sources. The CSSM [20] is a different approach for handling coherent signal sources. This approach begins by using FFT to break down the wideband array data into a number of narrowband components. The narrowband array manifold matrices are then converted into focusing matrices in order to create matrices matching to a chosen reference frequency. The use of narrowband DOA estimation techniques, like the spectral estimation approach [5], is then applied to determine the directions of arrival. The spectrum estimating techniques are favourable since they need less computing effort than other techniques (such those based on least squares, maximum likelihood, etc.). Preliminary DOA estimations close to the real directions of arrival are needed for the CSSM method's focusing matrix design.

 ISBN 978-9959-9703-2-9

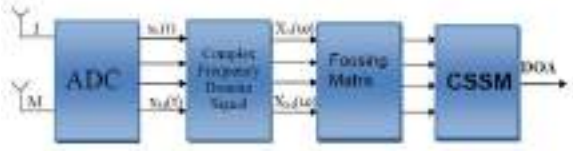

Fig. (6). Basic Principle of Coherent Signal Subspace Method.

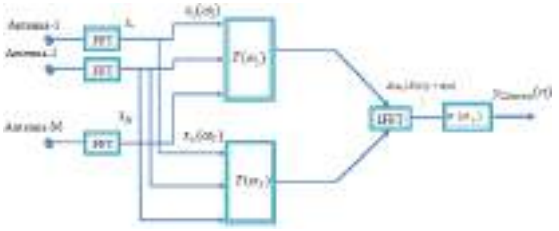

Fig. (7). Block Diagram of the CSSM Wideband Adaptive Beamformer.

The first method to coherently sum the correlation matrices of different frequency bins was CSSM, which Wang and Kaveh developed [5]. Using a transformation matrix (focusing matrix) that is dependent on the frequency bin, it merges the correlation matrices at various frequency bins into a single general correlation matrix at a single focusing frequency. This process is known as concentrating. Coherent techniques' general process is depicted in Figure (6-7).

A generic block architecture for the focused wideband adaptive beamformer is shown in Figure (7). In this method, a single time domain narrowband beamformer is used to concentrate the signal subspaces at various frequencies to a single frequency using a pre-processor that is implemented as a frequency dependent linear transformation matrix $T(\omega_j)$.

Low computing cost, the ability to address the signal cancellation issue, and enhanced convergence qualities are the key advantages of the coherent technique. Theoretically, the CSSM should utilize a focusing matrix $T(\omega_j)$ fulfilling [5].

$$T(\omega_j)A(\omega_j,\theta) \cong A(\omega_0,\theta) \quad (19)$$

Where (ω_j) are the frequencies within the bandwidth of the signals and w0 is the focused frequency, i.e. $T(\omega_j)$ focuses the signal subspaces $T(\omega_j)A(\omega_j,\theta)$ at frequencies (ω_j) onto the signal subspace $T(\omega_j)A(\omega_0,\theta)$. The matrices $T(\omega_j)A(\omega_j,\theta)$ and $T(\omega_j)A(\omega_0,\theta)$ contain the steering vectors of the sources in their columns at frequencies (ω_j) and (ω_0), respectively, where (θ) is the DOAs vector.

There are several approaches to design the focusing matrix $T(\omega_j)$ in the following sections, we describe several representative focusing methods. They propose Rotational signal subspace focusing transformation (RSS).In [6] a quantities measure for The ratio of the array's SNR following and before the focusing operation is used to determine the focusing loss. The benefit of employing unitary focusing matrices is emphasized by the authors since they have no focusing loss. In order to solve the following constraint minimization issue (Hung and Kaveh [6] devised a unitary focusing matrix), they suggest unitary transformations as follows:

$$\min_{T(\omega_j)} \left\| A(\omega_0,\theta) - T(\omega_j)A(\omega_i,\theta) \right\|_F$$

j=1,2,.....J (20)

Subject to $T^H(\omega_j)T(\omega_j) = I$

Where $\|\cdot\|_F$ is the Frobenious matrix norm [20]. The solution to (22) is given by.

$$T_{RSS}(\omega_j) = V(\omega_j)U(\omega_j)^H \quad (21)$$

Where the columns of $U(\omega_j)^H$ and $V(\omega_j)$ are the left and right singular vectors of $A(\omega_j,\theta)A(\omega_0,\theta)^H$ They named this focusing matrix the Rotational Signal Sub-space (RSS) focusing matrix. then the general focusing

 ISBN 978-9959-9703-2-9

correlation matrix as.

$$R_{focuing} = \sum_{j=1}^{J} T^{H}(\omega_j) R_{XX} T(\omega_j) \quad (22)$$

Therefore, the issue is how to identify focusing angles that should match the signal's DOA but are not accessible. Finding focusing angles $A(\omega_0, \theta)$ that ought to be sufficiently near to the genuine DOAs typically involves employing low-resolution DOA estimating techniques. Some closely spaced DOAs, however, cannot be addressed using this method. Furthermore, focusing angles may not always result in a solution with the right value, unlike beginning values in other iterative approaches. For accurate estimates, focusing angles should be near to the genuine DOA; however, if they are not the same as the true DOA and the focusing frequency is not at the center of the signal's band, the bias will never reach zero. For high resolution techniques, the bias could be absolutely crucial.

5- Eigen-value based Diagonal Loading

The EDL technique attempts to overcome the adaptive approach of the FDL technique by using the following equations to estimate [128]

$$R_{dl-eig}(k) = \mathbf{R}_{XX} + \alpha(k)\mathbf{I}_M \quad (23)$$

Where α is a positive diagonal loading factor. I represents a unit matrix. with RXX replaced by the signal free correlation matrix and the loading factor (7).

$$\alpha(k) = -\lambda_{\min} + \sqrt{(\lambda_{\min} - \lambda_M) - \quad (\lambda_{M-1} - \lambda_{\min})} \quad (24)$$

with $\lambda_1 > \lambda_2 > \ldots\ldots > \lambda_M$ denoting the ordered eigenvalues of signal-free R_{XX} with M the dimension of interference subspace [7].

The algorithm can improve the presence of random array manifold vector error Poor adaptive beamforming algorithm. However, this method the primary The question is how to choose the amount of discretion to load. Usually selected based on experience special Given value, the most typical is 10σ2, where said single sensor σ² The noise power, the paper loaded in the selected amount of sediment it was 10σ².The concept of diagonal loading is straightforward. We use,

$$R_{xx}(\omega,\theta)_L = \frac{1}{M}\sum_{n=1}^{M} X(\omega,\theta)X(\omega,\theta)^H + \sigma_L^2 I \quad (25)$$

In place of the estimated spectral matrix in order to design w. We use $R_{xx}(\omega,\theta)_L$ instead of $R_{xx}(\omega,\theta)$ because it is not used as an estimate of $R_{xx}(\omega,\theta)$.

based on eigen values Using diagonal loading factors, which are independent of direction inaccuracy, is the preferred method. The ways to estimate the loading factor using EDL need precise knowledge of the steering vector error, just as narrowband techniques, and adapt current techniques for wideband beamforming to appropriately estimate the loading factor. then using Eq. (18) to represent the new correlation matrix in beam-patterns or a pseudo spectrum.

6. Simulation Results

Under these circumstances, the result of the CSSM method is shown in the last assumption, where it is expected that the signal at -20° is a multipath variant of the signal at 20°. For each signal, the SNR is adjusted to -10 and 10 dB.

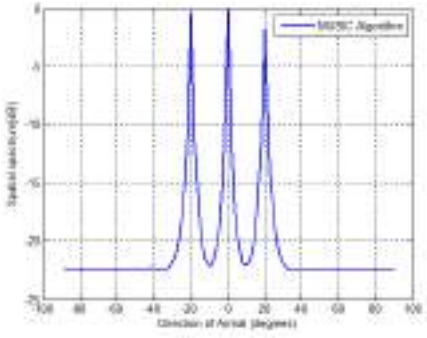

Fig. (8). Spatial Spectrum of the CSSM Algorithm in the Coherent Signals.

Figure (8) makes it evident that the spatial

ISBN 978-9959-9703-2-9

spectral function for the case of correlated signals was produced using the CSSM algorithm.

7. Behaviour Analysis for Different Algorithms

Methods for estimating DOA rely on either the array manifold's parametric structure or the signals' non-Gaussianity or cyclo-stationarity. These approaches include multiplying a weight matrix by the incoming data matrix in order to estimate the waveform of the signals. variables that have an impact on the DOA.

1. The array's element count.
2. Signal-to-Noise Ratio, second.
3. Quantity and the distance between array items.
4. The number of signals event sampled.

1- Effect number of elements of the antenna array on DOA's estimation

The number of array elements is assumed to be a varying variable during the simulation where it varies from 5 to 11 elements.

The other settings are SNR = 0dB and 128 snapshots. Figure (9) illustrates the relationship between the number of array elements and the DOA estimation. It is obvious that as the number of array elements rises, the MUSIC Method becomes more accurate in estimating the DOA of incident signals. This is due to the fact that adding more array components will result in a narrower beam around the directions of incident signals.

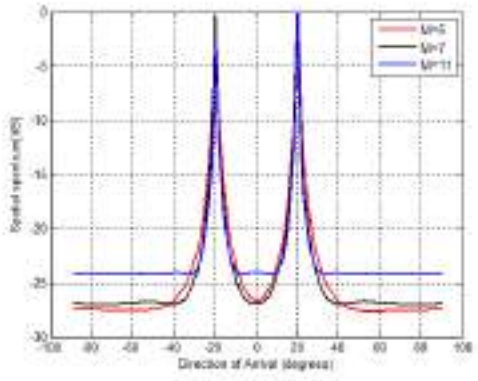

Fig. (9). The effect of the number of elements on DOA's on MUSIC algorithm.

2- Effect of The Signal to Noise Ratio (SNR)on DOA's Estimation

During the simulation, it is assumed that the signal to noise ratio is a variable that changes from -10 dB to 10 dB for each signal. The 11 elements in the array, which are spaced apart by half a wavelength, are regarded as making up a linear array. 128 snapshots are used to evaluate the array covariance matrix and the spatial spectrum of the MUSIC technique. In the figures below, the SNR's impact on DOA estimate is depicted. Figure (10), which shows that MUSIC Methods can precisely estimate the DOA of incoming signals as SNR increases, makes this point quite evident.

 ISBN 978-9959-9703-2-9

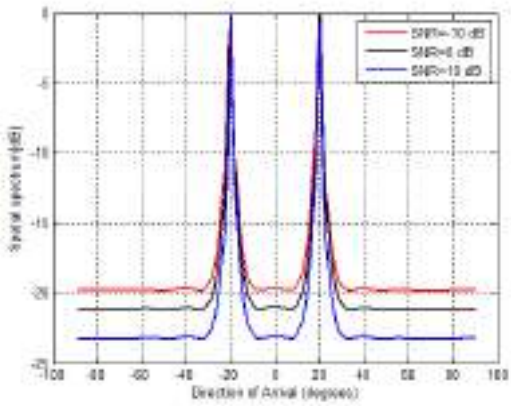

Fig. (10). The effect of the signal to noise ratio on DOA's MUSIC algorithm.

This is due to the fact that higher SNR will result in a narrower beam around incident signal directions. The peaks are sharper when the noise is lower. The peaks spread out as a result of the additional noise. As the SNR increased, the performance improved, indicating that the SNR had an impact on the resolution of the MUSIC technique. It is evident that the ratio of the output peaks to the noise level at the array's output grows correspondingly as SNR rises.

3- Effect the Number of Snapshots of The Signal on DOA's Estimation

To test the method algorithm estimator's capabilities with various signal snapshots, a simulation program was run. The number of snapshots is assumed to be a variable during the simulation with a range of 50 to 1000 snapshots for each signal. This differs from the assumptions we made in the earlier analysis of the influence SNR. Figure (11), which shows how the MUSIC algorithm can see that as the number of pictures increases, the peaks in the MUSIC spectrum get sharper, is abundantly evident.

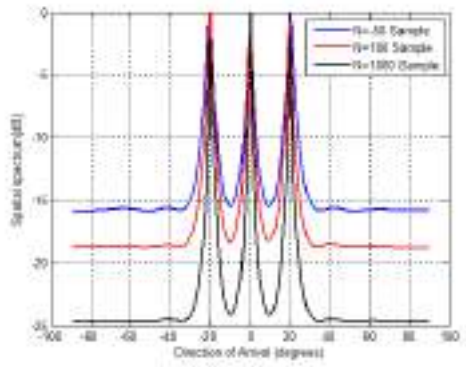

Fig. (11). The effect of number of snapshots signal on DOA's MUSIC algorithm.

4- Array antenna Spacing & resolution

The performance of the beamformer depends on the array's element spacing and number, as shown by an examination of the MUSIC algorithm equation from the Beam Pattern section.

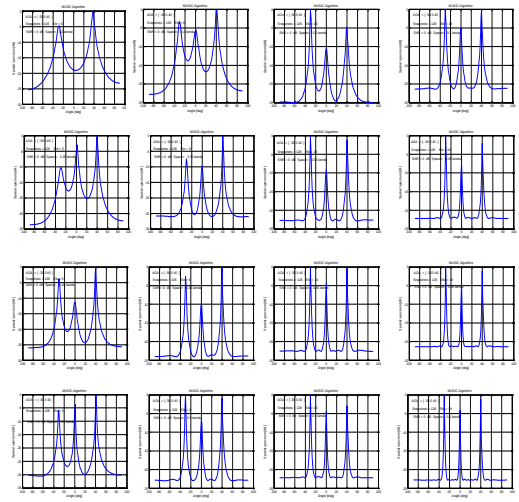

Fig. (12). Performance quantity music dependent on the spacing and array's elements.

Figure (12) above shows how altering these settings impacts the spatial filtering capability

ISBN 978-9959-9703-2-9

of the beamformer. Figures are influence the SNR and element count for DOA separation. The development of an adaptive antenna system based on direction of arrival benefits from this approach.

4. Conclusion

This article discusses the configurations of smart antenna systems as well as the reasons to use adaptive antenna array for DOA. It also describes the fundamental functions and parts of adaptive antenna array for DOA and interference cancellation for wideband signal. Wideband DOA performance was examined utilizing theoretical framework and simulation with MATLAB software.

The simulation results displayed in this study indicate that the uniform linear array-based DOA estimate approaches are effective. Computer simulation is used to study and examine two DOA estimation techniques for wideband signals. These techniques are incoherent signal subspace methods (ISSM), which are wideband DOA estimation techniques for high resolution estimate of angles of arrival of several wideband plane waves as part of the MUSIC algorithm. The CSSM, or second method, combines a solid, almost ideal data-adaptive statistic. To assure a statistically sound pre-processing of wideband data, this approach is employed in conjunction with improved focusing matrix design. The response of the MUSIC is not sharp at the peaks whereas it was sharp in the case of uncorrelated input signal condition, which is why incoherent approaches like IMUSIC fail when it comes to identifying correlated input signals. The source covariance matrix does not meet the complete rank constraint required by the MUSIC for Eigen decomposition, which leads to this issue. CSSM with TCT performs better, however it is not a fair estimate method. to lessen or eliminate bias and increase resolution. When array defects of any type are taken into consideration, Eigenvalue EDL is resilient. The higher performance of the suggested approaches on beam-pattern control, output SINR augmentation, and robustness against have been demonstrated by extensive numerical testing. When diagonal loading is used Wideband signals were used to study the situation of DOA estimating, and the impact of bandwidth on estimator accuracy was examined using computer simulations, the Incoherent method, and coherent subspace method-based techniques like MUSIC. It is obvious that the beamformer may be used to load correlated signals using the spatial spectral function produced by the CSSM method.

References

[10] P. H. Lehne and M. Pettersen, “An overview of smart antenna technology for mobile communications systems,” IEEE Communications Surveys, vol. 2, no. 4, pp. 2–13, Fall Quarter 1999.

[11] T. Do-Hong, F. Demmel, and P. Russer, “A method for wideband direction-of-arrival estimation using frequency-domain frequency- invariant beamformers,” in IEEE Int. Symp. Antennas and Propagation Dig., 2003.

[12] W. Liu and R. J. Langley, “An adaptive wideband beamforming structure with combined subband decomposition,” IEEE Trans. Antennas Propagat., vol. 57, Jul. 2009.

[13] R. Schmidt, “Multiple Emitter Location and Signal Parameter Estimation,” IEEE Trans. on Antennas and Propagation, Vol. AP-34, No. 3, March 1986.

[14] Wang, H. and Kaveh, M., “Coherent signal-subspace processing for the detection and estimation of angles of arrival of multiple wide-band sources," IEEE Trans. Acoust., Speech, Signal Processing, Aug. 1985.

[15] H. Wang and S. Kay, “A maximum likelihood angle-Doppler estimator using importance sampling,” IEEE Trans. Aerosp. Electron. Syst, Apr. 2010.

M. Alshulli, “Wideband direction of arrival estimation and interference cancellation”

 ISBN 978-9959-9703-2-9

المؤتمر الدولي الثاني للعلوم والهندسة
2nd International Conference on Science and Engineering
ICSE 2023
Faculty of Engineering - University of Bani Waleed
Bani Waleed, Libya

Paper Code: ICSE-033

PERFORMANCE ENHANCEMENT OF ORTHOGONAL FREQUENCY DIVISION MULTIPLEXING SYSTEM FOR MITIGATION OF NARROWBAND INTERFERENCE OVER ADDITIVE WHITE GAUSSIAN NOISE

Amal A. Salh[a] and Mohamed S. Alshulle[b]
[a]College of Technical Technology, Bani Walid, Libya.
[b]Military Industries Organization, Bani-walid, Libya.
*dr.engineeralshole@gmail.com

Abstract: An essential component of multicarrier digital data transmission systems is orthogonal frequency division multiplexing (OFDM), which divides a single data stream into a number of lower-speed subcarrier signals. This new standard for data transmission is the first to use OFDM in a communication system that uses data packets. To achieve high throughput and good transmission quality in wireless communication networks, parallel transmission of data symbols is implemented as an abstraction. A way to handle concurrent transmission is via OFDM.
The performance of the bit error ratio (BER) is improved in this paper when the transmission channel's SNR is altered. Here, SNR is increased while BER is decreased. However, OFDM does not exhibit resilience to narrowband interference (NBI) in its present implementation. It is advised to use an OFDM system with CI to lower the NBI of the OFDM system. Using orthogonal CI spreading codes, the CI code distributes each of the N low-rate symbol streams across all N subcarriers. With little system complexity increases, the high NBI is reduced. Furthermore, the system performs much better than the conventional method in terms of bit error rate (BER). A carrier-interferometry OFDM system's performance has been compared to that of OFDM. It has been found that one of these systems can minimize the symptoms of NBI. The development of a MATLAB software to simulate a basic OFDM system is used to support this work. An completed MATLAB application can be used to explore the characteristics of an OFDM system. This process of development may be used to study the workings of an OFDM system.

Keywords: (Orthogonal Frequency Division Multiplexing (OFDM), Bit Error Ratio (BER), NarrowBand Interference (NBI , Carrier Interferometry (CI))

Introduction

In wireless communication systems, it is frequently preferable to permit the subscriber to send data to the base station while simultaneously receiving data from the base station. A cellular system divides any given area into cells where a mobile unit in each cell communicates with a base station. The primary goal in the design of cellular systems is to be able to improve the channel's capacity, or to handle as many calls as feasible in a given bandwidth while maintaining an adequate degree of service quality. It is essential to have a framework in place for several users to access and use wireless

 ISBN 978-9959-9703-2-9

communication systems or cellular technologies at once. Different multiple access strategies have been employed as cellular technology has developed. They form the very core of the way in which the radio technology of the cellular system works. There are four main multiple access schemes that are used in cellular systems ranging from the very first analogue cellular technologies to those cellular technologies that are being developed for use in the future. Frequency Division Multiple Access (FDMA), Time Division Multiple Access (TDMA), Code Division Multiple Access (CDMA), and Orthogonal Frequency Division Multiplexing (OFDMA) are the four different multiple access systems [1],[2].

OFDM is a method of encoding digital data on multiple carrier frequencies. Since it saves the need for complex equalizers, it is best suited for channels with a non flat frequency response [2]. The OFDM technique enables a base station to bifurcate a bunch of radio spectrum into sub-channels. And the strength of the sub-channels and the no. of channels assigned to different be adjusted as required. The technique enables high data rates, miles away from a transmitter. Hence it suits with the radio interference that is normaly found in urban areas, where signals reflect off walls and generates confusing echoes [2]. The idea of OFDM is derived from Multi-Carrier Modulation (MCM) transmission technique. The principle of MCM is that to divide the input bit stream into several parallel bit streams and then they are used to modulate several sub carriers. Guard band is used to separate the sub-carrier so that they do not overlap with each other. Band pass filters are used at the receiver side, to separate the spectrum of individual sub-carriers. Spectrally efficient MCM techniques, such as OFDM, which use closely spaced orthogonal sub-carriers and overlapping spectrums, are a specific case of MCM. OFDM does not require the use of band pass filters because of the orthogonality of the subcarriers. As a result, the available bandwidth is utilized effectively while preventing ICI.

The fundamental idea behind the OFDM system is introduced and addressed in this work. Including its production and reception, the OFDM communication system This paper's goal is to use OFDM methods to investigate the impact of cyclic prefix on data rate. It has been suggested that the CI techniques [4], such as carrier-interferometry OFDM (CI-OFDM) and pseudo-orthogonal carrier-interferometry OFDM (POCIOFDM), can improve OFDM performance when NaBI is present. The creation of a MATLAB software that simulates a fundamental OFDM system achieves this goal. This work will introduce the CI-OFDM technique, which is thought to lessen the effects of NBI. The following sections stress the CI-OFDM system's primary concept.

1. Transmitter Structure

The CI-OFDM transmitter is shown in Figure 1 (Figure 1(a) and (b)). Each information symbol is modulated onto every N carrier in the CI-OFDM system following the S/P conversion procedure [3],[4]. The transmitter applies a different orthogonal spreading code to each information symbol when spreading is done in the frequency domain in order to ensure the separation of information symbols at the receiver side. These spreading codes line up with how (to the symbol) [3] is applied.

$$C^{(K)}(t) = \sum_{i=0}^{N-1} B_i^{(K)} e^{j2\pi i \Delta f t} . g(t) \quad (1)$$

where Δf is the carrier separation ($\Delta f = 1 / T_S$ to ensure carrier Orthogonality); $g(t)$is a rectangular pulse shape of duration T_S (where T_S is OFDM symbol length); and $B_i^{(K)}$,*i=0,..,N-1* refers to the k^{th} symbol's spreading sequence characterized by

$$\left\{B_0^{(k)}, B_1^{(k)}, \dots\dots\dots, B_{N-1}^{(k)}\right\} = \left\{e^{j\frac{2\pi}{N}.k.0}, \dots\dots, e^{j\frac{2\pi}{N}.k.(N-1)}\right\} (2)$$

The CI spreading codes defined in (1) and (2) are orthogonal spreading codes, that is,

 ISBN 978-9959-9703-2-9

$$R\left[\frac{\int C^{(k)}(t)\overline{C^{(l)}(t)dt}}{\int C^{(k)}(t)\overline{C^{(k)}(t)dt}}\right] = R\left[\frac{1}{N}.\sum_{l=0}^{N-1} e^{j(\frac{2\pi}{N}ki-\frac{2\pi}{N}Li)}\right] \quad (3)$$

where R is the real values.

$$C^k(t) = \sum_{i=0}^{N-1} B_i^{(k)} e^{j2\pi i\Delta f t}.g(t) \quad (4)$$

$$\overline{C^{(L)}(t)} = \sum_{i=0}^{N-1} e^{j2\pi i\left(\frac{l}{N}+\Delta f\right)}.g(t) \quad (5)$$

Multiplied Equation (4) by Equation (5).

$$C^{(k)}(t)\overline{C^{(l)}}(t) = \sum_{i=0}^{N-1} e^{j2\pi i(\frac{k}{N}-\frac{l}{N})}.g^2(t) \quad (6)$$

And

$$C^{(k)}(t)\overline{C^{(k)}(t)} = \sum_{i=0}^{N-1} e^{j2\pi i(\frac{k}{N}-\frac{k}{N})} = e^0 = 1 \quad (7)$$

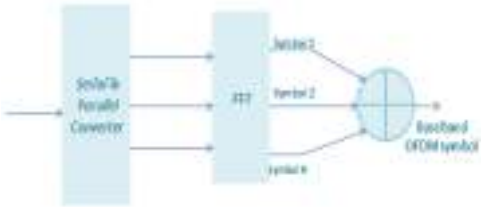

(a) Traditional OFDM transmitter.

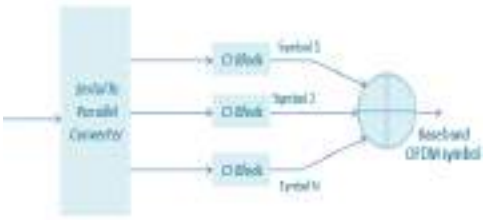

(b) Modified OFDM transmitter with CI blocks.

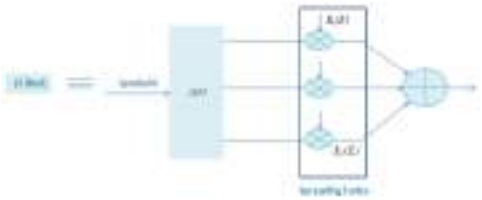

(c) Detailing the CI block.

Fig. 1: Traditional OFDM and CI-OFDM Transmitters.

In the CI-OFDM system, the sent signal for the k[th] symbol may be written as:

$$S^{(k)}(t) = R\left[\sum_{i=0}^{N-1} A\,.S^{(k)}.e^{j2\pi i\Delta f t}.e^{j\frac{2\pi}{N}.k.i}.e^{j2\pi f_c t}.g(t)\right] \quad (8)$$

where A is a constant that ensures symbol energy of unity, $S^{(k)}$is the k^{th} information symbol, an$S^{(k)} \in \{+1,_1\}$, and is the carrier frequency. The total transmitted signal for the CI-OFDM system can be written as:

$$S(t) = R\left[\sum_{k=0}^{N-1}\sum_{i=0}^{N-1} A\,.S^{(k)}.e^{j2\pi i\Delta f t}.e^{j\frac{2\pi}{N}.k.i}.e^{j2\pi f_c t}.g(t)\right] \quad (9)$$

2. CI-OFDM Receiver Structure

Figure (2) shows the receiver structure for the CI-OFDM kth symbol. The received signal is divided into its N carrier components and recombined in order to reduce both the ISI and the narrowband interference signal in the receiver [4].

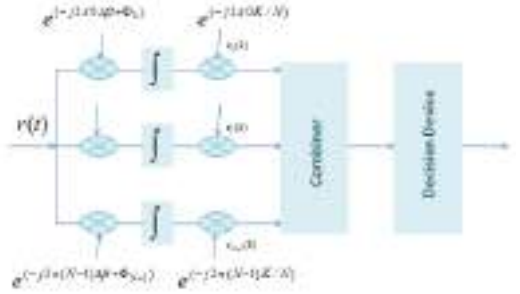

Fig. 2: Receiver Structure for CI-OFDM System for the k^{th} symbol.

ISBN 978-9959-9703-2-9

$$r(t) = \sum_{k=0}^{N-1}\sum_{0}^{N-1} A\alpha_i S^{(k)} \cos\left(2\pi f_c t + 2\pi\Delta f t + \frac{2\pi}{N}.k.i + \varphi_i\right) g(t) + I(t) + n(t) \quad (10)$$

where the frequency-selective Rayleigh fading channel introduces a fading gain and phase offset (a_i, φ_{ij} , respectively, into the ith carrier; n(t) is an AWGN with zero mean; and double-sided PSD is equal to $\frac{N_o}{2}$.

In order to reduce interference, the received signal is broken down into its N carrier components and recombined. The symbol estimate's (k) is then created using a hard decision device. By using a single FFT, the frequency decomposition is more effectively (and less expensively) done in practice. Here, we go into further depth about how the receiver works.

To mitigate the effects of narrowband interference (Ii), as well as the presence of both ISI and noise, a well constructed cross-carrier combiner is used. The combiner's standard configuration is

$$R(^{K}) = \sum_{i=0}^{N=1} W_i . r_i^{(k)} \quad (10)$$

It is simple to demonstrate that [5] and the Ith combining weight obtained using the MMSE criterion are equivalent.

$$W_i = \frac{A\,\alpha_i}{E\left[(r_i^{(k)})^2\right]} \quad (11)$$

when interference is present (i.e., when narrowband interference weakens the i^{th} carrier).

The $r_i^{(k)}$ with and without NBI can be written as:

$$r_i^{(k)} = A\alpha_i S^{(k)} + \sum_{\substack{l=0 \\ l\neq k}}^{N-1} A\,\alpha_i S^{(l)} \cos\left[\frac{2\pi}{N}(k-l).i\right] + n_i \quad 0.W \quad (12)$$

where is the NBI and is the AWGN.

$$\therefore W_i = \frac{A\alpha_i}{E\left\{\left(r_i^{(k)}\right)^2\right\}} = \frac{A\alpha_i}{NA^2\alpha_i^2 p_i + \sigma_i^2 + \frac{N_o}{2}} \quad (13)$$

It is important to notice that the combining weights are very closely matched by when the narrowband interference has very high power $\sigma_i^2 \gg NA^2\alpha_i^2$,[[5].

$$\therefore W_i = \begin{cases} 0 & , \ i \in \{m, m+1, \dots, m+M-1 \\ NA^2\alpha_i^2 p_i + \sigma_i^2 + \frac{N_o}{2} & , \quad 0.W \end{cases} \quad (14)$$

3. Performance of OFDM and CI-OFDM with Narrowband Interference in AWGN.

The likelihood of error is first calculated under the assumption that CI-OFDM and OFDM are being transmitted over an AWGN channel with narrowband interference across subcarriers.

For an OFDM signal, the decision variable for the i^{th} symbol is easily shown to be:

$$r_i = \begin{cases} AS^{(i)} + I_i + n_i \ , \in \{m, m+1, \dots, m+M-1\} \\ AS^{(i)} + n_i \ , \quad 0.W \end{cases} \quad (15)$$

The probability of error for OFDM in the presence of narrowband interference in an AWGN channel therefore corresponds to:

$$P(e) = \frac{N-M}{N}.Q\left(\sqrt{\frac{2E_b}{N_o}}\right) + \frac{M}{N}\left(\sqrt{\frac{2E_b}{N_o+2\sigma_I^2}}\right) \quad (16)$$

It is clear that the first term reflects the contribution of "interferred carriers," while the second term indicates the contribution of "carriers that do not experience interference." It is clear that the latter term dominates the typical BER. It has been observed that, for the CI-OFDM system, the impact of narrowband interference is equally dispersed over all information bits and is diffused throughout all sub-carriers. By presenting the decision statistic entering the hard decision device R((K)), we may start to compute the probability of mistake term. Assuming EGC at the combiner (an ideal choice in the AWGN channel), the decision variable $R^{(K)}$equates to:

$$R^{k} = \sum_{i=0}^{N-1} r_i^{(k)} = \sum_{i=0}^{N-1} AS^{(K)} + I_i + \sum_{i=0}^{N-1} n_i \quad (17)$$

where the intended signal is the first term, the contribution of interference is the second term, and the AWGN is the third term.Then, for CI-OFDM, the signal-to-interference-plus-noise-ratio (SINR) may be expressed as [6]$SINR = \frac{NE_b}{M\sigma_I^2 + N\frac{N_O}{2}}$ (18)

ISBN 978-9959-9703-2-9

Thus, the probability of error for CI-OFDM corresponds to [6]

$$P(e) = Q\sqrt{SINR} = Q\left(\sqrt{\frac{2E_b}{2\frac{M}{N}\sigma_I^2 + N_O}}\right)$$

(19)

4. Result

Extensive simulations are used to validate the BER performances of the OFDM and CI-OFDM systems in the presence of NBI. Assuming that the signal-to-interference ratio (SIR) is equal to -2dB, that the modulation is BPSK, that the channel model is vehicular outdoor channel, and that the number of run 10^3 and 10^4 as indicated in Figures (3).

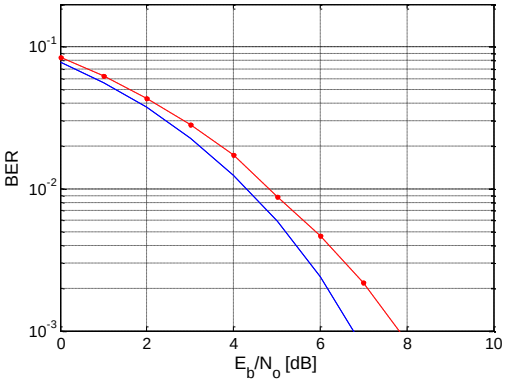

Fig. 3: Depicts the simulation blocks of the CI-OFDM system.

Fig. 4: Simulation blocks of the CI-OFDM system.

where the deterministic number of subcarriers used to form the NBI signal has a normal distribution and SIR.

The 0s and 1s are created at random to create the signal. Each data block is run through a BPSK modulator before being speeded up using CI code and having its symbols translated to the time domain and given subcarriers using IFFT.

5. Simulation results

After adding a cyclic prefix that is longer than the channel's maximum delay spread and serves as a guard interval to ensure circular convolution, the resulting block is broadcast across a wireless multipath channel. After that, the AWGN is added to the signal, and a chosen number of subcarriers interfere with the NBI signal.

The received signal is subsequently distributed using CI dispreading algorithm at the receiver side after the CP has been eliminated. Following the conversion of the received data block to the frequency domain in order to eliminate the ISI and the NBI induced by the channel using MMSE with correction term, the obtained received data block is provided as follows [6].

ISBN 978-9959-9703-2-9

$$C = \frac{conj(H)}{\left(H * conj(H) + \frac{1}{SNR}\right)} \quad (19)$$

After that, the demodulation is applied to the produced signal in order to approximate the original signal. the effectiveness of an OFDM system when NBI is present and interference effects are present on subcarriers 1, 2, and 4. Figure (5) shows how an OFDM system performs when NBI is present and interferes with the 1, 2, and 4 subcarriers.

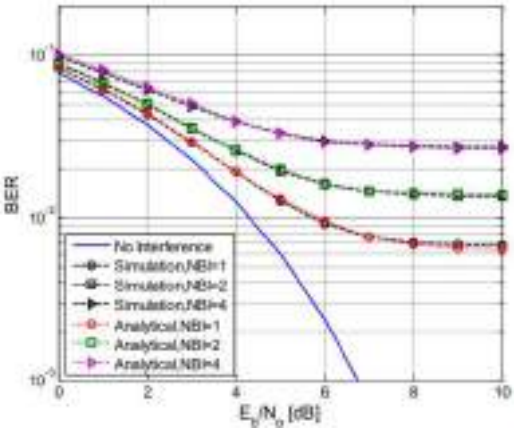

Fig. 5: BER Performance of an BPSK-OFDM system in the presence of NBI in an AWGN, SIR= -2[dB].

Figure (6) shows that the presence of interference significantly reduces an OFDM system's performance, and that this degradation worsens as the number of interference sub-carriers rises. Figure (6) shows the CI-OFDM system's performance when NBI is present for the same values of interference.

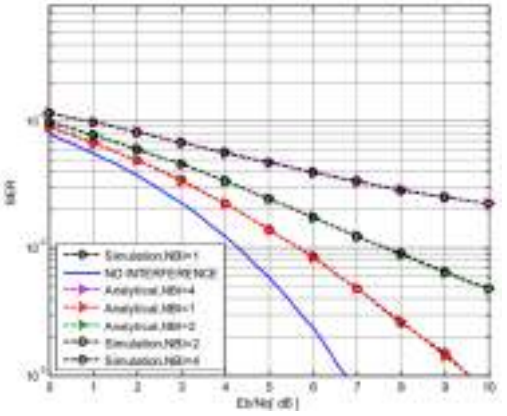

Fig. 6: BER Performance of an BPSK- CI-OFDM system in the presence of NBI in an AWGN, SIR= -2 [dB].

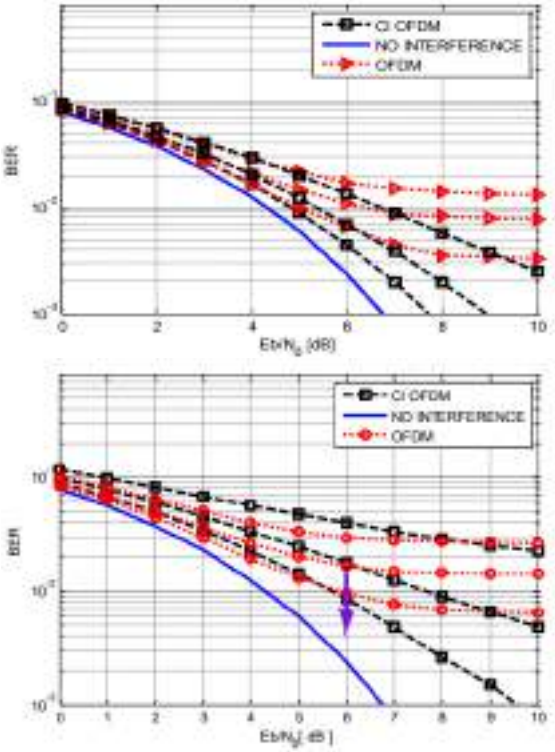

ISBN 978-9959-9703-2-9

Fig. 7: BER Performance of BPSK- OFDM Vs CI-OFDM systems in the presence of NBI in an AWGN (a) SIR= 2[dB], (b) SIR= -2[dB].

Figure (7) shows that the CI-OFDM system performs better than the OFDM system in the presence of interference because orthogonal codes are used; nevertheless, when the number of interference sub-carriers is increased, the performance of the CI-OFDM system becomes more susceptible to the effects of interference. As a result, although the impact of the NBI has been lessened, the additional complexity introduced to the system has not entirely eliminated it. The performance of the OFDM and CI-OFDM systems in the presence of NBI is shown in Figure (7) for the same values of interference.

6. Conclusion

In wireless networks and mobile communications, OFDM has a bright future. This technology was created in response to the expanding global market for wireless networks and the rising need for massive amounts of bandwidth. OFDM is already a key component of WLAN and will be in MAN as well. It will undoubtedly rule the communication sector in the years to come.

In this study, MATLAB is used to model an OFDM system. The main parts, benefits, and drawbacks of an OFDM system are reviewed. Additionally, the BER performance of OFDM over AWGN channel models in the current NBI has been examined, as well as the OFDM system simulation model.

This study has examined the fundamentals of narrowband interference cancellation methods and OFDM systems. Basic operations and characteristics of the CI and orthogonal systems are discussed. The architecture of the CI system and the justification for using adaptive interference cancellation are also discussed.

A theoretical framework and simulation using the MATLAB program have been used to examine the performance of OFDM Systems utilizing the CI approach. In order to mitigate narrowband interference over additive white gaussian noise and the impact of NBI, the CI-OFDM system is finally introduced. The performance of the orthogonal CI-OFDM system has been proven to be superior to either the OFDM, while both later systems are significantly degraded by the presence of NBI. In light of the previous systems shown, it can be said that the orthogonal CI-OFDM system is the best countermeasure method. When narrowband interference is present, CI-OFDM gives substantially less graceful performance deterioration, according to simulation results of OFDM and CI-OFDM systems over AWGN channel. This is a direct result of the information being spread evenly throughout the whole bandwidth using CI-OFDM.

References

[16] H. Lu, T. Xu and H. Nikookar, “Cooperative Communication over Multi-scale and Multi-lag Wireless Channels”, book chapter in “Ultra Wideband”, InTech publisher, ISBN 978-953-51-0781-1. Oct. 2012.

[17] A. R. Forouzan, and M. Moone, “Precursor inter-symbol interference removal by block transmission-based time-reversed equalization,” EURASIP Journal on Advances in Signal Processing , Dec. 2013.

[18] C. Zhang,“Cognitive Non-Continuous Carrier Interferometry Orthogonal Signal Division Multiplex Transmission In Autonomous Vehicular Communications”, IEEE Journal on Selected Areas in Communications, pp.:37-47,Vol.:29, Issue: 1, 2011.

[19] D. Wiegandt, Z. Wu, and C. R. Nassar, “High performance carrier Interferometry OFDM WLANs: RF testing,” IEEE International Conference on Communications (ICC), pp.: 203-207, vol. 1, 2003.

[20] A, SALEH,"The Bit Error Rate (BER) Performance in Multi-Carrier (OFDM) and Single-Carrier". Electronic Theses and Dissertations. Paper 744, 2012.

[21] S. Hara and R. Prasad, “Overview of multi-carrier CDMA”, IEEE Commun. Mag., pp

 ISBN 978-9959-9703-2-9

المؤتمر الدولي الثاني للعلوم والهندسة
2nd International Conference on Science and Engineering
ICSE 2023
Faculty of Engineering - University of Bani Waleed
Bani Waleed, Libya

Paper Code: ICSE-051

NETWORK SIMULATION AND IMPLEMENTATION OF 5G NR NETWORK IN TRIPOLI CITY

Osama M .Abuzaid[a], Ramadan A. M. Khalifa[b], Khaled ELgantri[c], Adel Issa Ben Issa[d]
[a] Faculty of Technical Science, Bani Walid, Libya
[b,c] High Institute of science and Technology-Suk Algumaa Tripoli, Libya
[d] Higher institute of engineering technologies Tripoli, Tripoli, Libya
(Osamamasuod233, Ramadanamharree, K.elgantri, adelissa.976) @gmail.com

Abstract: Recent tremendous rise in mobile communications is transforming the globe into a completely linked civilization. Current 4G networks account for about half of global mobile traffic, and overall mobile data traffic is likely to skyrocket in the coming years. The fourth generation (4G) mobile communication system is incapable of meeting some unique needs such as high traffic density, high traffic volume density, a large number of connections, and high mobility. This research is aimed to examine the deployment of 5G NR in various situations utilising the expert radio-planning tool Atoll in order to improve 5G NR Co-exists 4G in the neighbourhood of Tripoli City by building a 5G NR network. It is intended to cover the area with a 4G/5G network.

Keywords: Mmwaves, Link budget, SS-RSRP, SS-SINR, 5G topology, NRand Coverage

Introduction

Users have grown accustomed to wireless network connections in a variety of devices, including smartphones and smart watches, during the previous few decades. Mobile communications have progressed from a comparable first generation (1G) that employed circuit switched technology, through a third generation (3G) that featured packet switching, and lastly to the most current fifth generation (5G). Mobile communication users have growing wants and expectations, which pushes technology progress to meet those demands. Many never-before-seen services and applications, such as self-driving cars, remote surgery, and artificial intelligence, are now available. Wireless carriers must be prepared to handle a three-order-of-magnitude increase in data traffic in order to serve the new services. Researchers have to locate more capacity in additional new wireless spectrum to do this[1]

Since the new wireless spectrum needs a larger quantity of capacity, millimeter-wave frequencies will be taken into consideration for the 5G New Radio (5G NR) technology's spectrum. For 5G NR , the Third-Generation

 ISBN 978-9959-9703-2-9

Partnership Project (3GPP) defines two categories of frequency range: Frequency Range 1 (FR1), which covers 450 MHz to 6000 MHz in the sub-6 GHz range, and Frequency spectrum 2 (FR2), which covers 24250 MHz to 52600 MHz in the millimeter wave spectrum Channel bandwidths for the FR1 range form 5 MHz to 100MHz, while those for the FR2 range from 50MHz to 100MHz . Massive MIMO, mmWave beam steering, configurable time and frequency intervals, bandwidth sections, and mmWave propagation are just a few of the technical advances that will be available in future 5G networks. Prior to implementing any communications system, careful planning is required. For wireless network operators, the planning and optimization of the network is essential[1]. This report was developed for the 5G New Radio (NR) planning process using Atoll planning software. The findings of this study should help with the development of the 5GNR network as well as the monitoring of the Secondary Synchronisation Reference Signal Received Power (SS-RSRP) and Secondary Synchronisation Signal-to-Noise and Interference Ratio (SS-SINR) parameters in Tripoli, Libya.

Method

Research Method

For the sake of the 5G NR coverage estimates in Atoll, each pixel on the map is treated as a non-interfering user with a defined service, mobility type, and terminal. This analysis provides information on effective signal levels, signal quality, and throughput.

An accurate user distribution at a certain moment is the foundation of a simulation. A snapshot is the representation of the user distribution at a specific time. Based on this snapshot, Atoll estimates a number of network characteristics, including user throughputs, uplink noise increase, downlink and uplink traffic loads, and more. Iterative calculations are used to calculate simulations.

A simulation, as opposed to a forecast, refers to a specific distribution of 5G users. Figure 1 depicts the network planning in Tripoli town using 5G technology.

This study concentrated on 5G NR planning at a frequency of 26 and 3.5 GHz based on coverage area, i.e. Planning in terms of the capacity and coverage they are served at sites in the covered area. Calculating the route loss and signal level as part of coverage planning tries to determine the signal strength and attenuation between UE and base station. The downlink and uplink data rates as well as cell capacities are calculated during capacity planning.

 ISBN 978-9959-9703-2-9

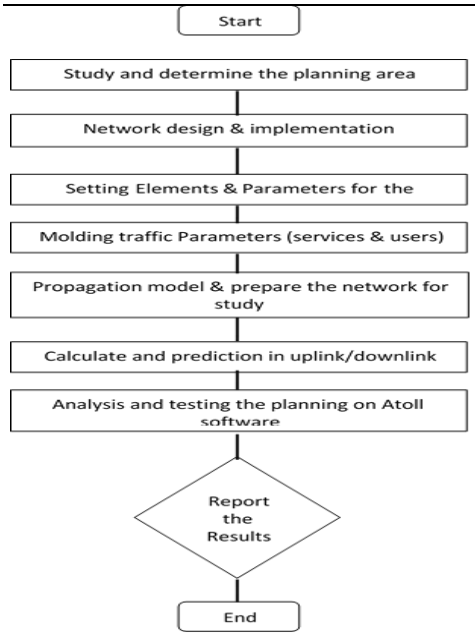

Fig 1: Flowchart of the paper

The number of sites needed to cover the target location was established by the study's findings. In the subsequent step, the parameters derived from the planning outputs were investigated. In reality, the first step in this study was to locate the area and create a digital map of Tripoli, Libya, where 5G New Radio (NR) network planning will take place. The area and geographic location of Tripoli were the data that were needed for this investigation. the taxonomy of services should also be determined. The analysis and execution of a planning simulation based on the data collected and the findings of the calculations served as the paper's concluding stage. Version 4.3 of the Atoll planning program was used to process the data.

A. *Coverage area*

The area that will be covered by a network serves as the basis for the computation used in the coverage planning. In reality, a number of variables, including transmit power, route loss, device sensitivity, radio link budget computation, and cell radius, might have an impact on this planning.

In this study, the network design tried to determine the ideal number of sites for the Tripoli region by estimating the coverage area for each site based on the propagation model to be used in the simulation.

TABLE 1: RSRP Value Category

Kategori	Range
Good	-70 dBm s/d -90 dBm
Normal	-91 dBm s/d -110 dBm
sBad	-110 dBm s/d -130 dBm

B. *Secondary Synchronisation- Reference Signal Received Power Parameter (SS-RSRP)*

The term "SS reference signal received power" (SS-RSRP) refers to the average power (Watts) measured on User Equipment (UE) from the cell transmitter's secondary synchronisation signal (SS).

The Secondary Synchronisation - Physical Broadcast Channel (SS-PBCH) window

 ISBN 978-9959-9703-2-9

duration constrains the measurement time resource for SS-RSRP[11].

C. *SS reference signal received quality (SS-RSRQ) parameter*

The phrase refers to the NSS-RSRP/NR carrier RSSI ratio (also known as secondary synchronisation signal reference signal received quality, or SS-RSRQ), where N is the number of resource blocks in the NR carrier RSSI measurement bandwidth. Both the numerator and denominator measurements must use the same set of resource blocks [11].

D. *The signal-to-noise and interference ratio (SS-SINR) of a system.*

The SS signal-to-noise and interference ratio (SS-SINR) is defined as the linear average of the power contribution (in [Watt]) of the secondary synchronisation signal-carrying resource elements divided by the linear average of the noise and interference power contribution (in [Watt]) of the secondary synchronisation signal-carrying resource elements within the same frequency bandwidth [11].

E. *The rate of data*

Data rate, which is defined in bits per second, is the number of bits of data that may be delivered during a transmission process in one unit of time. The maximum DL and UL data rates supported are computed using the combination supported by the EU.

RESULT AND ANALYSIS

A. *Model of 3GPP 38.900 propagation*

The Atoll GPP 38.900 is a propagation model that can handle frequencies up to 100 GHz. The technical report 3GPP TR 38.900 backs this up.

The 3GPP TR 38.900 as implemented in ATOLL is a semi-deterministic propagation model in that it uses empirical formulas to calculate path loss along transmitter-receiver profiles and determines LoS/NLoS status based on actual geo data (rather than the 3GPP TR 38.900's suggested LoS/NLoS probabilities) [10]. Our propagation scenarios, which include Rural Macro, Urban Macro, Urban Micro, and Indoor Hotspot, are defined by ATOLL 3GPP 38.900. Established sets of empirical formulae are used for both line-of-sight (LoS) and non-line-of-sight (NLoS) propagation under each propagation scenario, known as a configuration in Atoll. These formulae allow for the user-defined and automatic calibration of the route loss terms' coefficients using measurement data.

B. *Standard Propagation Model (SPM)*

The Standard Propagation Model (SPM) is based on the Hata formulas and is suited for scenarios in the 150 to 3500 MHz band over long distances.

 ISBN 978-9959-9703-2-9

This paper applied 5G mmwave a 24-100 GHz frequency range, which is a 3GPP 38901 propagation model used. Also 3.5 GHz that belong to new bands below 6 GHz, which Standard Propagation Model (SPM) used.

C. *Simulation Results*

This research have couple simulation scenarios, the first will be establishment of the 5G NR network In a certain area in the city of Tripoli. The second will be an upgrade from the fourth generation network to the fifth generation, 4G / 5G network will be deployed, there will be large macro cells and 5G small cells to cover the area in addition to the scenario of a crowded party or event.

The locations of the sites were determined using the Site Placement feature of the Atoll programme. The simulation results showed the parameters' values for SS-RSRP and SS-SINR, the average data rate achieved throughout, and the number of gNodeBs necessary to fully cover the selected region of Tripoli.

TABLE 2: THE ESSENTIAL SYSTEM PARAMETERS [4] [6] [7].

Parameters	**Settings**	
	Scenario1 ***5G***	*Scenario2* ***5G/4G***
Frequency band	n78 3.5)/n256 (26) GHz	*5G* (3.5 / 26 GHz) *4G* (900 MHz)
Carrier BW (MHz)	100/200/400	*5G* (100/200/400) *4G* (20/15/10)
Duplex Mode	TDD	TDD
Propagation Model	3GGP / SPM	3GGP / SPM/Cost_Hata
Max power (dBm)	50	50/43 for both
SSS EPRE (dBm)	15	15
Antenna H (m)	30	30
Layer	*5G* Macro cell / small cell	*LTE* Macro cell /*5G* small cell
The type of cell	P-Cell	P-Cell
Minimum SS-RSRP	-140	-140
SS/PBCH numerology	(15 KHz)/ (120 kHz)	(15 kHz)/ (120 kHz)
Number of gNodeB	6 Sites * 3 sectors	12 Sites * 1 sectors
Planning Area	25.11 km²	1.31 km²
Traffic numerology	2 (60 /120 kHz) Normal CP	2 (60 /120 kHz) Normal CP
Radio equipment	5G NR Radio Device	5G NR and LTE Radio Device
Scheduler	Proportional Fair	Proportional Fair
Diversity support (DL)	Transmit Diversity; SU-MIMO; MU-MIMO	Transmit Diversity; SU-MIMO; MU-MIMO
Diversity support (UL)	Receive Diversity; SU-MIMO; MU-MIMO	Receive Diversity; SU-MIMO; MU-MIMO

1. Scenario 1 5G NR network Downlink

A. SS-RSRP

ISBN 978-9959-9703-2-9

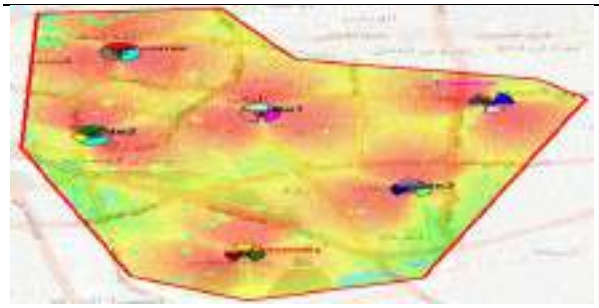

Fig 2: Scenario 1 SS-RSRP Parameter

TABLE 3: Statistical Calculation Scenario 1 SS-RSRP Parameters

Raster Statistic	Value (dBm)
Minimum	-140
Maximum	-70
Mean	-95

Results of the SS-RSRP simulation on coverage area can be seen at Table below.

TABLE 4: The Results of SS-RSRP Scenario 1

SS-RSRP Value	Percentage%	Area km2)	Color
-70 to 80 dBm	44.054	13.406	
-80 to 90 dBm	41.2	11.144	
-90 to 100 dBm	11.6	3.041	
-100 to 110 dBm	1.7	0.24	
-120 to 140 dBm	0.88	0.142	

The forecast utilising 6 sites, each with 3 gNodeB, yielded an average SS-RSRP of -82.02 dBm. This indicates that the preceding technology (5G) has excellent signal strength. SS-RSRP, on the other hand, was measured in this investigation with a minimum value of -140 dBm and a maximum value of -70 dBm.

A. Data Rate

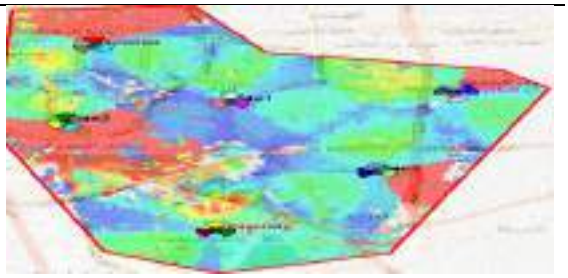

Fig 3: Scenario 1 Data Rate

TABLE 5: STATISTICAL CALCULATION SCENARIO DATA RATE PARAMETERS

Raster Statistic	Value (Mbps)
Minimum	20
Maximum	250
Mean	120

As shown in Table VI the results of the data rate based on coverage area.

TABLE 6: The RESULTS OF SS-RSRP SCENARIO 1

Data Rate Value	Percentage %	Color
250_200 Mbps	28.79	
200_150 Mbps	7.28	
150_100 Mbps	18.38	
100_50 Mbps	25.82	
50_20 Mbps	19.7	

The data rate average that obtained from the prediction using 6 sites each with 3 of gNodeB was 140 Mbps . This means that the data rate is good in the previous technology (5G). Meanwhile, this research showed SS-

 ISBN 978-9959-9703-2-9

RSRP with a low value of 20 Mbps and a high value of 250 Mbps.

C. SNR

Fig4: gNodeB mapping scenario 1 SS-SINR parameter

TABLE 7: Statistical Calculation Scenario 1 SS-SINR Parameters

Raster Statistic	Value by (dB)
Low	-20
High	30
Mean	10

Results of the SS-SINR simulation based on coverage area can be seen at Table below.

TABLE 8: SIMULATION RESULTS OF SS-SNR SCENARIO 1

SS-SNR Value	Percentage %	Area (km2)	Color
30 to 20 dB	96.93	24.18	
20 to 10 dB	1.86	0.48	
10 to 0 dB	0.81	0.2	
0 to -10 dB	0.36	0.1	
-10 to -20 dB	0	0	

The average SS-SNR obtained from the prediction using 6 sites each with 3 sectors of gNodeB was 25 dB. This means that the signal strength is very good in the technology of (5G). Meanwhile, this study showed SS-RSRP with a minimum value of -20 dB and a maximum value of 30 dB

2. *Scenario 2 upgrade from the fourth generation to the fifth generation network, 4G& 5G NR network.*

In this case study, the scenario is proposed 4G & 5G network work together, and a party or festival is supposed to be covered in a certain square in Tripoli. As well as the advent of mmWave bands for 5G NR Small cells, collaboration between 5G, 4G macro cells, and 5G Small cells alone will be necessary in this situation. (i.e. creating the 4G network, as if the present network and then upgrading and developing it to the 5G network on top of the 4G network).

The locations of the sites were chosen to cover as much of the region as feasible in order to have a uniform distribution of users across all cells. The total size of the selected area is 1.31 km² it is a different area than the one in the first scenario 1.

As indicated in the graphic below, six separate transmitters dispersed across several sites will provide LTE coverage for the whole region.

ISBN 978-9959-9703-2-9

Fig5: Distribution of the LTE Sites and Transmitters.

As indicated in the graphic below, 4 separate transmitters dispersed across several sites will provide 5G NR coverage for the whole region. The 4 5G sites will be radiating as macro cells

Fig6: Distribution of the 5G NR Sites and Transmitters.

5G NR limited cell deployment Because the event or festival will take place in a very limited area, small cell deployment at higher frequencies, notably millimeter range frequencies, has been chosen as the means to cover it.

Small cells are pieces of radio equipment that may be mounted on buildings, traffic signals, or other objects.

It is first necessary to choose the Martyrs Square where the ceremony would take place. Martyrs' Square will be used as the location for the festival simulation because it is where the Tripoli City Festival and performances are held. Then, as indicated in the image below, the traffic map is constructed as precisely as possible to make it as realistic as feasible.

Fig 7: The festival area, Martyrs Square

The following figure shows the creation and orientation of the small cells in the festival area (Martyrs Square) in Tripoli.

Fig 8: 5G NR Small cells.

Finally, the "Default Beamformer" is used by all transmitters in both LTE and 5G NR. However, 5G NR need 128 for both

ISBN 978-9959-9703-2-9

transmission and reception antennas, compared to 4 transmission and 4 reception antennas for LTE transmitters

Each transmitter also uses its mechanical azimuth value to direct its beam towards a particular spot.

A. Coverage by SS-RSRP and Transmitters

Using Atoll's prediction, the area that each transmitter will cover in a 4G/5G network can be determined as shown in the following figures.

Fig 9: Area Covered by LTE Transmitters

The prediction chosen depends on the received reference signal strength (SS_RSRP), a common indicator of coverage quality.

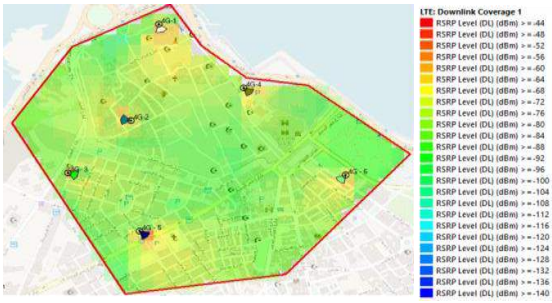

Fig 10: LTE Coverage by SS-RSRP

TABLE 9: LTE SS -RSRP Statistical Calculation PARAMETERS

Raster Statistic	Value (dBm)
Minimum	-140
Maximum	-44
Mean	-96

The forecast made using 6 sites of gNodeB yielded an average SS-RSRP of -79.72 dBm. The bulk of the region seems to be covered by a pretty strong reception signal for the older technology (4G). A minimum value of -140 dBm and a maximum value of -44 dBm were found for SS-RSRP in this investigation.

Fig 11: Area Covered by 5G NR Transmitters

The prediction chosen depends on the received reference signal strength (SS_RSRP), to indicate the coverage quality of 5G gNodeB Transmitters.

ISBN 978-9959-9703-2-9

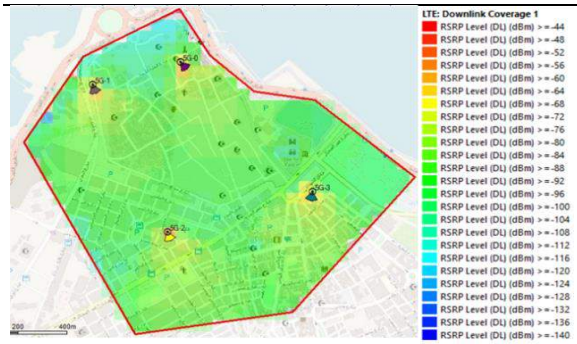

Fig 12: 5G NR Coverage by SS-RSRP

TABLE 10: 5G SS -RSRP Statistical Calculation PARAMETERS

Raster Statistic	Value (dBm)
Minimum	-140
Maximum	-44
Mean	-96

The forecast made using 6 sites of gNodeB yielded an average SS-RSRP of -88.72 dBm. In the previous technology (5G), the vast majority of the region is covered by a pretty strong reception signal. A minimum value of -140 dBm and a maximum value of -44 dBm were found for SS-RSRP in this investigation. A forecast of 5G NR Downlink footprint was developed and is provided as shown below in order to see if the full party or festival can be covered by just two 5G small cells.

Fig 13: 5G Small Cells Coverage by SS-RSRP

This graph demonstrates that a strong SS-RSRP signal level of roughly -90 dBm will cover the party area.

B. 3D Simulator

The simulations will assist in determining weather the deployment was effective or whether the small and macro cells distribution is insufficient to simultaneously cover a concert and this computation zone.

The results of the final simulation, which was run using the two traffic maps of the 5G/4G network's macro and small cells, are depicted in the following image.

Fig 14: 5G/4G Network Simulation Result.

3,565 people are included in this simulation shows that the bulk of them are connected

ISBN 978-9959-9703-2-9

(green dots). with only a small proportion having no coverage or service. The specifics of these percentages are depicted in the image below.

Fig 15: Breakdown of the Rejected Users

Out of 3,565 users, 7 have been denied in total, giving the rejection rate a 0.9% value. It can be observed that 0 have no service and 7 have no coverage in the figure below.

For the concert users, a zoomed image will be presented below because the data above do not depict whether the concert users were accepted by the network or not.

Fig 16: Simulated Concert Users

It appears to be a decent proportion, however in order to do a more thorough research, no concert attendees were turned away from the network owing to any issues. The tables below provide comparisons.The lowest and maximum demand for each service will be compared in the table with the outcomes.

TABLE 11: COMPARISON OF DEMAND AND ACHIEVED SIMULATION RESULTS

Service	Demand connected users	obtained connected users	Min Throughput Demand (UL) Mbps	Max Throughput Demand (UL) Mbps	obtained Throughput (UL) Mbps	Min Throughput Demand (DL) Mbps	Max Throughput Demand (DL) Mbps	obtained Throughput (DL) Mbps
Broadband	2,205	2,203	899.9	8,999	5437.43	1,055.8	10,558	7,881.94
Internet	345	345	11	11	11	44.6	446	205.13
Video	11	11	594	900	900	0	0	0
Voice	377	376	1.41	1.41	1.41	1.71	1.71	1.71
Concert service	33	33	0	1,700	1,700	0	800	800

The table demonstrates that each throughput value obtained falls between the lowest and maximum demand for each service.

Conclusion

This work designed and improved 5G NR networks, models and parameters NR planning was studied and the main objective was to develop a study allowing to implement the dimensions of 5G networks, and then implement the 5G NR network planning for some areas in Tripoli using the simulation program Atoll.for tthis paper Atoll was used to implement coverage predictions, quality predictions, amplitude predictions, and realistic simulations in order to study signal propagation using different propagation models and the benefits of using beamforming and massive MIMO. As a consequence of the 5G NR network design based on coverage area by watching SS-RSRP and SS-SINR parameters, has satisfactory and normal network performance. The average data rate of downlink 140 Mbps. The second case study,

 ISBN 978-9959-9703-2-9

on the other hand, similarly offered coverage in a different location via a 4G/5G network, but this time it also addressed the difficulty of handling a scenario in which several individuals are crammed into a small region, the outcomes in terms of rejected users in this case were successful because the network displayed a 0.2% offline user percentage with no coverage on the map's edges. The majority of service consumers were then pleased with the network's throughput performance.

References

[1] T. Chapman, E. Larsson, P. von Wrycza, E. Dahlman, S. Parkvall, J. Skold, "HSPA Evolution The Fundamentals for Mobile Broadband," Academic Press, 2015.

[2] ITU-R, IMT Vision—Framework and overall objectives of the future development of IMT for 2020 and beyond. Recommendation ITU-R M.2083, September 2015.

[3] D.Jyotsna Agrawal, Evolution of Mobile Communication Network: From 1G to 4G,Physics and Electronics Department, India, Nov 2015 - 11

[4] ITU-R, Future technology trends of terrestrial IMT systems. Report ITU-R M.2320, November 2014.

[5] Dahlman E, Parkvall S, Skld J. 4G LTE-Advanced Pro and the Road to 5G Elsevier 2016.

[6] ITU-R, Guidelines for evaluation of radio interface technologies for IMT-2020. Report ITU-R M.2412 November 2017.

[7] ITU-R, Minimum requirements related to technical performance for IMT-2020 radio inter-Face (s). Report ITU-R M.2410 November 2017.

[8] Shttp://www.dolphmicrowave.com/news/%E3%80%905g%E3%80%915g-spectrum-range-of-3gpp protocol /, September 2020.

[9] 3GPP, "System Architecture for the 5G System (Release 15), TS 23.501; june-2018.

[10] 3GPP, "Release 15, TR 21.915; September-2019.

[11] Rozé, Antoine. Massive MIMO, an angular approach for future multi-user systems at millimeter wavelengths. Diss. INSA of Rennes, 2016.

[12] Dahlman E, Parkvall S, SK LD J. 5G NR: The Next Generation Wireless Access Technology Elsevier 2018.

[13] Benosman. Radia. Sidhoum. Amel. "Studies and simulation of the performance of small cells in 5g systems". Diss. 2013.

[14] P. Nagaraj, "Impact of atmospheric impairments on mmWave based communication, "arXiv.org, 2018. [Online].

[15] http://www.techplayon.com/5g-duplex/, May 2020

[16] 3GPP TS 38.211, NR, Physical Channels and Modulation (Release 15), December 2018.

[17] http://www.techplayon.com/5g-nr-cell-search-and-synchronization-acquiring-system-information/.May 2020

[18] http://www.techplayon.com/5g-network-rf-planning-link-budget-basics/, September 2020.

[19] September 2020.

[20] BOUCHERIT Yassamine, MADANI Samir, LTE RAN Design and Optimization, Institute National Telecommunications and Information and Communication Technologies, 2015.

 ISBN 978-9959-9703-2-9

المؤتمر الدولي الثاني للعلوم والهندسة
2nd International Conference on Science and Engineering
ICSE 2023
Faculty of Engineering - University of Bani Waleed
Bani Waleed, Libya

Paper Code: ICSE-058

PERFORMANCE OPTIMIZATION AND ANALYSIS OF MICROSTRIP PATCH ANTENNA ARRAY FOR 5G AND BEYOND

Mohamed, S, Alshulle[a], Boshra. A. Abdalslam[b]
[a]Military Industries Organization, Bani-walid, Libya.
*dr.engineeralshole@gmail.com

Abstract: Modern smartphones demand a very high bandwidth, making the 5G communication technology a revolution in the wireless communication business. Researchers are motivated to advance communication technology, whether in the software or hardware sectors, by this quick transformation. Additionally, antenna design is regarded as a fundamental topic that requires constant advancement to support 5G wireless communication systems.
This paper's major objective is to create a planner microstrip antenna array that will support 5G communication systems by including all crucial aspects of current wireless communication systems and making use of huge MIMO antenna. The suggested antenna is built to function at 28GHz, a high frequency (mm-waves). The suggested design's large bandwidth (>1 GHz) and high realized gain (>8 dB) satisfy the key aspects of 5G. A two antenna array design with horizontal series-feed components to a planar configuration design is offered as an antenna array to improve the directivity and realized gain of the antenna design. The 11x112 element array (11V12H) design of the proposed antenna must achieve a high gain and high bandwidth at the operating band. A phase shifter (transmission line) is included into the eleven series-feed element configuration to enable beam steering. With this upgrade, the option to tilt the primary radiation pattern in a certain direction was added.
The outcomes demonstrate It is discovered that the suggested antennas accomplish strong pattern diversity, high gain, great directivity, high radiation efficiency across the working band, and very tolerable bandwidth in the aforementioned range, making them extremely suited for 28 GHz band use. The suggested antenna has an 8.71 dB gain and an 8.83 dB directivity. By utilizing a large MIMO antenna, these capabilities are particularly beneficial for wireless communication equipment used in 5G and beyond. Using Ansoft HFSS, the suggested antennas' simulation was performed.

Keywords: (Fifth generation (5G), Voltage Standing Wave Ratio (VSWR), Return Loss (S))

Introduction

The launch of 5G devices that use mm-wave frequencies has posed tough problems for the communications sector, especially for mobile devices. Compared to low frequency bands, mm-wave bands have a higher path loss. Using antenna arrays with higher gains to make up for the significant path loss is one possibility. High-gain antennas provide narrow beamwidth because the gain is inversely related to radiation beam width. Beam scanning is therefore necessary to increase spatial coverage. Although phased arrays may be used to perform beam scanning, they are often narrow-band, expensive, hard to install since phase shifters are used, and take up more space in contemporary wireless

 ISBN 978-9959-9703-2-9

terminals. Therefore, a substitute for phased arrays at mm-wave frequencies is provided by multi-port antennas MIMO, which provide numerous directional beams [1]. Figures (1a) and (1b) compare a standard phased array, which requires phase shifters to direct the beam, and a switchable antenna array, which requires a switch to excite a particular antenna to cover a certain section of the space.

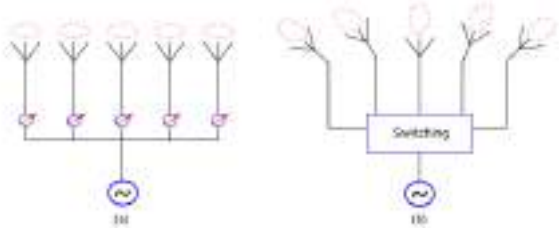

Fig. 1: Antenna array. (a) Phased and (b) switchable [19].

The antenna array's array element consists of several subarrays. A 2D array is made up of several horizontal rows and vertical columns of subarrays. The fundamental concepts and technologies of massive MIMO in the 5G NR system are represented by this huge MIMO antenna. A huge number of antennas are used, which produces precise, user-specific beams and boosts the received signal power. It also lessens the degree of interference with other users. Therefore, a large number of antennas can enhance the overall signal quality. Massive MIMO systems can come in a variety of shapes and sizes depending on where the antenna pieces are positioned. It is possible to assess the features of the huge MIMO radio gear by dissecting it into its various parts. One of the key elements that affects how well a large MIMO system performs is angular coverage, particularly when the system is installed in a building like a stadium or skyscraper and the connected users are dispersed in both horizontal and vertical directions. Antennas A base station may focus its broadcast power into a series of tiny beams by using a lot of antennas. The form and direction of the broadcast signals can be controlled by the base station if it has the capacity to dynamically change the phase and amplitude of (groups of) antenna components. The advantages listed below can thus be anticipated in cellular systems.

1. Enhancement and structuring of the coverage.
2. Enhanced throughput for a single user.
3. Cell throughput increase with numerous spatial divisions.

Dimensions of Massive MIMO Because the antenna array of a base station comprises of subarrays, applying separate digital beamforming (BF) to every antenna element is inefficient in terms of development costs and cell angular coverage. The azimuth and elevation angles would be constrained to a specific range depending on the geometric distribution of the users even if one were to operate a 2D AAS utilizing numerous antenna components. Additionally, since base station antennas are frequently situated in high places like rooftops or masts, their elevation angle does not need to be in the whole range of -90° to 90° in the vertical direction, which would result in excessive transmission power loss. Thus, a subarray is formed by connecting just a single RF transmit/receive chain, which includes a power amplifier and a low noise amplifier, to a small number of neighboring antenna components that are normally oriented in a vertical orientation. Figure (2) shows a 32T32R massive MIMO radio with a subarray made up of three antenna components (N_{sub} = 3).

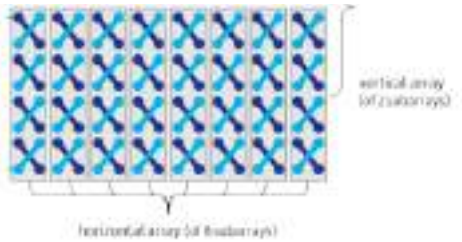

Fig. 2: An example of massive MIMO radio

ISBN 978-9959-9703-2-9

configuration.

A phase shifter or other extra RF device is needed to change a subarray's steering angle since only one digital BF weight is applied inside the subarray [2].
This study introduces the design and analysis of a large MIMO antenna that uses a microstrip antenna array. It is intended to operate at 28 GHz, which is the band used for 5G applications. It succeeds in one band. The suggested antenna is a base station antenna with a good gain at a reasonable price and weight. The prototype antenna array's characteristics, including return loss (RL), bandwidth, VSWR, gain, directivity, and radiation pattern, have been examined.

13. Microstrip Antenna

Microstrip antennas have emerged as one of the most cutting-edge areas of antenna theory and design in recent years, and they are increasingly being used in a variety of contemporary microwave systems [3]. This study gives a general review of the fundamental properties of array and MIMO-style microstrip antennas. Also considered is a new antenna arrangement for better performance.

14. Microstrip Antenna Analysis

The transmission line model, cavity model, and full wave model [4] (which predominantly uses integral equations/Moment Method) are the three models that are most frequently used for the study of Microstrip patch antennas. The transmission line model is the most straightforward and provides the best physical understanding, but it is also the least accurate. Although more complicated in nature, the cavity model is more precise and provides useful physical understanding. Full wave models can handle single elements, finite and infinite arrays, stacked components, arbitrary shaped elements, and coupling. They are also incredibly precise and adaptable. These are far more complicated and provide less information than the two models listed above. This model depicts the microstrip antenna as two slots that are separated by a transmission line that is L in length and W in width. In essence, the microstrip is a non-homogeneous line made of two dielectric materials, usually the substrate and air. Figure (3), which has a thickness of t, depicts the distribution of electric field lines in a transmission line mode.

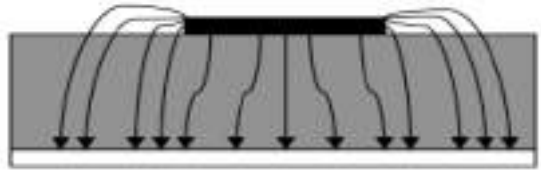

Fig.3: Electric field lines in a transmission line.

Since TEM refers to the direct transfer of electric field lines to the dielectric, it results in the fact that transmission lines cannot support transfer-electric-magnetic TEM. This cannot be allowed, as can be shown in Figure 4, as part of the electric field lines exit into the atmosphere before reaching the dielectric substrate[4, 5].
Relative permittivity will be substituted by _reff, which is somewhat less than _r and is supplied in relation to this issue of transferring field lines into air before it penetrates the dielectric. as [5].

$$\varepsilon_{reff} = \frac{\varepsilon_r+1}{2} + \frac{\varepsilon_r-1}{2\sqrt{1+\frac{12h}{W}}} \quad W/h>1 \qquad (1)$$

Where ε_r h, w, are the substrate dielectric constant, the dielectric substrate height and the patch width respectively. The affective dielectric constant is also a function of resonant frequency fr equation (2).

$$f_r = \frac{v_0}{2\sqrt{\varepsilon_{eff}}(L+2\Delta L_{eff})} \qquad (2)$$

Since there is just one dielectric substrate under and above the transmission line and working at high frequencies makes the microstrip line more homogenous, the effective

 ISBN 978-9959-9703-2-9

dielectric constant is also closer to the real dielectric constant.

According to the plan, the patch's length will be increased on both sides as a result of the movement of electric field lines through the atmosphere, as shown in Figure (4). Figure (4) shows that with vertical polarization (Ev), the electric field lines are oriented in opposing directions on both of the width's edges. Actually, because of the out-of-phase situation, they annihilate one another. The horizontal polarization, on the other hand, is in phase. By combining the resultant fields, the maximum radiated field is produced. It makes sense to assume that the Microstrip Patch Antenna's two slots are what generate the antenna radiation.

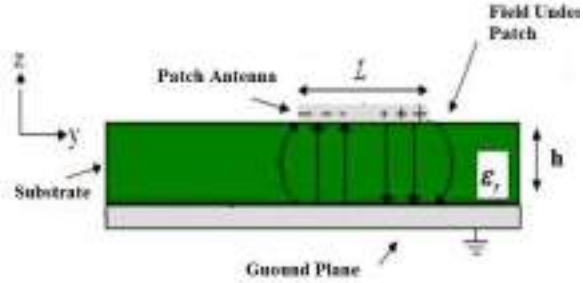

Fig. 4: The Electric Field lines on both edges of microstrip antenna.

A relatively common relation for the normalized extension of the length is [3, 5], which is used to calculate the extension of the length ΔL.

$$\Delta L = 0.412h\frac{(\varepsilon_{reff}+0.3)(\frac{W}{h}+0.264)}{(\varepsilon_{reff}-0.258)(\frac{W}{h}+0.8)} \quad (3)$$

The characteristic impedance of the microstrip line can be written as:

$$Z_o = \frac{120\pi}{\sqrt{\varepsilon reff}(1.393+\frac{W}{h}+\frac{2}{3}\ln(\frac{W}{h}+1.444))} \quad (4)$$

A relatively common relation for the normalized extension of the length is [3, 5], which is used to calculate the extension of the length L:

Antenna Width

The following equation is used to compute the width w [6]:

$$W = \frac{C}{2f_c\sqrt{\frac{\varepsilon_r+1}{2}}} \quad (5)$$

Where, c is the speed of light, f and ε_r are respectably the resonance frequency and the dielectric constant of the substrate.

Antenna Length

The effective length L_{eff} can be calculated by the following equation [6]:

$$L_{eff} = \frac{C}{2f\sqrt{\varepsilon_{reff}}} \quad (6)$$

Then the actual length of the patch is given by the following equation [6]:

$$L = (L_{eff} - 2\Delta L) \quad (7)$$

Ground Planes

The transmission line concept is essentially limited to an unlimited ground plane. However, it has been proven that a finite ground plane may also be employed, if the ground plane is six times greater than the height of the dielectric substrate, plus the needed length or breadth. The ground plane width and length may now be estimated correspondingly as [6]:

$$W_g = 6.h + W \quad (8)$$

$$L_g = 6.h + L \quad (9)$$

15. Microstrip series-feed linear antenna array for 5G application

A 12-element series-feed linear array of rectangular microstrip antenna is presented in this paper. The suggested design comprises of 12 identical rectangular microstrip patches linked with each other by meandering series lines. About half of a wavelength's worth of feed lines link the devices. This permits in-phase fields in the neighboring patches. The array is fed at the middle patch, resulting in a broadside radiation pattern with no beam tilt and symmetrical amplitude distribution. Rectangular microstrip patch antenna comprises of a rectangular shape radiating patch on one side of dielectric substrate which positioned on a ground plane. For acquiring the high performance of patch antenna we must attentive about the height, dielectric

ISBN 978-9959-9703-2-9

constant of material and operating frequency.

16. Antenna Design

The design of the suggested array starts with a design of a conventional antenna utilized to function in 5G frequency range (centered at 28 GHz) in the section 3. The geometry uses linear array of rectangular microstrip antenna, as illustrated in Figure (5). The microstrip series-feed line is used to improve the impedance matching between the element and the feed line. The dimensions of the antenna are: W = 18 mm, L = 19.3 mm. The feed is obtained through a microstrip line with 2.5x 0.4 mm. The two parts of antenna are joined together with little distance between them as indicated Figure (5), as it helps the integration of the array with other RF circuits. The substrate employed was the Duroid 5880 with εr= 2.2, and h=1.6 mm.

Fig.5: Proposed A 12-element series-feed linear array of rectangular microstrip antenna.

After simulation and optimization using HFFS Software, the final dimensions are shown in the Figure (6).

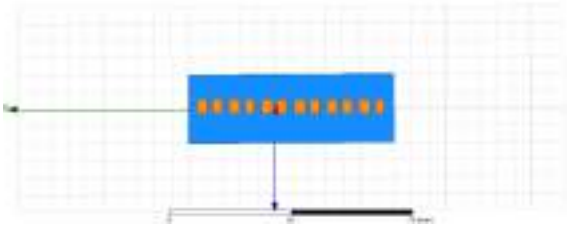

Fig.6. View of A 12-element series-feed linear array of rectangular microstrip antenna, dimensions (mm).

The published structure is carried out in HFSS. The appropriate simulations are carried out to acquire the scattering parameters. The collected findings matched the published results which completes the antenna validation.

16.1 Simulated Results

The simulated reflection coefficient of the series-feed linear array of rectangular microstrip antenna is illustrated in Figure (7). It is clear that the described antenna can functioning band (under -10 dB) at centered 28GHz (-12 dB),with bandwidth which runs from 26.4GHz to 28.7GHz (FBW 8.2%). So, it is pretty evident that this operating band fulfill the design criteria of 5G standard operating frequency.

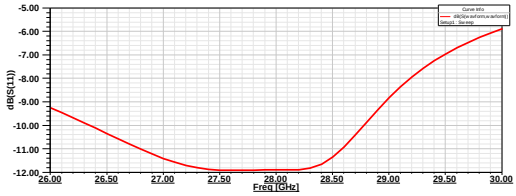

Fig.7: Simulation results of the series-feed linear array of rectangular microstrip antenna.

Figure (8), illustrate the VSWR for 5G microstrip antenna array with good values, we had 1.6 at 28 GHz, this signifies good received signals.

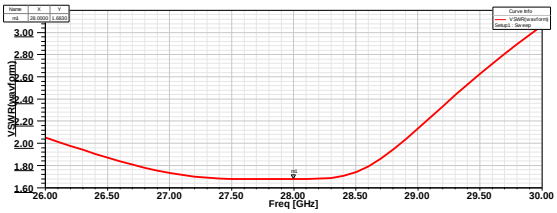

Fig. 8: VSWR of the series-feed linear array of rectangular microstrip antenna.

17. Phased microstrip Linear Antenna Array for 5G Application

One key objective of creating phased-array antennas is to perform beam guiding electronically and therefore to remove the

ISBN 978-9959-9703-2-9

mechanical movement of an antenna system. Electronic beam steering in an array antenna can be done via time delay scanning, frequency scanning or phase scanning methods. However, ease of implementation, inexpensive digital control circuits, rapid reaction time and great sensitivity make the phase scanning approach the most preferred. For optimal operation, a wise alternative for a phase shifter is a switched line or ferrite phase shifter with analog or digital control. A proper decision for the positioning of phase shifters along the feed line is also a very essential element. The orientation may be in series or in parallel. Although the series phases have the advantage of sharing equal power, the downside is the phase compensation circuit since the fundamental inter-element phase shift must be multiplied by the number of elements and the attenuations of the phases build up along the feed line. On the contrary, with parallel combination, although each phase shifter does not share the same power, the key advantage is all phases are independent of each other and therefore modeling of the control circuit becomes easier.

A 11-element linear array of rectangular microstrip antenna identical individual microstrip patch antennas functioning at 28 GHz have been developed and produced as a part of the test platform. These 11 antennas can be implemented as an array.

6.1 Antenna Design

The design of the suggested array starts with a design of a conventional antenna utilized to function in 5G frequency range (centered at 28 GHz). The geometry uses linear array of rectangular microstrip antenna, as illustrated in Figure (9). The microstrip feed line is used to enhance the impedance matching between the element and the feed line. The dimensions of the antenna are: W = 55 mm, L = 8 mm. The distance between the center of two elements has been reached to > 0.5 $\boldsymbol{\lambda}$., as it enables the integration of the array with other RF circuits. The substrate employed was the Rogers RT/duroid5880™, with ⟦εr⟧_= 2.2, and h = 1.6 mm.

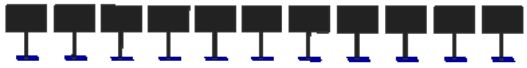

Fig. 9: Proposed A 11-element linear array of rectangular microstrip antenna.

After modeling and optimization using HFFS Software, the final dimensions are presented in the Figure (10).

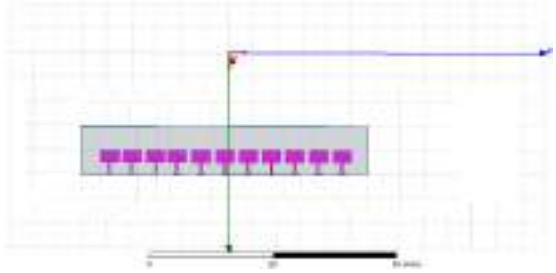

Fig. 10: View of A 11-element linear array of rectangular microstrip antenna, dimensions.

The published structure is carried out in HFSS. The appropriate simulations are carried out to acquire the scattering parameters. The collected findings matched the published results which completes the antenna validation.

6.2 Simulated Results

The simulated reflection coefficient of the series-feed linear array of rectangular microstrip antenna is illustrated in Figure (11). It is clear that the stated antenna can operate band (under -10 dB) at centered 28 GHz (-11.9 dB), with bandwidth which ranges from 26.4 GHz to 28.7 GHz (FBW 8.2%). So, it is pretty evident that this operating band fulfill the design criteria of 5G standard operating frequency.

 ISBN 978-9959-9703-2-9

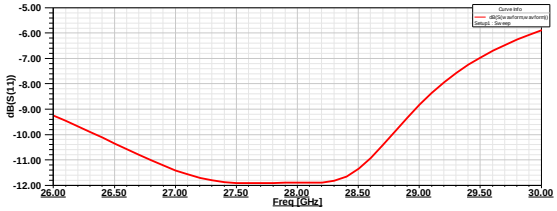

Fig. 11 .Simulation results of rectangular microstrip antenna array.

Figure (12), demonstrate the VSWR for 5G microstrip antenna array with good values, we had 1.6 at 28 GHz, this signifies good received signals.

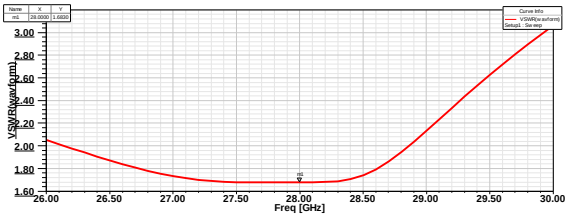

Fig. 12 .VSWR of rectangular microstrip antenna array.

The goal of this study is to develop a microstrip antenna with high directional gain for band 28 GHz applications. Initially we configured our antenna as a single element microstrip patch antenna and after assessing the outcomes of antenna characteristics, operating frequency, radiation patterns, reflected loss, efficiency and antenna gain, we turned it to a series-feed linear array of rectangular microstrip antenna. To enhance more directivity, gain, efficiency, and have better radiation patterns, we designed and studied horizontal arrays of rectangular microstrip antennas and series-feed linear arrays in the following section.

18. Phased Microstrip Antenna Array (1V11H) for 5G Application

Using HFSS, a rectangular microstrip patch antenna array is created by arranging identical horizontal and series-feed components in a planar arrangement. 11x11 (1V11H) shaped patches are arranged into an array to make up the specified element array. the same impedance matching feeding method using a microstrip line. With this method, each antenna element receives an identical amount of power.

7.1 Design Principles

According to Figure (13), the suggested antenna is made up of 11x112 components (1V11H). All of the planned arrays' feeding networks are the same size as a single patch antenna.

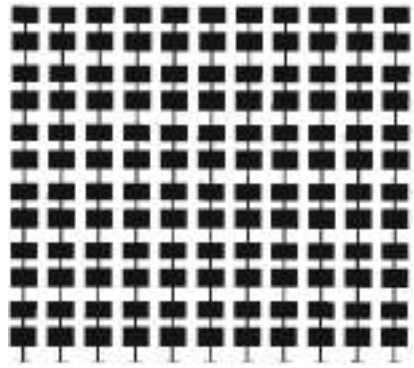

Fig. 13. Proposed geometry of microstrip antenna array.

The antenna is made of a Duroid 5880 substrate with an ε_r value of 2.2 and has dimensions of 166 mm in length and 84 mm in breadth. It may be readily integrated onto the same substrate. Every two vertical components now have a gap between them of greater than 0.5. The patches are designed to improve gain and return loss directivity. The suggested is quite inexpensively and simply fabricatable. The array's shape is shown in Figure 13 using all available dimensions.

After simulation and optimization using HFFS Software, the final dimensions are shown in the Figure (14).

ISBN 978-9959-9703-2-9

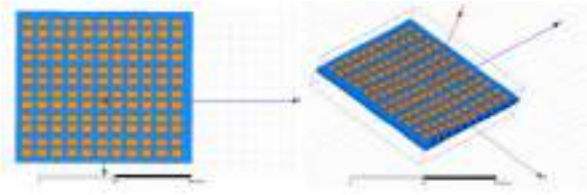

Fig. 14 .View of proposed microstrip antenna array, dimensions (mm).

7.2 Simulated Results of Proposed Antenna

The planned microstrip patch antenna array has already been designed. Using electromagnetic full wave simulation (HFSS), this has been verified.

a- Antenna Return Loss

Figure (15) displays the 11x12 microstrip patch antenna array's simulated reflection coefficient. It is clear that the stated antenna is capable of using the 5G frequency. The operational band's bandwidth ranges from 26.4 GHz to 30.2 GHz (FBW13.5%), with a central frequency of 28 GHz (under -10 dB) and a slope of -14.36 dB. Therefore, it is abundantly obvious that this operating band complies with the 5G standard operating frequency design criteria.

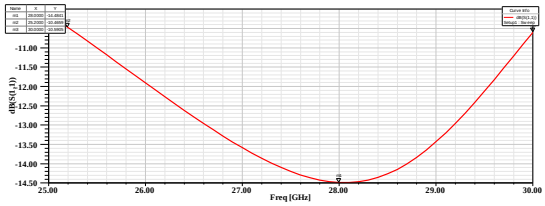

Fig. 15 .The return loss of the proposed microstrip antenna array.

b- Voltage Standing Wave Ratio (VSWR)

Figure (16) displays the VSWR for a 5G application with favorable results; we got a range of 1.4 in the 28 GHz band, which indicates excellent received signals (no reflection).

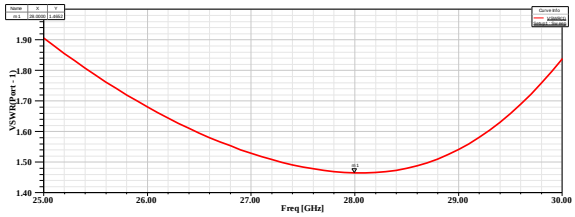

Fig. 16 .VSWR of the proposed microstrip antenna array.

c- Radiation Pattern

Figure (17) depicts the radiation patterns for the proposed microstrip patch antenna array for 5G. Since the antennas are patch type, the radiation patterns in the phi=0 deg (x-y plane) and phi=90 deg (y-z plane) planes are directional as would be expected. The antenna's directional pattern is present in every component.

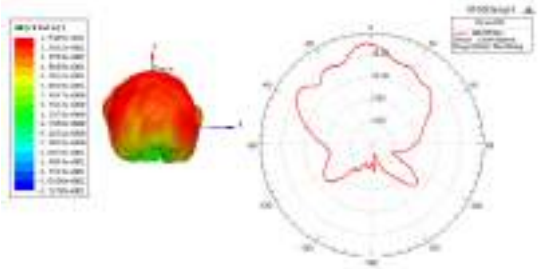

Fig. 17 .2D and 3D radiation pattern of the proposed microstrip antenna array.

d- Gain and Directivity

Peak measured gain for the proposed design is 8.71 dB, whereas peak simulated directivity is 8.83 dB.

ISBN 978-9959-9703-2-9

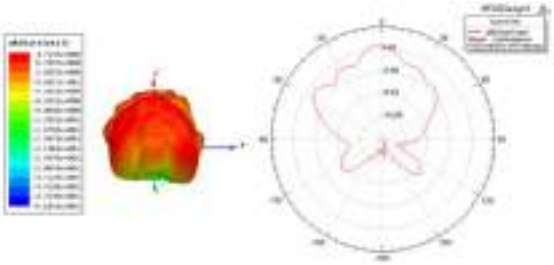

Fig. 18 .2D and 3D gain of the proposed microstrip antenna array.

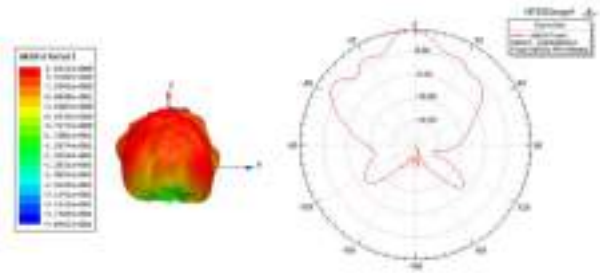

Fig. 19 .2D and 3D directivity of the proposed microstrip antenna array.

The maximal antenna efficiency is also around 97%. Figures (18) and (19) below show 2D and 3D far field plots of the planned antenna's radiating gain and directivity. The antenna's gain and directivity are also good.

e- Current Distribution on the proposed antenna.

The red arrows in Figure (20), which depicts the current distribution pattern at 28 GHz, indicate the strongest current spread in the antenna patch.

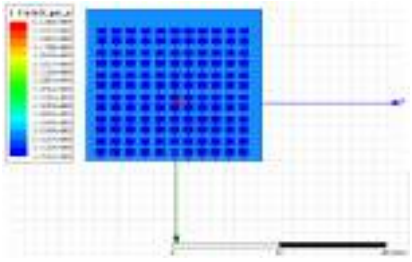

Fig. 20 .Current distribution on the microstrip antenna array.

Conclusion

In this study, we present the findings for the linear, horizontal, and series-fed planned rectangular microstrip patch antenna array constructed using HFSS for the 28 GHz band. The influence on the gain, directivity, and scattering pattern is seen.

The constructed of element antenna arrays in series-feed elements array antennas consists of 12 shaped patches with proportions equivalent to those of a single shaped antenna. With a bandwidth of 26.4 GHz to 28.7 GHz (FBW 8.2%), the simulated return loss parameter is better than -10 dB (-12 dB), and the minimum value of VSWR is around 1.6 at 28 GHz. Finally, in order to further optimize the parameters, planner microstrip array antennas are introduced. In order to create the rectangular microstrip patch antenna array, identical horizontal and series-feed components were arranged in a planar manner. The 11x12 ((11V12H) shaped patches that make up the intended planner array are arranged into an array. the same impedance matching feeding method using a microstrip line. With this method, each antenna element receives an identical amount of power. When designing the array, a space between elements greater than 0.5 is employed. The bandwidth of the return loss, which ranges from -14.36 dB to 30.2 GHz (FBW13.5%), is 26.4 GHz to 26.4 GHz. The better VSWR is 1.56 dB. The antenna's field gain is 8.71 dB, and its directivity is 8.83 dB. The suggested antennas can be made quickly and cheaply and have directed emission patterns, which are valuable. Utilizing a substrate material with a low dielectric constant, the antennas are small and thin. The suggested antennas are simple and inexpensively fabricatable. For usage in huge MIMO antenna and 5G wireless communication equipment, these properties are particularly beneficial. All simulations in this study were done using the electromagnetic

ISBN 978-9959-9703-2-9

program Ansoft HFSS. In addition, the antenna is small and can cover the whole 5G frequency spectrum.

References

[1] T. Beijing, "A Design of Phased Array Antenna Based on the Vivaldi Antenna," pp. 334–337, 2010.

[2] M. Tegegn, "Design and Analysis of a 28 GHz Microstrip Patch Antenna for 5G Communication Systems", International Research Journal of Engineering and Technology (IRJET) e Volume: 08 Issue: 02 | Feb 2021.

[3] G.J.Foschini, "Layered space-time architecture for wireless communication in a fading environment when using multi element antennas",BLTJ, Autumn, 1996.

[4] Primer "Wi-Fi: Overview of the 802.11 Physical Layer and Transmitter Measurements", Copyright © 2013,

[5] P. Ngocle, "Antenna selection for energy effivent MIMO OFDM wirless systems ", university of wollonogong thesis collection, 2015.

[6] C. A. Balanis "Antenna Theory Analysis and Design", John Wiley & sons, inc., Publication, 3rd Edition, ISBN: 0-471-66782, 2005.

 ISBN 978-9959-9703-2-9

المؤتمر الدولي الثاني للعلوم والهندسة
2nd International Conference on Science and Engineering
ICSE 2023
Faculty of Engineering - University of Bani Waleed
Bani Waleed, Libya

Paper Code: ICSE-005

STUDY ON DIFFERENT TYPES OF CAR COOLANT USED IN LIBYAN MARKET: ADDITIVES DROPOUT

Salem M. Embaya [a], Zayad M. Sheggaf[b], Omar A. Addbeeb[c] , Al-Moataz Billah Muhammad[c], and Suhaib Ghaith[c]

[a]Department of mechanical engineering /Higher Institute of Engineering Technologies, Bani Walid, Libya

[b]Libyan Center for Engineering Research and Information Technology Bani Walid, Libya,

[c]Department of mechanical engineering /Bani Walid University, Bani Walid, Libya

*Crosspnding author: salemdalla89@gmail.com

Abstract: In this research, the effect of four types of coolants used in the local market, (namely Abrad, Freezetone, Algabl Green, and Algabl Red), on the rate of additive dropout quantity was studied, and the cylinder block alloy of the Chevrolet Optra engine car was used as the study material, The results of the chemical analysis technique show that the investigated material is Al-Si alloy. The cylinders have a rectangular cross-section. The samples were placed inside a glass container for each type of coolant, three samples were used. A sensitive balance was used with an accuracy of 1/10000 to measure the weight of the samples before testing and their weight after the immersion process for different periods of time to calculate the rate of additive dropout in g/h/cm2. Preliminary results showed that the additives were deposited on the samples surfaces in different quantities. In addition, after cleaning the samples with distilled water and drying them, these deposits remained stuck to the samples. Through the results obtained after weighing, it was found that the Algabl green coolant has the lowest rate of sedimentation. The additive dropout quantity was about 0.00000478 g/hr/cm^2, followed by Freezetone with 0.00000713 g/hr/cm^2, while the amount of additive dropout with the Abrad type was 0.00002543 g/hr/cm^2. The additives dropout causing deteriorating cooling system performance, where deposit the additive on cylinder block wall will reduce the transferred heat generated inside composition chambers, cylinder heads and blocks are highly and dynamically loaded structures that transfer a lot of heat, so the choice of coolant type for engine is very important to ensure that engine is operating properly.

Keywords: (additives dropout, engine car coolant)

Introduction

Liquid coolants like water and ethylene glycol are used into cooling system of internal combustion engines, and to improve their thermo physical properties metal oxides is added. Generally, a coolant is diluted by city water and well water. Since the quality of the waters is largely differ from place to place, a special care must be exercised when a

 ISBN 978-9959-9703-2-9

corrosive water, which includes a lot of sulfate ion and chlorine ion, or a hard water, which includes a large of calcium and magnesium, is used [1, 2]. The quality of water in Japan is regarded as generally good, while water in Europe and Asia is hard and that in America the chance is high that water containing a high degree of sulfuric acid ion and chlorine ion is used for dilution, which can reflect on additives of coolant, and should be considered [3]. Additives for coolant are classified into the following four types. The first is called an anode type that becomes immobilized after forming an oxidation film or adsorption film on a metal surface. The second is called a cathode type that covers the metal surface with hydroxide deposited due to a chemical reaction or electrochemical reaction and thereby inhibits rust. The third is called an adsorption type that forms an anticorrosive film of a single molecule through combining with metal. The last is a film-forming type that forms insoluble polymer after reacting to copper [2, 4]. Engine was made of cast iron because of ease casting and nonappearance of appreciable shrinkage of volume, vibration damping wear resistance and machinability. Recently, aluminum used in automobiles to produce many engine parts such as piston and cylinder block to save weight [5, 6]. Engine coolant used in vehicle to minimize the degradation of nonmetals and prevent the corrosion of the metals in the cooling system. Various forms of corrosion could occurred in cooling systems of engine, including uniform corrosion, galvanic corrosion, crevice corrosion, pitting corrosion, intergranular corrosion, erosion corrosion, and cavitations corrosion [7]. An applicable treatment is used to give the cooling water the correct properties that prevents service problems. cooling water that has not had treatment can soon cause problems in the cooling system such as corrosion, sediment or hard particles. Corrosion protection oils (emulsion oils) are not recommended for the treatment of the cooling water. If instructions about the use of corrosion protection oils are not obeyed and coolant checks are not sufficient, then water / oil emulsion can occur. This can cause the cooling system to become clogged. Recently, there are a lot of coolant liquids in the Libyan market, some of which are manufactured locally and others are imported. Some of these liquids caused problems in car engines, such as corrosion and blockage of the engine or radiator caused by additives dropout. In this study, the percentage of additives dropout for four different coolants will be determined and the corrosion at core plug measured.

Experimental procedure

 ISBN 978-9959-9703-2-9

A consumed car engine cylinder block used in the present study. The chemical composition of the alloy was determined using FOUNDARY-MASTER Pro emission spark spectrometer. Table 1 shows the chemical composition of cylinder block alloy.

Table1: the chemical composition of cylinder block alloy

Element	Cr	Zn	Mg	Mn	Cu	Fe	Si	AL
Wt.%	0.0260	0.714	0.257	0.151	3.59	0.702	11.5	Bal.

Twelve specimens are taken from cylinder block, three for each coolant type, which are cut into plates (35 mm×35 mm×12 mm) and then grounded and polished. Subsequently, they are immersed into engine coolants, which are Abrad, Freeztone, Algabl green, and Algabl Red for 72, 120, 216, , and 360 hr at room temperature as shown in Figure 1. The weight of additives dropout, and that precipitated on specimens is measured using a 1/10000 electronic balance.

Fig. 1 : Experimental setup

Results and discussion

Figure 2 shows the surface morphologies of samples after 360 hr of immersion in coolants.

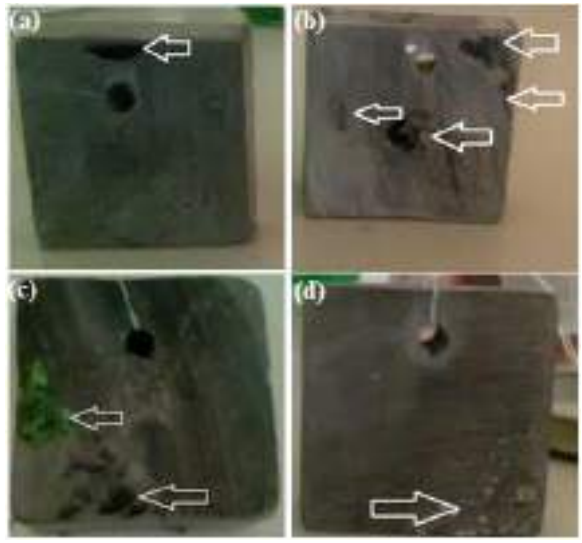

Fig. 2 : Effect of coolant type on surface of cylinder block alloy (a) Algabl green, (b) Algabl red, (c) Abrad, and (d) Freeztone

As can be seen, the surfaces of the alloys extremely affected by the extension of immersion time, and the surface revealed significant additives dropout. It has been reported that many coolant additives like silicate and phosphate, which used as corrosion inhibitors in engine coolant, have limited solubility [8]. That meant that if the antifreeze or additives got too concentrated in

ISBN 978-9959-9703-2-9

the coolant, then the excess phosphate and/or silicate would "dropout" of the coolant. These dropout problems caused premature water pump failures, radiator blockages, and heater core problems. Table 2 shows weight of samples before and after immersion on coolant liquids during 72, 120, 216 and 360 hrs.

Table 2 : Weight of samples before and after immersion in coolants

	ABRAD			Algabl Red		
sample No.	1	2	3	1	2	3
original Wt. g	38.2874	35.7261	35.7255	35.4405	32.3886	36.2103
Area, cm^2	43.30458	42.6451	42.3577	40.4787	40.3726	42.74574
time, hr						
72	38.2918	35.7933	36.0393	35.4587	32.507	36.4925
120	38.2961	35.7975	36.046	35.4626	32.3112	36.4646
216	38.3217	35.8651	36.1334	35.5072	32.5955	36.4817
360	38.319	35.8621	36.123	35.5094	32.5926	36.4885

	Algabl Green			FREEZETONE		
sample No.	1	2	3	1	2	3
original Wt. g	34.8777	30.7508	37.0199	38.9742	31.85	34.2368
Area, cm^2	42.934642	41.7195	45.4320	42.9275	43.8436	42.8007
time, hr						
72	34.8968	30.7724	37.0483	38.998	31.8863	34.2843
120	34.898	30.7685	37.0471	39.0057	31.8881	34.2833
216	34.9232	30.7845	37.0845	39.1735	31.9316	34.3781
360	34.9144	30.7884	37.0652	39.1755	31.9322	34.3783

Fig. 3 shows three samples average of additives dropout quantity for four types of coolant. Indeed, considerable differences are noticed in the case of Algabl Green and Freeztone compared with Abrad and Algable Red, which were 0.00000478, 0.00000713033 g/hr/cm^2 for Algabl Green and Freeztone, respectively, while 0.00002.54304 and 0.0000263792 g/hr/cm^2 for Abrad and Algable Red, respectively.

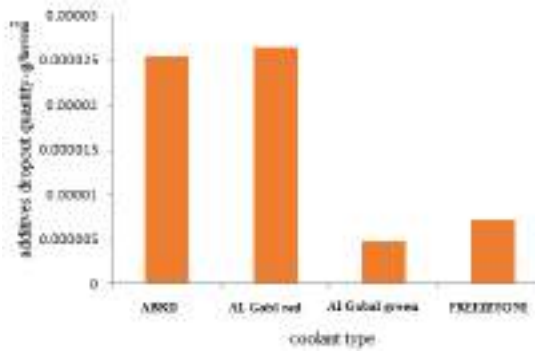

Fig. 3 : Effect of coolant type on additive dropout quantity

The additives can drop out of solution, causing deteriorating cooling system performance and wear in the coolant pump. This situation is greatly aggravated by poor coolant

ISBN 978-9959-9703-2-9

maintenance. In fact, more than 40% of diesel engine downtime is caused by cooling system failure. Even with good maintenance, conventional automotive or heavy duty coolant should be replaced every 2 or 3 years [9]. Most cooling system water contains calcium and/or magnesium from drinking water supplies. Water that contains over 100 ppm of these minerals is considered “hard water”. It is wonderful to drink, but these minerals can form scale in engine cooling systems. As the concentration of these minerals increases, so does the probability that you will have cooling system scale problems. The level of dissolved solids in coolant water is generally referred to as the “total hardness” reported in parts per million (ppm). Cooling system additives that contain anti-scale chemicals can allow the use of moderately hard water. It is best to use water that is at least as good as the recommended water quality listed in the ASTM standards [10].

Conclusion

In this study, the effects of engine coolant car on quantity of additive dropout were investigated. A significant notes observed using visual inspection, as the additives precipitate on the samples with different colors, However, these deposits were in different quantities with the different type of coolant used. Weight measurements showed that Al Gabal green was the lowest in dropout rate, which produced locally, compared with Abroad coolant type that import from overseas. In addition, the high dropout rate of Al Gable red compared with Al Gable green could be related to the dye type, as both coolants are produced by the same local company.

Acknowledgment

References

1. Alves, L.O.F.T., et al., Comparative performance analysis of internal combustion engine water jacket coolant using a mix of Al2O3 and CuO-based nanofluid and ethylene glycol. Energy, 2022. 250: p. 123832.

2. Iijima, K. and S.O.K. Iwakata, Development of Non-Amine Type Engine Coolant. Komat’s Technical Report, 2002. 48(149).

3. Cape, J.N., D. Fowler, and A. Davison, Ecological effects of sulfur dioxide, fluorides, and minor air pollutants: recent trends and research needs. Environment International, 2003. 29(2-3): p. 201-211.

4. Kokilaramani, S., et al., Microbial influenced corrosion of processing industry by re-circulating waste water and its control measures-A review. Chemosphere, 2021. 265: p. 129075.

5. Eyre, T., Wear resistance of metals. Treatise on Materials Science and Technology, 2013. 13: p. 363-442.

6. Alakoul, K.A., A.R.H. Wetaify, and A.N. Huseein, Protection of engine cylinder against thermal and mechanical failure by nano-oxide coating.

 ISBN 978-9959-9703-2-9

7. Rowe, L., Automotive Engine Coolants: A Review of Their Requirements. Engine Coolant Testing: State of the Art, 1980. 705: p. 3.

8. Рузимов, С. and Д. Муйдинов, STUDY ON CAR ANTIFREEZE AND COOLANT: MAIN PROBLEMS, MAINTAINING, REPAIRING AND DIAGNOSING SERVICES. Журнал Технических исследований, 2020. 3(5).

9. Hudgens, R. and R. Hercamp. Test Methods for the Development of Supplemental Additives for Heavy-Duty Diesel Engine Coolants. in Engine Cooling Testing: Second Symposium. ASTM STP. 1986.

10. Ruzimov, S. and D. Muydinov, STUDY ON CAR ANTIFREEZE AND COOLANT: MAIN PROBLEMS, MAINTAINING, REPAIRING AND DIAGNOSING SERVICES. ТЕХНИКА ФАНЛАРИ. 5(3): p. 46.

 ISBN 978-9959-9703-2-9

المؤتمر الدولي الثاني للعلوم والهندسة
2nd International Conference on Science and Engineering
ICSE 2023
Faculty of Engineering - University of Bani Waleed
Bani Waleed, Libya

Paper Code: ICSE-014

RECYCLABILITY OF ALUMINIUM PISTON ALLOY

Mohammed A. Abuqunaydah[a], Zayad M. Sheggaf[b], Muheieddin Meftah Elghanudi[c], Salem A. Salem[d]

[a]High Vocational Libyan Center of Casting, Libya
[b]Libyan Centre for Engineering Research and Information Technology, Bani Walid, Libya
[c]Mechanical Engineering Department/Surman College of Science and Technology, Surman, Libya
[d]Mechanical Engineering Department/College of Technical Sciences, Bani Waild, Libya
*Crosspnding author: zayad1976@gmail.com

Abstract: One of the most recycled and recyclable materials now in use is aluminium. Frequently, aluminium cans, automobile components, and window frames are recycled back into itself. A vital component of the contemporary aluminium industry is recycling. Recycled aluminium production uses only around 5% of the energy required to produce new aluminium, resulting in lower carbon emissions and cost savings for both corporations and end users. As a result, today's use of roughly 75% of all aluminum created throughout history. Recycling rates for aluminium exceed 90% in the majority of industrial sectors, including the construction and automobile industries. Every year, the United States saves more than 90 million barrels of oil equivalent through industry recycling. Capability to re-melting aluminium alloys scrap without losing its alloying elements and finding optimum pouring temperature are the purpose of this paper, and the results will determine the possibility of reusing piston alloy to make components similar to those they were recycled from. Automotive cast aluminium scrap obtained from pistons were used as experimental specimens, which were melted via an electrical furnace then poured at four different temperatures, namely 680, 720, 760, and 800 °C into a strip fluidity steel mould. The chemical composition of the four specimens were examined using spark emission spectrometer and the length of melted metal that flowed through the mould strips was measured as well to determine fluidity. Also, an optical microscope was used to detect microstructure defects. The chemical composition ratios of alloying elements before and after recycling showed that the resulting alloys could be closely equivalent to the commercial alloy that was originally used to make the components. In addition, the higher the pouring temperature the greater the casting fluidity. Generally, the consumed aluminium piston alloy can be re-melted and used to produce many parts.

Keywords: (casting, recycling, aluminium alloys)

Introduction

Due to their unique properties, such as low density, high thermal conductivity, simple net-shape fabrication techniques (casting and forging), ease of machinability, high reliability, and excellent recycling characteristics, aluminum alloys are the preferred material for pistons in both gasoline and diesel engines. Al-Si casting alloys are chosen often to produce

 ISBN 978-9959-9703-2-9

engine parts due to their great castability, where silicon plays an important role, particularly, having high thermal properties, which increases fluidity [1, 2]. Castability is the ability of an alloy to be cast without formation of defects such as cracks, segregations, pores and porosity. In addition, loss-alloying element during re-melting could occur. Therefore, casting characteristics of AI-Si alloys require careful melting, degasifying, and pouring. Failure to exercise adequate control during the melting and casting processes is one of the most prominent problems [3]. The pouring of molten metal into the mold and subsequent filling are crucial processes in the casting process. It has been noticed in foundry practice that some alloys fill the mould cavity completely and reproduce its intricacies in the finished casting better than others do when filling moulds of sophisticated design, particularly those that involve thin portions. Therefore, testing for mould filling capacity is crucial since it not only aids in choosing the right alloy composition for a certain application, but also helps with quality control and lowers the likelihood of casting rejections. A lack of fluidity could contribute to the development of mistune castings or the absence of surface characteristics [4, 5]. The characteristics of mould and metal jointly are involved in determining fluidity, and pouring temperature is one of the factors related to metal. G. Timelli et. al [6] investigated the fluidity of four different high pressure die cast Al–Si and Al–Si–Cu alloys at a pouring temperature range of 580–760 °C. They found that fluidity linearly increases at increasing temperatures. In the other study, Chennakesava Reddy et. al [4] found out that influence of pouring temperature on fluidity of Al-Si-Mg cast alloys is positive, whereas the higher the pouring and mould pre-heat temperature the greater the casting fluidity, as pouring temperature range is between 650 and 850 °C, and the mould was preheated before pouring to 400 °C. An effective recycling temperature in the aluminium foundry has been investigated in this study, which shows that the alloy chemical composition of the melted piston scrap is consistently equivalent to original piston alloy, also the strip fluidity of Al-Si piston alloy with different pouring temperature has been studied, that is used for gravity die casting, the strip fluidity test measures the ability of alloy to fill a mould of different cross sections and thus provides a wider specification of actual casting conditions.

Experimental

A consumed car engine's pistons were used in the present investigations. The chemical composition of the samples was determined

 ISBN 978-9959-9703-2-9

using FUNDARY-MASTER Pro emission spark spectrometer before and after recycling. The pistons were cut into small pieces then melted in an electrical furnace, and the tests were carried out in the pouring temperature range of 680 – 800 °C with a step of 40 °C. Because fluidity is an empirical measure of a processing characteristic, this property measures in one of the several types of fluidity tests. Two common types are the mould fluidity spiral and the strip fluidity test. According to previous studies [4, 8], a strip fluidity testing mould (a tool steel strip type mould) was chosen for this investigation, the design of which is shown in Fig. 1, which includes four strips, a pouring basin, and a running system. Each strip was of 10 mm width and 200 mm length. The thicknesses of the strips were 1, 3, 5, and 7 mm.

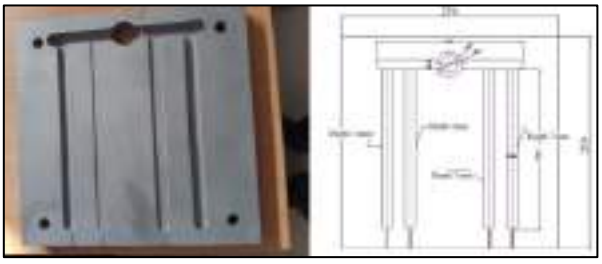

Fig. 1: Fluidity test mould

Results and Discussion

Figure 2 shows the ingot after solidified, the molten metal flow can be seen through the strips with 5 and 7mm depth only, as the mould is not heated (casting with mould at room temperature). The same results were found by A. Heidarzadeh et. al [7] as the molten metal did not pass through the strip with 1 mm thickness and solidified at running system which was cast without preheating the mould. However, the length of the metal flow in strips mould of 5 and 7 mm depth are taken as a measure of casting fluidity.

Fig. 2: Photographic view of strip fluidity test casting

The effect of pouring temperature on the fluidity alloy is shown in Figure 3. It can be seen that the fluidity increases with raising pouring temperature. The degree of super heat of the alloy grows with increasing pouring temperature, this leads to keeping the alloy as a molten form for a longer period, also the

 ISBN 978-9959-9703-2-9

super heating of alloy decrements the fluid viscosity, so the liquid melt is able to flow over a longer distance due to increase in fluid life [4, 7]. In addition, increasing the pouring temperature delays the nucleation and growth of fine grains at the tip of the flowing metal into the mould channel, which leads to increment of the fluidity. [8]. On the other hand, an increase in the fluidity of the alloy as a result of an increase in the pouring temperature may lead to one of the most important defects of the microstructure, which is porosity. Porosity in castings mainly occurs due to gas entrapment in the melt at a highly turbulent flow of liquid metal into the die cavity [9].

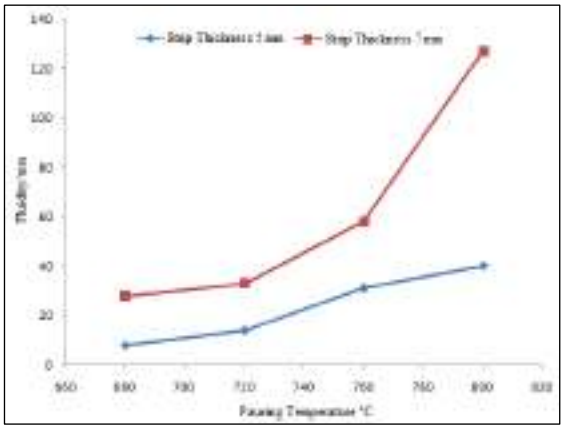

Fig. 3: Effect of pouring temperature on fluidity

Table 1 gives the chemical composition of alloys, original alloy and alloys pouring at different temperatures, which were obtained from recycled aluminium piston.

Table 1: Chemical composition of alloys

Temp °C	Si	Fe	Cu	Mn	Mg	Zn	Cr	Ni	Ti	Al
Orig.	10.1	0.288	3.13	0.614	0.742	0.0579	0.0168	0.28	0.0163	Bal
890	10.8	0.467	1.85	0.338	0.727	0.387	0.0191	0.592	0.0191	Bal
720	11.2	0.508	1.91	0.411	0.787	0.0405	0.0182	0.469	0.0134	Bal
760	13.4	0.516	1.08	0.0621	1.13	0.0732	0.0636	0.971	0.0106	Bal
800	13.9	0.668	1.29	0.133	0.719	0.221	0.0167	0.676	0.0118	Bal

It can be observed that the alloy chemistries of the alloys obtained from recycled pistons are well within the normal specifications for pistons. It is noteworthy that the alloy chemistries are fairly consistent, the Cu content is slightly low, whereas its content varies from a low of 1.08 wt.% for alloy poured at 760 °C to a high of 3.13 wt.% for original alloy. Furthermore, it is anticipated that alloys made from piston scrap will include between 10.1 and 13.4 wt of Si. Typically, near eutectic Al-Si cast alloys with significant amounts of Cu, Mg, and Ni are used to cast pistons. Because of their outstanding fluidity and feedability and close to zero solidification range, eutectic alloys are chosen. High dimensional stability, scuff resistance, wear resistance, and lower thermal expansion are further benefits of the high Si content to the alloy. These are essential functional specifications that pistons must meet in order

 ISBN 978-9959-9703-2-9

to work properly across a large operating temperature range. In some cases, pure alloying element could be added during melting to prevent the loss of that element, which is caused by oxidation [12, 13]. Finally, it is seems that the consumed piston alloys can be reused to cast components similar to those they were recycled from without significant loss of performance. Furthermore, it has been reported that rapid cooling during casting may cause segregation defect at surface of re-melted alloys, as shown in Figure 4, this defect can be fixed by removing a few millimeters from specimen surface using milling process ref. A study on the recycling 7075. Segregation process may occur at the end of solidification [14].

Fig. 4: Segregation process at surface of alloy poured at 800 °C, x50

When the aluminum alloys are melted at high temperatures, gases like hydrogen are easily formed in the molten metal and cause defects such as gas porosity and shrinkage porosity [10]. The increased porosity can cause a reduction in the mechanical properties [11]. As shown in the above results, melting the alloy at a high temperature caused an increase in fluidity; on the other hand, it led to form common casting defects, which can no longer be treated.

Conclusion

1. Casting fluidity of alloys increases with increasing pouring temperature of melt.
2. The mould with strips less than 5 mm of thickness needs pre-heating where the molten metal did not reach the strips.
3. Alloy addition is not required in the melting process
4. No significant change in the chemical composition after re-melting can be observed.
5. Segregation process can be reduced to a minimum with slow cooling during casting process.
6. The consumed aluminium piston alloy can be re-melted and used to produce many parts, as recycling is one of the most effective ways to produce alloys in our country.

 ISBN 978-9959-9703-2-9

Acknowledgment

The authors would like to express their deepest gratitude to the foundry and metallurgical lab technicians at High Vocational Libyan Center of Casting.

References

1. Davis, J.R., Aluminum and aluminum alloys. 1993: ASM international.
2. Stefanescu, D., J. Davis, and J. Destefani, Metals Handbook, Vol. 15--Casting. ASM International, 1988, 1988: p. 937.
3. Sigworth, G., The modification of Al-Si casting alloys: important practical and theoretical aspects. International Journal of Metalcasting, 2008. 2(2): p. 19-40.
4. Sumanth, M., A.C. Reddy, and V. Murti, FLUIDITY TESTING ON Al-Si-Mg CAST ALLOYS. life. 1: p. 2.
5. Radwan, B., Treatment of a Liquid Al-Si Alloy: Quality Control and Comparison of Two Melt Degassing Processes. 2020.
6. Timelli, G. and F. Bonollo, Fluidity of aluminium die castings alloy. International Journal of Cast Metals Research, 2007. 20(6): p. 304-311.
7. Heidarzadeh, A., et al., The effect of copper addition on the fluidity and viscosity of an Al-Mg-Si alloy. Journal of materials engineering and performance, 2014. 23(2): p. 469-476.
8. Srinivasa, R. and R. Patil, Characterization of Casting and Deformation Process of a Metal Alloy. International Research Journal of Engineering and Technology, 2017. 4(2).
9. Wilczek, A., P. Długosz, and M. Hebda, Porosity characterization of aluminium castings by using particular non-destructive techniques. Journal of Nondestructive Evaluation, 2015. 34(3): p. 1-7.
10. Ahmad, R., N. Talib, and M. Asmael. Effect of pouring temperature on microstructure properties of Al-Si LM6 Alloy sand casting. in Applied Mechanics and Materials. 2013. Trans Tech Publ.
11. Irfan, M., et al., Porosity reduction and mechanical properties improvement in die cast engine blocks. Materials Science and Engineering: A, 2012. 535: p. 108-114.
12. Barnes, S. J., & Lades, K. (2002). The evolution of aluminium based piston alloys for direct injection diesel engines (No. 2002-01-0493). SAE Technical Paper.
13. Özer, G., Burgucu, S., & Marsoğlu, M. (2012). A study on the recycling of aluminium alloy 7075 scrap. Materials Testing, 54(3), 175-178.
14. Otani, L. B., Matsuo, M. M., Freitas, B. J. M., Zepon, G., Kiminami, C. S., Botta, W. J., & Bolfarini, C. (2019). Tailoring the microstructure of recycled 319 aluminum alloy aiming at high ductility. Journal of Materials Research and Technology, 8(4), 3539-3549.

 ISBN 978-9959-9703-2-9

المؤتمر الدولي الثاني للعلوم والهندسة
2nd International Conference on Science and Engineering
ICSE 2023
Faculty of Engineering - University of Bani Waleed
Bani Waleed, Libya

Paper Code: ICSE-026

REDUCING DRAG IN TRUCK TRAILER USING NACA PROFILE

Wanis M. Shibani[a], Abdulhakim A. Abidat[b], Khaled S. ALwaer[b]
[a]Mechanical Engineering, Higher Institute of Science and Technical Mesallata, Libya
[b]Mechanical Engineering, Higher Institute of Science and Technical Al-Garabulli, Libya
*Corresponding author: wanismustafa@yahoo.com

Abstract: Almost seventy percent of all goods are transported with the help of commercial vehicles with tractor-trailer combinations. Despite the fact that intensive aerodynamic studies have been taken into account for a few decades within the automotive industry. In theory the engine will only deliver fifty percent of the power to move the vehicle forward as the other fifty percent will be wasted against the significant and contrasting drag force. Computational Fluid Dynamics, often known as CFD, is a very powerful and effective tool which is used in engineering practice to find solutions to aerodynamic problems. The ANSYS Fluent (version 2016) software has been used to conduct the analysis throughout this paper and solidworks (version 2016) software to draw all model used. This article contains an in-depth study involving the usage of NACA aerofoil on the critical area of a trailer to help reduce the drag coefficient and hence exploit the fuel saving potential. Various different NACA aerofoils have been used in the study of the effectiveness of each profile for the given purpose. The best choice of NACA profile concluded from the CFD results is NACA 0012 with five parts attached to the truck trailer.

Keywords: (Aerodynamics, CFD, Truck Trailer)

Introduction

Commercial vehicles have not been the main area of research and application of aerodynamic advancements. The aerodynamic design of commercial/heavy vehicles has only been active for around thirty years [1]. Since commercial vehicles are the biggest fossil fuel consumers, most fleet operators are forced to improve the aerodynamic styling of their vehicles. Aerodynamic efficiency is directly proportional to the frontal area, the density of the head wind, the speed the vehicle is travelling at and the coefficient of drag, which is simply dependent on the shape of the vehicle.

It can be noticed from the above formula of drag force that at velocities higher than thirty miles per hour, drag force becomes significantly strong and hence important and up to fifty percent of engine power can be consumed to overcome this drag force.

At the present time, the tractor-semitrailer is one of the most common forms of transport. It

 ISBN 978-9959-9703-2-9

plays a crucial role in cargo transportation because it is flexible and faster when compared with railway transportation [2].

One of the important ways which it used in order to conserve energy and to protect the global environment is improving the aerodynamic drag, so the main concern of the automotive industry is to reduce fuel consumption. The evolution of the vehicle body and the reduction of drag is fundamental for developing fuel consumption and driving performance so that it will increase the vehicle's capacity.

In spite of this, recent studies have shown that saving 3% in fuel consumption could be the result of reductions of 10% in aerodynamic drag [3].

In a lot of cases, the most dominant resistive forces for over 50% of overall resistance to motion are the drag force, thus it influences the fuel efficiency of the vehicle [4].

The one way that may be used to reduce fuel consumption for heavy vehicles can be attained by modifying truck shapes to reduce the aerodynamic resistance (drag) [5]. As result of that, the vehicle design is still a controlling worker when creating vehicle body shapes. In last year's achieved flow amendments and drag decreases without the need to change a physical shape by use an active flow control techniques [3], General, the flow field created around a vehicle shape, which it will influence the aerodynamic force system generated [4].

The drag of heavy vehicles is commonly decreased by using a range of methods, for example streamlining airflow, covering exposed under body structures, decreasing wake and flow separation, all of which could be achieved by cab and trailer mounted devices, for example cab roof and side fairings, trailer-front fairings and base-flaps. Despite the availability of these solutions, it not all these solutions have been exactly appropriate in the automotive industry, because there are some issues, such as cost, maintenance, safety and efficiency, which reduce the alternatives available to fleet operators [6].

The need for truck aerodynamic improvement was realized almost four decades ago when NASA's Dryden Flight Research Centre at Edward Sir Force Base started the research in this particular area. The initial work was carried out by Kenworth (1985) and proved the importance of cad-fairing adding onto the trailer in order to achieve reduced aerodynamic drag force.

Model Construction

Figure 1 shows the key dimensions of the semi-trailer model that was used in this analysis, which was created Solidworks V.2016. The height of the semi-trailer has been

 ISBN 978-9959-9703-2-9

taken as a standard 4.2 m based on commonly found dimensions and was taken as the baseline configuration. The dimensions of the semi-trailer, wheels and ground clearance are typical of real conditions, the length of the semi-trailer 16.28 m, the width 2.6 m and the length of the trailer 12.73 m, with wheels diameter 0.5 m.

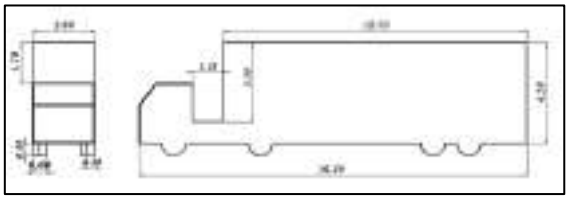

Fig. 1: The model dimensions by meter

The dimension of the NACA Airfoil, variations were created in the model by the application of the same foil, once with the usage of three equal splits, once with the usage of five equal splits and finally without any split along the entire height of the trailer end.

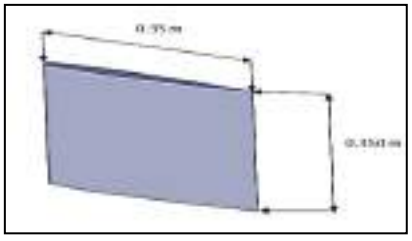

Fig. 2a: The NACA airfoil model 1

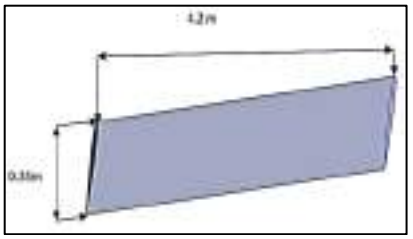

Fig. 2b: The NACA airfoil model 2

NACA Aerofoil Profiles

Three different NACA airfoils were used to analyses the effectiveness of each profile and its validity for the application. The three NACA airfoils used for the study are as given, NACA airfoil 0006, NACA airfoil 0012, and NACA airfoil 2412.

The semi-trailer with three NACA airfoils on each side of the semi-trailer.

The NACA length is 0.35 m and width 0.35 m, the gap between the NACA airfoil and the trailer is 0.2m, the position of the NACA airfoil on each side of the semi-trailer are one on the top and one on the bottom of the trailer and the last one was put in the middle, between the top and bottom NACA.

ISBN 978-9959-9703-2-9

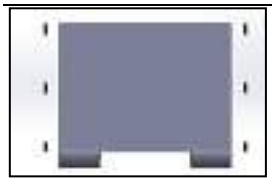

Fig. 3: The tractor trailer with three NACA profile

The semi-trailer with five NACA airfoils on each side of the semi-trailer.

The NACA has length of 0.35 m and width of 0.35 m, the gap between the NACA airfoil and the trailer is 0.2 m, the positions of the NACA airfoil on each side of the semi-trailer are two on the top and the bottom of the trailer and the last three were put between the top and bottom NACA, so as the distance between each NACA was 0.6125 m.

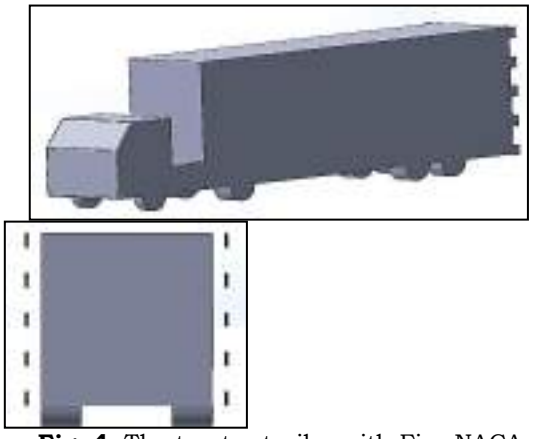

Fig. 4: The tractor trailer with Five NACA profile

The semi-trailer with one NACA airfoil on each side of the semi-trailer.

The NACA has width of 0.35 m and length of 4.2 m, the same as the length of the trailer of the truck, the gap between the NACA airfoil and the trailer is 0.2m.

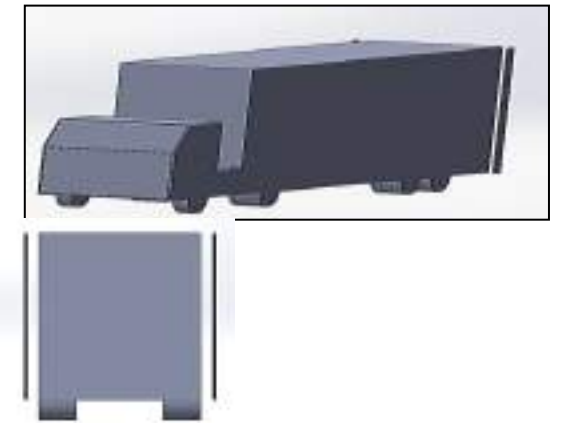

Fig. 5: The tractor trailer with one NACA profile

Computational Domain

The various models of the semitrailer formation under test were each imported into a three-dimensional, geometrically generated flow domain. The flow domain consisted of a rectangular cuboid volume containing the semitrailer model, as shown in the figure. The flow domain had a length of 260.48 m, such that the inlet of the flow domain was 5.L upstream and the outlet was 10.L of the semi-trailer models (where L is the total length of the semi-trailer model). The longitudinal side walls

 ISBN 978-9959-9703-2-9

of this area were at a distance of 3.W from the model (where w is the total width of the semitrailer model), so the width of the flow area was 18.2 m, and the distance between the horizontal top wall of the area and the top of the semitrailer was 4.H (where H is the total height of the semitrailer model), so the height of the flow area was 22 m.

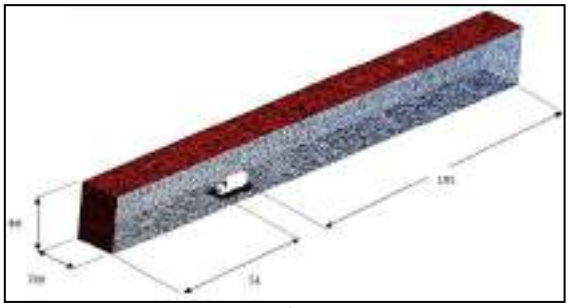

Fig. 6: Domain Geometry

Justification of Mesh

Mesh generation is the second step of CFD and is considered one of the main steps in CFD after the definition of the domain geometry. At this stage the CFD will divide the domain into a number of smaller elements, to resolve the flow physics within the domain geometry that has been created. This leads to the creation of a mesh (or grid) of cells overlying the whole domain geometry. The number of elements in the mesh within the computational domain will have an effect on the accuracy of a CFD solution, which means increasing the number of cells will increase the accuracy of the CFD solution [7]. The first step in the mesh before choose the correct size of mesh is a justification of mesh, which was used during the study as it holds a vital impact in the results in terms of not only the accuracy of results obtained, but also the computational time, which has been one of the most critical elements in the success of this article. This was achieved by using different elements of face size, so it was done by using the bigger element face size to domain and smaller elements face size to the body of the semi-trailer without NACA airfoil. The mesh independence test was done at meshes of 1.25 million, 2.5 million and 5.6 million with velocity of 40MPH (17.88m/s) and angular velocity of rotation wheels (35.76 rad/s) was used for this test. The results of the mesh independence test are shown in the table below.

Table. 1: The justification of mesh

Number of Case	Size of Mesh (m)			Number of elements	Force (N)			Drag coefficient
	Min	Max	Body of semi-trailer		Pressure	Viscous	Total	
1	0.1	1	0.165	1256890	2504	60	2504	1.057

ISBN 978-9959-9703-2-9

2	0.1	1	0.07	2514836	2319	93	2413	1.019
3	0.02	1	0.04	5564584	2232	115	2348	0.99

It may be seen from the table that the accuracy of the results has been increased by increasing the number of elements. Mesh was chosen for this article with approximately 5.6 million elements, and also it has been used 12 million elements for model and the result was far less in comparison, that it was 0.9% difference with used 5.6 million elements. To save time required for the analysis, mesh with 5.6 million elements was selected as standard for all the remaining results for the article with a quality of mesh 96%.

Boundary Conditions

In this article, the velocity of the domain of the semi-trailer was defined as a velocity inlet with three different velocities at three different cases, which are 17.88 m/s (40 M/h), 22.35 m/s (50 M/p) and 25 m/s (56 M/h). The side face of the domain behind the model was defined as pressure outlet zero, and the bottom face of the domain flow was defined as moving wall by velocity 17.88 m/s (40 M/h), 22.35 m/s (50 M/p) and 25 m/s (56 M/h). The wheels of the domain flow were defined as rotation wheels with angular velocity as 35.76 rad/s, 44.7 rad/s and 50 rad/s. The figure 7 shows the names of all the faces of the semi-trailer.

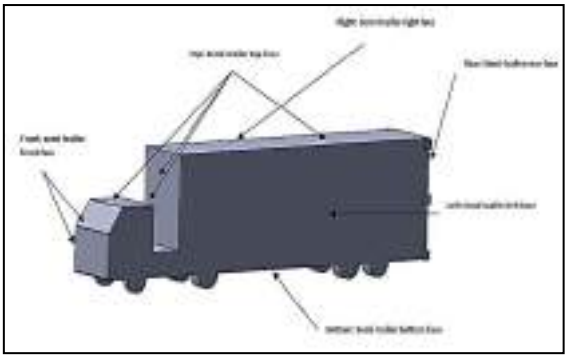

Fig. 7: Truck areas of aerodynamic interest

Results And Analysis

There have been rather interesting result trends found during the study, details of which can be found in next section. Data collection and representation has been carefully chosen to convey the results in the most direct manner. All the NACA foil profiles are compared side by side showing the drag force, density of air, frontal area of the commercial vehicle and, most importantly, the aerodynamic drag percentage reduction, which has been critical information since it highlights in black and white that which NACA foil is the most appropriate for the purpose within the NACA air foils used in this research.

Flow Velocity Variation

 ISBN 978-9959-9703-2-9

Three different flow velocities were used to ensure the in-depth study corresponding to the effect of flow velocity change with the maximum flow velocity used as the maximum motorway speed limit for commercial vehicles in the UK.

The three flow velocities used for the analysis are as follows 17.88 m/s (40mph), 22.35 m/s (50mph), and 25.03 m/s (56mph).

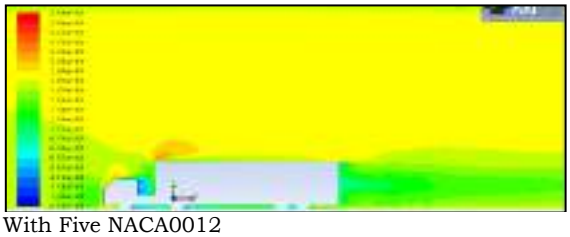

With Five NACA0012

Fig. 8: Contours of velocity magnitude, Semi-trailer at velocity of 17.88 m/s

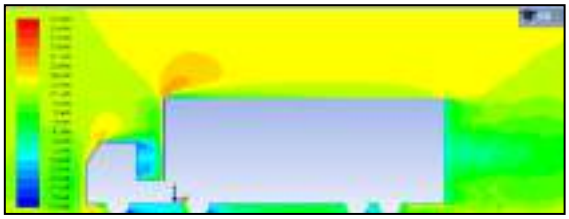

With Five NACA0012

Fig. 9: Contours of velocity magnitude, Semi-trailer at velocity of 22.35 m/s

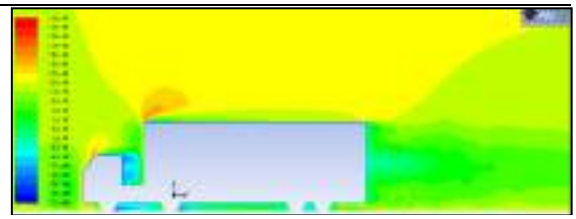

With Five NACA0012

Fig. 10: Contours of velocity magnitude, Semi-trailer at velocity of 25 m/s

The tables below are contained the data collected from CFD results and other calculations for various speeds suggested.

Table 2: shows different velocities with various DRAG and drag coefficient reading

Velocity = 17.88 m/s					
Type of NACA	Drag (N)	Air density (kg/m3)	Area (m sq.)	Drag coefficient	Drag coefficient (%) Decrease
Truck without NACA	2348	1.225	12.09	0.992	0.000
Truck with three NACA 0006	2351	1.225	12.13	0.990	0.203
Truck with five NACA 0006	2360	1.225	12.16	0.991	0.059
Truck with one NACA 0006	2362	1.225	12.17	0.991	0.095
Truck with three NACA 0012	2359	1.225	12.17	0.990	0.236

ISBN 978-9959-9703-2-9

Type of NACA	Drag (N)	Air density (kg/m3)	Area (m sq.)	Drag coefficient	Drag coefficient (%) Decrease
Truck without NACA	4569	1.225	12.09	0.987	0.000
Truck with three NACA 0006	4571	1.225	12.13	0.984	0.310
Truck with five NACA 0006	4586	1.225	12.16	0.985	0.202
Truck with one NACA 0006	4590	1.225	12.17	0.985	0.239
Truck with three NACA 0012	4584	1.225	12.17	0.983	0.402
Truck with five NACA 0012	4601	1.225	12.23	0.982	0.511

Velocity = 25 m/s

Truck with one NACA 2412	3759	1.225	12.26	1.001	1.271
Truck with five NACA24 12	3696	1.225	12.23	0.987	0.165
Truck with three NACA 2412	3682	1.225	12.17	0.988	0.069
Truck with one NACA 0012	3708	1.225	12.26	0.988	0.068

Type of NACA	Drag (N)	Air density (kg/m3)	Area (m sq.)	Drag coefficient	Drag coefficient (%) Decrease
Truck without NACA	3657	1.225	12.09	0.989	0.000
Truck with three NACA 0006	3659	1.225	12.13	0.986	0.300
Truck with five NACA 0006	3672	1.225	12.16	0.987	0.183
Truck with one NACA 0006	3675	1.225	12.17	0.987	0.224
Truck with three NACA 0012	3671	1.225	12.17	0.985	0.354
Truck with five NACA 0012	3684	1.225	12.23	0.984	0.481

Velocity 22.35 = m/s

Truck with one NACA 2412	2418	1.225	12.26	1.007	1.480
Truck with five NACA24 12	2376	1.225	12.23	0.992	0.016
Truck with three NACA 2412	2366	1.225	12.17	0.993	-0.056
Truck with one NACA 0012	2384	1.225	12.26	0.993	-0.071
Truck with five NACA 0012	2367	1.225	12.23	0.988	0.387

ISBN 978-9959-9703-2-9

Truck with one NACA 0012	4632	1.225	12.26	0.987	0.089
Truck with three NACA 2412	4599	1.225	12.17	0.986	0.095
Truck with five NACA2412	4616	1.225	12.23	0.985	0.201
Truck with one NACA 2412	4693	1.225	12.26	0.999	-1.201

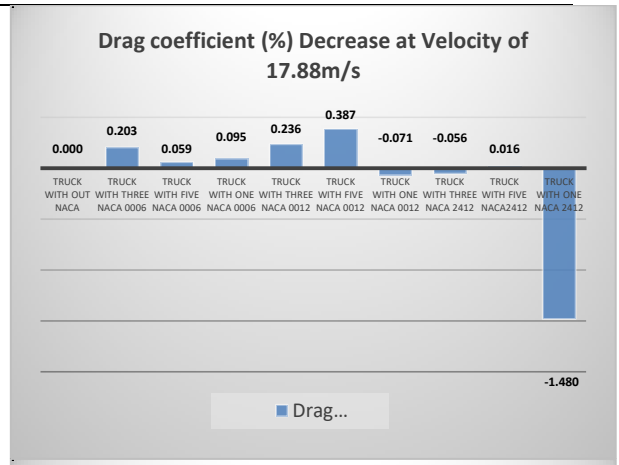

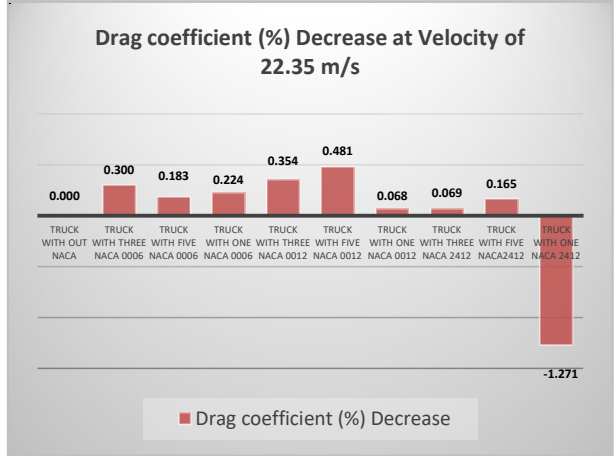

Individual Effects and Velocity Effect

Tables and the charts below show that the drag coefficient (%) decrease at various velocities. Indeed, the best NACA profile showed good results is NACA 0012 with five parts distributed at the back of truck-trailer. As can be seen from fig. 11 the values percentage of drag coefficient decrease are 0.387 % at speed of 17.88 m/s, and 0.481 % at speed of 22.35 m/s, and 0.511 % at speed of 25 m/s. Actually, it can be concluded that the drag coefficient % decreases more at high speed suggested.

ISBN 978-9959-9703-2-9

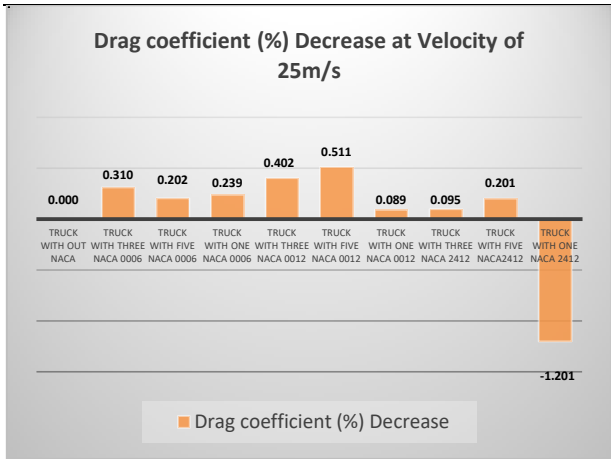

Fig. 11: Shows drag coefficient (%) decrease at velocities of (17.88 m/s, 22.35 m/s, and 25 m/s) respectively.

Tables and coming charts showed drag coefficient at different velocities. It's clear that the lowest drag coefficient appointed at truck with five NACA 0012 compared to other models of NACA shapes attached to the truck. Fig. 12 shows that, the lowest drag coefficient for the truck with five NACA 0012 is 0.988 at velocity of 17.88 m/s, and the lowest drag coefficient for the truck with five NACA 0012 is 0.984 at velocity of 22.35 m/s, and the lowest drag coefficient for the truck with five NACA 0012 is 0.982 at velocity of 25 m/s. where it can be concluded that, the best choice of NACA profile for the truck trailer is NACA 0012 with five parts attached to truck trailer.

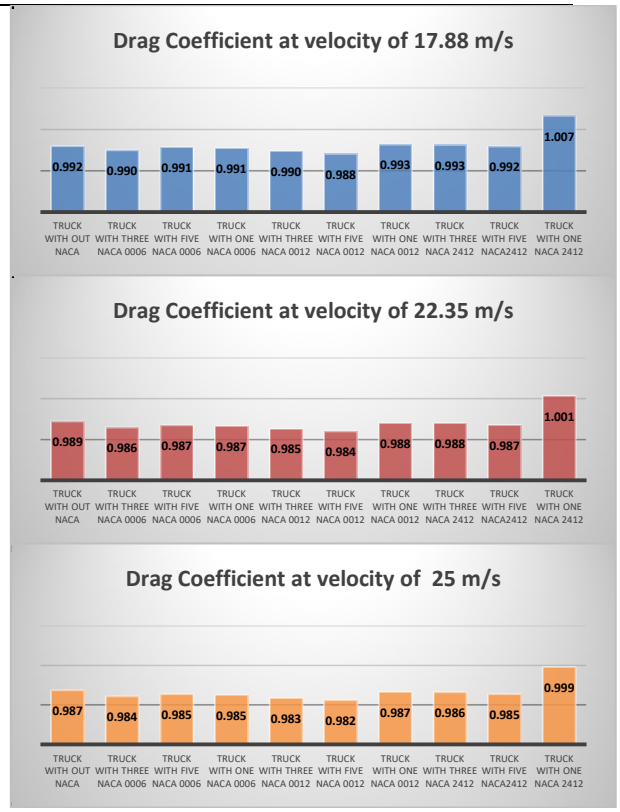

Fig. 12: Shows drag coefficient at velocities of (17.88 m/s, 22.35 m/s, and 25 m/s) respectively.

CFD Results Validation

Since it is a novel concept, unfortunately the study cannot be directly validated with the desired accuracy. However, the magnitude of the total impact involving both the effect of velocity on the aerodynamic drag on commercial vehicles and the range of NACA airfoils can be compared to match the trends. As the results suggest, the application of NACA

ISBN 978-9959-9703-2-9

airfoil has a considerable beneficial effect on the commercial vehicle's aerodynamics and significantly helps to reduce aerodynamic drag, and hence the fuel economy can be increased with the usage of this phenomenon. It can also be noticed that the NACA feature has a far greater impact on higher velocity, hence maximum benefit can be obtained at the top speed limit of 56 mph.

Conclusion

The results from the article involve the baseline model with the incorporation of cab fairing. This was important as it represents the best industry practice for further aerodynamic improvement of the vehicle design, in this case the trailer aerodynamic efficiency against drag force. Now another novel concept is being applied to significantly reduce the wake region with the help of NACA airfoils. Airfoils help to keep the flow attached to the foil and hence dipping more into the wake region before the flow separates from the rear end of the trailer. Once the wake region or rear end turbulence region is decreased significantly in area, drag force onto the trailer will also be achieved, which has been proven through results obtained with the help of CFD analysis for this article.

The conclusions which can be drawn after the study has been carried out to reduce aerodynamic drag using NACA airfoil can be described in the following points:

1) Aerodynamic drag can be significantly reduced with the application of NACA airfoil onto the body of the trailer near the wake region.

2) As proved with the in-depth CFD analyses, NACA airfoil provides the benefit of reducing aerodynamic drag and hence helps to reduce fuel consumption.

3) It can be seen that, by usage of NACA airfoils, drag force is increased due to increment of the front area of the vehicle and the drag coefficient is increased simultaneously. Therefore, with presence of NACA airfoil, an unusual and inverse relationship between drag force and drag coefficient is established.

4) The best choice of NACA profile concluded from the CFD results is NACA 0012 with five parts attached to the truck trailer.

Abbreviations and Acronyms

CFD	Computational Fluid Dynamic
NACA	National Advisory Committee for Aeronautics
NASA	National Aeronautics and Space Administration
MPA	Meter Per Hour

ISBN 978-9959-9703-2-9

m	Meter
s	second
rad	radian
L	The total length of the semi-trailer model
W	The total width of the semi-trailer model
H	The total height of the semi-trailer model

References

[1] V. Modi, "Moving surface boundary-layer control: a review," Journal of fluids and structures, vol. 11, pp. 627-663, 1997.

[2] S. Matěj and N. Jiří, "Aerodynamic devices to reduce the base-and underbody drag of semitrailer unit," in AED2004: sborník příspěvků 4th International Conference on Advanced Engineering Design na CD, 2004.

[3] R. Littlewood and M. A. Passmore, "Aerodynamic drag reduction of a simplified squareback vehicle using steady blowing," Experiments in fluids, vol. 53, pp. 519-529, 2012.

[4] V. Malviya, R. Mishra, and J. Fieldhouse, "CFD investigation of a novel fuel-saving device for articulated tractor-trailer combinations," Engineering Applications of Computational Fluid Mechanics, vol. 3, pp. 587-607, 2009.

[5] I. S. Ali and A. A. Mahmood, "Improvement of aerodynamics characteristic of heavy trucks," in 3rd international conference on recent trends in engineering and technology, 2013, pp. 246-255.

[6] Z. Mohamed-Kassim and A. Filippone, "Fuel savings on a heavy vehicle via aerodynamic drag reduction," Transportation Research Part D: Transport and Environment, vol. 15, pp. 275-284, 2010.

[7] G. H. Yeoh and K. K. Yuen, Computational fluid dynamics in fire engineering: theory, modelling and practice: Butterworth-Heinemann, 2009.

 ISBN 978-9959-9703-2-9

المؤتمر الدولي الثاني للعلوم والهندسة
2nd International Conference on Science and Engineering
ICSE 2023
Faculty of Engineering - University of Bani Waleed
Bani Waleed, Libya

Paper Code: ICSE-027

WEAR RESISTANCE EVALUATION OF PUNCHING PROCESS IN BANI WALID INDUSTRIAL FACTORY

Mahmod Gomaha* ¸Mohamed Alaalam, Abdussalam Ali Ahmed[b]
[a,b] Mechanical and Industrial Engineering Department, Bani Waleed University, Bani Walid, Libya
*Corresponding author: samadmssamad@gmail.com

Abstract: The process of punching has become prominent in the manufacturing industry because of its ability to make highly specialized parts that minimize waste and cost. With punching process, the goal is to use what is stamped/punched out rather than what is left after going through the die. In this paper, the evaluation of wear resistance and productivity of cutting die that uses to make holes in gun safety part is discussed and studied. The results of this work showed that, there is attempts by some engineers in the factory to teach a high productivity of the die, but they failed, Where the dies used had many problems, including the decrease in the toughness of the punch, and an error in the design of the punch, To solve the problems that occur in the die, which were the reason for reducing productivity, we suggest choosing other wear-resistant materials to design new dies and making a suitable design for the die by applying the shear angle and suitable clearance between the bunch and the die.

Keywords: Blanking process, Wear, Cutting die, clearance

Introduction

Bani Walid Industrial Factory is one of the important factories in Libya. It is located in Bani Walid City about 10 Km from the city center. It has been opened in (1982) to produce light machine guns such as revolvers, pistols, rifles, general-purpose rifles and some special equipment for army. The planning section in the Factory has reported some defect problems in one of the production lines especially for the Klachenkov rifles. This production line is to fabricate one of the parts, which is the safety part in the rifles. This part consists of a ring fixed on a small bar, which is fixed on the rifle body. To fix the safety part on the rifle, a hole on the ring and bar should be drilled. To make this hole, the safety part pass through the cutting process by the cutting die to obtain an initial hole and then the hole is machined to obtain the right and accurate measurements. The production strategy for the safety part is to produce 3000 pieces daily (i.e., 1500 pieces per shift). These pieces pass under the pressing bar which contains the cutting die to the pulling machine. The cutting die is sharpened between the shifts (i.e., after producing 1500 pieces). This has been achieved by the old cutting dies, which are made in Russia. Once the old cutting dies run out of the stores, the Factory has fabricated these dies locally due to difficulties to obtain them from abroad. Unfortunately, those locally fabricated dies did not perform well when they have been used in the production line.

There are some problems related to this die such as:

 ISBN 978-9959-9703-2-9

1-The productivity of those dies have been decreased to 430 pieces before sharpening.
2-The percentage of defected parts is increased. The ring separates from the bar during the cutting process or following processes. The quality control team does not accept this percentage.
3- The Broaching tool failure before the expected lifetime during the brushing process. The productivity of this tool has dropped rapidly from 1200 pieces to 250 pieces.

Since these problems appeared, the planning section in the Bani Walid Industrial Factory has tried to overcome them but without any success. Therefore, the main goal of this study is to investigate and solve the problems concerning the cutting dies. Reverse engineering played a major role in collecting the data for the cutting dies. But since the original dies are not available, the locally fabricated dies are used. The strategies that have been tried by the planning section were studied to benefit from them and realize the failure reasons to avoid them in the new study. In order to improve the cutting die, it is required that all dimensions should be measured and prepare all drawings using computer.
Mechanical properties such as surface roughness, hardness have been measured. Metallographic examination was carried out to study the microstructure of the old die. Once all data have been obtained, many experiments have been carried out with some modifications to solve the problems.

Reverse Engineering

Reverse engineering is the disassembly, measurement and documentation of all the parts of an existing product unlike conventional forward engineering which begins with a problem or idea and works toward a solution or product, reverse engineering begins with a product and results in understanding, documentation or idea. (1)
Reverse engineering is a four-stage process in the development of technical data to support the efficient use of capital resources and to increase productivity. The stages, all of which are conducted after a rigorous prescreening of potential consist of data evaluation, data generation, design verification, and design implementation.
This process is typically applied for the improvement of production lines manufacturing capabilities; ideally, groupings of parts by system or subsystem produce the best pool of candidates for reverse engineering.
Accurate data development for long-term maintenance and support of technical capabilities is the cornerstone of reverse engineering. This process provides a level of technical support. Since reverse engineering requires the investment of capital, reverse engineering projects are carefully prescreened to ensure a high probability of success.
Those projects, which do not meet prescreened criteria, are typically not considered, berceuses success in reverse engineering is generally measured by return no investment. Figure (1) illustrates the difference between the traditional design process and the reverse engineering process. (2)

 ISBN 978-9959-9703-2-9

Figure 1: Traditional versus Reverse engineering design process (1)

Blanking and punching Operation

Whether the die shown in figure (2) is a blanking die or a punching die depends solely upon its intended use. it is called a blanking die if it is meant to produce blanks *B* of a desired contour and size by cutting them out of the required type of material *A*. the blanks are the desired product (piece parts) made by the die. In most cases, the material remaining after the blanks have been cut out is considered scrap.

If the purpose of the die is to make openings of a desired contour and size in the required material *A*, it is called a piercing die. In this case *A* represents the piece part and *B* is called the slug. The slug is usually considered scrap.

The basic elements of both dies are identical. The name of the die is derived from its intended use. The physical effects of the tool upon the stock material are the same whether it is punching in a piece part or whether it is punching out blanks which are the desired product of the die. (11)

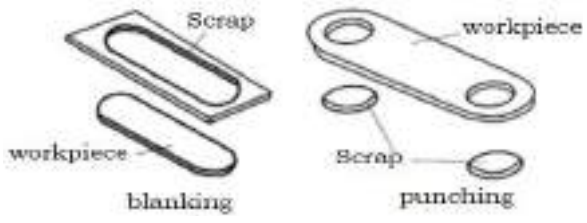

Fig. 2: Differences between blanking and punching (11)

Proper cutting clearance is necessary to the life of the die and the quality of the piece part. Excessive cutting clearance results in objectionable piece-part characteristics; insufficient cutting clearance causes undue stress and wear on the cutting members of the tool because of the greater punching effort required. (12)

The clearance between the punch and the die plays an important role in the blanking process.

The selection of clearance will influence the life of the die or punch, the blanking force, the quality of the workpiece.

In figure (3) blanking force-punch stroke curves for different clearance are presented. For material considered as rigid-plastic, the blanking force arising from the elastic deformation of the material is omitted. From fig (3) it can be seen that an increase in the clearance causes a decrease blanking force (13)

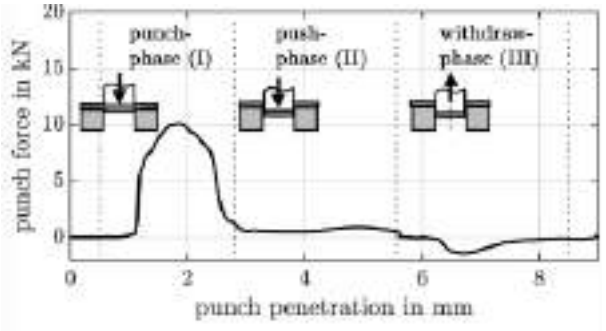

Fig. 3: The simulated punch stroke-blanking load curve. (10)

Determining cutting clearance

The physical properties and the thickness of the stock material are the factors that determine the amount of cutting clearance. The thickness is easily measured but the physical properties in relation to cutting clearance are not. Therefore, the optimum clearance must often be determined by actual experiment. (12)

The die-clearance chart figure (4) may be used to find the recommended die clearance to be allowed, and to be provided for, in designing a die for service as determined by the materials groups which follow and for the reestablished percentage of material thickness of the original part which the die is designed to produce. (12)

Group1. 1100and 5052 aluminum alloys, all tempers. An average clearance of 4.5 % of material thickness is recommended for normal punching and blanking.

ISBN 978-9959-9703-2-9

Group2. 2024 and 6061 aluminum alloys; brass, all tempers; cold rolled steel, dead soft; stainless steel soft. An average clearance of 6 % of material thickness is recommended for normal punching and blanking.

Group3. Cold-rolled steel, half hard; stainless steel, half hard and full hard. An average clearance of 7.5% is recommended for normal punching and blanking.

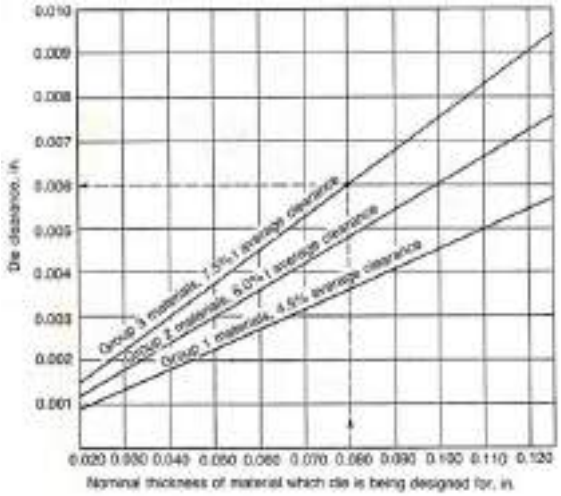

Fig. 4: Die-clearance chart by groups of materials, using the recommended of metal thickness. (12)

Experimental work

The Industrial Factory in Bani Walid is facing problems in one of its production lines that is specialized in producing one part of the Klashenkove rifle which is called the safety part as shown in figure (5). The problems include the following:

Fig. 5: The safety part

1- The Broaching Tool failure which is used in the broaching process.
2- The Productivity of the cutting die (figure 6) is not satisfying the planning department in the factory.
3- The percentages of the defects were high, which is produced by this die. Also, the problem of separation of the ring which is fixed to the safety port by spot welding was 8.6%.

Fig. 6: The cutting die

Problem Identification:

Four different dies were chosen as samples to study the problems mentioned above as Shown

ISBN 978-9959-9703-2-9

in table (1)
The first die (Da) is the original one, the other were modified.

Table 1: Show four different dies

Dies	Productivity (Pieces)	Accepted (Pieces)	Rejected (Pieces)	Defect percentage	Problem
Da	430	393	37	8.6%	Wear on the punch and die block.
Db	65	62	3	4.6%	Fracture of punch
Dc	80	84	6	7.5%	Fracture of punch
De	85	76	9	10.6%	Wear on the edges of the punch

In order to investigate these problems, the dies were dies disassembled to carry out tests and measurements.

Figure (7) shows the basic elements of a blanking or piercing die. These elements are the die block in which the proper female die opening has been made, the punch, and stripper. (The back gage which locates the back edge of the stock material is, in this instance, a part of the stripper.) They are mounted on a die set in order to achieve and retain proper matching of the punch and the die opening. The die block and stripper are secured to the die shoe by means of screws and dowels. The punch is screwed and doweled to the punch holder.

When the die is set up or mounted in the punch press, the punch holder is secured to the ram of the press and, of course, moves with the ram. The die shoe is secured to the press bed and remains stationary.

The stock material *A* is fed or loaded in the proper position on the top surface of the die block. When the press is tripped, the ram drives the punch through the stock martial *A* into the die opening, thereby producing an opening in the stock material by cutting out the blank or slug *B*. this blank or slug remains in the die opening when the punch is withdrawn and is pushed through the die by the blanks or slugs produced subsequently.

Fig. 7: The basic element of a blanking or piercing die.

Disassembly of Blanking Die

This component is composed of five main parts, which are:

1-Die Block

The die block (figure 8-part D) is the female part of a complete blanking die which is used to produce piece parts consistently to required specifications.

2- Punch

A punch is a male member of a complete die which mates or acts in conjunction with the female die to produce a desired effect upon the material being worked. a die can be a simple tool composed of punch, die block, and stripper, or it can be an extremely Factory mechanism which performs many and varied operations. (Figure 8-part B)

3- Punch Holder

This part is shown in figure (8-part A). It is used to fixing the punch of longitude for insuring no deflection from die block.

4- Stripper

ISBN 978-9959-9703-2-9

The purpose of this part is to insure no moving of the punch of the cycle (figure 8-part C)

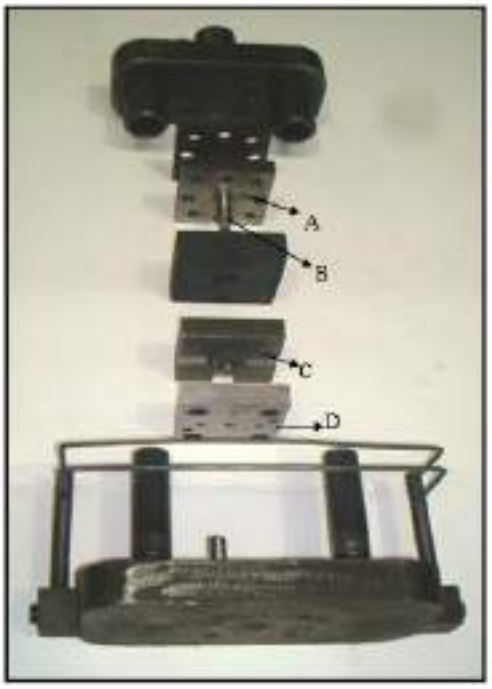

Fig. 8: Disassembly of blanking die, A- Punch holder, B- Punch, C- Stripper, D- Die block

Measurements and Drawing

The dimensional measurements were taken using calipers, micrometers, and coordinate measuring CMM as shown in figures (9).

Fig. 9: Measurement Tools.

Fig. 10: Die block.

ISBN 978-9959-9703-2-9

Fig. 11: punch

Hardness Measurement

The Rockwell hardness (scale C) measurements were taken on polished samples. Tests were mode using a standard a Rockwell hardness test machine and a load of 150 kg.

The hardness values are the average of 10 minimum reading this method is the most widely used hardness test. Its general acceptance is due to its speed, freedom from personal error, ability to distinguish small hardness differences in hardened steel, and the small size of the indentation, so that finished heat-treated parts can be tested without damage.

This test utilizes the depth of indentation, under constant load, as a measure of hardness. A minor load of 10 kg is first applied to seat the specimen. This minimizes the amount of surface preparation needed and reduces the tendency for ridging or sinking in by the indenter. The major load is then applied, and the depth of indentation is automatically recorded on a dial gage in terms of arbitrary hardness numbers.

Impact Test

In general Impact tests are designed to measure the resistance to failure of a material to a suddenly applied force such as collision, falling object or instantaneous blow. The test measures the impact energy, or the energy absorbed prior to fracture.

Charpy test specimens of dimensions 55x10x10mm were cut from the dies. The sample have a V-sharp notch, 2mm deep, with 45 angle and 0.25 mm radius along the base

Surface Roughness Measurement

Surface topography is of great importance in specifying the function of a surface. A significant proportion of component failure starts at the surface due to either an isolated manufacturing discontinuity or gradual deterioration of the surface quality. Typical of the former is the laps and folds which cause fatigue failures and of the latter is the grinding damage due to the use of a worn wheel resulting in stress corrosion and fatigue failure. The most important parameter describing surface integrity is surface roughness. In the manufacturing industry, surface must be within certain limits of roughness. Therefore, measuring surface roughness is vital to quality control of machining work piece. Surface roughness measurement is performed on Sutronic 3+ devise as it can be seen in figure 12

Fig. 12: Sutronic 3+devise.

Chemical Analysis

Spark emission spectrometry is a rapid, precise and reliable method for elementary analysis of conducting solids, whose discovery dates back to the last century.

Today this technique is used on a systematic basis in the steel, metallurgy and foundry industries for developing, producing and providing quality control of metals and alloys.

In spark spectrometry, the emission source consists of a sparking stand and a spark generator.

The sample to be analyzed, hard faced with an abrasive, is a held on the support plate by an attachment device.

Spark emission spectrometry is an analytical technique which is routinely used in the metal industry.

Chemical composition of the samples under investigation were measured using spectrophotometer.

 ISBN 978-9959-9703-2-9

(Cutting Die Lowness of Productivity)

To study the low productivity of the selected dies manufactured at Bani Walid Factory, tests and measurements were carried out as can be seen in table 2.

Table 2: shows an old dies specification

Dies	AISI Steel Type	Hardening temperature °C	Hardness HRC	Clearance mm	Productivity	Rejected	% of Rejected parts
Da	W1	800	59.8	0.008	430	37	8.6%
Db	W1	790	69.4	0.009	65	3	4.6%
Dc	W1	800	59.4	0.008	80	6	7.5%
De	W1	815	51.1	0.008	85	9	10.6%

Regarding the die Da wear occurred on the edges of the Punch and the Die block as shown in figures (13, 14(a, b)) due to pressure on the edges.

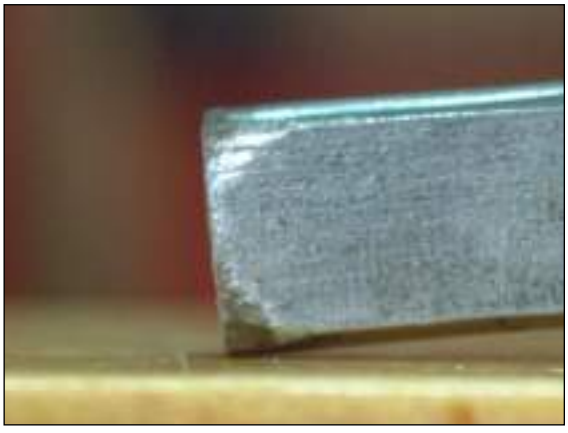

(**A**)

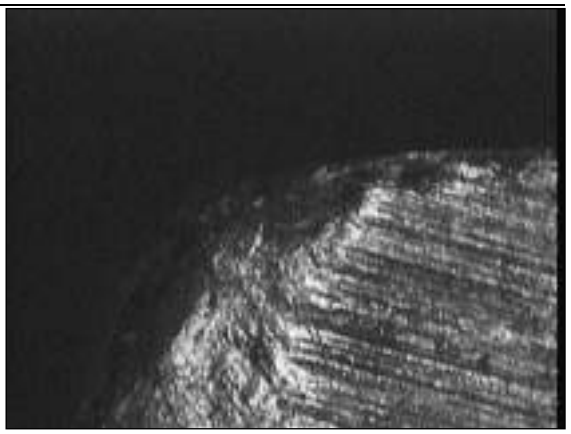

(**B**)

Fig. 13 A, B: Shows wear defect on the punch.

(**A**)

ISBN 978-9959-9703-2-9

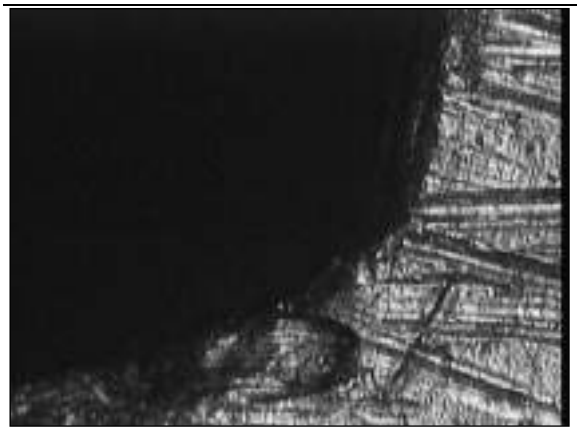

(**B**)

Fig/ 14 A, B: Shows wear effect on the die block

-Regarding the die Db, it was a try from the planning department in the factory to increase productivity by raising the hardness of the die to 68 HRC without considering that; if the hardness is high, the impact strength of the die will be less which causes fracture.
-To sharpen the die Dc more than two times, the planning department made the punch longer to raise the dies entire productivity, this caused the punch bend and fracture.
-Low hardness of De die caused wear on the edges of the punch and die block.
The main reason for low productivity is the wearing that occurs to the punch and die block. To increase productivity, we have to decrease wear problem. To obtain optimum specification many experiments were made.

Hardness Measurement

Hardness measurements were performed on old dies and new dies. The locations are shown in figure 15.
The hardness values of old dies (Da, Db, Dc, and De) are illustrated in table (3).

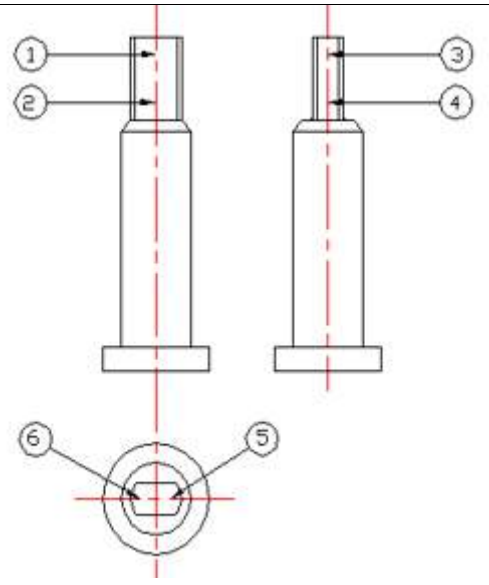

(**A**)

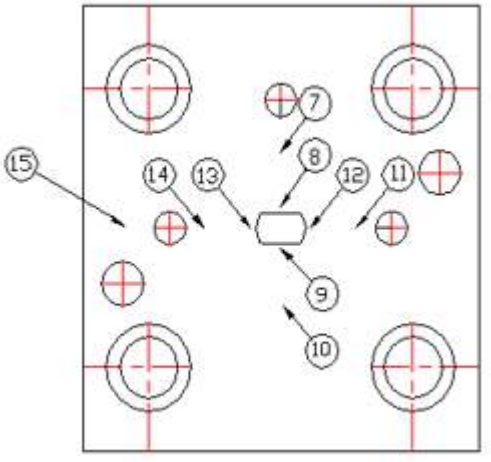

(B)

Fig. 15 A and B: Locations of hardness measurements

It can be seen that the hardness measurements of Da and Dc are equal. However, die Db has higher hardness and the lowest hardness was obtained for die

 ISBN 978-9959-9703-2-9

en the hardness is high, the die Db is fractured and productivity was 50 pieces.
contrast that the productivity of die De was 80 ces this due to low hardness values.

ble 3: Rockwell hardness test results for Da, Db, Dc,

Location	Hardness Value (HRC)			
	Da	Db	Dc	De
1	60	71	60	52
2	61	69	60	51
3	59	67	59	51
4	58	70	59	51
5	60	68	61	50
6	59	70	60	52
7	62	69	59	50
8	60	69	60	51
9	58	68	58	51
10	59	70	59	52
11	60	71	60	51
12	61	71	60	52
13	60	70	58	50
14	59	69	59	51
15	61	69	61	51
Average	59.8	69.4	59.5	51.1

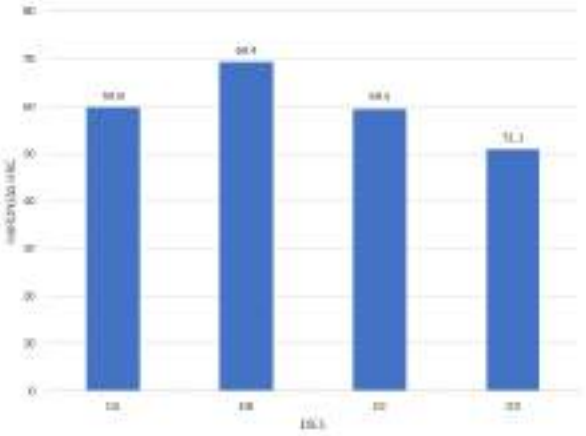

Fig. 16: Hardness measurements of dies

Impact Energy Results

The impact energy is one of the important properties, which needs to study to avoid the punch fracture during the operation. The impact result of old dies are given in table (4). The samples were taken from the dies with dimensions. And as can be seen from figure 17, the relationship between hardness and toughness.

The impact energy increases as the hardness values decreases.

Table 4: Impact test results for Da, Db, Dc, and De.

Sample No.	Energy absorbed x 10(J)			
	Da	Db	Dc	De
1	0.25	0.1	0.20	0.42
2	0.25	0.1	0.20	0.41
3	0.20	0.1	0.25	0.40
Average	0.23	0.1	0.22	0.41

ISBN 978-9959-9703-2-9

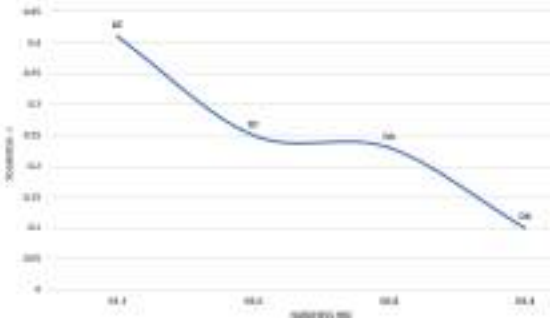

Fig. 17: Relationship between hardness and toughness.

Surface Texture Measurement Results

The surface roughness of the old dies and the dies used in the study are given in tables (5). The surface of the new dies was smothered than the surface of the old dies. These surface measurements were carried out to avoid fatigue problem.

Table 5: Surface Roughness Values for Da, Db, Dc, and De.

Location	The Value of Surface Roughness (μm)							
	Da		Db		Dc		De	
	Punch	Die block	Punch	Die block	Punch	Die block	Punch	Die block
1	0.40	0.48	0.40	0.47	0.39	0.44	0.40	0.46
2	0.42	0.49	0.40	0.47	0.40	0.45	0.42	0.46
3	0.41	0.48	0.41	0.48	0.40	0.45	0.40	0.45
Average	0.41	0.483	0.40	0.473	0.396	0.446	0.41	0.456

Chemical Analyses

In this study the chemical compositions of these alloys are shown in table 6.

Table 6: Chemical composition analysis of Da

Element	C	Mn	Si	Cr	Ni	V	Fe
Content%	1.031	0.207	0.452	0.112	0.107	0.054	97.98

Productivity

Table (7) shows the productivity results of different dies used in this work compared with dies produced by Bani Waleed Industrial Factory.

However, the optimum productivity of the old dies made by Da is 430 pieces.

Table 7: Productivity Results

Dies	Germany W.Nr.	AISI	Cutting clearance	effect Length of punch	Angle	Productivity	No. Defects	Defect percentage
Da	1.1550	W1	0.008mm	15mm	0°	430	37	8.6%
Db	1.1550	W1	0.009mm	15mm	0°	65	3	4.6%
Dc	1.1550	W1	0.009mm	28mm	0°	80	6	7.5%
De	1.1550	W1	0.008mm	15mm	0°	85	9	10.6%

Conclusion

Through this work and from the chemical analysis of the metal used in the manufacture of the die, it was found that the percentage of chromium is low, and this affects the wear resistance, so it is necessary to choose another metal that is better to obtain high productivity. It was also found that the clearance in the die used is insufficient and small in relation to the thickness of the insurance to be cut, and this increases the pressure on the edges of the pieces in the die and leads to rapid wear. We expect that increasing the length of the bunch to solve the problem is not an appropriate option because this increase weakens the bending resistance of the bench. We advise the factory administration to make dies from other materials, pay attention to the bunch design, and choose a suitable clearance in the die.

References

1) Otto, Kevin, and Wood, Kristin. Product Design Techniques in Reverse Engineering and New Product Development. Prentice Hall, 2000.

 ISBN 978-9959-9703-2-9

2) Ingle, K. A. Reverse Engineering, McGraw-Hill, 1994.
3) Chilling effects clearinghouse-www.chillingeffcts.org disclaimer/privacy
4) www. Reveres engineering. Com
5) H. James de St. Germain, Reverse Engineering utilizing domain specific knowledge, 2002.
6) Mahmoud M. Farag, Materials selection for engineering design, Prentice Hall. 1997.
7) D.T.Llewellyn and R.C.Hudd, Steels: metallurgy and applications, BH, 1998.
8) David A. Smith, Die design handbook, Society of manufacturing engineers, Third edition, 1990.
9) IVANA SUCHY, Handbook of Die design, Mc Graw Hill Companies, 1998.
10) George Schneider, Jr. CMfgE catting tool applications, 1991.
11) www.toolingandproduction.com
12) D. Eugene Ostergaard, Basic Diemaking, Mc Graw-Hill Book Company, 1963.
13) T.M.Chang Finite element simulation of the effect of clearance on the forming quality in the blanking process
14) G. Krauss STEELS. Heat treatment and processing principles, ASM international, November 2000.
15) Evaluation of ductile fracture models for different metals in blanking
16) http://www.metalravne.si/selector/OC100.html
17) http://www.metalravne.si/selector/OCR12VM.html
18) http://www.metalravne.si/selector/MERILO.html
Mahmod Gomah, Murat Demiral, An Experimental and Numerical Investigation of an Improved Shearing Process with Different Punch Characteristics, *Corr. Author's Address: College of Engineering and Technology, American University of the Middle East, Kuwait, Murat.Demiral@aum.edu.kw 375Strojniški vestnik - Journal of Mechanical Engineering 66(2020)6, 375-384

 ISBN 978-9959-9703-2-9

المؤتمر الدولي الثاني للعلوم والهندسة
2nd International Conference on Science and Engineering
ICSE 2023
Faculty of Engineering - University of Bani Waleed
Bani Waleed, Libya

Paper Code: ICSE-050

IMPROVE THE SURFACE ROUGHNESS OF PETG PRODUCTS IN FDM 3D PRINTING PROCESS WITH ADDITION OF CARBON FIBER

Abraheem Hadeeyah[1], Ibrahim Emhemed[2], ,Fouzi Alhader[3] , Neila Masmoudi [4] , Monder Wali[5]*
[a,c] dept. Mechanical Engineering/National Engineering School of Sfax, Tunisia -The Higher Institute for Technical Siences Tarhuna, Libya
[b] dept. physics, Education Faculty/Azzaytuna University, Tarhuna, Libya.
[d,f] dept Mechanical Engineering/ National Engineering School of Sfax, Tunisia
*Crosspnding author: ibrahem27777@gmail.com, I.emhemed@azu.edu.ly, alhadar7533@gmail.com, neila.masmoudikhabou@enis.tn, mondherwali@yahoo.fr

Abstract: The aim of this study is to improve the surface properties of PETG material in 3D printer products by adding Carbon-Fiber (CF). Carbon-Fiber is a material that can be added to PETG, PLA, ABS, Nylon and Polycarbonate PC filaments to increase their strength and stiffness. The main contribution of this study is to provide a comprehensive evaluation of the surface roughness of PETG and PETG/carbon-Fiber filaments printed by fused deposition modeling (FDM) technique. The surface roughness is measured using surface roughness PCE-RT20000 tester. By adding 15% weight of Carbon-Fiber to PETG material, the surface roughness value was reduced by 32.7% in the final 3D printed product. This resulted from Carbon-Fiber's capacity to improve the material's flexibility and strength as well as its capacity to close gaps between PETG material threads by enhancing flow and adhesion. The chemical interaction between Carbon-Fiber and PETG contributed to increased flow and adhesion of the material. This interaction plays a role in obtaining good surface properties.

Keywords: (3 D printing, materials, surface roughness, PETG, PETG/Carbon-Fiber)

Introduction

The increasing popularity of 3D printing, also known as additive manufacturing (AM), rapid prototyping (RP), or solid free-form technology (SFF), in a variety of applications has led the modern manufacturing industry to seek to replace conventional techniques with this innovative technology where suitable. This is due to the numerous advantages that 3D printing offers in comparison to conventional, energy-intensive techniques, such as the ability to fabricate complex geometries as a single unit with no joints, reduced material and labor costs, improved surface finish, decreased energy demand, single-step processing temperature, simplified processing (CAD model-Print-Install), near-net shape finish, quick production time, short lead time, and lower overall cost [1]. One of the main benefits of 3D printing is the capability to produce near-net shape products without the

 ISBN 978-9959-9703-2-9

need for physical molding to achieve the desired shape of the product. Designs can be created as 3D objects using software such as AutoCAD and SolidWorks, which are commonly used for designing prototypes for 3D printing applications. Once created, the 3D soft files can then be converted into the stereolithography (STL) format, a format that can be interpreted by a 3D printer [2]. The main advantages of this technology are the ability to develop complex shapes without geometric limitations and the conversion from the 3D solid model to the manufactured part with only a few parameters. The generic term AM encompasses several technologies such as fused filament fabrication (FFF), selective laser sintering (SLS), electron beam melting (EBM), and stereolithography (SLA). FFF is by far the most extensively used technology due to its ability to manufacture complex parts with a broad range of thermoplastic polymers at relatively low production costs. FFF accounts for 69% of all AM processes [3]. Surface roughness is a critical parameter that affects the mechanical and physical properties of materials, such as friction, wear, corrosion, adhesion, and reflectivity. In 3D printing, surface roughness also determines the accuracy, quality, and appearance of the printed parts. Therefore, it is essential to understand and control the surface roughness of 3D printed materials for enhancing their performance and functionality [4]. Among the various 3D printing materials, polyethylene terephthalate glycol (PETG) is a thermoplastic polymer that exhibits high strength, toughness, and chemical resistance. However, PETG may have high surface roughness due to its low viscosity and high shrinkage during printing. To overcome this limitation, PETG can be blended with carbon fiber reinforced filament (carbon Fil), which can improve the stiffness, dimensional stability, and thermal conductivity of PETG [5]. The main contribution of this study is to provide a comprehensive evaluation of the surface roughness of PETG and PETG/carbon Fil filaments printed by FDM technique. This study can help in selecting the appropriate materials for different 3D printing applications that require high surface quality. This research aims to improve the mechanical properties of PETG by adding carbon fibers to it. It is expected that this research will lead to the development of polymer materials based on PETG with improved mechanical properties, which can be used in various applications, including the automotive industry, aviation, and 3D printing.

2. Methodology

2.1. Materials

In this study the PETG and PETG\CF

 ISBN 978-9959-9703-2-9

materials commercially available industrially common 3D printing material was used: Polyethylene Terephthalate Glycol - Carbon Fiber (PETG - CF). This filament of 1.75 mm in diameter.

Carbon fibers are added to materials in different ratios and are commonly available in 3D printers and other products. In this study, PETG material was chosen with 15% carbon fiber added to it.

2.2. Experimental procedures

2.2.1 Specimen preparation

Samples were printed using the ENDER 3D printer. Figure 1, shows the 3D printer used in this study.

Fig:1, 3D printer (FDM)

And the printer settings are given in the following table1:

Table 1: shows the printer settings Parameter.

printer settings		
1-	Infill	100%
2-	Printing temperature	240C^0
3-	Build plate temperature	80C^0
4-	Print speed	55 mm/s
5-	Fan speed	100 mm/s
6-	Layer height (mm)	0.2 mm

The samples were designed using SolidWorks software 2023 and converted into stereolithography (STL) format. The printer's operating program (G-Codes) was then produced to control the printer's operation and execute the models. Six samples were prepared, three of which were made of PETG material and the other three were made of PETG material with 15% Carbon-Fiber added to them. The surface roughness of each sample was measured and the average value was taken for the sake of accuracy. The surface roughness is measured using a roughness tester. The following figure shows the PCE-RT 2000 Roughness Tester.

Fig.2. Surface Roughness Tester

 ISBN 978-9959-9703-2-9

RESULTS:

The surface roughness test results for PETG and PETG-CF materials are:

PETG are: (6.853 , 6.339 , 7.236) μm, $Ra = 6.886 \mu m$ and PETG+15% carbon-Fiber are: (5.144 , 4.765 , 4.010) μm, $Ra = 4.639 \mu m$. The improvement percentage in surface roughness is: 32.7%.

The appearance of the 3D printed surface roughness test PETG and PETG-CF specimens are shown in Fig3(a,b):

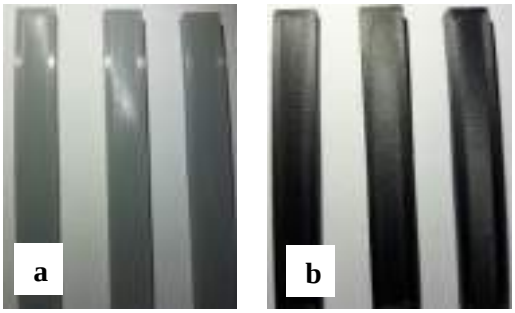

Fig. 3 (a) the surface of PETG sample, and (b) the surface of PETG-CF sample

Discussions

By adding 15% carbon-Fiber to PETG material, surface roughness was reduced by 32.7% during the 3D printing process. This was due to carbon-Fiber's ability to reinforce the strength and flexibility of the material, as well as fill gaps between PETG material threads by increasing flow and adhesion. This corresponds to references [6,7]. This resulted in improved surface smoothness and regularity. Carbon-Fiber has different functional groups than PETG material, which contributed to the formation of new bonds and breaking old bonds between polymer chains. These properties also contributed to the flow and adhesion of the material to the surface, thus leveling the surface or filling gaps between threads. This is consistent with what (Eunseob Kim et al) [8] found that Carbon-Fiber is more viscous than PETG at temperatures close to 3D printing temperature. This makes Carbon-Fiber flow better from the nozzle and form better on the surface, leading to improved surface smoothness. However, material viscosity may also be affected by other factors such as particle shape and composition in the material due to their manufacturing method and their physical and chemical properties This corresponds to references [6].

Conclusion

1- Addition of carbon Fil into to PETG material made it stronger and more rigid, thus making it less prone to deformation or breakage during 3D printing. This may lead to improved surface smoothness and regularity.

2- The surface properties of PETG material improved by 32.7% when 15% carbon-Fiber was added to PETG.

3- One of the most important factors that contributed to improving surface roughness is

 ISBN 978-9959-9703-2-9

that carbon-Fiber has higher viscosity than PETG.

4- The small particle size of carbon-Fiber filled the gaps and voids in PETG material.

5- Good mixing between the two materials contributed to forming a smoother and more regular surface.

6- The printer's Settings calibration was very compatible with the printed material, which effectively contributed to obtaining good results.

7- Increased surface leveling and filling gaps between threads due to increased flow and adhesion of the material by carbon-Fiber.

8- The chemical interaction between carbon-Fiber and PETG contributed to increased flow and adhesion. This interaction played a role in obtaining good surface properties.

References

[1] Abraheem, H, Amir K, Fouzi A, Ibrahim A, Neila K, and Mondher W, The effect of ambient temperature on the quality of three-dimensional printer products in FDM technology for ABS material, First Libyan international Conference on Engineering Sciences & Applications (FLICESA_LA) 13 – 15 March 2023, Tripoli – Libya.

[2] I. Gibson, D. Rosen, B. Stucker, in: Additive Manufacturing Technologies, Additive Manufacturing Technologies: 3D Printing, Rapid Prototyping, and Direct Digital Manufacturing, second ed., 2015, https://doi.org/10.1007/978-1-4939-2113-3.

[3] E. García, P.J. Núñez, M.A. Caminero, J.M. Chacón, S. Kamarthi, Effects of carbon fibre reinforcement on the geometric properties of PETG-based filament using FFF additive manufacturing, Composites Part B: Engineering, Vol 235, 2022,

[4] M. S. Khan, M. A. Qazi, M. A. Khan, M. A. Khan, and M. A. Khan, “Surface Roughness Analysis of 3D Printed Parts: A Review,” Materials Today: Proceedings, vol. 46, pp. 103–108, 2021.

[5] ScienceDirect. (2022). Effects of carbon fiber reinforcement on the geometric properties of 3D printed PETG parts. [online] Available at: https://www.sciencedirect.com/science/article/pii/S1359836822001494.

components: fused deposition modeling”, Vol, 22 · No. 6 · 887–894.

[6]- Yang L, Li S, Li Y et al (2019) Experimental investigations

for optimizing the extrusion parameters on FDM PLA printed

parts. J Mater Eng Perfor

[7]- Hooshmand MJ, Mansour S, Dehghanian A (2021) Optimization

of build orientation in FFF using response surface methodology

and posterior-based method. 27:967-994https:// doi.

 ISBN 978-9959-9703-2-9

org/ 10. 1108/ RPJ- 07- 2020- 0162

[8] Eunseob, K, Yong-Jun S, Sung, H. A. (2016), "The effects of moisture and temperature on the mechanical properties of additive manufacturing.

 ISBN 978-9959-9703-2-9

المؤتمر الدولي الثاني للعلوم والهندسة
2nd International Conference on Science and Engineering
ICSE 2023
Faculty of Engineering - University of Bani Waleed
Bani Waleed, Libya

Paper Code: ICSE-037

STUDYING THE QUALITY OF TRANSMITTED SIGNAL VIA A WIRELESS AND WIRED LINES

Rajab Algheetah[a], Ahseen Naser Aldeeb[b]
[a] Electrical Engineering Department, Higher Institute of Engineering Technology Bani Walid, LibyaName
[b] Mechatronics Department, Higher Institute of Engineering Technology Bani Walid, Libya
*Crosspnding author: ahssinaldeeb@gmail.com

Abstract: A communication system refers to the process of exchanging information between two or more parties. Wired communication systems use physical cables or wires to transmit signals, while wireless communication systems transmit signals through the air without the use of physical cables. Both wired and wireless communication systems have their advantages and disadvantages, and the choice of system depends on the specific requirements of the application. In this research, a full compression between wired and wireless signals are discussed.

Keywords: (optical, wire, wireless, control, system, communication)

Introduction

A communication system conveys information from its source to a destination some distance away. There are so many different applications of communication systems that we cannot attempt to cover type. Nor can we discuss in detail all the individual parts that make up a specific system.

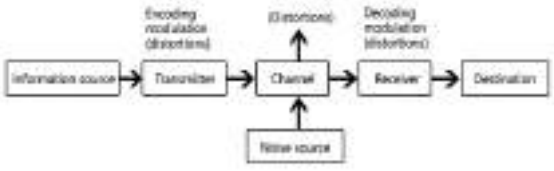

Figure 1: Functional block diagram of a communication system

The Transmitter. The transmitter converts the electrical signal into a form that is suitable for transmission through the physical channel or transmission medium.
The Channel. The communications channel is the physical medium that is used to send the signal from the transmitter to the receiver. In wireless transmission, the channel is usually the atmosphere (free space).
The Receiver. The function of the receiver is to recover the message signal contained in the received signal.

Optical communication system

optic communication is such as any communication system with one different where, this kind uses light pulses to transfer information from one point to another through communication channel.

 ISBN 978-9959-9703-2-9

In this kind of communication system, the transmission could be by two different ways, either using optical Fiber by means of wired communication medium as shown in figure.2 or letting the signal propagating in atmosphere direct to destination by means of wireless communication medium as figure.3.

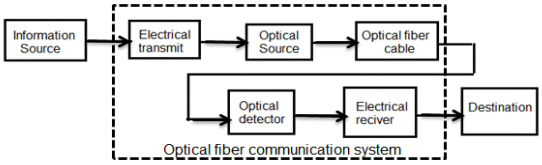

Figure2: Optical Fiber communication system

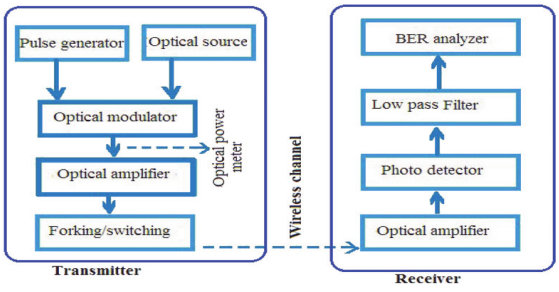

Figure 3: Optical wireless communication system.

The signal is transferred from an electrical signal into an optical form by using one kind of light either in both wire or wireless. As the signal transferred into optic and transmitted through one types of communication medium then the light detector plays great role, where the light detector is the device that converts the light into electrical signal or regenerate the optical signal back to its original signal (massage signal).

COMMUNCATION MEDIUM

The communication medium could be one of two ways whether wired which presented by optical fiber or wireless which represented in atmosphere.

Optical Wireless Communication

Wireless technologies are one of the great success stories in the history of technology, realizing the dream of humans to communicate from anywhere at any time. While voice communication was the primary service some ten years ago, wireless data and mobile Internet have become pervasive much more rapidly than anyone could have imagined and augmented voice communication experience with much richer multimedia content. Today, the term "wireless" is widely used as a synonym of radio frequency (RF) technologies as a result of the worldwide domination of RF devices and systems in the market. The RF band lies between 30 kilo Hertz (kHz) and 300 Giga Hertz (GHz) of the electromagnetic spectrum and its use is strictly regulated by the local and international authorities. In most cases, sub-bands are exclusively licensed to operators, e.g., cellular phone operators, television broadcasters, point-to-point microwave links etc. With the ever-growing demand for data heavy wireless applications and services, the demand for the RF spectrum is outstripping the supply, thus leading to the spectrum congestion. In the light of the spectrum bottleneck at both the network access and backhaul levels, the time has come to seriously consider the upper parts of the electromagnetic spectrum for wireless communications. By doing so, we move into the optical band which includes infrared (IR), visible (VL) and ultraviolet (UV) sub-bands, see Fig. 4.

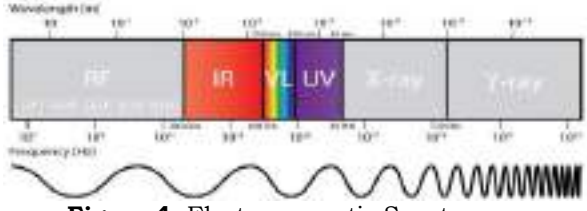

Figure 4: Electromagnetic Spectrum

Transmitter and receiver circuits

To study the wireless and wires signals, a transmitter and receiver circuits are applied. The transmitter circuit consists of four stages as shown on figure 5.

ISBN 978-9959-9703-2-9

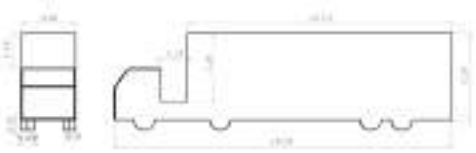

Figure 5: transmitter stages

The first stage in transmitter is low pass filter to pass frequencies blew 80KHz. Second stage (signal supply voltage) is alternative way to compensate the reverse bias for the op-Amp. Third stage is active band bass filter to pass frequencies between nearly 10Hz and16 KHz and amplify signal in this range. Where the R5 and R6 controlling the gain of op-amp and these resistors with C4 and C5 are controlled the frequencies cut off. Fourth stage is the last stage which are used to amplify the current which feeds LED, the current should deliver to LED.

The receiver circuit consists of two stages as in figure 5.

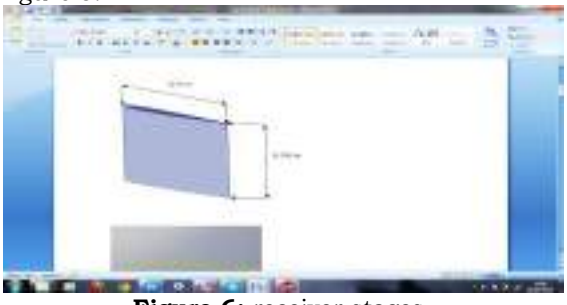

Figure 6: receiver stages.

The received signal is weak so, it needs to be amplified. The first stage would amplify the signal ten times where, R7 and R6 to control the gain of op-amp so, R7 should be ten times of R6. Second stage is band pass filter is used to pass frequencies in range 1.5 Hz to 16KHz. Where R9 and R10 controlling the gain of op-amp and these resistors with C7and C12 are controlled the frequencies cut off.

RESULTS

A sine wave with 1 KHz frequency and 50mVp-p is supposed as an input to check the implemented practical transmitter and receiver in lab and we get these results:

At transmitter:

The output at stage **1** (low pass filter):

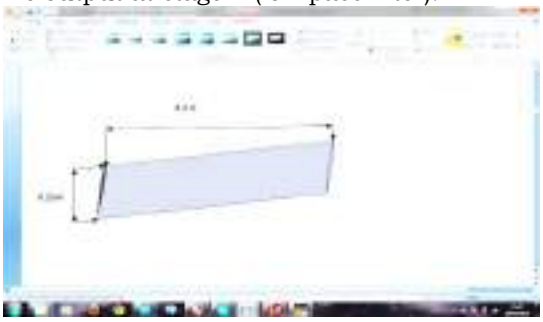

Figure 7: Reading at stage 1

Amplitude in figure 7 = 60 *mV*

The output at stage **3**(amplifier):

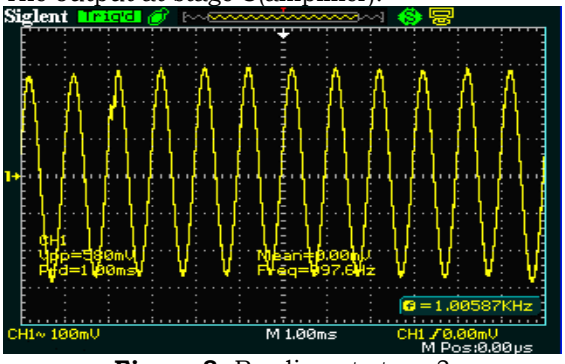

Figure 8: Reading at stage 3

Amplitude in figure 8 = 580 *mV*

The output at stage 4(LED):

ISBN 978-9959-9703-2-9

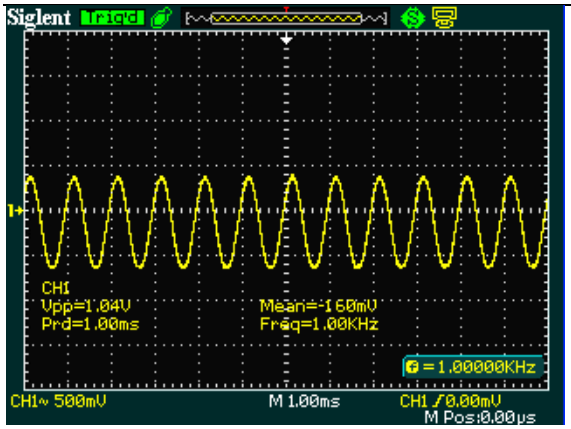

Figure 9: Reading at stage 4

Amplitude in figure 9 = 1.04*V*

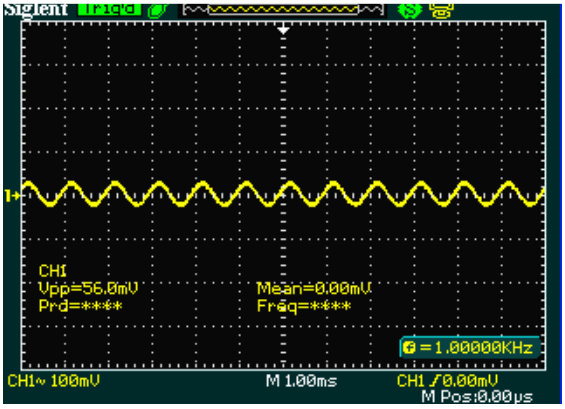

Figure 10: Reading before stage 1

Amplitude in figure 10 = 56 *mV*

The output at stage 1(amplifier):

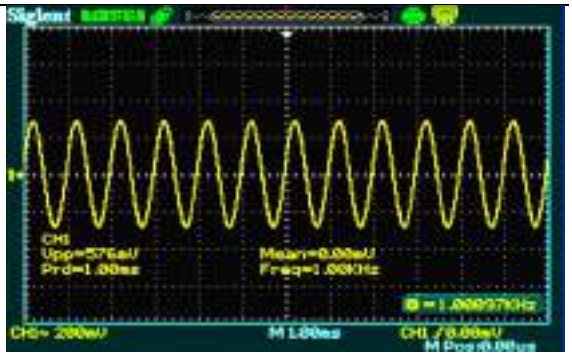

Figure 11: Reading at stage 1

Amplitude in figure 11 = 576 *mV*

The output at stage 2(active band pass filter):

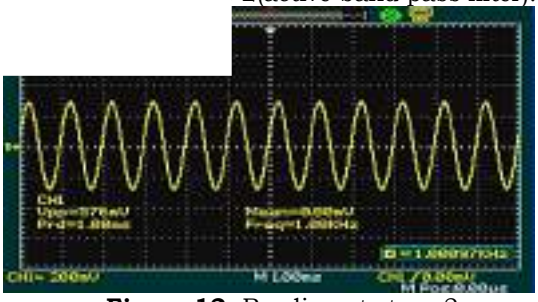

Figure 12: Reading at stage 2

Amplitude in figure 12 = 576 *mV*

Using the whole circuit (transmitter and receiver) in wired (optical fiber) case at different lengths using the same check signal above we get the results below:

After distance 0.5 m:

Figure 13: Output receiver after 0.5 m from

ISBN 978-9959-9703-2-9

transmitter by optical Fiber

Amplitude in figure 13 = 4.48*V*

After distance 1 m:

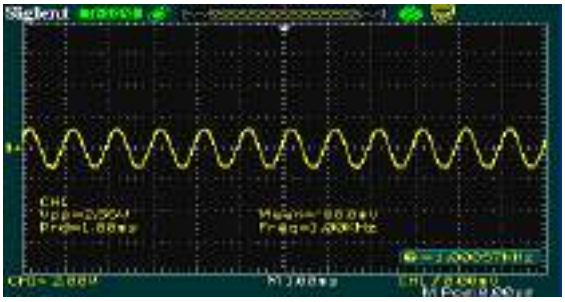

Figure 14: Output receiver after 1 m from transmitter by optical fiber

Amplitude in figure 14 = 2.56*V*

After distance 3 m:

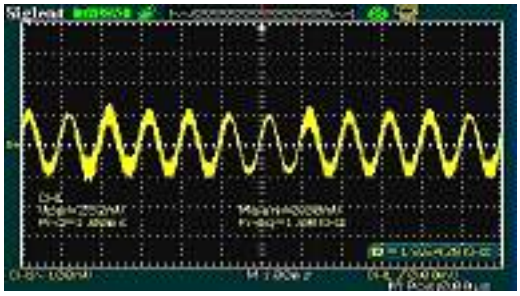

Figure 15: Output receiver after 3 m from transmitter by optical fiber

Amplitude in figure 15 = 252 *mV*

After distance 0.1m:

Figure 16: Output receiver after 0.1 m from transmitter by wireless

Amplitude in figure 16 = 820 *mV*

Then using wireless channel (free space) and changing LED and photodiode types at different lengths and we get these results below:

After distance 0.1m:

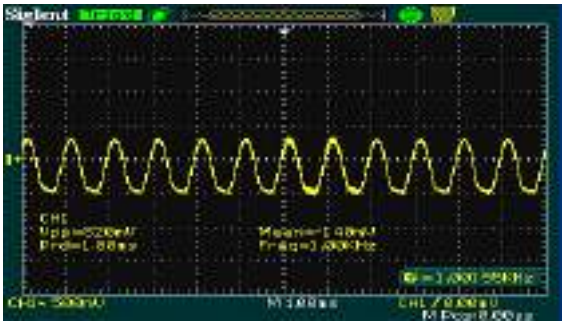

Figure 17: Output receiver after 0.1 m from transmitter by wireless

Amplitude in figure 17 = 820 *mV*

After distance 0.5m:

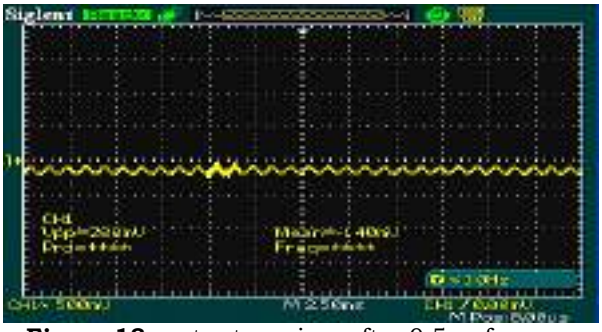

Figure 18: output receiver after 0.5 m from transmitter by wireless

Amplitude in figure 18 = 200 *mV*

After distance 1m:

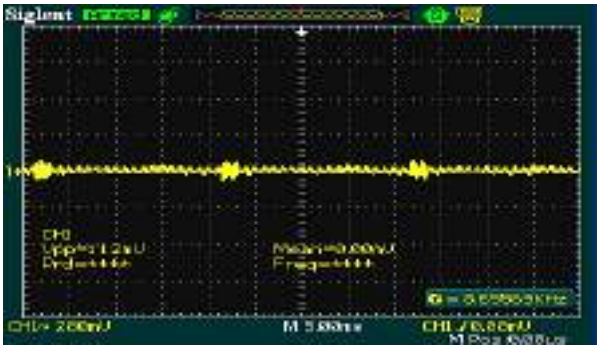

ISBN 978-9959-9703-2-9

Figure 19: Output receiver after 1 m from transmitter by wireless

Amplitude in figure 19 = 112 *mV*

Also, we sent voice signal on both medium and get these results:

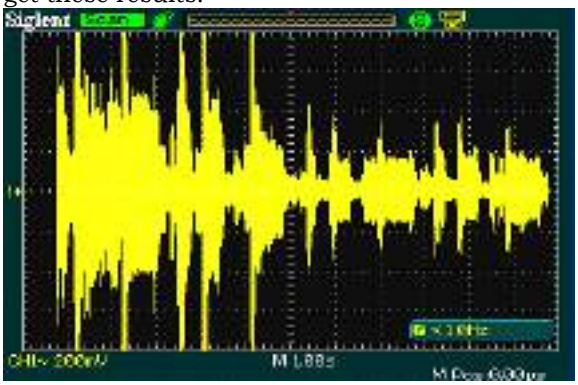

Figure 20: Input voice signal

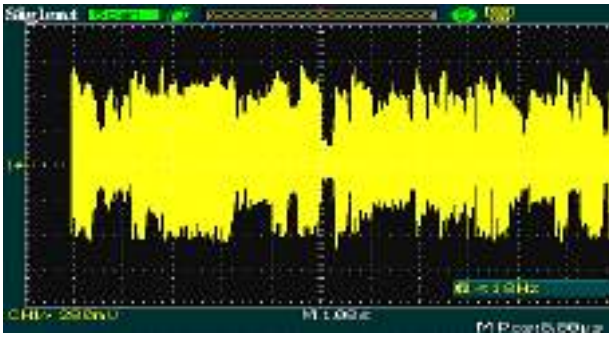

Figure 21: Output voice signal at 1m by optical Fiber

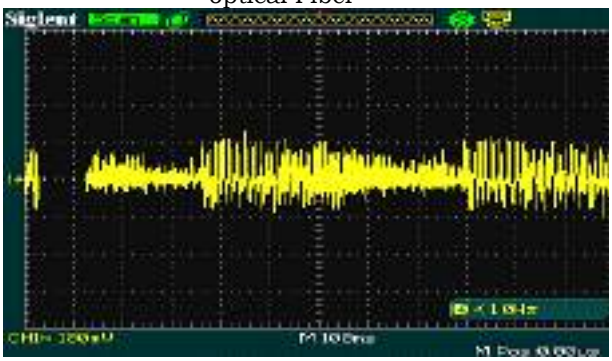

Figure 22: Output voice signal after 1m wireless

Conclusion

The transmitter and receiver electronic circuits have been built successfully and the main purpose of this project has satisfied effectively. Through also thru test and observes the circuits, they give robust results.

Signal degradation in optical Fiber depends on various parameters such as Fiber type, length of Fiber and wavelength. by using optical Fiber more efficient than wireless channel because it's noise less channel.

Many useful notes and deductions are concluded from this work, and could be summarized as follows:

1) The distance of optical fiber has a great effect on degrading the signal as noted from results.
2) From results, there is notable different in received signal when changing communication medium.
3) We have a prospect for practical use if the transmission distance is within about 3 meters for wired and 1.5 meters for wireless.
4) From the wired results we noted a bit of attenuation, and we discovered that is the results of the side cutter that we used. The side cutter that we used meant to be a cupper cable which is use not suitable for optical cables.

In final, this kind of simple circuits could be used in (Indoor application) due to its efficiency and low cost.

References

[**1**] Lee F.C., "*Power Electronics System - Introduction*", Virginia Tech,2005.

[**2**] "*Power Electronics System-A Joint Course*", taught by Virginia Polytechnic Institute and State University (Virginia

 ISBN 978-9959-9703-2-9

Tech), 2005.

[**3**] J. M. Tour, M. Kozaki and J. M. Seminario, "Molecular Scale Electronics:

A Synthetic/Computational Approach to Digital Computing", J Am Chem

Soc, pp. 8486-8493, 1998.

[**4**] 'P.O.12.3 Requirements Regarding Wind Power Facility Response To Grid

Voltage Dips Proposal Sent To Ministry,' BOE, Num. 254, Oct. 2006, pp. 37017-

37019.

[**5**] T. Kostyrko, B. Bułka, "Current fluctuations of polymeric chains", Phys.

Rev. B, Vol. 67, 2555-2561, 2003.

[**6**] W. B. Davis, W. A. Svec, M. A. Ratner and M. R. Wasielewski, "Molecular-wire

behaviour in p-phenylenevinylene oligomers", Nature, Vol. 396, pp. 60-63, 1998.

[7] R. A. Marcus, Chem. Phys. Lett., Vol. 133, pp. 471, 1987.

[**8**] K. V. Mikkelsen, M. A. Ratner, "Molecular Electronics", Chem. Rev, Vol. 81, pp.

113, 1987.

 ISBN 978-9959-9703-2-9

المؤتمر الدولي الثاني للعلوم والهندسة
2nd International Conference on Science and Engineering
ICSE 2023
Faculty of Engineering - University of Bani Waleed
Bani Waleed, Libya

Paper Code: ICSE-061

MICROGRID ENERGY DISTRIBUTION SIZING AND MANAGEMENT CONSIDERING PV/WT/BT INTEGRATION UNDER RESIDENTIAL LOAD

Moamer Musbah Mohamed Ahmed
Dept. of Electrical and Electronics Eng ,Faculty of Engineering , University of Bani waleed , Libya
Moamer125@ gmail.com

Abstract: This study presented Microgrid (MG) model considering Photovoltaic (PV), Battery (BT), and Wind Turbine (WT) connected through DC/AC inverter and controlled by Energy Management Strategy (EMS). Where the aforementioned components are playing a crucial role in the management and sizing of MG energy distribution. Whereas previous studies have introduced nature-inspired metaheuristic algorithms along with supervisory control algorithms. The sizing algorithm namely Particle Swarm Optimization (PSO) is utilized while the supervisory control is considering a Rule-Based Energy Management Strategy (RB-EMS). In the simulation result, the RES could run the system and overcome the challenges in the proposed system when the PV Produces (5kW) and WT is also estimated to produce 5kW. Furthermore, our results give insight into the effects of different strategies and microgrid configurations.

Keywords: (MG, PV, WT, RB-EMS)

Introduction

Hybrid renewable energy sources are promising systems to address energy barriers that consist of primary sources and batteries and diesel generators [1]. However, hybrid systems face several barrios such as environmental, social, technical, economic, policy, intermittency, and fluctuation. Integrating a proper hybrid system could complement each other and overcome the aforementioned issues when one of the sources experiencing fluctuation or intermittency [2]. Libyan climate is one of the most blessing among African countries [3]. The literature covers numerous Integrating forms of the RESs, the main two integration forms are stand-alone and grid-connected [4]. The former is totally isolated from the grid and suitable for rural and isolated locations. While the latter is the most preferable system due to its flexibility and can be exploited in urban areas [5]. RESs sizing and optimization have been investigated in various studies considering multiple nature sources [6]. The performance of RES. the MG drivers are categorized in terms of deployment and development into three groups, which are energy security, economic benefits, and clean

 ISBN 978-9959-9703-2-9

energy integration [7]. The growth was incremental in the examination of PV and WT to get demand satisfaction, meet sustainable goals and environmentally friendly life free of Greenhouse Gas (GHG) [8].

Microgrid energy distribution sizing and management involves the design and control of a localized electrical network that integrates various energy sources and enables efficient distribution within a specific geographical area [9]. Moreover, the EMS coupled with the sizing techniques to meet the main objectives of gaining a cost-effective system and renewable [10]. Integrate battery storage to address the intermittent nature of renewable energy sources and provide a stable power supply [11]. Size the battery capacity based on the estimated energy deficit during periods of low generation or high demand. Consider factors like depth of discharge, round-trip efficiency, and battery lifespan [12]. Hybrid systems have been evaluated by many scholars because of their flexibility in integrating many sources such as PV, WT, BT, and other generation sources [13]. Furthermore, several merits are provided for integrating MG systems such as enhancing energy efficiency, increased reliability, cost saving, energy resilience, and environmental benefits [14].

The knowledge contribution of this article is addressing the intermittency of the solar and wind turbine by integrating energy storage batteries along with analysis of the climatology collected data for easy understanding from the consumers. Moreover, the main of the RESs to meet the load which mean being renewable system. While the rest structure of the article is organized as follows: the implementing methodology to size and monitor the power flow are discussed in Section 2. The acquired result has been plotted and discussed in Section 3. Eventually, the article is closed with the conclusion and list of literature-cited sources.

Methodology

Based on the load assessment and renewable energy potential, the sizing of the system components will be considered. Microgrids are small-scale, localized power systems that can operate independently or in conjunction with the main power grid. In such systems, energy distribution sizing involves evaluating factors such as load demand, available generation capacity, storage capacity, and the characteristics of the distributed energy sources. The presented components in Figure 1 are the interconnected components of the proposed system that is hybridized and controlled by EMS to manage the flow of power in the system [5]. Furthermore, the system has been connected through DC/AC due to its flexibility, simplicity, and balance of the energy

 ISBN 978-9959-9703-2-9

flow to connect PV, WT, BT, and the grid, despite the DC bus bar system that connects DC appliances only. Besides, alternatively integrating more converters that may increase the cost and make the complexity of the circuit.

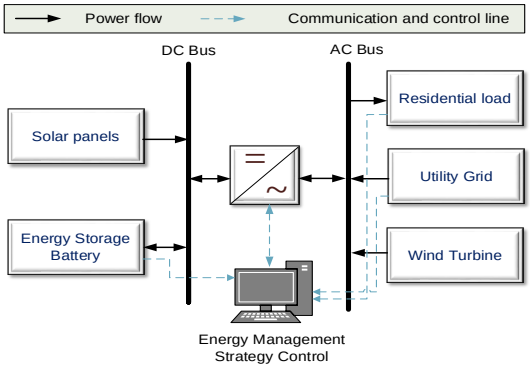

Fig. 1 Proposed microgrid hybrid diagram.

Based on International Energy Agency (IEA), the generation cost of electricity from the RESs (PV and WT) is decreasing throughout the years from 2010-2021 as demonstrated in Figure 2.

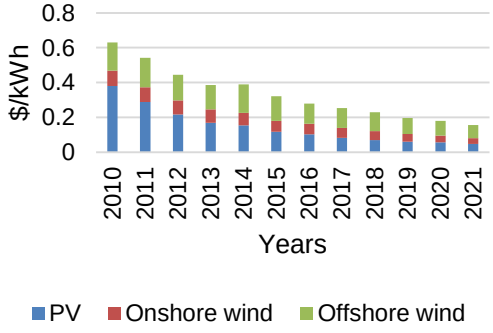

Fig. 2 Global PV and wind turbine generation costs (2010-2021) based on IEA.

According to the collected climatology data for the considered site of the study that recorded by the PVWatt web page [15], while the hourly recorded data of solar irradiance and wind speed data have presented in Figure 3 and Figure 4, respectively.

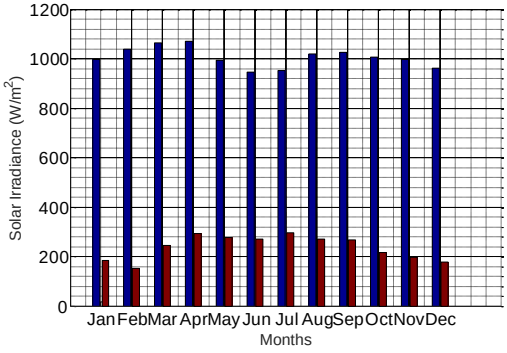

Fig. 3 Annual solar irradiance.

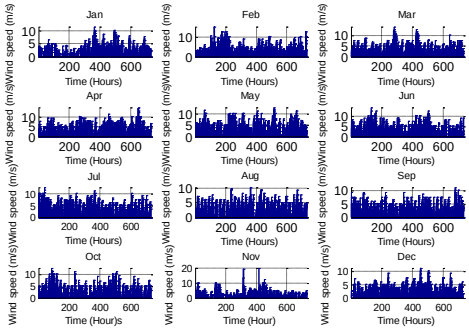

Fig. 4 Annual wind speed.

The aforementioned data has been implemented with the help of mathematical equations that presented in the literature [9].

ISBN 978-9959-9703-2-9

To size the system components, nature-inspired metaheuristic algorithms as part of Artificial Intelligent (AI) tools are exploited [16]. The PSO is originally introduced in 1995 by Kennedy and Eberhart to address various problems in several fields [17]. The EMS is based on IF-THEN statements and considered due to its simplicity as human knowledge based rules and does not have a complex mathematical equations [18]. Additionally, classified into three main groups, Rule-Based, Optimization-Based, and Learning-Based [19], [20]. The EMS proposed rules can be as listed:

1. RESs power home appliance (the priority to run with RESs).
2. Battery to run home appliance.
3. Grid supply the home appliances.

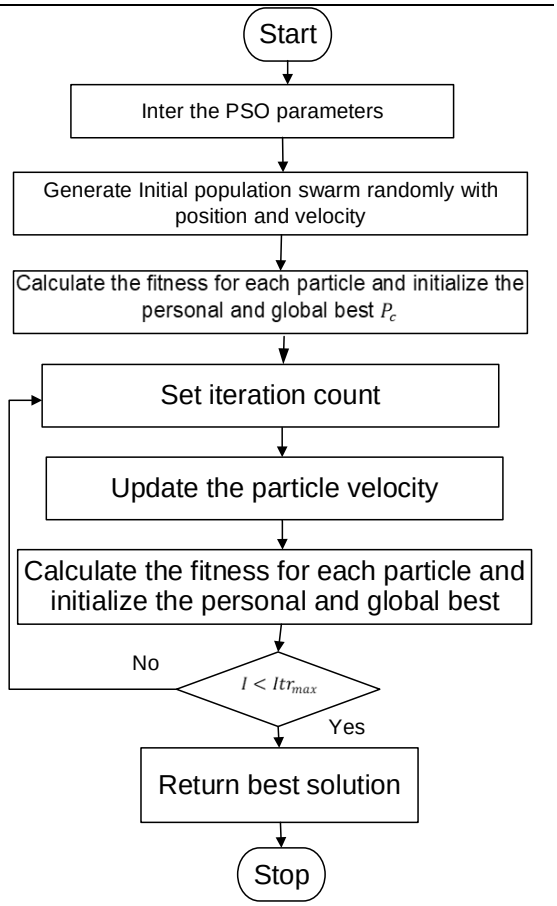

Fig. 5 Particle Swarm Optimization flowchart [17].

Results and Discussion

Based on the proposed modal system in Figure 1, the acquired result for the iteration number that refers to the annual cost that equals to USD 0.03/kWh during 1000 times of iteration. The comparison result of the output generated power from the sources is demonstrated in Figure 7. The operation shows the charge,

 ISBN 978-9959-9703-2-9

discharge, PV output, WT output, and the main load. The integrated sources produced power during the year based on the main factor which is the climate changes. When the sources are not sufficient to meet the demand, the battery as backup system will run the system appliances.

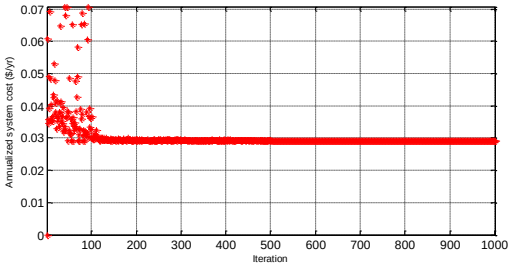

Fig. 6 convergence

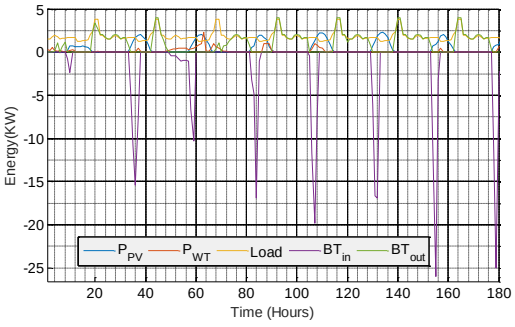

Fig. 7 Comparison result of the generated output power.

Conclusion

In conclusion, microgrid distributed systems are preferable generation systems because they hold great potential for promoting sustainable energy optimizing resource utilization and achieving reliable and cost-effective energy supply systems. Nature-inspired methos coupled with EMS to meet the objectives with smoothly flow the power in the proposed system based on if-them statements. Based on the collected data and obtained result, the study area is rich with sources to generate electricity using nature sources instead of conventional sources. For future studies direction by considering smart systems acquire decarbonization systems to improve the power and environmental systems which integrated more RESs.

References

[1] A. A. Khan, A. F. Minai, R. K. Pachauri, and H. Malik, “Optimal Sizing, Control, and Management Strategies for Hybrid Renewable Energy Systems: A Comprehensive Review,” Energies, vol. 15, no. 17, p. 6249, Aug. 2022, doi: 10.3390/en15176249.

[2] M. S. Javed et al., “Economic analysis and optimization of a renewable energy based power supply system with different energy storages for a remote island,” Renew. Energy, vol. 164, pp. 1376–1394, 2021, doi: 10.1016/j.renene.2020.10.063.

[3] A. O. M. Maka, S. Salem, and M. Mehmood, “Solar photovoltaic (PV) applications in Libya: Challenges, potential, opportunities and future perspectives,” Clean. Eng. Technol., vol. 5, p. 100267, 2021, doi: 10.1016/j.clet.2021.100267.

[4] B. K. Das and M. Hasan, “Optimal sizing of a stand-alone hybrid system for electric and thermal loads using excess energy and waste heat,” Energy, vol. 214, p. 119036, Jan. 2021, doi: 10.1016/j.energy.2020.119036.

[5] M. M. Khaleel, A. A. Ahmed, and A. Alsharif, “Energy Management System Strategies in Microgrids: A Review,” North African J. Sci. Publ., vol. 1, no. 1, pp. 1–8, 2023.

[6] F. A. Khan, N. Pal, and S. H. Saeed, “Optimization and sizing of SPV/Wind hybrid

 ISBN 978-9959-9703-2-9

renewable energy system: A techno-economic and social perspective," Energy, vol. 233, p. 121114, 2021, doi: 10.1016/j.energy.2021.121114.

[7] A. Hirsch, Y. Parag, and J. Guerrero, "Microgrids: A review of technologies, key drivers, and outstanding issues," Renew. Sustain. Energy Rev., vol. 90, no. September 2017, pp. 402–411, 2018, doi: 10.1016/j.rser.2018.03.040.

[8] S. Singh, M. Singh, and S. C. Kaushik, "A review on optimization techniques for sizing of solar-wind hybrid energy systems," Int. J. Green Energy, vol. 13, no. 15, pp. 1564–1578, Dec. 2016, doi: 10.1080/15435075.2016.1207079.

[9] A. Alsharif et al., "Impact of Electric Vehicle on Residential Power Distribution Considering Energy Management Strategy and Stochastic Monte Carlo Algorithm," Energies, vol. 16, no. 3, p. 1358, Jan. 2023, doi: 10.3390/en16031358.

[10] A. R. Battula, S. Vuddanti, and S. R. Salkuti, "Review of Energy Management System Approaches in Microgrids," Energies, vol. 14, no. 17, p. 5459, Sep. 2021, doi: 10.3390/en14175459.

[11] A. Alsharif, A. A. Ahmed, M. M. Khaleel, A. S. D. Alarga, O. S. M. Jomah, and A. B. E. Alrashed, "Stochastic Method and Sensitivity Analysis Assessments for Vehicle-to-Home Integration based on Renewable Energy Sources," in 2023 IEEE 3rd International Maghreb Meeting of the Conference on Sciences and Techniques of Automatic Control and Computer Engineering (MI-STA), IEEE, May 2023, pp. 783–787. doi: 10.1109/MI-STA57575.2023.10169210.

[12] O. Ellabban, H. Abu-Rub, and F. Blaabjerg, "Renewable energy resources: Current status, future prospects and their enabling technology," Renew. Sustain. Energy Rev., vol. 39, pp. 748–764, 2014, doi: 10.1016/j.rser.2014.07.113.

[13] W. Ma, X. Xue, and G. Liu, "Techno-economic evaluation for hybrid renewable energy system: Application and merits," Energy, vol. 159, pp. 385–409, 2018, doi: 10.1016/j.energy.2018.06.101.

[14] M. E. T. Souza Junior and L. C. G. Freitas, "Power Electronics for Modern Sustainable Power Systems: Distributed Generation, Microgrids and Smart Grids—A Review," Sustainability, vol. 14, no. 6, p. 3597, Mar. 2022, doi: 10.3390/su14063597.

[15] NREL, "PVWatts®," 2020. https://pvwatts.nrel.gov/pvwatts.php (accessed Oct. 19, 2020).

[16] M. Khaleel, A. A. Ahmed, and A. Alsharif, "Artificial Intelligence in Engineering," Brill. Res. Artif. Intell., vol. 3, no. 1, pp. 32–42, Mar. 2023, doi: 10.47709/brilliance.v3i1.2170.

[17] F. Marini and B. Walczak, "Particle swarm optimization (PSO). A tutorial," Chemom. Intell. Lab. Syst., vol. 149, pp. 153–165, Dec. 2015, doi: 10.1016/j.chemolab.2015.08.020.

[18] A. Alsharif, C. W. Tan, R. Ayop, K. Y. Lau, and A. M. Dobi, "A rule-based power management strategy for Vehicle-to-Grid system using antlion sizing optimization," J. Energy Storage, vol. 41, no. July, p. 102913, Sep. 2021, doi: 10.1016/j.est.2021.102913.

[19] Y. E. García Vera, R. Dufo-López, and J. L. Bernal-Agustín, "Energy Management in Microgrids with Renewable Energy Sources: A Literature Review," Appl. Sci., vol. 9, no. 18, p. 3854, Sep. 2019, doi: 10.3390/app9183854.

[20] A. Alsharif, C. W. Tan, R. Ayop, A. Dobi, and K. Y. Lau, "A comprehensive review of energy management strategy in Vehicle-to-Grid technology integrated with renewable energy sources," Sustain. Energy Technol. Assessments, vol. 47, no. xxxx, p. 101439, Oct. 2021, doi: 10.1016/j.seta.2021.101439.

 ISBN 978-9959-9703-2-9

المؤتمر الدولي الثاني للعلوم والهندسة
2nd International Conference on Science and Engineering
ICSE 2023
Faculty of Engineering - University of Bani Waleed
Bani Waleed, Libya

Paper Code: ICSE-062

NUCLEAR ENERGY AND OPPORTUNITIES TO BENEFIT FROM IT IN LIBYA

Abdalfettah Aljedk
Electrical and Electronics Engineering, Faculty of Engineering / Bani waleed University, Libya
Abdalfettahaljedk@bwu.edu.ly

Abstract: The exponential growth in population requires a parallel increase in the total electrical energy to feed all loads with electrical energy. Diversity, independency of resources and global warming call for installing renewable and nuclear energy plants.. Where there are many renewable energy sources that can be used in Libya, including nuclear energy; Yet nuclear power with its many attractive features is not used at all. This study presents the energy resources available in Libya and reviews the main challenges and opportunities in the field of nuclear energy. At the end of this paper some conclusions are mentioned.

Keywords: (electrical energy, renewable energy, nuclear power plants, nuclear energy)

Introduction

Nowdays, The population of Libya 8,732,299 million people in 2023, has been as a small country in the world than have population. [Head of the Civil Registry Authority in Libya] Despite the remarkable growth in energy consumption in the last five years due to the large population base, the rate of domestic energy generation still lags behind that of other neighboring countries. Thus, Libya depends mainly on non-renewable energy sources (fuel energy). Because energy is one of the most important strategic requirements for developing countries . Libya's primary energy resources include hard coal, oil and natural gas.

Libya is also witnessing a rapid growth in the demand for electricity and potable water at a low cost, and according to the recent studies. the demand for electricity in Libya will exceed 10,000 MW by the year 2030, unless alternative energy is produced and systems are applied to conserve energy sources.

In order to build or establish a program that provides a huge amount of increasing demand and the development of technical knowledge, skills and experience, Libya needs a balanced and feasible mixture between renewable energies , nuclear energy and fossil fuels so that it is effective, practical, economically serious and sustainable in order to produce

 ISBN 978-9959-9703-2-9

energy, which in turn will allow the preservation of energy resources Libya of oil and gas for the future of future generations.

The future of nuclear energy in the world

Nuclear energy supplies the countries of the world with more than 16% of the electrical energy; It supplies 35% of the needs of the European Union. Japan obtains 30% of its electricity needs from nuclear energy, while Belgium, Bulgaria, Hungary, Slovakia, South Korea, Sweden, Switzerland, Slovenia and Ukraine depend on nuclear energy to supply a third of its energy needs. Because the amount of nuclear fuel required to generate a large amount of electrical energy is much less than the amount of coal or oil needed to generate the same amount[1]. One ton of uranium generates energy Electricity greater than millions of barrels of oil or millions of tons of coal. Solar energy cost is much greater than the costs of nuclear power. It does not release harmful gases into the air, such as carbon dioxide, nitrogen oxide or sulfur dioxide, which cause global warming, acid rain and smog. The source of nuclear fuel (uranium) is readily available and easy to obtain and transport, while the sources of coal and oil are limited [2]. Nuclear power generation plants occupy small areas of land compared to power plants that depend on solar energy or wind energy. However, the use of nuclear energy causes the production of harmful radiation and reduces The degree of its radioactivity After that, it can be recycled and reprocessed to recover the uranium and plutonium that have not yet fissioned, and use them again. For thousands of years, there is no safe system for the disposal of this waste, but nuclear research centers around the world are working on finding modern technology to solve this issue.

Nuclear energy and its future in Libya

The State of Libya does not need nuclear energy for the current generation because it does not have a problem in providing energy due to the presence of oil and gas, but how will future generations Will you manage? Oil is an important thing for human life, not only for engines or power generation, but even in the clothing industries, for example, which oil is threatened with depletion. As for solar energy, it is clean and excellent, but what do we do when evening comes and the sun sets? So we have to develop it in order to store it, but also that is not easy, so it is difficult to be a major source of energy. It is also financially expensive, and it is true that solar energy is widely available in Libya. But if we want to establish a solar power station, the price will be very expensive, reaching five or ten times the construction of a nuclear power station. The problem is that climate change is one of the challenges of energy use, which will require

 ISBN 978-9959-9703-2-9

us to use oil reasonably, a country that has abundant financial resources, which makes it have the ability to build nuclear plants for the benefit of future generations, as it will use oil to export and obtain revenues and use nuclear energy to generate electricity, which is strategic good. And if we calculate this, then one gram of uranium produces as much energy as it produces about 1800 liter of oil and three tons of coal [3].

Nuclear energy and how to succeed in Libya

Libya is one of the countries that showed good interest in this type of energy, and actively sought to establish a nuclear plant at the end of the eighties and the beginning of the nineties of the last century, and an agreement was reached with a Russian company in this regard to establish a nuclear plant with a capacity of MW 1000 south of the city of Sirt. However, the political circumstances and the country's foreign relations prevented the implementation of the project. Nuclear reactor projects are scientific and technical projects that will not be successful without the following considerations:[4].

1- Spreading scientific awareness among intellectuals and the general public of the importance of using and exploiting nuclear energy in generating electricity, and introducing them to the positive returns from that.

2- Supporting scientists and intellectuals towards directing the government and the state to the scientific policy that results in supporting and establishing scientific projects.

3- Benefiting from the experience of modern countries that use nuclear reactors to generate electric power.[5]

4- Negotiating well with private companies to build nuclear reactors and obtaining adequate international guarantees.

Comparison between nuclear energy and other energies

Nuclear energy is the best means today to provide the world with electric energy, and it is efficient compared to all other energy sources, and its production cost is the lowest compared to other energies. As the importance of relying on nuclear energy has increased in light of the relative consideration of its costs, and its facilities can be established next to the consumption sites easily without the need for complex transportation and supply arrangements. In addition, nuclear energy is not linked to specific climatic conditions, as is the case with solar energy, wind energy, and water energy. Nuclear energy is clean energy that does not contribute to global warming. In this regard, the former inspector of the International Atomic Energy Agency (IAEA), Hans Becks, stated, That "the danger of global warming is greater than the threat of weapons

 ISBN 978-9959-9703-2-9

of mass destruction to the environment," and he also stressed the need to reduce gas emissions and rely on peaceful nuclear energy to obtain electric power without polluting the atmosphere with gases [6][7].

Advantages of using nuclear energy

1 - Diversity and Security First and foremost, installing nuclear power plants on a system improves the security and diversity of that system. In the event of unexpected accidents or disasters, a system fed from several types of resources can be more stable and secure. Moreover, diversity provides more alternatives to unit commitment and spinning tanks, resulting in better economic operation of the power system for both producing companies and consumers[8].

2 – table[1] of shows carbon dioxide emission rates from coal, oil, gas, solar energy, wind energy and nuclear energy. Renewable resources and nuclear energy represent a friendly alternative solution to global warming. In fact, a very attractive feature of nuclear power plants is that about 10-30 grams of carbon dioxide is emitted per kilowatt-hour of energy through the entire energy chain. This is the same rate of emission as in wind power and much lower than coal, oil and natural gas [9], [10]. Accordingly, a large part of the global energy consumption is increased from renewable and nuclear resources, as it will be the least contribution to global warming.

Table 1: CO2 EMISSION RATES

Energy Resource	CO_2 Emission (gram/kWh)	Normalized Rate to nuclear (min-max)
Coal	900-1200	30-120
Oil	700-900	23-90
Gas	350-900	12-90
Solar	100-200	3-20
Wind	10-75	1-7
Nuclear	10-30	1

3- The Cost : The cost of nuclear energy is cheaper than other alternatives. This has been confirmed by independent studies by the Ontario Energy Authority (OPA) and the Organization for Economic Co-operation and Development[19]. Recent global trends toward higher fossil fuel prices combined with lower interest rates, lower inflation, and the increasing importance of carbon emissions as a direct cost of power generation have improved the relative economics of nuclear power [11].

although gas, coal and nuclear are the lowest cost options according to global surveys, the discount rate plays a significant role in determining overall cost effectiveness. With the large initial capital costs of developing nuclear generation and the relatively low cost of fuel on a per kilowatt-hour basis, the discount rate

 ISBN 978-9959-9703-2-9

plays an important role in determining the relative costs across these options. At a discount rate of 5%, the stable cost of nuclear power is $29/MWh compared to $47 for natural gas. But at a 10% discount rate, nuclear generation costs $43/MWh compared to $51 for natural gas"[12].

4- Other advantage of using nuclear energy which involve it's strong performance record over decades of experience and continuous improvements in its reliability, safety and lower operating costs. Moreover, stability of supply and KWh price is ensured and this can help in hydrogen economy. In addition to the fact that nuclear plants have minimal environmental impacts, since waste volumes are small and manageable, spent fuel storage is no longer a technical issue but rather a political decision [13].

Need to take into consideration In the cost of using nuclear

There are three main issues need to be taken into account during the use of nuclear energy

1. Nuclear safety and security Like the Chernobyl plant accident in 1986, the ever-desired end to nuclear plants. Indeed, when such a catastrophe strikes, many lives can be lost and thousands suffer health disorders, as well as serious environmental impacts that can add to long-term concerns. In the case of Chernobyl, it was clear that poor management and outdated reactor design were the main culprits. After the accident of 1986 in particular, international agreements and the nuclear safety system were reviewed and some of them were concluded to enhance the safety of nuclear activities [14]. Nuclear security at the same time is another major concern. That is, nuclear facilities must be protected and nuclear materials and radioactive sources must be well monitored.

2. Nuclear materials as a source of radiation All types of nuclear materials involved in the nuclear energy chain may emit beta, gamma, and/or protons, neutrons, alpha particles, and fission fragments. These radiations can pose risks to workers and the environment [15]. Hence, ensuring that nuclear material is well managed and controlled at all stages from production to storage under an authorized regulatory regime is essentially a national task. In addition, international systems may be parallel to national systems to improve global nuclear safety. Considering the disposal of spent fuel, about 10,000 tons of spent fuel annually is a small amount compared to the 28 billion tons of waste carbon dioxide from fossil fuels that are released directly into the atmosphere. However, being a highly hazardous material, radioactive waste is a matter of concern to the public despite experts stressing the safety of geological disposal.

 ISBN 978-9959-9703-2-9

3. Natural disasters: Natural disasters may threaten nuclear plants if they are not well designed to withstand expected natural disasters. For example, the Cooper Nuclear Power Plant experienced flood waters on the Missouri River near Brownville in July 1993 and the operator was forced to shut down the reactor [16]. In addition, hurricanes and tornadoes are another threat to nuclear plants; The Davis Base Nuclear Power Plant near Toledo, Ohio, was hit by a hurricane and winds caused an off-site power loss that automatically shut down the reactor [17]. Moreover, the recent disaster in Japan (the Fukushima nuclear accident in 2011) has resulted in a relapse in the republic's public opinion towards nuclear power.

The economic aspect of using nuclear energy

1-The nuclear reactor construction project has been considered one of the long-term projects from the economic, strategic and national perspectives.

2- Availability of means of protection and safety more than before as a result of avoiding defects and shortcomings in old nuclear reactors, the most famous of which is the Chernobyl reactor accident in the former Soviet Union and the nuclear reactor disaster in Fukushima, Japan, following the earthquake.

3- Increased global demand for electric power.

4- The rapid increase in the cost of electric power generation generated by fossil fuels, which makes nuclear power generation an attractive economic option.[18]

Nuclear energy and it's development in Libya and the Arab world

Nuclear energy has countless peaceful uses, and all of them achieve great economic benefits for the countries that use them, and Libya and the Arab countries can achieve great economic gains if this energy is used on a large scale and in studied ways, and given the presence of vast areas of desert lands in Libya and the Arab world, storming the desert for the purpose Development is one of the basic purposes that must be taken into account in any direction of economic and social development in Libya and the Arab world, and in this regard nuclear energy can play a very important role in the development of desert areas by addressing the problems of the desert environment, especially energy, agriculture and water[19]. Nuclear energy is used in desert development by providing energy and clean water for the benefit of human, agricultural and industrial development in these arid regions.

Conclusion

Libya is a very large country with a land area of 1,800,000 Km^2 and a small population of 8,732,299 million in 2023. By 2030 the population of Libya will increase to 10 million,

 ISBN 978-9959-9703-2-9

this growing population definitely needs an increase in energy supply and it must be in parallel with The same rate of increasing electricity generation in general and installing new types of power stations is required and welcome in any energy supply system. Given the lack of nuclear energy resources in Libya, the installation of nuclear power plant(s) is important for diversity and national independence as well. Having much lower carbon dioxide emission rates than coal and gas plants adds another attractive environmental advantage. Moreover, the stability of energy prices and stability in generation invite investors to invest in nuclear energy. On the other hand, this energy resource involves challenges and issues that must be taken into account. Among these challenges, the establishment of a national regulatory system based on the results of the long experience gained by other countries in the use of nuclear energy and international or regional cooperation is also required to ensure security and safety. In addition, it must be disposed of. radioactive waste very safely. Finally, natural disasters also pose a critical challenge, if the National Nuclear Authority decides to build a nuclear plant(s), the site must be chosen carefully and the construction constructed in such a way as to take into account all natural disasters.

References

[1] Soyhan, H. S., "Sustainable energy production and consumption in Turkey: A review", Renewable and Sustainable Energy Reviews, 13 (6-7), 1350-1360, (2009).

[2] Yıldız, T., "Turkey's Energy Policy, Regional Role and Future Energy Vision", Insight Turkey, 12 (3), 33-38, (2010).

[3] Energy Market Regulatory Authority (EPDK), 1(2012).

[4] Ismail Shaaban Muhammad Maan Diop Louay Bahjat Dib; Nuclear energy and its impact on the economies of countries(2009).

[5] Güngör, Z., and Bozkurt, G., "Economical Comparison of Imported Energy Sources in Terms of Long Term Production Planning", Energy

International Journal, 24 (1), 31-42 (1999).

[6] Yılmaz, A. O., "Renewable energy and coal use in Turkey". Renewable Energy, 33(5), 950-959, (2008).

[7] Bilgin, M., "Energy and Turkey's Foreign Policy: State Strategy, Regional Cooperation and Private Sector Involvement", Turkish Policy

Quarterly, 9 (2), 81-92 (2010).

[8] World Nuclear Association, (2012).

[9] Rashad S. M., "Nuclear Power and the Environment Prospects and Challenges", Radio Science Conference, 2006, NRSC.

[10] Rashad S. M., and Hammad, F. H.

 ISBN 978-9959-9703-2-9

"Nuclear Power and the Environment: Comparative Assessment of Environmental and Health Impacts of Electricity Generating Systems", Applied Energy, 65 (2000), 211-229, (2000).

[11] I. Mahariq, Challenges and Opportunities in Nuclear Energy: Promising Option in Turkey?(2013)

[12] Tynan, P. and Stephenson, J., "Nuclear Power in Saudi Arabia, Egypt, and Turkey-how cost effective?", The Century Foundation, New York, (2007).

[13] Duffey R. B., Miller A.I., and Hopwood J., "Canadian solutions to global energy and environment challenges: green atoms", EIC Climate Change Technology, IEEE, (2006).

[14] Badawy, I., "Production of nuclear energy and the control of nuclear materials", Second Radiation Physics Conference, 59, 1994, Monoufia- Egypt.

[15] Semenov, B., "Executive summary; Key issues and findings", Senior. Expert Symposium on Electricity and the Environment, 1991, HelsiblEv, Finland,

[16] IAEA safeguards: an introduction, International Atomic Energy Agency, IAEA/SG/n\TF/3, Vienna, Austria, (1981).

[17] Gunter P., "Natural Disasters and Safety Risks at Nuclear Power Stations", Nuclear Information and Resource Service, November (2004).

[18] shukrieldabar, bakershikhi, aamtamtum Prospects and future of nuclear energy in Libya(2017)

[19] Euromonitor International, Economist Intelligence Unit, (2010).

 ISBN 978-9959-9703-2-9

المؤتمر الدولي الثاني للعلوم والهندسة
2nd International Conference on Science and Engineering
ICSE 2023
Faculty of Engineering - University of Bani Waleed
Bani Waleed, Libya

Paper Code: ICSE-002

ESP DESIGN OPTIMIZATION AND SENSITIVITY ANALYSIS FOR OIL WELL (E-05) USING PROSPER SOFTWARE

[a]Elnori Elhaddad, [b]Mohammed Garoom, [c]Hoosam lssa
[a]Petroleum Engineering Department, Faculty of Engineering, Bani-Waleed University
[b]Petroleum Engineering Department, Faculty of Engineering, Bani-Waleed University
[c]Petroleum Engineering Department, Faculty of Engineering, Bani-Waleed University
*Crosspnding author: norimab2014@gmail.com

Abstract: The natural reservoir pressure is often sufficient to lift the fluids to the surface. However, when excessive water and gas production occurs, the reservoir pressure may no longer be sufficient. In such cases, an artificial lift method is required to lift the fluids to the surface. The objective of this study is to improve the efficiency of the ESP system and to identify the critical parameters that affect the system's performance of oil well E.05 using Prosper software. Results were obtained and analyzed to determine the optimal design for the well. In this paper, we discussed the ESP model and its impact on productivity. The ESP model is designed to optimize parameters such as reservoir pressure, pump sitting depth, operation frequency, and number of stages. Specifically, the model recommends a reservoir pressure of 3100 psi, a pump sitting depth of 5000 ft, an operation frequency of 60 HZ, and number of stages of 225 stages. By implementing these parameters, the ESP model has been shown to significantly improve productivity. This model boasts best pump and motor efficiency, making it a reliable choice for optimizing production. The oil flow rate for the well has increased from 916 STB / D to 1008 STB / D, indicating a successful current design for the well. Further research is needed to better understand the factors that affect ESP performance, such as wellbore conditions, fluid properties, and pump design.

Keywords: 103 E oilfield, ESP, optimization, prosper software, Sensitivity Analysis

Introduction

The petroleum engineer can select the most suitable artificial lift method based on technical, economic, and other parameters

[1 ،2].

We require an artificial lift method the natural pressure of the reservoir is not sufficient to lift the fluids to the surface because of excessive water and gas production. But every method has specific requirements.[3 ،4]

If the Electrical Submersible Pump (ESP) does not operate at recommended parameters, the ESP efficiency will decrease and it may get failure [5].

This work aims to optimize the ESP design for the oil well E.05 and study the impact of various parameters on the well's performance using Prosper software, which is a crucial step in ensuring efficient oil production. By utilizing PROSPER software, we can analyze and optimize the design parameters of the ESP

 ISBN 978-9959-9703-2-9

system, including reservoir pressure, pump setting depth, operation frequency, number of stages, water cut, wellhead pressure, and gas oil ratio. This optimization process can greatly improve the performance of the well., resulting in an increased production rate and reduced operating costs. It is essential to study the impacts of various parameters on well performance.

ESP delivers high efficiency and reliability but with high maintenance and workover costs. The design model's results will have a significant impact on both the oil production and future performance of oil wells [6].

In the field of oil and gas production, the setting depth of electrical submersible pumps (ESPs) near the producing zone is a critical factor in optimizing flow efficiency and well completion. By setting the ESP close to the producing zone, we can improve the efficiency of fluid production and reduce the risk of damage to the wellbore, the less distance the fluid has to travel, reducing the pressure drop and increasing the flow rate. [7].

ESP provides operating flexibility for changing conditions, allowing for adjustments to be made as needed. This is particularly important in high water cut oil wells, where the water to oil ratio can vary greatly [8].

The productivity of a well is influenced by various parameters. These parameters include factors such as reservoir pressure, water cut, tubing size, and wellhead pressure. Each of these parameters plays a crucial role in determining the productivity of a well. It is essential to carefully consider and optimize to ensure maximum productivity of the well. Electrical submersible pumps (ESP) will also be impacted by the number of stages and operation frequency, these parameters can have a significant impact on the production of a well. [9].

The ESP design for oil well E.05 has been optimized and a sensitivity analysis has been conducted. Results indicate that the optimized design will lead to improved efficiency and performance. Further details on the specific changes made and the results of the sensitivity analysis are available.

In this paper, we present an optimization and sensitivity analysis of ESP design for the Oil Well (E-05) using Prosper software. The purpose of this study is to improve the efficiency of the ESP system and to identify the critical parameters that affect the system's performance. To achieve this, we use the Prosper software to simulate the ESP system and evaluate its performance under different operating conditions. We also perform a sensitivity analysis to identify the critical parameters that affect the system performance. Our results show the optimal ESP configuration for the E-05 well.

Methodology

In this paper, several steps were run to achieve the main objectives of this research. These steps start with gaining the technical and practical knowledge about aspects of production engineering, then proceed through software training for PROSPER software, and finally processing data to be suitable for the project objectives and summarized as follows:

1. Collecting the required data for the study such as PVT, well schematic, production, and pressure tests. For example, GOR, Oil & Gas Gravity, Water Salinity, Bottom hole temperature and pressure, Oil Volume Factor, Oil Viscosity, and Bubble Point Pressure.

 ISBN 978-9959-9703-2-9

2. Study the performance of a well's productivity using production and pressure history. As Total fluid, Water cut, Total Gas, wellhead pressure, Casing Pressure, Flowing Line Pressure, and Choke.

3. Matching the data of the well with correlations in PROSPER starts with PVT through the IPR curve and VLP matching process.

4. Building the well model in PROSPER after completing the matching with less error percentage.

5. Prediction of future production performance as optimization of reservoir parameters and its effect on well productivity using the ESP method as one of the artificial lift methods.

6. Optimization of ESP parameters such as pump setting depth, frequency of pump, wellhead pressure, and pump stages.

7. Selecting the best pump type and optimum ESP parameters to improve well productivity.

Reservoir (A), is limestone with a rather high porosity and low permeability, the oil system is medium to light and is highly under-saturated. The Reservoir (A) Data can be summarized in the following tables.

Table 1: Shows Reservoir (A) Data.

Reservoir (A)		units
Formation Depth, (D)	6764	Ft
Avg. Net Pay, (h)	100	Ft
Initial Pressure, (P_i)	3002	Psia
Current Pressure, (P)	2576	Psia
Reservoir Temperature, (T_{res})	196	F°

Table 2: Shows Rock Properties Data.

Rock Properties		Units
Avg. Porosity, ($\phi_{avg.}$)	25	%
Initial Water Saturation, (S_{wi})	27	%
Avg. Permeability, ($k_{avg.}$)	13	Md

Table 3: Shows Fluid Properties Data.

Fluid Properties		Units
Saturation Pressure, ($P_{sat.}$)	435	Psia
Gas Oil Ratio, (GOR)	185	SCF/STB
FVF @ Initial Pressure, (B_{oi})	1.169	RB/STB
Oil Viscosity, (μ_o)	1.74	Cp
Oil Gravity, (API)	33	API°

Table 4: Shows Fluid Reserves Data.

Reserves		
Original Oil in Place, (N)	172	MMSTB
Initial Oil Reserves, (N_p)	64	MMSTB
Original Gas in Place, (G)	29	BSCF
Initial Gas Reserves, (G_p)	12	BSCF

The Reservoir (A) started production in early 1976 with six producer wells. In 1979, after severe pressure decline was observed, the two peripheral injectors were put into operation.

From 1976 until the end of 1991, (10.87 MMSTB) of the reserves, have been produced which equals (16.93%) of the initial oil reserves with, a recovery (6.32%) of the original oil in place which, representing a low pool recovery.

In the early 1990s, production development projects were initiated in a reservoir consisting of nine vertical producer wells, six horizontal producer wells, and ten injectors. This marked a significant step forward in the field of reservoir engineering, as the use of both vertical and horizontal wells allowed for more efficient extraction of oil and gas. The injectors, meanwhile, were used to maintain reservoir

ISBN 978-9959-9703-2-9

pressure and increase production rates.

1. PROSPER Software

PROSPER is the industry standard single well-performance design and optimization software. It can model most types of well completion and artificial lifting methods. PROSPER is used by major operators worldwide. The software allows the building of well models with the ability to address all variables such as well configuration, fluid characteristics (PVT), multiphase VLP correlations, and various IPR models. Tuning of the models is possible by matching real field production data. The benefit of matching is the ability to model different scenarios with increased accuracy [10], **Figure (1)**.

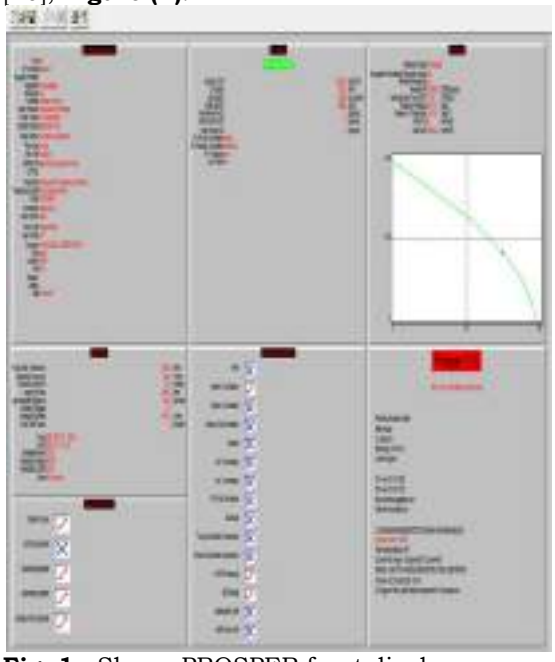

Fig. 1: Shows PROSPER front display

Calculation of VLP using multiphase flow correlations with the evaluation of VLP variables is the major application of the PROSPER software. Sensitivity analysis on future changes of parameters that affect VLP and IPR is easily assessed.

A full range of well types can be modeled in PROSPER including gas, oil, water, condensate, and steam. Different configurations such as angled, multi-layer, and multi-laterals can also be modeled. A full range of IPR models can be used in Prosper including PI entry, Vogel, Composite, Fetkovich, Jones, horizontal well model, and several others. Various completion configurations such as gravel pack, open, cased, and perforated hole are also available [11-13].

2. Building a base model

The first step when modeling a new well in PROSPER is to fill out a system summary as shown in **Figure (2)**. The Black Oil model, with the oil and water option describing the fluid. It is also here the choice of artificial lift method is made, we can input the necessary data and create a design.

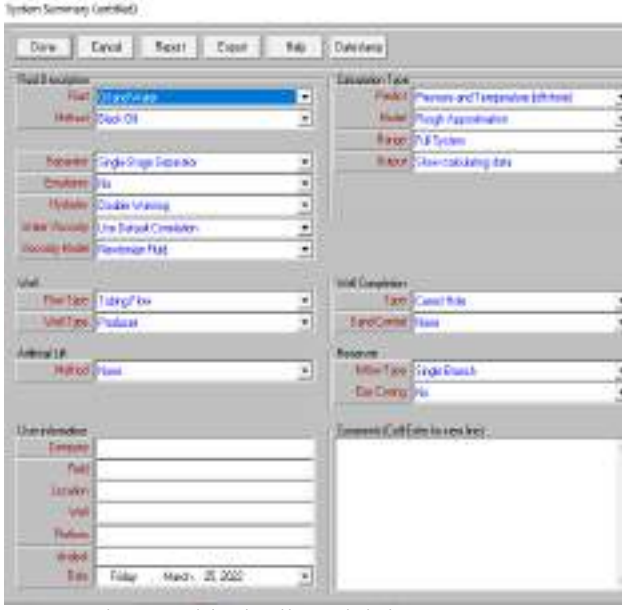

Fig. 2: Shows a black oil model data

RESULTS and DISCUSSION

ISBN 978-9959-9703-2-9

1. Well Modeling

The well has been successfully modeled after all input data was completed. The results of the PVT data were found to match the laboratory results when compared using empirical correlations which are shown in **Figure (3)**, **Figure (4)**, and **Figure (5)**.

1.1 PVT Modeling

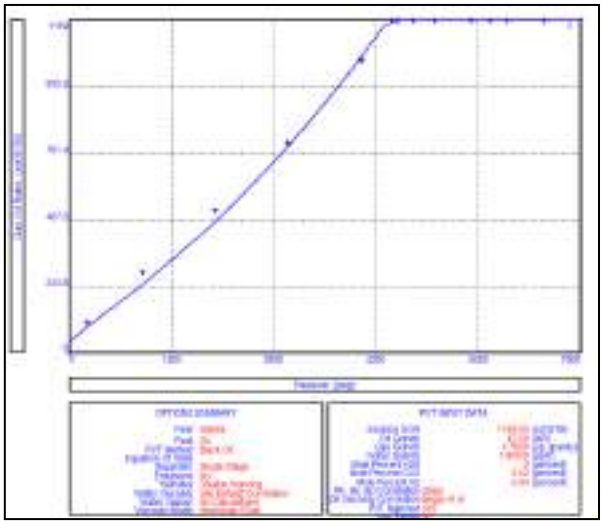

Fig. 3: Shows Gas Oil Ratio vs pressure

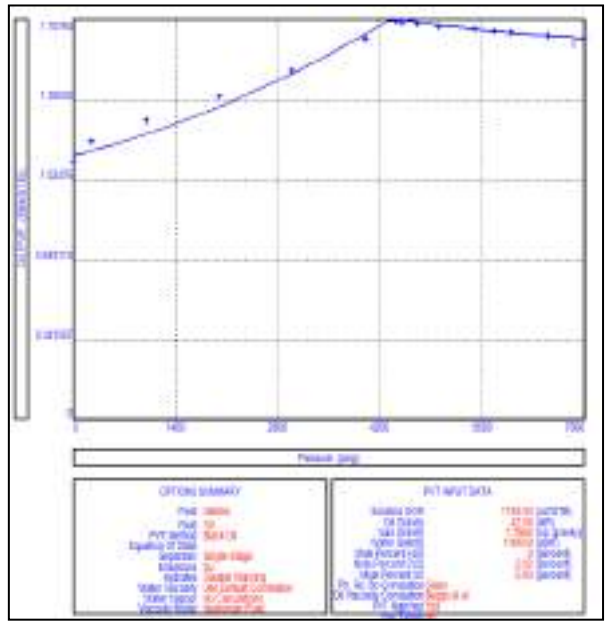

Fig. 4: Shows Oil Formation Volume Factor vs. Pressure

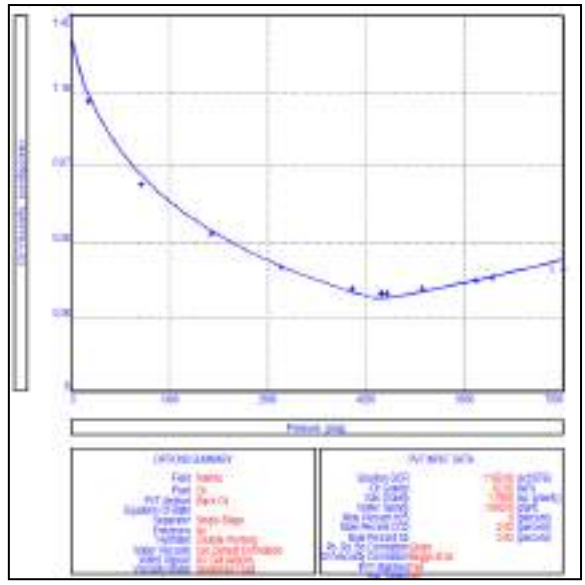

Fig. 5: Shows Oil Viscosity vs. Pressure

ISBN 978-9959-9703-2-9

1.2 IPR and VLP Modeling for E.05

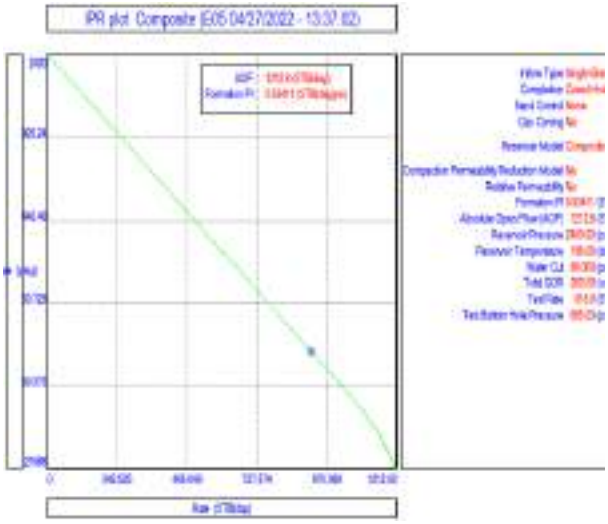

Fig. 6: Shows Inflow perfofmance relation ship (IPR) plot for the well E-05

After several trials and steps using various correlations, the matching of Inflow performance (IPR) and Outflow performance (VLP) was successfully improved. The most effective correlation was found to be Francher Brown, **Figure (7)**.

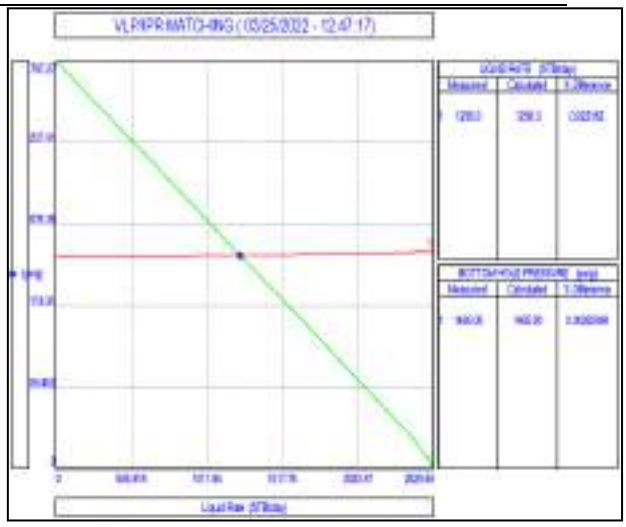

Fig. 7: Shows VLP/IPR matching for the well E-05

2. Sensitivity Analysis

Sensitivity analysis is a valuable method for determining the impact of parameters that will affect ESP performance such as operation frequency, water cut, number of stages, pump setting depth, wellhead pressure, and reservoir pressure for the well (E-05) to identify key variables and assess the impact of uncertainty on the output.

2.1 Operation Frequency

The operation frequency of the pump shown in **Figure (8)**, has a significant effect. In order to understand the impact of the frequency, it is important to consider the specific application and the desired flow rate. A higher frequency typically results in a faster flow rate but also increases energy consumption and can lead to premature wear and tear on the pump. Conversely, a lower frequency may result in a slower flow rate but can reduce energy consumption and extend the lifespan of the pump. Careful consideration of the operational frequency is crucial in optimizing the

ISBN 978-9959-9703-2-9

performance and efficiency of the pump.

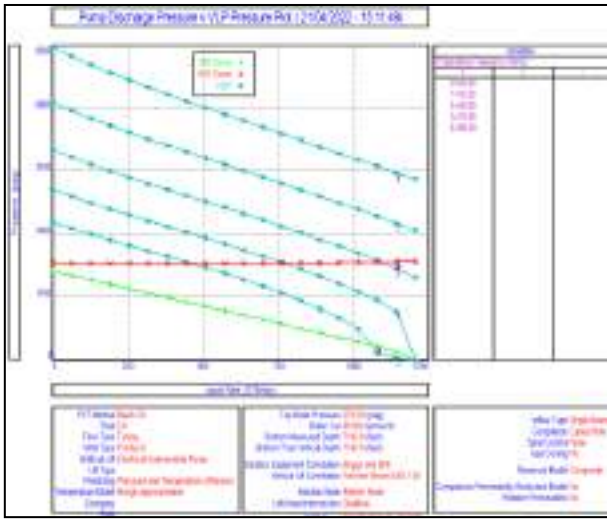

Fig. 8: Shows the effect of operation frequency on ESP performance for the well E-05

The study on the effect of operation frequency on production performance for well E.05 using ESP has revealed that the optimum operating frequency is 60 HZ. This frequency has been identified as the maximum value for the operation, as the well ceases to produce beyond this point.

Table 5: Optimization results of operation frequency

Well No	Operation Frequency	Current Liquid Production	Optimum Liquid Production
E.05	54-60 HZ	916 STB/D	1091STB/D

2.2 Water Cut

Water cut can have a significant impact on the performance of the Outflow (VLP) and ESP systems, as demonstrated in **Figures (9)**. It is important to consider the effect of water cut when analyzing the efficiency and productivity of these systems.

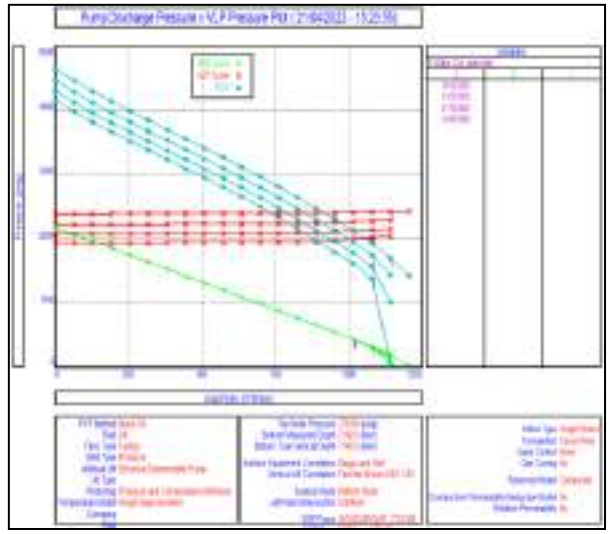

Fig. 9: Shows the effect of water cut on ESP performance for the well
E-05

After conducting a study on the impact of water cut on production performance using ESP for the well E.05, it has been determined that the high water cut is negatively affecting both oil production and ESP performance. Therefore, it is necessary to reduce the water cut to improve overall production efficiency.

Table 6: Shows the Optimization results of water cut

Well No	Water cut	Current Liquid Production	Optimum Liquid Production
E.05	88-30 %	110 STB/D	627 STB/D

2.3 Number of Stages

In this section, we analyzed the impact of multiple pump stages on the overall performance of the pump, as illustrated in **Figure (10)**. As we know, the number of stages

ISBN 978-9959-9703-2-9

in a pump can significantly affect its efficiency and effectiveness. By increasing the number of stages, the pump can generate a higher pressure head and flow rate, but this also results in higher energy consumption. On the other hand, reducing the number of stages can lead to lower pressure head and flow rate, but also lower energy consumption. Therefore, it is crucial to carefully consider the number of pump stages required for a particular application to achieve the desired performance while minimizing energy consumption.

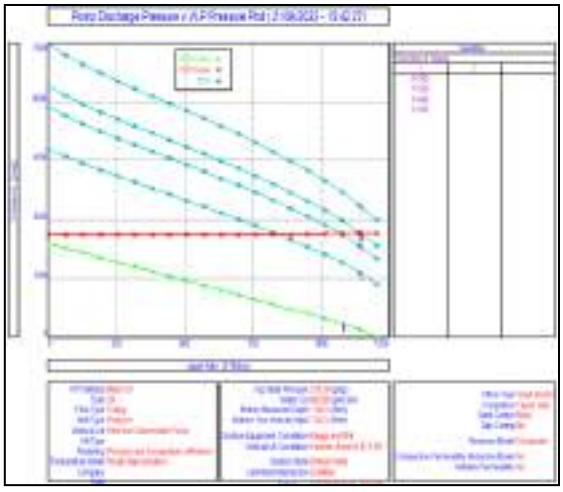

Fig. 10: Shows the effect of pump number of stages on ESP performance for well E-05

In this study, we present an analysis of the impact of the number of stages on production performance using ESP for well E.05. Our results indicate that the optimal performance of ESP was achieved by utilizing 400 stages for this particular well. We observed that the increased number of stages is dependent on the pump and pump depth and that increasing the number of stages can lead to improved ESP efficiency. These results are significant as they provide valuable insights for optimizing ESP performance in oil and gas production. Our study highlights the importance of considering the number of stages when designing ESP systems, as it can have a significant impact on production performance. By understanding the relationship between the number of stages and ESP efficiency, operators can optimize their systems to achieve maximum production performance. Overall, our study contributes to the ongoing efforts to improve oil and gas production efficiency and provides a foundation for future research in this area.

Table 7: Optimization results of pump number of stages

Well No	No of stages	Current Liquid Production	Optimum Production
E.05	277-400	916 STB/D	1148 STB/D

2.4 Pump setting depth

We examined the impact of pump setting depth on pump performance, as illustrated in **Figure (11)**. Our results reveal that the pump setting depth can significantly affect the pump's performance. Specifically, as the pump setting depth increases, the pump's efficiency decreases, resulting in a reduction in a flow rate. This decrease in efficiency is due to the increased head required to lift the fluid to the pump intake, resulting in higher energy consumption. Therefore, it is crucial to consider the pump setting depth when designing and operating a pumping system to ensure optimal performance.

We set ESP's close to the producing zone for various reasons related to flow efficiency and well completion. The setting of ESPs is crucial for the optimization of production rates and the longevity of the well. By setting the ESP close to the producing zone, we can reduce the pressure drop between the formation and the

ISBN 978-9959-9703-2-9

pump, which leads to higher flow rates. Additionally, the close proximity of the ESP to the producing zone allows for better control of the fluid level in the wellbore, which helps to prevent gas locking and other issues that can impede production. Furthermore, the placement of the ESP close to the producing zone can also aid in the prevention of sand production, which can damage the pump and decrease production rates. Overall, the setting of ESPs close to the producing zone is a critical factor in the success of the well and should be carefully considered during the design and completion phases.

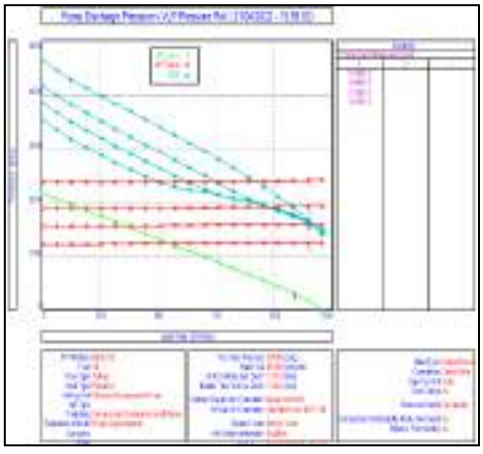

Fig. 11: Shows the effect of pump setting depth on ESP performance for well E-05

In this study, we analyzed the impact of setting pump depth on production performance using ESP for the well E-05. Our results indicate that the higher the pump, the better the performance of ESP. Specifically, we observed the best performance of ESP by setting the pump depth at 5000 ft, which resulted in a significant increase in ESP efficiency. These results suggest that carefully selecting the pump depth can have a significant impact on the overall production performance of ESP.

Table 8: Shows Optimization results of pump setting depth

Well No	Pump depth	Current Liquid Production	Optimum Production
E.05	5000 ft – 6500 ft	916 STB/D	967 STB/D

2.5 Reservoir pressure

We analyzed the impact of reservoir pressure on the performance of the pump, as illustrated in **Figure (12)**. It is well known that the pressure of the reservoir plays a crucial role in determining the efficiency and effectiveness of the pump. The higher the pressure, the better the performance of the pump. This is because the pump can extract more fluid from the reservoir, resulting in a higher flow rate. However, it is important to note that there is a limit to the pressure that can be applied, beyond which the pump may become inefficient and even fail. Therefore, it is necessary to carefully monitor and regulate the reservoir pressure to ensure optimum pump performance. In the conclusion, the relationship between reservoir pressure and pump performance is a critical factor that must be taken into consideration in any pumping system.

 ISBN 978-9959-9703-2-9

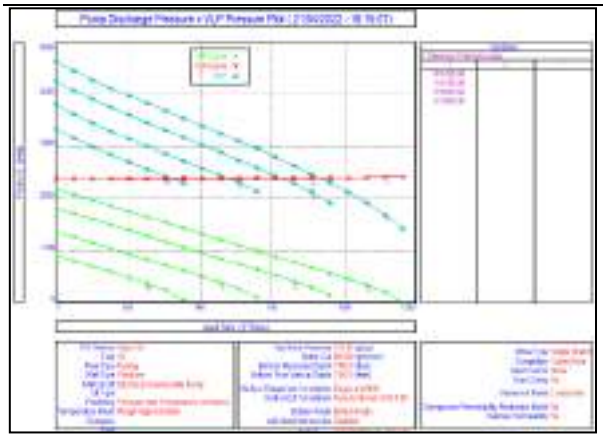

Fig. 12: Shows the effect of reservoir pressure on ESP performance for well E-05

We present the results of our study on the impact of reservoir pressure on production performance using ESP for the well E-05. Our results demonstrate that an increase in reservoir pressure leads to a corresponding increase in the productivity index, resulting in enhanced oil production. This highlights the importance of monitoring and supporting the reservoir pressure to ensure optimal production performance. Our study emphasizes the significance of reservoir pressure management in the oil industry and provides valuable insights for future research in this field. These results have significant implications for the oil industry.

Table 9: Shows the Optimization results of reservoir pressure

Well No	Reservoir Pressure	Current Liquid Production	Optimum Production
E.05	2400 – 3100 psi	916STB/D	1576 STB/D

2.6 Well Head Pressure

We have explored the impact of wellhead pressure on pump performance. As depicted in **Figure (13)**, the pressure at the wellhead has a significant influence on the efficiency of the pump. If the pressure value exceeds a certain threshold, it can ultimately affect the overall production of oil and gas. Our study focused on small values of wellhead pressure ranging from 100 psi to 400 psi. It is imperative to understand this relationship to optimize pump performance and maximize production. Through careful analysis and experimentation, we can determine the optimal wellhead pressure for a given pump and ensure that it operates at its highest efficiency. This understanding is critical for the success of any oil and gas operation and can lead to significant improvements in production.

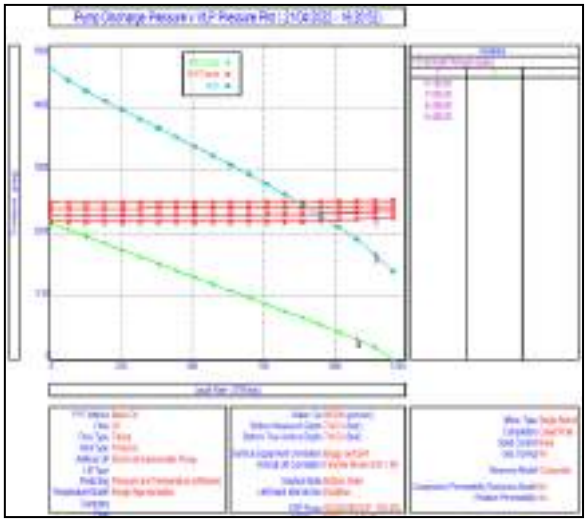

Fig. 13: Shows the effect of wellhead pressure on ESP performance for the well E-05

In this study, we investigated the effect of wellhead pressure on production performance using ESP for the well E-05. Our results indicate that the wellhead pressure has no clear effect on production performance. These results suggest that other factors, such as reservoir pressure and water cut, may have a

ISBN 978-9959-9703-2-9

greater impact on production performance. Overall, our study contributes to the growing body of knowledge on optimizing oil and gas production through efficient well design and operation.

2.7 Gas Oil Ratio

In this study, we investigated the impact of Gas Oil Ratio (GOR) on pump performance. As shown in **Figure (14)**, GOR, defined as the ratio of gas volume to oil volume, plays a crucial role in determining the efficiency of the pump. IF GOR increases, the pump performance decreases due to the reduction in fluid density. This reduction in fluid density leads to a decrease in the pump's head and efficiency. Conversely, as the GOR decreases, the pump performance improves due to the increase in fluid density. It is worth noting that the effect of GOR on pump performance is more pronounced at higher flow rates. Therefore, it is imperative to consider the GOR when designing and operating pumps in the oil and gas industry. However, it is important to mention that in our study, we used a small amount of GOR that had no effect on the pump performance. These results highlight the importance of considering GOR in pump design and operation to ensure optimal performance and efficiency in the oil and gas industry.

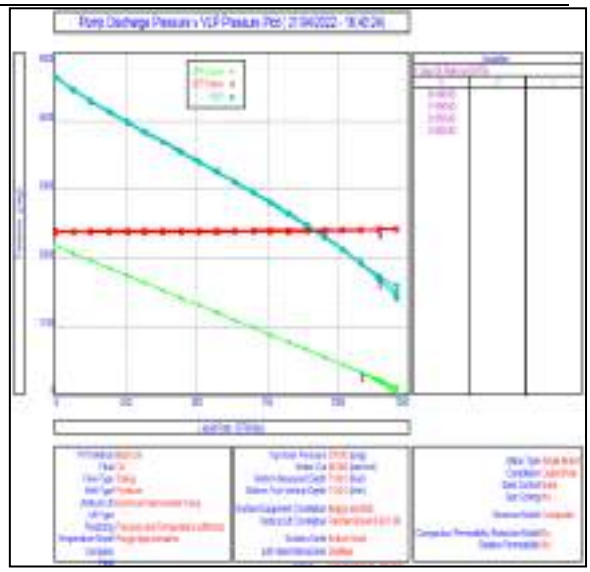

Fig. 14: Shows the effect of GOR on ESP performance for the well E-05

3. Final Optimization for the well E-05

In order to investigate the impact of various parameters on the performance of ESPs, it is necessary to carefully select the optimal operating parameters. As depicted in **Figure (15)**, we can observe the best operation parameters that have been identified through our research. By studying each parameter individually, we can gain a deeper understanding of its influence on ESP performance. This analysis is crucial for optimizing the performance of ESPs and improving their efficiency.

 ISBN 978-9959-9703-2-9

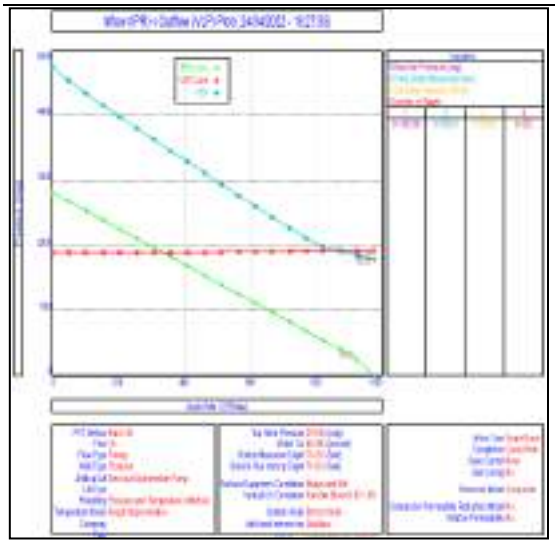

Fig. 15: Shows Final Optimization for the well E-05

We present the optimization results of the installed ESP and their impact on the production rate. As shown in **Tables (10) and (11)**, the results indicate a moderate increase of 92 STB/D after the optimization process. Although this increase may not seem significant, it is important to note that even small improvements in ESP performance can have a positive impact on overall production. These results highlight the importance of regularly monitoring and optimizing ESPs to ensure maximum efficiency and productivity in oil production operations.

Table 10: Shows Final Optimization Results for the Well E-05

Well No	Reservoir Pressure	Operation Frequency	Number of stages
E.05	3100 psi	60 HZ	225

Table 11: Shows Final Optimization Results for the Well E-05

Well No	Current Production	Pump Depth	Optimum Production
E.05	916 STB/D	5000 ft	1008
			STB/D

We have completed the selection process for the ESP model that improves production. After careful consideration of all available options, we have selected the TYEP model based on the required power of 28.35hp. This model has the lowest power requirement compared to other models and provides the best pump and motor efficiency with 63% and 83%, respectively. The expected operation oil rate is approximately 1500 STB/day. The pump type selected is the CENTURION - P17 4 inches, while the motor type is CENTRLIFT 450 30HP. The cable type chosen for this setup is Aluminum 50 A. Our selection process was based on thorough analysis and consideration of all available options, ensuring that we have made the best decision for our needs.

CONCLUSION

We present the results of our study on ESP design optimization and sensitivity analysis for oil well (E-05) using Prosper software.

Our study highlights the importance of conducting sensitivity analyses during the design phase of ESP systems to ensure optimal performance and efficiency. We believe that our results will be useful to engineers and researchers working in the field of oil well production optimization.

We have completed our study and have arrived at the following conclusion:

1. The frequency of the pump is directly related to its flow rate. A higher frequency results in a faster flow rate, while a lower frequency may result in a slower flow rate. However, it is important to note that a higher frequency also increases energy consumption and can lead to

ISBN 978-9959-9703-2-9

premature wear and tear on the pump. On the other hand, a lower frequency can reduce energy consumption.

2. We have addressed the issue of high water cut and their negative impact on both oil production and electric submersible pump (ESP) performance. High water cut can lead to decreased oil production and increased wear and tear on ESPs. To improve overall production efficiency, it is necessary to reduce the water cut.

3. In our observation that the number of stages in an ESP system is heavily reliant on the pump and pump depth. Increasing the number of stages has been shown to have a positive impact on the efficiency of the ESP system.

4. The benefits of setting the Electric Submersible Pump (ESP) close to the producing zone in oil wells. By doing so, we can significantly reduce the pressure drop between the formation and the pump, resulting in higher flow rates. This is due to the fact that the closer proximity of the ESP to the producing zone allows for better control of the fluid level in the wellbore.

5. Our results indicate that an increase in reservoir pressure leads to a corresponding increase in the productivity index, which in turn enhances oil production. This highlights the critical importance of monitoring and supporting the reservoir pressure to ensure optimal production performance. Our observations suggest that maintaining optimal reservoir pressure is crucial for the sustainable production of oil.

6. By studying each parameter individually, we can gain a deeper understanding of its influence on ESP performance. This analysis is crucial for optimizing the performance of ESPs and improving their efficiency. Through our research, we aim to contribute to the advancement of this important technology and its applications in various industries.

7. One of the main advantages of ESP Design Optimization is its ability to optimize designs with multiple objectives. This is achieved by using a multi-objective optimization that can simultaneously optimize multiple objectives, such as minimizing cost of maintenance, increasing efficiency and maximizing performance. However, there are also limitations to ESP Design Optimization. One limitation is the need for accurate models of the system being optimized. If the model is inaccurate, the optimization may produce suboptimal results or even fail to converge. Another limitation is the computational cost of the optimization process. ESP Design Optimization can be computationally expensive, especially when optimizing complex systems with many design variables.

8. Sensitivity Analysis is another useful tool that can be useful in identifying critical parameters that have a significant impact on the performance of the system. Sensitivity Analysis can also be used to identify areas where further research and development is needed. However, like ESP Design Optimization, Sensitivity Analysis also has limitations. One limitation is the assumption of linearity. Sensitivity Analysis assumes that the relationship

 ISBN 978-9959-9703-2-9

between the input parameters and the output of the system is linear. This may not be the case for all systems, and non-linear relationships may be missed. Another

RECOMMENDATIONS

1. As academic researchers, it is important to continue to study and analyze the effects of various factors on production performance, in order to improve the efficiency and effectiveness of oil production.
2. Further research is needed to fully understand the complex interactions between wellhead pressure and production performance using ESP.
3. Further research is needed in this area to fully understand the underlying mechanisms and optimize the use of ESP in oil and gas production.
4. Our research provides a foundation for future studies in this area. We believe that our results will be valuable to those in the oil and gas industry who are looking to improve their production processes. Overall, our study provides important insights into the factors that impact oil and gas production efficiency and lays the groundwork for future research in this area.
5. We recommend implementing regular monitoring and support measures to maintain the reservoir pressure at optimal levels. By doing so, we can ensure the continued success of oil production operations.
6. Further research is needed to better understand the factors that affect ESP performance, such as wellbore conditions, fluid properties, and pump design.

REFERENCES

[1].Nguyen T, Artificial Lift Methods: Design, Practices, and Applications. 1st (Edn), Springer Nature, Germany, (2020), pp-347.

[2]. Nguyen H, Del Mundo F, Improving Artificial Lift Design Through Dynamic Simulation, SPE North America Artificial Lift Conference and Exhibition, Society of Petroleum Engineering, Texas, USA, (2016) .

[3].Alemi M, Jalalifar H, Kamali G, Kalbasi M, (2010) A prediction to the best artificial lift method selection based on TOPSIS model. Journal of Petroleum and Gas Engineering Vol. 1(1), pp 009-015.

[4].Brown K E. Technology of artificial lift methods. Volume 1. Inflow performance, multiphase flow in pipes, the flowing well. United States: N. P., 1977.Web.

[5]. O.J. Romero, "Subsea Electrical Submersible Pump Significance in Petroleum Offshore Production", Universidade Federal do Espírito Santo, March 2013.

[6]. Abdelhady A, Gomaa S*, Ramzi H, Hisham H, Galal A and Abdelfattah A, (2020), Electrical Submersible Pump Design in Vertical Oil Wells, Petroleum & Petrochemical Engineering Journal, ISSN: 2578-4846, Volume 4 Issue 5, MEDWIN PUBLISHERS.

[7].Bader Abdullah Alqahtani; et al. Electric Submersible Pump Setting Depth

 ISBN 978-9959-9703-2-9

Optimization- A Field Case Study, Paper presented at the SPE Middle East Artificial Lift Conference and Exhibition, Manama, Bahrain, October 2022. https://doi.org/10.2118/206934-MS

[8]. A. Suat Bagci, SPE, Murat Kece, SPE, ESP Performances for Gas-Lifted High Water Cut Wells, SPE Annual Technical Conference and Exhibition, Florence, Italy, 19–22 September 2010.

[9]. Hamzah Amer Abdulameer, et al, (2020), Production Optimization for Natural Flow and ESP Well A Case Study on Well NS-5 Mishrif Formation-Nasriya Oil Field, ISSN: 2710-1096. Journal of Petroleum Research and Studies. VOL. 10 NO. 2: ISSUE 27. DOI: https://doi.org/10.52716/jprs.v10i2.342

[10]. https://www.petex.com/products/ipm-suite/prosper/

[11]. Kermit E. Brown, "The Technology of Artificial Lift Methods- Volume 2b"1980

[12]. Brown, K.E. et al.: "The Technology of Artificial Lift Methods", "Production Optimization of Oil and Gas Wells by Nodal Systems Analysis," Penn Well Publishing Co., Tulsa, OK(1984), Vol. 4. (2)
[13]. T. Ahmed, Reservoir engineering handbook (Gulf Professional Publishing, (2006), (3).

تحسين تصميم المضخة الغاطسة (ESP) وتحليل الحساسية للبئر النفطي (E-05) باستخدام برنامج Prosper

النوري الحداد ، محمد قروم ، حسام عيسى
جامعة بني وليد – كلية الهندسة – قسم هندسة النفط والغاز

الملخص

غالبًا ما يكون ضغط المكمن النفطي طبيعي وكافي لرفع السوائل إلى السطح. ومع ذلك ، عند حدوث زيادة مفرطة في إنتاج الماء والغاز ، قد لا يكون ضغط المكمن النفطي كافياً. في مثل هذه الحالات ، يلزم استخدام احدى طرق الرفع الاصطناعي لرفع السوائل إلى السطح. الهدف من هذه الدراسة هو تحسين كفاءة نظام المضخة الغاطسة (ESP) وتحديد المتغيرات الحرجة التي تؤثر على اداء المضخة في البئر النفطي E.05 باستخدام برنامج Prosper. تم الحصول على النتائج وتحليلها لتحديد التصميم الأمثل للبئر. في هذه الورقة ، ناقشنا نموذج للمضخة الكهربائية الغاطسة (ESP) وتأثيره على الإنتاجية. تم تصميم نموذج ESP لتحسين المتغيرات مثل ضغط الخزان وعمق المضخة وتردد التشغيل وعدد المراحل للمضخة. على وجه التحديد ، يوصي النموذج بضغط خزان يبلغ 3100 رطل لكل بوصة مربعة ، وعمق المضخة 5000 قدم ، وتردد التشغيل 60 هرتز ، وعدد المراحل 225 مرحلة. من خلال تنفيذ هذه المتغيرات ، ثبت أن نموذج المضخة الكهربائية الغاطسة (ESP) يحسن الإنتاجية بشكل كبير. يتميز هذا النموذج بأفضل مضخة وكفاءة للمحرك ، مما يجعله خيارًا موثوقًا به لتحسين الإنتاج. زاد معدل تدفق الزيت للبئر من 916 STB / D إلى 1008 STB / D ، مما يشير إلى التصميم الحالي ناجح للبئر. هناك حاجة إلى مزيد من البحث لفهم العوامل التي تؤثر على أداء المضخة الكهربائية الغاطسة بشكل أفضل ، مثل ظروف تجويف البئر ، وخصائص السوائل ، وتصميم المضخة.

الكلمات المفتاحية: الحقل 103أي ، المضخة الكهربائية الغاطسة (ESP) ، تحسين ، برنامج بروسبر ، تحليل الحساسية

ISBN 978-9959-9703-2-9

المؤتمر الدولي الثاني للعلوم والهندسة
2nd International Conference on Science and Engineering
ICSE 2023
Faculty of Engineering - University of Bani Waleed
Bani Waleed, Libya

Paper Code: ICSE-017

A CASE STUDY OF SELECTION OF CORROSION INHIBITORS FOR WATER SOURCE OF WAHA FIELD

SALIM .O. MIFTAH
Petroleum Engineering Department , Engineering college/University Of BANI-WALEED, LIBYA
*Crosspnding author: salem_agal@yahoo.com

Abstract: WAHA oil field is an important oilfield in Libya is operated by WAHA company . In this oil field water is being used for reinjection in reservoir to increase the pressure in the reservoir and hence increase production of crude oil. This water is produced from the water source wells drilled in oil field. Injection water contains dissolved carbon dioxide and hydrogen sulphide and hence it has corrosive characteristic .Moreover the temperature of water is high .A study has been performed to select suitable corrosion inhibitor for inhibition of corrosion. This paper presents the results of corrosion inhibition studies of water source wells in WAHA field. The concentration of selected corrosion inhibitors has been optimized for economical consideration.

Keywords: (Corrosion inhibitor, water source, optimization)

Introduction

WAHA oil field is operated by WAHA company and it is the important oil fields in Libya . The unique nature of this oil field is that has no liquid effluents. Whatever water is produced it is again injected to reservoir together with some other water for enhanced oil recovery . WAHA oilfield has about twenty water source wells at W-59 and nine water source wells at N.DEFA . These wells are producing water about 85000 bbl/day . The geological formation of all water source wells are either TAZERBO formation or SARIR formation . The temperature of water from the well of TAZERBO formation was measured as 72.7 C while the temperature of the water fro well of SARIR formation was 98.9 C . The typical analysis of both type of water are given in Table 1 and 2 . Both type of water acid gases water has acidity and becomes corrosive. The acid corrosion in water flood is controlled by addition of chemicals corrosion inhibitors.

A wide variety of inhibitor formations [1,4] is available for corrosion control in water flood and brine disposal system . However most of these inhibitors are produced from only a few types of starting materials. Fatty acid and rosin acids some form of basic nitrogen precursor and ethylene oxide are active ingredient sources .

After transformation into final product the resulting ingredients are usually dissolved in alcohol (often isopropyl alcohol) water solution.

Table 1 : Typical water analysis from a well of

 ISBN 978-9959-9703-2-9

TAZERBO formation:

Property	Units	Result
Cations		
Calcium (Ca^{+2})	Mg/L	50.0
Magnesium (Mg^{+2})	Mg/L	13.4
Sodium (Na^{+})	Mg/L	1538.8
Anions		
Chloride (Cl^{-})	Mg/L	2300.0
Sulphate (SO_4^{-2})	Mg/L	0.0
Carbonate (CO_3^{-2})	Mg/L	0.0
Bicarbonate (HCO_3^{-})	Mg/L	457.5
Miscellaneous		
Total hardness	Mg/L as $CaCO_3$	180
Calcium hardness	Mg/L as $CaCO_3$	125
Magnesium hardness	Mg/L as $CaCO_3$	55
Phenolphthalein alkalinity (P Alkalinty)	Mg/L as $CaCO_3$	0
Methyl orange alkalinity (M alkalinity)	Mg/L as $CaCO_3$	375
Ph at 25 C°		6.59
Total dissolved	Mg/L	4430
Conductivity at 25 C°	mhos/cmμ	7120
Specific gravity		1.0031
Dissolved Gases (on site)		
Carbon dioxide (CO_2)	ppm	108
Hydrogen sulphide (H_2S)	ppm	4
Oxygen (O_2)	ppm	0

Table 2 : Typical water analysis from well of SARIR

Property	Units	Result
Cations		
Calcium (Ca^{+2})	Mg/L	330.0
Magnesium (Mg^{+2})	Mg/L	394.9
Sodium (Na^{+})	Mg/L	3585.5
Anions		
Chloride (Cl^{-})	Mg/L	6800.0
Sulphate (SO_4^{-2})	Mg/L	620.0
Carbonate (CO_3^{-2})	Mg/L	0.0
Bicarbonate (HCO_3^{-})	Mg/L	305
Miscellaneous		
Total hardness	Mg/L as $CaCO_3$	2450
Calcium hardness	Mg/L as $CaCO_3$	825
Magnesium hardness	Mg/L as $CaCO_3$	16.25
Phenolphthalein alkalinity (P Alkalinty)	Mg/L as $CaCO_3$	0.0
Methyl orange alkalinity (M alkalinity)	Mg/L as $CaCO_3$	250
Ph at 25 C°		6.13
Total dissolved	Mg/L	12215
Conductivity at 25 C°	mhos/cmμ	14690.0
Specific gravity		1.0085
Dissolved Gases (on site)		

ISBN 978-9959-9703-2-9

Carbon dioxide (CO_2)	ppm	96.0
Hydrogen sulphide (H_2S)	ppm	5.5
Oxygen (O_2)	ppm	0

2.CORROSION INHIBITORS STUDIED

In this study tow commercial inhibitors are studied . We have given identification number S1 and S2 for the selected corrosion inhibitors . The description of these corrosion inhibitors are follows:

CORROSION INHIBITOR (S1) :
It is a commercial product . This is a water soluble filming amine corrosion inhibitor containing (morpholine basis and dimer acid) as active materials formulated to give good film persistency in fresh water , sea water and heave brine systems.
CORROSION INHIBITOR (S2):
This is also a commercial product . It is water soluble filming amine corrosion inhibitor it has the similar blend as S1 except does not contain dimer acid.

3.CORROSION INHIBITORS TESTING METHOD

There are different techniques for testing of corrosion inhibitors such as: [2,3]

. Weight Loss Specimens.

. Electrical Resistance Probes.

. Polarization.

. Galvanic Corrosion Probes.

In present study Linear Polarization Resistance Technique (LPR) has been used. This method of evaluating corrosion rates employs galvanic cell the test water being the electrolyte and the two carbon steel rods providing the electrodes. In the (Result) mode the two ranges the electrodes are initially coupled for a period of 14 seconds .This is to allow the coupling polarization current to fall to a small static value . The cell is then polarized to +20 mV for about 15 seconds towards the of this time a reading of the current flowing is taken. The cell potential is then reversed to – 20 mV for about 15 seconds and another reading of the current flow is taken at the end of time . An average of the two current reading is then calculated . This current is then processed by the meters electronics an displayed as a corrosion rate in Mils Per Year (MPY) . Experimental conditions used are summarized in table 3

Test Temperature	70 C°
Water Phase	Water from water source wells
Gas Phase	CO_2 saturated
Coupon Material	1018 M/S

Both the corrosion inhibitors (S1 and S2) have been tested at different concentrations ranging 0 to 50 ppm . The results are summarized in Table 4-5 and Fig 1-2.

Table 4: Corrosion inhibition of water source wells(TAZERBO) using S1 and S2 corrosion inhibitors

Dose Rate (ppm)	Percent Corrosion Inhibition	
	S1	S2
0	0.0	0.0
5	93.03	88.85
10	97.01	92.87
25	98.63	96.31
50	99.20	97.62

Table 5: Corrosion inhibition of water source wells(SARIR) using S1 and S2 corrosion inhibitors

Dose Rate (ppm)	Percent Corrosion Inhibition	
	S1	S2

ISBN 978-9959-9703-2-9

0	0.0	0.0
5	88.89	84.98
10	92.91	90.86
25	95.56	93.38
50	97.88	96.01

Fig.1.Corrosion Inhibition in Water Source Well TAZERBO formation

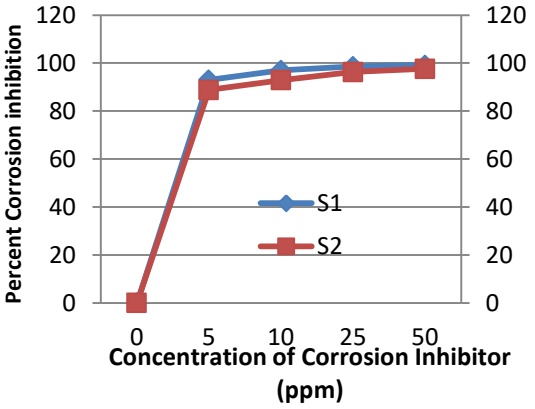

Fig .2. Corrosion Inhibition in Water Source Well SARIR formation

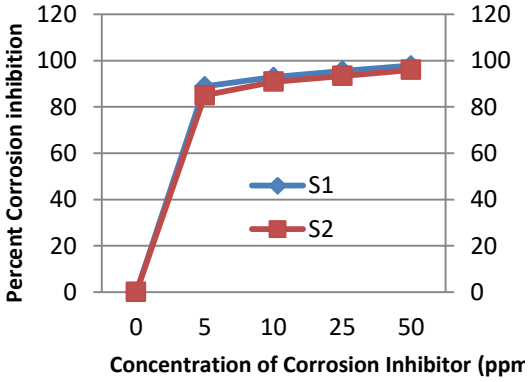

- In from the results it is clear that both corrosion inhibitors S1 and S2 showed corrosion inhibition for waters from water source wells of Waha oilfield.
- Bothe corrosion inhibitor S1 performed better compared at the same concentrations of corrosion inhibitor S2 .
- This is because corrosion inhibitor S1 contains dimer acids but the corrosion inhibitor S2 does not contain dimer acids and other components the same.

CONCLUSION:

REFERENCES:

1.C . C. Nahtan (1962) , Correlation of oil soluble water dispersable corrosion inhibitors in oilfield fluids, Corrosion 18 , 282 .
2. R.J. Meakins (1963) , Alkyl quaternary ammonium compounds as inhibitors of acid corrosion of steel , J. Appl, Chem.,13, 339.
3. N.Hackerman . R. M. Hurd and R.R annand (1962). Some structural effects of organic N- containing compounds on corrosion inhibition , Corrossion 18, 37 t.
4. P.A . Wolf and F. J. Bobalek (1970). Synergistic amine mixtures for inhibition of (acid) corrosion in aqueous systems , US Patent 3,373, 170.

 ISBN 978-9959-9703-2-9

المؤتمر الدولي الثاني للعلوم والهندسة
2nd International Conference on Science and Engineering
ICSE 2023
Faculty of Engineering - University of Bani Waleed
Bani Waleed, Libya

Paper Code: ICSE-001

DEVELOPMENT OF AN ONLINE EXAMINATION SYSTEM CASE STUDY: CYPRUS INTERNATIONAL UNIVERSITY

Mabrouka Algherinai [a]
[a] Information Technology, The Higher Institute of Sciences and Technology, Aljofra-sokana, Libya
*Crosspnding author: kokyrbab1@gmail.com

Abstract: The study set out to develop an online examination system. System design made use of entity relation diagrams (ERDs), case diagrams, site diagrams and object oriented (class) design to model system processes and entities. MYSQL was used to implement the server based database, md5 for encryption. PHP (Hypertext pre-processor) web scripting language was used to enforce interaction with the database. The online examination is an Internet based questionnaire, with questions compiled from different libraries. Its mission is to offer a quick, easy and safe way for students to take the exam. The resulting system was tested and validated. It was able to meet the required specifications and address some limitations of the previous system such as data confidentiality and security.

Keywords: System design, ERD, MYSQL, HTML, Specifications

Introduction

Test or an examination is an assessment, administered on paper or on a computer, intended to measure the test-takers' knowledge, skills, or aptitudes. Tests are often used in education, professional certification, counselling, psychology, the military and many other fields. The goal of testing is a measurement that is called a test score, which is a summary of the evidence contained in an examinee's response to the items of a test that are related to the construct or constructs being measured [1].

New technologies have been widely used in higher education to deliver curriculum content, [2].

Statement of the Problem

1) Current pen-and-paper evaluation systems are very time consuming; students' scripts must be marked manually.
2) It is difficult to analyze examinations manually.
3) When many candidates sit for an examination, more invigilators are required, which increases cost.
4) Results are not precise because calculations and evaluations are subject to human error.

 ISBN 978-9959-9703-2-9

5) Result processing takes more time as it is done manually.
6) The likelihood of an examination paper being leaked is greater in the current system compared to the proposed system.

Aim and Objectives

The main aim of the proposed project is to develop an effective online examination system for a university.

The objectives of the research are:

1. To survey the latest computer-based examination management systems.

To develop a software application for an online examination system.

2. To implement the system using active server pages (ASP).

Significance and Contributions of the System

With the proposed system the following contributions would be made to teaching professionals and educational institutions:

1) It is possible to monitor how much progress a student has made.
2) The progress of many students can be judged immediately.
3) Problematic topics that need revision can easily be identified.
4) A large number of students can assessed fairly and objectively.
5) Opportunities for cheating are reduced.
6) Marking load of teachers is reduced: an assessment for a semester can be made based on students' output over a 2 or 3 hour period.
7) Examinations are more reliable and cheaper to administer.

Scope of the System

This project would be very useful for a university course where regular evaluation of students is required. Further it can also be useful for anyone who requires feedback based on objective type responses, in the corporate world as well as in educational institutions. The project can be used anywhere, as it is a web based application; user location does not matter. The examiner or invigilator does not have to be present when candidates take the examination. The implementation will be based on the three areas: Computer architecture, Performance evaluation Network and Java.

Literature Review

Overview

An electronic examination (e-Exam) system is an examination conducted using the Internet or an intranet. It reduces much of workload involved in examining, training, grading and reviewing. The set of questions commonly used in the e-examination system are multiple choice objective tests and quizzes that can be formally and easily evaluated online [1].

Many institutions are re-evaluating traditional

 ISBN 978-9959-9703-2-9

methods and are providing pedagogical materials through the Internet. Several studies have been carried out on distance education, which encompasses web classrooms and web-based online examinations [3]. The development of web-based testing and assessment is an important and growing area of application of web technology [6].

Electronic Examination Systems

An Electronic Examination System (e-Exam) is a cost-effective and popular means of mass evaluation system [4]. Computer based testing can achieve significant cost-savings due to the speed at which results are analysed and presented. The e-Exam is web based system that provides the facility to conduct examinations and view the results of these exams online [8]. Only two categories of people participate in this system: one is the user and the other is the administrator. With the online examination and result processing system users can create and administer exams, tests, quizzes in a secure client/server environment. Candidates will be thoroughly and efficiently evaluated through a fully automated system that not only saves lot of time but also gives fast results [9].

Institutional learning management system (LMS) such as Blackboard is used in many cases for online assessment. Web CT, or an in-house product [10]. There are several advantages that institutions and also learners get from online assessment. These include:

1) Time analysis of responses to the question level to better discriminate between candidates [11].
2) Question banks and randomization of questions and response orders to reduce cheating.
3) Automated analysis of results from entire candidate cohorts.
4) Immediate feedback can be given.

However, there are also some difficulties associated with various forms of online assessment [11]. Online assessment may not be effective for evaluating creativity, problem solving ability, critical thinking, reflection, or authentic learning; collectively the characteristics of deep and effective learning. The delivery technology itself creates problems of inter-candidate interaction and is prone to technical malfunctions which can affect many students simultaneously. Should the whole network fail, the examination needs to be rescheduled.

Justification for Online Examinations

Nevertheless, E-exams can be justified in a number of ways. It can help avoid the stresses associated with current paper-based systems; it can assess valuable life skills; it can be better for users – for example by providing on-demand tests with immediate feedback, and perhaps

 ISBN 978-9959-9703-2-9

diagnostic feedback, and more accurate results via adaptive testing; it can help improve the technical quality of tests by improving the reliability of scoring[12].

A detailed historical background of online education was presented in by Gaytan and McEwen [15], which discussed its potentials and limitations that could lead to the advancement of the scholarship of teaching and learning.

They stressed the need for online instructors to understand the way online education has evolved over the years from previous conceptions of education and the wide array of implications and assumptions involved in the delivery of online education. They also presented some recommendations for the advancement of online education.

Existing System at the Cyprus International University (ciu)

Until recently, examinations in Cyprus followed traditional pen-and-paper practices: students were given question papers and wrote their answers in answer booklets. The whole process of assigning tests and evaluating the scores after the test was done manually. Processing the test paper, i.e. checking and distributing respective scores took a long time. The existing system at CIU is the product of a mini-project entitled "Online Examination System" carried out by Niraj Lola [13], a 5th semester MCA student at the National Institute of Technology, Calicut in November 2004. He designed an Online Examination system for conducting multiple choice online tests. This system only has three sections which are: English language, Mathematics, and Chemistry, with a time limit for each section. In this system examinees take the exam and are able to view their results immediately after each section. This system also allows the examinee to know both correct and incorrect answers at the end of each section. The system was developed using Adobe Dreamweaver (CS4), MySQL (Database), Apache Tomcat Server (Server). Its implementation involved two modules; one for the Administrator and the second for the Examinee.

Difficulties with the Existing System

A review of the system identified some difficulties.

1) There is no mechanism to control the number of times a candidate/student can take the exam.
2) Each candidate has only twenty minutes to answer twenty questions in each section. However, a student who is very slow in answering questions might waste the twenty minutes on only one question.
3) Only the Administrator can register each candidate/student for the examination.

In a situation where there are thousands of students to sit for the test, it is very difficult for the Administrator to register and assign an

 ISBN 978-9959-9703-2-9

Exam ID to each student, sequentially.

In the university, the first problem encountered in organizing a test is that reams of hard copied documents are still generated. This raises the age-old discussion of keeping information in the form of databases versus keeping the same on sheets of paper. Information's that are being kept in hard-copied documents leads to the following problems:

1. Lack of space: Because academic assessments have legal significance, the documents generated must be carefully stored.
2. Filing poses a problem; Due its tediousness
3. Filtering is difficult: It is hard to filter relevant documents from irrelevant ones when the number involved is very large [16]. Reviewing becomes time consuming: The entire process is carried out manually at the centres and all the records are maintained on the papers. So the maintenance of records is very difficult in the departments, and furthermore, it is very difficult to check the records.

The existing system is paper based, time consuming, inflexible and labor intensive.

System Development

Introduction

This section explains how the new proposed system will be carried out and implemented to ensure the system will work smoothly and effectively.

Need For the New (proposed) System

All the limitations mentioned in the existing system will be addressed by the proposed system. This will be achieved through the following measures in the proposed system:

1. Each candidate will be able to take the exam only once. If the candidate attempts to log in a second time to take the exam, a web page will be displayed with a message informing the candidate he can only take the exam one time and directing him back to the home page. This improvement will control the number of times a candidate can sit for the test.
2. Each question in each section will be assigned one minute. This is to help the candidate to be time conscious and manage his time in answering questions. This should increase the number of questions answered by the candidate.
3. The Examination ID for each candidate is generated automatically and stored in the database after the candidate has successfully registered for the exam. Candidates can register by themselves, without the help of the Administrator. In

 ISBN 978-9959-9703-2-9

this way, time will not be wasted on the registration process.

4. In the existing system the site is limited to only three sections of questions which are Performance Evaluation Network, Computer Architecture, and Java. In the proposed system there will be more than three sections and the answer to each question will be displayed before the student attempts the next question. The grade of the exam will be displayed when the administrator clicks on the grade button after the student has answered the question on that particular section.

To solve these problems, a computerized system is required. A web based application will provide a flexible working environment that will be easy to use and will reduce the time for report generation and other paper work. This online examination system will also provide an efficient computerized solution for the student that wants to sit for the test. The system will be easy to administer, reliable and cost effective.

The main purpose of the proposed system, therefore, is to provide a comprehensive computerized system that can capture, collate and analyze the data from these tests. The new system is needed to solve the limitations discovered in the previous system.

System Analysis & Design

System analysis is a problem-solving technique that decomposes a system into its component pieces for the purpose of studying how well those component parts work and interact to accomplish their purpose [16]. The design of the online examination and result processing system will be broken down into two key facets with the following identified functions:

A. System Analysis

1) Preliminary investigation
2) Problem analysis
3) Requirement analysis

B. System Design

1) Design
2) Overview of the new system
3) Construction
4) Implementation

C. Preliminary Investigation

The preliminary investigation must define the scope of the project and the perceived problems, opportunities, and directives. This phase is not intended to take much time [17]. The preliminary investigation typically includes the following tasks:

1) Definition of the study approach (interview or observation)
2) Development of problem statement

D. Development of Problem Statement

The following information was obtained from a study of the existing system.

a) Information Data

ISBN 978-9959-9703-2-9

Input

1) Wastage of resources
2) Too much paper work
3) Information may not be accurate
4) Delay in viewing scores

Output

1) Candidates not answering examination questions in time allotted
2) Limited to only three subject areas
3) Too much paper work generated

Stored data

1) Data organization is very poor (too much paper work)
2) Stored data not easily retrieved
3) Result/scores not immediately accessible by students
4) Year-to-year comparisons difficult

Efficiency

1) Do not improve student's efficiency
2) Do not improve quality of CIU test system

Control

1) Data or information not adequately secure
2) Chance of question paper being leaked before the examination day
3) Crimes (e.g. alterations can be made to data).

Finances

1. Cost of purchasing papers and printing materials are high.

The number of staff required is large.

Problem Analysis

The goal of problem analysis is to study and understand the problem domain well enough to thoroughly analyze its problems, opportunities and constraints.

Requirement Analysis

The requirement analysis defines the requirements for the proposed system. The key here is what, not how. The requirement analysis phase answers the question, what do the users (candidates and the administrator) need and want from the new system. Design of the logical model of the E-exam (the proposed system) will be carried out by drawing the Case Diagram, and the State Diagram.

Characteristics of the Proposed System

The Online Examination System created for taking CIU exam has following features:

1) In comparison to the existing system, the proposed system will be less time consuming and more efficient.
2) The proposed system will provide instant feedback to students
3) Analysis at many levels will be very easy because it is automated.
4) Results will be precise and accurate, and will be available within a very short span of time because calculations and evaluations are done by the simulator itself.
5) The proposed system is very secure with no chances of leakage of the question paper

ISBN 978-9959-9703-2-9

because it is dependent on only one person, the administrator.

6) Each candidate can sit for the examination only one time.
7) The logs of registered candidates and their marks are stored and can be backed up for future use.

What are the user's demonstrable needs?

The user needs a system which will remove all the problems mentioned earlier. The user wants a web-based system which will reduce the bulk of paperwork, provide ease of work, flexibility, fast record finding, ability to modify, add, and remove items, and generate reports.

How can the problem be redefined?

Our proposed conception of the system, taking into account the problems of the existing system, is set out on paper. We matched the problems and needs of the existing system and requirements to the structure of the proposed system. We further updated the layout on the basis of redefined the problems.

In the feasibility study phase we had undergone through various steps, which are described as under.

How feasible is the system proposed?

This was analyzed by comparing the following factors with both the existing systems and proposed system.

Effort

Compared to the existing system, the proposed system will provide a better working environment in which there will be ease of work and the effort required will be comparatively less than the existing system.

Time

The time required generating a report or for doing any other work will be comparatively much less than in the existing system. Record finding and updating will take less time than the existing system.

Labor

In the existing system, the number of staff required for completing the work is large; the new system will require a smaller number of staff.

System Design

This stage involves creating the structure of modules that best solves the problems specified above; that is, the development of specifications or a 'blueprint' of how the system will work.

Design Approach

In the software development process, the system design phase involves decomposing a software system into modules and defining the relationship among these constituent modules. Usually, combinations of two or more design approaches are employed in the execution of a project [18]. In the case of the examination and result processing system, the following design approaches were employed:

Modern Structure (site) Design

This is a process-oriented technique for breaking up a large program into a hierarchy

ISBN 978-9959-9703-2-9

of modules that result in a computer program that is easier to implement and maintain (change) [19]. It is considered a process-oriented technique because its emphasis is on the process building blocks in the E-exam.

Object-Oriented Design

The first thing is to identify the object that represents actual data with its domain. Once the object's behaviors and responsibilities have been determined, the next step is to create a detailed model of how the objects will interact with each other [20].

System Implementation

Introduction

If the proposed system is to be implemented holistically, it is a departure from the old ways of writing exams in CIU. Introducing such a system has to be done with care. After the completion of the coding processes, it is necessary to perform a wide range of activities before the E-exam system can be operational.

Fig. 1: Activity diagram for the system

Such activities include system testing, system implementation, system maintenance, functional requirements, specification report for the system, software system attributes.

Overview of the System

The online examination and result processing system created for taking the online WAEC test a different sequence of activities for candidates and for the administrator. The following are stages for candidates:

1) Login with username and password / Register
2) New User Registration
3) Edit Profile/View Result

 ISBN 978-9959-9703-2-9

4) Select Subject
5) Examination
6) View my score
7) Log out

The system has the following stages for the administrator:

1) Login

View user (edit, delete and reset exam for candidate)

2) Edit Subjects
3) View All Subjects
4) Add Questions
5) View all scores
6) Log out

Modular Design

A software system is always divided into several sub systems that facilitates its development. A software system that is structured into several subsystems is easier to develop and test. The different subsystems are known as modules and the process of dividing an entire system into subsystems is known as modularization, or decomposition.

The different modules are.

1) Login Module
2) Registration module
3) Question paper creation Module
4) Examination Module
5) Student Module
6) Administrator Module

Design Stages for Candidates

Login/And New User (registration for candidates).

There is a quality login window because this is more secure than other login forms: in a normal login window, multiple logins are available so that more than one person can access the test with their individual login. In this project, each user can login with his/her username and his/her password to enter the site. Hence it is more secure and reliable than the previously used online exam simulator.

Registration

This is the web page where the registration process will be done by each candidate before sitting for the exam. The registration page has the following items that each candidate must fill in correctly: Candidate's Email address, User Name, Password. Retype Password, Contact number, Address, City, pin code. After the candidate has successfully registered, he/she will have to login with a valid username and password.

Change Password

Each candidate has the opportunity to change his/her password after login is successful as often as he/she wishes. The effect of this change will also be updated in the database.

Edit Profile/View Result

At this initial stage the candidate cannot view a result but he can edit his profile and change

 ISBN 978-9959-9703-2-9

his password if he wants to

Subject Selection

The test page is the most important page in this project. From the given choices, the candidate can select his subject (like Performance Evaluation Network, Java) to take the exam.

Examination

After the candidate has selected a subject, the next web page will display the questions. Only one multi-choice question will be displayed at a time. A timer is set for each multi-choice question. If the candidate fails to select an answer to the question from the options given within one minute, then the next question will be displayed automatically. This improvement in the system will help the candidates to be time conscious and he/she will be able to answer more questions. Poor time management was one of the limitations in the existing system.

View My Scores

After the candidate has answered the last question, he/she will be instructed to click on the grade button which will display the student's grade. The student will be instructed to print out this page.

Log Out For Candidate

Each candidate will be advised to log out after finishing the exam to exit the examination site.

Design Stages for the Administrator

Login

The administrator has a unique User Name and Password which he/she can use to login to the site and perform some administrative task. If the wrong username and password is entered by the administrator, he/she will not be able to login.

View Users

Only the administrator has the privilege to view all users (candidates). The administrator has the ability to manage users, manage subjects, manage results, prepare questions and reset exams for any candidate if the need arises. All these tasks can be performed on the web page (front end). There is no need to manipulate the database (back end).

Edit Subjects

The administrator is able to add subjects, if and when the need arises. The effect of this change will be updated automatically in the database.

View Subjects

The administrators can view all subjects and decide to edit or add more

View All Scores

Only the administrator has the access to view the scores of all candidates. The scores will be displayed on a single web page. The date each candidate sat for the exam will be displayed along with each candidate's names and score.

Log Out Admin

It is advisable for the administrator to log out of the site as soon as he/she has finished the

 ISBN 978-9959-9703-2-9

task to prevent other unauthorized users from manipulating the site.

Database Design

Data storage is a critical component of this system. All information systems create, read, update and delete data, which are stored in a database. The most popular from a database used is the relational database. For the purpose of this project, Microsoft Access version will be used for data storage. The name of the database is "configure _test".

Home Page:

This is the first page to be viewed by the examinee (usually a student). It is the page introducing the examinee to the task ahead.

Login Page:

This is the page where examinees who are registered users log in their username and password. Successful login leads the examinee to the next page. If the examinee is not yet a registered user, he/she clicks on the click here link below the login link, and will be directed to the Registration Page.

Registration Page:

This is where the unregistered user becomes a registered user. It requests the candidate to provide: his/her first name, last name, e-mail address, user name, and password, re-type password, and phone number. After successful registration of this information, the examinee will be redirected to the Login page and asked to log in with a valid username and password.

Select A Subject Page:

This is the next page after the Login page. It asks the candidate to select a subject from the list of three subjects in the dropdown menu.

Question Interface Page:

After the candidate has selected a subject, the questions will be displayed on the next web page. Only one multi-choice question will be displayed at a time. The Next Question icon on this page when clicked automatically brings up the next question from the database. A timer is set for each multi-choice question. If the candidate fails to select an answer to the question from the options given within one minute, the next question will be displayed automatically. The series of questions that is displayed to a candidate is drawn randomly from the database. It has a score reader which records the number of correct answers in the examination but does not record the incorrect answers in the examination.

Result Interface Page:

After candidates have answered the last question, they will be automatically taken to this page, where they will see their scores.

System Testing

Testing is often seen as a means of establishing that a program is error-free and that it performs as planned. However, it is almost impossible to test a program so

 ISBN 978-9959-9703-2-9

thoroughly that it can be claimed to be free of errors. Unit testing is carried out by testing all the events and modules that have been coded and sub tested for a program as an integrated unit.

Fig. 2: Admin dashboard page

Fig.3: Login page for Admin

Fig. 4: Login page for student

ISBN 978-9959-9703-2-9

Fig. 5: Registration Page for student

The types of tests carried out fall into the following categories:

Test that there are no errors in syntax and language in the program code.

Fig. 6: Student dashboard page

1) Test that data which are valid are entered into the system.
2) Test each module with sample data to determine actions and reactions in a real life situation.
3) Test the performance of the system, such as the speed of response ties and handling of large volumes of data.
4) Test that the examination score is automatically generated immediately after exams.
5) Test that each candidate can answer the test only one time.
6) Test that the administrator can view all the student data and scores.
7) Test that the administrator can edit, delete, and reset exams for candidates if the need arises.

Functional Requirements

For the proposed system to be implemented properly the following hardware and software requirements must be available.

Hardware Requirements

Network: a local area network (LAN) is required to be constructed in the university. If the application is to be run at more than one exam center, a wide area network link between the LANs of the university's exam centres is needed. The LAN is constructed using wireless technology. The wireless LAN requires wireless network cards for each system.

 ISBN 978-9959-9703-2-9

1) *Client system:* Pentium IV, 2.4GHz processor, IGB RAM, 80G HDD (Hard Disk Drive).
2) *Laptops:* Intel Centurion 2.0 GHz processor, 2GB RAM, 120GB, wireless NIC (Network Interface Card) card.

Software Requirements

A. Operating systems

1) windows 8 – for server
2) MySQL (WAMPP version 2.5) – for server.

B.Windows Vista/XP for clients and laptops.

Specification Report for the Oroposed System

The specification report for the proposed system is illustrated below:

System Interface

The application would be a self-contained system. It will not access data from any other application, nor will other application have access to its data.

User Interface

Application will be accessed through a Browser Interface. The interface would be viewed best using 1024 x 768 and 800 x 600 pixels resolution setting. The software would be fully compatible with Microsoft Internet Explorer version 6 and above. No user would be able to access any part of the application without logging on to the system.

Communication Interface

The system should be accessed over a LAN specifically on an Intranet. For clients to access the application server, the network should be running TCP/IP protocol.

Conclusion

This project report entitled "Online Examination System" has come to the final stage. The system has been carefully developed; it is free of errors and at the same time it is efficient and time-saving for candidates, lecturers and administrators. It is important that the system is robust, and provision is provided for future development in the system. The entire system is secured. The e-Exam is a small but effective system for conducting online examinations. Once the test has been distributed, completed submissions are electronically sent to the online exam data processing engine, which stores, scores, and tabulates them. Results are published by the reporting module. Detailed records of all data turned in by each respondent are readily accessible by authorized users from the online exam Microsoft Access database. It is cost effective; it can be easily modified, and it can be converted for other testing purposes. For example it can be converted to an online quizzing system, qualification tests for industrial workers, or an online Feed Back System.

 ISBN 978-9959-9703-2-9

References

[1] S.D. Achtemeier, L.V. Morris, L. V. and C.L. Finnegan. (2003). "Considerations for developing evaluations of online courses." Journal of Asynchronous Learning Networks, 7(1), 1-13.

[2] BabatundeIpaye (2009), "E-Learning in a Nigerian Open University", National Open University bipaye@gmail.com

[3] A. Huszti and A. Petho (2008), "A Secure Electronic Exam System", Informatika

[4] M. Ibrahiem, M. El Emary, A.A. Jihad. And Abu Al Sondos (2006), "An Online Website for Tutoring and E-Examination of Economic Course", American Journal of Applied Sciences 3 (2): Page 1715-1718

[5] T. Schramm (2008), "E-Assessments and E-Exams for Geomatics Studies", Department of Geomatics Hafen City University Hamburg Hebebrandstraße 1, 22297 Hamburg, Germany

[6] YuanZhenming, Zhang Liang, Zhan Guohua (2003), "A Novel Web-Based Online Examination System for Computer Science Education", 33rd ASEE/IEEE Frontiers in Education Conference, S3F-7-S3F-10

[7] J. C Adams and A. A. Armstrong (1998), "A Web-based testing: A study in integrity," World Wide Web, vol. 1, no. 4, pp. 193-208.

[8] J.S. Iyilade and W.O. Odekunle. (2005). "A web-based student testing and assessment system". In Proceedings of the International Conference on Application ofIctto Teaching, Research, and Adminstration, AICTTRA (Vol. 1, pp. 16-24).

[9] VijayIndoria, Prashant Sharma, AnoopSoni, (2004), project report on online examination, international school of informatics and management.

[10] D. Pullen and B.Cusack. (2007). "Schooling without borders". Technology and teaching, 101-114.

[11]E. Gvozdenko and D. Chambers. (2007). "Applying Computerised Testing & Certainty Based Assessment to Reveal More about Student Learning: From Theory To Practice". International Journal of Learning, 13(12).

[12]C. Rogers (2006) "Faculty perceptions about e-cheating during online testing,"J.Comput. Sci. Colleges, vol.22, no. 2, pp. 206-212.

[13] J. *Gaytan* and B.C. *McEwen*. (2007). "Effective online instructional and assessment strategies". American Journal of Distance Education, 21(3), 117–132.

[14]NirajLola.(2004), e-Exam: the online examination system, Y2m004. Department of Computer Science and Engineering National Institute of Technology, Calicut, pp. 7-11.

[15] Niraj Lola. (2004), e-Exam the online examination system, Y2m004. Department of computer science and engineering national institute of technology, Calicut, pp. 7-11.

[16]Smarty,Navin,(2009) (http://.answer.yahoo.com> other-education, (2010).

[17] Thefreewikipedia,Test(studentassessment),(2010), (http"//en.wikipedia.org/wiki/Test_ (student _assessment), (2010).

[18] Thomas Schramm (2008), "E-Assessments and E-Exams for Geomatics Studies", Department of Geomatics Hafen City University Hamburg Hebebrandstraße 1, 22297 Hamburg, Germany

[19] Vijay Indoria, Prashant Sharma, AnoopSoni, (2004), project report on online examination, international school of informatics and management.

[20] Yuan Zhenming, Zhang Liang, Zhan Guohua (2003), "A Novel Web-Based Online Examination System For Computer Science Education", 33rd ASEE/IEEE Frontiers in Education Conference, S3F-7-S3F-10 Fels ő oktatásban. Page 1-7. Of Nigeria, page 1-11.

Mabrouka M. Al geryani was born in the city of Sawknah in 1985, she graduated from the Higher Institute for Comprehensive Careers Al Jufrah-Sawknah. She worked as a tutor in the Institute from 2009 to 2012, and is currently pursuing her master's degree in Cyprus, Cyprus International University in Information Technology.

 ISBN 978-9959-9703-2-9

المؤتمر الدولي الثاني للعلوم والهندسة
2nd International Conference on Science and Engineering
ICSE 2023
Faculty of Engineering - University of Bani Waleed
Bani Waleed, Libya

Paper Code: ICSE-003

FLUIDITY OF ALUMINUM PISTON ALLOY WITH DIFFERENT AMOUNT OF POURING TEMPERATURE

Zayad M. Sheggaf[a], Sharafaddeen S. Wanis Ehzazat[b], and Almabrouk A. Dhaw Esdeira[a]
[a]Libyan Center for Engineering Research and Information Technology, Libya
[b]College of Technical Sciences, Bani Waild, Libya
*Crosspnding author: zayad1976@gmail.com

Abstract One of the principal attributes of the aluminum-silicon alloys is their excellent fluidity, or the ability to fill a mold cavity. Fluidity is a complex characteristic that is influenced by surface tension, viscosity, alloy freezing range, melt, cleanliness, superheat, and solidification conditions. Chemical modifiers are generally considered to be detrimental to fluidity despite the fact that all the chemical modifiers commonly in use decrease surface tension. This investigation has been carried out to study the influence of pouring temperature of aluminum piston alloy on casting fluidity and microstructure defects. A strip type of fluidity testing mould was used in this study, and optical microscope to find microstructure defects. The results showed that higher the pouring temperature greater the casting fluidity. Otherwise, the overheating caused porosity, solidification shrinkage, and dross formation into the microstructure of the alloys melted at temperature higher than 760 C°.

Keywords: aluminum alloys, casting, fluidity

Introduction

Due to their unique properties, such as low density, high thermal conductivity, simple net-shape fabrication techniques (casting and forging), ease of machinability, high reliability, and excellent recycling characteristics, aluminum alloys are the preferred material for pistons in both gasoline and diesel engines. Due to their excellent castability, where silicon plays a significant role, especially having high thermal characteristics that increase fluidity, Al-Si casting alloys are frequently utilized to create engine parts. [1-3]. Otherwise, casting characteristics of AI-Si alloys requires careful melting, degasifying, and pouring. Failure to exercise adequate control during the melting and casting processes is one of the most important problems [4, 5]. Pouring molten metal into the mold and then filling it are two crucial processes in the casting process. It has been noticed in foundry practice that some alloys fill the mould cavity completely and reproduce its intricacies in the finished casting better than others do when filling moulds of sophisticated design, particularly those that

 ISBN 978-9959-9703-2-9

involve thin portions. Therefore, testing for mould filling capacity is crucial since it not only aids in choosing the right alloy composition for a certain application, but also helps with quality control and reduces casting rejections. Mistune castings or the absence of surface characteristics may be caused by inadequate fluidity [6, 7]. The characteristics of mould and metal jointly are involved in determining fluidity and pouring temperature is one of the factors related to metal. The aluminum-silicon alloys containing 8.5 to 13% Si are widely used to produce automotive parts. Generally, the higher the silicon content, up to the eutectic composition (12.6% Si), the greater the fluidity and, consequently, the easier an alloy is to cast [2]. The previous research found that pure Si would have been expected to have over 21 times the fluidity of pure aluminum as a result of its higher latent heat. However its greater rate of heat loss, seen to be nearly 5 times faster as a result of its higher freezing temperature, reduces this significantly. The low density of silicon also reduces the effect somewhat further [8]. G. Timelli et. Al [9] investigated investigate the fluidity of four different high pressure die cast Al–Si and Al–Si–Cu alloys at pouring temperature range of 580–760 °C. They found that fluidity linearly increases at increasing temperatures. At the other study, Chennakesava Reddy et. Al [6] found out that influence of pouring temperature on fluidity of Al-Si-Mg cast alloys is positive, where higher the pouring and mould pre-heat temperature greater the casting fluidity, as pouring temperature range is between 650 and 850 °C, and the mould preheated before pouring to 400 °C. They also found that silicon content in the alloy raises the surface tension resulting resistance to tearing of liquid layers and iron content favors the streamline flow of metal in the channels. The aim of the present study is to investigate the strip fluidity of Al-Si piston alloy with different pouring temperature used for gravity die casting, the strip fluidity test measures the ability of alloy to fill a mould of different cross sections and thus provides a wider specification of actual casting conditions.

Experimental Procedure

A consumed car engine pistons were used in the present investigations, The chemical composition of the piston alloy was determined using FOUNDARY-MASTER Pro emission spark spectrometer. Table 1 shows the chemical composition of alloy.

Table 1: The chemical composition of investigated alloy.

Element	Cr	Zn	Mg	Mn	Cu	Fe	Si	AL
Wt.%	0.0260	0.714	0.287	0.151	2.59	0.762	11.5	Bal.

ISBN 978-9959-9703-2-9

For the purpose of preparing specimens at various pouring temperatures, the pistons were cut into small pieces and remelted. The tests were conducted in the pouring temperature range of 680 - 860 °C with a step of 10 °C after the pieces had been melted in an electrical furnace fitted with a graphite crucible. Since one of the many different types of fluidity tests uses fluidity as an empirical measure of a processing characteristic, this attribute is measured. Two common types are the mould fluidity spiral and the strip fluidity test. According to the previous studies [6, 10, 11], a strip fluidity testing mould (a tool steel strip type mould) was chosen to use in this investigation, whose design is shown in Fig. 1, which including four strips, a pouring basin, and running system. Each strip was of 10 mm width and 200 mm length. The thicknesses of the strips were 1, 1.25, 1.55, and 1.85 mm.

Fig. 1: Fluidity test mould

The temperature of the melt was measured using a K-type thermocouple. The melt was finally poured into the mould, then, the length of fluidity was measured. The samples were examined via an optical microscope to detect the formed porosity into microstructure of specimens.

Results and Discussion

Figure 2 shows the ingot after solidified, it can seen the molten metal did not flow through the strips but does flow into the running system for both sides due to the mould is not heated (casting with mould at room temperature), same result where found by A. Heidarzadeh et. Al **[10]** as the molten metal did not pass through the strip with 1 mm thick and solidified at running system which was cast without preheat the mould. However, the length of the metal flow in all strip mould summed together is taken as a measure of casting fluidity.

Fig. 2: Photographic view of strip fluidity test casting

The effect of pouring temperature on the fluidity alloy is shown in Figure 3. It can be seen that the fluidity increases with increasing

ISBN 978-9959-9703-2-9

pouring temperature. The degree of super heat of the alloy increases with increase in pouring temperature, this leads to keep the alloy as a molten form for a longer period, also the super heating of alloy decrements the fluid viscosity, so the liquid melt is able to flow over a longer distance due to increase in fluid life [6, 10]. In addition, increasing the pouring temperature delays the nucleation and growth of fine grains at the tip of the flowing metal into the mould channel, which lead to increment of the fluidity. [12, 13].

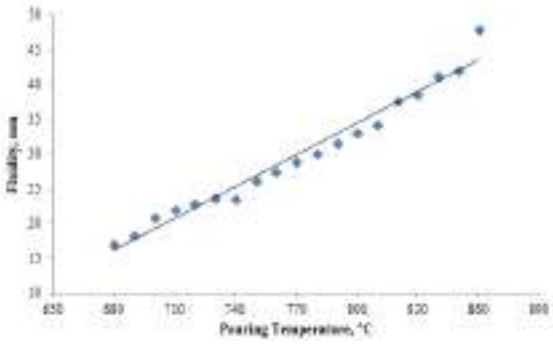

Fig. 3: Effect of pouring temperature on fluidity

On the other hand, an increase in the fluidity of the alloy as a result of an increase in the pouring temperature may lead to one of the most important defects of the microstructure, which is porosity. Porosity in castings mainly occurs due to gas entrapment in the melt at a highly turbulent flow of liquid metal into the die cavity [14, 15]. Figure 4 showed the microstructure of alloys with different pouring temperatures. The images showed that the porosities were formed at higher values of pouring temperature. The overheating in aluminum foundry causes gas porosity, solidification shrinkage, and dross formation [16]. In Figure 4 (a, b and c) no structure defects have been detected, otherwise in Figure 4 (d, e and f) some drosses were formed during solidification which referred with the circles.

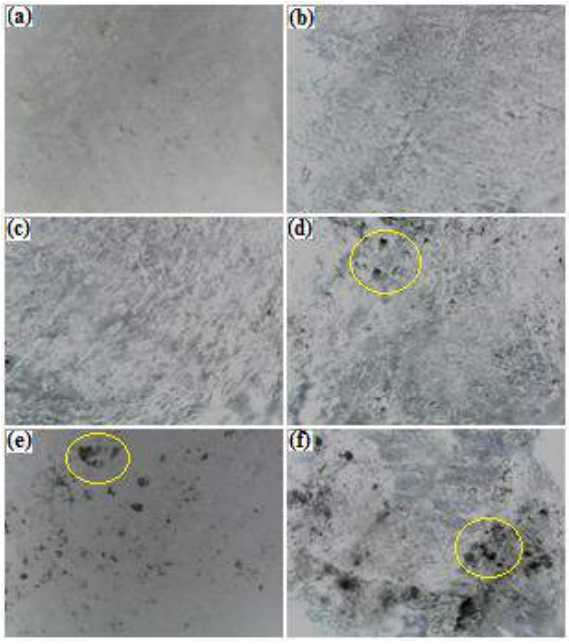

Fig. 4: Microstructure images of (a) 680, (b) 720, (c) 760, (d) 800, (e) 830 and (f) 860 °C pouring temperature, 50x.

Figure 5 showed formation of the solidification

ISBN 978-9959-9703-2-9

shrinkage defects caused by overheating at 840 °C pouring temperature.

Fig. 5: Microstructure images of the alloy melted at 840 °C, 50x.

Furthermore, the images of microstructure for the alloys were pouring at a high temperature also showed another structure defect, which was porosity, as shown in Figure 6 as clusters noted by circles. Porosity in cast parts is primarily caused by gas entrained in the melt as the liquid metal flows in a highly turbulent flow within the mold cavity. [16, 17]. In liquid metal die casting, the main filling mode is turbulent flow, so it is easy to form entrained gas in the cavity, which leads to the formation of porosity defects inside the casting, which greatly affects the compactness and mechanical properties of the casting structure [18, 19].

Fig. 6: The formed porosity into microstructure of the alloy at 840 °C, 50x.

When the aluminum alloys are melted at high temperatures, gases such as hydrogen are likely to be generated in the molten metal, causing defects such as gas pores and shrinkage pores. [20]. The increased porosity can cause a reduction in the mechanical properties [21]. As shown in the above results, melt the alloy at a high temperature caused increase in fluidity; on the other hand, led to form common casting defects, which can no longer be treated.

Conclusion

The effect of pouring temperature on strip fluidity of aluminum piston alloy was investigated. From the analysis, the following can be summarized:

 ISBN 978-9959-9703-2-9

1. Casting fluidity of alloys increases with increasing pouring temperature of melt.

2. The mould with strips less than 3 mm thicknesses needs pre-heating, where the molten metal did not reach the strips.

3. Casting defects were observed for the alloys with pouring temperature more than 760 °C.

4. The consumed aluminum piston alloy can be re-melted and used to produce many parts, as a recycling is the most effective ways to produce the alloys in our country.

Acknowledgment

The authors would like to acknowledge the machining workshop technicians and metallurgy laboratory technicians in college of technical sciences Bani Walid Libya, also, High vocational Libyan for casting.

References

1. Davis, J.R., Aluminum and aluminum alloys. 1993: ASM international.

2. Stefanescu, D., J. Davis, and J. Destefani, Metals Handbook, Vol. 15--Casting. ASM International, 1988, 1988: p. 937.

3. Kalemtas, A., et al., Thermal properties of pressureless melt infiltrated AlN–Si–Al composites. Transactions of Nonferrous Metals Society of China, 2013. 23(5): p. 1304-1313.

4. Sigworth, G., The modification of Al-Si casting alloys: important practical and theoretical aspects. International Journal of Metalcasting, 2008. 2(2): p. 19-40.

5. Sigworth, G., The modification of Al-Si casting alloys: important practical and theoretical aspects. International Journal of Metalcasting, 2008. 2: p. 19-40.

6. Sumanth, M., A.C. Reddy, and V. Murti, FLUIDITY TESTING ON Al-Si-Mg CAST ALLOYS. life. 1: p. 2.

7. Radwan, B., Treatment of a Liquid Al-Si Alloy: Quality Control and Comparison of Two Melt Degassing Processes. 2020.

8. Campbell, J., Review of fluidity concepts in casting. Cast Metals, 1995. 7(4): p. 227-237.

9. Timelli, G. and F. Bonollo, Fluidity of aluminium die castings alloy. International Journal of Cast Metals Research, 2007. 20(6): p. 304-311.

10. Heidarzadeh, A., et al., The effect of copper addition on the fluidity and viscosity of an Al-Mg-Si alloy. Journal of materials engineering and performance, 2014. 23(2): p. 469-476.

11. Di Sabatino, M., L. Arnberg, and D. Apelian, Progress on the understanding of

 ISBN 978-9959-9703-2-9

fluidity of aluminium foundry alloys. International Journal of Metalcasting, 2008. 2(3): p. 17-27.

12. Srinivasa, R. and R. Patil, Characterization of Casting and Deformation Process of a Metal Alloy. International Research Journal of Engineering and Technology, 2017. 4(2).

13. Di Sabatino, M., Fluidity of aluminium foundry alloys. 2005.

14. Wilczek, A., P. Długosz, and M. Hebda, Porosity characterization of aluminium castings by using particular non-destructive techniques. Journal of Nondestructive Evaluation, 2015. 34(3): p. 1-7.

15. Cao, H., et al., The influence of different vacuum degree on the porosity and mechanical properties of aluminum die casting. Vacuum, 2017. 146: p. 278-281.

16. Prukkanon, W., N. Srisukhumbowornchai, and C. Limmaneevichitr, Influence of Sc modification on the fluidity of an A356 aluminum alloy. Journal of Alloys and Compounds, 2009. 487(1-2): p. 453-457.

17. Shivkumar, S., L. Wang, and D. Apelian, Molten metal processing of advanced cast aluminum alloys. JOM, 1991. 43: p. 26-32.

18. Li, M., Y. Li, and H. Zhou, Effects of Pouring Temperature on Microstructure and Mechanical Properties of the A356 Aluminum Alloy Diecastings. Materials Research, 2020. 23(1).

19. Li, M., Y. Li, and H. Zhou, Effects of pouring temperature on microstructure and mechanical properties of the A356 aluminum alloy diecastings. Materials Research, 2020. 23.

20. Ahmad, R., N. Talib, and M. Asmael. Effect of pouring temperature on microstructure properties of Al-Si LM6 Alloy sand casting. in Applied Mechanics and Materials. 2013. Trans Tech Publ.

21. Irfan, M., et al., Porosity reduction and mechanical properties improvement in die cast engine blocks. Materials Science and Engineering: A, 2012. 535: p. 108-114.

 ISBN 978-9959-9703-2-9

المؤتمر الدولي الثاني للعلوم والهندسة
2nd International Conference on Science and Engineering
ICSE 2023
Faculty of Engineering - University of Bani Waleed
Bani Waleed, Libya

Paper Code: ICSE-009

METEOROLOGICAL AND HYDROLOGICAL DROUGHT ANALYSIS OF SINOP, KASTAMONU, BARTIN PROVINCES IN THE WESTERN BLACK SEA

Amhmmed Anbeeh Albaqoul1, Allam Musbah Al Allam2, Waleed Ahmoda3
Tülay Ekemen KeSkin4
1,2Engineering and Information Technology Research Center, Bani Walid, Libya
1,4Universiti Karbuk,Turkey
3College of Technical Sciences, Bani Walid
*Corresponding Author: alamalallam8@gmail.com
*Corresponding Author: amhmedalwarfally@gmail.com
*Corresponding Author: tekemen@gmail.com

Abstract: In recent years, a significant change has been observed in the climate characteristics of Turkey. These changes, which are compatible with the general trend of global climate change, are also felt in the Western Black Sea Basin. This paper reported on the calculation of drought indices, with emphasis on two recently developed indices, the Reconnaissance Drought Index (RDI) and the Stream flow Drought Index (SDI) using specialized software package, named Drin C (Drought Indices Calculator). Additionally, Drin C includes a module for the estimation of potential evapo transpiration (PET) through temperature-based methods (Hargreaves, Blaney - Criddle, and Thornthwaite) that can be used for the calculation of RDI. Therefore, in this study carried out in the Western Black Sea region, meteorological drought analyzes for1-, 3-, 6- ve 12 months were made for 3 precipitation observation stations in the provinces of Sinop, Kastamonu, Bartın, and monthly total precipitation and monthly average temperature data were used to determine the meteorological drought.

Keywords: Drought analysis, Standard Precipitation Index (SPI), Reconnaissance Drought Index (RDI), Stream flow Drought Index (SDI), Sinop, Kastamonu, Bartın ,West Black Sea Region

Introduction

Drought is defined as a phenomenon that may be related to the area under investigation and should be addressed using a specific application. The region can faces environmental, economic, and social challenges and so, many definitions of the dangerous drought have been developed [1]. During a drought, a lack of moisture usually results in a severe hydrological imbalance. The areas can had also experienced dry weather and long-term water scarcity due to water scarcity. According to Hagman (1984), drought is the most common natural disaster [2]. The event are the most complex of all-natural disasters that have affected man, but the nature of drought has been described as the event observed in a specific period and circumstances. Every year, various regions of the world are affected by the drought [3,4]. Considering the severity, duration, and effects

 ISBN 978-9959-9703-2-9

of the drought, there are certaindroughttypes; meteorologicaldrought,agriculturaldrought,hydrologicaldrought,andsocioeconomic drought[5]. Meteorological drought is defined by the severity and duration of the drought. Depending on rainfall data, it is the first type of drought we encounter. Because its effect is dependent on rainfall, the period of rainfall corresponds to an average level in that drought type. Because the climate regime of the regions is an important factor, meteorological droughts vary in different locations. Taking two regions with different precipitation amounts as an example, the average annual rainfall in the first region is estimated to be 500 mm/year for longer years. In contrast, the annual rainfall in the second region is estimated to be around 1500 mm/year. If the amount of rainfall in the region in the same year is 750 mm/year, then the first region is experiencing a humid year, while the second region is experiencing a dry year. The main reason for this is due to atmospheric conditions that caused a lack of precipitation based on the climatic regime. Furthermore, meteorological drought had recorded monthly rainfall data. It is assessed on a seasonal, water-year, and annual time scale [6]. As a result, the researcher observed the significant socioeconomic impact of such frequent changes.

Agricultural drought is investigated due to a lack of rainfall due to meteorological drought and soil water deterioration. The water demand of a plant is determined by its biological properties, as well as the growth or stages of the soil's physical and biological properties [7].

A lack of water in the hydrological system was referred to as a hydrological drought. It was a type of drought in which water levels in rivers, lakes, reservoirs, and groundwater were unusually low [8].

The hydrological drought indicated that the total flow of the dry year was lower than the previous year's average flow. Furthermore, the frequency and severity of hydrological drought are typically defined at the river basin scale. Hydrological drought is considered to be ongoing if the actual flow in a river during a specified time period falls below a certain threshold. As a result, the effects of hydrological drought upstream of a river basin may reduce downstream flow and vice versa [9].

For example, after years of severe drought in a river basin, many years of normal rainfall were required to replenish the reservoirs. Therefore, the socioeconomic drought occurred due to meteorological, hydrological, and agricultural drought factors being linked to the supply and demand for certain economic goods or services. Water, food, and hydroelectric energy supply, for example, are all affected by weather conditions. In most cases, demand for these goods is increasing due to rising per capita consumption. As a result, droughts are typically caused by an increase in demand for supply goods and a decrease in climate factors [10].

Gümüş (2017) used the Stream Arid Index approach to conduct drought studies in the Asi Basin. Data from four flow monitoring sites between 1954 and 2005 were analyzed in the research. In the basin, the flow drought index calculations for the 3, 6, and 12-month time series indicated the dry, humid, and wet times of year. There were many more broken years between 1980 and 2005 than in prior years, according to the statistics. In addition, 2000 and 2001 were shown to be very dry years.[11].

Gümüş ve diğ., (2019),by the Ceyhan-Ceyhan area of Turkey conducted a study aimed to investigate the meteorological and hydrological drought, Standardized Precipitation Index, the method (SPI) and Current Drought Index (SDI) method in the region that was favored and methods gave similar results It is stated that they help to understand the drought better [12].

Bakanoğulları (2020) used SPEI (Standardized Precipitation Evapo transpiration Index) and SPI Indices to analyze the Istanbul-Damlca Stream Basin droughts. When determining drought frequency and severity in the study, researchers used the (SPEI) and (SPI). The

 ISBN 978-9959-9703-2-9

Thornthwaite technique was used to determine the SPEI drought index evapotranspiration in the basin between 1982 and 2006, using meteorological data. It is statistically noteworthy that the coefficient of determination (R2) between the yearly SPEI and SPI indices (0.977) is substantial. Drought patterns differed across the one, three, and six-month time frames, however. Study findings show a more accurate SPEI Drought Index regarding agricultural productivity and its usage is healthier [13].

In research by Coşkun (2020), a long-term precipitation trend analysis in the Van Lake basin was performed. The long-term recorded precipitation data from Van-Bölge, Muradiye, Erçiş, Gevaş, zalp, Tatvan, and Ahlat meteorological stations were used to evaluate both yearly and seasonal patterns in precipitation. Gevaş and Ahlat stations have declined yearly precipitation since the MannKendall Test, Spearman's Rho, and en Tests were used to analyze the data. Van-District station had an increase in annual precipitation. However, this time the rise was negligible. Erciş and Ahlat stations have had a considerable fall in precipitation, whereas Van-Region has seen a slight rise [14].

2. Material and Method

This study presented the methodology used to collect and analyze the data of the study. The scope of the study is to determine drought sensitivity and calculate drought years to show the driest year in the western Black Sea region with the help of data from 8 precipitation and 4 flow observation stations data. In order to track changes in drought index values through time, drought analysis was used. The Standard Precipitation Index (SPI), the Reconnaissance Drought Index (RDI) and the Stream flow Drought Index (SDI) used for this aim. Sinop, Kastamonu and Bartın provinces in the Western Black Sea region was selected for research due to sometimes the scarcity of precipitation. Analyzes for meteorological and hydrological drought analysis were performed with the help of data between 1969-2019, and 1965-2915, respectively. Missing precipitation, temperature and flow data were completed with regression analysis.

Station Number	Station Name	Connected Province	Height (m)	Coordinate	Observation Period
17020	Bartın	Bartın	33	41°K 32°D	1965-2015
17074	Kastamonu	Kastamonu	800	41°K 33°D	1965-2015
17026	Sinop	Sinop	32	42°K 35°D	1965-2015

2.1. Methodology

A meteorological and hydrological drought analysis will be conducted for 8 precipitation and 4 flow observation stations data in the study area. Missing data were completed with regression analysis. The Standard Precipitation Index (SPI) method is used to determine meteorological drought using monthly total rainfall data. The Reconnaissance Drought Index (RDI) method used to determine meteorological drought using average monthly temperature data and total monthly precipitation data. Also The Stream flow Drought Index (SDI)method is used to determine hydrological drought using monthly mean flow data A drought analysis were performed using Drin C software at the study areas for 1, 3, 6, and 12 months.

2.2. Data

Monthly total precipitation and mean temperature data for stations 8 in the Sinop, Kastamonu and Bartın provinces were obtained

ISBN 978-9959-9703-2-9

from the General Directorate of Meteorology and monthly mean flow data for stations 4 in the study area were obtained from the General Directorate of State Hydraulic Works. The average annual temperatures, the total annual averages of precipitation, and the average flow data obtained from these stations are shown in Table 1.

Table 1. Precipitation and flow monitoring stations and its geographic locations.

2.3. Standardized Precipitation Index

The Standard Precipitation Index (SPI) was developed by (McKee et al. 1993). to determine the effects of the reduction in precipitation on groundwater, reservoir storage, soil moisture, snow drifts, and streams. It is obtained by dividing the precipitation difference from the mean, which is converted to normal distribution within the specified time period by the standard deviation. In fact, SPI provides a standardized conversion of the observed precipitation probability and could be calculated for desired time periods such as 1, 3, 6, 9, 12, 24, and 48 months. The formula and classification of the method are given below [15]

$$SPI = (X_i - X_i) / \sigma \qquad (1)$$

Where:

- SPI: Standard Precipitation Index
- Xi: amount of precipitation
- Xi: average of precipitation
- σ:standarddeviation

Table 2. Index values and classification of SPI method [15]

SPI	SPI
≤ 2.0	Extremly wet
1.50-1.99	Severely wet
1.00-1.49	Modetraly wet
0-0.99	Mildly wet
-0.99-0	Mild drought
-1.49- -1.00	Modarate drought
-1.99- -1.50	Severe drought
≤ - 2.00	Extreme drought

2.4. Reconnaissance Drought Index

ThereconnaissanceDroughtIndex(RDI)isdevelopedtoapproachthewaterdeficitinamoreaccuratemanner,asasortofbalancebetweeninputandoutputinawatersystem[16]. The initial value (α k) of RDI was calculated for the year on a time basis of k (months) as follows:

$$\alpha_k^{(i)} = \frac{\sum_{j=1}^{k} P_{ij}}{\sum_{j=1}^{k} PET_{ij}}, \text{i} = 1(1)\text{N and j} = 1(1)\text{k} \qquad (2)$$

Where:

- Pij and PETij are the precipitation and potential e-vapo transpiration of the j-thmonthofthei-thyear
- Nis the total number of years of the available data
- The values of αk satisfactorily follow both the lognormal and the gamma distributions in a wide range of locations and different time scales, in which they were tested.

$$RDI_{st}^{(i)} = \frac{Y^{(i)} - \overline{Y}}{\hat{\sigma}_y} \qquad (3)$$

Where:

- $y^{(i)}$ is the $\ln(a_k)^{(i)}$
- y is its arithmetic mean
- σy is the standarddeviation of y

Table 3. Corresponding boundary values of RDIst[29].

Mild	Moderate	Severe	Extremeclasses

ISBN 978-9959-9703-2-9

-0.5 to -1.0	- 1.0 to -1.5	-1.5 to -2.0	< -2.0

2.5. The Stream flow Drought Index

The index is a hydrological drought analysis. According to Nalbantis and Tsakiris (2009), if a time series of monthly stream flow volumes Qi,j is available, in which i denotes the hydrological year and j the month within that hydrological year (j = 1 for October and j = 12 for September), Vi,k can be obtained based on the equation [17].

$V_{i,k} = \sum_{j=1}^{3k} Q_i \; i = 1,2,\ldots.12 \; k = 1,2,3,4$ (4)

in which Vi,k is the cumulative stream flow volume for the i-th hydrological year and the k-th reference period, k = 1 for October-December, k = 2 for October-March, k = 3 for October-June, and k = 4 for October-September. Based on the cumulative stream flow volumes Vi,k, the Stream flow Drought Index (SDI) is defined for each reference period k of the i-th hydrological year as follows[18]

$$SDI_{i,k} = \frac{y_{i,k} - \overline{y}_k}{s_{y,k}} \quad i = 1, 2, \ldots \quad k = 1, 2, 3, 4$$

Table 3 .Definition of states of hydrological drought with the aid of SDI [34]

State	Description	Criterion
0	Non-drought	SDI ≥ 0.0
1	Mild drought	-1.0 ≤ SDI < 0.0
2	Modarate drought	-1.5 ≤ SDI < -1.0
3	Severe drought	-2.0 ≤ SDI < -1.5
4	Extreme drought	SDI < -2.0

3.Result Discussion

Within the scope of this research, SPI, RDI and SDI values for 1, 3, 6, and 12 months were calculated and evaluated using the Precipitation, Reconnaissance and Stream flow Drought Index method respectively. The process used the values of the total monthly precipitation, the average monthly temperature and mean monthly discharge for total 12 monitoring stations of the Sinop, Kastamonu and Bartın provinces.

3.1 Bartin Precipitation Monitoring station (17020) meteorological drought analysis (SPI)

SPI values were examined during periods 1, 3, 6, and 12 months using monthly total precipitation data measured continuously between 1965 -2019 of the Bartın station.

Figure 1 and Figure 2 show the rates of dryness and humidity of monthly, 3-, 6-, and 12-months, respectively. Figure 1 show that the monthly dryness ranged between 45% and 59% according to SPI values. The highest dry period is 59% in Nov and Feb, with the lowest dry 45% period in Mar. When analyzed, the wet periods were the period with a high moist of 41% in Nov, Feb. The periods of drought and moisture for each of 3-, 6-, and 12-months for the SPI values are shown in Figure 3.2.The most. Dry periods with the highest SPI -3 values are SPI3-3 in Oct of 59%, and the lowest dry period is SPI3-3 Jan with 48%. For the periods SPI3- in JAN and SPI6- in April, the droughts were 52% and 55%, respectively. SPI-12 calculated according to 12-month values dryness is 50%, and moisture is 50%.

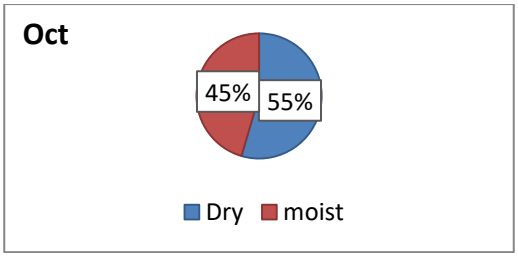

ISBN 978-9959-9703-2-9

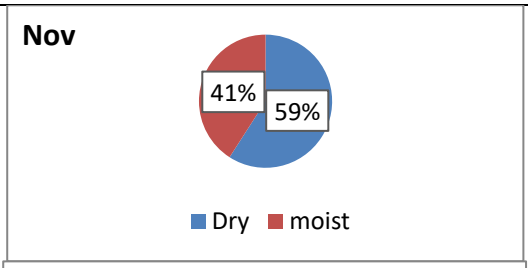

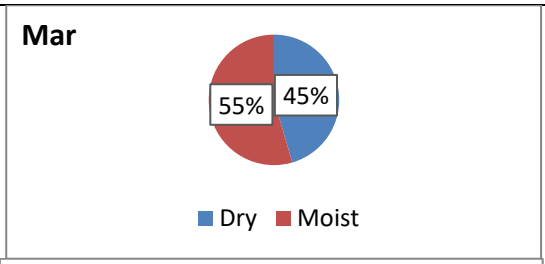

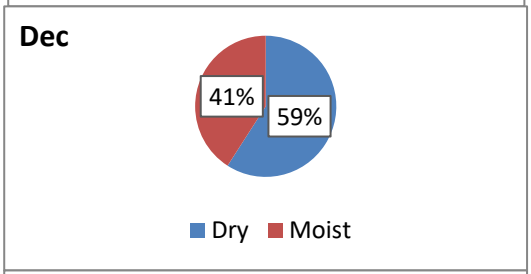

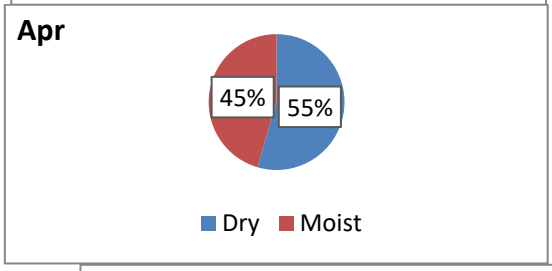

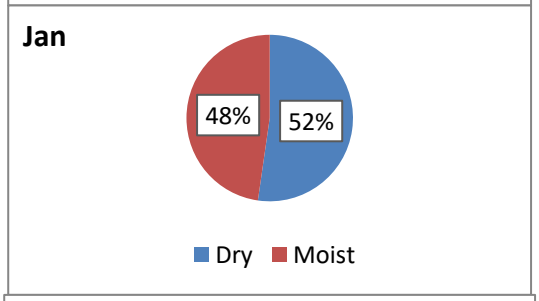

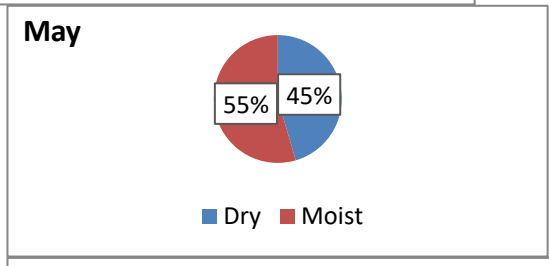

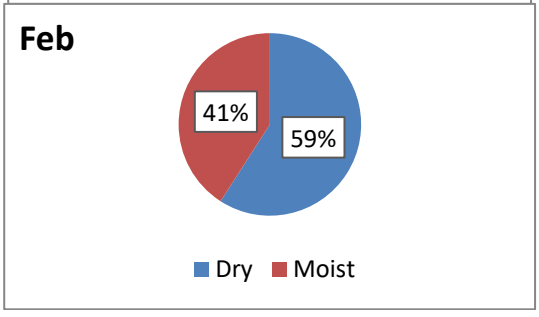

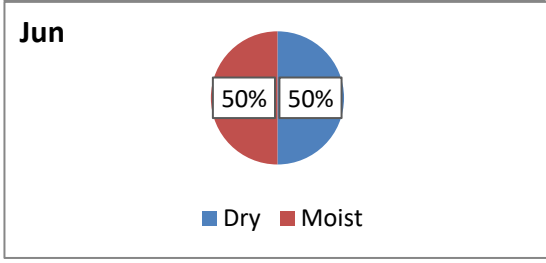

ISBN 978-9959-9703-2-9

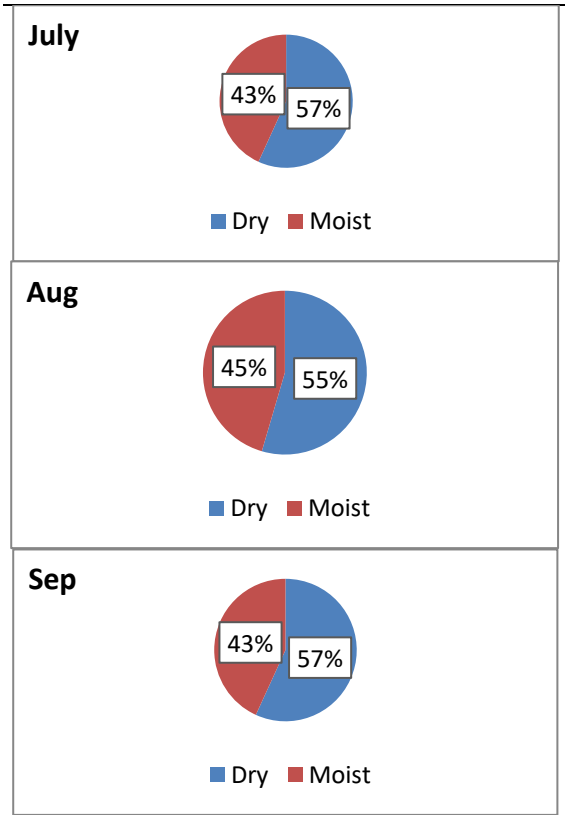

Figure 1. Dry - moist period distributions according to the monthly SPI values for the BARTINstation (No. 17020)Form 1965 to 2019.

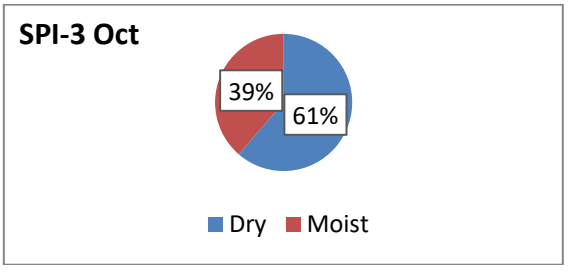

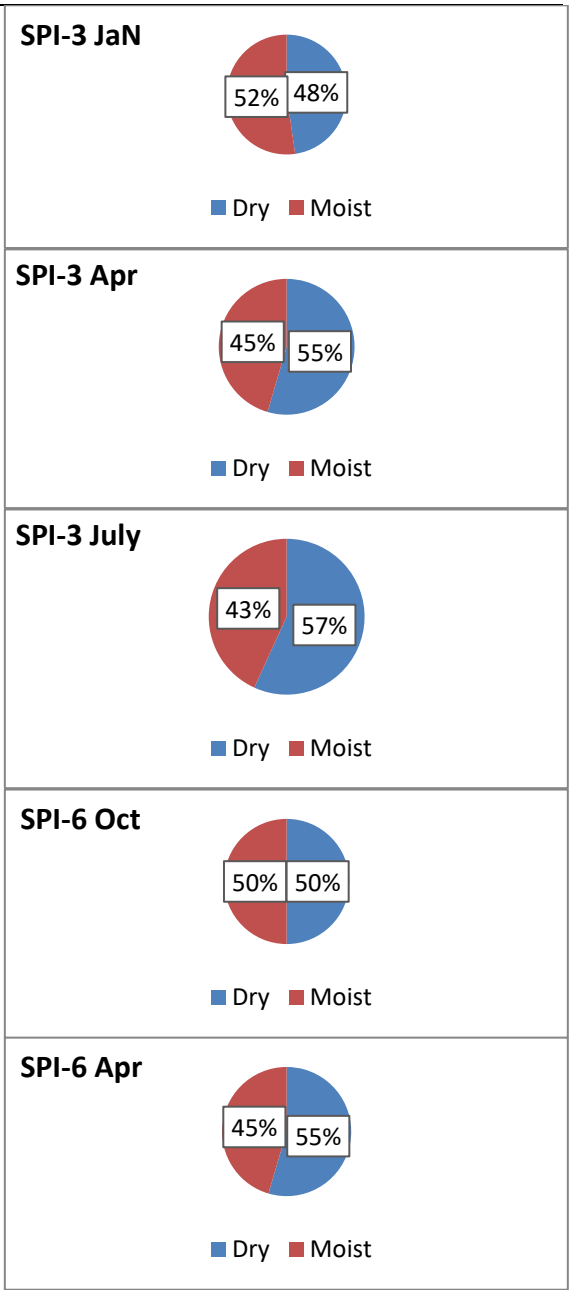

ISBN 978-9959-9703-2-9

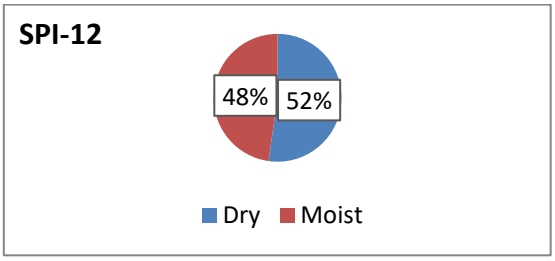

Figure 2. Dry - moist period distributions according to the 3,6,12month SPI values for the BARTINstation (No. 17020)Form 1965 to 2019

3.2.Kastamonu Precipitation Monitoring (17074)meteorological drought analysis (SPI)

SPI values were examined during periods 1, 3, 6, and 12 months using monthly total precipitation data measured continuously between 1965 -2019 of the Kastamonu station. Figure 3. and Figure 4 are shown the rates of monthly dryness and humidity 3-, 6-, and 12-months. In Figure 3.3, monthly dryness ranged between 52% and 73% according to SPI values. The highest dry period was 73% in Nov and 70% in Oct, with the lowest 52% dry period in Mar. The wet periods when analyzed were the period with a high moist of 69% in Dec, and the lows wet period was 5% in May. The periods of drought and moisture for each of 3-, 6-, and 12 months for the SPI values are shown in Figure 3.4. The driest periods with the highest SPI -3 values are SPI3-2 in Oct of 58%, and the lowest dry period is SPI3-3 Apr with 50%. For the two periods of SPI of every six months SPI-6, the dry period was SPI6-1 October and SPI6-2 April with 52%. SPI-12 calculated according to 12-month values dryness is 56%, and moisture is 44%.

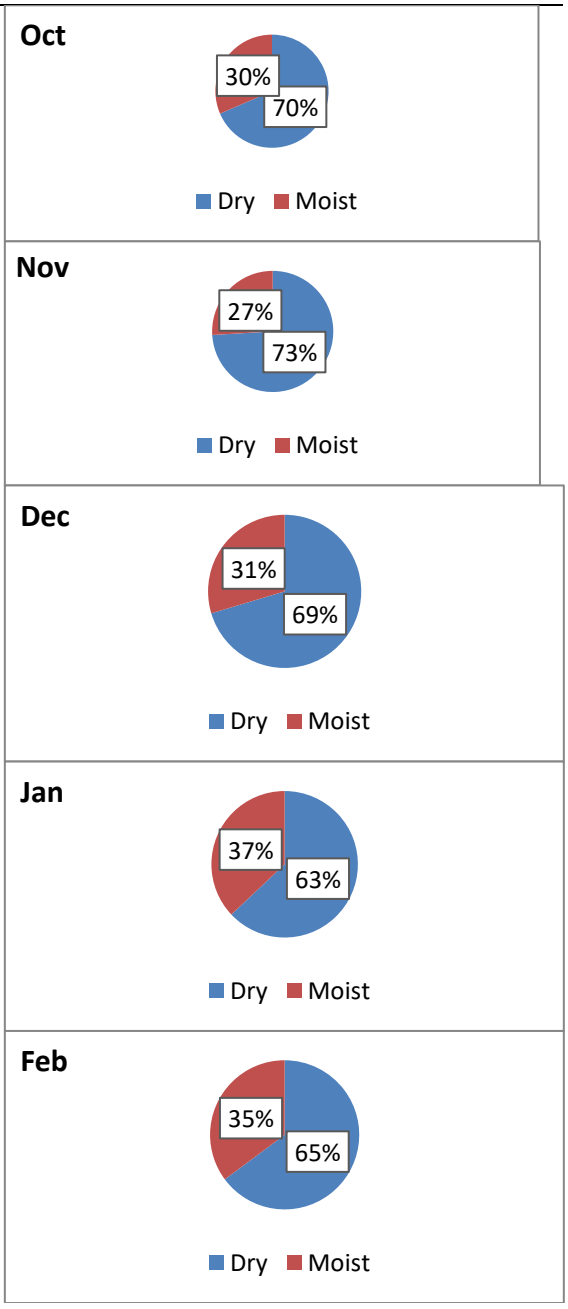

ISBN 978-9959-9703-2-9

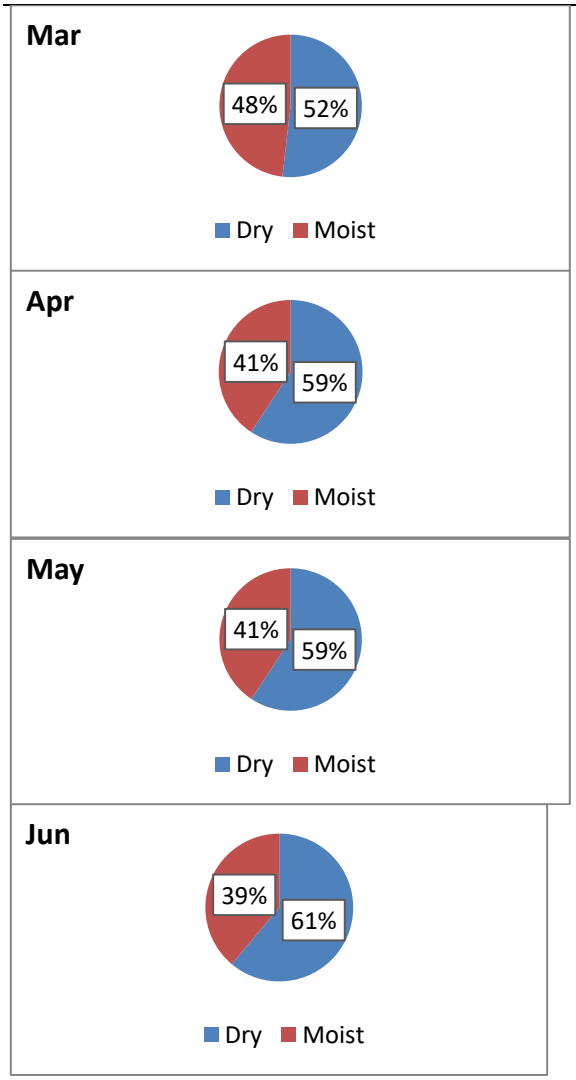

Figure.3. Dry - moist period distributions according to the monthly SPI values for the KASTAMONU station (No. 17074)Form 1965 to 2019.

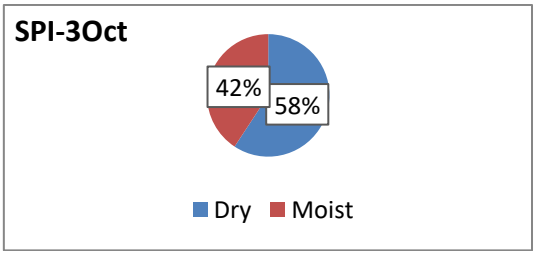

ISBN 978-9959-9703-2-9

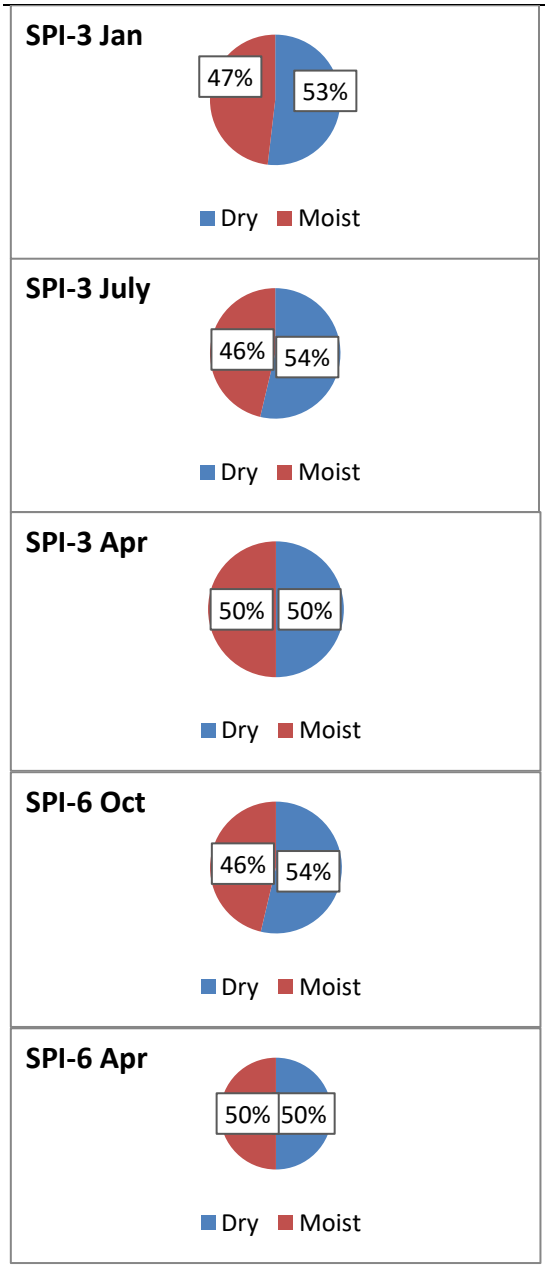

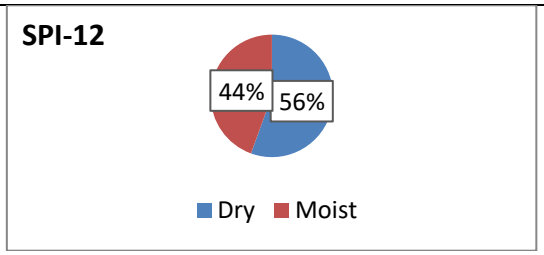

Figure 4. Dry - moist period distributions according to the 3,6,12month SPI values for the KASTAMONUstation (No. 17074)Form 1965 to 2019.

3.3.Sinop Precipitation Monitoring Station (17026)Meteorological Drought Analysis (SPI)

SPI values were examined during periods 1, 3, 6, and 12 months using monthly total precipitation data measured continuously between 1965 -2019 of the Sinop station. Figure 5 and Figure 6 are shown the rates of monthly dryness and humidity 3-, 6-, and 12-months. In Figure 3.5, monthly dryness ranged between 52% and 74% according to SPI values. The highest dry period was 74% in Nov and 70% in Dec, with the lowest 52% dry period in Mar. The wet periods when analyzed were the period with a high moist of 69% in Dec, and the lows wet period was 7% in May. The periods of drought and moisture for each of 3-, 6-, and 12 months for the SPI values are shown in Figure 3.6. The driest periods with the highest SPI -3 values are SPI3-1 in Oct of 59%, and the lowest dry period is SPI3-3 Apr with 50%. For the two periods of SPI of every six months SPI-6, the dry period was SPI6-1 October 54% and SPI6-2 April with 50%. SPI-12 calculated according to 12-month values dryness is 56%, and moisture is 44%.

ISBN 978-9959-9703-2-9

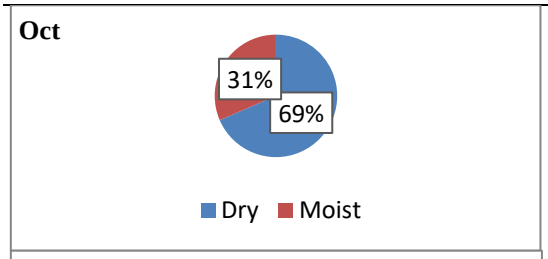

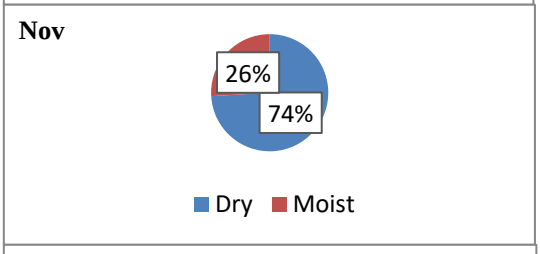

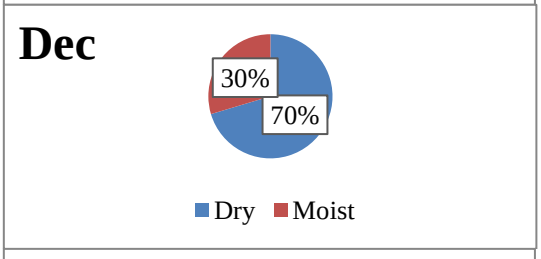

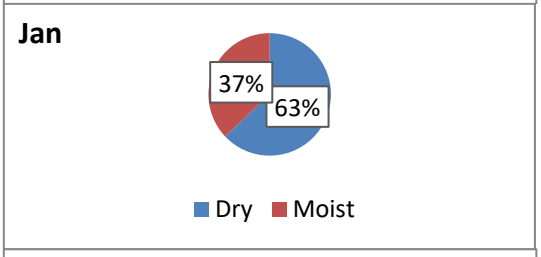

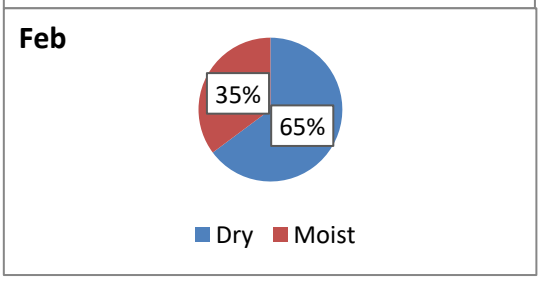

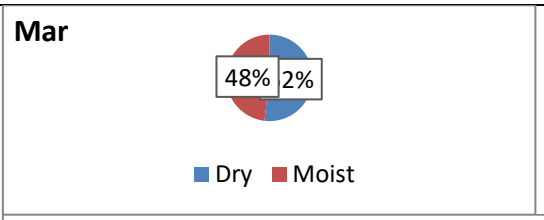

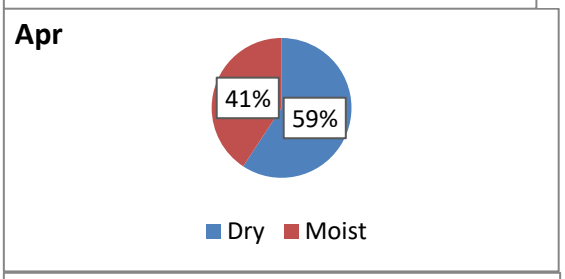

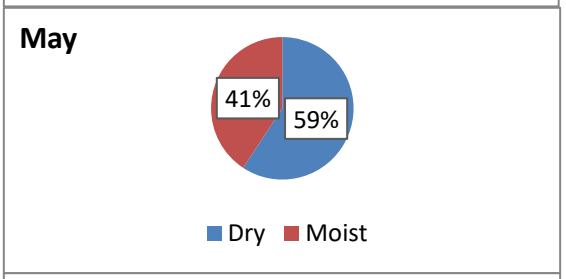

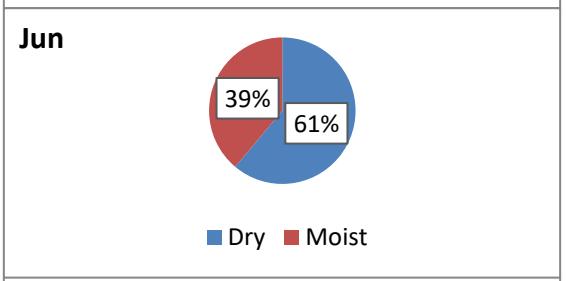

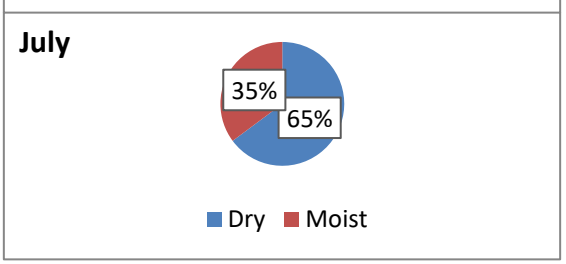

ISBN 978-9959-9703-2-9

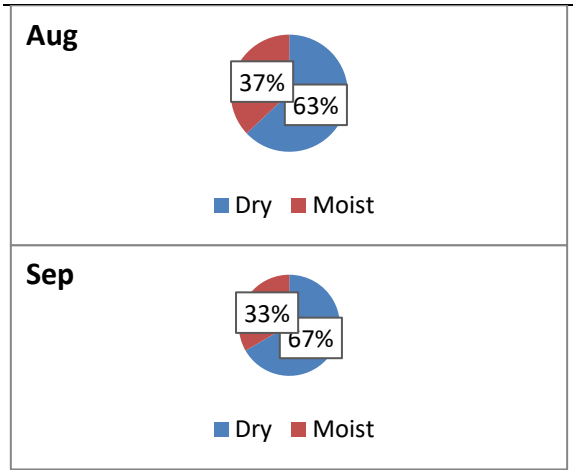

Figure 5. Dry - moist period distributions according to the monthly SPI values for the SINOP station No. 17026Form 1965 to 2019.

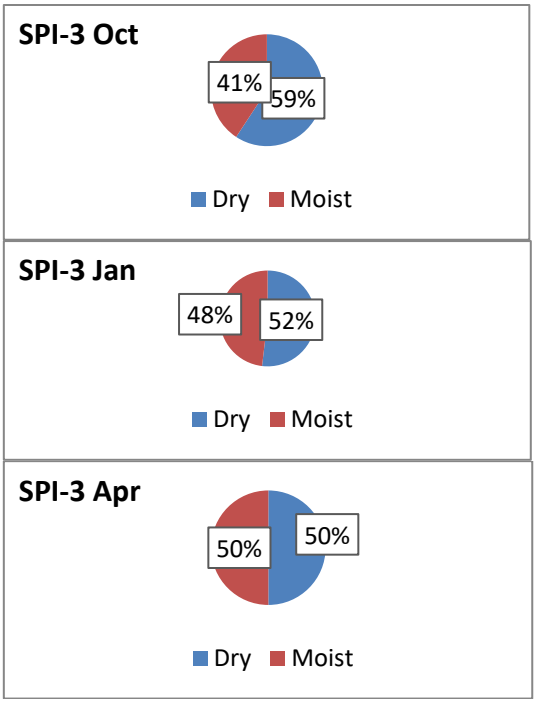

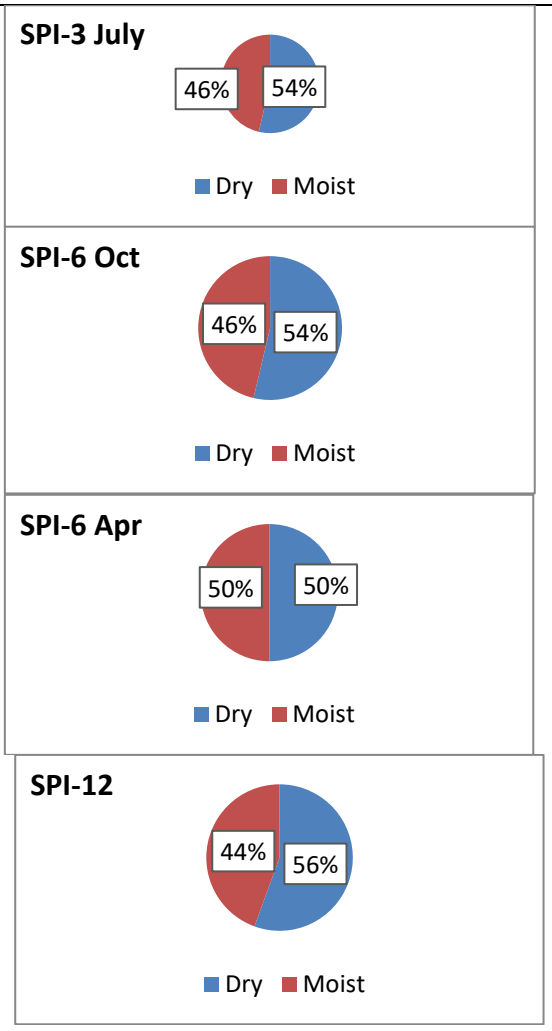

Figure 6. Dry - moist period distributions according to the 3,6,12month SPI values for the SINOP station (No. 17026)Form 1965 to 2019.

4. Conclusion

According to the precipitation efficiency index, the climate types in BARTIN are in the humid

ISBN 978-9959-9703-2-9

climate class, and there is no change. Work according to the evaluation of the temperature index on the basis of annual evaporation In the 54-year period between 1965 and 2019, the average-temperature climate type is observed quite consistently. Offers. The classification of drought index designed for rainy climates is generally in the summer period in BARTIN. One of the biggest impacts of global climate change occurs on precipitation, This is the case in some areas. While causing drought due to lack of precipitation; Some floods and overflow as a result of extreme rains in regions manifest itself. In this study, the climate The effect of the change in the West Black Sea Basin is innovative. It was investigated by the SPI method. This method is based on the precipitation of the basin, applied to the data. This precipitation data Obtained from the General Directorate of Meteorology Affairs. In the SPI analysis of all stations on a monthly basis, in Bartin station it is found that Dec, Nov, Feb is drier with 59% ratio and for Kastamonu station it was recorded that Nov was drier with 73%, at Sinop station it is discovered that Nov was drier than other months with 74%. In calculating SPI-3 for all stations based on the monthly rainfall data in SINOP station the highest value for drought in SPI3-1 Oct in 59% extremely dry, , and the highest value for BARTIN in SPI3-1 October In 59% exceptionally moist. Was in SPI3-4 July in 1985-1986 exceptionally moist. In calculating SPI-6 for all stations in BARTIN station, the highest value of dryness and humidity is observed in SPI6-2 in Apr, the highest value of drought in 52% extremely dry and the highest value of humidity in 55 exceptionally moist; and the highest value of humidity is in the54% in Oct, exceptionally moist; in SINOP station, the highest value of drought was in SPI6-2 in April in the year 1983-1984 exceptionally dry. SPI-12 values range between 50-57% in all the mentioned stations.

REFERENCES

1. Marimon, Cristina Domingo. "Contributions to the knowledge of the multitemporal spatial patterns of the Iberian Peninsula droughts from a Geographic Information Science perspective." *Geofocus: Revista Internacional de Ciencia y Tecnología de la Información Geográfica*" 17: 9 (2016).

2. Palmer, W.C., "Meteorological drought", ***US*** *Department of Commerce, Weather Bureau,* USA, 20-25 (1965).

3. McKee, T. B., Doesken, N. J., & Kleist, J., "The relationship of drought frequency and duration to time scales", *In Proceedings of the 8th Conference on Applied Climatology*, Colorado, USA, 179-183 (1993).

4. Nalbantis, I., "Evaluation of a hydrological drought index", *European Water***,** 23(2): 67-77 (2008).

5. Wilhite, D. A., & Glantz, M. H., "Understanding: the drought phenomenon: the role of definitionsv, *Water International***,** 10(3): 111-120 (1985).

6. Şen, Z., 2009, Kuraklık Afet ve Modern Hesaplama Yöntemleri, Su Vakfı Yayınları, İstanbul, 248s. Şen, Z., "İklim değişikliği içerikli taşkın afet ve modern hesaplama yöntemleri", *Su Vakfı Yayınları***,** Istanbul, 248 (2009).

7. Wilhite, D. A., "Drought as a natural hazard: concepts and definitions", *Routledge***,** London, 34-41 (2000).

8. Van Loon, A. F., "Hydrological drought explained", *Wiley Interdisciplinary Reviews: Water***,** *2*(4): 359-392 (2015).

9. Aksoy et al., "Drought Analysis in Gediz Basin", *Scientific Congress of the Turkish*

 ISBN 978-9959-9703-2-9

National Union of Geodesy and Geophysics (TUJJB), İzmir, 28-31 (2018).

10. Al-Faraj, Furat AM, and Bassam NS Al-Dabbagh. "Assessment of collective impact of upstream watershed development and basin-wide successive droughts on downstream flow regime: The Lesser Zab transboundary basin." *Journal of Hydrology*" 530: 419-430, (2015).
11. Tigkas D, Vangelis H, Tsakiris G. 2012. "*Drought and climatic change impact on stream flow in small watersheds*". Sci. Total Environ. 440: 33–41
12. Veysel Gumus , "*Spatio temporalprecipitation and temperature trend analysis of the Seyhan – Ceyhan River Basins, Turkey, Meteorological Applications*", 10.1002/met.1768, **26**, 3, (369-384), (2019).
13. Yenigun, Kasım, and Wlat A. Ibrahim. "Investigation of drought in the northern Iraq region." *Meteorological Applications* "26.3: 490-499 (2019).
14. Gujarati, D. N. (2004). "*Basic Econometrics (4. Baskı)* " New York : The Mc-Graw Hill Companies.
15. Bayazıt M., Yeğen Oğuz E.B., (2005), "*Mühendisler için İstatistik, Birsen Yayınevi*", İstanbul, 198ss.
16. Tsakiris, G., Vangelis, H., & Tigkas, D., "*Drought impacts on yield potential in rainfed agriculture*", *In Proceedings of 2nd International Conference on Drought Management Economics of Drought and Drought Preparedness in A Climate Change Context*, Greece, 4-6 (2010).

McKee, T. B., Doesken, N. J., & Kleist, J., "*The relationship of drought frequency and duration to time scales*", *In Proceedings of the 8th Conference on Applied Climatology*, Colorado, USA, 179-183 (1993).

 ISBN 978-9959-9703-2-9

المؤتمر الدولي الثاني للعلوم والهندسة
2nd International Conference on Science and Engineering
ICSE 2023
Faculty of Engineering - University of Bani Waleed
Bani Waleed, Libya

Paper Code: ICSE-016

COMPARISON OF ENSEMBLE LEARNING ALGORITHMS IN PREDICTING HEART DISEASE

Bader N. Awedat [a], Ali M. Abumrfgh [b]
[a] computer science, faculty of Information Technology / Azzaytuna University, Libya
[b] Computer science, faculty of Information Technology / Azzaytuna University, Libya
*Corresponding author: bader_najep@yahoo.com

Abstract: The main objective of this research is enhancing accuracy of predictive analysis for cardiovascular diseases (CVDs) through the implementation of ensemble learning algorithms. Ensemble learning is a strong approach that combines predictions from multiple models to amelioration overall performance. In this research, we compare the effectiveness of three ensemble learning algorithms: Random Forest, AdaBoost, and Stacking. We evaluate their performance using five criteria: Recall, Precision, F-score, Roc Auc, and Accuracy. The obtained results indicate that the AdaBoost algorithm has achieved the highest performance in the field of diagnosis using the available data. This signifies the high effectiveness of this algorithm in disease prediction and diagnosis. It is also notable that the Stacking algorithm has demonstrated strong performance, particularly in comparison to the Random Forest algorithm. Other performance standards such as Accuracy, Recall, Cohen's kappa, F-measure, Precision, and Specificity also exhibit good performance for the different algorithms. The ROC Curve metric reveals that the AdaBoost algorithm has attained the highest value (97.64), indicating its capability to effectively discriminate between true and false instances.

Keywords: Bagging, Boosting, Ensemble learning, ROC curve, Stacking

Introduction

Cardiovascular diseases (CVDs) are a significant global cause of mortality, accounting for approximately 17.9 million deaths annually, representing 31% of all global deaths. The majority of these deaths result from heart attacks and strokes, with a significant proportion occurring prematurely in individuals under the age of 70. This presents a major public health concern that necessitates attention and effective preventive measures. CVDs frequently lead to heart failure, and the provided dataset contains 13 features that can be utilized to predict the possibility of heart disease. [1]

Heart failure is commonly observed as a result of cardiovascular diseases. This dataset comprises 13 features that aid in predicting the likelihood of heart disease. Early detection and effective management are essential for individuals with cardiovascular disease or those at a high risk of developing it, given the presence of risk factors like hypertension, diabetes, hyperlipidemia, or pre-existing conditions. Machine learning models can

 ISBN 978-9959-9703-2-9

significantly contribute to addressing this issue.

Ensemble learning improves performance by creating and combining multiple distinct base learners using dedicated approaches. These individual models are commonly referred to as base learners, while the process of combining them is known as integration strategy. In the context of combining multiple models to improve predictive performance, ensemble learning techniques are employed. In this approach, the individual performance of each base learner doesn't need to be exceptionally strong; rather, it should surpass random guessing. Based on how the base learners are generated, ensemble learning methods can be broadly classified into two categories: 1. Parallel methods, such as Bagging, and 2. Sequential methods, such as Boosting. [2]

The concept of "wisdom of the crowd" involves merging multiple weak models or learners into a single predictive model. This methodology aims to address bias, reduce variance, and enhance accuracy by leveraging the collective knowledge and predictions of the individual models.

The aim of this research is to improve the accuracy of predictive analysis for heart disease. While individual machine learning models may have limitations in their prediction capabilities, ensemble learning methods, such as collaborative learning, strive to address this issue by training multiple models successively to enhance the overall accuracy of the system. Additionally, ensemble learning approaches are well-suited for datasets of different sizes, making them effective in data mining tasks. These methods have demonstrated promising performance in tackling the challenges of variance and bias that are commonly encountered in data mining algorithms. In our study, we specifically concentrate on the complex task of heart disease prediction and diagnosis, which involves understanding various contributing factors.

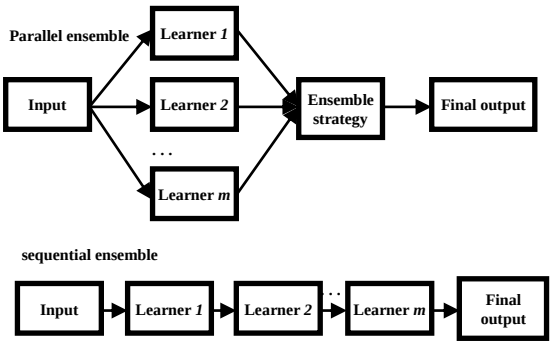

Fig. 1: Flowchart of Parallel and Sequential ensemble.[2]

Related Work

A concise overview of recent research papers comparing various machine learning algorithms and examining their outcomes.

In the study conducted by Madhumita Pal and Smita Parija [3], the random forest algorithm was employed to predict heart disease. The researchers utilized a dataset comprising 13 features for their analysis. The obtained results revealed an accuracy of 86.9%, a sensitivity value of 90.6%, and a specificity value of 82.7%. The receiver operating characteristics analysis demonstrated a diagnosis rate of 93.3% for heart disease prediction using the random forest algorithm. These findings highlight the high effectiveness of the random forest

 ISBN 978-9959-9703-2-9

algorithm in accurately classifying heart disease [3].

In a recent study conducted by Asfandyar Khan et al. [4], a novel ensemble approach known as the 'Stacking Classifier' was proposed to enhance the performance of integrated individual classifiers and reduce the likelihood of misclassification for individual instances. The Stacking Classifier utilizes Random Forest and SVM as meta-classifiers. The experimental results indicated that the proposed stacking classifier achieved a remarkable accuracy of 0.9735 percent in diagnosing diabetes, surpassing the performance of existing models such as Naive Bayes (0.7646 percent), KNN (0.7460 percent), DT (0.7857 percent), and LDA (0.7735 percent). Similarly, in the context of cardiovascular disease, the suggested stacking classifier demonstrated superior performance compared to current models, including KNN (0.8377 percent), NB (0.8256 percent), DT (0.8426 percent), LDA (0.8523 percent), and SVM (0.8472 percent). The stacking classifier achieved a higher accuracy of 0.8871 percent [4].

T. R. Mahesh, et al [5], the researcher used the synthetic minority over-sampling technique (SMOTE). The results of the study indicate that the AdaBoost-Random Forest classifier achieves a high accuracy of 95.47% in the early detection of heart disease.

Md. Maidul Islam, et al [6], In this research, 9 algorithms were compared, including 5 Ensemble Learning algorithms, and gave the best results, the best of which was the stack algorithm.

The Stacked Ensemble Classifier showcases outstanding performance, achieving an accuracy of 0.910, sensitivity of 0.934, specificity of 0.883, best F1-score of 0.916, minimum Log Loss of 3.08, and the highest ROC value of 0.909 [6].

Among the various evaluated metrics, Random Forest demonstrates the highest sensitivity, followed by XGBoost [6]. The Stacked Classifier model attains an accuracy of 91.06%, along with an F1 score of 0.9163. In comparison, the XGBoost and Random Forest algorithms achieve accuracies of 89.78% and 89.36%, respectively, with corresponding F1 scores of 0.8972 and 0.8911. The Extra Tree Classifiers, CART, GBM, MLP, SVC, and KNN algorithms exhibit accuracies of 88.51%, 85.10%, 82.97%, 82.12%, 81.27%, and 80.00%, respectively [6].

Types of Ensemble Learning:

1.Bagging:

In the ensemble learning approach called "majority voting," multiple weak models (N in total) are trained in parallel using non-overlapping subsets of the input dataset. In the testing phase, each model is assessed individually, and the label that receives the highest number of predictions is chosen as the final prediction. This approach aims to merge the predictions from multiple models to achieve a more robust and accurate prediction.

2.Boosting:

Boosting is a machine learning technique that trains N different weak models sequentially on the entire dataset. These weak models are typically of the same type (homogeneous). In each iteration, data points that were misclassified by the previous weak model are assigned higher weights to prioritize their correct classification by the subsequent weak learner. During the testing phase, the predictions of each model are combined by assigning weights based on their test error, enabling a voting mechanism. Boosting methods are known to effectively reduce prediction bias.

3.Stacking:

In the ensemble learning approach, multiple weak models (N in total) are trained simultaneously, often of different types

 ISBN 978-9959-9703-2-9

(heterogeneous). This training process is performed using one subset of the dataset. Once the weak models are trained, a meta learner is trained using their predictions to perform the final prediction. The meta learner utilizes the other subset of the dataset. During the testing phase, each individual model predicts its label, and these predicted labels are combined and provided to the meta learner, which generates the ultimate prediction.

Materials and Methods:

We employed group learning algorithms to predict heart failure diseases, including the utilization of the random forest algorithm and AdaBoost. Additionally, we incorporated four stacked algorithms for enhanced performance. The applied algorithms in this study are based on the analysis of a Heart Failure dataset obtained from the Kaggle repository. The dataset comprises 304 patient samples, each representing medical records. The heart failure dataset includes a wide range of features. To enhance the algorithm performance, a comprehensive analysis of these features is conducted, considering factors such as importance scores, accuracy, sensitivity, and specificity. The dataset was split into a training set comprising 70% of the data and a testing set comprising the remaining 30%.

In this study, Google Colab Notebook was utilized as the simulation tool for conducting the experiments and constructing the models. Google Colab Notebook is a convenient platform for Python programming projects, offering a wide range of features such as rich text components, code integration, and real-time data analysis capabilities. It enables the seamless integration of descriptive analysis, findings, equations, and visualizations. Similar to Jupyter Notebook, Google Colab Notebook provides a web-based interactive interface for creating and sharing interactive graphics, maps, plots, visualizations, and narrative texts. This tool proved to be invaluable in facilitating the analysis process and enhancing the efficiency of the research workflow. Moreover, Google Colab Notebook is an open-source tool, making it accessible and freely available for researchers.

Five features were used out of a total of 13 features in our study. These features are as follows: Age, resting blood pressure (trestbps), Cholesterol level (chol), Maximum heart rate achieved (thalach, ST depression induced by exercise relative to rest (oldpeak).

In addition, the target feature was utilized to determine the presence (1) or absence (0) of heart disease."

Ensemble techniques:
Ensemble techniques refer to methods that employ multiple learning algorithms or models to create an optimal predictive model. The resulting model exhibits superior performance compared to the individual base learners used independently. Ensemble learning has various other applications, such as feature selection and data fusion, among others. Additionally, ensemble techniques can be categorized into three main types: Bagging, Boosting, and Stacking.

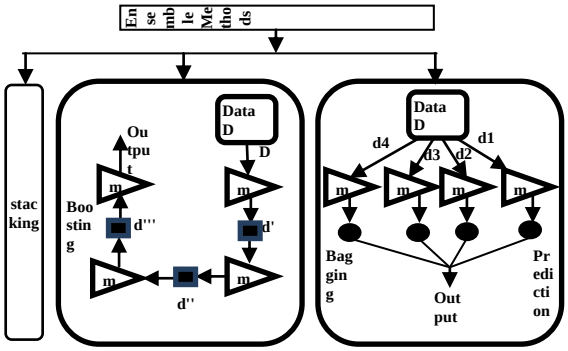

Fig. 2: Representing the types of ensemble methods.[7]

1.Bagging (Bootstrap Aggregating):

 ISBN 978-9959-9703-2-9

Bagging is a short form of bootstrap aggregating. It is an ensemble technique that divides a dataset into n samples with replacement. The dataset is divided into n samples, and each sample is trained individually using separate machine learning models. Then the output of all the separate models is combined into one single output by using voting (Figure 3). [8]

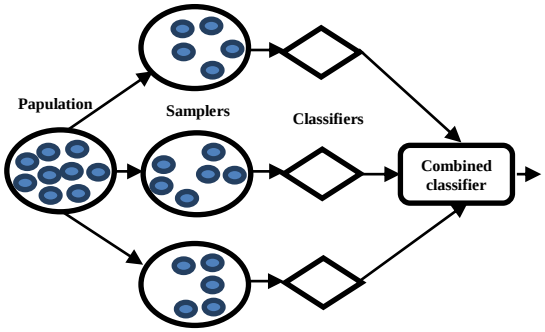

Fig. 3: Bagging with sampling [8]

Random Forest (RF) is a powerful machine learning technique that employs an ensemble of decision trees to tackle classification and regression problems. It combines multiple decision trees using bootstrap sampling, and the final classification or regression outcome is determined through majority voting or averaging [9][10]. RF is widely recognized for its robustness in handling imbalanced, missing, and multicollinear data [2][9]. The analysis process consists of two stages:

Stage 1: The random forest is constructed by randomly selecting samples with replacement from the initial dataset (training data). Subsets are created, and regression trees are built based on these smaller datasets. During the training stage, various parameters can be adjusted, including the number of variables (mtry) and the number of trees (ntree).

Stage 2: Once the random forest model is trained, predictions can be generated. The input variables for each regression tree are combined, and the final prediction is obtained by averaging the predictions from all the trees [10].

Majority Voting, also known as Hard Voting, is a classification technique in which the predicted class label $\hat{y}$ is determined by taking the majority vote of multiple classifiers C_j. In other words, the class label that is predicted by the majority of the classifiers is selected as the final prediction:

$$\hat{y} = mode\ \{C_1(x), C_2(x), \ldots., C_m(x)\}\ [11]$$

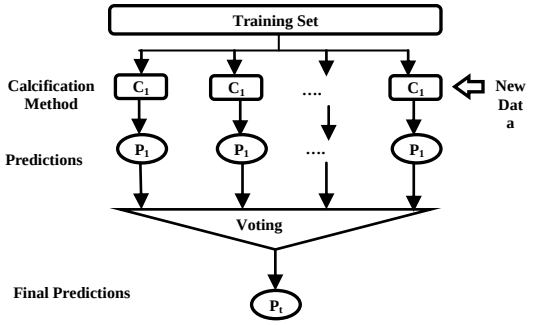

Fig. 4: Random Force Algorithm. [12]

2.Boosting:

There are primarily three types of boosting algorithms commonly used in Machine Learning:

- AdaBoost algorithm,
- Gradient descent algorithm,
- Xtreme gradient descent algorithm [7].

In 1995, Freund and Schapire introduced the Adaboost (adaptive boosting) algorithm. This algorithm operates by adjusting weights without requiring any prior knowledge of the learner's training process [13].

ISBN 978-9959-9703-2-9

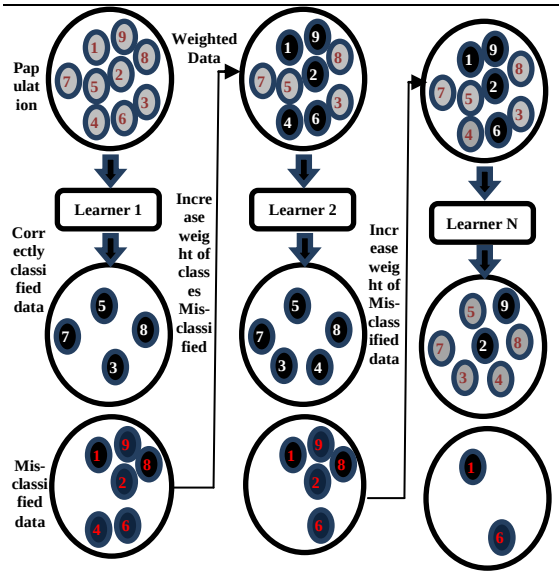

Fig. 5: AdaBoost boosting. [8]

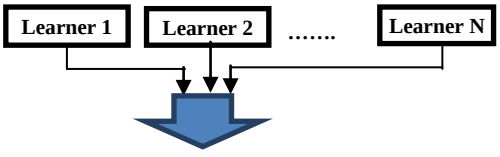

Fig. 6: Voting of n learners in AdaBoost boosting.[8]

Basic Algorithm for Boosting:

1. **Initialize:** set all examples to have equal weights
2. **For each** t = 1, …, T,
3. Learn a hypothesis h_t from weighted examples
4. **Decrease weights** of examples h_t classifies **correctly**
5. Calculateα_t, the weight of the current weak learner, h_t
6. $\boldsymbol{Return}\ h(x) = \sum_{t=1}^{T} \alpha_t\ h_t(x)$

3.Stacking:

Stacking is a powerful technique for combining predictions in ensemble learning. It involves training multiple models, referred to as base learners, to generate individual predictions. These predictions are then used as input for another model, known as the meta learner or aggregator, which learns to combine the base learners' predictions (Figure 7). Think of stacking as building a stacked architecture of machine learning models, where each layer learns to aggregate the predictions of the previous layer. Unlike traditional ensemble methods that use simple functions like majority voting to aggregate predictions, stacking leverages a model to perform this aggregation, resulting in improved performance and flexibility.

ISBN 978-9959-9703-2-9

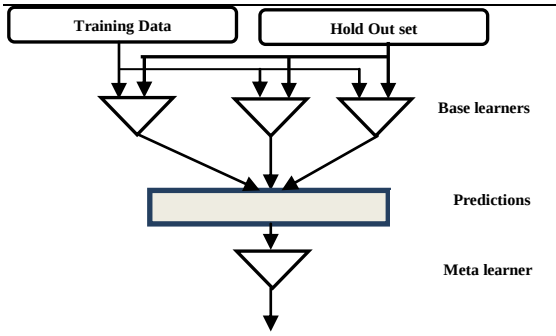

Fig. 7: Stacking. [8]

Stacking Algorithms: Two algorithms, xgboost and random forest, were used as stack algorithms and Logistic Regression was used as mate algorithm.

Dataset Description

The Heart Failure Dataset utilized in this study is sourced from the Kaggle platform [14]. The dataset used in this study is a combination of five distinct datasets, resulting in a comprehensive and diverse collection of attributes. Specifically, we focused on employing attributes that are highly relevant in predicting a patient's heart condition for this specific experiment. Furthermore, the dataset file comprises 13 medical variables for a total of 304 patients. A comprehensive description of each attribute, along with the respective value count, is presented in Table 1. The exploratory data analysis is further depicted in Table 2, accompanied by a figure illustrating the features with less than 5 columns, and another figure displaying the features with more than 5 columns. The heatmap representation can be observed in Figure 2.

Table 1. Description of Features

N.	Features	Description
1	Age	"The age of the individual, expressed in years". (Source: Ramadan A.M. Elghalid et al., 2022)
2	Sex	"The gender of the person, represented as a binary variable where 1 indicates male and 0 indicates female". (Source: Ramadan A.M. "Elghalid et al., 2022)
3	chest_pain_type	"0: asymptomatic 1: atypical angina 2: non-angina pain 3: typical angina" (Source: Ramadan A.M. Elghalid et al., 2022)
4	RestingBP	"The person's resting blood pressure upon admission to the hospital, measured in millimeters of mercury (mm Hg)". (Source: Ramadan A.M. Elghalid et al., 2022)
5	Cholesterol	"The measurement of the person's cholesterol level, expressed in milligrams per deciliter (mg/dL)". (Source: Ramadan A.M. Elghalid et al., 2022)
6	FastingBS	"Indicates whether the person has a fasting blood sugar level higher than 120 mg/dL. It is represented as a binary variable, where 1 indicates true (blood sugar > 120 mg/dL) and 0 indicates false (blood sugar ≤ 120 mg/dL)". (Source: Ramadan

 ISBN 978-9959-9703-2-9

7	RestingECG	A.M. "Elghalid et al., 2022) Resting Electrocardiographic Results: 0: Indicates probable or definite left ventricular hypertrophy based on Estes' criteria. 1: Represents a normal resting electrocardiogram. 2: Indicates the presence of ST-T wave abnormalities, such as T wave inversions and/or ST elevation or depression exceeding 0.05 mV". (Source: Ramadan A.M. "Elghalid et al., 2022)
8	MaxHR	The maximum heart rate achieved by an individual". (Source: Ramadan A.M. Elghalid et al., 2022)
9	ExerciseAngina	"The presence of exercise-induced angina, represented by a value of 1 for 'yes' and 0 for 'no". (Source: Ramadan A.M. Elghalid et al., 2022)
10	Oldpeak	"The magnitude of ST depression induced by exercise relative to rest. Note that 'ST' refers to specific positions on the ECG plot. For more information, please refer to the provided resource". (Source: Ramadan A.M. "Elghalid et al., 2022)
11	ST_Slope	The slope of the peak exercise ST segment: 0: Represents a downsloping ST segment. 1: Indicates a flat ST segment. 2: Indicates an upsloping ST segment". (Source: Ramadan A.M. "Elghalid et al., 2022)
12	Heart Disease	The Target (1 = no, 0= yes)". (Source: Ramadan A.M. Elghalid et al., 2022)

Table 2. Exploratory data analysis

age	sex	cp	trestbps	chol	fbs	restecg	thalach	exang	oldpeak	slope	ca	thal	target
63	1	3	145	233	1	0	150	0	2.3	0	0	1	1
37	1	2	130	250	0	1	187	0	3.5	0	0	2	1
41	0	1	130	204	0	0	172	0	1.4	2	0	2	1
56	1	1	120	236	0	1	178	0	0.8	2	0	2	1
57	0	0	120	354	0	1	163	1	0.6	2	0	2	1
...	...	...	...	...	...	...	...	...	...	...	...	...	...
57	0	0	140	241	0	1	123	1	0.2	1	0	3	0
45	1	3	110	264	0	1	132	0	1.2	1	0	3	0
68	1	0	144	193	1	1	141	0	3.4	1	2	3	0
57	1	0	130	131	0	1	115	1	1.2	1	1	3	0
57	0	1	130	236	0	0	174	0	0.0	1	1	2	0

303 rows × 14 columns

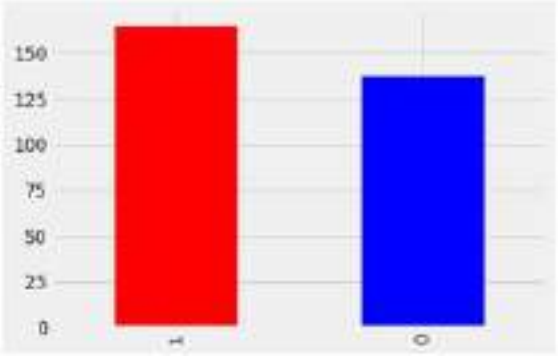

Fig. 8: Percentage of Heart Disease

ISBN 978-9959-9703-2-9

We have 165 persons with heart disease and 138 persons without heart disease, so our problem is balanced. [Kaggle Inc]

Fig. 9: Heatmap depiction of the dataset.

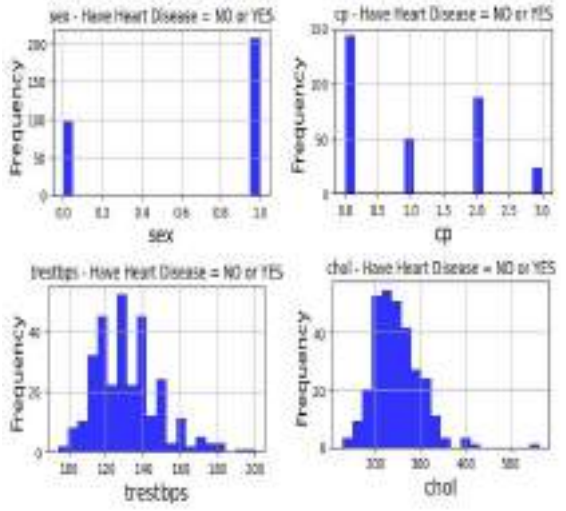

Fig. 10: Properties with less than 5 variables.

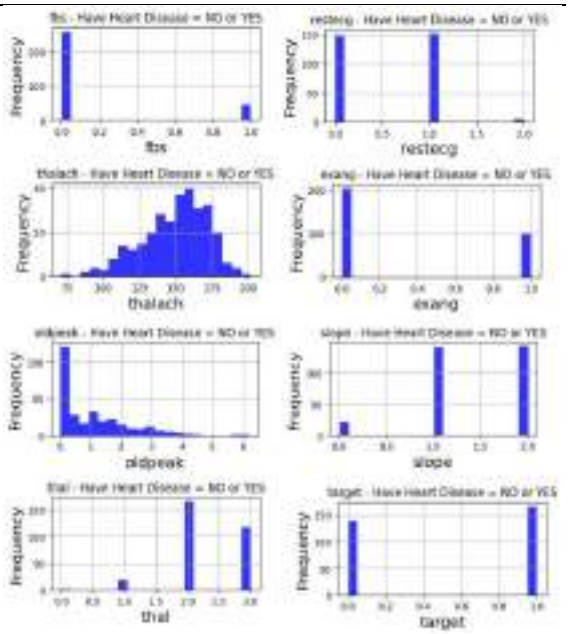

Fig. 11: Properties that have more than 5 variables.

Evaluation Metrics:

The dataset is divided into two subsets for evaluation purposes: the training dataset and the test dataset. The training dataset is used to construct the classifier, while the test dataset is employed for prediction using the trained classifier. Typically, this split allocates 80% of the data for the training dataset and 20% for the test dataset.

Table 3. Exploratory data analysis

		Predicted Class	
Actual Class	Total population = P + N	Positive (PP)	Negative (PN)
	Positive (P)	True positive (TP)	False negative (FN)
	Negative (N)	False positive (FP)	True negative (TN)

ISBN 978-9959-9703-2-9

True Positive (TP): Represents the number of correctly classified positive instances.

False Negative (FN): Indicates the number of positive instances incorrectly classified as negative.

False Positive (FP): Refers to the number of negative instances incorrectly classified as positive.

True Negative (TN): Represents the number of correctly classified negative instances.

Accuracy: It represents the percentage of test tuples that are correctly classified.[15]

$$\text{Accuracy} = \frac{\text{Number of correct predictions}}{\text{Total Number of predictions}} \text{ [15]}$$

Precision: Measures the exactness of a classifier by calculating the percentage of positive predictions that are correct in relation to the total positive predictions [16].

$$\text{Precision} = \frac{TP}{TP+FP} \text{ [16]}$$

Recall: also referred to as sensitivity or true positive rate, is a metric that quantifies the completeness of a classifier by calculating the percentage of actual positive tuples in the test dataset that the classifier correctly identifies as positive.[16].

$$\text{Recall} = \frac{TP}{TP+FN} \text{ [16]}$$

F1-Score: The F1-Score is a measure that combines precision and recall using their harmonic mean.[16]

$$F1 = \frac{2*\text{Precision}*\text{recall}}{\text{Precision}*\text{recall}} \text{ [16]}$$

Performance Analysis of Classifiers using Area under the ROC Curve: The AUC-ROC is a crucial metric used to evaluate the accuracy of classifiers.

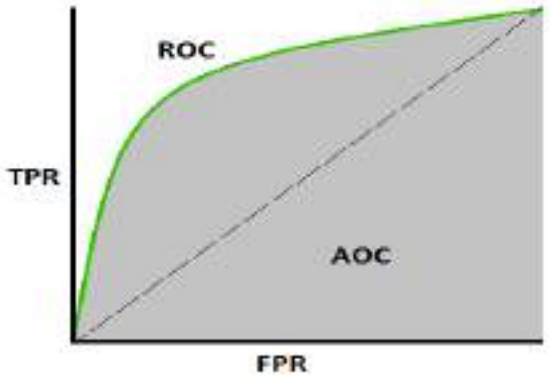

Fig. 12: ROC Curve

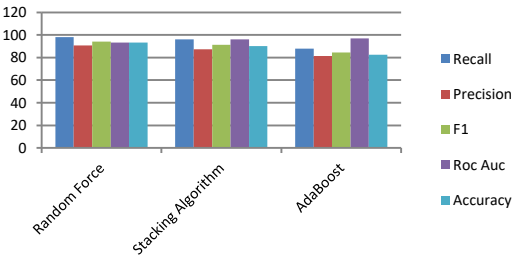

Fig. 13: Weighted average recall, precision, F-score, ROC AUC, and accuracy of the cardiovascular diseases dataset.

ISBN 978-9959-9703-2-9

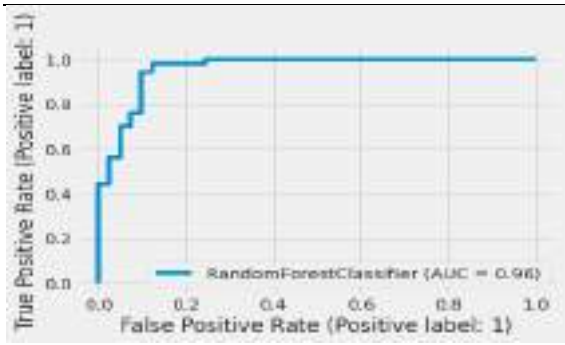

Fig. 14: ROC Curve for Random Forest Model.

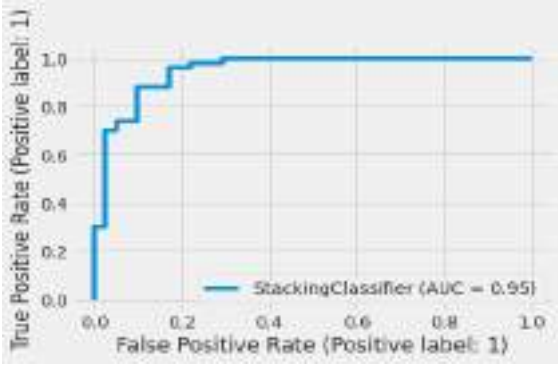

Fig. 15: ROC Curve for Stacking Model.

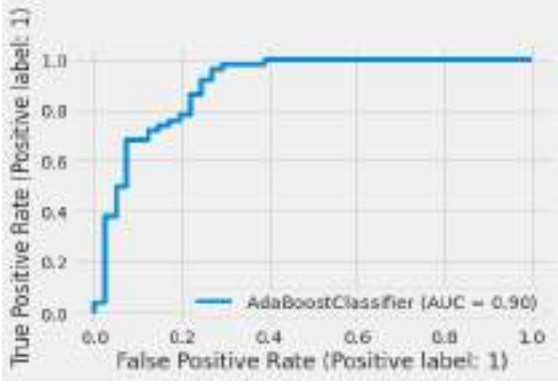

Fig. 16: ROC Curve for AdaBoost Model.

Results:

By working on the Heart Failure dataset using Python and machine learning libraries, the findings were as follows

In Table4, Table 5, the algorithms were compared in terms of Accuracy, Precision, Recall, F1-Score, ROC curve and it was found that all algorithms are equal in the total of True Positive and False Positive and the highest Accuracy of the AdaBoost Algorithm was the same as that given by ROC curve, which means that the model is able to predict the correct positive states TPR and predict the correct negative states FPR significantly.

While the Stacking Algorithm gave the lowest result and was Accuracy=84.61 while ROC curve=98.0 which means that the model is unable to predict the correct positive states TPR and predict the correct negative states FPR correctly.

Table 4. Compare Train Result of algorithms.

	Random Force Algorithm	Stacking Algorithm	AdaBoost Algorithm
TP	76	97	95
FP	21	0	2
FN	11	0	3
TN	104	115	112
Accuracy	84.91	100	97.64
Recall	90.43	100	97.39
Cohen's kappa(k)	69.34	100	95.25
F-measure	86.67	100	97.82
Precision	83.20	100	97.25
Specificity	78.35	100	97.94
Sensitivity	90.34	100	97.39
ROC Curve	91.91	100	99.56

Table 5. Compare Test Result of algorithms.

ISBN 978-9959-9703-2-9

	Random Force Algorithm	Stacking Algorithm	AdaBoost Algorithm
TP	36	30	31
FP	5	11	10
FN	1	3	6
TN	49	47	44
Accuracy	93.41	84.61	97.64
Recall	98.0	94.0	88.0
Cohen's kappa(k)	86.56	68.37	68.37
F-measure	94.23	87.03	84.61
Precision	90.74	81.03	81.48
Specificity	90.0	81.03	80.0
Sensitivity	98.0	94.0	88.0
ROC Curve	93.19	0.98	97.64

Discussions

Based on the presented results, we can highlight some potential discussions and conclusions:

1. AdaBoost Algorithm Performance: The AdaBoost algorithm demonstrates excellent performance in the evaluation of heart failure-related diseases. With high accuracy, recall, and precision rates observed in both the training and testing datasets, the algorithm showcases its strong ability to accurately identify such conditions.

2. Stacking Algorithm Performance: Although the Stacking algorithm demonstrated ideal performance in the training dataset, its performance was slightly lower in the testing dataset. Two algorithms, Random Forest and XGB, were used as the stack, with Logistic Regression as the output. The small number of stacked algorithms may be the reason behind this performance difference.

3. Random Forest Algorithm Performance: The results show that the Random Forest algorithm has achieved good performance but slightly lower than AdaBoost in the testing dataset. There may be a need to review and improve the factors influencing the performance of this algorithm.

4. Importance of Feature Analysis and Selection: Based on the use of only five features out of a total of 13 in the study, it can be said that accurate feature analysis and selection play a significant role in improving the performance of algorithms. Further studies should be considered for more analysis and verification of the importance of different features.

5. Statistical Metrics Performance: The values of statistical metrics such as Cohen's kappa and F-measure indicate that the statistical models used have a good ability to predict heart failure-related cases. There may be additional improvements to be considered to enhance the values of these metrics.

Conclusion

In this paper, 3 Ensemble learning algorithms were compared and the AdaBoost algorithm gave the highest prediction in the dataset cardiovascular diseases (CVDs). It can be said that in diagnosing diseases using data mining algorithms, it is not possible to rely on Accuracy scales as a measure of the model's accuracy in prediction, the important thing is to know the degree to which the model fully understands the positive correct and negative correct states to give a correct and reliable accuracy ratio. The AdaBoost algorithm has proven to work in medical datasets more than the Random Force Algorithm and the Stacking Algorithm.

Arabic section:

مقارنة خوارزميات التعلم الجماعي في تنبؤ أمراض القلب

ISBN 978-9959-9703-2-9

بدر نجيب عويدات، علي ابومرفق

الملخص: يهدف هذا البحث إلى تحسين دقة التحليل التنبؤي لأمراض القلب والأوعية الدموية (CVDs) من خلال تنفيذ خوارزميات التعلم الجماعي. التعلم الجماعي هو نهج قوي يجمع بين التنبؤات من عدة نماذج لتحسين الأداء العام. في هذه الدراسة، نقارن فعالية ثلاث خوارزميات للتعلم الجماعي: الغابة العشوائية (Random Forest)، وخوارزمية التعزيز التكيفي (AdaBoost)، وخوارزمية المكدس (Stacking). سيتم تقييم أدائها باستخدام خمسة معايير: الاستدعاء (Recall)، الدقة (Precision)، مقياس (F-score)، ومنحنى AUC-ROC، ونسبة صحة خوارزمية التصنيف (Accuracy). تشير النتائج التي توصلنا إليها إلى أن خوارزمية AdaBoostقد حققت الأداء الأعلى في مجال التشخيص باستخدام البيانات المتاحة. وهذا يشير إلى فعالية عالية لهذه الخوارزمية في التنبؤ وتشخيص الأمراض. ويمكن ملاحظة أن خوارزمية Stacking أظهرت أداءً قويًا أيضًا، خاصة في مقارنتها بخوارزمية Random Forest. معاملات الأداء الأخرى مثل Accuracy، Recall، Cohen's kappa، F-measure، Precision، و Specificity، تظهر أيضًا أداءً جيدًا للخوارزميات المختلفة. يظهر معامل ROC Curve أن خوارزمية AdaBoostحققت أعلى قيمة (97.64)، مما يشير إلى قدرتها على التمييز بين الصحيح والخاطئ بشكل فعال.

الكلمات المفتاحية: التكييس، التعزيز، تعليم المجموعات، منحنى الاستجابة التشغيلية، المكدس.

Abbreviations and Acronyms

CVDs: cardiovascular diseases. SMOTE Technique: SMOTE stands for Synthetic Minority Over-sampling Technique. ROC Curve: ROC refers to Receiver Operating Characteristic. XGB Algorithm: XGB stands for Extreme Gradient Boosting, CART Algorithm: CART stands for Classification and Regression Trees. GBM: Gradient Boosting Machine. MLP: Multi-Layer Perception. SVC: Support Vector Machine. KNN: K-Nearest Neighbors. TP: True Positive, FN: False Negative. FP: False Positive. TN: True Negative, AUC-ROC (Area Under the Receiver Operating Characteristic Curve)

References

[1] Kaggle David Lapp, 2019, Heart Disease Dataset, Kaggle, Date Access 29-9-2022, direct Link: https://www.kaggle.com/datasets/johnsmith88/heart-disease-dataset,

[2] Yiheng Li, Weidong Chen. A Comparative Performance Assessment of Ensemble Learning for Credit Scoring. Mathematics 2020, 8, 1756.

[3] Madhumita Pal, Smita Parija, 2021, Prediction of Heart Diseases using Random Forest, J.Phys.:Conf.Ser.1817 012009.

[4] Asfandyar Khan,. et al, Cardiovascular and Diabetes Diseases Classification Using Ensemble Stacking Classifiers with SVM as a Meta Classifier, Diagnostics, 2022, https://doi.org/10.3390/diagnostics12112595

[5] T. R. Mahesh, et al, AdaBoost Ensemble Methods Using K-Fold Cross Validation for Survivability with the Early Detection of Heart Disease, Computational Intelligence and Neuroscience ، Volume 2022.

[6] Md. Maidul Islam, Tanzina Nasrin Tania, Sharmin Akter, and Kazi Hassan Shakib, 2022, An Improved Heart Disease Prediction Using Stacked Ensemble Method, CC BY-NC-ND 4.0.

[7] Yash Khandelwal, 2021, Ensemble Stacking for Machine Learning and Deep Learning, Analytics Vidhya, Date Access 2-9-2022, direct Link: https://www.analyticsvidhya.com/blog/2021/08/ensemble-stacking-for-machine-learning-and-deep-

[8] Alok Kumar, Mayank Jain, (2020), Ensemble Learning for AI Developers Learn Bagging, Stacking, and Boosting Methods with Use Cases, Apress, ISBN-13 (electronic): 978-1-4842-5940-5.

[9] Byeon, H. Exploring Factors for Predicting Anxiety Disorders of the Elderly Living Alone in South Korea Using Interpretable Machine Learning: A Population-Based Study. Int. J. Environ. Res. Public Health 2021, 18, 7625.

[10] Ahmad, M., Kamiński, P., Olczak, P., Alam, M., Iqbal, M., Ahmad, F., Sasui, S., Khan, B. Development of Prediction Models for Shear Strength of Rockfill Material Using Machine Learning Techniques. Appl. Sci. 2021, 11, 6167.

[11] S. Raschka. Python Machine Learning. Packt Publishing Ltd, Third Edition, 2019.

[12] Dharmaraj Patil, Jayantrao Patil, 2018, Malicious URLs Detection Using Decision Tree Classifiers and Majority Voting Technique, Cybernetics and Information Technologies 18(1):11-29.

[13] Saini, A. (2021, September 15). Master the AdaBoost Algorithm: Guide to Implementing & Understanding AdaBoost. Analytics Vidhya. Retrieved January 15, 2023, from https://www.analyticsvidhya.com/blog/2021/09/adaboost-algorithm-a-complete-guide-for-beginners/

 ISBN 978-9959-9703-2-9

[14] Ramadan A.M. Elghalid, Ahmed Alwirshiffani, Abdelhafid Ali I. Mohamed, Fatimah Husayn, Amir Aldeeb, Aisha Andiasha. "Comparison of Some Machine Learning Algorithms for Some Machine Learning Algorithms for Predicting Heart Failure", 2022 International Conference on Engineering & MIS (ICEMIS.

[15] Muhammad Sakib Khan Inan, Istiakur Rahman, (2022), Integration of explainable artificial intelligence to identify significant landslide causal factors for extreme gradient boosting based landslide susceptibility mapping with improved feature selection., Machine Learning Applied to Geo-technical Engineering, arXiv, v1.

[16] Nabeela Ashraf1, Waqar Ahmad2, Rehan Ashraf3, A Comparative Study of Data Mining Algorithms for High Detection Rate in Intrusion Detection System, Annals of Emerging Technologies in Computing (AETiC) Vol.2, No.1, 2018.

 ISBN 978-9959-9703-2-9

المؤتمر الدولي الثاني للعلوم والهندسة
2nd International Conference on Science and Engineering
ICSE 2023
Faculty of Engineering - University of Bani Waleed
Bani Waleed, Libya

Paper Code: ICSE-007

A COMPUTERIZED SYSTEM FOR MONITORING AND INFORMING ABOUT ANY UNAUTHORIZED DRILLING OPERATIONS NEAR THE CABLES

Selah Abufana, Emad ZARGOUN
Computer Department College of science Bani waleed University Bani waleed/ Libya
Computer Department College of science Bani waleed University Bani waleed/ Libya
*Crosspnding author: emadzargoun@bwu.edu.ly

Abstract: The biggest challenge is to protect the cables in cities and villages from random excavations, as the protection of these cables by traditional methods such as concrete and some cement stones is not sufficient. It has become necessary to search for effective and alternative protection techniques that can protect the cables. In this paper, a novel method is proposed to design a drill monitoring system for early warning using fiber optic distributed acoustic sensing systems (DAS) based on phase OTDR. The proposed method has three stages. The first stage is to use buried fiber optic cable as a sensing system to detect any activity such as drilling or digging near the cable. The second stage is the processing system; in this stage, the sensed signal is de-noised using a wavelet transform, and then the difference is used for high pass filtering. This phase includes the autocorrelation to improve the interferometric visibility of the movements or threats near the goal area via a fiber optic cable. Moreover, the correlated signal power is computed and sent to the test and comparison stages. In the last stage, all signals are compared with a predefined threshold; if the average exceeds the threshold, the discrete signal is considered to be high, and there is drilling near cables; otherwise, the signals are considered to be undesired signals. Different types of activities were used at different SNR levels to assess the effects of the proposed method on detection performance. The results show the effectiveness of the used system for early drilling detection to protect the cables.

Keywords: (Acoustic sensing, DAS systems, sensing, monitoring system)

Introduction

The usage of fiber optic distributed acoustic sensing (DAS) in recent years has attracted extreme attention in the discipline of acoustic and vibration detection in current years. essentially, it's miles based on the measurement of Rayleigh scattered light, which happens while the light traveling in fiber optic cables scatters again alongside the sensor cable path because of imperfections (referred to as "scattering centers") measured at the sender end [1]. According to a theory, mechanical vibrations take place because of threat movements or physical activities, which happen around the buried fiber cable because they create fluctuations in the form of backscattered light. Researchers have

 ISBN 978-9959-9703-2-9

investigated such fluctuations and classified them. For this purpose, a phase-sensitive technique called "optical time-domain reflectometry (Phase-OTDR) was developed over the last 25 years to conduct distributed acoustic sensing [2, 3]. Contrary to the traditional OTDRs, Phase-OTDR pulses have coherent lights, which are transmitted through fiber optic cables; so, sensing is done through the relative phases of reflected fields of the scattering centers. For monitoring multi-point acoustic vibrations throughout a fiber cable, it gives an efficient method. For DAS, phase-sensitive OTDR is not only the used method in DAS system. Many other methods are used, which apply optical frequency domain reflectometry (OFDR). Both these major approaches differ based on the used detection method; some of them use direct detection while the other uses coherent (heterodyne) detection. The former is easier-to-implement because it uses a low-constraint optical signal as compared to the later. The coherent detection method assures a longer dynamic range and higher SNR [3]. The effectiveness of the DAS system can also be assessed by its different applications, for example, it is used in structural crack detection [4], railroad and safety monitoring [5, 6], Long Perimeter Monitoring [7], location information of intruder [8], structural health monitoring [2], intrusion detection and security mentoring [9, 14], detection performance improvement in complicated noisy environments [10, 11]. A backscattered signal, which is sensed in a phase-OTDR DAS system, has significantly lower signal-to-noise ratio (SNR) that influences the systems vibration detection [12], monitoring multiple dynamic events in real time [15], Networking of underwater acoustic sensors is the technology behind a wide range of applications including coastal surveillance, oil platform monitoring, earthquake and tsunami early warning [16].

Background (Literature Survey)

The method is a combination of correlation matching and Short Time Fourier Transform (STFT) to detect and analyze events using OTDR. This method achieves high accuracy and efficiency .

Continuous Wavelet Transform (CWT) has been proposed as another used method for detecting non-stationary signals using a distributed phase OTDR based vibration sensor. The time-frequency information regarding a event can be obtained through continuous wavelet transform methods. The wavelet ridge detection method gives information about the frequency evolution with the help of the CWT scalogram. This reported time-frequency analysis is a powerful tool for stationary/non stationary vibration signals in the system.

 ISBN 978-9959-9703-2-9

A technique called “curvelet de-noising” has been proposed for noise removal in the time domain, and also for improving the system’s detection performance using phase-sensitive optical time-domain reflectometry. In this context, gray image means raw data traces while curvelet transformation means removed noise. The vibration detection in a sensing path has been shown. In this method, the SNR has increased to 7.8dB.

A new technique to remove the effect of fading noise has been discovered, which his now used in distributed acoustic sensing systems [11]. This method has used the temporal adaptive f-OTDR signal processing method. In this context, the fundamental theory suggests SNR maximization, and the results have demonstrated that it is possible to achieve above 10dB SNR values without system bandwidth reduction and it does not need any optical amplifier.

A novel empirical mode separation method has been used in the detection system of wireless communication signal transceivers. The empirical mode method is used in the detection system to separate signal modes and then component analysis is applied to extract certain properties. This system is successful for low SNR transient signals and is certainly superior to other techniques. The system is successful in classifying specific transmitters and they can also be used for wireless communication for security purposes.

Distributed acoustic sensing system

In distributed acoustic sensing system the whole fiber acts like a multi-sensor, so it is very sensitive to environmental noise and all vibrations that happen near the cable path. The main idea of this system is to process and locate the backscattered light in an optical fiber to detect and extract changes, which happened at a specific point along the sensing path in DAS. Typically, one of the backscattered lights that occurred in the optical fiber is called Rayleigh scattering [3], which is a form of elastic scattering, in which, the scattered light frequency is similar to the incident light. Distributed acoustic sensing (DAS) is a technology that uses Rayleigh backscattering in a buried fiber-optic cable to detect vibration signals around the sensing path by sending laser pulses along the buried fiber cable. Small imperfections within the fiber cause light backscatter. Many activities cause vibration around the sensing path such as moving vehicles, hitting, or digging by different tools besides many other vibrations with

 ISBN 978-9959-9703-2-9

distinct acoustic characteristics. Threat vibration along the fiber path causes this backscattering light then, Rayleigh backscattering measured and processed to localize and extract the threats [1, 3].

Proposed Method

The proposed method as shown in the block diagram as shown in Fig. 1.

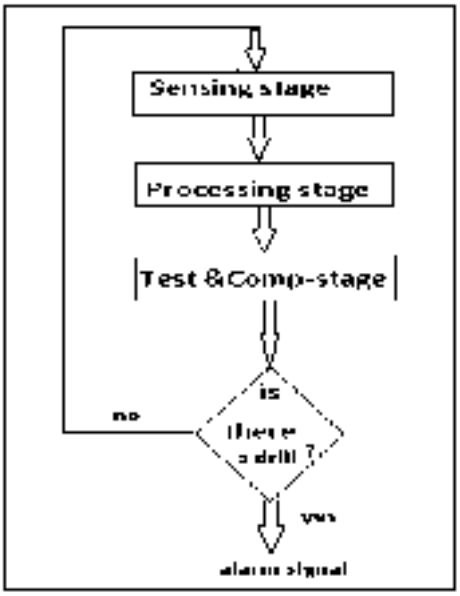

Fig. 1: The proposed method.

- Sensing stage

The main idea of sensing stage is to sense any activity or drilling near the cable by locating the backscattered light using phase OTDR. Phase OTDR measures the Rayleigh backscatter for each transmitted pulse. The characteristics change due to any mechanical vibrations that interact with the buried fiber optic cable and any changes that happened at a specific point along the sensing path are send to the processing stage.

- Processing stage

The goal in this stage is to identify and extract the event y (t) that was sensed near the cable from the whole signal x (t) by removing the noise g (t), as illustrated in equation (1).

$$x(t)=y(t)+g(t)$$

where x(t) is the backscattered signal, y(t) is the event signal (drill signal), and g(t) is the noise. The goal is to extract the event signal y(t) from the backscattered signal while suppressing the noise g(t). The technique starts with noise reduction g(t) from x (t) to find the goal signal y(t) using wavelet de-noising method [3, 16]. On different scales, wavelets can localize the signal features; so, during the noise removal, preserving important signal features is possible, using Symlets at level 5, sym5 wavelets are used to decompose the DAS data for each channel [13]. Effectively remove the noise of the

 ISBN 978-9959-9703-2-9

system and other environmental interferences. Then the difference is used for high pass filtering and extracting the changes as shown in Fig. 2.

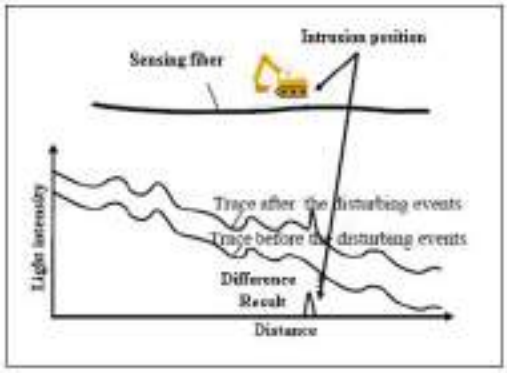

Fig. 2: Difference in time domain.

This phase includes autocorrelation to improve the interferometric visibility of the digging near the cable in all areas over a fiber optic cable. Moreover, the correlated signal power is computed and then sent to the next stage.

Test and comparison stage

In the third stage, all signals are compared with a predefined threshold, if the average of these signals exceeds the threshold, the discrete signal is considered to be high, and there is drilling near the cables, then an alarm signal sent from the system to the main system to show the position of the threat and alarm messages sent to all units. If the signals do not exceed the threshold, they are deemed undesirable and ignored. The drill detection architecture system is depicted in Fig. 3.

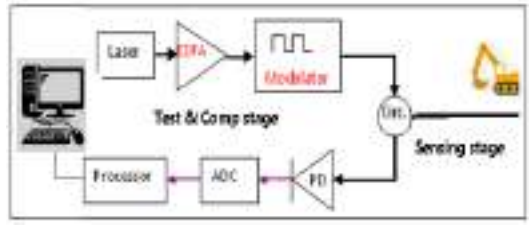

Fig.3: Drill Detection architecture system

Experimental results

The proposed method tested with different captured data called this called raw data as shown in Fig. 4.

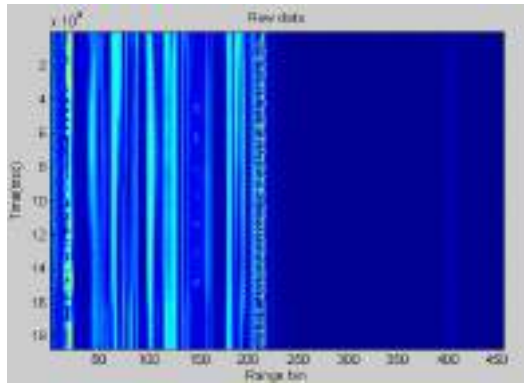

Fig. 4: The waterfall graph of raw data.

ISBN 978-9959-9703-2-9

As an illustration, the activity near the cable that have been tested in this study and de-noised by applying Wavelet method as shown in Fig. 5.

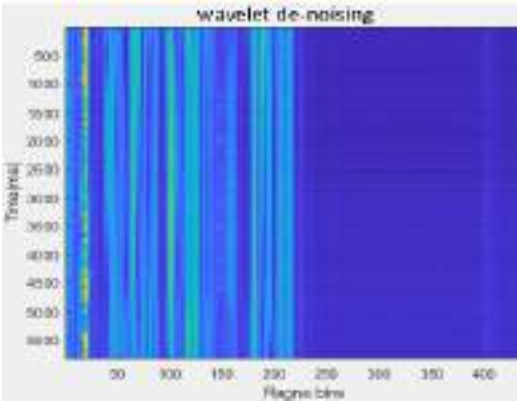

Fig. 5:De-noising data using wavelet.

Then difference in the time domain approach is used to find the abrupt changes in the signal Then the power of each signal is estimated. It is based on relation of Parseval that can be expressed as in equation (2).

$$\sum_{m=0}^{N-1} |y_{dtf}[c,m]|^2 \quad (2)$$

where m is the digital time index, and c is the measurement point on the cable and ydif is the drill signal and N is the number of samples used for signal power estimation as shown in Fig. 6.

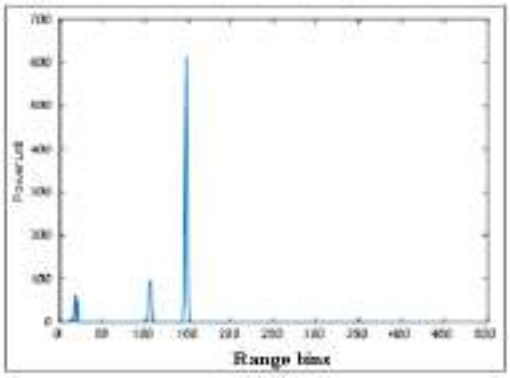

Fig. 6: The power of signals at each bin.

Finally, the data is sorted, and we found the maximum- valued bins, which correspond to the drilling events as illustrated in Fig. 7.

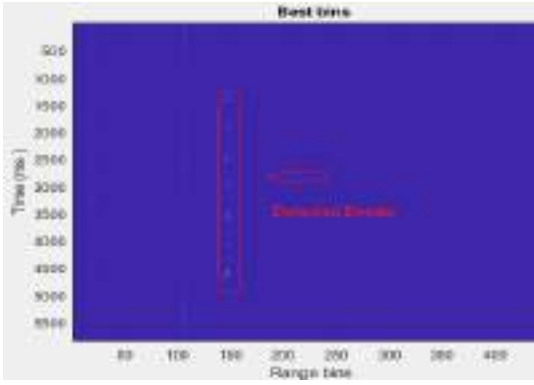

Fig. 7:The best events detected in the range bins(7 drilling hits).

Conclusion

The current paper has presented a new

ISBN 978-9959-9703-2-9

technique to detect any unauthorized drilling operations near the cables using phase-OTDR-based fiber optic distributed acoustic sensing systems, which combines the difference in the time domain and the wavelet de-noising with autocorrelation, which is conducted during the detection stage. We applied a series of tests for recorded and created data sets collected from different tools, hammer, pickaxe, and shovel. This technique uses a different approach to event detection that combines Wavelet de-noising and difference-in-time-domain methods with the autocorrelation process. Since wavelet de-noising is used for removing noise from measured backscattered signals, we used difference in time domain approach between the consecutive pulses to extract abrupt signal changes and to perform high-pass filtering in the signal, and then, to decide whether the signal should be removed, we used the autocorrelation function in all the ranges throughout the sensing fiber cable, which compares a signal with its own time-delayed version in every bin. Then, each of the calculated values is compared to a predefined threshold. If it exceeds the threshold, the discrete signal is considered as highly correlated while others are considered as undesired (uncorrelated) signals. We calculated the power of the correlated signal in the last phase at each bin and sorted it in a vector form in descending order, which shows that the maximum-valued bins were event signals. These signals are sent to the main system, and the system sends alert signals to all control systems, providing them with all information about the threat and its location to take the necessary action. System performance is evaluated at various SNR levels. The results shows that the method is quite effective in reducing the strong background noise and making it easy to detect any unauthorized drilling operations near the cables. This technique can be easily generalized to identify different types of threats of interest for many security applications.

Arabic section:

د.صالح ابوفانة – أ.عماد زرقون
قسم الحاسب الآلي كلية العلوم جامعة بني وليد / ليبيا
قسم الحاسب الآلي كلية العلوم جامعة بني وليد / ليبيا

الملخص: التحدي الأكبر هو حماية الكابلات في المدن والقرى من الحفريات العشوائية ، حيث أن حماية هذه الكابلات بالطرق التقليدية كالخرسانة وبعض أحجار الأسمنت غير كافية. أصبح من الضروري البحث عن تقنيات حماية فعالة وبديلة يمكنها حماية الكابلات. في هذا البحث ، تم اقتراح طريقة جديدة لتصميم نظام مراقبة الحفر للإنذار المبكر باستخدام أنظمة الاستشعار الصوتي الموزعة بالألياف الضوئية (DAS) على أساس المرحلة .OTDR الطريقة المقترحة لها ثلاث مراحل. تتمثل المرحلة الأولى في استخدام كابل الألياف الضوئية المدفون كنظام استشعار لاكتشاف أي نشاط مثل الحفر أو الحفر بالقرب من الكابل. المرحلة الثانية هي نظام المعالجة ؛ في هذه المرحلة ، يتم إزالة الضوضاء من الإشارة المحسوسة باستخدام تحويل مويجي ، ثم يتم استخدام الفرق لتصفية التمرير

 ISBN 978-9959-9703-2-9

العالي. تتضمن هذه المرحلة الارتباط التلقائي لتحسين رؤية قياس التداخل للحركات أو التهديدات بالقرب من منطقة الهدف عبر كابل ألياف بصرية. علاوة على ذلك ، يتم حساب قوة الإشارة المرتبطة وإرسالها إلى مرحلتي الاختبار والمقارنة. في المرحلة الأخيرة ، تتم مقارنة جميع الإشارات بعتبة محددة مسبقًا ؛ إذا تجاوز المتوسط العتبة ، تعتبر الإشارة المنفصلة عالية ، وهناك حفر بالقرب من الكابلات ؛ وبخلاف ذلك ، تعتبر الإشارات إشارات غير مرغوب فيها. تم استخدام أنواع مختلفة من الأنشطة على مستويات مختلفة من SNR لتقييم آثار الطريقة المقترحة على أداء الكشف. أظهرت النتائج فاعلية النظام المستخدم للكشف المبكر عن الحفر لحماية الكابلات.

References

[7] D. Hill, Distributed Acoustic Sensing (DAS): Theory and Applications, pp. 4,5, 2015.

[8] Y. Liu et al., Distributed fiber optic sensors for vibration detection, Sensors, vol. 16, no. 8, 1164, 2016.

[9] Abufana. S. A et al., Variational mode decomposition based threat classification for fiber optic distributed acoustic sensing, IEEE Access,2020.8:100152-100158J.

[10] H. Yue et al., Simultaneous and signal-to-noise ratio enhancement extraction of vibration location and frequency information in phase sensitive optical time domain reflectometry distributed sensing system, Optical Engineering, vol. 54, no. 4, 047101, Apr. 2015

[11] F. Peng et al., Real-time position and speed monitoring of trains using phase-sensitive OTDR, IEEE Photonics Technology Letters, vol. 26, no. 20, pp. 20552057, Oct. 2014.

[12] Z. Wang et al., Novel Railway-Subgrade Vibration Monitoring Technology Using Phase-Sensitive OTDR, in Proc. SPIE 10323,25th International Conference on Optical Fiber Sensors, Jeju, SouthKorea, 2017.

[13] J. C. Juarez, E. W. Maier, and H. F. Taylor, Distributed fiber-optic intrusion sensor system, Journal of Lightwave Technology, vol. 23,no. 6, pp. 20812087, June 2005.

[14] H. Liu et al., Traffic flow detection using distributed fiber optic acoustic sensing, IEEE Access, vol. 7, pp. 6896868980, 2018.

[15] F. Peng et al., Ultra-long high-sensitivity-OTDR for high spatial resolution intrusion detection of pipelines, Optic Express, vol. 22, no.11, pp. 1380413810, Jun. 2014.

[16] H. Wu et al., Separation and determination of the disturbing signals in phase-sensitive optical time domain reflectometry (Φ-OTDR),"Journal of Lightwave Technology, vol. 33, no. 15, pp. 3156–3162,Aug. 2015.

[17] I. Olcer, I. and A. Oncu, "Adaptive temporal matched filtering for noise suppression in fiber optic distributed acoustic sensing, Sensors,vol. 17, no. 6, 1288, 2017.

[18] Z. Qin, L. Chen, and X. Bao, Wavelet de-noising method for improving detection performance of distributed vibration sensor,.IEEE Photonics Technology Letters, vol. 24, no. 7, pp. 542544, Apr.2012.

[19] M. Aktaş et al., "Deep learning based multi-threat classification for phase-OTDR fiber optic distributed acoustic sensing applications," in Proc. SPIE 10208, Fiber Optic Sensors and Applications XIV,Anaheim, California, United States, 2017.

[20] A. Makarenko."Deep learning algorithms for signal recognition in long perimeter monitoring distributed fiber optic sensors" 2016 IEEE 26th International Workshop on Machine Learning for Signal Processing (MLSP). IEEE, 2016.

[21] Y. Muanenda."Recent advances in distributed acoustic sensing based on phase-sensitive optical time domain reflectometry" Journal of Sensors 2018 (2018).

P. Kumar and K. Preetam. "DCT based OFDM for underwater acoustic communication. " 2012 1st International Conference on Recent Advances in Information Technology (RAIT). IEEE, 2012.

 ISBN 978-9959-9703-2-9

المؤتمر الدولي الثاني للعلوم والهندسة
2nd International Conference on Science and Engineering
ICSE 2023
Faculty of Engineering - University of Bani Waleed
Bani Waleed, Libya

Paper Code: ICSE-024

DESIGN AND IMPLEMENTATION OF A SELF-CHECKING ROTATOR USING BERGER CODE

A. M. Ejamaila, A. A. Khalleefahb , A. M. Salimc A. H. Maamard
aComputer engineering & IT, College of Technology Sciences, Bani-Walid -Libya
bDepartment of Computer engineering, College of ELECTRONIC TECHNOLOGY, Bani-Walid –Libya
cComputer engineering & IT, College of Technology Sciences, Bani-Walid -Libya
dDepartment of Computer engineering, College of ELECTRONIC TECHNOLOGY, Bani-Walid-Libya
aAdel.m.Ejamail@gmail.com bgrimida2008@gmail.com
cabuojaylahbendalla@gmail.com cAli_h_maamar@yahoo.uk.com

Abstract: The advances in semiconductor generation have greatly improved the scale of integration. Today virtual systems are extra complicated than ever earlier than. These complex circuits are greater susceptible temporary and intermittent faulty. The complexity of the digital circuits results in extra crosstalk, noise, and different assets of temporary errors during normal operations. Conventional off-line testing techniques cannot guarantee detection of these faults; they can be detected by using on-line or concurrent error detection (CED). Concurrent error detection methods allow digital systems to affirm the correctness in their effects in the course of regular operation. Berger Code is one of the famous codes for CED applications because it could stumble on all unidirectional errors in digital structures. This paper proposes a layout to achieve the self-checking checker used of Berger code as a means of incorporating CED right into a self-checking for the rotate register.

Keywords: Berger Code, rotator register, Two-Rail Checker (TRC), Self-checking

Introduction

Since the 1960s, concurrent error detection techniques have been used extensively in commercial digital systems [1]. Concurrent error detection's primary goal is to perform real-time checks on system outputs to ensure data integrity by identifying temporary or permanent faults while the system is functioning normally. Concurrent error detection makes it possible to find errors as the system is running. is essential for a broad range of applications, from avionics and space to telephone switching networks, online transaction processing, etc. An online error detector of your choice can be added to a computer system. These detectors operate under the fundamental principle of redundancy in hardware replication, information (redundant codes), software, or execution time. Redundancy is the use of additional resources above and beyond what is necessary for an unchecked system [2]. By some other words this redundancy can take the form of additional hardware (hardware redundancy), additional software (software redundancy), additional information (information redundancy), or multiple code executions on a single piece of hardware (time redundancy) [3]. Only information redundancy using Berger code checkers in Totally Self-Checking (TSC) is the focus of this paper.

 ISBN 978-9959-9703-2-9

1. Rotate register

A rotate register is a virtual circuit includes a cascade of flip flops, wherein the output of one flip flop is connected to the input of the subsequent turn flop. The data stored within the rotate register can be shifted from one location to the following vicinity. An N-bits rotate register can be shaped by means of connecting N-flip- flops where each flip- flop keep a single bit of data. Registers are used for data storage or for the motion of data; they're normally used interior Calculators or computer systems to save data inclusive of two Binary numbers before they're added together, or to convert data from both a parallel to serial or serial to parallel layout [4]. Figure 1 shows the impact of facts motion from left to right through a rotate register.

Since the 1960s, concurrent error detection techniques have been used extensively in commercial digital systems [1]. Concurrent error detection's primary goal is to perform real-time checks on system outputs to ensure data integrity by identifying temporary or permanent faults while the system is functioning normally. Concurrent error detection makes it possible to find errors as the system is running. is essential for a broad range of applications, from avionics and space to telephone switching networks, online transaction processing, etc. An online error detector of your choice can be added to a computer system. These detectors operate under the fundamental principle of redundancy in hardware replication, information (redundant codes), software, or execution time. Redundancy is the use of additional resources above and beyond what is necessary for an unchecked system [2]. By some other words this redundancy can take the form of additional hardware (hardware redundancy), additional software (software redundancy), additional information (information redundancy), or multiple code executions on a single piece of hardware (time redundancy) [3]. Only information redundancy using Berger code checkers in Totally Self-Checking (TSC) is the focus of this paper.

1. Rotate register

A rotate register is a virtual circuit includes a cascade of flip flops, wherein the output of one flip flop is connected to the input of the subsequent turn flop. The data stored within the rotate register can be shifted from one location to the following vicinity. An N-bits rotate register can be shaped by means of connecting N-flip- flops where each flip- flop keep a single bit of data. Registers are used for data storage or for the motion of data; they're normally used interior Calculators or computer systems to save data inclusive of two Binary numbers before they're added together, or to convert data from both a parallel to serial or serial to parallel layout [4]. Figure 1 shows the impact of facts motion from left to right through a rotate register.

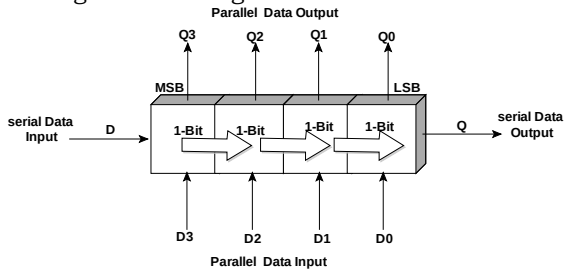

Fig. 1: rotate register.

Figure 2 shows rotate right operation, the serial output of the register is connected to the serial input of the register.

 ISBN 978-9959-9703-2-9

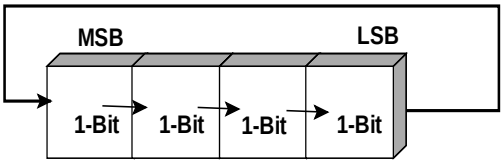

Fig. 2: rotate Right register.

By applying clock pulses data is shifted right. The data shifted out of the serial out pin at the right hand side is recirculated back into the shift register input at the left hand side. Thus the data is rotated right within the register. Figure 3 shows rotate left operation, the serial output of the register is connected to the serial input of the register.

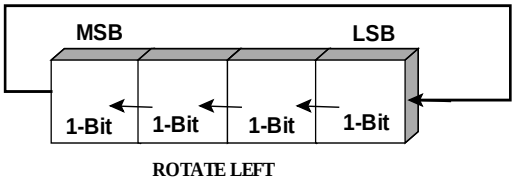

Fig. 3: rotate Left register.

By applying clock pulses data is shifted left. The data shifted out of the serial out pin at the left hand side is recirculated back into the shift register input at the right hand side. Thus the data is rotated left within the register.

2. SELF-CHECKING CIRCUITS

Self-checking is the capability of a logic component (chips, boards, or assembled system) to automatically check for errors [5]. Self-checking circuits enable on-line error detection, which enables faults to be found as the circuit is being used normally. It has the ability to identify both temporary and irreversible faults [6]. To the original circuit (functional unit), it is intended to add some circuitry. If there is an error in the functional unit, this additional circuit will check the output of the functional unit to ascertain it [7]. Self-checking circuits can be designed using a variety of codes. Only separable codes that separate the information bits from the check bits are the focus of this paper. The Berger code converts a word's number of 1s into a binary representation. The count is added to the data after the binary word is completed. The best AUED (All Unidirectional Error Detecting) codes are called Berger codes. It can identify all unidirectional bit errors, such as when one or more ones become zeros, but it cannot recognize when zeros become ones. The error won't be noticed if the same number of bits flip from one to zero as they do from zero to one [8]. Two-Rail Checker (TRC) A one bit output is insufficient for a Totally Self-Checking (TSC) circuit because a stuck-at-fault on the output resulting in the "good" output could not be detected [2, 9, 10, 11]. A two rail (1-out-of-2) code is typically used to encode the output of a TSC circuit. Two complementary codewords are compared using a two-rail checker unit (TRC). The checker decides whether the functional circuit's output is an acceptable or unacceptable codeword [2]. Figure 4's block diagram depicted the suggested design for the self-checking rotator register checker. The proposed 4-bit Rotator Left/Right register resembles a shift register with taps added to each stage of input and output in a serial-in/serial-out design. Din (Serial Input) is where serial data shifts in. The first Din bit data appears at (Q4) after a certain number of clocks that is equal to the number of bits. Start by entering the rightmost bit of the four bits (1001) into the register. As soon as data are entered into the register, the Check Symbol Generator (CSG) generates a code word for the data, which is then stored in the 3-bit register and used to compare the inputs from the two rails.

Self-checking can be defined as the ability to automatically check logic (chip, board, or assembled system) for errors [5]. A self-checking circuit allows online fault detection. This means that faults can be detected during normal operation of the circuit. It can detect the presence of both transient and permanent errors [6]. The idea is to add some circuits to the original circuit (functional unit). This

 ISBN 978-9959-9703-2-9

additional circuitry examines the outputs of the functional units and determines if the functional units are faulty [7]. Many codes can be used to design self-checking circuits. This article will only focus on separable code where the information bit is separated from the check bit. A Berger code counts the number of ones in a word and represents it in binary. Complement binary words and add counts to the data. The Berger code is the best systematic AUED (All Unidirectional Error Detecting) code detects all unidirectional errors. If one or more 1's are converted to 0's, they can be identified, but if 0's are converted to 1's at the same time, they are not. If the same number of bits changes from 1 to 0 as they change from 0 to 1, no error is detected [8]. A 1-bit output is not sufficient for a full self-test (TSC) circuit because it cannot detect stuck-at faults in the output that lead to a 2-Rail Checker (TRC) "good" output [2, 9], 10, 11]. The output of the TSC circuit is typically encoded with a two-rail (1 of 2) code. A Two-Rail Checker Unit (TRC) is used to compare two complementary codewords. A validator determines whether the output of a functional circuit is a valid or invalid codeword [2]. The block diagram in Figure 4 shows a proposed design for implementing a self-checking rotator register checker. The proposed 4-bit rotator left/right register looks like a serial-in/serial-out shift register with additional taps at each input and output stage. Serial data is inserted into Din (serial input). After a number of clocks equal to the number of bits, the first Din bit data appears on (Q4). Enter 4 bits (1001) into the register, starting with the rightmost bit. As data enters a register, a check symbol generator (CSG) generates codewords for the data. A 3-bit register contains complementary codewords used at the two rail inputs for comparison.

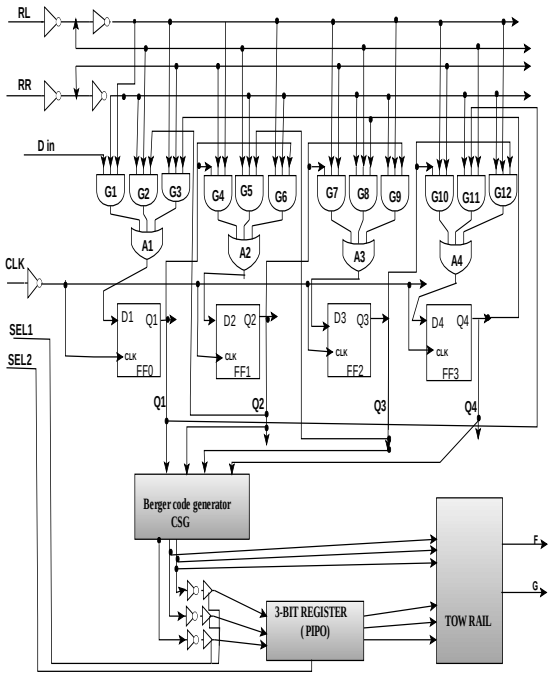

Fig. 4: 4 Bit Rotator Left/Right register.

Since no information bit is discarded except for their position the Berger check of the result of rotate operation is simply the Berger check of the operand, since no information bit and the numbers of 1's is the same, if no error is detected. After the operation of register rotate (left/right) done, the CSG generates new check bits code for that word. In order to detect faults on the word after the operation we drive the stored check bits code and the inverted created one to the Two -rail checker. The steps in the checking procedure can be implemented as shows the flowchart in figure 5. The designs are implemented in Verilog HDL for simulation and synthesis. The Waveforms below shows the output of the Simulation Processor. The waveform in Figure 6 shows the Reset register, loading data to the rotator register and execute the rotate left / rotate right to the loaded Data, so the signals as follow:

 ISBN 978-9959-9703-2-9

CLK: clock signal. Din: Data in shows the input data into the register.Q1: first Bit of the output data shows the value of first bit in the register.Q2: second Bit of the output data shows the value of second bit in the register. Q3: third Bit of the output data shows the value of third bit in the register.Q4: fourth Bit of the output data shows the value of fourth bit in the register. The table 1 shows the control state for the used register. The waveform in

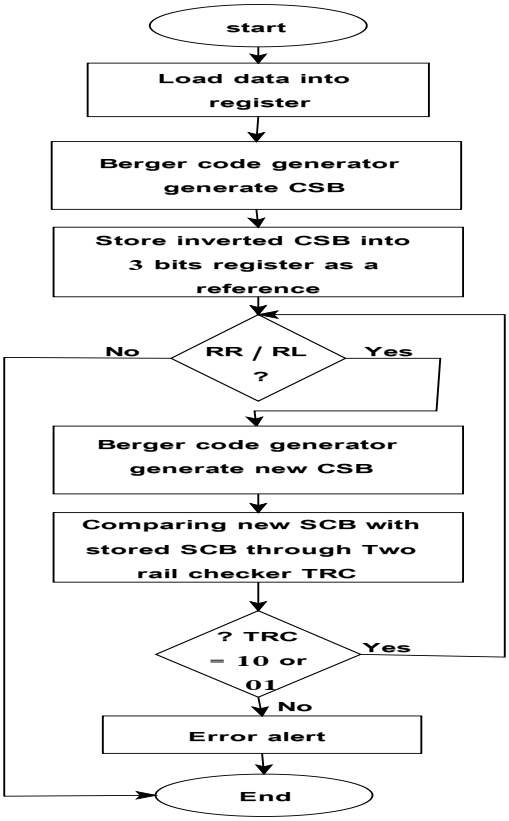

Fig. 5: Flowchart shows steps in the checking procedure.

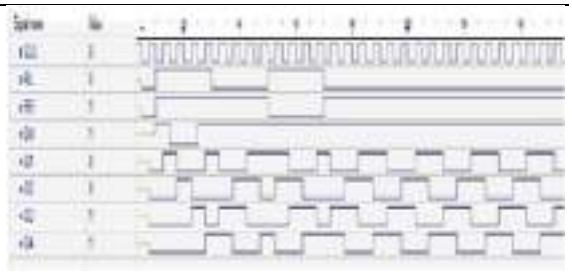

Fig. 6: Waveform shows loading data to the rotator register.

Table 1: control state for the register.

RL	RR	Operation
0	0	Reset register
0	1	rotate right
1	0	rotate left
1	1	Load data

Figure 7 shows the Berger Code check symbol Generator for 4-bit, where the input for CSG is the output for the 4-bit rotator register, the signals as follow:
CLK: clock signal. Q1: first Bit of the output data shows the value of first bit in the register.Q2: second Bit of the output data shows the value of second bit in the register.

Fig. 7: Waveform shows Berger code check symbol generator.

Q3: third Bit of the output data shows the value of third bit in the register. Q4: fourth Bit of the output data shows the value of fourth bit in the register.Sig21: first Bit of the CSG output shows the value of first bit in the CSG

ISBN 978-9959-9703-2-9

output. Sig22: second Bit of the CSG output shows the value of second bit in the CSG output. Sig23: third Bit of the CSG output shows the value of third bit in the CSG output. The waveform in the Figure 8 shows the implementation loaded data to the register, generate the check symbol bits word, pushed in complement of the check symbol bits word to 3-bit register, rotate left/right the register, drive data to two rail checker, and obtain the result.

Fig. 8: Waveform shows the Simulation of rotator implementation processor.

3. Conclusion

This paper presents a technique for implementing fault secure rotators based on Berger code. In this design Berger code generator generates check bits code for each input word of the shift register, since no information bit and the numbers of 1's is the same, if no error is detected. After the operation of register rotate left/right done, the Berger code generator generates check bits code for that word. In order to detect faults on the word after the operation we drive the stored check bits code and the inverted created one to the Two -rail checker. This design achieves high levels of reliability by means of moderate hardware cost. The system can detect all Unidirectional Error in the rotator.

1. References

[1]. Subhasish Mitra, "Diversity Techniques for Concurrent Error Detection", Technical Report, Center for reliable computing, May 2000.

[2] P. K. Lala. Self-Checking and Fault-Tolerant Digital System Design. Morgan Kaufman Publishers, San Francisco, 2001.

[3]. Manoj Franklin, "A Study of Time Redundant Fault Tolerance Techniques for Superscalar Processors" Department of Electrical & Computer Engineering, Clemson University, Clemson, USA, 1995 IEEE.

[4]. Tony R. Kuphaldt Lessons In Electric Circuits, Volume IV Digital Fourth Edition, last update November 01, 2007, openbookproject.net/ electricCircuits.

[5] Huda Abugharsa, and Ali Maamar," Self Checking Systolic LIFO Stack",7th WSEAS Int. Conf. on Instrumentation Measurement, Circuits and Systems (IMCAS '08), Hangzhou, China, April 6-8, 2008.

[6] KHADIJA F. O. ALGHEITTA. AMAL J. MAHFOUD. ALI H. MAAMAR. Design of a Self-Checking Up Counter. International Conference on Advanced in Computing, Engineering and Learning Technologies, Abu Dhabi, UAE, 2013.

[7] Mustafa Abd-El-Barr," Design and Analysis of Reliable and Fault-Tolerant Computer Systems ", Imperial College Press, 2007, ISBN 1-86094-668-2.

[8] VARADAN SAVULIMEDU VEERAVALLI. Diagnosis And Error Correction For A Fault-Tolerant Arithmetic And Logic Unit For Medical Microprocessors, Graduate School- New Brunswick Rutgers, The State University of New Jersey October, 2008.

[9] B. W. Johnson. Design and Analysis of Fault Tolerant Digital Systems. Addison-Wesley, Reading, MA, 1989.

[10] D. K. Pradhan. Fault-Tolerant Computing:

 ISBN 978-9959-9703-2-9

Theory and Techniques, volume I. Prentice Hall, Englewood Cliffs, New Jersey, 2003.

[11] T. R. Stankovic, M. K. Stojcev, and G. Ordjevic. Design of Self-Checking Combinational Circuits. In Proc. of the International Conf. on Telecommunications in Modern Satellite, Cable and Broadcasting Services, volume 17, pages 763-768, October 2003.

 ISBN 978-9959-9703-2-9

المؤتمر الدولي الثاني للعلوم والهندسة
2nd International Conference on Science and Engineering
ICSE 2023
Faculty of Engineering - University of Bani Waleed
Bani Waleed, Libya

Paper Code: ICSE-039

DEVELOPING THE SKILLS OF USING CLOUD COMPUTING AMONG UNIVERSITY STUDENTS: A PROPOSED PROGRAM

Halima Aboobaker, Abobaker Zargoun
Computer Engineering & IT, College of Electronic Technology Baniwalid, Libya
Control Engineering, College of Electronic Technology Baniwalid, Libya
*Crosspnding author: halimabobaker@bit.org.ly

Abstract: The study aimed to build a proposed e-training program to develop the skills of using cloud computing (Google Drive apps) among university students using the Moodle e-learning system and according to the instructional design system ADDIE, the program included five training modules.

To achieve the objective of the study, the extent to which students possess the skills of using cloud computing applications was measured through a questionnaire about the study, where the sample of the study was 98 students from Bani Walid University.

The results showed that many students do not have the skills to use cloud computing applications, which led to the proposal to design and build an e-training program that will have an impact and effectiveness on the development of these skills among students. At the conclusion of the study, the researcher recommended a set of recommendations that could contribute to the development of the skills of using cloud computing among students in the teaching and learning processes in various curricula, whether at the undergraduate or graduate level.

Keywords: (Cloud computing, E-learning system, E-training program, Google Drive applications, Skill)

Introduction

Cloud Computing applications are an important thing because they offer a solution to some of the barriers to adoption of e-learning by providing you with a large public resource that can be used by all members of an educational institution without requiring an infrastructure, in addition cloud computing applications provides communication and collaboration tools between users such as e-mail, contact list, calendar and notepad, as well as office applications such as storing documents, creating documents and sharing with others, and a working platform Applications, for example: support for creating websites, using educational management systems.

This study aims to highlight on the most important technological applications that have

 ISBN 978-9959-9703-2-9

a significant impact on the teaching and learning processes, it is cloud computing applications and how to benefit from it for the learner, through building a proposed e-training program to develop the skills of university students using these applications, which meet the required and constantly changing training needs, overcome the boundaries of time and space, and provide an interactive e-training environment.

Problem of study

Through my work, noticed that most students do not use cloud computing applications and do not know the importance of these applications in the teaching and learning processes, which they must have to keep up with the technological development in education.

Objectives of study

The study aims to achieve the following goals:

- Building an e-training system using Moodle that includes educational content and training courses focused on enhancing students ' cloud computing skills.
- Encourage students to use cloud computing applications in study and work, analyze their benefits, disadvantages and compare them with traditional computing.
- Provide the necessary technical support and guidance to students in case they encounter problems while using cloud computing applications.

Importance of study

The importance of the study is the following:

- The proposed e-training program using the Moodle helps students to use cloud computing applications in collaborative learning through collective participation among themselves.
- The proposed e-training program provides an opportunity to provide faculty members with a practical program that includes how to use cloud computing applications in teaching.
- The results of this study benefit curriculum developers in building e-courses using cloud computing applications.

Cloud computing

Rashid and Chaturvedi [1] define Cloud Computing "is the use of hardware and software to deliver a service over a network (typically the Internet) with cloud computing, users can access files and use applications from any device that can access the Internet".

According to the researcher, all the previous definitions agreed between them on the existence of a virtual place as a computer frame storage platform, accessed via the internet, which is an essential element to

 ISBN 978-9959-9703-2-9

access the cloud, this place contains storage space in addition because it converts computer programs and technologies from productive technologies to services that provide fast processing through a series of devices and servers somewhere, thus saving the user storage space, software purchase, maintenance and development costs, and therefore the user's focus is on using this services only.

Cloud computing types

Cloud computing has several types for providing services and applications to educational and other institutions, this can be illustrated as follows:

- Software as a service (SaaS)

Namely, you use a specific application stored in the cloud, for example, a word program located in the data centre, and you connect to it via the internet and write in it, modify and add data, and then get the output from it, and all this while you are in the cloud and your device is only the communication tool, and the user here cannot control the operating system in the cloud and does not control the hardware nor the network connection, and YouTube can be considered within this classification.

- Platforms as a service (PaaS)

Using the cloud as a platform to put several applications on it and can work on all of them, you can also put a complete operating system as well, and there is integration between applications, for example, something can be designed with Photoshop and then inserted to another application, which moves and adds effects, so you get a video clip with sound like Google Apps, a platform that allows you to add applications as desired.

- Infrastructure as a service (IaaS)

Here the cloud is treated as an infrastructure limited by a certain processing capacity, storage space and a certain number of users, and you are free to use it in the way that suits you, for example, you can install several operating systems, install several applications on each system and allow a certain number of users to enter each operating system to use its applications without allowing confusion between them.

The diversity of the former cloud components and the multiplicity of their services can serve the educational process very effectively, as these components provide the educational institution with the infrastructure for computing education, as well as the high cost of creating huge servers, purchasing programs and facilitating the preparation of electronic courses in accordance with the electronic capabilities of students. In computing, we have free applications that are easy to access collectively from several users via the internet and do many educational services, such as Google applications, which have created many

 ISBN 978-9959-9703-2-9

educational applications in its cloud and allocated a special section for them, and we also have free electronic platforms through which we can develop applications and software for the institution affiliated with electronic courses and various auxiliary enrichment programs that excite students and give an atmosphere of fun with benefit, as well as we have an infrastructure that has a processing capacity that may not be available within the institution's network and exceeds its computing capacity, in addition to huge storage spaces such as that provided by Google, which starts from 15 GB for free and reaches to 16 TB for a certain amount is considered cheap in front of the size of the benefit to the organization due to the use of these spaces and applications.

Services provided by cloud computing for universities

- Accommodate the dependencies of the rapid increase in the use of the mobile device.
- Storage of expanded amounts of sensitive data and easily accessible information.
- Getting the latest software and Application Updates.
- Simplify the enrolment and admission processes at universities, which are expensive and time-consuming processes.
- It allows more flexibility and multiple options that enhance Effectiveness, raise efficiency in organizations by increasing productivity and reducing cost.
- Taking advantage of the huge infrastructure provided by cloud services to carry out practical tests and experiments, so it copes with the great developments that have occurred in recent years in the computer industry.
- Some complex calculations take years to perform on high-end computers, while companies such as Google and Amazon and their clouds of thousands of servers connected to each other make it possible to perform such calculations in minutes or hours from anywhere in the world where internet service is available.

Construction and design of the proposed e-training program

The process of building training programs is a key stage in the methodology of the training process, during which the objectives of the program are formulated, its content is determined in terms of topics, activities, events, diagnostics of training methods for its implementation, identification of other requirements required by the implementation process, and all this is done in the light of scientific assessment of the actual training

 ISBN 978-9959-9703-2-9

needs of participants in these programs.

There are many educational design models related to the production of electronic training programs, and among these models are: ADDIE Instructional design model, Kemp model, Waterfall model and others.

During this study, the researcher chose the ADDIE Instructional design model for the following reasons:

- Clarity of the form steps and their sequence.
- A general model based on its steps is considered to be the dominant of other models. The model establishes a specific, structured and flexible framework for the design of training programs.
- All these steps are suitable for building a training program based on the Moodle course management system, and it is considered one of the models with high flexibility to build research tools and materials.

The model consists of five steps that represent its name, namely:

Analysis, design, development, implementation, evaluation. The following are the steps to build the e-training program that was designed and built in this study.

1. The analysis phase

It represents the basic and important stage for all other stages. The most important training needs were identified in order to design an electronic training program to develop the skills of using cloud computing applications for university students. The results of the study showed through a questionnaire to measure students ' possession of the skills of using cloud computing applications conducted on 98 students from Baniwalid University, that 69 students, 70.4%, do not have the skills of using cloud computing applications. Therefore, the study highlighted the need for students to learn cloud computing skills, through electronic training programs that bring them those knowledge and skills. Through the above, the training needs of the e-training program have been identified as follows:

- The cognitive aspect of students:
  - Knowledge about cloud computing and how to use it in education.
  - Knowledge of the Google Drive application and how to use it in education.
  - Knowledge of Google Docs and how to use them in education.
  - Knowledge of Google presentations and how to use them in education.
  - Knowledge of Google models and how to use them in education.
- The skill side of students:

ISBN 978-9959-9703-2-9

- Special skills of the Google Drive application.
- Special skills using Google Docs.
- Special skills using Google presentations.
- Special skills using Google Forms.

2. Defining the general objectives of the E-Training Program

The general objectives of any training program are one of the most important procedural steps in the design of the program, as they play an important role in determining the elements of the content of the program, as well as choosing the appropriate means and methods to achieve the desired goals of this program. The general goal of the program was set, which is to develop the skills of using cloud computing applications among university students, and then set the goals for the training program as follows:

- Students acquire theoretical knowledge of cloud computing, its applications and its importance in education.
- Students acquire knowledge and skills related to the Google Drive application and employ it in education.
- Students acquire the skills to deal with Google presentations and employ them in education.
- Students acquire the skills to deal with Google documents and employ them in education.
- Students acquire the skills to deal with Google Forms and employ them in education.

3. Development of the training content of the program

After defining the general outlines of the training program and formulating the goals, the scientific content of the training program was determined, formulated and organized based on the method of task analysis. The training content included five modules arranged according to the skills to be learned in a sequential and graduated manner from easy to difficult, from simple to complex, from knowledge to performance, and related to the previous experiences of students.

The content sequence has been organized in the form of training modules as shown in the following table:

Table1: Training modules for the proposed e-training program.

Training Modules	Sub-elements

 ISBN 978-9959-9703-2-9

Introductory module	The concept of cloud computing. The basic components of cloud computing. Characteristics of cloud computing. Types of cloud computing. Cloud computing services in education.
Google Drive app	The concept of the Google Drive app. Types of documents that can be edited through the Google Drive app. Advantages of using the Google Drive app. Create a Gmail email. Login to Google Drive. The main components of the Google Drive screen.
Google Docs	Create the document. Change & Copy the document language. Convert the document type. Publish the document on the web. Document settings change. Print the document. Insert photos into the document. Insert an equation into the document. Insert a drawing into the document. Insert a table into the document. Control the properties of the table. Add written comments. Add audio comments. Insert the table of contents. Format the text. Proofreading the document by spelling. Search for the topic in Google. Send the file by e-mail as an attachment. Share files with others electronically.
Google Slides	The capabilities of the Google presentations editor. Create a presentation. Import slides. Display format. Publish the offer on the web. Add movements to the presentation. Insert photos to the display. Insert a video to the presentation. Add a comment to the offer. Add & Delete a new slide. Change the background. Change the appearance. Change the order of the slides. Turn on the display.
Google Forms	Definition of Google Forms. The possibilities of the Google Forms editor. Create the form. Rename the form. Change the appearance of the model. Write form questions. Determine the type of question. Add a new question. Add photos of the model. Add a video to the form. Send the form by e-mail. Share the form via Facebook, Twitter, Google+. Accept responses. View responses in spreadsheets.
Google Forms	Definition of Google Forms. The possibilities of the Google Forms editor. Create the form. Rename the form. Change the appearance of the model.

ISBN 978-9959-9703-2-9

	Write form questions. Determine the type of question. Add a new question. Add photos of the model. Add a video to the form. Send the form by e-mail. Share the form via Facebook, Twitter, Google+. Accept responses. View responses in spreadsheets.

4. Design and implementation of the e-training program

The proposed e-training program is designed and built according to the following steps:

- The choice of the e-learning management system (Moodle), where the latest version (4.2) was chosen to be the e-training environment for the current study, where the Moodle system is one of the e-learning management systems (LMS) available for free and open source, and its tools can be customized according to the requirements of the study, and this system aims to create an interactive environment through which trainers and trainees communicate with each other through many means such as delivering the training material to trainees or adding activities, assignments, tests or communication and dialogue through discussion forums.
- Preparing a preliminary scheme for designing the e-training program in the form of stages and steps to help organize the e-training environment, and also facilitates the implementation of this scheme at the development stage.

Fig. 1: The first scheme for the design of the e-training program

- After the preparation of the design scheme is completed, the scheme is reviewed to ensure that all the necessary topics, elements and tools are available to achieve the goals of the E-Training Program.
- Assembling some multimedia elements necessary to build the electronic training program from various electronic sources such as Google search engine as well as Pinterest website that provides photo sharing service.

 ISBN 978-9959-9703-2-9

- Download the Moodle version and install it to start building the E-Training Program, and then implement the design scheme and produce the proposed e-training program for this study.

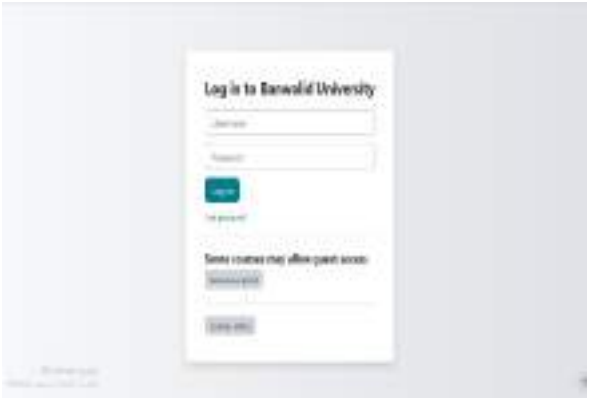

Fig. 2: Login screen

- After completing the registration process, the main screen of the program is accessed as shown in Figure (3).

Fig. 3: Main screen for entering the e-training program

- Then, entering the main screen, click on the icon of the e-training program and then enter the main page of the program as shown in Figure (4).

Fig. 4: Main page of the e-training program

5. Evaluation of the e-training program

After the completion of the process of building and designing the proposed e-training program, the evaluation process of the contents and elements of the program comes to ensure the accuracy, clarity and effectiveness of all the contents and elements of this e-training program.

6. Modification of the e-training program

This step comes in order to review the most important strengths and weaknesses of the program and its aim is to increase the effectiveness of the proposed electronic training program.

Conclusion

We conclude from this study that:

- The subject of the e-training program is one of the modern technological

 ISBN 978-9959-9703-2-9

innovations in the field of e-learning, which prompts students to learn the knowledge and skills related to this program in addition to their aspiration to deal with cloud computing applications.

- The method of using cloud computing applications (Google Drive app) is a fun and easy way that makes it easy for students to understand, which leads to an increase in students ' achievement.
- The possibility of providing training according to the appropriate time and place for the student and also getting rid of the restriction of time and place that may restrict the student to receive training in the traditional way .
- Giving the student the opportunity to repeat the application several times without getting bored by entering the e-training program via tablets or smartphones more than once at any time he wants and from anywhere, and this may not be available to students in other training programs, as most other programs are done by viewing only .

Recommendations

According to the conclusions of the study, some of the following recommendations were made:

- The possibility of applying the E-Training Program proposed in this study to faculty members and students at universities in order to develop their skills in using cloud computing applications and help employ them in education.
- Expanding the use of cloud computing applications in education in general and the university stage in particular, due to its potential in developing a collaborative learning environment among students, in addition to increasing the effectiveness of learner-centered learning, it also reduces students ' dependence on learning methods based on teacher activities.
- Guiding and motivating students to use cloud computing applications, including (Google Drive application) to complete projects and study assignments, which makes them able to learn from each other as well as see the work of other groups participating in (Google Drive) projects.

E-learning centers at universities implement multiple strategies to employ cloud computing applications.

- Working on spreading awareness of cloud computing applications, employing them and relying on them in providing some courses that can be offered through these environments through holding conferences

 ISBN 978-9959-9703-2-9

and workshops at various educational institutions.

References

[1] Rashid, Amit Chaturvedi, (2019), Cloud Computing Characteristics and Services: A Brief Review, International Journal of Computer Sciences and Engineering, 421.

[2] Michael Rowe, Vivienne Bozalek, Jose Frantz, (2013), Using Google Drive to facilitate a blended approach to authentic learning, British Journal of Educational Technology.

[3] Vipin Kumar Choudhary, (2018), Cloud Computing and its Applications: A Review, International Journal of Emerging Trends & Technology in Computer Science.

[4] Awaneesh, Manmohan Mishra, Priyana P. Shinde, Surabhi Srivastava, A. Deepak, (2023), Role of cloud computing in management and education.

[5] A.-I. Neicu *et al, (2020),* Cloud Computing Usage in SMEs. An Empirical Study Based on SMEs Employees Perceptions.

[6] Alieva Nodira, Djuraeva Saida, Abdusamatova Gulchekhra, (2023), Use of Cloud Technologies In The Educational Process, european journal of multidisciplinary research and management studies.

[7] Ashraf Ali, (2022), An Overview of Cloud Computing For the Advancement of the E-Learning Process, Journal Theoretical and Applied Information Technology.

[8] Hui Han, Silvana Trimi, (2022), Cloud Computing-based Higher Education Platforms during the COVID-19 Pandemic, International Conference on E-Education, 83-89.

 ISBN 978-9959-9703-2-9

المؤتمر الدولي الثاني للعلوم والهندسة
2nd International Conference on Science and Engineering
ICSE 2023
Faculty of Engineering - University of Bani Waleed
Bani Waleed, Libya

Paper Code: ICSE-056

PHISHING ATTACK ON CREDENTIAL HARVESTER (GOOGLE)

Haytham F. Dhaw[a], Alhadi A. Alajeilib, Khalid M. Ajbrahc, Abdesalam A. Almarimi[d]
Mohammed A. Abdulsalam[e]
[a]Dept. of General Section/ Higher Institute of Medical Technology Baniwalid, Libya
Email: h.mondo89@gmail.com
[b]Libyan Center for Engineering Research and information Technology, Baniwalid, Libya
Email: h.alajeili@outlook.com
[c]Dept. of Computer Engineering & IT/ College of Electronic Technology Baniwalid, Libya
Email: khaledajbarh267@gmail.com
[d]Dept. of Computer Engineering & IT/ Higher Institute of Engineering Technologies Baniwalid, Libya
Email: belgasem_2000@yahoo.com
[e]Libyan Center for Engineering Research and information Technology, Tripoly, Libya
Email: Mo.18892mr@gmail.com

Abstract: Vulnerabilities and weaknesses of web applications are targeting by attackers. Therefore, penetration testing techniques are very important for building strategies which make the system is secure. This paper proposes a penetration testing model for phishing attack which is a common these days. The proposed model was implemented using the latest versions of VMware-machine, kali-Linux, and Windows 10. The Hiddeneye, Ngrok, and bitly tools were used. This was achieved by information gathering method. The obtained results of the phishing attack were identified and their appropriate countermeasures were defined.

Keywords: Computer security, Web security, Ethical hacking

Introduction

This Phishing is a cybercrime in which scammers send a malicious email to individual(s) or mass users of any organization by impersonating a recognized individual or a business partner or a service provider, these emails are carefully created such that it is opened it without any suspicion. Criminals have countless methods and types of phishing emails to fake email users. Phishing is the electronic version of social engineering and has found a huge market in our email-obsessed world. Hackers send fraudulent emails out to literally millions of people, hoping a few will click on the attached links, documents, or pictures, with the goal of getting recipients to willingly provide valuable private information such as; social security numbers, passwords, banking numbers, PINs, credit card numbers and so on [1].

 ISBN 978-9959-9703-2-9

This can be achieved through a few different methods. Sometimes, cybercriminals trick email recipients into opening an email attachment that loads harmful malware onto their system. Other times, they fool recipients into providing sensitive personal information directly via web forms. Either way, these seemingly small mistakes could send serious ripples across an organization, compromising a corporate or personal security. These types of phishing attacks open the door for attackers to enter into the victim system and access confidential data like bank account details, credit card numbers, social security number, passwords, etc. [2].

Once the information is obtained, the phishers immediately send or sell it to people who misuse them. Sometimes, phishing not only results in loss of information but also injects viruses into the victim's computer or phone. As soon as infected, phishers gain control over devices, through

which they can send emails and messages to other people connected through the server.

According to the APWG report, the number of unique phishing websites had reached 73.80% from October 2017 to March 2018, and, 48.60% of the reported phishing incidents had used ".COM" domain. The domains and websites that interacted with assumed are safe, but hackers do trick us with different types of phishing attacks, by using impersonated domains and cloned websites. Scammers use Social Engineering to know the online behavior and preferences of the potential victim [3]. This helps them to craft a sophisticated attack.

According to the Kaspersky report in the second quarter of 2019, the average share of spam in global mail traffic cut down to 57.64%, while the Anti-Phishing system prohibited more than 130 million redirects to phishing sites, up 18 million during the previous reporting period. Throughout the second quarter of 2019, their security solutions detected a total of 43,907,840 malicious email attachments. The most prevalent malware in mail traffic was Exploit.MSOffice.CVE-2017-11882.gen with a share of 7.53%, while Backdoor.Win32.Androm, with an 8% share, was the most common malicious family [4].

In the third quarter of 2019, first place by prevalence in mail traffic went to the Office malware Exploit.MSOffice.CVE-2017-11882.gen (7.13%); in second place was the Worm.Win32.WBVB.vam worm (4.13%), and in third was another malware aimed at Microsoft Office users, Trojan.MSOffice.SAgent.gen (2.24%). In the third quarter of 2019, the Anti-Phishing system prevented 105,220,094 attempts to direct users to scam websites. The

 ISBN 978-9959-9703-2-9

percentage of unique attacked users was 11.28% of the total number of users of Kaspersky products worldwide. The rating of categories of organizations attacked by phishers is based on triggers of the Anti-Phishing component on user computers. It is activated every time the user attempts to open a phishing page, either by clicking a link in an email or a social media message, or as a result of malware activity. When the component is triggered, a banner is displayed in the browser warning the user about a potential threat. This is the first time, in 2019, the share of attacks on organizations in the Global Internet Portals category (23.81%) exceeded the share of attacks on credit organizations (22.46%). Social networks (20.48%) took third place [5].

PHISHING ATTACK

Phishing can take many forms and can be achieved with many tools and techniques. Here, we highlight the most common tools and techniques that are used to carry out phishing scams. There are many sophisticated types of phishing involving email fishing [6].

1. **Email Phishing**

Most phishing attacks are sent by email. The crook will register a fake domain that impersonators a genuine organization and sends thousands out thousands of common requests. The fake domain often involves character substitution, like using ‘r’ and ‘n’ next to each other to create 'rn' instead of 'm'.

There are some reasons why phishing attacks are frequently conducted through email:

Wide Reach: Email is a widely used communication channel, with billions of emails sent and received every day. Attackers leverage this extensive reach to target a large number of potential victims simultaneously.

• Easy Spoofing: Attackers can easily spoof the sender's information in an email, making it appear as if the email is coming from a reputable source or a trusted organization. They may manipulate the display name, email address, or even use techniques like email header forgery to make the email seem legitimate.

• Social Engineering: Phishing emails often employ social engineering techniques to manipulate recipients into taking desired actions. They may use urgency, fear, curiosity, or the promise of rewards to entice users into clicking on malicious links, opening infected attachments, or disclosing sensitive information.

• Link Manipulation: Phishing emails commonly contain manipulated or fraudulent links. As mentioned earlier, attackers alter the URLs to lead recipients to fake websites that mimic legitimate ones. These fake sites are designed to collect login credentials or personal information.

• Malicious Attachments: Phishing emails may

 ISBN 978-9959-9703-2-9

also include attachments that contain malware or viruses. These attachments often masquerade as harmless files, such as PDFs, documents, or invoices, but they can infect the recipient's device once opened.

• Automation and Scalability: Phishing attacks can be automated, allowing attackers to send a large volume of emails quickly and easily. They can use tools to generate phishing emails en masse, targeting a broad range of recipients and increasing the chances of success.

It's important to stay vigilant and exercise caution when interacting with emails, especially those that appear suspicious or unexpected. Be wary of unsolicited emails asking for personal information, urging immediate action, or containing suspicious links or attachments. Verify the legitimacy of emails independently, by contacting the supposed sender through a trusted source or using official contact information.

Alternatively, they might use the organization's name in the local part of the email address such as 'google@domainregistrar.com' in the hopes that the sender's name will simply appear as 'google' in the recipient's inbox.

There are several ways to spot a phishing email. Here are some common signs to look out for:

Phishing: Phishing attacks involve sending deceptive emails that appear to be from legitimate sources, such as banks, online services, or trusted organizations. The goal is to trick recipients into divulging sensitive information, such as login credentials, credit card numbers, or personal data.

• Spear Phishing: Spear phishing attacks are targeted phishing attempts aimed at specific individuals or organizations. Attackers gather information about their targets to create personalized and convincing emails, making it more likely for recipients to fall for the scam.

• Whaling: Whaling attacks are a form of spear phishing that specifically targets high-profile individuals like CEOs or senior executives. Attackers craft sophisticated emails pretending to be from trusted sources, aiming to trick these individuals into divulging sensitive information or performing actions that benefit the attacker.

Email Spoofing: Email spoofing involves forging the sender's email address to make it appear as if the email is coming from someone else. Attackers can manipulate the "From" field to make it seem like the email is from a trusted source, tricking recipients into trusting the message and taking action.

• Malware Attachments: Attackers may send emails with malicious attachments, such as infected documents or executable files. Opening these attachments can result in the installation of malware on the recipient's device, leading to unauthorized access, data theft, or other malicious activities.

 ISBN 978-9959-9703-2-9

• Man-in-the-Middle (MitM) Attacks: In a MitM attack, an attacker intercepts communication between the sender and recipient of an email. The attacker can eavesdrop on the conversation, modify the content of the emails, or even impersonate one of the parties involved.

- Email Account Compromise: Attackers may gain unauthorized access to someone's email account by guessing or stealing login credentials. Once they gain control, they can use the compromised account to launch further attacks, send spam, or access sensitive information.

- Phishing Sub-Domains Attackers can create sub-domains that mimic legitimate websites to launch phishing attacks. For example, they may create a sub-domain like "login.example.com" that looks similar to a legitimate login page. Unsuspecting users who enter their credentials on such sub-domains unknowingly provide their information to the attacker.

2. Hidden URL phishing attack is a technique used by attackers to deceive users by hiding the actual destination of a URL within a seemingly legitimate one. This manipulation aims to trick users into clicking on the link, thinking it leads to a trusted website when, in reality, it redirects them to a malicious or fraudulent webpage. Here's how a hidden URL phishing attack can occur:

- Text masking: Attackers can hide the actual URL by using text masking techniques. They may display a text hyperlink that appears legitimate but, when clicked, directs the user to a different website. For example, the displayed link may show "www.example.com," but the actual URL leads to a malicious site.

- HTML anchor tags: Attackers can leverage HTML anchor tags to manipulate the URL. By using code, they can specify a different URL in the anchor tag's "href" attribute than what is displayed to the user. This allows them to show a legitimate-looking link while redirecting users to a different site.

- URL shorteners: Attackers often use URL shortening services to mask the actual destination of a link. They generate a shortened URL that appears harmless or intriguing, but it leads to a malicious website. Users may not be able to discern the true

 ISBN 978-9959-9703-2-9

destination before clicking on the shortened link.

3. pop-up phishing attack, also known as a pop-up scam or pop-up phishing, is a tactic employed by attackers to deceive users through fraudulent pop-up windows. These pop-ups are designed to mimic legitimate websites or system messages in order to trick users into revealing sensitive information or downloading malware. Here's how a pop-up phishing attack typically works:

    - Unauthorized Pop-up Windows: Attackers create pop-up windows that appear during browsing sessions or when visiting specific websites. These pop-ups may overlay the current page or open in new browser windows.

    - Mimicking Legitimate Sources: Pop-up windows are designed to imitate trustworthy sources, such as legitimate websites, software updates, or system alerts. They may use logos, branding, or language similar to those used by reputable organizations to appear convincing.

    - Urgency and Fear Tactics: Attackers often employ urgency or fear tactics to prompt users into taking immediate action. The pop-up may claim that the user's computer is infected, personal data has been compromised, or their account is at risk. This creates a sense of urgency and can lead users to make hasty decisions without proper scrutiny.

    - Soliciting Personal Information: Pop-up phishing attacks may request users to enter sensitive information, such as login credentials, credit card details, or personal identification information. The intention is to trick users into providing their confidential data, which can later be misused for identity theft or fraud.

    - Malware Downloads: Pop-up windows can also trick users into downloading and installing malware-infected files or applications. These malicious downloads can compromise the user's device, leading to unauthorized access, data theft, or other harmful consequences.

THE PROPOSED MODEL

In this paper, a penetration testing model was proposed as a model to test the integrity and confidentiality of data on the network security throughout a particular four phases of

 ISBN 978-9959-9703-2-9

procedures as shown in “Fig. 1”. Several tools and techniques are used for social engineering and information gathering to generate the domain and attacks on the intended network security. Therefore, the test network laboratory was setup in attempt to simulate attacks on the given network with a few information about the target system or network, hence, the used type of penetration testing known as a grey-box approach. It reduces the number of irrelevant tests and minimize the possibility of damage to the system or network.

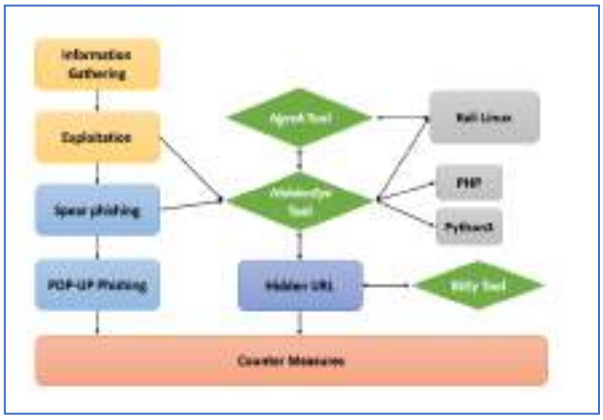

Fig. 1: The Proposed Penetration Testing Model

The overall process of penetration testing is divided into several phases collectively they form a comprehensive penetration testing methodology. Different methodologies may have different nomenclature for various phases, but these methodologies share the same objective. There are four phases as shown in "Fig. 2", to be used by the network penetration tester.

LABAROTORY SETUP

The proposed penetration testing model is implemented using specific tools and techniques. First, we have installed the VM Ware version 15.5, which is virtualization software that allows us to use different operating systems on the virtual machine, to emulate a cross-platform environment. Second, two machines OSs (Kali Linux and Windows 10) software were installed and the firewall is activated with each machine as depicted in "Fig. 2". Moreover, this OS software served as a target or victim machine throughout the test.

The HiddenEye, Ngrok, and Bitly are the main tools that were used to conduct the penetration test. The HiddenEye modern tool requires PHP and Python3 to be installed. The We have installed Ngrok tool on Kali machine, as one of the penetration testing tools during the victim exploitation process.

 ISBN 978-9959-9703-2-9

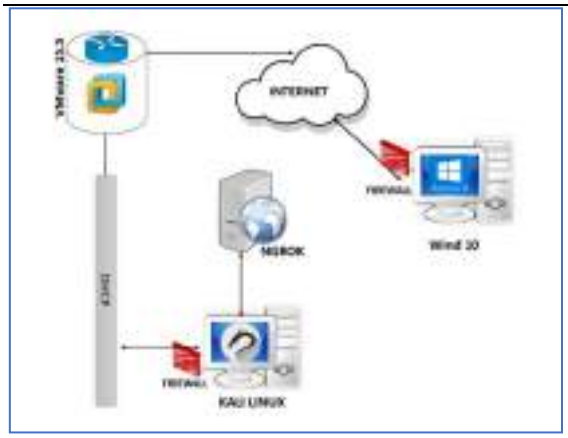

Fig. 2: Laboratory Infrastructure

EXPERIMENTAL RESULTS

In this section, the implementation of phishing attack of the proposed model is presented with the obtained results. Such an attack is carried out as following:

• Step 1: the phishing attack is started by downloading the hiddeneye tool. We have selected the Google site to test the username and password against broken based on the hiddeneye sequence number which is 2 for the Google service as shown in "Fig. 3".

Fig. 3: Selecting Google Page

• Step 2, Ngrok tool (multiplatform tunneling) is selected as reverse proxy software to establishe secure tunnels from a public endpoint such as Internet to a locally running network service while capturing all traffic for detailed inspection and replay [8]. "Fig. 4" shows establishing secure tunnels.

Fig. 4: Establishing Secure Tunnels.

• Step 3: Identifying reverse connecting port of the victim machine for making redirects

ISBN 978-9959-9703-2-9

connection via port 8080 using Ngrok tool for Kali Linux machine with domain generator. "Fig. 5" shows the implantation of this task.

Fig.5: Redirecting Connection Port

• Step 4: Inserting a custom redirect URL 'google.com' as shown in "Fig. 6".

Fig. 6: Redirecting URL

• Step 5: A new URL is generated as shown in "Fig. 7". Then, it will be hided using bitly tool, that make the victim does not expect that such a link is sent from a server as shown in "Fig. 8". The hidden URL is sent either by creating a fake-email or through social media to make the user of a victim website clicking the link to confirm some information.

Fig. 7: Generating URL by Ngrok.

Fig. 8: Hiding the URL.

• Step 6: Finally, once the link is clicked by the victim, then user name and the password are obtained using hiddeneye tool. Moreover, specifications of the victim's device, the public IP, and the state/country are displayed as shown in the "Fig. 10".

ISBN 978-9959-9703-2-9

Fig. 9: The Result of the Success Attack

COUNTERMEASURES

The victim machine became compromised. So, the below proposed techniques should be considered and highly recommended as countermeasures to make a victim machine protected from phishing attack. Such techniques are listed as following:

• To make a victim machine protected from the pop-up phishing, users should avoid the responding for the popup windows that appear spontaneously and clicking a hyperlink. Moreover, block pop-ups in the browser settings and always log out of the banking sessions and other sensitive accounts as soon as the work is completed [9].

• Filter emails for phishing threats using multi software tools to detect a lot of malwares in an email and to detect known malicious URLs and security analytics to alert on unknown ones such as 'Rapid7 UserInsight' tool.

• Updating client-side, software, and plug-ins in

• Updating the operating systems, browsers, and its plug-ins such as Flash and Java. This is required due to some phishing emails include URLs to exploit vulnerabilities.

• Implementing 2-factor authentication and adding 2-factor authentication (2FA) to any external device to stop attackers from using stolen passwords.

• Training employees on security awareness due to any phishing attack can succeed only if a target victim clicks on the link. So, creating awareness and educating the employees and other users about the types of phishing attacks in the network is the best way to prevent phishing attacks.

• Reading sender's email address carefully is also a way to prevent phishing attacks.

• Copying and pasting characters in an email address in the notepad to check the use of numeric or special characters.

• Checking the website address to avoid a fake address which is a very similar to the real one. For example, there is a typo in the link that people can easily miss: 'www.citiibank.com' instead of 'www.citibank.com', and 'amazon.com,' that will be redirected to 'arnazon.com', which belongs to the attacker.

CONCLUSIONS

ISBN 978-9959-9703-2-9

We have presented a penetration testing model for phishing attack. Such a model was implemented and suitable counter measures were defined. We have found that security methodologies and tools, if properly utilized, can prove their usefulness for understanding the weaknesses of the network or system and how they might be exploited. Penetration testing is not an alternative to other security measures however, it can be used to complement the defence in depth principle. Moreover, the use of old systems should be avoided as it may have serious vulnerabilities.

Absolute security cannot be achieved, this is one of the fundamental principles of security, but a high rate of safety could be achieved through the implementation of network penetration testing periodically. Therefore, penetration testing techniques is very useful for building strategies for measuring the extent of securing data in order to improve the management performance, through the filtration of data.

Finally, in order to perform a successful penetration tests, the underlying methodology should use different security tools.

REFERENCES

[1] L. Irwin, "The 5 most common types of phishing attack," July.09.2019. Available: https://www.itgovernance.eu/blog/en/the-5-most-common-types-of-phishing-attack. [Accessed Dec.26.2019].

[2] H. Farag. and A. Almarimi, "Investigation of Threats for Common Network Attacks," In the Proceeding of LICTEE2019'02, Tripoli, Libya, Mar, 2019.

[3] Apwg, "Phishing Activity Trends Reports," Oct.26.2019. Available: https://apwg.org/trendsreports/. [Accessed: Dec.25.2019].

[4] Maria V. and other, "Spam and phishing in Q2 2019," Nov.26.2019. Available: https://securelist.com/spam-and-phishing-in-q2-2019/92379/ [Accessed: Dec.30.2019].

[5] Maria V. and other, "Spam and phishing in Q3 2019," Nov.26.2019. Available: https://securelist.com/spam-report-q3-2019/95177/ [Accessed: Dec.30.2019].

[6] S. Phirashisha, G. Mary, K. Ushamary, S. Bobby. "Phishing-An Analysis on the Types, Causes, Preventive Measuresand Case Studies in the Current Situation," Journal of Computer Engineering (IOSR), p-ISSN: 2278-8727, 2015, PP. 01-08.

 ISBN 978-9959-9703-2-9

[7] B. Jan-Willem, M. Lorena, J. Marianne, H. Pieter, "Spear phishing in organisations explained," Information and Computer Security. 25. 00-00. 10.1108/ICS-03-2017-0009, 2017, pp. 593-613.

[8] "Ngrok," Dec.3.2019. [online]. Available: https://ngrok.com/product. [Accessed: Dec.30.2019].

[9] B. Gupta, A. Nalin, P. Kostas. "Defending against Phishing Attacks: Taxonomy of Methods, Current Issues and Future Directions," Telecommunication Systems. 2017, 10.1007/s11235-017-0334-z.

 ISBN 978-9959-9703-2-9

المؤتمر الدولي الثاني للعلوم والهندسة
2nd International Conference on Science and Engineering
ICSE 2023
Faculty of Engineering - University of Bani Waleed
Bani Waleed, Libya

Paper Code: ICSE-059

PERFORMANCE COMPARISON OF IMAGE NOISE REDUCTION AND FILTERING ALGORITHMS

Khaled Almarimi[1] , Ibrahim Elwarfalli[2*], Moammer H.Daw[3]
[1]Department of Computer Science, Science College, Baniwaleed University, Libya
almaimekhaled@gmail.com
[2]* West Virginia University, US
* Crosspnding : ieelwarfalli@mix.wvu.edu
[3]Department of Computer Science & IT , Technical Sciences College of Baniwalid , Libya

Abstract: Image noise poses a significant challenge in digital image processing, impacting the quality and reliability of various applications. To address this issue, researchers have developed a multitude of noise removal techniques. In this article, we propose a Modified Wiener filter as a novel approach to combat image noise. Additionally, we explore and compare its performance with other well-known noise removal techniques, including the Adaptive Lee filter, adaptive median filter, and adaptive Wiener filter. By examining the unique characteristics, advantages, and limitations of each method, we aim to provide valuable insights into their effectiveness and applicability in real-world scenarios.

Keywords: adaptive Wiener filter, Modified Weiner Filter, Adaptive Lee filter, adaptive median filter

Introduction

As digital images continue to play a vital role in fields such as medical imaging, remote sensing, and computer vision, the demand for robust noise removal techniques becomes increasingly important. To achieve this, researchers have devised advanced noise removal techniques such as the Adaptive Lee filter, adaptive median filter, and adaptive Wiener filter. These methods leverage adaptive algorithms and statistical approaches to estimate local image statistics and optimize noise reduction. Each technique employs adaptive algorithms and statistical approaches to adaptively estimate local image statistics and optimize noise reduction. By understanding the strengths and limitations of these techniques, researchers and practitioners can make informed decisions when selecting an appropriate method for their specific image denoising needs. In this article, we study these filters in addition to a proposed Modified Wiener filter, shedding light on their mechanisms and discussing their performance in various scenarios.

 ISBN 978-9959-9703-2-9

Literature Review

Image processing techniques play a crucial role in enhancing the quality of digital images by removing noise and artifacts. The adaptive median filter is an important method widely employed for noise reduction and preserving edge details. here, we explore relevant studies and developments in the field of adaptive median filtering [1].

The adaptive median filter is an effective technique for noise removal, particularly in images with varying levels of noise and complex backgrounds. In their seminal work, P. K. Sahoo, S. Soltani, and K. C. Wong (1988) proposed the concept of the adaptive median filter, which analyzes the local neighborhood of pixels and adjusts the filter window size accordingly to adapt to different noise levels. Their method demonstrated superior noise reduction performance compared to traditional fixed-size median filters. Since the introduction of the adaptive median filter, several extensions and improvements have been proposed to enhance its capabilities. K. G. Cortelazzo and M. L. Trivedi (1994) introduced a modified adaptive median filter that incorporates spatial information to achieve better noise suppression in textured and non-textured regions. S. S. Again et al. (2007) presented an improved adaptive median filter that utilizes morphological operations to enhance the filtering process and handle impulse noise effectively. The adaptive median filter finds extensive applications in medical imaging, where preserving fine details and reducing noise are crucial for accurate diagnosis. In their study, R. Raju et al. (2014) applied the adaptive median filter to denoise magnetic resonance images, leading to improved image quality and more reliable analysis. Y. Wang, H. Yu, and Y. He (2020) proposed an adaptive median filtering approach for ultrasound image enhancement, enhancing the visibility of structures and improving diagnostic accuracy.

Materials and Methods:

1- Adaptive Lee Filter (ALF)

The Adaptive Lee filter is a widely used technique in image processing for speckle noise reduction in remote sensing and ultrasound imaging. This section provides an overview of the Adaptive Lee filter, its applications, and key studies in this field.

The Adaptive Lee filter is a statistical filtering technique that effectively suppresses speckle noise while preserving image details. It adaptively estimates the local statistics of the image, adjusting the filter parameters to achieve optimal noise reduction results. This filter is particularly useful in applications

 ISBN 978-9959-9703-2-9

where preserving image features and maintaining fine details are crucial.

Lee introduced the concept of the sigma filter, which is the foundation of the Adaptive Lee filter. The sigma filter estimates local statistics to adaptively adjust the filter parameters, providing effective speckle noise reduction [8].

Wu, Huang, and Liao proposed a new adaptive filter based on the Lee filter for speckle noise reduction in ultrasound images. The filter adaptively estimates the local statistics and incorporates a novel weight function to enhance noise reduction performance [14].

Bae and Kang developed an adaptive Lee filter specifically for polarimetric synthetic aperture radar (SAR) data. The filter adaptively estimates the covariance matrix to effectively reduce speckle noise in SAR images, improving image quality and interpretation [2].

Qu, Huang, and Xu proposed an adaptive polarimetric Lee filter for speckle noise reduction in polarimetric SAR images. The filter adaptively estimates the covariance matrix of polarimetric data to achieve optimal noise reduction while preserving polarimetric information [11].

These studies by Lee, Wu et al., Bae and Kang, and Qu et al. have contributed significantly to the development and application of the Adaptive Lee filter in different domains. These studies showcase the effectiveness of the Adaptive Lee filter in enhancing image quality while suppressing speckle noise.

The Lee filter (LF) stands as an adaptive filter for noise diminution that conserves the edges of the image for effective used. The mathematical illustration for LF denoising is formulated as given in equ (1).

$$H = \overline{m} + W \times \left(C - \overline{m}\right) \qquad (1)$$

Where, represents a denoised image, indicates mean intensity of the filter window, implies the weight function and is a central element in the filter window[6].

By applying the ALF, each pixel on an image is considered and supplanted by the center value of its surrounding pixels. Initially, the center value is estimated by sorting the whole pixel values as of the filter window in to numerical order[6]. On the off-chance that the neighborhood pixels consist of an even number of pixels, the pixel values' average is utilized as the center value. Then the old center pixel value in filter window is swapped with the newly sorted pixel value. This helps to replace the noisy pixels on an image. To ameliorate the performance in edge areas, a refinement is done to the original LF, wherein the neighborhood used in high variance areas for the calculation of the local statistics took on board the orientation of a possible edge. Therefore, the weighting function of LF is written as given in eq. (2).

 ISBN 978-9959-9703-2-9

$$W = \frac{\sigma^2}{\sigma^2 + \rho^2} \quad (2)$$

Here, denotes a weighting function, indicates variance of the image, in which represents the variance of pixels in filter window.

Adaptive Median Filter(AMF)

The adaptive median filter is a widely used technique in image processing for noise reduction and preserving image details. This section review aims to provide an overview of the adaptive median filter, its applications, and key studies in this field.

Adaptive Median Filter is a nonlinear filtering technique that adjusts the filter size based on the local characteristics of the image. It is effective in removing different types of noise, including salt-and-pepper noise and impulse noise, while preserving important image details. The filter adaptively analyzes the pixel neighborhood and applies a variable-sized window to obtain better noise reduction results.

Lee proposed the adaptive median filter for impulsive noise removal in highly corrupted images. The filter adjusts the window size based on the local noise characteristics, achieving effective noise reduction[7].

Huang and Russell introduced new algorithms for adaptive median filters, improving their noise removal capabilities. The study presented various techniques for selecting the window size, enhancing the adaptivity of the filter[4].

Bhargava and Shah proposed an adaptive impulse noise removal method using progressive switching median filters. The technique effectively detects and removes impulse noise while preserving image details[3].

Zhang and Wang introduced an adaptive fuzzy switching weighted median filter for salt-and-pepper noise removal. The filter adapts the weights based on the local image characteristics, resulting in improved noise reduction performance[15].

The adaptive median filter is a powerful tool for noise reduction in image processing. Through adaptive window sizing and analysis of local image characteristics, it effectively removes noise while preserving important image details. Previous studies by Lee, Huang and Russell, Bhargava and Shah, and Zhang and Wang have made significant contributions to the development and improvement of adaptive median filters.

In AMF procedure, the size of filter window is modified in accordance to the noise density. Median filters changes the SPN values and retains the grey values of the image as it is. In the process of detecting the noise points, pixels are just divided into two categories based on

 ISBN 978-9959-9703-2-9

Pmax and Pmin, thereby making it easy to sort image of pixels into noise points. To prevent sorting Pmax into noise point, a variable (LS) least set difference is introduced and Ω represents the set of non pollutant points.

$$LS = \min\{|P_{ij} - P_{zk}|\} \quad (3)$$

Where Zk is pixel values in neighborhood of non pollutant points.

The first step computes the value of Pmin and Pmax by sorting the gray values of pixels in the working window Wij . The minimum pixel value is assigned Pmin and the maximum value is assigned Pmax . The average intensity values of the pixels is assigned Pmed. The next step checks if Pij is a pulse or noise point. If it is a pulse it is then added to the set of non pollutant set. If the size of the window is less than maximum window size, the width of the working window is increased by two. If it is greater than the maximum window size, Pij remains unchanged (if Ω is empty) otherwise LS is computed and the filter output is Pij (If LS ≤ Threshold) else Pij becomes a noise point and the output is Pmed (median value of Ω). Figure (1) illustrates the AMF procedure

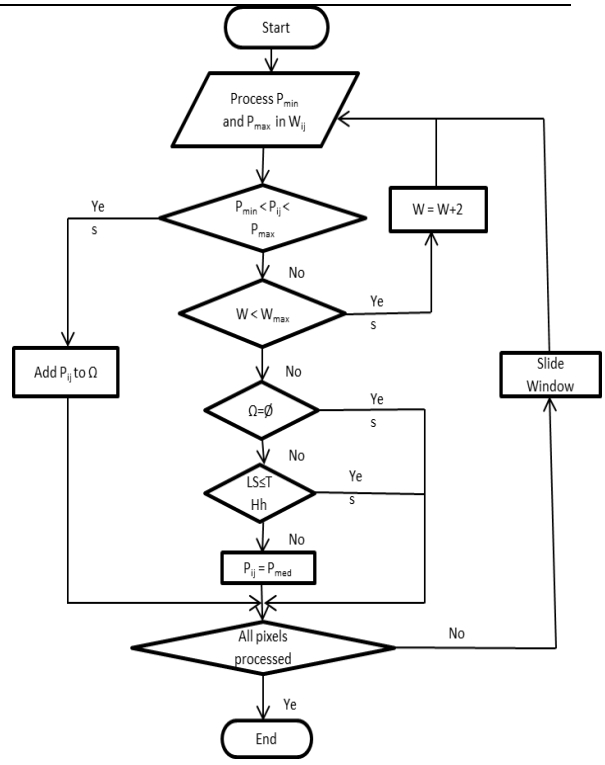

Utilizing this algorithm the SPN is removed and the noise-free $I_f^{'}$ image is obtained.

Let Pij be the pixel value of point (i,j) of the original image If (N), Wij be the present working window. Let Pmin, Pmed, Pmax be the minimum, intermediate and maximum pixel value respectively. Suppose maximum window is Wmax , LS of threshold, Th, with window set to Wij, Width W=3 and Ω = Ø.

Step 1: Compute the values of Pmin and Pmax with Wij for current pixel.

 ISBN 978-9959-9703-2-9

Step 2: If Pmin < Pij < Pmax

Then Pij remains unchanged and Add the non pollution point from Wij into Ω

Step 3: If W < Wmax

Set W= W +2 (increment width by 2)

Step 4: If W ≥ Wmax

Check if Ω = Ø

Pij remains unchanged

Otherwise Compute LS of Pij by eq (3)

If LS ≤ Th

Filter output is Pij

Else

Pij is the noise point and filter output is Pmed (median value of set Ω)

Proceed to Sep 5

Step 5: The procedure is recursed until all pixels are processed.

Utilizing this algorithm the SPN is removed and the noise-free $I_f^{'}$ image is obtained.

1- Existing Adaptive Wiener Filtering(AWF)

The inverse filtering is a restoration technique for deconvolution, i.e., when the image is blurred by a known lowpass filter, it is possible to recover the image by inverse filtering or generalized inverse filtering[10]. However, inverse filtering is very sensitive to additive noise. The approach of reducing one degradation at a time allows for the development of a restoration algorithm for each type of degradation and simply combine them. The Wiener filtering executes an optimal tradeoff between inverse filtering and noise smoothing. The Wiener filter removes the additive noise and inverts the blurring simultaneously. The Wiener filter is based on a statistical approach. The WF stands as a linear estimation of the original image [9]. The block diagram of wiener filter is given in figure(2).

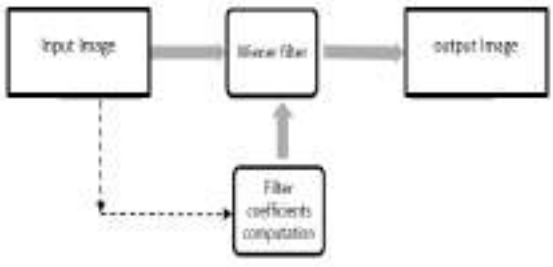

Figure 1: Block diagram of the Wiener Filter

The Wiener filtering is optimal in terms of the mean square error. In other words, it minimizes the overall mean square error in the process of inverse filtering and noise smoothing [5]. Wiener filters are usually applied in the frequency domain. Given a degraded image x(n,m), one takes the Discrete

 ISBN 978-9959-9703-2-9

Fourier Transform (DFT) to obtain X(u,v). The original image spectrum is estimated by taking the product of X(u,v) with the Wiener filter G(u,v):

$$\hat{s}(u,v) = G(u,v)X(u,v) \quad (4)$$

The inverse DFT is then used to obtain the image estimate from its spectrum. The Wiener filter is defined in terms of these spectra:

$H(u,v)$ Fourier transform of the point-spread function (PSF).

$P_{ɞ}(u,v)$Power spectrum of the image process, obtained by taking the Fourier transform of the image autocorrelation.

$P_{\Omega}(u,v)$Power spectrum of the noise process, obtained by taking the Fourier transform of the noise autocorrelation.

The Wiener filter is expressed below

$$G(u,v) = \frac{H(u,v)*P_{ɞ}(u,v)}{H(u,v)^2 P_{ɞ}(u,v) + P_{\Omega}(u,v)} \quad (5)$$

For the case of additive white noise and no blurring, the wiener filter simplifies to:

$$G(u,v) = \frac{P_{ɞ}(u,v)}{P_{ɞ}(u,v) + \sigma_{\Omega}^2} \quad (6)$$

Where σ_{Ω}^2 is the noise variance.

Also Proposed a technique for removal of speckle noise from images using a combination of hybrid wiener-median filter[12].

Initially logarithmic transform of the noisy image was computed. This step is performed because speckle noise is a multiplicative noise.

The Mean-squared Methods uses the fact that the Wiener Filter is one that is based on the least-squared principle, i.e.the filter minimizes the error between the actual output and the desired output. To do this, first the variance of the data matrix is to be found. Then, a box of certain size is passed around the matrix, moving one pixel at a time[13]. For every box, the local mean and variance is found. And the filtered value of each pixel is found by the following formula:

Weiner Filter estimates the local mean and variance around each pixel

$$M' = \frac{1}{NM} \sum_{i,j \in \eta} G(i,j) \quad (7)$$

$$\sigma^2 = \frac{1}{NM} \sum_{i,j \in \eta} G^2(i,j) - M'^2 \quad (8)$$

Where η is the $N - by - M$ Local neighborhood of each pixel in the image G, this creates a pixel-wise Wiener Filter using these estimates.

Weiner Filter based on mean squared method is expressed by using the equation:

 ISBN 978-9959-9703-2-9

$$b(i,j) = M' + \frac{\sigma^2 - r^2}{\sigma^2}\left(G(i,j) - M'\right) \quad (9)$$

Where, $b(i,j)$ represent the MWF in the time domain, M' is the local mean around each pixel, σ^2 denotes the variance and also r^2 represents the noise variance. The frequency domain (FD) representation of the image G_i is $G(u,v)$.

1- Proposed Modified Wiener Filter(MWF)

Weiner filter (WF) is effectual in the existence of random noise like the Gaussian noise. The inverse filtering stands as a restoration method for deconvolution, explicitly when the image is blurred via a known low pass filter; it is probable for recovering the image by means of inverse filtering or else generalized inverse filtering. Nevertheless, inverse filtering is exceptionally responsive to additive noise. It eradicates the additive noise and also inverts the blurring concurrently. The general Weiner filter produces results that are often too blurred and spatially invariant. A modified Wiener Filter (MWF) was proposed to overcome this problem.

The gray scale image G_i is imposed as the input to the MWF. Here the quantity of noise that exists in the image was minimized. This was performed by comparing the received image with an assessment of a preferred noiseless signal. This involves the diminishment of the median square error.

The original wiener filter uses the mean value (M') for the filtering process. In this approach , the filter continuously looks at its nearby neighbours to decide whether or not it is a representative of its surroundings, if it is not that pixel value is replaced with the mean of its neighbouring pixel values. This approach leads to a wide discrepancy in some pixel values thus affecting the image preservation details. A different approach was utilized for computing M' in our proposed wiener filter. The median was utilized. This approach preserves the image details better. Instead of just replacing pixel values with mean of their neighbourhood, we utilized the median and M' is derived as follows:

Sort all the pixels in ascending order , if a pixel is not a representative of its neighbourhood. The neighbourhood is sorted in ascending order and the pixel value is simply replaced by the median value of its neighbourhood. This will allow the noisy pixel to take a value that is closer to its neighbourhood pixels thus preserving the image details.

The median is calculated by first sorting all the

 ISBN 978-9959-9703-2-9

pixel values from the surrounding neighborhood into numerical order and then replacing the pixel being considered with the middle pixel value. (If the neighborhood under consideration contains an even number of pixels, the average of the two middle pixel values is used.) Figure illustrates an example calculation.

123	125	126	130	140
122	124	126	127	135
118	120	150	125	134
119	115	119	123	133
111	116	110	120	130

Neighbourhood values:

115, 119, 120, 123, 125, 126, 127, 150

Median value: 124

Figure 2: An example of pixel median computation

From the above formula (9), it can be seen that if the original pixel value is similar to the local variance then the filtered value will be that of the local median, if the original pixel value is very much different from the local median, then it will be filtered to give a higher/lower intensity pixel depending on the differences. Also, if the local variance is similar to the matrix variance, which is around 1 (i.e. only noise exists in the box) then the filtered pixel will be that of the local median, which should be close to zero.

The filter is a slight modification of equation (10). In this approach we compute median and also the added with the noise variance to get the smoothed image.

The filtered image is mathematically written as shown below.

$$W(u,v) = M' + \frac{\sigma^2 + r^2}{\sigma^2}\left(G(i,j) - M'\right) \quad (10)$$

Where, represent the MWF for filtered value of each pixel, is the local median around each pixel, denotes the variance and also represents the noise variance. The G(i,j) represent the 'gray scale image' on the time domain.

$$P(u,v) = W(u,v).G(u,v) \quad (11)$$

Where, is the 'filtered image' on the FD, is the 'modified wiener filter' on the FD and is the 'gray scale image' on the FD. Figure (3) Shows the block diagram of the proposed wiener filter.

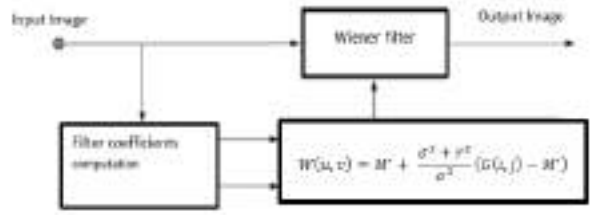

Figure 3 : Block diagram of Modified Wiener Filter (MWF)

 ISBN 978-9959-9703-2-9

Results and Discussions

This paper focuses on the evaluation and comparison of various image filters, including the Modified Wiener Filter, Wiener Filter, Median Filter, and Adaptive Lee Filter. These filters are widely used in image processing applications for noise reduction and image enhancement.

The Modified Wiener Filter is a variant of the traditional Wiener Filter that incorporates additional modifications to improve its performance in noisy environments. It utilizes statistical properties of the image and noise to achieve optimal noise reduction results.

The Wiener Filter is a classical linear filter used for image denoising. It assumes a stationary signal and stationary noise in the frequency domain, and it aims to minimize the mean square error between the filtered image and the original image.

The Median Filter is a non-linear filter that replaces each pixel value with the median value of its neighborhood. It is effective in removing impulse noise and preserving edges, but it may result in blurring of fine details.

The Adaptive Lee Filter is a statistical filter that adapts to local image characteristics and effectively reduces speckle noise while preserving important image details. It estimates local statistics and adjusts filter parameters for optimal noise reduction.

This section of the paper compares and evaluates the performance of the proposed modified wiener filter in terms of PSNR. The proposed filters performance is contrasted with other existing filters say wiener filter, median filter and averaging filter.

The preprocessing uses the MWF to abolish noise. The PSNR ('Peak Signal to Noise Ratio') that is associated with the application of each filter is estimated for database. These values are contrasted with the existing filters like the Wiener Filter, Median Filter , Lee Filter and MWF,. The PSNR determines the image quality. The higher PSNR value denotes high quality.

Table 1: PSNR values for the proposed MWF filter and the other existing filters that are implemented using database .

Frames	PSNR Values			
	MWF	ALF	AWF	AMF
1	46.0367	38.18555	37.66491	36.78769
2	46.034	38.06246	37.66592	36.78691
3	46.0699	38.08859	37.67718	36.81163
4	46.09185	38.13165	37.67269	36.77833
5	46.08754	38.00522	37.68014	36.75052
6	46.06611	38.03343	37.66249	36.76345
7	46.04962	38.09444	37.63714	36.74512
8	46.0495	38.99484	37.62195	36.7016

ISBN 978-9959-9703-2-9

9	46.052	38.12629	37.61009	36.71103
10	46.04714	38.13046	37.60655	36.7027

Figure 4: Performance evaluation of MWF on database

Figure 4 above shows the PSNR values of the proposed and existing techniques. The proposed MWF has the highest PSNR value of 46.09185 at fourth frame, while AMF has the lowest PSNR value of 36.7016 at eighth frame. AWF has the highest PSNR value of 37.60655at tenth frame.

Conclusion

In conclusion, the research paper comprehensively evaluated and compared the performance of four image filters: the Modified Wiener Filter, Wiener Filter, Median Filter, and Adaptive Lee Filter. The findings of this study contribute to the understanding of these filters and their suitability for various image processing applications.

The Adaptive Lee filter is a statistical filtering technique that effectively reduces speckle noise while preserving important image features. It adaptively estimates local statistics and adjusts filter parameters to achieve optimal noise reduction results. On the other hand, the adaptive median filter addresses impulse noise by replacing pixel values with the median of neighboring pixels, effectively smoothing out noise while preserving edges. The adaptive Wiener filter utilizes the statistical properties of the signal and noise to remove noise from images, assuming a stationary signal and stationary noise. Lastly, our proposed modified Wiener filter introduces modifications to enhance its performance in noisy environments. This filter combines the principles of the Wiener filter with additional enhancements to achieve improved noise reduction and image quality. Moreover, the PSNR values that were attained by the employment of the MWF were much above the values that were obtained using other filters.

References

[1] Razaque, F. H. Amsaad, M. Abdulgader, V. C. Mannava, I. Elwarfalli and P. T. Kilari, "Automatic Tampering Detection Paradigm to Support Personal Health Record," 2016 IEEE First International Conference on Connected Health: Applications, Systems and Engineering Technologies (CHASE), Washington, DC, USA, 2016, pp. 388-393, doi: 10.1109/CHASE.2016.77.

[2] Bae, H., & Kang, M. G. (2015). Adaptive Lee filter for polarimetric synthetic aperture radar data. IEEE Transactions on Geoscience and Remote Sensing, 53(4), 1931-1945.

[3] Bhargava, M., & Shah, H. (2011). Adaptive impulse noise removal using progressive switching median filters. International Journal of Computer Science and Information Security, 9(5), 133-138.

[4] Huang, T. S., & Russell, D. (1997). Adaptive median filters: New algorithms and results.

 ISBN 978-9959-9703-2-9

IEEE Transactions on Image Processing, 6(3), 404-417.

[5] J. Jaybhay and R. Shastri, A STUDY OF SPECKLE NOISE REDUCTION FILTERS, An International Journal (SIPIJ) Vol.6, No.3, June 2015.

[6] K. Abdalhamid and W. Jeberson(2019) Pose-Invariant Face Recognition By Means Of Artificial Bee Colony Optimized Knn Classifier, Jour of Adv Research in Dynamical & Control Systems, Vol. 11, Special Issue-08.

[7] Lee, J. S. (1980). Adaptive median filtering for the removal of impulsive noise from highly corrupted images. IEEE Transactions on Acoustics, Speech, and Signal Processing, 28(6), 744-747.

[8] Lee, J. S. (1983). Digital image smoothing and the sigma filter. Computer Vision, Graphics, and Image Processing, 24(2), 255-269.

[9] Marapareddy R (2017) Restoration of blurred images using wiener filtering, Proceedings of WRFER International Conference, 25th June, 2017, Bengaluru, India.

[10] Mohamed Jabarulla, and Heung-No Lee (2018) Speckle reduction on ultrasound liver images based on a sparse representation over a learned dictionary, Applied Sciences, 8(6): 903.

[11] Qu, Y., Huang, X., & Xu, L. (2018). Adaptive polarimetric Lee filter for speckle noise reduction in polarimetric SAR images. IEEE Transactions on Geoscience and Remote Sensing, 56(2), 1011-1022.

[12] Sarita and Surab (2016) " Despeckling of Images using Weiner Filter and Hybrid Median Filter", International Journal of Computer Applications (0975 – 8887), Volume 154 – No.7, November 2016.

[13] Saroj Kumar Gupta and Surya Bahadur(2010) Noise Load Adaptive Filter Using Neural Network, International Journal of Mathematics and Engineering 10 (2010) 115-121, ISSN 0976 – 1411.

[14] Wu, X., Huang, X., & Liao, S. (2011). A new adaptive filter for speckle noise reduction in ultrasound images. IEEE Transactions on Medical Imaging, 30(1), 85-94.

[15] Zhang, H., & Wang, Z. (2014). Adaptive fuzzy switching weighted median filter for salt-and-pepper noise removal. Journal of Visual Communication and Image Representation, 25(1), 13-20.

 ISBN 978-9959-9703-2-9

المؤتمر الدولي الثاني للعلوم والهندسة
2nd International Conference on Science and Engineering
ICSE 2023
Faculty of Engineering - University of Bani Waleed
Bani Waleed, Libya

Paper Code: ICSE-055

TRIBE ENVIRONMENT, BUILT ENVIRONMENT AND URBAN PRIVACY BANI WALID CITY AS A CASE STUDY

Fawzi Mohamed Agael [a] , Hamza ALKHAZMI[b,] Omar Ali Alameen [c]
fawzi6664@gmail.com,hammtmh@gmail.com, omar3228570@gmail.com
a,b,c Department of Architecture & urban planning, Faculty of Engineering, Elmergib University, Libya
*Corresponding author email: fawzi6664@gmail.com

Abstract: This research examines the relationship between cultural and social interactions, as cultural societies have unique characteristics that are reflected in their cultural expressions and their impact on the built environment, and vice versa, using Space Syntax measures (Intelligibility and synergy), which are links between some of the most important measures of Space Syntax theory. The city of Bani Walid was chosen as a case study because it has lower values of Intelligibility and synergy than traditional pedestrian cities.
Analyzes of the Space Syntax theory were used, as it was noted that there is a strong relationship between local integration and Global integration, as well as between Connectivity and Global integration ,which in turn reflects knowledge of the degree of privacy and the impact of people's cultural background on planning their cities.
The relationships between roads, spaces and their syntactic values are very important issues to understand the impact of social and cultural interactions on the spaces and streets of the city.

Keywords: Cultural interactions, Space Syntax measures, Bani Walid, Global integration, Syntactic values

Introduction

Researchers have shown an increasing interest in understanding how the individuals' behavior influences built environment and how it can be proactively utilized to impact specific behavior, such as improving socio-cultural interaction or reducing felonies. This relevant research spans different fields, including design, geography, urban planning, and sociology, resulting in a diverse set of concepts, hypotheses, and techniques for understanding how the built environment can improve socio-cultural interaction[1].
A similar definition is also given by the Webster's Online Dictionary; privacy is the quality of being secluded from the presence or view of others or the condition of being concealed or hidden [2].
The idea of distinguishing spaces according to their degree of privacy is very common for architecture. It is traced back to the beginning of the seventeenth century [3].
For today's architectural practice, this distinction, seems self-evident and almost an essential precondition when approaching a design problem. Nevertheless, in most cases dealing with it ends up in separating social spaces from private spaces. This separation of social and private is pinpointed by Nathan Witte in his thesis on privacy "Within the architecture discourse, privacy is seen as

 ISBN 978-9959-9703-2-9

something to be provided or withheld" [4].

The concept of privacy is complex and multifaceted, and its definition varies depending on the context and interpretation. Scholars from various fields, including law, philosophy, sociology, environmental psychology, anthropology, biology, zoology, and architecture, have studied privacy extensively. In recent years, the field of computer science has also focused on privacy as a critical issue [5].

Privacy serves as a vital mechanism for controlling overcrowding in the animal kingdom, and it is necessary for developing and maintaining healthy relationships within society. According to Irwin Altman and Westin, one of the major functions of privacy is to serve the individual's self-identity by creating personal boundaries. In other words, privacy allows individuals to establish a sense of control over their personal space and information, which is essential for maintaining autonomy and individuality [6].

In today's digital age, privacy has become a critical concern due to the widespread use of technology and the internet. With the constant collection and dissemination of personal data, individuals are at risk of losing control over their privacy. Therefore, it is essential to implement measures to protect personal information and ensure individuals have the right to control their data. This can be achieved through the development of privacy policies and regulations, as well as the use of encryption and other security measures to safeguard personal data [7].

Overall, privacy is a vital aspect of personal identity and autonomy, and it is essential to protect it in all contexts, whether in the physical or digital world [8].

Today, cities around the world are experiencing different ways of living, and the development and progression of urban areas, along with various social changes, have greatly increased the complexity of urban design [9].

As sociocultural practices of any society depend on the willingness of the people to continue practicing them and the impact of resettlement programs on such activities, there is a need for urban open spaces at the local urban level to reduce social stresses by increasing direct interactions and building linguistic connections [10].

The most essential parts of a social framework are activity spaces, as these are spaces where social interaction occurs. Therefore, it is important for towns and cities to create specific places where social effectiveness can happen, and individuals can freely choose. Previous studies have shown that any communicative activity can influence the quality of life and personal satisfaction. Additionally, there is a critical relationship between open spaces and physical well-being, including good health and public interaction [11].

Furthermore, the experience of space in the urban environment is directly influenced by what is seen and how it is viewed, and the urban image in human reason, thus human behavior, can be oriented through all furniture components to be made in urban places. The environment is a condition that employs social support, and culture matters since people have distinctive qualities and diverse inclinations concerning administration and leadership, that are identified with their cultural foundation [12].

Lastly, individuals need relationships to develop a sense of self, and relationships are important for their ability to help individuals build up a feeling of self. The relational self is the part of an individual's self-concept that comprises the emotions and beliefs that one has regarding oneself that develops based on interactions with others.(Lubis and Primasari, 2012). Urban image in human reason in this manner the human practices and behaviors can be oriented through all furniture components to be made in urban places (Lang, 1994). Environment is the condition that employs social support (Laurens, 2012). One approach emphasizes the importance of culture in cross-cultural interactions. In this

 ISBN 978-9959-9703-2-9

viewpoint, culture matters since people have distinctive qualities and diverse inclinations concerning administration and leadership that are identified with their cultural foundation (Hofstede, 2001). Studies have demonstrated that national culture impacts an individual's mentality, conduct and convictions (Harrison and Huntington, 2000; Hofstede, 2001; Kirkman et al., 2006.(Also develop a sense of self of individuals need more Relationships; relationships are important for their ability to help individuals build up a feeling of self. The relational self is the part of an individual's self-idea that comprises of the emotions and convictions that one has in regards to oneself that creates in light of collaborations with others [13].

Cultural of communities

Cultural communities have unique characteristics that are reflected in their cultural expressions, including language, folklore, traditional food and clothing, and customs related to celebration and gathering. In order to prevent the loss of their cultural identity due to increasing global cultural openness, many communities make efforts to preserve their traditional heritage and cultural traits [14].

The Urban Formation

Urban formations are a favorite theme of many regions, and different types of urban formations can be found in different areas. In addition to the nature of the relationship between the Blocks and spaces in the city, attention is also given to the urban relationships between the blocks themselves and the shapes, sizes, and proportions of the blocks and spaces. In The region of ban Walid and other tribe traditional Arab cities, these characteristics can be seen in the relationship between blocks and spaces, such as closed streets (like tree) and alleys, reflecting the social concepts and relationships of the residents and their environmental methods in response to climatic conditions and their social composition [15].

The social field

is the realm of interaction that occurs between individuals and their social environment. It differs from the urban field in that urban formation are the result of interactions that occur within the social field [16].

According to Bourdieu, the social field encompasses markets, social relations, individuals, institutions, capital, and domination. This social field can be divided into subfields such as education, economy, cultural production, religion, and bureaucracy. Bourdieu compares society to a universe, where each group, like the galaxies of the universe, has a social status related to its surrounding circumstances [17].

Thus, Bourdieu views society as a social space, and the relative position of a group within that space determines its identity. It determines the identity of the dominant layer in the community, and thus the characteristics of this layer have a significant impact on the shape and distribution of urbanization [18].

The cultural model

The cultural model is represented that it is the collection of perceptions, expressions, values, and ideas that a society creates in its interaction with reality. Thus, the model relates to society as a whole in a particular historical period. The transition from one historical period to another indicates that the content of this model, including its perceptions, expressions, values, and ideas, may be changing. For us, the cultural model is a collection of representations, values, and ideas produced by the social field that work to frame symbolic and dialogical actions in this field. These actions are shaped according to the specificity of this cultural content that attributes identity to the individual or is considered simultaneously with the social field itself.

The culture

The definition of culture is a way of life shared by the members of a society or community and a acquired through membership and participation in the community's way of life.

 ISBN 978-9959-9703-2-9

Culture can be learned through interaction with others and includes two aspects: the material aspect, such as invention and production, and the moral aspect, such as beliefs, attitudes, values, and rules of behavior. These are examples of the moral aspects of culture [19].

Culture is a complex whole consisting of customs, traditions, beliefs, values, practices, and all the inventions and innovations that exist for human existence, among others [20].

Bani Walid City

Bani Walid is a city situated in the Tripoli region, specifically in the sub-region of Misurata, which is positioned east of the AL-Khums sub-region along the coastal area. The primary settlement in this sub-region is the city of Misurata, while Bani Walid is regarded as the second city of the Baladiya, located to the south of Misurata. Figure (1) The city is predominantly inhabited by the Warfalla tribe, which was a mother tribe that has since split into sub-tribes. These sub-tribes have divided the lands amongst themselves, with each tribe being aware of its own borders, except for the central area of the city, known as 'Alsuqe' or the market area. This region serves as a hub for the local population to fulfill their shopping needs, trade their goods, animals, and other products.

Figure (1) location of Bani Walid city

Bani Walid is located on both banks of the Wadi Alblad, which experiences seasonal rainfall that alters the usually dry valley. The dams in the city, which are all outdated, are believed to have been constructed during the third century CE, possibly as part of the Roman Empire's frontier zone development in the area [21].

Agricultural products were transported to Leptis Magna, a significant port that developed into a major city in Roman Africa. Apart from the dams and tombs near Msletten, no other ancient remains are identifiable in the modern-day Bani Walid. However, the city does host a small museum that displays many antiquated models from neighboring archaeological sites. These models often feature agricultural motifs,

 ISBN 978-9959-9703-2-9

such as a man climbing a palm tree or a peasant plowing with a dromedary, which were commonly found throughout the Roman Empire's frontier zone. Another prevalent theme in the museum's exhibits is fish, which can also be seen in Qasr Banat. In the semi-desert landscape, water, life, and eternity are symbolic themes. The museum's green area showcases two ancient olive presses from Bir Tarsin that date back to the third or fourth century. Other ancient artifacts in the museum originate from Leptis Magna, Oea (modern-day Tripoli), and Ghirza [22].

In the past, Bani Walid was a desert region with scarce water, and its inhabitants relied on livestock such as camels, sheep, and goats for their livelihoods. They constructed their homes using stones found on the banks of the valleys, including Almardom, Tininai, and Chmikh. The city center, or market, was sparsely populated, with only a few residents who did not own the land they farmed or the cattle they raised. These residents built their homes along the banks of the valley, which provided a source of food for the city due to the fertility of its soil.

Today, the people of Bani Walid continue to build their homes in the same locations alongside the old buildings. The city has grown and developed, with improved infrastructure and services, but it still maintains a connection to its past and traditions. The residents still rely on livestock and agriculture, with the valley remaining an important source of food and water. Despite the changes, Bani Walid remains a unique and fascinating place, rich in history and culture.

Bani Walid Urban morphology

The urban morphology of Bani Walid is characterized by scattered settlements along the banks of a valley, with separate villages forming a discontinuous pattern on either side of the zigzagging valley terrain. The steep terrain has resulted in the main roads, usually one per village, following the contours of the valley and culminating in a cul-de-sac within the village itself. Each village, representing a tribe, is shaped like a tree, figure (2) , with the main road serving as the trunk and branching out into smaller roads that support urban control and privacy[22].

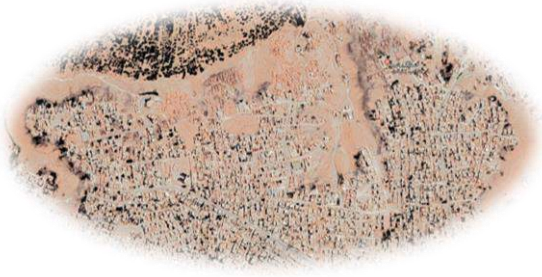

Figure (2) Top view of the main part of Bani Walid

Satellite images of the city reveal a lack of a specific pattern of buildings and spaces, with random buildings occupying the land. This absence of a clear pattern may contradict established theories about building and patterns of urban areas due to the random growth of the city. figure (3) The city's growth was not governed by specific controls, whether natural or human, resulting in a fabric characterized by gathering and overlapping in most of its parts [22].

 ISBN 978-9959-9703-2-9

Figure (3) the built environment of the city

Space syntax

Space syntax is widely recognized as a valid and authentic theoretical and methodological analyzer for studying how space affects human development by measuring spatial configuration (Hillier & Hanson, 1984). It has also become a computer language for describing the spatial pattern of cities. From the perspective of human activities, urban space can be divided into two categories: closed space and free space. Obstructed spaces consist of spatial obstacles, such as buildings, within which people cannot move freely.

Open space, on the other hand, is a part of urban space in which people can move freely. The spaces analyzed by Space Syntax focus on the connections and syntax of spaces; it measures patterns, connections, and arrangements of spaces that cannot be measured with simple Euclidean geometry [23].

Space syntax focuses on the topological relationships of space, including interconnectivity and accessibility, but not on physical distance. Space syntax analysis was carried out as part of the analysis of human perception in Bani Walid City. The analysis of the built environment is at the heart of this research. The results will help us measure the

 ISBN 978-9959-9703-2-9

intelligibility and synergy of parts and spaces of the city, among other measures. In addition, it helps us explain why people perceive places differently, and why some places are meaningful while others are easily forgotten (see figure and table). The aim is to describe the syntactic configuration of the city of BaniWalid, analyzing how each space in the spatial structure is related, connected each other to show how urban patterns support urban privacy.

This study explores the relationship between sociocultural interactions and the built environment using measures of space syntax, such as correlation, connectivity, global integration, intelligibility, and synergy between local and global spaces. The city of BANI WALID was chosen as a case study for its low integration and synergistic value (high privacy).

The results show a strong correlation between local and global integration and between connectivity and global integration. Due to these linkages, a certain type of planning hinders understanding (privacy) and synergy thereby hindering the development of good relations between city dwellers and visitors, increasing the privacy of urban planning.

Understanding the relationship between routes, spaces, and their syntactic values is critical to determining how urban spaces and streets affect sociocultural interactions.

Space syntax is generally considered an important hypothesis and method of analysis in examining how space affects human development by measuring spatial configurations (Hillier et al., 1984). In spatial configuration studies, the basic methodology is to divide space according to scale and human visual capabilities. From this perspective, space is divided into extensive and small-scale spaces (Montello, 1993; Egenhofer et al., 1995). The extent of these small-scale spaces in a city is beyond human visual capabilities and cannot be seen from a single point. Some small-scale spaces, for example,aroom, are larger than the human body , but one would still be able to comprehend the whole [24]

These measures are used to analyze the urban form of a city. Connectivity refers to how well different parts of a city are connected by an efficient transportation network. Global integration measures the extent to which all streets of the city is integrated with the wider region or the sity through transportation hubs. Local integration measures how well different parts of the city are connected to each other, including pedestrian routes. The intelligibility indicator measures how easy it is for people to navigate and understand the layout of the city, including the arrangement of streets and landmarks. The synergy indicator measures the extent to which the city's urban form fosters social interaction and community building.

These measures can be used to assess the quality of urban form and to compare the urban form of different cities. By comparing the measures of Bani Walid with the averages of other local and global cities around the world table (1), it is possible to gain insights into the strengths and weaknesses of its axial lines and the overall urban form.

Table (1) comparing the measurements of Bani Walid with the averages of other cities

Category	connectivity	local integration	global integration	intelligibility	synergy
	C	[n]	[n]	R(n)	R1(n)
U.S Cities	5.808	2.980	1.81	0.225	0.099
Euro Cities	4.008	2.264	0.916	0.137	0.266
English Cities	3.713	2.146	0.72	0.129	0.232
Arabic Cities	2.075	1.013	0.92	0.231	0.16
Libyan Cities	3.03	2.03	0.864	0.192	0.269
Old Bengazi	4.03	2.5	1.15	0.232	0.4041
Tripoli	4.46	2.529	0.992	0.1963	0.3284
Old Tripoli	3.82	2.209	0.948	0.1875	0.4286
Misrata	3.716	1.842	1.289	0.3286	0.7729
Bengazi	3.09	1.893	0.999	0.2134	0.3563
Ghat	2.77	1.691	0.9317	0.2828	0.4009
Ghadames	2.69	1.593	0.8837	0.1967	0.191
Bani Walid	2.667	1.355	0.744	0.1824	0.1747

Discussion and Results of Syntactic analysis of Bani Walid built environment:

CONNECTIVITY VALUE C

The city of Bani Walid has a connectivity value of 2.667, which is lower than the average connectivity value of the traditional pedestrian

ISBN 978-9959-9703-2-9

city of Ghadames. This is because the tribal settlements in Bani Walid tend to prioritize privacy, resulting in a street network that resembles a tree with many cul-de-sacs within each tribe. As a result, the limited number of paths available for observers to choose from restricts the diversity of travel options within the city. Figure (4)

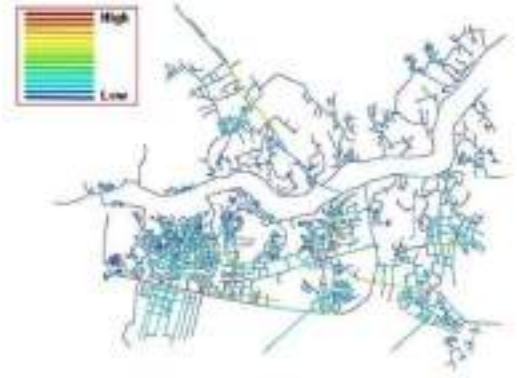

figure (4) Bani Walid city- connectivity value-c

Global integration Rn

The level of global integration in Bani Walid has significantly decreased and is below the average for traditional cities, with a value of 0.348. This suggests that the urban plan of Bani Walid does not promote easy movement between different parts of the city, and instead, limits mobility within the confines of each neighborhood or tribe. The linear streets that serve as traffic axes connecting different parts of the city are the most integrated spaces in Bani Walid. figure (5)

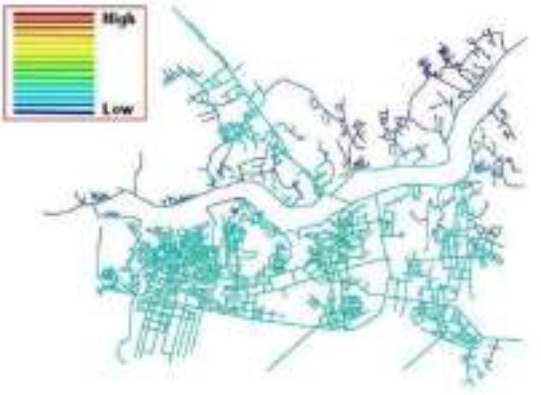

Figure (5) Bani Walid city- global integration-Rn

local integration-R3

This indicator has been calculated on the basis 3 steps depth, Bani Walid city was (1.842) Slightly higher than the average of Arabic cities, this value means that the city has straight and connected streets. For this indicator was very low, less than average of compact traditional towns, this mean that the city has short, curved streets. Figure (6)

Figure (6) Bani Walid city- local integration-R3

Intelligibility Rn **vs. C**

ISBN 978-9959-9703-2-9

In terms of intelligibility, Bani Walid has a very weak score of 0.0624 compared to other cities, including traditional ones. This indicator is derived from a combination of the global integration and connectivity values. Intelligibility refers to an observer's ability to comprehend the entire city by viewing only a few select areas. However, in the case of Bani Walid, the spatial structure requires viewing a large portion of the city to understand it as a whole. figure (7)

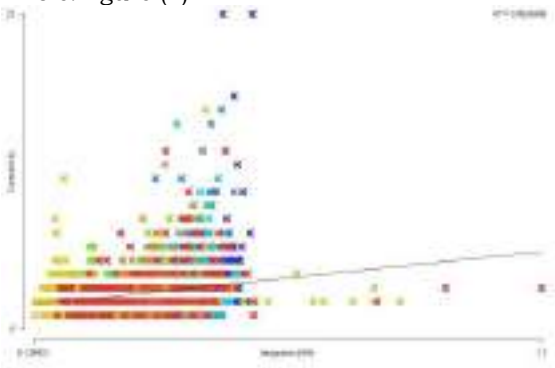

Figure (7) Bani Walid city Intelligibility Rn vs. C

SYNERGY R3 vs. Rn

This indicator is a reflection of the relationship between global integration and local integration values. It aims to determine whether the spatial structures of a city support or prevent the flow of movement between local inhabitants and global visitors. Additionally, it assesses if the city's spatial structures promote integration and cultural exchange among users of urban spaces.

Surprisingly, Bani Walid has a lower score of 0.2247, which suggests that its spatial structures hinder the relationship between the local and global levels. This is mainly due to the tribal settlements' emphasis on privacy as a way of life, which limits the interaction between the local and global communities. figure (8)

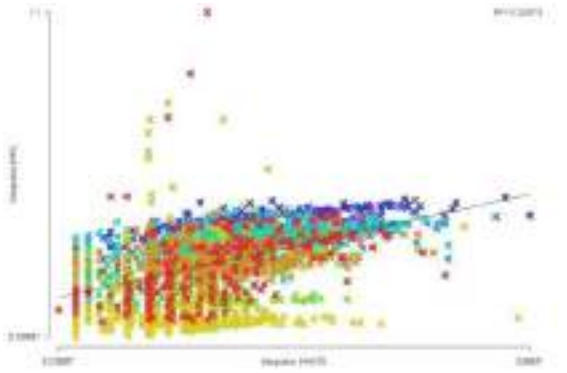

Figure (8) Bani Walid city Synergy R3 vs. Rn

The relationships within the tribes in Bani Walid city

The traditional social structure of Bani Walid is reflected in its spatial layout, as seen in the axial analysis. However, this analysis falls short in reflecting the local centers of the tribes, and thus segment analysis has been conducted to observe the tribal structure in local measures.

The results of the segment analysis indicate that the angular integration increases as the distance decreases, as shown in Figures 46a, b, c, and d. This is due to the close relationships within the tribes, which are confined to narrow areas. The angular analysis also highlights the emergence of new integration cores as the diameter of the analysis decreases, confirming the tribes' enclosure in a limited area with excessive privacy for each tribe.

The majority of integration cores appeared within a radius of 250 meters, which is much less than the limits of walking distance on foot. This confirms the existence of strong relationships within very narrow limits. Therefore, the traditional social structure of Bani Walid deeply ingrained in its spatial layout, with close relationships confined to limited areas. figure (9)

 ISBN 978-9959-9703-2-9

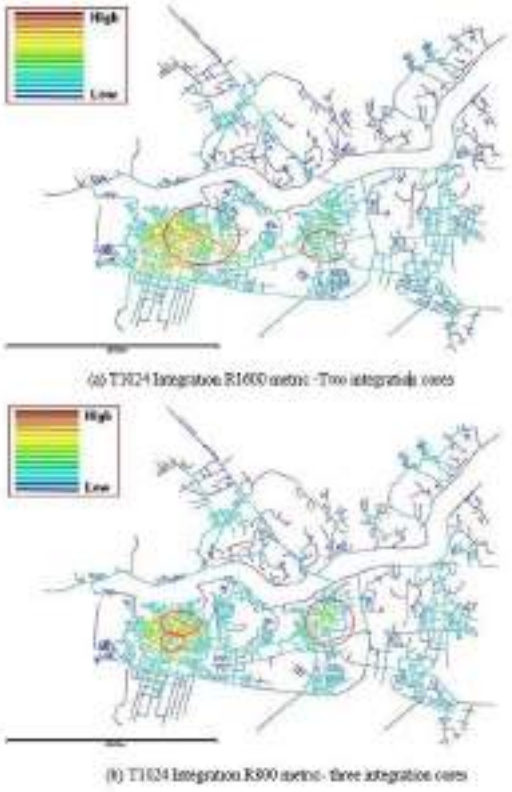

Figure (9) angular integration of Bani Walid city

CONCLUSION:

The physical environment plays a significant role in shaping the perceived quality of a city. The study suggests that urban design must take into account the culturally and socially specific needs of the people who inhabit the city, as well as their mentality. It is important to consider both the hidden features and visual aspects of urban design and architecture, including the combination of structures and areas with other city elements like streets, buildings, and uncovered spaces.

The design of urban interfaces and spatial relations is crucial to creating good urban environments. The requirements for interaction shape any designed environment, which should aim to support various social and cultural possibilities.

ISBN 978-9959-9703-2-9

In the case of Bani Walid, the city's spatial structure is not easily intelligible and is less legible in terms of visuals and structures. The city contains short, curved axes, compact spaces, and various changes in directions, resulting in a large axial size that is difficult to understand and requires a lot of effort to comprehend. Additionally, it is challenging to move from one part of the city to another due to the high level of privacy within the tribes, which acts as a significant obstacle to linking residents and visitors.

References

[1] Johnston R .J. et. al. The dictionary of human geography. Oxford: Blackwell (2000).

[2] **Webster's Online Dictionary**, *"definition of privacy"*, [online], Available from: <http://www.websters-online-dictionary.org/>, [Accessed August 2006]

[3] Riley Terence., "*the Un-Private House"*, the Museum of Modern Arts, New York (1999).

[4] Witte Nathan, "*Privacy: Architecture in Support of Privacy Regulation"*, University of Cincinnati, doctoral dissertation, (2003).

[5] Madanipour **A**, "*Public and Private Spaces of the city"*, Routledge, London(2003).

[6] Helen Greenwood, *"less privacy, please"*, The Sunday Morning Herald, (2004). [online], Available from: <http://www.smh.com.au/articles/2004/01/09/1073437460981.html?from=storyrh>, [Accessed August 2006]

[7] Bill Hiller**,** Julienne Hanson, "*the Social Logic of Space"*, Cambridge University Press, Cambridge,(1984).

[8] Hall**,** E.T., "*the hidden dimension, man's use of space in public and private"*, The bodley head, London, Sydney, Toronto (1969).

[9] Abdul Karim, H., &Hashim, A. H.) The effect of a resettlement scheme on the social-cultural changes of the Temuan Community.Procedia - Social and Behavioral Sciences (2012).

[10] Moeini, M. (2012). Attitudes to urban walking in Tehran. Journal of E&PB.

[11] Das, D. (2008). Urban quality of life: A case study of Guwahati, Springer Science+Business Media B.V., Soc Indic Res. 88, 297–310

[12] Nasution, A. D., &Zahrah, W. (2014). Community perception on public open space and quality of life in Medan, Indonesia. Procedia - Social and Behavioral Sciences, 153, 585 – 594.

[13] Andersen, S. M., & Chen, S. (2002). The relational self: an interpersonal social-cognitive theory. Psychological review, 109(4), 619.

[14] Butina Watson G. and Bentley, I. Identity by Design, Oxford, Elsevier Ltd, (2007)

[15] Medjdoub Benachir and Yannou Brnard**,** (2000), *"Separating Topology and Geometry in Space Planning"*, CAD COMPUT AIDED DES. Vol. 32, no. 1, pp. 39-61., [online], Available from: <http://www.lgi.ecp.fr/~yannou/Publis/CAD%202000%20-%20Medjdoub%20&%20Yannou.doc>, [Accessed August 2006]

[16] بيار بورديو ، اسباب عملية ، ترجمة انور مغيث ، الدار الجماهيرية للطبع و النشر ،طرابلس ،1996.

[17] حكيمة بولعشب ، تحديات الهوية الثقافية العربية في ظل العولمة ، جامعة جيجل ، الجزائر

[18] موريس انجرس ، منهجية البحث العلمي في العلوم الانسانية)تدريبات عملية (ترجمة بوزيد صحراوي واخرون ، دار القصبة للنشر ، الجزائر ،2004

[19] سامية محمد جابر ، منهجية البحث في العلوم الاجتماعية ، دار المعرفة الجامعية ، الاسكندرية .

[20] فاروق احمد المصطفى ، محمد عباس ابراهيم ، الانثروبولوجيا الثقافية ، دار المعرفة الجامعية 2008 .

[21] *Agael fawzi , ozer ozlem , Human perception in the Libyan built environment: Al-Khums and Bani Walid Cities as case studies*, **Archnet-IJAR**: **International Journal of Architectural Research**, vol 11, No 2, (2017).

[22] *Agael fawzi , ozer ozlem , Human*

 ISBN 978-9959-9703-2-9

perception in the Libyan built environment: Al-Khums and Bani Walid Cities as case studies, **Archnet-IJAR**: **International Journal of Architectural Research**, vol 11, No 2, (2017).

[23] Hillier , B, Hanson, J and Peponis, J. The syntactic analysis of settlements. Architecture et Comportement/Architecture and Behavior. vol. 3, 1987, Vol. no. 3.

[24] Jiang B, B, Claramunt , C and Klarqvist , B. An integration of space syntax into GIS for modeling urban spaces. International Journal of Applied Earth Observation and Geoinformation. 2, 2000.

 ISBN 978-9959-9703-2-9

المؤتمر الدولي الثاني للعلوم والهندسة
2nd International Conference on Science and Engineering
ICSE 2023
Faculty of Engineering - University of Bani Waleed
Bani Waleed, Libya

Paper Code: ICSE-057

UTILIZATION OF BESHR SILICA IN FILTRATION

*Hatim A. Sasi[a], Abdelhafed A. Adernawe[b] , Ahlam A. Ben Taher[c], Hajer Bark[d]
[a,b,c,d] Mining department, Faculty of Engineering/University of Tripoli, Tripoli, Libya
*Corresponding author: H.Issa@uot.edu.ly

Abstract: Due to the environmental regulations and scarcity of water resources, it's important to find ways for wastewater treatment for reusing in different purposes. Sand and media filtration is a commonly applied technology for the removal of suspended substances from water and is frequently used for drinking and process water production. In this research the silica sand deposits from Besher-Libya location were physically and chemically characterized as a prelim study to investigate its suitability as a wastewater-filter, the properties studied are; porosity, permeability, specific gravity, grain size distribution and chemical analysis. The obtained results were compared with the standard specifications according to Manvile (1986) and concluded that the results are promising and could be used as a wastewater-filter.

Keywords: (filtration, grain size, silica, wastewater)

Introduction

With the pace of life accelerating, filtration has become a part of daily life. We deal with filtration, filters and its equipment permanently in homes, factories and various government facilities. Filters, in addition to being barriers that remove solids from wastewater, help in obtaining a uniform flow of runoff. This changes the nature of the water and makes it suitable for drinking, Agriculture, boiling or cooling make-up. Moreover, wastewater filtration helps users meet the requirements of more stringent environmental restrictions in discharge. Although filtration, considered as a simple mechanical process, in fact it includes the mechanisms of adsorption (physical and chemical), straining, sedimentation, interception, diffusion, and inertial impaction [1]. Sand media filters are one of the most popular filters used in micro-irrigation systems, especially for filtering water with big amounts of organic impurities [2]. Silica and industrial sand are used in filtration processes of drinking water, wastewater treatment and water production from wells. Uniform grain shapes and grain size distributions are the most physical characteristics control the filter efficiency, which are responsible of producing efficient filtration bed operation in removal of contaminants from potable and wastewater. The filter bed is graded by size and density which are describes the type of filters to "multilayer", "in-depth", and "mixed media". The used technique is to put light coarse particles at the top of the filter bed and fine denser particles are at the bottom [1]. Fortunately silica is chemically inactive and will not react with acids, pollutants, volatile organics or solvents. Coarse silica is used as packing material in deep-water wells to increase yield from the aquifer because it's preventing the infiltration of fine particles from the formation and so expanding the permeability around the well screen [2].

 ISBN 978-9959-9703-2-9

Moreover, the mechanical strength of silica sand makes it a high durable material and that will ensure the filter media will be long lasting, even under high pressure in pressure filter, and lowering maintenance costs. The aim of this paper is to investigate the characterization of Besher sand deposits as a filter media according to Manvile 1986.

Location of study area

The area where the sample had been taken is located in the Centre part of Libya beside the coastal road close to the Brega oil port (Beshr soil).

Experimental and methodology

During the geological survey in the sedimentary basin of Central Libya, several samples of Beshr soil deposits were collected. The material expected to be chemically and mineralogical homogeneous throughout the area, therefore four samples about 20 kg were collected from distal parts of the basin. The samples were low in density, friable, and white to yellowish in color in spatial distribution, as shown in figure (1).

Fig. 1: Beshr soil samples

Raw materials used in this paper which obtained from the Beshr site were dried for 24 hour at 105° C, and weighted in dry room condition [3], samples were tested to obtain some physical properties; density, specific gravity, porosity, permeability and Grain size analysis which have been carried out according to American Society for Testing and Materials "ASTM". To determine the size distribution of the sample's particles, a sieve analysis test was carried out. Moreover, a loss of Ignition test was performed to measure the organic content in the soil.

Results and discussion

1. Physical Properties:

Porosity is defined as volume fraction of voids within the silica sand's layer and can be determined easily by weight measurement [4]; the sample's mean porosity was 1.085%. The apparent density is the mass per total volume, the bulk density of soil depends greatly on the mineral make up of soil and the degree of compaction, the average of bulk density for the samples studied were 2.4 g/cm^3. Specific Gravity of sand is the ratio of the density or mass of sand to the density or mass of a reference substance at a fixed temperature and the volume should be the same, the middle specific gravity of the target samples were 2.054. Soil permeability is the property of the soil to transmit water and air, the samples show permeability of 0.0625 cm/sec.

2. Grain size analysis:

The grain size analysis test is done to determine the percentage of each size of grains contained within a soil sample as shown in table (1), then the results of the test are used to draw the grain size distribution curve as shown in figure (2).

Table 1: Grain size analysis results

ISBN 978-9959-9703-2-9

Sieve No.	Diameter mm	Weight %	Cumulative oversize %	Cumulative Undersize %
4	4.75	6.66	6.5	93.5
10	2	9.44	15.8	84.2
20	0.850	24.02	39.4	60.6
40	0.425	23.19	62.2	37.8
60	0.250	13.68	75.6	24.4
100	0.150	10.13	85.6	14.4
200	0.075	9.02	94.5	5.5
pan	-			-

The grain-size distribution of the soil sample obtained by plotting the percent finer with the corresponding sieve on semi-log graph paper, as shown above which is used to calculate the uniformity coefficient of the sample. From the grain size distribution curve, the values of D10, D30, and D60, which are the diameters that correspond to the percent finer of 10%, 30%, and 60%, respectively can be determined [5], [6].

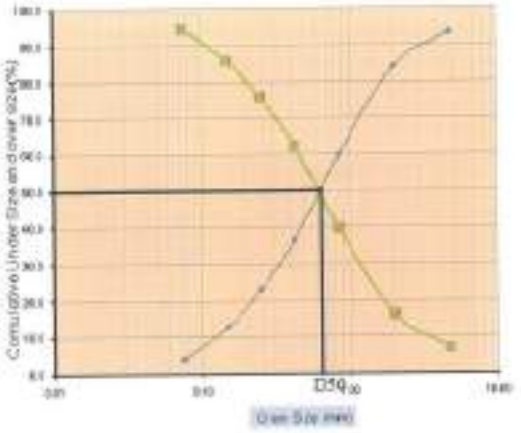

Fig. 2: Grain size distribution curve

The values of the uniformity coefficient Cu and the coefficient of gradation Cc can be calculated using the following equations:

$Cu = D60 \div D10 = 0.85 \div 0.26 = 3.27$

$Cc = (D30)^2 (D10 \times D60) = (0.32)^2 (0.26 \times 0.85) = 0.463$

3. Loss of Ignition (LOI):

This test is designed to measure the amount of moisture or impurities Lost when the sample is ignited under the conditions specified in the individual monograph. Then, the difference of weight is divided by the original weight. The results of samples's loss of ignition are presented in table (2) below.

Table 2: Loss of ignition results

Sa. No.	LOI
R5-1	0.44
R5-2	0.30
R5-3	0.37
R5-4	0.34
R5-5	0.34

4. Chemical analysis:

The chemical analysis of the bulk samples was done in Zleten cement factory and the results shown in the Table (3).

Table 3: Chemical analysis results

Sa. No.	R5-1	R5-2	R5-3	R5-4	R5-5
Na_2O %	0.14	0.13	0.11	0.12	0.12
MgO %	1.15	1.16	1.11	1.11	1.14
SiO_2 %	74.17	74.24	74.24	74.09	74.4
Fe_2O_3%	3.74	3.49	3.45	3.34	3.41
Al_2O_3%	5.80	5.82	5.77	5.76	5.81
K_2O %	0.44	0.45	0.44	0.44	0.44
CaO %	14.78	14.67	14.8	15.11	14.65

Silica, alumina, iron oxide Were the main constituents of the samples. The Sio_2 content corresponds to related aluminum silicate minerals present in the sample and the existence of Al_2O_3, Fe_2O_3 to the high amount of chlorite and vermiculite present in the sample. The contents of CaO and MgO are slightly high due to the existence of carbonate minerals, the loss of ignitions (LOI) of the sample is mainly attributed to loss of H_2O contained in clay minerals, the sodium oxide (Na_2O) and potassium oxide (K_2O) are mainly attributed to the presence of feldspar, illite and clay mineral.

5. The XRD analysis:

ISBN 978-9959-9703-2-9

X-ray powder diffraction (XRD) is a rapid analytical technique used for phase identification of a crystalline material. The samples are finely ground, homogenized, and average bulk composition is determined. The samples are characterized as clay-silica deposits as these minerals are composed of amorphous silica (SiO_2nH_2O) which has biological origin.

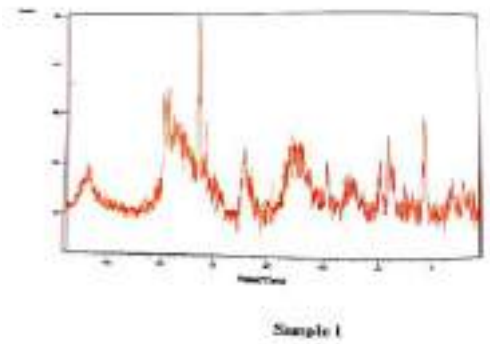

Fig. 3 (a): XRD analysis of sample 1

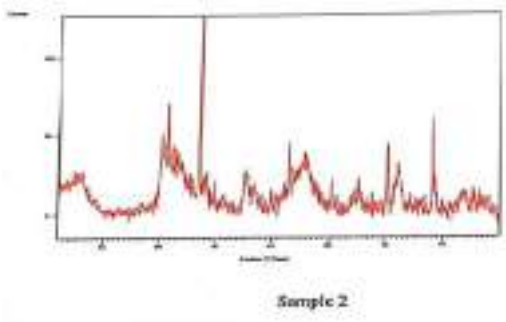

Fig. 3 (b): XRD analysis of sample 2

The XRD analysis of the four bulk samples are presented in figure (3. a,b,c,d). Referring to the XRD analysis, other clay minerals such as chlorite $(MgFe)_3$,(Si Al)4010(OH) and illite are also present in variable amounts and smectite (Ca,Mg,Na).

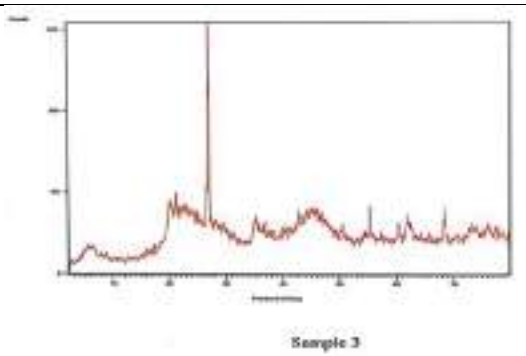

Fig. 3 (c): XRD analysis of sample 3

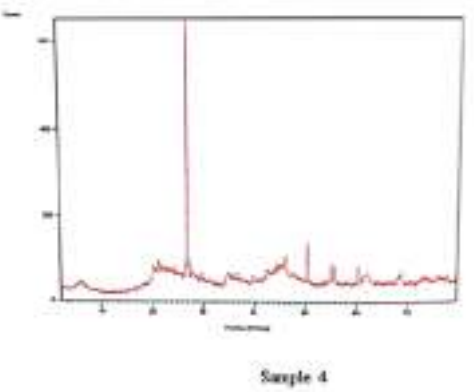

Fig. 3 (d): XRD analysis of sample 4

The results show the contents of the samples are different phases of silicate minerals i.e Quartz, Cristobalite, Tridymite, accompanied to the feldspar (microline) and vermiculite.

Conclusion

In this research some physical and chemical properties of Besher silica were studied to investigate its possibility to use in water filtration, these properties are permeability, porosity, specific gravity, grain size distribution. The results compared with standard specification of filtration according to Manvile 1986 and concluded that the results are promising and in line with standard specifications.

ISBN 978-9959-9703-2-9

Acknowledgment

Thanksgiving to Zliten cement factory.

References

[1] H. Barka, Applicability of Besher Silica in Filtration Process, Bachelor's project, Tripoli University, Libya 2016.

[2] M. Elbana, F. Ramírez de Cartagena, J. Puig-Bargués, (August, 2012), Effectiveness of sand media filters for removing turbidity and recovering dissolved oxygen from a reclaimed effluent used for micro-irrigation, Agricultural Water Management, 111, 27-33, DOI:10.1016

[3] MD Sahadat Hossain, Ph.D., P.E.; Md Azijul Islam; Faria Fahim Badhon, (2018). Network, [online], Available at: https://uta.pressbooks.pub/soilmechanics/open/download?type=xhtml

[4] F. G. Bell, Engineering geology and geotechnics. Newnes Butterworths, London, 1980, pp. 11-93.

[5] L. Mazogy, Studying the possibility of using silica sand in the Abu Ghailan region for the glass industry, Bachelor's project, Tripoli University, Libya 2009.

[4] John T. Germaine, Amy V. Germaine, (2009, May 20). Network, (2nd ed.) [online]. Available at: https://www.google.com.ly/books/edition/Geotechnical_Laboratory_Measurements_for/Ln5EpwZooPQC?hl=en&gbpv=1

 ISBN 978-9959-9703-2-9

المؤتمر الدولي الثاني للعلوم والهندسة
2nd International Conference on Science and Engineering
ICSE 2023
Faculty of Engineering - University of Bani Waleed
Bani Waleed, Libya

Paper Code: ICSE-015

AXIOM COUNTABILITY OF VIA SEMI- OPEN SETS

Nagah A. Elbhilil *
Mathematics Department, Faculty of Science/ Tripoli University, Tripoli-Libya
*Corresponding author : nagahdow@gmail.com

Abstract: The paper intends to present a s-open sets and discuss some of its properties. and its relationship to open sets. also, they are used to introduce a specific form of countable space axioms called s-countable axioms, these include; S- separable spaces, s-first countability and s-second countability. Through the classical concept of topology, the properties of these spaces have been studied; moreover, we study the enumerated s-compounds and their behavior in some special spaces.

Keywords: Topological spaces and generalization, s- open sets, subspace, Countability Axiom Separability

Introduction

Many researchers have introduced different types of generalized countability axioms: g-countability axiom, b-countability axiom, D-countability axiom and finally R-countability axiom. The cared Siwiec in a year 1974 [1] The g-(first, second) countable space are defined by using weak basis in (X,τ) space, and showed their relationship with measurability. A year later, Siwiec [2] wrote an overview that generalized the concept of first countable space and studied the relationship between these generalizations.

In the year1991, Jian-ping [3] studied some of them Generalization of the first countability; Call it namely ω_k- spaces, when he states The relationship between the T_1 spaces , ω-spaces and first countability. In 2013, Selvarani [4] advance guard the b-countable axiom on b-open sets, and then Elbhilil and Arwini[5] defined generalize types of countability axiom. is called pre-first countability, and they define these axioms in terms of sets, proving that pre-separable spaces and pre-second countability are equivalent to separable spacesIn general topology, several distinct understandings of open sets have been explored.

Some of these concepts, including i-open set $(i = \alpha, s, pre, b)$,have been defined in a similar manner using operations involving the closure and the interior. Of these, the notion of preopen (or locally dense) sets is particularly significant. "Locally dense" sets were first identified as preopen sets by Corson and Michael in 1964 [6]. In 1982, Mashhour, and others [7] used

 ISBN 978-9959-9703-2-9

the term "preopen" instead of "locally dense" set. Introduced by Csaszar [8], a set X can have a generalized topology - abbreviated as GT - which is typically represented as (X,μ), in this terminology, the μ-open sets indicate the elements of the generalized topology. The concept of μ-countability axioms, which are specific to GT, were established in 2013 by Ayawan and Canoy [9]. In their research, they explored the qualities of these ideas and determined the characteristics of μ-first (μ-second) countable space in the context of GT product. See [10,11] for details on fundamental properties in generalized topology. In 1963, Levine [12] took an interest in the concept of s-open sets.

The study of general closed sets was started by C.E.Aull [13] in 1968, We consider the set of closed sets that belong to each superset as open. Arya and Noor introduced the concept of generalized closed set. [14] In 1987, Bhattacharyya and Lahiri defined and tested the concept of s-generalized closed sets based on the concept of s-closed sets. This class was introduced of α -generalized closed sets by Maki, Devi and Balachandran [15] in 1994.

In this study we used s-open sets to define a countability axiom, it is called s-countability axioms, where this class consists of the axioms: s-separability, s-first countability and s-second countability.

It is illustrate the relationship between the countable axioms and the s-countability axioms, then we examine the hereditary properties of these spaces and their images under special functions, and the properties of these spaces: submaximal spaces, partitioned spaces, extreme separation spaces, solvability. The article is divided into seven main parts: s-open sets, s-dense, s-continuous functions, s-separability spaces,s-first countability, s-second countability, properties of s-countability, and final state.

2. SEMI OPEN SETS

Definition 2.1. [16] A subset η of space X it's say s-open if and only if there exists u an open set such that $u \sqsubseteq \eta \sqsubseteq \bar{u}$.

Theorem 2.1. [16] A subset η in X space is s-open if and only if $\eta \sqsubseteq \overline{\eta^{o}}$.

The all of s-open sets and s- closed sets in $(X,\tau)$are denoted by SO(X) and SC(X), respectively.

Theorem 2.2. [12] Let η be s-open in the space X and suppose $\sqsubseteq \xi \sqsubseteq \bar{\eta}$. Then ξ is s-open.

Definition 2.2. [16] The s-closed set is complement of a s-open set.

Proposition 2.1. [17]

1) X and ϕ are s-open sets.
2) Arbitrary union of s-open sets is s-open.
3) Intersection of s-open sets need not be s-open.

Examples 2.1.

1) If $X = \mathbb{R}$ with usual topology space and let $A = \{x: 0 < x < 3\} \cup \{4\}$, $B = \{x: 2 < x < 5\} \cup \{1\}$ A and B are not s-open, but $A \cup B$ are s-open

 ISBN 978-9959-9703-2-9

set.

2) Let $=\{a,b,c\}$, $\tau=\{X,\phi,\{a\}\}$ is topology space then $\{b\}$ is s–open but is not open set.

Definition 2.3. [18] The intersection of all s-closed sets of X containing η is called the s-closure of η and is denoted by $\bar{\eta}^{semi}$.

Definition 2.4. [18] The union of all s-open of sets of X contained in η is called the s-interior of η and is denoted by $\eta^{o\,semi}$.

Proposition 2.2. [19] A s-open set is the intersection of an open set and a s-open set.

Definition 2.5. [6] A subset P of a space (X,τ) is say preopen if $P\subseteq \bar{P}^{O}$, the preclosed set is complement of preopen set.

In [6] the following diagram (1) shows the relationship between the open, peropen set and dense set.

open $\Longrightarrow$ preopen

Dense$\Longrightarrow$ preopen

Diagram (1)

Proposition 2.3. A set η in a space(X,τ) then

1) In [20] $\eta\subset \bar{\eta}^{-semi}\subset\bar{\eta}$.

2) If η is s-open [21] in X and P is preopen in X such that $\eta\cap P=\phi$, then $\eta=\phi$ or $P=\phi$.

Theorem 2.3. [12] Let $\eta\subseteq Y\subseteq X$ where X is a space and Y is a subspace. Let $\eta\in SO\,(X)$. Then $\eta\in SO\,(Y)$.

Definition 2.6. [22] A set is regular open if and only if it is preopen and s-closed.

Theorem 2.4. [22] For a subset η of (X,τ) the following sentences are equivalent:

1) η is preopen.

2) The s-closure of η is a regular open set.

Definition 2.7. [23] A subset η of a space X it is said to be s-regular if a subset η is s-open and s-closed .

The set of all s-regular sets of X is denoted by SR (X).

The following diagram (2) shows the relationship between the regular sets and s-open sets.

regular sets $\Longrightarrow$s-regular sets $\Longrightarrow$ s-open sets

Diagram (2)

Proposition 2.4. [24] If (X,τ) is topological space, and $\eta\subset P\subset X$, where P is preopen. Then η is s-open (s-closed) in P if and only if $\eta=S\cap P$, for some s-open (s-closed) set S.

Proposition 2.5. [25] Let η be a subset of a space X. Then:

1) $\bar{\eta}^{semi}=\eta\cup\bar{\eta}^{O}$.

2) $\overline{X-\eta}^{semi}=X-\eta^{o\,semi}$.

3) $(X-\eta)^{o\,semi}=X-\bar{\eta}^{semi}$.

Definition 2.8. [26] A subset B of a space X is say b-open if $B\subseteq\overline{B^{O}}\cup\bar{B}^{O}$.

Theorem 2.5. if (Y,τ_Y) be a subspace of a space (X,τ) and let $\eta\subseteq Y$. If η is s–open in X , then η is s -open in Y.

Proof. Let η is s-open in , there exists an open set u in X such that $u\subseteq\eta\subseteq\bar{u}$. Then $u^{Y}=u\cap Y\subseteq\eta\subseteq\bar{u}\cap Y=\bar{u}^{Y}$ Thus η is s-open in

ISBN 978-9959-9703-2-9

Y.

Definition 2.9. [27] A subset w of a space X is Called a weak open, if there is an open set u such that $\overline{w} = \overline{u}$.

Remark 2.1. 1) IN [27] All s-open sets are weakly open set.

2) A [6] set is an open if and only if it is s-open)and preopen.

The following diagram (3) shows the relationship between the open sets and i-open sets $(i = \alpha, \text{pre}, \text{s}, b)$

$$\text{Open set} \Longrightarrow \alpha\text{-open set} \Longrightarrow \begin{matrix} \Longrightarrow \text{s} - \text{open set} \\ \Longrightarrow \text{pre open set} \end{matrix} \Longrightarrow b - \text{open set}$$

Diagram (3)

Proposition 2.6. [6] If η is s-open in space X and P is preopen in space X, then $\eta \cap P$ is s-open in P and preopen in η.

3. S-DENSE SET.

Definition 3.1. [28] let D a subset of X a space is said to be dense if $\overline{D} = X$.

Definition 3.2. [29] A subset B of X is called b-dense if $\overline{B}^b = X$.

Definition 3.3. [30] let D a subset of X a space is said s-dense if $\overline{D}^{semi} = X$.

Proposition 3.1. [20] Every non-empty preopen subset of X space is s-dense.

Corollary 3.1. let (X, τ) topology space then:

1) Any s-dense set is dense.

2) Any b -dense set is s-dense.

Proof. 1) if D be a s-dense subset of a space X, i.e. $\overline{D}^{semi} = X$, since $\overline{D}^{semi} \subseteq \overline{D}$ then $\overline{D} = X$.

2)if B be a b-dense subset , i.e. $\overline{B}^b = X$, since $\overline{B}^b \subseteq \overline{B}^{semi}$ such as $\overline{B}^{semi} = X$.

The following diagram (4) shows the relationship between the b–Dense and s-open sets.

b-Dense $\Longrightarrow$ s-Dense $\Longrightarrow$Dense$\Longrightarrow$ preopen$\Longrightarrow$ s-open

Diagram (4)

Corollary 3.2. If A subset of (X, τ) is s-dense if and only if any non-empty s-open set in contains points from A.

Proof. $\Longrightarrow$ If A be a s-dense subset in , and if Bbe a non-empty s-open set. Since $B \neq \phi$ and there is $\bar{A}^{semi} = X$ there is $x \in B$ and $x \in \bar{A}^{semi}$,we get $A \cap B = \phi$.

$\Longleftarrow$ If x be any element in X ,then any s-open set that contains x intersect A , i.e. $x \in \bar{A}^{semi}$ we get $\bar{A}^{semi} = X$.

Corollary 3.3. Let (X, τ) topology space then:

1)Every subset of X space that contains a s-dense set is s -dense.

2) If A is s-dense set in B,and B is s-dense in X, then A is s-dense in X.

Proof. 1) verified $\bar{A}^{semi} \subseteq \bar{B}^{semi}$for every sets A and B satisfy $A \subseteq B$.

2) Let N is s-open set in X,then $A \cap B \neq \phi$ since B is s-dense in X ,by corollary (3.2) we have $N \cap B$ is s-open set in B. Since A is s-dense in , then we have $(N \cap A) \cap B \neq \phi$,i.e. $(N \cap B) \cap A = N \cap A \neq \phi$,Therefore, A is s-dense in X.

ISBN 978-9959-9703-2-9

Theorem 3.1. [31] A set $\eta \subseteq X$ is nowhere s-dense if and only if $(\bar{\eta}^{semi})^{O} = \phi$.

Theorem 3.2. [30] Let (X,τ) be a space and $D \subset X$.Then D is dense in X if and only if $D \cap \eta \neq \phi$.

For any non-empty $\eta \in SO(X)$

Proposition 3.3. [30] Let (X,τ) be a space and $\in SO(X)$, $U \in \tau$ and $U \cap \eta \neq \phi$. Then for dense set , $U \cap \eta \cap D \neq \phi$.

Remark 3.1.[30] If D is dense in the space (X,τ) and U is open in (X,τ) then $\overline{(D \cap U)}$ is a s-open set.

Theorem 3.3. The union of finite number of non- s-dense set is non s-dense sets.

Proof. Let A,B are non-s–dense sets, we put $W = (\overline{A \cup B}^{\text{semi}})^{o}$ so that

$W \cap (\bar{B}^{\text{semi}})^{C} \subseteq (\bar{A}^{\text{semi}} \cup \bar{B}^{\text{semi}}) \cap (\bar{B}^{\text{semi}})^{C}$

that is $W \cap (\bar{B}^{\text{semi}})^{C} \subseteq (\bar{A}^{\text{semi}} \cup \bar{B}^{\text{semi}}) \cap (\bar{B}^{\text{semi}})^{C}$

$\bar{A}^{\text{semi}} \cap (\bar{B}^{\text{semi}})^{C} \subseteq \bar{A}^{\text{semi}}$. Since $\bar{B}^{\text{semi}} \cap (\bar{B}^{\text{semi}})^{C} = \phi$.then $(W \cap (\bar{B}^{\text{semi}})^{C})^{o^{\text{semi}}} \subseteq (\bar{B}^{\text{semi}})^{C} \subseteq \left(\text{scl}(A)\right)^{o^{\text{semi}}} = \phi \subseteq \emptyset^{o^{\text{semi}}}$. Since A is non s-dense. But

$(W \cap \left(\bar{B}^{semi}\right)^{C})^{o^{\text{semi}}} = W \cap (\bar{B}^{\text{semi}})^{C}$.

Since $W \cap (\bar{B}^{\text{semi}})^{C}$ is s–open set, it follows that $W \cap (\bar{B}^{\text{semi}})^{C} = \phi$, which implies $W \subseteq \bar{B}^{\text{semi}}$ then $w^{o\ \text{semi}} \subseteq \left(\bar{B}^{\text{semi}}\right)^{o^{\text{semi}}} = \phi$, Since B is non s–dense. But $w^{o\ \text{semi}} = \overline{A \cup B}^{\text{semi}o^{\text{semi}}\ o^{\text{semi}}} = \overline{A \cup B}^{\text{semi}o^{\text{semi}}}$. So that $\overline{A \cup B}^{\text{semi}o^{\text{semi}}} = \phi$ .Hense A ∪ B is non s-dense.

Theorem 3.4. If A be a subset of(X,τ) spaces then A is non s– dense in X if and only if $X - \bar{A}^{\text{semi}}$ is s- dense in X.

$A^{o\ \text{semi}} = X - \overline{X - A}^{\text{semi}}$

Proof. by Proposition 2.6. it follows that $\bar{A}^{\text{semi}} = X - (X - A)^{o\ \text{semi}}$ and

$\bar{A}^{\text{semi}o^{semi}} = X - \overline{X - \bar{A}^{\text{semi}}}^{\text{semi}}$

Sinse A is non s–dense then $\bar{A}^{\text{semi}o^{\text{semi}}} = \phi$.

then $X - \overline{X - \bar{A}^{\text{semi}}}^{\text{semi}} = \phi$, we get $\overline{X - \bar{A}^{\text{semi}}}^{\text{semi}} = X$,then $\overline{X - \bar{A}^{\text{semi}}}^{\text{semi}}$ is s–dense.

4.S-CONTINUOUS FUNCTION.

Definition 4.1. [12] let $F:(X,\tau) \to (Y,\sigma)$ function is called s-continuous if is $F^{-1}(V)$ a s-open set of (X,τ) for any open set V of (Y,σ) .

Corollary 4.1. Any continuous function is s–continuous function.

Theorem 4.1. [12] Let $F:(X,\tau) \to (X,\sigma)$ be the s-continuous function. Then for any dense subset D of (X,τ) , $D \cap F^{-1}(O) \neq \phi$, for any0 $\in \sigma$.

Definition 4.2. [33] A function $F:X \to Y$ is said to be:

1)irresolute if the inverse image of every s-open set in Y is s-open in X.

2)pre-s-open if the image of every s-open set in X is s-open in Y.

Definition 4.3. [33] if $F:X \to Y$ function is said to be s-homeomorphism if F is irresolute

ISBN 978-9959-9703-2-9

and pre-s-open.

Theorem 4.2. [33] If $F: X \to Y$ then:

1)An open and continuous then F is irresolute and pre s-open.

2) a homeomorphism then $F$is also a s-homeomorphism.

Theorem 4.3. [34] Let A is s–open set in X space, if $F: X \to Y$ be a continuous open mapping where X and Y are spaces . then $F(A)$ is s-open set in Y.

5. APPLECATION OF SEMI-OPEN SET

5.1.In Partition Spaces.

Definition 5.1.1. [28] A (X, τ) be a space is say partition space if any open subset of X is closed.

Proposition 5.1.1. In partition space (X, τ) , any subset of X is s-open, i.e $SO(X, \tau) = P(X)$.

Proof. Suppose A is a subset of X ,then $A \subseteq \bar{A}$, every closed set in partition space is also open, then $\bar{A}$ is open set, i.e. $\overline{A^O} = \bar{A}$, so $A \subseteq \overline{A^O}$, then A is s-open set.

Corollary 5.1.1 In Partition space X is s-separable space if and only if the space X is countable space.

Proof. clear that $\{\{x\}\}$ is a countable s-local base at every point x in X .

Definition 5.1.2. [39] A topological space (X, τ) is say s-partition if any s-open subset of X is s-closed.

5.2.In Submaximal Spaces.

Definition 5.2.1. [35] Let (X, τ) is Say submaximal space if each dense set in X is open.

Theorem 5.2.1. [36] If (X, τ) is submaximal and $A \in SO(X)$ then (A, τ_A) is submaximal.

Corollary 5.2.1. In (X, τ) is submaximal, any s-open set is open, i.e. $SO(X, \tau) = \tau$.

Proof. If A be a s-open subset in a space , then from proposition (2.4) (1) A is preopen set in X in [5] we get A is open set.

Corollary 5.2.2. In a submaximal space X, if D is dense if and only if D is s-dense in X.

Definition 5.2.2. A space (X, τ) is called s-submaximal if any s-dense subset of X is s-open.

Definition 5.2.3. [37] A subset η of a space $(X, \tau)$is say s-preopen if $\eta \subseteq \overline{\eta^o}$, s-preclosed set is the complement of s-preopen set .The family of all s-preopen sets and s-preclosed sets in X are denoted by $SO(X)$ and $SC(X)$,respectively.

Theorem 5.2.2. If (X, τ) be a space, then the following properties are holds:
1) (X, τ) is s-submaximal;

2)any s-preopen set is s-open.

Proof. 1) $\Rightarrow$ 2): if $N \subseteq X$ be a s-preopen set. Then $\subseteq \overline{N^{O^O}}$, let $\overline{N^{O^O}} = M$, say.

This implies $\overline{M}^{\text{semi}} = \overline{N}^{\text{semi}}$ and hence $\overline{((X-M) \cup N)}^{\text{semi}} = \overline{(X-M)}^{\text{semi}} \cup \overline{N}^{\text{semi}} = \overline{(X-M)}^{\text{semi}} \cup \overline{M}^{\text{semi}} = X$ and thus $(X-M) \cup N$ is s-dense in .

$N = ((X-M) \cup N) \cap M$ is s-open.

Now

$(X-M) \cup N$

 ISBN 978-9959-9703-2-9

and N is the intersection of two s-open sets and hence N is s-open.

2) $\Rightarrow$ (1 : Let M be a s-dense subset of X.

Then $\overline{M}^{\text{semi}^O} = X$, then $M \subseteq \overline{M}^{\text{semi}^O}$ and M is s-preopen,M is s-open.

5.3.In extremely disconnected

Definition 5.3.1. [43] A space (X, τ) is called extremelly discometed if the closure of evrey coopen set is open.

Theorem 5.3.1. [20] In a topological (X, τ) the following nditions are equivalent:

1) X is extremally disconnected.

2)Any regular closed subset of X is preopen.

3)Any s-open subset of X is preopen.

Corollary 5.3.1. [21] A topological (X, τ) is said to be extremally disconnected if and only if for any s-open set $A \subseteq X$ and every s-preopen set $\subseteq X$, then set $A \cap B$ is s-open.

Definition 5.3.2. A space (X, τ) is called extremally s-disconnected if the s–closure of any s-open subset of X is s-preopen.

Definition 5.3.3. Let subset N of a space (X, τ) is said to be regular s-open if $N = (\overline{\text{N}}^{\text{semi}})^{o^{\text{semi}}}$.

The complement of a regular s-open set is called regular s-closed.

Proposition 5.3.1. Let (X, τ)be a topological space and $N \subseteq X$.If N is a regular s-open set, then it is s-open.

Proof. Clearly.

Theorem 5.3.2. Let (X, τ) be a space, then the following are equivalent:

1)(X, τ) is extremally s-disconnected;

2)Any regular s-open set is s-clopen.

Proof. 1) $\Rightarrow$2): Let (X, τ) is extremally s-disconnected and Let N be a regular s-open set, then $N = (\overline{\text{N}}^{\text{semi}})^{o^{\text{semi}}} = \overline{N}^{semi}$ Hence N is s-closed ,we have N is s-clopen.

1) $\Rightarrow$2) : Let $N \in SO(X)$. Then $\overline{N^O}$is a regular s-closed set which is s-clopen. Hence is $\overline{N^O}$ s-open.

2) 5.4.On Resolvability

Definition 5.4.1. [40] A space (X, τ) is said to be resolvable if there is dense subset $D - X$ for which $X - D$ is also dense. A space which is not resolvable is called irresolvable.

Corollary 5.4.1. [40] Every subset of X is resolvable (irresolvable)if it is resolvable (irresolvable) as a subspace.

Corollary 5.4.2. [41] Any submaximal space is irresolvable and in fact hereditarily irresolvable.

Theorem 5.4.1. [41] Any s-open subset of a resolvable space is resolvable.

6.S-SEPARABILITY.

Definition 6.1. [29] A topological (X, τ) is said to be separability if it has a countable dense subset in X.

Theorem 6.1. [29]

1)Every open subspace of a separability is separability.

ISBN 978-9959-9703-2-9

2) The continuous image of a separability space is separability.

Definition 6.2. [30] A space X is said to be b-separability space if it has a countable b −dense subset of X.

Definition 6.3. A space X is say s-separability if it has a countable s-dense subset of X.

Corollary 6.1. 1) Any s-separability is separability.

2)Any b-separability space is s-separability.

Theorem 6.2. Every s–open subspace of s-separability is s-separability.

Proof. Let Y is a s-open subspace of s-separability X , then X has a countable s-dense subset η , since Y is a s-open subspace, then $Y \cap \eta$ is s-dense and countable subset in Y ,hence Y is s-separability.

Remark 6.1. An open subspace of s-separability is s-separability.

Proof. Direct since any open set is s-open.

Theorem 6.3. A s-irresolute image of s-separability is s-separability.

Proof. Let $F: X \to Y$ be a s-irresolute function from a s-separable.

Be a s-irresolute function from a s-separability space , then X has a countable s-dense subset η , so $F(\eta)$ is countable. Now suppose N is a s-open set in $F(X)$ since $F$is s-irresolute is a non-empty s-open set in X, so $F^{-1}(N) \cap \eta \neq \emptyset$,hence $N \cap F(\eta) \neq \emptyset$. We have $F(\eta)$ $F^{-1}(N)$ is a countable s-dense subset of $F(X)$.

7.S-FIRST COUNTABILITY

Definition 7.1. [28] A space X has a countable basis at x if there is a countable collection $\mathcal{B}_x$ of neighborhoods contains x is say basis at X if for each neighborhood U such that $x \in U$ there exists B_x in $\mathcal{B}_x$ such that $x \in B_x \subseteq U$.

Definition 7.2. [28] A topological space X having a countable basis at each of its points is said to first countability if for any $x \in X$ there is a countable local base $\mathcal{B}_x$ at X.

Theorem 7.1. [28] 1) Every subspace of first countability is first countability.

2) The continuous image of a first countability and open map is first countability.

Definition 7.3. In a space X, a collection N_x of s-open sets that contains an element x is called s-local basis at X if for any s-open set B such that $x \in B$ there is $N_x$in N_x such that $x \in N_x \subseteq B$.

Definition 7.4. A topological space X is called s-first countability if for any $x \in X$ there is a countable s-local base at X.

Theorem 7.2. A s-open subspace of s-first countability is s-first countability.

Proof. Let Y be a s-open subspace of a s-first countability X, then any $y \in Y\ (\subseteq X)$ has a countable s-local base $\aleph_y$ for X.

Let M is a s-open set in Y that contains y, then form theorem (2.6)then M is s-open in X ,

 ISBN 978-9959-9703-2-9

since $\aleph_y$ is a s-local base at y , there exists a s-open set $N_y \in \aleph_y$ such that $y \in N_y \subseteq M$, then $y \in N_y \cap Y \subseteq M \cap Y = M$therefore $N_y \cap Y$ is a countable s-local base at y in the subspace Y.

Theorem 7.3. Image of s-first countability under s-irresolute and M-s-open map is s-first countabililty.

Proof. Suppose $F: X \longrightarrow Y$ is a s-irresolute, M-s-open map from a s-first countabililty X onto a space Y. Then for any $y \in F(X)$ there is a countable s-local base $\aleph_{F^{-1}(y)}$ at $F^{-1}(y)$ for , since F is M-s-open map the collection $F(\aleph_{F^{-1}(y)})$ is countable collection of s-open sets in $F(X)$, and since F is s-irresolute, then $F(\aleph_{F^{-1}(y)})$ is a countable s-local base at y .

8. S-SECOND COUNTABILITY

Definition 8.1. [29] A space X has a countable basis if there is a countable collection $\mathfrak{B}$ of subsets of X that is a basis for on X space. In this case X is said to satisfy the second countability axiom, or to be second-countable.

Theorem 8.1. [29]

1) Second-countability implies first countability.

2) Every subspace of a second-countability is second-countability.

3) The continuous image of a second countability and open map is second countability.

Definition 8.2. The collection $\aleph$ of s-open sets in a space (X,τ) is say s-base for if each s-open set can expressed as a union of members of $\aleph$.

Examples 8.1.

1)Let $X = \mathbb{R}$ with $\tau = \{\mathbb{R}, \mathbb{Q}, \mathbb{K}, \emptyset\}$ the collection $\{\mathbb{Q}, \mathbb{K}\}$ is base for $\mathbb{R}$ but not s-base, while the collection is $\{\{x\}\}_{x\in\mathbb{R}}$s-base for $\mathbb{R}$ but not base.

2)Let $\tau = \{\mathbb{R}, \emptyset\}$ on $\mathbb{R}$ the collection $\{\{x\}\}_{x\in\mathbb{R}}$ is s-base but not base.

Definition 8.3. A space (X, τ) is say s- second countability if X has a countable s-base.

Examples 8.2.

1) Let $X = \mathbb{R}$ with $\tau = \{\mathbb{R}, \mathbb{Q}, \mathbb{K}, \emptyset\}$ is second countability but not s-second countability.

2) The trivial space on uncountable is second countable space but not s-second countability.

3) The space $X = \mathbb{R}$ with $\tau = \{\mathbb{R}, \mathbb{Q}, \emptyset\}$ is s-second countability, since $\{\mathbb{R}\} \cup \{\{x\}\}_{x\in\mathbb{Q}}$ is a s-local base for $\mathbb{R}$.

Definition 8.4. Let (X, τ) be a space is say s-countabiity if the collection $SO(X, \tau)$ is countability.

Corollary 8.1. Any s-countability is s-second countability.

Proof. Direct since $SO(X, \tau)$ is a countability s-local base for X.

Remark 8.1. Any s-countable space is s-first countability space and s-separability.

Examples 8.3.

1) Let $X = \mathbb{R}$ with $\tau = \{\phi\} \cup \{A \subseteq \mathbb{R}: 1 \in A\}$ is s-separability(since {1} is countable s-dense set

 ISBN 978-9959-9703-2-9

in $\mathbb{R}$), but X is not s-second countability since $\{1, x\}$ is s-open set for any $x \in \mathbb{R}$, $x \neq 1$.

2) If $X = \mathbb{R}$ and $\tau = \{\phi, \mathbb{R}, \{1\}\}$ then X is s-first countability (since $\{\{1, x\}\}$ is a countable s-local base at any point $x \in \mathbb{R}$), but not s-second countability. Note that, the space X is countable but not s-second countability.

Theorem 8.2. Any s-open subspace of s-second countability is second countability.

Proof. If Y be a s-open subspace of a s-second countability of X, then X has a countable s-base $\aleph$. Now we need to prove that the collection $\aleph_Y = \{N \cap Y : N \in \aleph\}$ is a countable s-base for Y Let M is a s-open set in Y , then form theorem (2.3) we get M is s-open in X, since $\aleph$ is a s-base for X, there exist s-open sets $N_\alpha \in \aleph$ such that $M = \cup N_\alpha$, then $M = M \cap Y = \cup (N_\alpha \cap Y)$, therefore $\{N_\alpha \cap Y\}$ is a countable s-base for the subspace Y.

Theorem 8.3. The s-irresolute image of s-second countability and M–s-open map is s-second countability.

Proof. Let $F: X \to Y$ is a s-irresolute and M-s-open map from a s-second countability X onto space Y . Then X has a countable s-base $\aleph$, since the map F is $M-$ s-open map the collection $F(\aleph)$ is a countable collection of s-open sets in $F(X)$, and since F is s-irresolute, then $F(\aleph)$ is a countable s-local base for $F(X)$.

Example 8.4. Let $X = Y = \mathbb{R}$ with $\tau_1 = \{\mathbb{R}, \mathbb{Q}, \phi\}$ then $SO(X, \tau_1) = P(\mathbb{Q}) \cup \mathbb{R}$,and $\tau_2 = \{\mathbb{R}, \mathbb{Q}, \phi\}$, then $SO(X, \tau_2) = P(\mathbb{R})$. Then the identity map from $(\mathbb{R}, \tau_1)$onto the space $(\mathbb{R}, \tau_2)$ is M –s-open map, however the space $(\mathbb{R}, \tau_1)$ is s-second countability while $(\mathbb{R}, \tau_2)$ is not s-second countability.

Conclusion

We introduce the notion of dense countability axioms; namely semi-countability axioms. We study the basic properties of s-countability axioms, as their subspaces and their continuous images. In addition, we discuss the relations between s-countability axioms and countability axioms, and we prove that the axioms of separability, s-separability and s-second countability are equivalent.

Outline some of our results:

- s-dense set is dense.
- In submaximal space, any s- open set is open set.
- In partition space, any subset is s-open.
- s-separability is separability, but not conversely.
- b-separability is s-separability space, but not conversely.
- A s-open subspace of s-first countability is s–first. countability.
- s-countability space is s-first countability and s-separable space.
- s-Second Countabililty is s-First Countability.

 ISBN 978-9959-9703-2-9

- s-open subspace of s-second countability is second countability.

References

[1] Frank Siwiec, On Defining a Space By A Weak Base. Pacific Journal of Mathematics, 52 (1) (1974) 233-245

[2] Frank Siwiec, Generalization of The First Axiom Of Countability. Tocky Mountain Journal of Mathematics, 5 (1) (1975)

[3] Zhu Jian-Ping, The Generalizations of First Countable Spaces. Tsukuba J. Math., 15 (1) (1991) 167-173

[4] Ponnnuthai Selvarani. S, Generalization of Urysohn's Lemma and Tietze Extension Theorem in b-Finitely Additive Space. International Journal of Computer Application, 3 (2) (2013) 1-19.

[5] Nagah A. Elbhilil , Khadiga A. Arwini,(2021),Countability Axioms Via Preopen Sets. An International Scientific journal, 111-125.

[6] H. H. Corson, E.Michael,(1964), Metrizability Of Certain Countable Unions. IIlinois J. Math.,8 (2), 351-360.

[7] A. S. Mashhour, M. E. Abd El-Monsef and S. N. El-Deeb, On Precontinuous and Week Precontinuous Mappings. Proceedings of Mathematical and Physical Society of Egypt, 53 (1982) 47-53

[8] A. Csaszar, Generalized Topology, Generalized Continuity. Acta Math Hungar, 96 (2002) 351-357

[9] John Benedict T. Ayawan and Sergio R. Canoy, Jr., Axioms Of Countability In Generalized Topological Spaces. International Mathematical Forum, 8 (31) (2013) 1523-1530

[10] S. Ersoy, I. Ince and M. Bilgin, Strongly k -Spaces. Bulletin of The Iranian Mathematical Society, 43 (3) (2017) 727-734

[11] R. Khayyeri, R. Mohamadian, On Base for Generalized Topological Space. Int. J. Contemp. Math. Sciences, 48 (2011) 2377-2383

[12] N. Levine., (Jan., 1963), Semi-Open Sets and Semi-Continuity in Topological Space, The American Mathematical Monthly , Vol. 70, No.1, pp. 36-41.

[13] C.E. Aull, Paracompact and countably paracompact subsets, General Topology and its relation to modern Analysis and Algebra, Proc. Kanpur Topological Con., (1968), 49-53.

[14] S.P. Arya and T. Nour, Characterizations of s-normal spaces, Indian J. Pure Appl. Math., 21 (1990), 717-719.

[15] H.Maki ,R.Devi and K.Balachandran, Associated topologies of generalized α − closed sets and α − generalized closed sets , Mem.Fac. Sci.Kochi Univ.Ser.A.Math.,15(1994), 51-63.

[16] S. G. Crossley, S. K., (1971), Hildebrand, Semi-closure, Texas J. Sci., 22, 99-112

[17] Al-Khazraji, R.B., (2004), On Semi-p-Open Sets, M.Sc. Thesis, University of Baghdad.

[18] T. Noiri, (2003), Remarks On δ -Semi-Open Sets And δ –Preopen Sets, Demonstration Mathematica, Vol. XXXVI No 4.

[19] O. Njastad, (1965), On Some Classes Of Nearly Open Sets, Pacic J. Math. 15, 961-970.

[20] S.N. Maheshwari, R. Prasad, (1975),Some New Separation Axioms, Annals de laSociete Scientfique de Bruxelles,T.89.III, 395-402.

[21] J. Dontchev,(1998)Survey On Preopen Sets. The Proceedings Of The Yatsushiro Topological Conference, 1-118.

 ISBN 978-9959-9703-2-9

[22] T. Noiri,(1984), Hyperconnectedness And Preopen Sets, Rev. Roumaine Math. Pures Appl., 29 (4), 329–334.

[23] G. Di Maio, T. Noiri,(1987), On s-closed spaces, Indian J. Pure Appl. Math. 18 (1987), 226-233

[24] M. S. Sarsak, (2009),On Semi Compact Sets And Associated Properties, Int. J. Math. Math. Sci., 465387. DOI: https://doi.org/10.1155/2009/465387.

[25] El-Maghrabi , Nasef ,(2009) , Between Semi-Closed And GS-Closed Sets , Available online at www.jtusci.info ISSN: 1658-3655, 2: 78-87.

[26] D. Andrijevi c, (1996), On b-Open Sets, Mat. Vesnik 48, 59-64.

[27] U.V.Fatteh , D. Singh,(1983), A note on D-Spaces, Bull, Cal, Math, Soc,75, 353- 358.

[28] J. N. Sharma and A.R. Vasishtha ,(1976), Functional Analysis", meerut.

[29] S. Willard, General Topology. Addison-Wesley Publishing Company, United States of American (1970).

[30] Ponnnuthai Selvarani. S,(2013), Generalization Of Urysohn's Lemma and Tietze Extension Theorem in b-Finitely Additive Space. International Journal of Computer Application, 3 (2) 1-19.

[31] Shyamapada Modak ,(2011) , Remarks On Dense Set , International Mathematical Forum,Vol. 6, no. 44, 2153 – 2158 .

[32] T.M. NOUR ,(1998), A Note On Some Applications Of Semi-Open Sets, Internat. J. Math. & Math. Sci. , VOL. 21 NO. 205-207 .

[33] S. G. Crossley, S. K. Hildebrand, (1972), Semi-topological properties, Fund. Math. 74, 233-254.

[34] Thomas , Semi – open sets ,Thesis , ,August 1965 .

[35] N. Bourbaki,(1996), General Topology. Addison Wesley, Part 1, Reading, Massachusetts.

[36] D. A. Rose, R. A.Mabmoud,(1994) , On Spaces Via Dense Sets And Smpc Functions , Kyungpook Mathematical Journal, Vol.34, No.l, 109- 116.

[37] D. Andrijevic, (1986), Semi-Preopen Sets, Mat. Vesnik 38, 24-32.

 ISBN 978-9959-9703-2-9

المؤتمر الدولي الثاني للعلوم والهندسة
2nd International Conference on Science and Engineering
ICSE 2023
Faculty of Engineering - University of Bani Waleed
Bani Waleed, Libya

Paper Code: ICSE-019

MOLECULAR DOCKING, DFT, MEPS AND IN VITRO INVESTIGATIONS OF NI(II), PD(II) AND CU(II) COMPLEXES CONTAINING THIOSEMICARBAZONE MOIETY

Amrajaa S. Abubakr [a*], Salima A. BenGuzzi[b], Safaa S. Hassan[c]
[a]Department of Chemistry, University of Ajdabiya, Libya
[b]Department of Chemistry, University of Benghazi, Libya
[c]Department of Chemistry, University of Cairo, Egypt
*Crosspnding author: amrajaa.shahhat@uoa.edu.ly and amrajaa.shahhat@gmail.com

Abstract: Metal complexes of 3-acetylpyridine thiosemicarbazone ligand (3-APT) with Ni(II), Cu(II), and Pd(II) chlorides were screened against bacterial strains *Staphylococcus aureus*, *Bacillus subtilis*, *Escherichia coli* and *Pseudomonas aeruginosa*. Cytotoxic activities showed that the Pd (II) complex exhibited more effective cytotoxic activity against human breast cancer cell line MCF-7 with (IC_{50}=20.72 µg/ml. The nucleophilic and electrophilic location interactions in the investigated ligand were described using the molecular electrostatic potential (MEPs) map. The density functional theory (DFT) was also carried out. Molecular docking investigation displayed the interactions between the active site amino acids of ribosyltransferase with the studied complexes. Besides, the cytotoxic modes of action by the active chelates with epidermal growth factor receptor tyrosine kinase were studied.

Keywords: 3-Acetylpyridine, Thiosemicarbazone, Microbiological screening, Molecular docking

Introduction

Bacterial and viral mutations, as well as resistance to existing drugs, have emerged as significant challenges in the medical field. This necessitates the development of novel drugs and medicines to combat such a threat. It has been observed that metal complexes with thiosemicarbazone (TSC) ligands and their derivatives exhibit respectable medicinal properties and seem advantageous in terms of generating less toxic and more potent medications [1-4]. Significantly, detailed studies have shown that the biological activity of thiosemicarbazones is related to their ability to coordinate with metal centers in proteins and enzymes in a variety of ways, whether in the neutral form of thione or in the negative form of thiol. On chelation, the polarity of the metal ion will be reduced to a greater extent due to the overlap of the ligand orbital and partial sharing of the positive charge of the metal ion with the donor [5]. This increased lipophilicity enhances the penetration of the

 ISBN 978-9959-9703-2-9

complexes into lipid membranes and thus blocks the metal binding sites on enzymes of microorganisms [6]. When the nitrogen atom of the imine group of TSCs forms a hydrogen bond with the active centers of cellular components, it may disrupt typical cellular functions. These metal complexes also disturb the respiration process of the cell and thus block the synthesis of proteins, which restricts further growth of the organism [7]. It also correlates with the nature of the N-C=S group, which is of great interest in chemotherapeutics [8]. Palladium has complexes that demonstration a noticeable cytotoxic activity comparable to that of platinum-based drug references [9]. Consequently, the complexes formed by coordination of thiosemicarbazone derivative with various metal ions specially Pd(II) ion are expected to have potent antitumor properties [10]. However, there are only few previous reports on 3-acetylpyridine thiosemicarbazone [11-14]. So, this work constitutes a fertile and exciting area for further investigations. The present article gives an insight into the antibacterial and antitumor activities of copper(II), nickel(II) and palladium(II) complexes derived from 3-acetylpyridine thiosemicarbazone (3-APT). The nucleophilic and electrophilic location interactions in the investigated ligand were described. The density functional theory (DFT) is also described. The molecular docking study will be completed at the end to demonstrate the various hydrogen bonds that have been formed between our compounds and the selected proteins.

1- Methods

a. Theoretical Method

The investigated complexes are optimized using the density functional theory B3LYP and the basis set LANL2DZ [15]. The structures were visualized using GaussView 5.0.8 after the calculations were completed using the Gaussian09 package [16]. For molecular docking studies, the Molecular Operating Environment (MOE) 2009.10 program was utilized. The binding free energy of the inhibitor inside the macromolecule was calculated. The protein crystal structure of the ribosyltransferase (antimicrobial activity) (PDB: 3GEY) and epidermal growth factor receptor tyrosine kinase EGFR (antitumor activity) (PDB code: 1M17) was obtained from Protein Data Bank (PDB). The nucleophilic and electrophilic location interactions were descripted using the molecular electrostatic potential (MEP) map [17].

b. Experimental Method

In vitro antibacterial activities of the ligand and its complexes were studied using the Kirby-Bauer disc diffusion method [18]. After being incubated at 35–37 °C for 24–48 hours

 ISBN 978-9959-9703-2-9

with Gram (+) bacteria like *Staphylococcus aureus* and *Bacillus subtilis* and Gram (-) bacteria like *Escherichia coli* and *Pseudomonas aeruginosa*, the diameters of the inhibition zones were measured in millimeters. The growth of the tested bacteria was reached to approximately 10^7 cells/ml using Mueller Hinton media and counted by using plate counter [19]. The volume used from microbial suspension was 100 µl that spread onto agar plates. The volume used from the tested samples was 10 µl that placed on agar media with the help of blank paper disks. The influence of ligand and their chelates on the used bacteria were compared with sensitivity to a common antibiotic (Gentamicin).

$$\text{Activity Index (A)} = \frac{\text{Inhibition zone of prepared compound(mm)}}{\text{Inhibition zone of standard drug(mm)}} \times 100\%$$

The antitumor activity of 3-APT and its complexes against the MCF-7 breast cancer cell line was established through by MTT assay method which measures the cellular metabolic viability [20]. The MTT assay technique is based on the reduction of the tetrazolium salt MTT to insoluble purple formazan by metabolically active cells, making their activities quantifiable by spectrophotometry. Cells were cultured in 96-well plates and were treated with different concentrations of test compounds after incubation. Another group of cells was treated with small concentrations of doxorubicin, After 48 h treatment, the cells were incubated with MTT (0.5 mg mL^{-1}), and formazan crystals were dissolved in DMSO. Results are expressed in terms of the concentration required to inhibit cell growth by 50% relative to untreated cells (IC_{50}).

2- Results and discussion

a. Theoretical results

In order to better understand how well novel compounds exhibit bioactivity against the target, we can use molecular docking to identify the potential mechanisms of interaction and binding affinities of these therapeutic molecules. We validate the docking procedure by docking the co-crystalized ligand in its binding pocket. The co-crystalized ligand in the ribosyltransferase (code: 3GEY) was P34 (N~2~,N~2~-dimethyl-n~1~-(6-oxo-5,6 dihydrophenanthridin-2-yl)glycinamide. The docking results are seen in (Table 1) and (Figure 1). Side chain acceptor interaction type was observed between the terminal amino group proton with carbonyl oxygen of Thr-A622 amino acid in the case of ligand and with carbonyl oxygen of Asp-A623 in both Cu and Ni chelates. Cu chelate observed various interactions as side chain donor between the N of py ring with terminal amino group of Lys-A518, Backbone acceptor between the terminal NH_2 proton of ligand with Gln-B549 carbonyl

 ISBN 978-9959-9703-2-9

oxygen and arene-cation interaction between the aromatic pyridine ring with both (Ly-A518 & His-B550) amino acid residues. Moreover, the aromatic pyridine ring interacts with both His-B550 and the Pd chelate in an arene-cation fashion. Molecular docking study of the standard Gentamicin drug observed high scoring energy value which compatible with its antibacterial activity. It demonstrates the side chain donor interactions of the amino acids Asn-B508 (carbonyl oxygen), Lys-A518 (terminal amino), and Gln-B549 (carbonyl oxygen) with the ring oxygen atoms OH and NH_2It was observed that the OH groups of gentamicin and Gln-B549 (carbonyl oxygen) amino acid had a backbone acceptor interaction type. The redocking results mentioned variable poses with acceptable RMSD values. Most values are lower than 2 Å with high docking score. The best pose with high scoring energy and lower RMSD show interaction between NH group of P34 and Asn-B508 (carbonyl oxygen) as side chain acceptor interaction type manner. The Arene-cation interaction type was observed with His-B550. The previous docking results for Gentamicin and P34 were seen in (Figure 2). The hydrogen bonds values of most of observed results were written in (Table 1). All chelates have more negative scoring energy than the ligand itself. Backbone acceptor was observed in the ligand by hydrogen formation between Gln-767 (carbonyl oxygen) residue with NH proton and Arg-752 with the terminal amino proton. Solvent contact interaction was observed in Cu-L and Pd-L compounds. Ni-L chelate formed the hydrogen bond between the terminal amino protons with Asn-818 residue. Molecular docking study of both cisplatin and doxorubicin against the same protein revealed higher negative scoring energy value for doxorubicin than the cisplatin. The chelates have comparable values to the standard doxorubicin drug. The docking results are seen in (Table 2 and Figure 4). Doxorubicin (OH) interacted with Thr-830 (OH) while the cisplatin (NH_3) was interacted with the main chain oxygen of two different amino acids (Asp-831 and Glu-738). We validate the docking procedure by docking the co-crystalized ligand in its binding pocket. The co-crystalized ligand in the EGFR tyrosine kinase receptor (PDB Code: 1M17 (was 4-anilinoquinazoline (AQ4). The redocking of the (AQ4) revealed good poses with RMSD as seen in (Table 2 and Figures 3, 4). The RMSD is lower than 2 Å with high docking score. The docking results cleared the interaction between the (N1) quinazoline ring of (AQ4) inhibitor with the terminal amino group of Lys-721 amino acid. The hydrogen bond values were mentioned in (Table 2).

DFT calculations were performed for the 3-APT

 ISBN 978-9959-9703-2-9

ligand and its complexes. The optimization molecular properties were mentioned in Figures (5, 6) and (Table 3, 4). Some bond lengths were increased as [(N9-C7), (N9-N10) and (C11-S12)] and others were decreased as [(C1-N7), (N10-C11) and (C11-N13)] to optimize the coordination through N9 and S12 donor sites. New bonds were formed due to chelation as M-N9 and M-S12 bonds in all chelates with the appearance M-Cl bond in palladium and copper chelates. The bond angles of ligand were changed by the coordination to metal ions as pointed out in (Figure 5). Angles surrounding the metal change dramatically when the metal center is changed. The negative charge was mostly delocalized over N7 and S12 atoms with calculated charges -0.176 and -0.07 respectively to form the energetically stable five-membered ring. After coordination, the electron density over the previously mentioned atoms was decreased due to the transfer of charge from the donor sites of ligand to the central metal ions i.e. (L→M). The case of an increase in electron density may be due to the back donations from metal to ligand. These calculated charges converted to [Ni= (-0.217&+0.210), Cu= (-0.221 & +0.092) and Pd= (-0.15 &+0.170)] for N7 and S12 atoms respectively. The metal charges converted to +0.097, +0.067 and -0.083 in the case of Ni, Cu and Pd after coordination respectively. The molecular orbitals are identified as the frontier molecular orbitals (FMOs) as seen in (Figure 6). The HOMO-LUMO energy gap has been identified as an important stability descriptor. The large HOMO-LUMO energy gap is consistent with systems that are stable and have little reactiveness. The orbital frontier eigenvalues and HOMO-LUMO gaps are inserted in (Figure 6). A molecule with a small HOMO-LUMO gap is more reactive and is a softer molecule because the smaller hardness values imply higher reactivity. The complexes were more reactive than the parent ligand, as shown by energy gaps. The negative chemical potential is indicative of their stabilities. The electron cloud of (3-APT)'s HOMO is mainly localized on the aliphatic part concluding the thiosemicarbazone part but LUMO electron cloud extended to both the aliphatic and aromatic parts. The electron cloud with respect to the HOMO orbital was distributed after coordination over the aromatic pyridine ring with the coordination center in case of nickel chelate but distributed over the aliphatic part with the coordination center in case of copper and palladium chelates. The LUMO electron distribution of palladium chelate localized over the whole molecule while in nickel and copper chelates was limited to the aliphatic part with the coordination center. As indicated by the

 ISBN 978-9959-9703-2-9

magnitude of their dipole moments, the polarity of the ligand increased after chelation by bonding to palladium (II) metal ion and vice versa by coordination with nickel (II) and copper (II). Many ground state parameters can be calculated using the formulas below:

$I = - E_{HOMO}$ $A = - E_{LUMO}$

Where, I= Ionization potential of the compound, A= Electron affinity of the compound

I (Ionization potential) = $-E_{HOMO}$,

A (Electron affinity) = $-E_{LUMO}$

η (hardness)=((I-A))/2,

S (Softness) =1/2η,

μ (Chemical potential) =(-(I +A))/2,

x (absolute electronegativity) =((I + A))/2

Also, we noticed that Ni and Cu chelates had the lowest dipole values (See Table 4). The dipole moment property of a substance classically indicates its polarity. Drug solubility in water increases with increasing the dipole moment, suggesting that dipole moment is a crucial factor in determining drug penetration through the organism's cell membrane and the rate of excretion. The ability of a compound to penetrate the lipid layer of a microorganism more effectively is influenced by its liposolubility, attacking the cell constituents and become more dangerous and toxic in the cellular environment.

The electron density is polarized as seen in the three-dimensional view of MEP. Additionally, we can get the size and geometry of the molecules [21]. MEP is computed to estimate specific structural reactive sites by the change of color that indicates the electron density along the different positions in the molecule. The red or orange areas indicate locations with high density of electrons while the blue color provides positions with the low electron densities. N7 and S12 atoms have great negative electrostatic potential on the studied ligand, while the rest of the ligand molecule has the highest positive electrostatic potential, as seen in (Figure 7). It means the previously mentioned atoms can attracted to the positive electrostatic potential membrane structure of the cells and are active sites for metal ion coordination. We can say that the investigated chelates exhibit positive electrostatic potential (ESP) maps on their skeletons and negative ESP on its coordination centers, as shown in (Figure 7). Therefore, they can bind tightly into the investigated microorganism having the negatively electrostatic potential. This may be necessary in order to produce an optimal docking pose of the drug inside the binding pocket of the tested microorganism in order to form a stable complex.

a. Experimental results

The organisms used consist of two of each Gram positive (*Bacillus Subtilis&*

 ISBN 978-9959-9703-2-9

Staphylococcus aureus) and two Gram negative (*Escherichia coli & Pseudomonas aeruginosa*). All investigated compounds have at least similar inhibition zone value to the standard antibiotic. The most of inhibition zones exceed the standard antibiotic (*Gentamicin*) against all tested organisms as represented in (Figures 8, 9) and pointed out in (Table 5). Nickel chelate observed the best result against the *Escherichia coli* organism with an inhibition percentage 177.8 % relative to the standard antibiotic values (Gentamicin). The other compounds give 150 %, 155.5 % and 144.4 % for Cu, Pd and ligand respectively that compatible with the docking scores sequence is Ni > Pd ~= Cu > 3-APT. The free ligand was more effective than the standard drug at inhibiting the *Staphylococcus aureus* organism, with an inhibition percentage of 133.3%, but their complexes exhibit weaker antibacterial activity, with respective inhibition percentages of 118.5%, 103.7%, and 100% for Ni, Cu, and Pd complexes. When compared to the values for standard antibiotics, it also saw the best results against the *Pseudomonas aeruginosa* organism with an inhibition percentage of 171.4%. The remaining compounds give 161.9 %, 157.1 % and 157.1 % for Cu, Pd and nickel complexes with the sequence is: 3-APT > Cu > Pd ≈ Ni. Additionally, against the *Bacillus Subtilis* bacterial strain, all chelates and ligand demonstrated appreciable activity, as shown by the values in (Table 6).

The cytotoxicity order is Pd > Cu > L≈Ni depending on the IC_{50} values (See Table 6 and Figure 10). The lower IC_{50} of the compound, the less you consume from this active compound to achieve the favored effect. The most notable cytotoxic activity against the cancer cell was achieved by the palladium chelate. The isoelectronic property of Pd (II) to platinum (II) with similar square-planar geometry as cisplatin, the palladium (II) compounds expected to have a potential to be anti-cancer agent. One of the interesting observation that found, in spite of nickel and palladium are from the same group but palladium indicates more effective inhibition for the progression of cancer cells. It may be due to the facilely process of aquation of the Pd-compounds when enter the cancer cell and consequently inhibit its progress. Also, it may be due to the smaller size of the palladium complex as attached to one molecule of ligand only but nickel metal was attached to two molecules of ligand which maybe affect the membrane permeability of cancer cells and then the cell mortality that is called “cell apoptosis” [22]. The same observation was noticed by comparing nickel and copper activities, both complexes were attached to two ligand molecules but the copper ion with a

 ISBN 978-9959-9703-2-9

smaller size than a nickel. Therefore, copper chelate observed a higher cytotoxic effect. The anticancer activity of our compounds was in good agreement with earlier studies that suggested the anticancer effects of sulfur-containing compounds depend heavily on apoptosis [23]. In a previous study testing the cytotoxic properties of 2-APT ligand, the comparison of the cytotoxic activities indicates that 2-APT shows lower IC_{50} value than 3-APT [24].

Conclusion

The significance of thiosemicarbazones and their metal complexes, apart from their diverse chemical and structural characteristics, stems from not only their potential but also their proved application as biologically active molecules. The antibacterial screening showed the superiority of studied compounds over the well-known standard drug, gentamicin. This could be due to the presence of active function groups as NH_2, NH, and N-pyridine which help in the formation of hydrogen bonds with the active center of cell constituents. In particular, among the three complexes, the palladium (II) complex show noteworthy anticancer activity with a lower IC50 value (IC_{50} = 20.72 µg/ml) than its free ligand.

Arabic section:

الهـــدف والخلاصـــة: توضح هذه الورقة الفعالية المضادة للبكتيريا والمضادة للأورام لمعقدات أحادية المشتقة من 3- اسيتيل بيريدين الثايوسيميكارباز ون. تم استخدام النظرية الوظيفية للكثافة (DFT) لتحسين التركيب الهيكلي لليجاند ومعقداته. تم وصف تفاعلات الموقع المحب للنيوكليوفيلي والالكتروفيلي في الليجند الذي تم فحصه باستخدام خريطة الجهد الكهروستاتيكي الجزيئي (MEPs). تم إجراء مزيد من دراسة الالتحام الجزيئي النظرية لمراقبة المواقع النشطة في البروتينات المختارة أثناء تفاعلها مع مركباتنا. أظهر الفحص المضاد للبكتيريا تفوق المركبات المختارة على العقار القياسي المعروف ، الجنتاميسين. قد يكون هذا بسبب وجود مجموعات وظيفية نشطة مثل NH_2 و NH و N- في حلقة pyridine والتي تساعد في تكوين روابط هيدروجينية مع المركز النشط لمكونات الخلية. على وجه الخصوص ، من بين المخلبيات الثلاثة ، يُظهر معقد البلاديوم (II) نشاطًا مضادًا للسرطان جديرًا بالملاحظة مع قيمة IC_{50} أقل (IC_{50} = 20.72 ميكروغرام / مل).

Abbreviations and Acronyms

TSCs (Thiosemicarbazones), IC_{50} (half-maximal inhibitory concentration), µg/ml (Microgram per milliliter unit), MEPs (molecular electrostatic potentials), L (Ligand) Ni (Nickel), Cu (Copper), Pd (Palladium), MCF-7 (Michigan Cancer Foundation-7), FMOs (frontier molecular orbitals), .

Acknowledgment

The simulation in this work was performed at Cairo University's High-Performance Computing Center (accessed on 30 December 2022).

References

[1] García-Tojal, J., et al., Biological activity of complexes derived from thiophene-2-carbaldehyde thiosemicarbazone. Crystal structure of [Ni ($C_6H_6N_3S_2$) 2]. 2001. 86(2-3): p. 627-633.

[2] Prabhakaran, R., et al., Structural and biological studies of mononuclear palladium (II) complexes containing N-substituted thiosemicarbazones. 2008. 43(2): p. 268-273.

[3] Rodríguez-Argüelles, M.C., et al., Copper complexes of imidazole-2-, pyrrole-2-and indol-3-carbaldehyde thiosemicarbazones: inhibitory activity against fungi and bacteria. 2005. 99(11): p. 2231-2239.

[4] West, D.X., S.B. Padhye, and P.B. Sonawane, Structural and physical correlations in the biological properties of transition metal heterocyclic thiosemicarbazone and S-alkyldithiocarbazate complexes, in Complex

 ISBN 978-9959-9703-2-9

Chemistry. 2005, Springer. p. 1-50.
[5] Green, M.A., et al., In vivo quantitative whole-body perfusion imaging using radiolabeled copper (II) bis (thiosemicarbazone) complexes and positron emission tomography (PET). 2022: p. 751-771.
[6] Patil, S.A., et al., Comprehensive Review on Medicinal Applications of Coumarin-Derived Imine–Metal Complexes. 2022. 27(16): p. 5220.
[7] Vashi, K. and H.J.J.o.C. Naik, Synthesis of novel Schiff base and azetidinone derivatives and their antibacterial activity. 2004. 1: p. 272-275.
[8] Pelosi, G.J.T.O.C.J., Thiosemicarbazone metal complexes: from structure to activity. 2010. 3(1).
[9] Matesanz, A.I., I. Leitao, and P.J.J.o.I.B. Souza, Palladium (II) and platinum (II) bis (thiosemicarbazone) complexes of the 2, 6-diacetylpyridine series with high cytotoxic activity in cisplatin resistant A2780cisR tumor cells and reduced toxicity. 2013. 125: p. 26-31.
[10] Milewski, S., H. Chmara, and E.J.A.o.m. Borowski, Antibiotic tetaine—a selective inhibitor of chitin and mannoprotein biosynthesis in Candida albicans. 1986. 145: p. 234-240.
[11] Čobeljić, B., et al., Analysis of the structures of the Cu (I) and Cu (II) complexes with 3-acetylpyridine and thiocyanate. 2014. 69: p. 77-83.
[12] Mendes, I., et al., Structural and spectral studies of thiosemicarbazones derived from 3- and 4-formylpyridine and 3-and 4-acetylpyridine. 2001. 559(1-3): p. 355-360.
[13] Alwi, M.A.M., et al., Gravimetric and electrochemical statistical optimizations for improving copper corrosion resistance in hydrochloric acid using thiosemicarbazone-linked 3-acetylpyridine. 2022. 12(43): p. 27793-27808.
[14] El-Ayaan, U.J.J.o.C.C., Transition metal complexes of 3-acetylpyridine 4 N-(2-pyridyl) thiosemicarbazone (HAPS); structural, spectroscopic, and biological studies. 2012. 65(4): p. 629-642.
[15] Becke, A.D.J.T.J.o.c.p., Density-functional thermochemistry. I. The effect of the exchange-only gradient correction. 1992. 96(3): p. 2155-2160.
[16] Zheng, G., et al., Gaussian 09. 2009: p. 48.
[17] Al-Janabi, A.S., et al., Spectroscopic, anti-bacterial, anti-cancer and molecular docking of Pd (II) and Pt (II) complexes with (E)-4-((dimethylamino) methyl)-2-((4, 5-dimethylthiazol-2-yl) diazenyl) phenol ligand. 2023. 27(3): p. 101619.
]18] Biemer, J.J.J.A.o.C. and L. Science, Antimicrobial susceptibility testing by the Kirby-Bauer disc diffusion method. 1973. 3(2): p. 135-140.
]19] Hassan, S.S.J.A.O.C., Antibacterial, DFT and molecular docking studies of Rh (III) complexes of Coumarinyl-Thiosemicarbazone nuclei based ligands. 2018. 32(3): p. e4170.
[20] Ali, A., et al., Ligand substituent effect on the cytotoxicity activity of two new copper (ii) complexes bearing 8-hydroxyquinoline derivatives: Validated by MTT assay and apoptosis in MCF-7 cancer cell line (human breast cancer). 2021. 11(24): p. 14362-14373.
[21] Abdelaziz, A., et al., Ag (I), In (III), and Sn (II) chelates of azo mesalamine drug: Characterization, DFT studies, molecular docking and biological evaluation. 2023. 37(2): p. e6944.
[22] Salama, S.K., et al., Molecular docking simulation and anticancer assessment on human breast carcinoma cell line using novel bis (1, 4-dihydropyrano [2, 3-c] pyrazole-5-carbonitrile) and bis (1, 4-dihydropyrazolo [4′, 3′: 5, 6] pyrano [2, 3-b] pyridine-6-carbonitrile) derivatives. 2017. 71: p. 19-29.
[23] De Gianni, E. and C. Fimognari, Anticancer mechanism of sulfur-containing compounds, in The Enzymes. 2015, Elsevier. p. 167-192.
[24] Pal, S.J.P., Pyridine: A useful ligand in transition metal complexes. 2018. 57: p. 57-74.
[25] Wang, H., et al., A computational study of adsorption and activation of CO2 and H2 over Fe (1 0 0) surface. 2016. 15: p. 107-114.

Figures and Tables

 ISBN 978-9959-9703-2-9

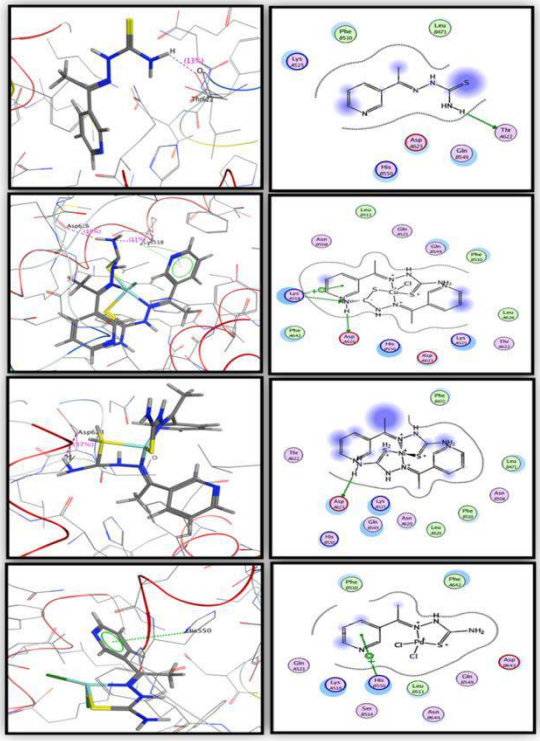

Fig. 1: Docking structures of with proteins ribosyltransferase.

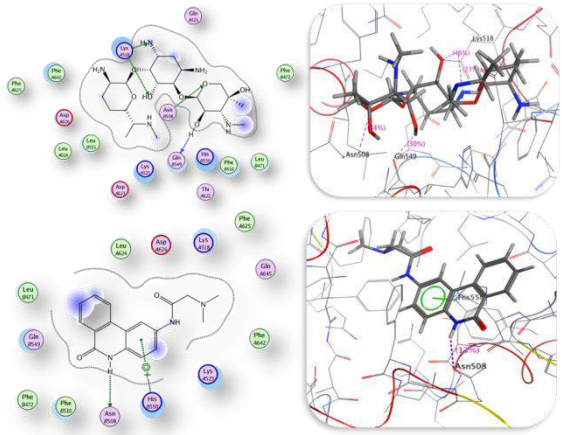

Fig. 2: 2D and 3D Docking structures of Gentamicin and P34 compounds with ribosyltransferase (code: 3GEY).

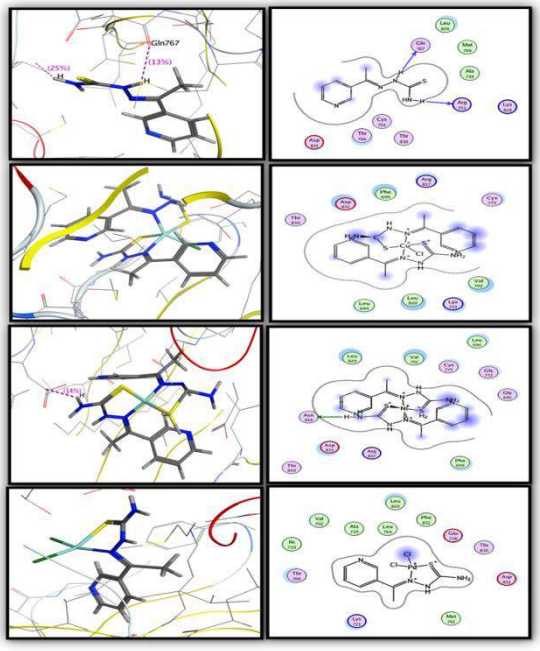

ISBN 978-9959-9703-2-9

Fig. 3: Docking structures of with proteins EGFR tyrosine kinase.

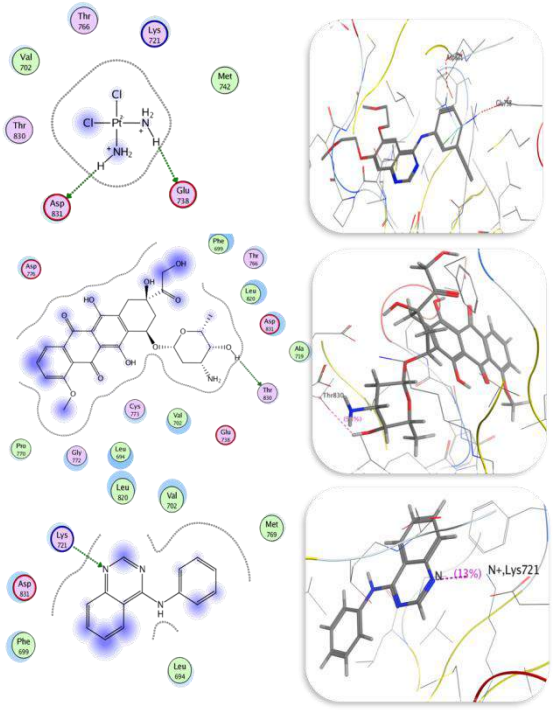

Fig. 4: 2D and 3D Docking structures of cisplatin, doxorubicin and AQ4 compounds respectively against EGFR tyrosine kinase (PDB ID: 1M17).

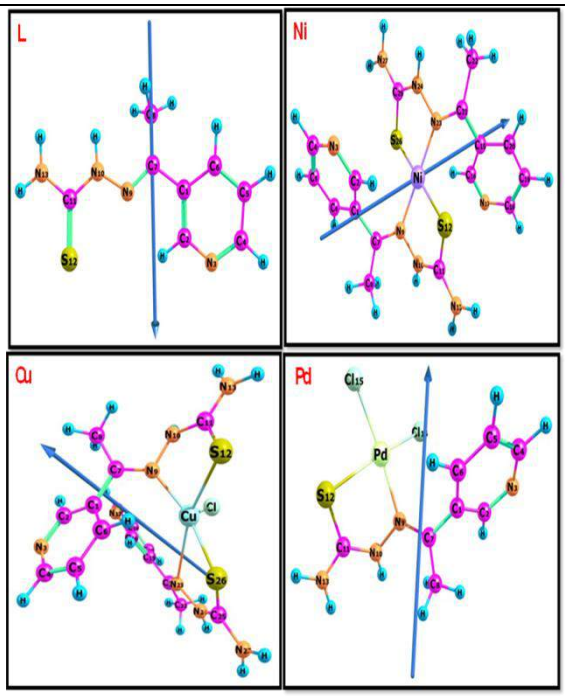

Fig. 5: Optimized geometry of ligand and its metal complexes.

ISBN 978-9959-9703-2-9

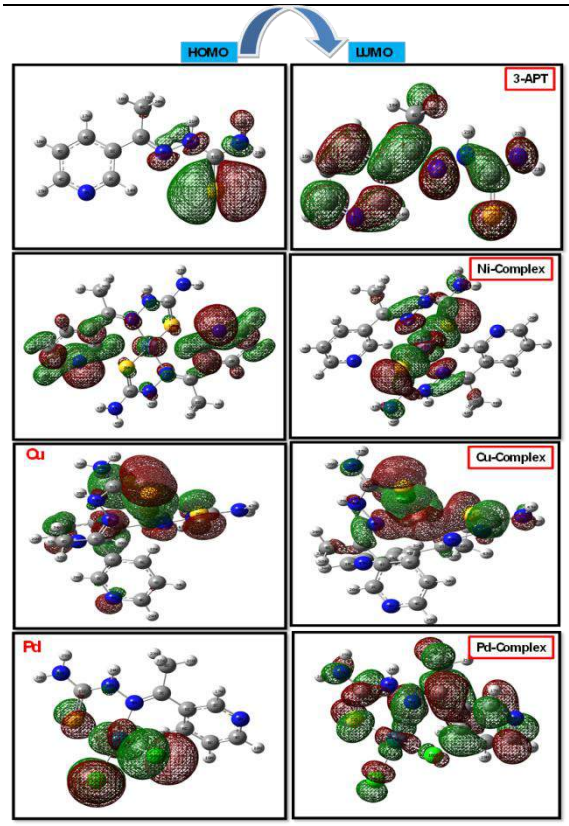

Fig. 6: Molecular graphs of ligand and complexes.

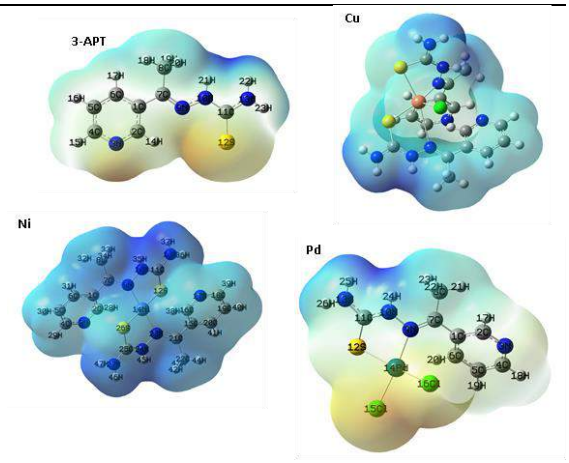

Fig. 7: The molecular electrostatic potentials (MEPs) of the ligand and its metal chelates.

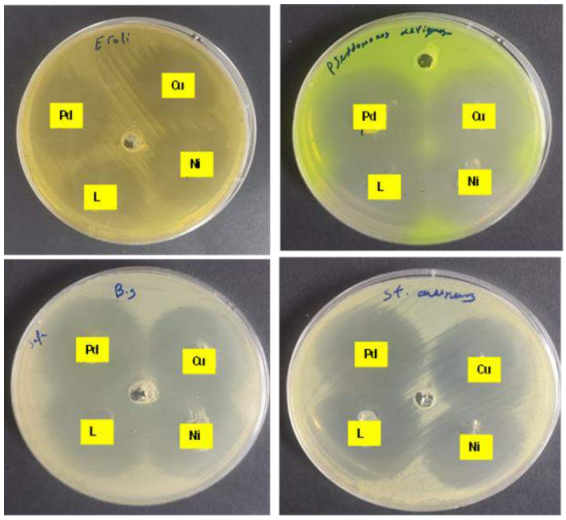

Fig. 8: Photographic representation of zone of inhibition of the ligand and their Ni(II), Pd(II) and Cu(II) towards different types of bacterial strains

ISBN 978-9959-9703-2-9

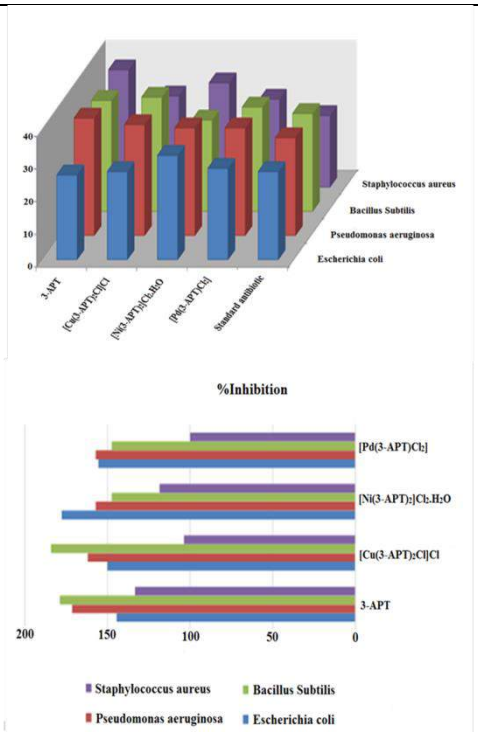

Fig. 9: Biological activity and percentage inhibition of the compounds towards different types of bacterial strains.

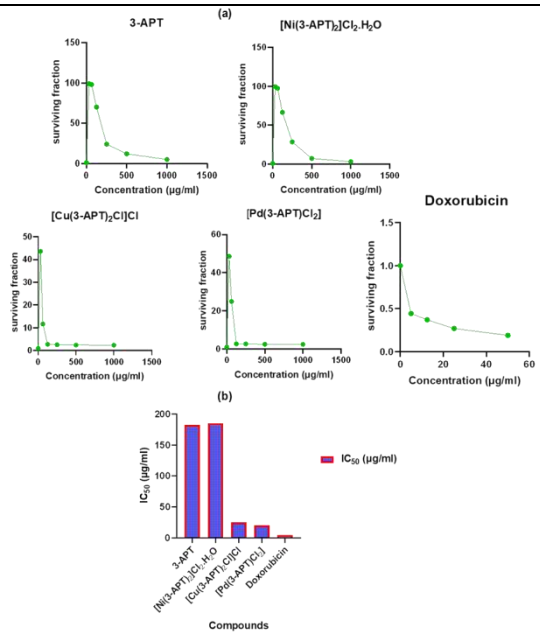

Fig. 10: Surviving fraction of 3-APT ligand and its metal complexes at different concentrations (µg/ml) on MCF-7 human breast cancer cell. B) IC_{50} values against the MCF-7 breast cancer cell line.

Table 1: Comparison of binding affinity of thiosemicarbazone ligand and their complexes against ribosyltransferase.

Compound	Scoring energy (RMSD)	Involved amino acids	Type of interaction
Ligand	-2.60(0.78)	Thr-A622 (2.43 °A)	Side chain acceptor
Cu-Complex	-4.42(2.25)	Asp-A623, Lys-A518 (2.78°A), Gln-B549 (1.88 °A) and (Ly-A518 & His-B550)	side chain acceptor, sid chain donor Backbone acceptor, an Arene-catio interaction
Ni-Complex	-5.71(1.36)	Asp-A623 (1.83 °A)	Side chain acceptor-

ISBN 978-9959-9703-2-9

Pd-Complex	-2.46(2.53)	His-B550	Arene-cation interaction
Gentamicin	-7.00(1.73)	(Asn-B508 (2.39 °A) & Lys-A518) and Gln-B549 (2.18 °A), Asn-B508 (1.80 °A)	side chain donor and Backbone acceptor, side chain acceptor
P34	-4.78(1.31) -3.31(2.49) -3.25(1.19) -2.66(1.21)	Asn-*B*508 and His-*B*550 N	side chain acceptor and Arene-cation interaction

Table 2: Comparison of binding affinity of complexes against EGFR tyrosine kinase receptor

Compound	Scoring energy (RMSD)	Involved amino acids	Type of interaction
Ligand	-3.04(1.58)	Gln-767 (2.29 °A) and Arg-752	Backbone acceptor
Cu-Complex	-5.57(2.48)		Solvent contact
Ni-Complex	-6.27(1.40)	Asn-818	Side chain acceptor-
Pd-Complex	-4.92(1.03)	His-B550	Solvent contact
Cisplatin	-1.92(2.01)	Asp-831 (2.08 °A) and Glu-738 (1.87 °A)	Side chain acceptor
Doxorubicin	-5.45(2.62)	Thr-830 (2.44 °A)	Side chain acceptor
4-anilinoquinazoline (AQ4)	-3.30(1.26) -3.91(2.54)	Lys-721 (3.30 °A) Lys-721	Side chain donor Arene-cation

Table 3: Some of the optimized bond lengths, Å and bond angles, degrees, for (3-APT) and complexes using B3LYP/6-311G and B3LYP/LANL2DZ respectively.

Bond length (A°)	Ligand	Ni-complex	Cu-complex	Pd-complex
R(M-N9)	-	1.93101	2.01961	2.11753
R(M-S12)	---	2.33752	2.60474	2.46697
R(M-Cl)	---	1.85452	2.32858	2.38765
R(C1-N7)	1.48037	1.46809	1.48031	1.47483
R(N9-C7)	1.30333	1.32968	1.31705	1.32077
R(N9-N10)	1.36739	1.42904	1.42550	1.42078
R(N10-C11)	1.38393	1.36297	1.37943	1.36863
R(C11-S12)	1.71220	1.77562	1.76001	1.75210
R(C11-N13)	1.36616	1.34157	1.35087	1.36231
A(C1-C7-N9)	115.723	119.011	117.531	119.770
A(C7-N9-Nl0)	119.732	116.951	118.787	116.862
A(N9-N10-Cl1)	121.350	116.416	115.095	119.928
A(N10-Cl1-S12)	125.366	117.854	121.286	122.192
A(N13-C11-S12)	121.728	122.162	121.685	121.124
A(C11-S12-M)	123.293	90.569	83.458	92.015
A(S12-M-N23)		96.833	164.996	---
A(S12-M-N9)	---	83.170	76.729	82.127
A(S12-M-S26)	---	179.994	97.444	---
A(N9-M-N23)	---	179.996	118.269	---
A(S12-Pd-Cl15)	---	55.550	---	91.810
A(N9-S12-Cl)	---	---	95.202	86.695

Table 4: Ground state properties of ligand and its metal complexes using B3LYP/6-311G and B3LYP/LANL2DZ respectively..

ISBN 978-9959-9703-2-9

Bond length (A°)	Ligand	Ni-complex	Cu-complex	Pd-complex
E_T, Hartree	-927.85681323	-1248.60316966	-1290.70834423	-696.596206139
E_{HOMO}, eV	-5.43	-12.40	-0.33	-5.97
E_{LUMO}, eV	-1.66	-9.11	-0.26	-2.99
ΔE, eV	3.77	3.29	0.07	2.98
I=- E_{HOMO}, eV	5.43	12.40	0.33	5.97
A= - E_{LUMO}, eV	1.66	9.11	0.26	2.99
χ, eV	1.88	6.54	8.16	3.01
η, eV	1.89	1.65	0.04	1.49
S, eV^{-1}	0.27	0.30	13.58	0.34
μ, eV	-3.54	-10.76	-0.30	-4.48

Table 5: Antibacterial activity data in (mm) of ligand and their chelates in various bacteria organisms and comparison with Gentamicin.

Compound	B. subtilis	S. aureus	E.coli	P. aeruginosa
Ligand	34	36	26	36
Cu- Complex	35	28	27	34
Ni-Complex	28	32	32	33-
Pd-Complex	32	27	28	33
Standard antibiotic Gentamicin	19	27	18	21

Table 6: Inhibitory activity (IC_{50}) of the ligand and their chelates against human breast cancer cell (MCF-7).

Compound	IC_{50} (µg/ml)	IC_{50} (µM)
Ligand	182.68	940
Cu- Complex	25.21	48.21
Ni-Complex	185.17	345
Pd-Complex	20.72	55.76

ISBN 978-9959-9703-2-9

المؤتمر الدولي الثاني للعلوم والهندسة
2nd International Conference on Science and Engineering
ICSE 2023
Faculty of Engineering - University of Bani Waleed
Bani Waleed, Libya

Paper Code: ICSE-046

ESTIMATION OF SOIL POLLUTION WITH WASTEWATER BY MEASURING THE CONTENT OF HEAVY ELEMENTS IN SOME VEGETABLES GROWN IN IT

Tawfik A. Al-Shohiby
Chemistry, Education/University of Tobruk, Libya
E-mail- bluo85@gmail.com

Abstract: : This research was conducted to estimation of soil pollution with wastewater by measuring heavy metals (Lead, Chromium, Copper, Zinc and Manganese) in Samples of imported vegetables (from Egypt), and the vegetables that we sampled are: cucumbers, tomatoes, eggplants, zucchini, onions and carrots, collected from the central vegetable market in Tobruk City. The samples prepared by dry-ashing digestion method and the concentrations of heavy metals were determined by using atomic absorption spectroscopy (AAS). The results showed a significant increase in the levels of heavy metals that were measured in the samples.

Keywords: pollution, wastewater, vegetables, heavy metal

Introduction

Environmental pollutants are substances or energy introduced into the environment that have adverse effects, or adversely affects the usefulness of a resource. These can be both naturally forming (i.e., minerals or extracted compounds like oil) or anthropogenic in origin (i.e., manufactured materials or byproducts from biodegradation). Pollutants result in environmental pollution or become public health concerns when they reach a concentration high enough to have significant negative impacts [1].

Untreated wastewater is a term used to describe wastewater that has not been treated to remove harmful pollutants. This type of wastewater can contain a variety of contaminants, including bacteria, viruses, parasites, heavy metals, and other chemicals. The use of untreated wastewater to irrigate vegetable fields is a common practice in many parts of the world. This is because wastewater is a readily available source of water, and it can be used to grow crops throughout the year. However, the use of untreated wastewater can also pose a number of risks to human health and the environment [2,3].

Growers are often unaware of the health risks associated with growing vegetables on

 ISBN 978-9959-9703-2-9

sewage and industrial effluents, which can lead to a buildup of heavy metals in the food chain [4].

Heavy metal pollution in water and soil is a serious problem that is of great concern to both the public and scientists, as these metals can be extremely toxic to human health and biological systems [5].

Research has shown that the rate at which plants absorb metals increases as the concentration of metals in the soil increases. In soils with low levels of metals, there is often a linear relationship between the concentration of metals in the soil and the concentration of metals in plants. For example, a study found that the concentration of Zn and Cd in bean leaf tissue increased with the amount of metals added to the soil through sludge applications. The concentration of metals in the plant tissue reached a maximum level, however, and did not increase further with additional applications of metals [6,7].

Urban agriculture can introduce new risks to public health, but it is also exposed to environmental hazards that can affect producers, traders, and consumers. These hazards are not unique to urban agriculture, as other activities in urban areas can also expose people to contamination. The list below summarizes the potential health hazards associated with urban agriculture, as identified by regional researchers in Africa, Asia, and Latin America [8].

1. Contamination of crops grown on polluted soils or irrigated with river water contaminated with industrial and chemical byproducts.
2. Microbial and heavy metal contaminants in untreated or improperly treated urban waste and human and animal excreta used in agriculture.
3. Zoonotic diseases associated with urban livestock keeping.
4. Encouragement of vector breeding sites.

The urban food system is at risk from industrial and chemical byproducts that can pollute crops, soil, and water. These pollutants can cause health problems for people of all ages, but children are especially vulnerable. Heavy metals are a major source of pollution in soils, and they can enter the food chain through irrigation, solid waste disposal, fertilizer and pesticide application, and atmospheric deposition [9].

Hardoy and Satterthwaite argue that chemical pollution is a major environmental concern in urban areas. Industrial and chemical pollutants are often disposed of in local bodies of water or vacant land without adequate measures to protect human health.

 ISBN 978-9959-9703-2-9

This can lead to a variety of health problems, including respiratory problems, cancer, and reproductive disorders [10]. They claim that "reports from Third World Cities of severe health problems arising from human contact with toxic or hazardous wastes are increasingly common".

Urban agriculture is a major source of heavy metal exposure for people living in urban industrial areas. This is because urban agriculture often takes place on contaminated land, and the produce grown on this land can contain high levels of heavy metals. The World Health Organization (WHO) and Polish researchers have found that 60-80% of heavy metal toxins found in human bodies in urban industrial areas are the result of consuming contaminated foods, rather than air pollution. [11].

Heavy metals are of considerable environmental concern due to their toxicity and cumulative behavior [12]. Trace quantities of certain heavy elements, such as Cr, Co, Cu, Mn, and Zn, are essential micronutrients for higher animals and for plant growth [13]. On the other hand, they are easily assimilated and accumulate in plants and animals' bodies [14]. Vegetables absorb heavy metals from the soil as well as from surface deposits on the parts of vegetables exposed to polluted air [14]. Moreover, the presence of heavy metals in fertilizers contributes an additional source of metal pollution for vegetables [15].

MATERIALS AND METHODS

Samples of the edible vegetables that were imported from Egypt collected from Tobruk Central Vegetable Market in April 2023, the samples were randomly collected included: Cucumber, Tomato, Eggplant, Zucchini, Carrots and Onion.

The vegetables were first washed in fresh running water to remove any dirt, dust, or parasites. They were then washed with distilled water to remove any remaining contaminants. The vegetables were then sliced and dried in an oven at 90 degrees Celsius for 48 hours. After drying, the vegetables were ground into a fine powder [16].

Also, we measured all sample wight before and after dried to determine the moisture content in all vegetable samples.

Two grams of dry matter for each sample was weighed in a porcelain crucible and burn it on hot-plate at 120°C. After burning, ash was obtained at 550°C in a muffle furnace for four hours [17]. Then the ash was dissolved with 5ml 1N Nitric Acid and after 2 hours the solution transferred to a 100-ml calibrated flask and filtered with filter paper and fill to 100 ml with same diluted acid.

Concentrations of heavy metals (Zn, Cu, Pb, Cr, Mn) were measured by Drawell DW-

 ISBN 978-9959-9703-2-9

AA320N Atomic Absorption Spectrophotometer.

RESULTS AND DISCUSSION

The moisture content in all vegetable samples is shown in table 1:

Table1: Moisture and solid contents in samples

Sample / Content	Zucchini	Eggplant	Carrots	Cucumber	Onion	Tomato
% moisture	93%	94.2 %	89.1 %	95.7%	89 %	93.9 %
% solid	7%	5.8%	10.9 %	4.3%	11 %	6.1 %

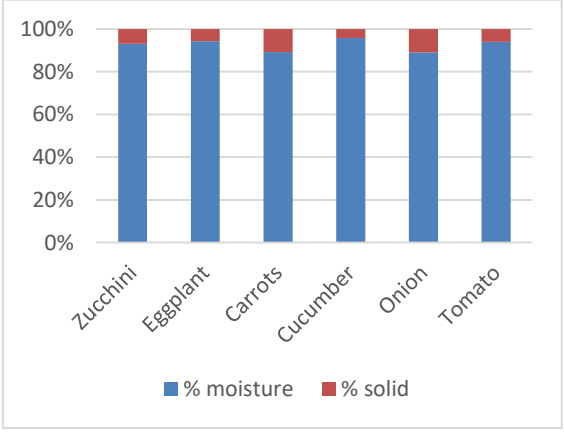

Figure 1: Comparing % of Moisture and solid contents in samples

Trace elements are essential in very small amounts for all life forms. However, they can also be toxic in higher concentrations, especially when they are present in organic compounds. Lead is a good example of a trace element that can be highly toxic, even in small amounts. It can cause a variety of health problems, including damage to the kidneys, liver, heart, and vascular and immune systems [18]. The presence of heavy metals in vegetables can be influenced by a number of factors, including the soil, fertilizers, and the proximity of industries or highways. It is important to be aware of the potential for heavy metal contamination in vegetables, as it can pose a health risk to humans, animals, and plants [19].

Copper and zinc are two trace elements that are essential for human health. They are required for a variety of biological functions, including the formation of enzymes and the maintenance of redox balance. However, even these essential nutrients can be toxic in high doses. It is important to consume copper and zinc in moderation, and to be aware of the potential for contamination in food [20].

The mean values of Zn, Pb, Mn, Cu, and Cr concentrations in 6 vegetable samples (Cucumber, Tomato, Eggplant, Zucchini, Carrots and Onion), are given in table 2 (Concentration mg/kg).

Table2: Concentrations of heavy elements in samples

Sample / Metal	Zucchini	Eggplant	Carrots	Cucumber	Onion	Tomato
Pb	0.771	0.962	3.13	1.132	1.329	0.66
Cr	0.218	0..818	4.7	0.449	0.271	2.929
Zn	7.4	2.562	9.13	5.38	6.98	3.82

ISBN 978-9959-9703-2-9

			3	8		4
Mn	0.504	1.479	3.144	1.378	1.313	0.732
Cu	N D	0.017	6.677	0.969	N D	N D

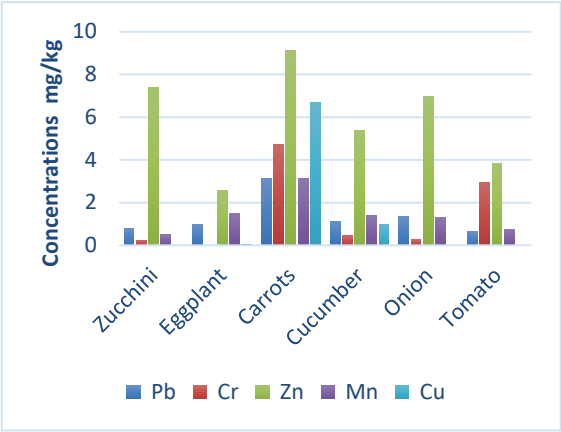

Figure 2: Concentrations of heavy elements in samples

The comparison between the main values of heavy metals in the samples with the values of the maximum normal value according to the Food and Agriculture Organization (FAO) [21], are in tables and figures 3, 4, 5, 6 and 7.

Table3: Lead concentrations in the samples and the maximum permissible value.

Sample \ Value	Value of Pb in sample	Normal value (Maximum)
Zucchini	0.771	0.1
Eggplant	0.962	0.1
Carrots	3.13	0.1
Cucumber	1.132	0.1
Onion	1.329	0.1
Tomato	0.66	0.1

Table4: Chromium concentrations in the samples and the maximum permissible value.

Sample \ Value	Value of Cr in sample	Normal value (Maximum)
Zucchini	0.218	0.1
Eggplant	0.818	0.1
Carrots	4.7	0.1
Cucumber	0.449	0.1
Onion	0.271	0.1
Tomato	2.929	0.1

Table5: Zinc concentrations in the samples and the normal value.

Sample \ Value	Value of Zn in sample	Maximum Normal value
Zucchini	7.4	8.3
Eggplant	2.562	1.6
Carrots	9.133	2.4
Cucumber	5.388	1.5
Onion	6.98	1.7
Tomato	3.824	1.7

Table6: Manganese concentrations in the samples and the normal value.

Sample \ Value	Value of Mn in sample	Maximum Normal value
Zucchini	0.504	2
Eggplant	1.479	2.3
Carrots	3.144	1.8
Cucumber	1.378	0.9
Onion	1.313	1.3
Tomato	0.732	1.2

Table7: Copper concentrations in the samples and the normal value.

Sample \ Value	Value of Cu in sample	Maximum Normal value
Zucchini	N D	1
Eggplant	0.017	0.9
Carrots	6.677	0.6
Cucumber	0.969	0.7
Onion	N D	0.4
Tomato	N D	1.8

ISBN 978-9959-9703-2-9

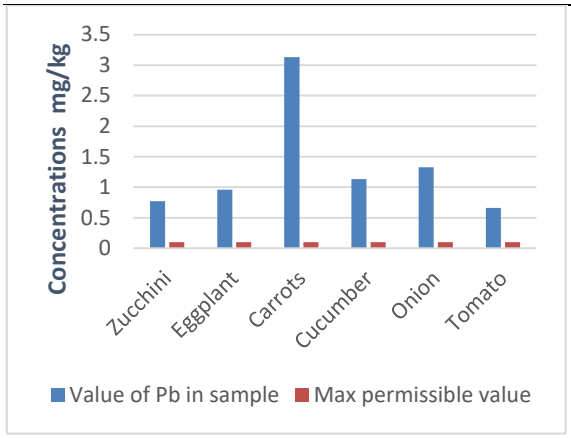

Figure3: Comparison of lead concentrations in the samples with the maximum permissible value.

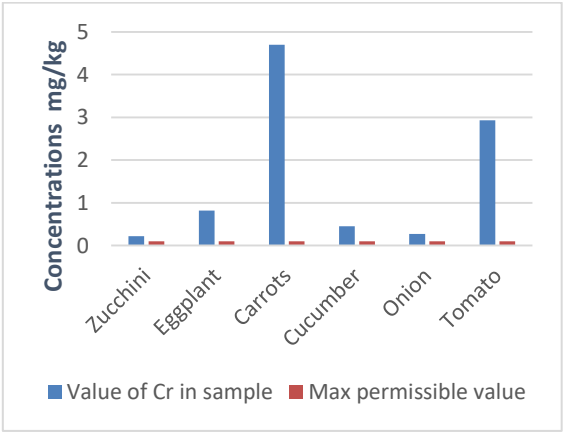

Figure4: Comparison of Chrome concentrations in the samples with the maximum permissible value

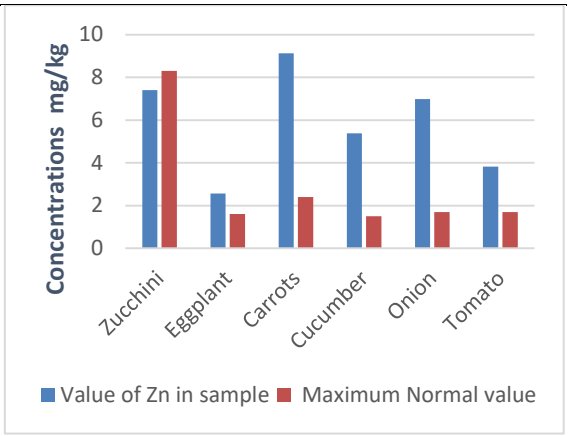

Figure5: Comparison of Zinc concentrations in the samples with the maximum normal value

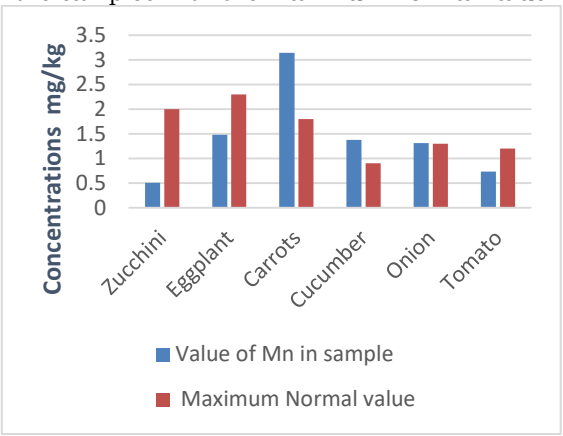

Figure 6: Comparison of Manganese concentrations in the samples with the maximum normal value

ISBN 978-9959-9703-2-9

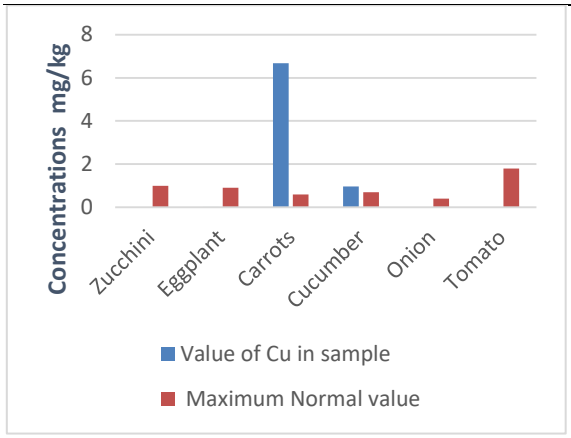

Figure 7: Comparison of Copper concentrations in the samples with the maximum normal value

From tables and figures 3, 4, 5, 6 and 7, we can see:

- Lead values recorded very high percentages in all samples when compared to the maximum permissible values, reaching more than 31 times the permissible rate in the carrot sample.
- Chromium values also recorded rises in all samples, some of which had a very high chromium percentage, as the carrot sample recorded a rise of 47 times the permissible value.
- Zinc, manganese and copper recorded high values in some samples, but they are not very high compared to lead and chromium, where zinc recorded the highest value in the onion sample which is 4.1 times the normal rate, while manganese recorded the highest value in the carrot sample and it reached only 1.74 times higher than the normal rate, while copper recorded readings in only three samples, one of which was in the carrot sample, and it was very high, as the rate of rise reached 11.1 times the normal rate.

Conclusion

The values of heavy metals in the samples recorded an increase in 22 out of 28. Lead and chromium, all of its readings recorded very high values, above the maximum allowable rate.

The large increase in the values of the heavy metal readings indicates a significant contamination in the soil used in cultivating the samples. This pollution in the soil leads us to the conclusion that its pollution was not only through the air, but there must be other reasons that increased the percentage of pollution, perhaps the most prominent of which is wastewater pollution, especially industrial wastewater that pollutes the water used in agriculture in that soil, which led to the occurrence of accumulation and high Levels of heavy metals in the soil with time. This could explain the high levels of minerals such as lead and chromium (and copper in some samples) to very high levels.

ISBN 978-9959-9703-2-9

In the end, it must be notes that the continued absolute dependence of the Libyan markets on imported vegetables contaminated with these high levels of heavy metals, without a strict mechanism to control quality standards in order to import this type of food, will lead to many public health problems for the citizen in the near future.

Arabic section:

تقدير تلوث التربة بمياه الصرف بقياس محتوى المعادن الثقيلة الموجودة في بعض الخضروات المزروعة بها.

توفيق ابريك الشهيبي
قسم الكيمياء، كلية التربية / جامعة طبرق – ليبيا

الملخص: تم إجراء هذا البحث لتقدير تلوث التربة بمياه الصرف عن طريق قياس المعادن الثقيلة (الرصاص والكروم والنحاس والزنك والمنغنيز) في عينات من الخضروات المستوردة (من جمهورية مصر العربية). الخضروات التي أخذنا عينات منها هي: الخيار والطماطم، الباذنجان، الكوسة، البصل والجزر، تم تجميعها من سوق الخضار المركزي في مدينة طبرق. تم تحضير العينات المحضرة بطريقة الهضم الجاف، وتم قياس تراكيز المعادن الثقيلة باستخدام جهاز قياس طيف الامتصاص الذري (AAS). أظهرت النتائج زيادة واضحة في مستويات المعادن الثقيلة التي تم قياسها في العينات.

الكلمات المفتاحية: التلوث، مياه الصرف، الخضراوات، المعادن الثقيلة.

Acknowledgment

This research was supported by Research Center of the University of Tobruk, as well as Aman Laboratory for Chemical Analysis. Thanks are due to Dr. Salah Mahjoub for his essential and helpful assistance in the laboratory.

References

1- Persson L, Carney Almroth BM, Collins CD, Cornell S, (2022), Outside the Safe Operating Space of the Planetary Boundary for Novel Entities, Environmental Science & Technology. 56, 1510–1521, DOI: 10.1021/acs.est.1c04158.
2- Wastewater engineering: treatment and reuse. *George Tchobanoglous, Franklin L. Burton, H. David Stensel, Metcalf & Eddy (4th ed.). Boston: McGraw-Hill. 2003.*
3- Danuta Witkowska, Joanna Słowik and Karolina Chilicka, (2021), Heavy Metals and Human Health: Possible Exposure Pathways and the Competition for Protein Binding Sites, Molecules (MDPI), 26, 6060, DOI: 10.3390/molecules26196060.
4- Gunnar F. Nordberg , Bruce A. Fowler and Monica Nordberg Handbook on the Toxicology of Metals , Academic Press, 2014, pp. 4-5.
5- Abdur Rashid, Brian J. Schutte, April Ulery, Michael K. Deyholos, Soum Sanogo, Erik A. Lehnhoff and Leslie Beck, (2023), Heavy Metal Contamination in Agricultural Soil: Environmental Pollutants Affecting Crop Health, Agronomy (MDPI), 13), 1521, DOI: https:10.3390/agronomy13061521
6- Sumira Jan, Javid Ahmad Parray, Heavy Metal Uptake in Plants, Springer, 2016, p. 3.
7- R. H. Dowdy, W. E. Larson, J. M. Titrud and J. J. Latterell, (1978), Growth and metal uptake of snap beans grown on sewage sludge-amended soil: a four-year field study, J. Environ. Qual, 39, 252,DOI:10.2134/jeq1978.00472425000700020020x.
8- K. Flynn, An overview of public health and urban agriculture: Water, soil and crop contamination and emerging urban zoonoses. International Development Research Centre (IDRC), 1999, p15.
9- H. Chen, Z. Chungrong, T. Cong and Z. Yongguan, (1999), Heavy metal pollution in soil in China: Status and countermeasures, Chemical Review, 28, 130-134, DOI: 10.1021/cr300135y.
10- J. E. Hardoy and D. Satterthwaite, Health and the urban poor in Gurinder. Springer Publishing, 1997, pp133, 123-162.
11- A. C. Bellows, Mustafa Koc, Rod MacRae, Luc Mougeot and Jennifer Welsh, (1999), Urban food health and the environment: The case of Upper

 ISBN 978-9959-9703-2-9

Silesia, Poland in International Development Research Centre (IDRC), pp132, 131-135.
12- J. A. Omgbu and M. A. Kokogbo, (1993), Determination of Zn, Pb, Cu and Hg in soils of Ekpan. Environment International, 11, 611-613, DOI: 10.1016/0160-4120(93)90312-6
13- E. Somers, 1974, The toxic potential of trace metals in foods. A review. Journal of Food Science, 70, pp 215-217, DOI: 10.1111/j.1365-2621.1974.tb02860.x
14- H. W. Nürnberg, The voltametric approach in trace metal chemistry of natural waters and atmosphere precipitation. Analytica Chimica Acta, 1984, pp1-21.
15- M. J. Buchaver, Contamination of soil and vegetation near zinc smelter by zinc, cadmium, copper and lead. Environmental Science and Technology, 1973, pp131-135.
16- A. A. Yusuf, T. A. Arawolo and O. Bamgbose, (2003), Cadmium, copper and nickel levels in vegetables from industrial and residential areas of Lagos Citu, Nigeria. Food and Chemical Toxicology, pp41, 375-378.
17- G. Fang, Y. Liu, S. Meng and Y. Guo, (2002), Spectrophotometric determination of lead in vegetables with dibromo-p-methyl-carboxy-sulfonazo. Talanta, 57, 1155-1160, DOI: 10.1016/s0039-9140(02)00195-9
18- Ab Latif Wani, Anjum Ara, and Jawed Ahmad Usmani, (2015), Lead toxicity: a review, PubMed, 8, 55–64, DOI: 10.1515/intox-2015-0009
19- Ahmed S. A. Asmoay, Salman A. Salman, Amr M. El-Gohary & Hassan S. Sabet, (2019), Evaluation of heavy metal mobility in contaminated soils between Abu Qurqas and Dyer Mawas Area, El Minya Governorate, Upper Egypt, Bulletin of the National Research Centre, 43, 88, DOI: 10.1186/s42269-019-0133-7
20- Harold M. Silverman, Joseph Romano and Gary Elmer, The Complete Guide to Vitamins, Minerals, and the Most Effective Herbal Remedies and Dietary Supplements Mass Market Paperback, Bantam books, 1999.
21- Food and Agriculture Organization of the United Nations (FAO), heavy metal regulation, legal notice No 66, 2003.

 ISBN 978-9959-9703-2-9

المؤتمر الدولي الثاني للعلوم والهندسة
2nd International Conference on Science and Engineering
ICSE 2023
Faculty of Engineering - University of Bani Waleed
Bani Waleed, Libya

Paper Code: ICSE-023

FLUORIDE CONTENT OF AVAILABLE BOTTLED DRINKING WATER IN TRIPOLI, LIBYA

Awatif Almaqrahi1, Hassan Eltaib1, Sundus Almontasir1, Insherah Idbeaa3.Gamila Elesvgh2, Fauzia Mohamed4, Abdurrahman Eswayah1
(1) Libyan Center for Biotechnology Research
(2) Food and Drug Control Center, Tripoli Libya
(3) Department of Botany. Faculty of science. Aljabal ALGharbi University.
(4) Department of Zoology. Faculty of science Tripoli University.
*Corresponding author: hassaneltybe993@gmail.com

Abstract: The present study was carried out to evaluate the fluoride content of bottled water brands available in the market of Tripoli city and to measure if it is consistent with local standards. A total of 23 commercially available brands were collected and examined for fluoride content. 22 samples were locally produced and one was imported. The average fluoride levels of each sample was determined using the procedure outline in the Palintest photometer method and then compared with the fluoride content printed on the bottle labels. In all bottled water brands investigated, 19 brands of the analyzed samples did not state the fluoride levels on the labels of the bottles. The determined fluoride concentrations ranged from 0 to 2.75 ppm. For each brand, the fluoride level was not similar to the labeled fluoride. 82.6% (19 brands) had a fluoride content lower than the Libyan standards, 1 brands had a fluoride content higher than the Libyan standards, and 7 brands had zero fluoride content. All the samples examined had fluoride content outside the range regulated by Libyan standards. There was a significant variation between the F levels stated by the manufacturer on the bottle labels and the values measured during the investigation.

Keywords: Fluoride, bottled water, oral health, Palintest

Introduction

Everything that lives on land, from plants to insects to humans, needs fresh water to survive. In fact, water is the main constituent in human body weight, on average, 60-70% of an adult's body weight is composed of water. Nowadays, the water demand that meets health requirements, and is free of contaminants has led to a new industry, the bottled water industry. Bottled drinking water is frequently used instead of tap water because of its convenience, pleasing taste, and perceived purity [11]. In the last few years, the consumption of bottled water has increased worldwide. Between 2006 and 2011, the world consumption changed from 178 billion to more than 231 billion liters. Drinking water is

 ISBN 978-9959-9703-2-9

usually the single largest contributor to daily fluoride intake [16].

Fluoride can be naturally found in natural water sources used for bottling at different levels, or can be added to reach the optimum content; it is a very effective mineral that has an influence on oral health; where it prevents decay in general when ingested and absorbed through the digestive system. The levels of fluoride ingested by humans differ from one individual to another according to the source they are exposed to, level, and amount ingested [9]. Excessive amounts of fluoride may cause health problems as well, the bottled water fluoride content may be highly variable among different brands, and that may lead to dental fluorosis especially in infants and children when receiving greater concentrations than the optimal levels recommended for their age group [1],[2]. An awareness of the exact concentration of drinking water whether public or bottled is required for an effective and safe preventive fluoride program [2]. Fluoride can sometimes be obtained from different sources in addition to drinking water, for example, in Karbala-Iraq black tea consumption is very common and the high content of fluoride in the tea leaves should be taken into consideration [13],[17]. As a result, all the sources of fluoride are important, and the total fluoride intake from all sources is critical in the development of fluorosis [10],[8],[18],[12],[4],[5]. Standards and limits have been developed by many international and local organizations to determine fluoride levels in drinking water that meet the needs of human health. In most of the early projects, it was found that most of the commercially available bottled water failed to list the content of fluoride [14],[20].

Fluoride, at some concentrations is known to influence many cellular functions in the human body in many ways. Some studies have demonstrated that high doses of fluoride can cause DNA damage, and change cell-cycle regulatory proteins, which in turn induce apoptosis [24]. However, the mechanism of apoptosis induced by fluoride is still unclear, especially in terms of identifying the signaling pathways that are closely involved in this process (Fig. 1) [24].

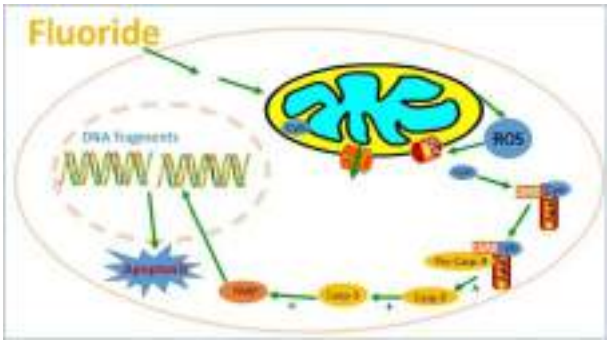

Fig.(1): Mitochondrion-mediated pathway of fluoride-induced cell apoptosis. Note: "+" means "activate"

Hence, this study is designed to discuss the

ISBN 978-9959-9703-2-9

fluoride concentration in commercially available bottled drinking water in Tripoli according to local standards, to find out if significant differences existed among the products, and to explore packaging date as a variable on the fluoride content in bottled waters.

1. Materials and methods

An experimental study was carried out to measure and discuss the fluoride content of commercially available bottled water in Tripoli, Libya. To assess the F measured, the results obtained were compared to the recommended optimal fluoride levels in water according to Libyan standards. The samples were analyzed at FADCC Laboratory; The F analysis was made by the photometric method using the plainest.

A total of 23 commercially available different bottled water brands, which were chosen from those available in major supermarkets and grocery stores in Tripoli, Libya, were collected and examined during (January-February) 2019. twenty-two brands were produced in Libya and one brand was imported (it was the only one brand found in the study area at the time of collecting samples). . twenty-one of the brands were within their expiration dates, while two did not state the expiration date. All the bottled water containers were made of plastic. Fluoride in the bottled water does not interact with the material of the bottle (glass or plastic) or the other minerals in the water [6,15]. The bottles were stored at room temperature in a dark place in their original closed container until they were examined. In order to check for the labelling of fluoride concentrations, the labels of the bottles were studied for comparison. The average for each sample was estimated, table (1). To assess the reliability of the method, a statistical analysis was employed to derive descriptive data using SPSS (Statistical Package for Social Science).

3. Results and discussion

Of the 23 samples of water examined, our findings are shown in Table (1), for each water sample, the fluoride concentration depicted on the label is shown in mg/L or (NM) if not mentioned. The mean F contents ranged between 0 and 2.751 ppm Table (1). Regarding the quality of the labeling of bottled waters, none of the samples had fluoride content listed on the labels. A clear variation between labeled and tested fluoride was estimated, which might be attributed to the soil mineral content of the underground reservoirs. Previous research attempts to evaluate the fluoride content of bottled water in several countries concluded that most of the early projects found that most of the commercially available bottled water failed to list the fluoride content[1],[21]. The

 ISBN 978-9959-9703-2-9

Fluoride content of each sample was judged according to the Libyan standard limits, where the standards have recommended that the fluoride in water in general be 1ppm without setting the minimum permissible level of F in drinking water. The World Health Organization (WHO) recommends that to maximize beneficial effects and minimize harmful effects, the level of F in drinking water should be ideally set between 0.7 and 1.2 ppm with a maximum of 1.5 ppm [22],[3]. Accordingly, a clear variation in fluoride concentration in the bottled water examined was found. The highest F concentration measured was 2.751 ppm, which is above the Libyan standard level recommended; the majority of tested samples had F levels below optimum health according to the standards used. All the samples examined, including the bottled water produced outside of Libya, have fluoride content outside the range regulated by the WHO, table (2). Hence, it is necessary that all concerned authorities take action to restrict the import and sale of these products.

Table (1): Fluoride levels in the analyzed bottled water (mg F/L).

Country of origin	Brand name	Labeled fluoride F(ppm)	Measured fluoride F(mean ± SD) ppm	Manufacture Expiry date
Local	1	NM	0 ± 0	M
Local	2	NM	0.2765 ± 0.0105	M
Local	3	0.24	0 ± 0	M
Local	4	0.97	0.181 ± 0.001	M
Local	5	NM	0.57 ± 0.0034	M
Local	6	0.2	0 ± 0	M
Local	7	NM	0 ± 0	M
Local	8	NM	0 ± 0	M
Local	9	0.02	0.0595 ± 0.0005	M
Local	10	NM	0.3708 ± 0.0002	M
Local	11	NM	0.396 ± 0.004	M
Local	12	NM	2.751 ± 0.009	M
Local	13	NM	1.952 ± 0.001	M
Local	14	NM	0.494 ± 0.006	M
Local	15	NM	0 ± 0	M
Local	16	NM	0.1565 ± 0	NM
Local	17	NM	0.036 ± 0.001	NM
Local	18	NM	0.502 ± 0.002	M
Local	19	NM	0.554 ± 0.014	M
Local	20	NM	0 ± 0	M
Local	21	NM	1.564 ± 0.006	M
Local	22	NM	2.05 ± 0.01	M
imported	23	NM	0.503 ± 0.003	M

NM: Not Mentioned.

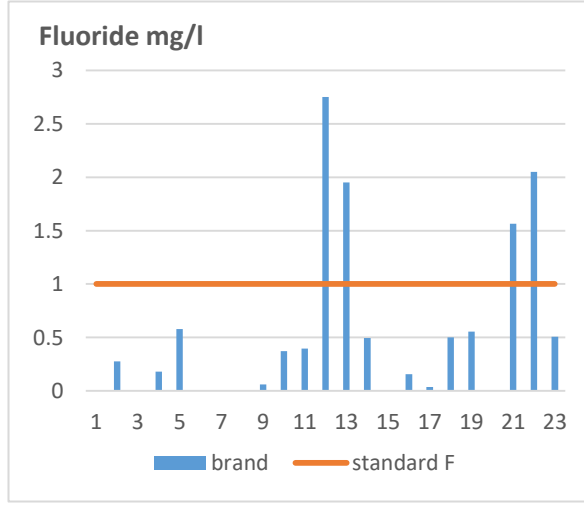

Fig. 2 Fluoride content compared to Libyan standard

ISBN 978-9959-9703-2-9

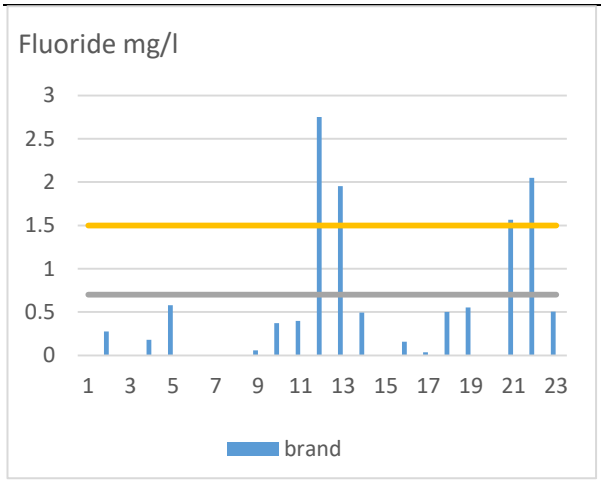

Fig.3 Estimated Fluoride compared to WHO

Table 2: International and local optimal fluoride level.

Standard	Fluoride mg/l Standard limit	References
Libyan standard	1	Libyan standards
World Health Organization	0.7-1.5	WHO 2011

4. Conclusion

This study concluded that all of the fluoride levels offered in the labels were different from the actual fluoride concentration tested; it is also noted that in most brands fluoride content is lower than the optimum level needed for human health; and sometimes above the level recommended according to the standards; especially for those who rely on bottled water as their main source of fluoride. It was also noted that for some brands the packaging date was not mentioned. Moreover there was a significant variation between the F levels stated by the manufacturer on the bottle label and the values measured during the investigation. However, there needs to be a public awareness so that the oral health care providers and consumers have accurate information on the fluoride content of the water they drink.

References

[1] Abdullah M. Aldrees, Saad M. Al-Manea, Fluoride content of bottled drinking waters available in Riyadh, Saudi Arabia. The Saudi Dental Journal (2010) 22, 189–193

[2] Ahiropoulos , V. , 2006. Fluoride content of bottled waters in North Greece. Int. J. Paediatr. Dent. 16(2)111-116

[3] American Dental Association (updated on June 5, 2002). American Dental Association Statement on Water Fluoridation Efficacy and Safety. Available from: <http://www.ada.org/prof/resources/positions/statements/fluoride2.asp> (accessed 29.08.09).

[4] Clark D. C., Hann H. J., Williamson M . F., Berkowitz J., Influence of Exposure to Various Fluoride Technologies on the Prevalence of Dental Fluorosis, Community Dentistry and Oral Epidemiology, 1994; vol. 22, 461–464.

[5] Clark D.C., Trends in prevalence of dental fluorosis in North America, Community Dentistry and Oral Epidemiology, 1994; vol. 22, 148–152.

[6] Centers for Disease Control and Prevention (CDC), 2013. Community water fluoridation. Division of Oral Health. Available: <http://www.cdc.gov>.

[7] David Robinson; Val Reed, The A-Z of social research jargon, Aldershot, Hants, England ; Brookfield, Vt., USA : Ashgate/ARENA, ©1998

[8] Fejerskov O., Thylstrup A., Larsen M . J., Clinical and Structural Features and Possible

 ISBN 978-9959-9703-2-9

Pathogenic Mechanisms of Dental Fluorosis, Scandinavian Journal of Dental Research, 1977, vol. 85, 510 – 534.

[9] Jagtap.S.,2012Yenkie,M.K. Labhsetwar, N.,Rayalu,S., 2012.Fluoride in drinking water and defluoridation of water. Chem. Rev. 112,2454-2466.

[10] Kiristy M . C., Levy S. M ., Warren J. J., Guha-Chowdhury N., Heilman J. P., Marshall T., Sources of Fluoride Intake in Children, Journal of the American Dental Association, 1996, vol. 127, 895 – 902.

[11] laiumandier JA, Ayers LW.Fluoride and bacterial content of bottled water s tap water. Arch Fam Med 2000;9:24

[12] Levy S. M ., Maurice T. J., Jakobsen J. R., Feeding Patterns, Water Sources and Fluoride Exposures of Infants and 1-Year-Olds, Journal of the American Dental Association, 1993; vol. 124, 65–69.

[13] Mahvi AH, Zazoli MA, Younecian M, Esfandiari Y. Fluoride content of Iranian black tea and tea liquor. Fluoride 2006;39(4):266-8.

[14] McFadyen, E.E., McNee, S.G., Weetman, D.A., 1982. Fluoride content of some bottled waters. Br. Dent. J. 153 (12), 423– 424.

[15] Mohamed Yehia Z. Abouleish, Evaluation of fluoride levels in bottled water and their contribution to health and teeth problems in the United Arab Emirates. The Saudi Dental Journal (2016) 28, 194–202.

[16] Murray JJ. Appropriate use of fluoride of human health. Geneva: world Health Organization, 1986

[17] Reza Fouladi Fard, Amir Hossein Mahvi, Sara Sadat Hosseini, Mohammad Khazaei, FLUORIDE CONCENTRATIONS IN BOTTLED DRINKING WATER AVAILABLE IN NAJAF AND KARBALA, IRAQ, Research report Fluoride 47(3)249–252 July- September 2014

[18] Richards A., Kragstrup J., Josephsen J., Fejerskov O., Dental Fluorosis Developed in Post-Secretory Enamel, Journal of Dental Research, 1986; vol. 65, 1406–1409.

[19] Rodwan-Junior JG. Bottled water 2011: the recovery continues [Internet]. New York: International Bottled Water Association; 2012. [cited 5 set 2014]. Available from: http://www.bottledwater.org/files/2011BWstats.pdf.

[20] Stannard, J., Rovero, J., Tsamtsouris, A., Gavris, V., 1990. Fluoride content of some bottled waters and recommendations for fluoride supplementation. J. Pedod. 14, 103–107.

[21] Studlick, J., Bain, R., 1980. Bottled waters-expensive ground water. Ground water 18, 340.

[22] WHO drinking-water quality series. Fluoride in drinking water. Edited by Bailey K, Chilton J, Dahi E, Lennon M, Jackson P, Fawell J, 2006.

[23] World Health Organization. Report of an expert committee on Oral Health Statues and Fluoride use and Oral Health. WHO Technical Report Series No 846. WHO:Geneva, Switzerland 1994.

[24] (Barbier O, Arreola-Mendoza L, Del Razo LM: Molecular mechanisms of fluoride toxicity. Chem Biol Interact 188(2): 319- 333, 2010 ..... DANIEL ARAKI RIBEIRO1,2, CAROLINE MARGONATO CARDOSO2, VERONICA QUISPE YUJRA2, MILENA DE BARROS VIANA1, ODAIR AGUIAR JR.1, LUCIANA PELLEGRINI PISANI1 and CELINA TIZUKO FUJIYAMA OSHIMA2 . Fluoride Induces Apoptosis in Mammalian Cells:In Vitro and In Vivo Studies. ANTICANCER RESEARCH 37: 4767-4777 (2017))

 ISBN 978-9959-9703-2-9

المؤتمر الدولي الثاني للعلوم والهندسة
2nd International Conference on Science and Engineering
ICSE 2023
Faculty of Engineering - University of Bani Waleed
Bani Waleed, Libya

Paper Code: ICSE-034

EFFECTS OF EXPOSURE CIGARETTE SMOKE ON THE CARDIAC TISSUES IN MALE ALBINO RATS AND THE IMPROVEMENT ROLE OF SIDR HONEY

Eda M. A. Alshailabi*[a] , Nura I. Al-Zail [a] and Afaf A. Alsalhin [b].
[a] Department of Zoology, Faculty of Science, Omar Al-Mukhtar University, Libya.
[b] Department of Zoology, Faculty of Science, Benghazi University, Libya.
*Crosspnding author: eda.muftah@omu.edu.ly

Abstract: The aim of this study was to investigate the effects of exposure cigarette smoke on the cardiac tissues in male rats and the improvement role of Sidr honey. Twenty eight male rats were divided into four groups; Group 1: control rats; group 2: rats were given Libyan Sidr honey (100 mg/kg b.w./d.) orally for 4 weeks.; group 3: rats were exposed to the five lit from sidestream of the Karelia red cigarettes (5 times/d.) by a machine smoking for 4 weeks.; and group 4: rats were received the Sidr honey (100 mg/kg b.w./d.) orally for 2 weeks, then the rats were exposed to the Karelia cigarettes generated by a machine smoking with given the Sidr honey for 4 weeks. The X-Ray radiography of rats showing, heart mildly enlarged size in the KC-exposed rats as compared with the NC rats. While, the POR rats showed normal heart size when compared with KC rats. Moreover, the KC group showed a significant increase ($P < 0.05$) in CK, CK-MB, and LHD as compared to the NC group, whereas the POR group showed a significant decrease ($P < 0.05$) in the CK, CK-MB, and LHD when compared with the KC group. Histological investigation of the heart tissues of the KC group showed different histopathological changes as compared to the NC group. Nevertheless, the POR group showed the marked improvement in the heart tissues as compared to the KC rats. Conclusion, results demonstrated that Libyan Sidr honey significantly reduced the toxic effects of KC-exposed on the heart structures.

Keywords: : Sidr honey, cigarette smoke, enzymes, heart tissues

Introduction

Cigarette smoke (CS) is one of the leading causes of death in many countries, which it is caused tissue damage, release of many substances in the body that have the direct potential of forming free radicals and activating inflammatory cells, such as macrophages and neutrophils, which also produces of reactive oxygen species (ROS) [1], [2], resulting in an imbalance in the cellular oxidant-antioxidant system [3], [4], and increasing the harmful substances concentration of tissues [1].

CS is a complex mixture composed of numerous harmful substances about 5000 chemical compounds. Among these substances

 ISBN 978-9959-9703-2-9

are nicotine, tar, carbon monoxide [5], [6], polycyclic aromatic hydrocarbons, cyanide, carbon-monoxide, lead, cadmium nitric oxide and nitric dioxide [7], where the nicotine is rapidly absorbed through the mucous membranes, respiratory tract, and gastrointestinal tract, and it is metabolized in the liver and caused oxidative cellular damage [8]. In addition, a long-term of CS exposure may be associated with myocardial dysfunction, heart failure, and increased mortality [9].

Antioxidants keeps the cells components from damage by resolving the free radicals. So, when antioxidants are consumed through the diet block damage to cells [10].

Honey is the natural product, and it has many nutritional, therapeutic and industrial values. it is contains a lot of bioactive substances such as amino acids, alkaloids, vitamins, proteins, phenolic compounds (PC), organic acids, flavonoids, and tocophrenols, where the PC counter oxidative stress, ROS [11], [12], and roughly limiting cell damage by their chemopreventive agents [13]. Moreover, PC might also display distinctive anticarcinogenic and cardioprotective effects linked to their free radical stopping properties [14].

In the light of these findings, the aim of this study is to investigate the effects of exposure cigarette smoke on the cardiac enzymes and tissues in male albino rats and the improvement role of Sidr honey.

Materials and Methods:

1. Chemicals:

•Libyan Sidr honey (SH) used was obtained from local market and analyzed by the Centre Lab of Omar Al-Mokhtar University, El-Beyda, Libya.

•Karelia red cigarettes (KC) were obtained from the local market.

2. Experimental animals:

28 healthy male albino rats, weighing 180-200 gm (10 weeks old) were used. Rats were obtained from the Zoology Department, Faculty Science, University of Omar Al-Mokhtar, El-Beyda, Libya. Animals were acclimatized for a period of 3 weeks and were housed in cages at standard laboratory conditions of room temperature (22 ± 2^{o} C). Rats were fed standard rat chow and water ad libitum. This experiment complied with the guide for the care and use of laboratory animals ethical guidelines.

3. Experimental design:

Male rats were randomly allocated into four groups of eight rats as follows:

Group 1: The normal control group (NC), rats were kept under standard laboratory conditions with ventilation and were not exposed to smoke.

 ISBN 978-9959-9703-2-9

Group 2: The Libyan Sidr honey group (SH), rats were given Sidr honey (100 mg/kg b.w./d.) [15], orally by gavage for four weeks.

Group 3: The Karelia red cigarettes group (KC). Cigarette smoke exposure was generated by a machine (bee smoker) device and a hole was connected to a smoking machine by the connection pipe to the glass box which was designed locally in the Zoology Department, Faculty Science, University of Omar Al-Mokhtar, El-Beyda, Libya (Fig. 1). The glass box is in a cube shape (aquarium shape) with the size of (length, 80 cm; width, 30 cm; height, 40 cm) for keeping the rats [16], [17]. The inhalation was performed in the closed glass box for condensation of the smoke a cover was removed to provide an unforced exchange of fresh air.

The KC was used five lit by using a smoking machine for fifteen minutes and exposing the rats to the sidestream of the KC for five minutes, then the rats were rested to ten minutes and ventilation by removing the box cover. This operation was repeated five times a day for four weeks, where the rats were exposed to the sidestream of the KC for six days in a week [18], [19].

Group 4: The protective group (PRO), rats were given SH (100 mg/kg b.w./d.) orally by gavage for two weeks then rats treated with the sidestream of the KC generated by a machine smoking (same group 3) with taking the Sidr honey for four weeks.

Fig. 1: The smoke-exposure system.

4. X-ray dark-field radiography:

At the end of the treatments, all rats were anesthetized with diethyl ether, then rats were taken to Tepa center in El-beyda city to investigate changes to the size heart can be precisely detected with imaging technique by X-ray dark-field [20].

1. Serum biochemical analysis:

At the end of the treatment, the blood samples were collected then centrifuged at 25^{o} C for 10 minutes with 4000 rpm to obtain the serum. The serum samples kept in deep freezer (-18^{o} C). The serum samples obtained analyzed to determine the concentration of creatine kinase (CK), lactate dehydrogenase (LDH) and creatine Kinase-myocardial (CK-MB) band of the control group and the experimental groups were performed in the Al-Beyda Laboratory for Medical Analysis, El-Beyda City by the methods of [21]. Plasma cardiac troponin T and I (cTnT and cTnI) were quantitatively

 ISBN 978-9959-9703-2-9

measured by means of a highly specific enzyme immunoassay using commercially available kits.

2. Histological examination:

Part of the heart tissue from all groups were fixed process in formalin (10 %), then dehydrated in graded alcohol and embedded in paraffin, and sections (5 µm) were prepared using a microtome device (model Leitz 1512, Germany). Sections were stained with hematoxylin and eosin by using standard procedures [22].

3. Statistical analysis:

All data were analyzed using Minitab statistical analysis package program (Minitab version 17). The parametric variables were displayed as the mean ± standard error (SE). We performed a one-way analysis of variance (ANOVA). In addition, means were separated using Turkey's test at $P < 0.05$. The T test also using for compared between two means.

Results:

1.X-ray dark-field radiography:

The X-Ray radiography of rats showing, normal heart size in the NC rats and SH rats after 4 weeks (Fig. 2, A & B). Moreover, heart mildly enlarged size in the KC-exposed rats after 4 weeks (Fig. 2, C) as compared to NC rats. While, normal heart size in the POR rats (Fig. 2, D) when compared with KC rats.

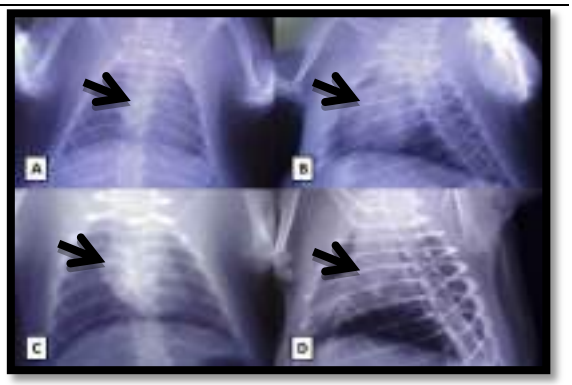

Fig. 2: X-Ray radiography of rats, showing, (A): Normal heart size (arrow), in the NC rats; (B): Normal heart size (arrow), in the SH rats; (C): Heart mildly enlarged size (arrow) in the KC-exposed rats; (D): Normal heart size (arrow) in the POR rats.

2.Determine of the enzymatic activities of heart:

2.1.Determination of the creatine kinase (CK) :

The results showed that there was a highly significant increase (P <0.05) in the expression of the mean values of CK level of the KC group (185.43 ± 3.05) as compared with the NC group (129.9 ± 1.72). Moreover, the mean values of the CK level in the PRO group (161.14 ± 2.45) showed a significant reduction (p<0.05) as compared to the KC group (Table 1).

2.2.Determine of the creatine kinase-myocardial band (CK-MB):

Data recorded for CK-MB levels were carried out in Table (1), a significant increase (P <0.05) were found in the mean values of the KC rats

 ISBN 978-9959-9703-2-9

(25.43±1.161) when compared with the NC rats (15.14 ± 0.77). Whereas, the mean values of CK-MB level in the PRO rats (19.71±0.71) showed a significant decrease (P <0.05) as compared with the KC rats.

2.3.Determine of the lactate dehydrogenase (LDH):

The mean values of LDH level of control and experimental animals were presented in Table (1). The mean values of LDH showed, a highly significant increase (P <0.05) in the KC animals (188.3 ± 3.70) as compared to the NC (151.9 ± 4.99). Nevertheless, the mean values of LDH showed, a significant inhibition (P <0.05) in the POR (171.49 ± 2.60) as compared to the KC animals.

Table 1: Average of mean values of CK, CK-MB, and LDH levels in the control and experimental groups.

Parameters	NC mean ± SE	SH mean ± SE	KC mean ± SE	PRO mean ± SE
CK (U/L)	129.9 ±1.72 C	130.29± 1.63 C	185.43 ±3.05 A	161.14 ±2.45 B
CK-MB (U/L)	15.14 ±0.77 C	15± 0.76 C	25.43± 1.161 A	19.71± 0.71 B
LDH (U/L)	151.9 ±4.99 C	139.29± 3.29 C	188.3± 3.70 A	171.49 ±2.60 B

*The means with different superscript were significantly different P < 0.05, were means superscripts with the same letters, mean that there is no significant difference (P < 0.05).
* NC =Normal control. SH= Libyan Sidr honey treated group. KC= Karelia red cigarettes group (PRO)= Protective group.

3. Histological investigation:

3.1. Histological preparations of the heart tissues

3.1.1. The heart sections of the NC group:

Microscopically, the heart sections of the NC group showed a normal histological architecture of the cardiomyocytes with well-organized and branched cardiac myofibers, centrally located oval nuclei, and minimal interstitial connective tissue with few interstitial fibroblasts (Fig. 3).

3.1.2. The heart sections of the SH group:

Light microscopic examination of the heart after administration of SH alone for 4 weeks revealed a normal histological structure: Normal histological architecture of the cardiomyocytes with well-organized and branched cardiac myofibers, centrally located oval nuclei, and minimal interstitial connective tissue with few interstitial fibroblasts (Fig. 4) as in the NC group.

3.1.3. The heart sections of rats exposure to KC:

Histological examination of the heart of rats after exposure to KC alone for 4 weeks showed different histopathological changes when compared with NC group such as arrangement of myocardial fibers was disordered as well as cellular oedema and breaks or necrosis were evident. In addition, perivascular mononuclear cell infiltration,

 ISBN 978-9959-9703-2-9

ragmentation of sacroplasm and degeneration changes, and congestion of blood vessels (Fig. 5). Hyaline degeneration of myocardial fibers, and highly thickened wall of blood (Fig. 6). Moreover, figure (7) showed congestion and dilatated of blood vessels, and hyperemia with inflammatory cells infiltrations. Also, degeneration of myocardial fibers and congestion of blood vessels with highly thickened wall was noted in the figure (8).

In the gross level, the heart of male adult rats after exposure to the KC after 4 weeks showed severe damage in the heart tissues.

3.1.4.The heart sections of POR rats:

The heart sections of animals that treated with SH for two weeks then the animals were exposure to KC by a machine smoking with taking the SH for 4 weeks manifested minimal histopathological alterations when compared with the KC group. The marked improvement in myocardial fibers with few degeneration of myocardial fibers and hyperemic interstitial blood vessels, and small number of necrosis (Fig. 9). The myocardial fibers which almost looks like the control with few degeneration of myocardial fibers these were apparent in the figure (10).

Finally, in many areas of heart tissues in the protective rats attained almost normal patterns.

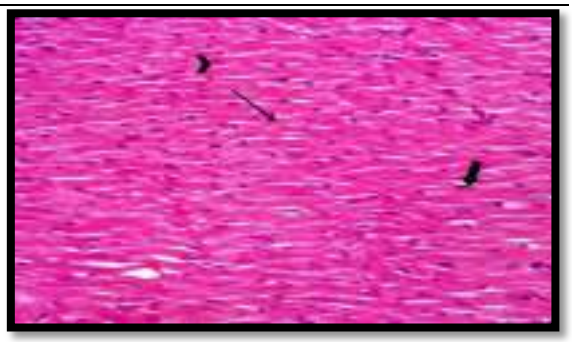

Fig. 3: Photomicrograph of heart tissues in the NC rats, showing the normal histological architecture of the cardiomyocytes with well-organized and branched cardiac myofibers (long arrow), centrally located oval nuclei (head arrow), and minimal interstitial connective tissue with few interstitial fibroblasts (thick arrow) in between. (H&E, ×400).

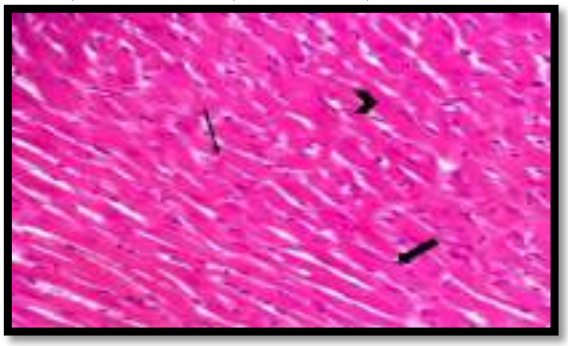

Fig. 4: Photomicrograph of heart tissues in the SH rats, showing the normal histological architecture of the cardiomyocytes with well-organized and branched cardiac myofibers (long arrow), centrally located oval nuclei (head arrow), and minimal interstitial connective tissue with few interstitial fibroblasts (thick arrow) in between. (H&E, ×400).

ISBN 978-9959-9703-2-9

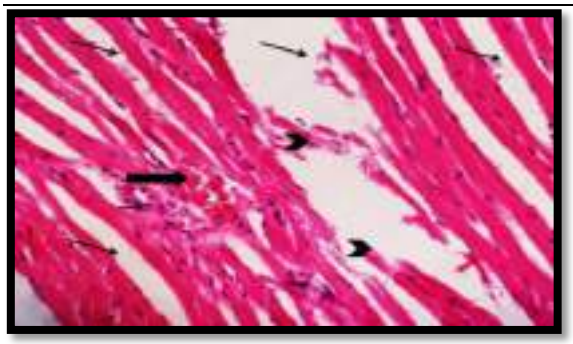

Fig. 5: Photomicrograph of heart tissues in the KC-exposed rats, showing the arrangement of myocardial fibers was disordered (long arrows) as well as cellular oedema and breaks or necrosis were evident. In addition, perivascular mononuclear cell infiltration (short arrows), ragmentation of sacroplasm and degeneration changes (head arrows), and congestion of blood vessels (long arrow). (H&E, ×400).

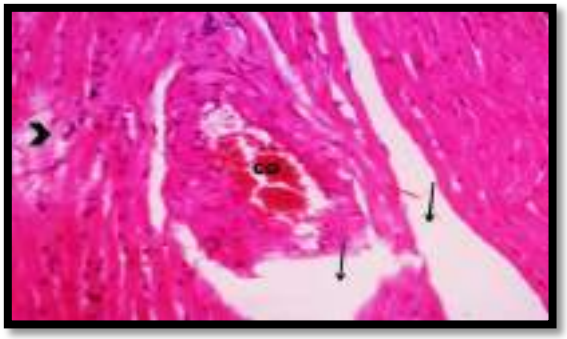

Fig. 6: Photomicrograph of heart tissues in the KC-exposed rats, showing the arrangement of myocardial fibers was disordered with oedema and necrosis (arrows), hyaline degeneration of myocardial fibers (head arrow), and congestion of blood vessels with highly thickened wall (long arrow). (H&E, ×400).

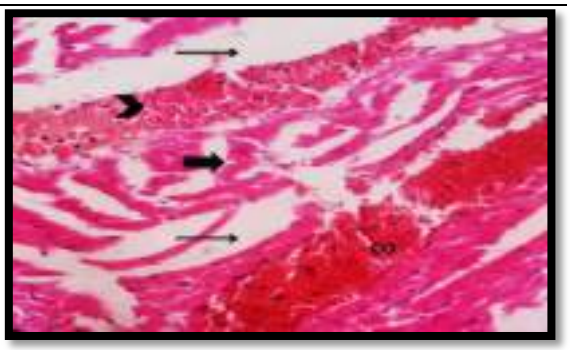

Fig. 7: Photomicrograph of heart tissues in the KC-exposed rats, showing the oedema (arrows) as well as ragmentation of sacroplasm and degeneration changes (thick arrow), hyaline degeneration of myocardial fibers (head arrow), and congestion and dilated of blood vessels (CO), and hyperemia with inflammatory cells infiltrations (head arrow). (H&E, ×400).

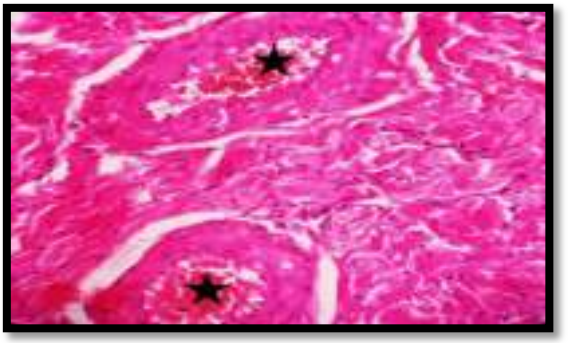

Fig. 8: Photomicrograph of heart tissues in the KC-exposed rats, showing the degeneration of myocardial fibers and congestion of blood vessels with highly thickened wall (stars). (H&E, ×400).

ISBN 978-9959-9703-2-9

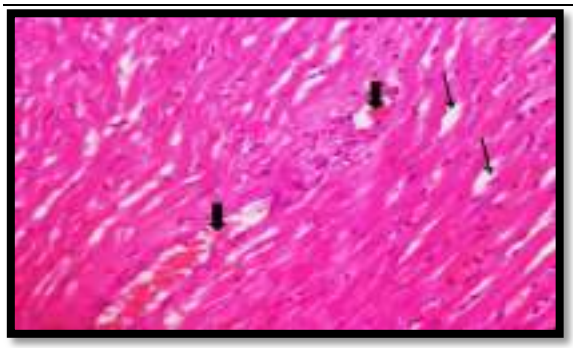

Fig. 9: Photomicrograph of heart tissues in the POR rats, showing the marked improvement in myocardial fibers with few degeneration of myocardial fibers and hyperemic interstitial blood vessels (thick arrows), and small number of necrosis (arrows). (H&E, ×400).

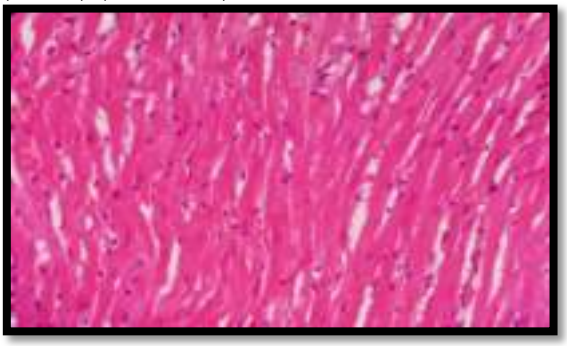

Fig. 10: Photomicrograph of heart tissues in the POR rats, showing the marked improvement in myocardial fibers which almost looks like the control with few degeneration of myocardial fibers (H&E, ×400).

Discussion:

CS exposure lead to many morphological changes in human and animal tissues [23]. Moreover, each puff of CS contains over 10^{15} free radicals, which include H_2O_2, reactive aldehydes, quinines, and benzo pyrene, because the CS had an estimated many toxic chemical compounds [24] such as nicotine, a highly addictive substance, where many of these compounds which are causally associated with deaths and diseases [25]. Furthermore, they said that about 11.1% of people deaths from cardiovascular disease occur exposed to sidestream cigarette smoke (SCS).

In this study, the X-Ray radiography of rats showed, heart mildly enlarged size in the KC-exposed rats after 4 weeks as compared with the NC rats. This is further supported by an experimental study showing that the 90 % of rats had hyperinflation in the CS exposure rats [20]. These changes may due to the toxic effect of KC on the structures of in the heart tissue. Moreover, several other factors could act as additional mechanisms to trigger cardiac hypertrophic process the generation of ROS induced by CS is cytotoxic to the myocardium, also nicotine and carbon monoxide has been shown linked to multiple effects to nervous and cardiovascular systems [26]. While, the POR rats showed normal heart size in when compared with KC rats. This might duo to by the antioxidant and radical scavenging activity of honey in endothelial cells induced by oxidative stress, where PC and flavonoids causes of the protective effect [27]. Besides that, honey has been proven reduce myocardial infarct size by reduce myocardial infarct areas [28].

 ISBN 978-9959-9703-2-9

On the other hand, the results indicated that, the mean values of CK, CK-MB, and LHD showed a significant increase in the KC group when compared with the NC group. These findings come in agreement with [29], [30], and [31] who found that the treated with CS caused a significant release of heart enzymes into circulation. This first goes to confirm that CS exposure toxicity can likely generate free radicals, hence, the elevated levels of CK, CK-MB and LHD [29], [31]. Also, [31] reported that the adverse effects of CS are mediated by the tar or by the particulate phase and the gas phase, which contain many numbers of free radicals, which resulting in oxidative stress. Moreover, the production of free radicals, other reactive oxygen and nitrogen species from the tar and gas phases of CS the contributory factors to smoke-related diseases such as cardio and cerebrovascular diseases, cancers, pulmonary diseases, and several others, where the sustained release of reactive free radicals of smoke imposes an oxidant stress, promotes lipid peroxidation and consequently perturbs the antioxidant defense systems in blood and tissues [29]. Furthermore, [30] found that the increased of LDH considered as indicator of tissues damage or cell necrosis or may be attributed on the CS chemical compounds induced cell damage in the body, which might carrer cellular contents with LDH into blood by cell damage. Additionally, [32] suggested that the CS-induced cardiac damage through the substantial rise of cardiac injury biomarkers (CK, CK-MB, and LDH) activities, reflecting cardiomyocyte membrane disruption and extensive cardiomyocyte damage.

In contrast, the results in this study showed a significant decrease in PRO group in the mean values of CK, CK-MB, and LHD when compared with KC group. This is accompanied with [28], [33]. These effects may due to the honey have suppressive effects on ROS, and inhibits the production of free oxygen radicals [34]. Moreover, honey has medicinal properties that plays a role in the prevention of vascular disorders such as cardiovascular [35].

Histological investigation of the heart tissues of KC group showed different histological changes as compared to NC group such as arrangement of myocardial fibers as well as cellular oedema and necrosis. In addition, perivascular mononuclear cell infiltration, ragmentation of sacroplasm and degeneration changes, congestion of blood vessels and hyperemia with inflammatory cells infiltrations. These results were supported by [26], [36] and [37]. The CS may have acted indirectly through generation of high levels of ROS or directly as toxin to the heart thereby affecting their cellular and functional integrity and associated with higherlevels of chronic inflammation [36].

 ISBN 978-9959-9703-2-9

Bocalini *et al.,* [26] stated that the effects of CS is associated with functional, structural cardiac changes and heart failure in rats. Moreover, the SCS contains a higher concentration of toxic gaseous chemicals cause vascular endothelial cell activation, dysfunction, and damage, also the CS caused an increase in oxidative stress, with effects on endothelial cells function and structure in the cardiovascular system, where, necrosis and apoptosis occur from the effect of ROS and other components of CS. Also, the necrotic death of cells leads to proteolysis of extracellular matrix through the release of lysosome proteases [25].

On the other hand, CS is associated with increases in inflammatory cells in the peripheral blood, and increased leukocyte recruitment to the vascular system [37]. However, [38] detected that the CS causes increased oxidative stress because of several mechanisms, including direct damage by radical species and the inflammatory response. Moreover, [32] established that the increase of free radicals output with excitotoxicity and lipid peroxidation accelerates inflammatory conciliators' synthesis and thus activates the inflammatory response in the heart tissues. So, they provoke leukocyte infiltration into the myocardium and aggravate inflammatory injury. In addition, [39] demonstrated that myocardial necrosis and oxidative stress trigger a cytokine by Tumor Necrosis Factor (TNF-α) and exacerbate myocardial injury which lead to a progressive and irreversible myocardial damage.

The POR group in the present study showed the improvement in heart tissues with the myocardial fibers which almost looks like the control with few degeneration of myocardial fibers.

The therapeutic potency of honey is due to the presence of many compounds as well as specific physicochemical properties that its associated with its wound healing effect, anti-inflammatory potency, antioxidant, and free radical scavenging ability, also it enhanced the healing process in damage tissue to rats and caused a significant decline in the levels of TNF-α. Moreover, it promote cell proliferation and neovascularization, with an overall pro-inflammatory effect [40].

Conclusion:

The present conclusions clearly demonstrate that the Libyan Sidr honey effects on protection in heart enzymes and tissues by the prevention of free radicals generation and it is an improved, and support wound healing, also it could tremendously enhance the treatment process and result in better outcomes against the tissues damage by CS.

References

 ISBN 978-9959-9703-2-9

[1] Diniz, M. F., Dourado, V. A., Silva, M. E., Pedrosa, M. L., Bezerra, F. S., Lima, W. G., (2013), Cigarette smoke causes changes in liver and spleen of mice newborn exposed during pregnancy. J Cytol Histol., **4**, 1-5. DOI:10.4172/2157-7099.1000168.

[2] Toklu, H., Şehirli, Ö., Şahin, H., Çetinel, Ş., Yeğen, B. C., Şener, G., (2010), Resveratrol supplementation protects against chronic nicotine-induced oxidative damage and organ dysfunction in the rat urogenital system. Marmara Pharm J., **14**, 29-40. DOI: 10.12991/201014462.

[3] El-Sokkary, G. H., Cuzzocrea, S., Reiter, R. J., (2007), Effect of chronic nicotine administration on the rat lung and liver: beneficial role of melatonin. Toxicol., **239**, 60-67. DOI: 10.1016/j.tox.2007.06.092.

[4] Sener, G., Toklu, H. Z., Cetinel, S., (2007),β-Glucan protects against chronic nicotine-induced oxidative damage in rat kidney and bladder. Environ Toxicol Pharmacol, **23**, 25-32. DOI: 10.1016/j.etap.2006.06.003.

[5] Brownson, R. C., Figgs, L. W., Caisley, L. E., (2002), Epidemiology of environmental tobacco smoke exposure. Oncogene, **21**, 7341-7348. DOI: 10.1038/sj.onc.1205809.

[6] Valsoni, B. C. G., Bonfim, M. R., Camargo, R. C. T., de Abreu, L. C., Souza, D. R. S., Filho, J. C. S. C., (2015), Effects of passive smoking associated with physical exercise in the skeletal muscles of rats during pregnancy and lactation. Int J Morphol., **33**, 497-506. DOI:10.4067/S0717-95022015000200015.

[10] Alshailabi, E. M. A., Abdalally, O. A., Majeed, S. F., (2021), Histopathological study on the protective effect of vitamin C against paracetamol-induced acute hepatic damage in rat. Global Libyan J., **53**,1-15.

[11] Augustine, I. O., Gertrude, O. N., Loveth, A. N., Al-Rashed, S., Obinna, U. O., Uchenna, E. K., Usman, I. M., Ogugua, E. A., Batiha, G. E., (2020), The role of garlic and honey on nicotine-induced toxicity on the cerebellum of adult Wistar rats. Res Squ., 1-18. DOI:10.21203/rs.3.rs-70046/v1.

[12] Ahmed, A., Khan, R. A., Azim, M. K., Saeed, S. A., Mesaik, M. A., Ahmed, S., Imran, I., (2011), Effect of natural honey on human platelets and blood coagulation proteins. Pak J Pharm Sci., **24**, 389-397.

[13] Alghazeer, R. , El-Saltani, H. , Saleh, N. , Al-Najjar, A., Hebail, F., (2012), Antioxidant and antimicrobial properties of five medicinal Libyan plants extracts. Nat Sci., **4**, 324-335. DOI: 10.4236/ns.2012.45045.

[14] Naili, M. B., Alghazeer, R. O., Saleh, N. A., Al-Najjar, A. Y., (2010), Evaluation of antibacterial and antioxidant activities of *Artemisia campestris (Astraceae)* and *Ziziphus lotus (Rhamnacea)*. Arabian J Chem., **3**, 79-84. DOI:10.1016/j.arabjc.2010.02.002.

[15] Kolawole, T. A., Oyeyemi, W. A., Adigwe, C., Leko, B., Udeh, C., Dapper, D. V., (2015), Honey attenuates the detrimental effects of nicotine on testicular functions in nicotine treated Wistar rats. Niger. J. Physiol. Sci., **30**, 11-16.

[16] Mohamed, M., Sulaiman, S. A., Jaafar, H., Sirajudeen, K. N. S., (2011), Antioxidant protective effect of honey in cigarette smoke-induced testicular damage in rats. Int. J. Mol. Sci., **12,** 5508-5521. DOI: 10.3390/ijms12095508.

[17] Al-Zail, N. I., Alshailabi, E. M.A., Abraheem, R. A., (2022). Changes in sexual hormone induced by cigarette smoke and the potential protective role of sidr LJBS., **19,** 19-28.

[18] Khalaf, G., Mostafa, H. K. K., (2012), Histological and immunohistochemical study on the effect of passive smoking on the skin of adult male albino rats and the possible protective role of Nigella sativa oil. Egypt J. Histol., **35**, 87-94. DOI: 10.1097/01.EHX.0000410719.45416.6f.

[19] Alshailabi, E. M. A., Abdalally, O. A., Majeed, S. F., (2021), Histopathological study on the protective effect of vitamin C against paracetamol-induced acute hepatic damage in rat. Global Libyan J., **53**,1-15.

[20] Dianat, M., Radan, M., Badavi, M., Mard, S. A., Bayati, V., Ahmadizadeh, M., (2018), Crocin attenuates cigarette smoke-induced lung injury and cardiac dysfunction by antioxidative effects: The role of Nrf2 antioxidant system in preventing oxidative stress. Respir Res., **19**, 1-20. DOI:10.1186/s12931-018-0766-3.

[21] Vennila, L. and Pugalendi, K. V., (2010), Protective effect of sesamol against myocardial infarction caused by isoproterenol in Wistar rats, Redox Rep., **15**, 36-42. DOI: 10.1179/174329210X12650506623168

[22] R. D. Lillie, Histopathological technigues and practical histochemistry. 3rd ed. McGraw-Hill,

 ISBN 978-9959-9703-2-9

New York, USA, 1954.

[23] Diniz, M. F., Dourado, V. A., Silva, M. E., Pedrosa, M. L., Bezerra, F. S., Lima, W. G., (2013), Cigarette smoke causes changes in liver and spleen of mice newborn exposed during pregnancy. J Cytol Histol., **4**, 1-5. DOI:10.4172/2157-7099.1000168.

[24] Goel, R., Bitzer, Z., Reilly, S. M., Trushin, N., Foulds, J., Muscat, J., Liao, J., Elias, R. J., Richie, J. P., (2017), Variation in free radical Yields from US marketed cigarettes. Chem Res Toxicol., **30**,1038-1045. DOI: 10.1021/acs.chemrestox.6b00359.

[25] Morris, P.B., Ference, B. A., Jahangir, E., Feldman, D. N., Ryan, J. J., Bahrami, H., El-Chami, M. F., Bhakta, S., Winchester, D. E., Al-Mallah, M. H., Shields, M. S., Deedwania, P., Mehta, L. S., Phan, B. P., Benowitz, N. L., (2015), Cardiovascular effects of exposure to cigarette smoke and electronic cigarettes clinical perspectives from the prevention of cardiovascular disease section leadership council and early career councils of the American College of cardiology. JACC., **66**, 1378-1391. DOI: 10.1016/j.jacc. 07.037.

[26] Bocalini, D. S., Luiz, R. S., Silva,K. A. S., Serra, A. J., Avila, R. A., Leopoldo, A. S., Lima-Leopoldo, A. P., da Cunha, M. R. H., Tucci, P. J. F., Santos,L. D., (2020), Short-term cigarette smoking in rats impairs physical capacity and induces cardiac remodelling. BioMed Res Int., **2020**, 1-7. Doi:10.1155/2020/2589892.

[27] Beretta, G., Orioli, M., Facino, R. M., (2007), Antioxidant and radical scavenging activity of honey in endothelial cell cultures. Planta Med., **73**, 1182-1189. DOI: 10.1055/s-2007-981598.

[28] Idrus, R. B. H., Sainik,N. O. A. V., Nordin, A., Saim, A. B., Sulaiman, N., (2020), Cardioprotective effects of honey and its constituent: An evidence-based review of laboratory studies and clinical trials. Int J Environ Res Public Health. 17, 3613. DOI: 10.3390/ijerph17103613.

[29] Anbarasi, P. K., Sabitha, K. E., Devi, C. S. S., (2005), Lactate dehydrogenase isoenzyme patterns upon chronic exposure to cigarette smoke: Protective effect of bacoside A. Envir Toxicol Pharm., **20**, 345-350. DOI:10.1016/j.etap.2005.03.006.

[30] Raddam, Q. N., Zeidan, M. M., Abdulrahman, M. A., Asaad, N. K., (2017), Smoking effects on blood antioxidants level: Lactate dehydrogenase, catalase, superoxide dismutase and glutathione peroxidase in university students. J Clin Exp Pathol., **7**, 331-337. DOI:10.4172/2161-0681.1000331.

[31] Tasdogan, A. M., Pancar, Z., (2020), Some biochemical responses in cigarette addicts who receive royal jelly supplement. EJMI., ,4, 204-208. DOI: 10.14744/ejmi.2020.28402.

[32] Elblehi, S. S., El-Sayed, Y. S., Soliman, M. M., Shukry, M., (2021), Date Palm pollen extract avert doxorubicin-induced cardiomyopathy fibrosis and associated oxidative/nitrosative stress, inflammatory cascade, and apoptosis-targeting bax/bcl-2 and caspase-3 signaling pathways. Animals, 11, 1-28. DOI:10.3390/ani11030886.

[33] Khalil, M. I., Tanvir, E. M., Afroz, R., Sulaiman, S. A., Gan, S. H., (2015), Cardioprotective effects of Tualang honey: Amelioration of cholesterol and cardiac enzymes levels. Biomed Res Int., **2015**, 1-8. DOI: 10.1155/2015/286051.

[34] Ahmad. A., Khan, R. A, Mesaik, M. A., (2009), Antiinflammatory effect of natural honey on bovine thrombin induced oxidative burst in phagocytes. Phytother Res., **23**, 801-808. doi: 10.1002/ptr.2648

[35] Ahmed, A., Khan, R. A., Azim, M. K., Saeed, S. A., Mesaik, M. A., Ahmed, S., Imran Imran, I., (2011), Effect of natural honey on human platelets and blood coagulation proteins. Pak. J Pharm Sci., **24**, 389-397.

[36] Adedayo, A. D., Tijani1, A. A. Musa, A. A., Adeniy, T. D., (2011), Histological study of smoke extract of *Tobacco nicotiana* on the heart, liver, lungs, kidney, and testes of male Sprague-Dawley rats. Nigerian Med J., **52**, 217-222. DOI: 10.4103/0300-1652.93791.

[37] Cavusoglu, Y., Timuralp, B., Us, T., Yurdanur Akgün, Y., Kudaiberdieva, G., Gorenek, B., Unalir, A., Goktekin, O., Ata, N., (2004), Cigarette smoking increases plasma concentrations of vascular cell adhesion molecule-1 in patients with coronary artery disease. Angiol., **55**, 397-402. DOI: 10.1177/000331970405500406.

[38] Meity, A., Santoso, A., Hermawan, H. O., Nugraha, R. A., Pikir, B. S., Suryawan, I. G. R., (2021), Acute effects of cigarette smoke on Endothelial Nitric Oxide synthase, vascular

 ISBN 978-9959-9703-2-9

cell adhesion molecule 1 and aortic intima media thickness [version 1; peer review: awaiting peer review]. F1000Res., **2021**, 1-13. DOI: 10.12688/F1000Research.28375.1.

[39] Khorrami, A., Hammami, M., Garjani, M., Nasrin Maleki-Dizaji, N., Garjani, A., (2014), Tacrolimus ameliorates functional disturbances and oxidative stress in isoproterenol-induced myocardial infarction. DARU J Pharm Sci., **22**, 1-9. DOI: 10.1186/s40199-014-0068-3.

[40] Tashkandi, H., (2021), Honey in wound healing: An updated review. Open Life Sci., **16**, 1091-1100. DOI: 10.1515/biol-2021-0084.

 ISBN 978-9959-9703-2-9

المؤتمر الدولي الثاني للعلوم والهندسة
2nd International Conference on Science and Engineering
ICSE 2023
Faculty of Engineering - University of Bani Waleed
Bani Waleed, Libya

Paper Code: ICSE-004

RISK FACTORS OF CORONARY HEART DISEASE PATIENTS AT MISRATA: AWARENESS AND ORIENTATION

S.Elwahaishi[a], A. Mustafa[b] and N. Ali[c]
[a,b] Department of Therapeutic Nutrition, Faculty of Health Sciences, Misurata University
[c] Department of Radiological Sciences and Medical Imaging, Faculty of Applied Medical Sciences, Majmaah University, Riyadh, KSA
* Corresponding author: elwahaishi@nurs.misuratau.edu.ly

Abstract: Many prospective studies have examined the associations between intakes of individual foods and the risk of coronary heart disease (CHD), but few have evaluated the relation of overall dietary patterns to the risk. A descriptive hospital-based study was conducted to assess knowledge of CHD patients about risk factors in Misrata hospitals. The study has consisted of 100 patients with CHD, at different ages, who were selected randomly during 2019. The study data were collected using well-structured questionnaire, patient record, and anthropometric measurements. Pearson correlation was used to examine correlation between risk factors, blood fat profiles, and lifestyle. The results revealed that (52%) of patients fall within the age group 51-70 years, the CHD was widely prevalent among males (55%), most of the patients (41%) were illiterate, majority of patients (92%) were suffering from other chronic diseases such as diabetes, hypertension, and obesity. The majority of patients (63%) were considerably ignorant of the causes and risk factors for CHD (P≤0.05). The majority of patients (54%) have excess weight and engage in sporadic physical activity. When compared to fewer patients (8%) who follow up with a dietician, there is a significant difference (P≤0.05) between patients who have no knowledge of the CHD diet regimen and those who have not received any counseling themselves. The correlation between age groups, chronic illnesses, and blood fat profiles was significant (P≤0.05), according to the results. The majority of patients had no practiced therapeutic lifestyle and little physical activity towards control of CHD. The appropriate nutrition education and patients counseling should be recommended among outpatients of CHD.

Keywords: Awareness, Coronary Heart Disease, Lifestyle, Misrata, Risk factor

Introduction

Coronary heart disease is a disease of the blood vessels supplying the heart muscle. The primary cause of CHD is atherosclerosis that reduces blood flow through the coronary arteries to the heart muscle, [1]. In the Middle East and North Africa, cardiovascular disease is the most common cause of mortality, resulting in more than one third of all fatalities, or 1.4 million people annually [2]. However, little information is known about their CHD knowledge and CHD risk factors despite estimations proclaiming that heart

 ISBN 978-9959-9703-2-9

disease deaths will increase between the years 2010 and 2030 [3].

Many of the risk factors of CHD such as Diabetes Mellitus (DM), dyslipidemia, hypertension (HTN), physical inactivity, and smoking are prevalent in Libya [4, 5]. This places Libya at risk for developing CHD, which is the leading cause of their mortality. Lack of data on Libyan CHD knowledge may limit the assessment of their cardiovascular health status and may limit the ability to plan programs that reduce CHD. This may contribute to the increased morbidity and mortality of heart disease in Libya. Assessment of knowledge is an important first step in addressing the issue of heart disease in Libya. Therefore, additional studies indicated to assess the baseline knowledge of Libyan on CHD, to determine the variables that impact CHD knowledge, and to identify the CHD risk factors. Because of eliminating health disparities, reducing cardiovascular deaths, and encouraged to educate patients about CHD and promote a healthy lifestyle by counseling their Libyan patients to engage in healthy lifestyles to reduce CHD risk.

A lack of research on the epidemiology of CHD in Africa is another issue. However, modernity and changes in lifestyle have increased CHD prevalence. According to earlier research, the prevalence of coronary heart disease (CHD) has increased by 160% across the Middle East and North Africa, and the condition has a high mortality rate (120 per 100,000 people). Similar to Tunisia, where research shows that between 1997 and 2009, the mortality rates from coronary heart disease (CHD) increased by 11.8% for men and 23.8% for women [5].

Despite the growing numbers of Libyan in Misrata City, it considered a "hidden minority" because of the lack of research-based information on their health. Therefore, little known about their baseline knowledge of CHD even though many of them have at least one CHD risk factor. Which may be a contributing variable to their morbidity and mortality. Research shows individuals who are not aware of their risk for developing a disease are less likely to adopt preventive behaviors [6, 7]. Awareness of CHD and its risk factors are significant in preventing and reducing CHD deaths [6]. The purpose of this study is to examine the baseline knowledge and risk factors of CHD in Misrata City to describe the relationships between knowledge socio-demographic, and socioeconomic characteristic of patients.

II.MATERIAL AND METHODS

The headings and subheadings from introduction to Acknowledgement must be in 9 points, bold face, aligned left, don't underline

 ISBN 978-9959-9703-2-9

any words in your paper, subheadings are numbered with 1, 2, 3 etc, delete and type).

A. Area of study

This is study was carried out in some hospitals of Misrata, Libya. Misrata is a city in the Misrata District in northwestern Libya, situated 187 km (116 mi) to the east of Tripoli and 825 km (513 mi) west of Benghazi on the Mediterranean coast near Cape Misrata. With a population of about 550,000, it is the third-largest city in Libya, after Tripoli and Benghazi. It is the capital city of the Misrata District, and it called the trade capital of Libya. It has lied at a longitude is 32 o.377533" N and Latitude is 15o.092017" E. It is located is at 7-meter height, which is equal to 23 ft. above sea level.

B. Research Design

This is a hospital-based cross-section descriptive study, which used to identify the risk factors of coronary heart disease, thereafter, alter to therapeutic lifestyle to prevent progressions of CHD and to stay healthy longer. Thereafter the data conducted and collected from respondents with used questionnaires to investigate risk factors most likely of CHD.

C. Study population

All the participants informed about the study purpose and signed the study consent forms. The study proposal approved by the Therapeutic Nutrition Department board, and all procedures followed by the ethical standards of the Misrata University. The study interviewed about 100 (CHD) patients of both sexes, who selected randomly from some public hospitals (Safwa, Elshifa, Algarawy, Ras-Ali, and Almahjoub Clinical Campus) in Misrata City, Libya. The study was targeted all age groups. Eligibility was determined through who coronary heart disease patients are and who are living in Misrata.

D. Study duration

The study was conducted within six months. From December 2019 up to April 2020. The duration was distributed among designing of questionnaire, data collection, analysis and interpretation, and report writing.

E. Data collection procedures

1. Questionnaire

Well-designed questionnaire according to objectives of the study. Three parts of the questionnaire were compiled and face-to-face interviews of CHD patients in selected hospitals in Misrata. The first part of the questionnaire was included sociodemographic and socioeconomic, the second part was included medical history and lifestyle and the third part was included dietary practices.

2. Anthropometric data

ISBN 978-9959-9703-2-9

The weight and height are measured. The anthropometric data recorded then BMI calculated using the procedure of anthropometric measurements and evaluation [8].

3. Blood lipid profile

A lipid profile is a blood test that measures the amount of cholesterol and fats called triglycerides in the blood. The primary data of lipid profiles were collected from patient's files used to identify who would be included in the study.

F. Data quality management

A well-structured questionnaire was prepared according to study purposes and aims. A pre-test of the questionnaire was done before actual data collection just to check its accuracy, response to analysis, and estimate which time it is needed.

G. Statistical analysis

SPSS (version 18) and graphs were used for data analysis. Descriptive statistical methods are represented in the frequency and percent as well as Pie charts and histograms. Pearson Correlation was used to study the relationship between variables. The relationship between the two variables is significant if P-value is less than 0.05.

III.RESULTS AND DISCUSSION

The study was conducted to examine the knowledge about risk factors of coronary heart disease (CHD) of those were attended primary care services in selected hospitals at Misrata City, Libya. Also, it was described the relationship between socio-demographic and socioeconomic characteristics variables that influence knowledge of CHD risk factors.

A. The socio-demographic and socioeconomic characteristics

Table (1) shows the age groups of CHD patients, most patients 52% fall within the age group 51-70 years old. This finding was closed to the study reported that 85% of CHD patients were at range 51-70 years [9]. While CHD was greater prevalent among males 55% than females 45% thus was shown in gender groups. This is finings agreed with studies stated that CHD has been considered a disease of men. However, CHD is the leading cause of death both in men and in women [9,10]. However, the reason for gender variation is not clear; it may be attributed to the protective effect of estrogen [11]. It is estimated that 82 percent of people who die of coronary heart disease are 65 and older at the same time, the risk of stroke doubles every decade after age 55 [12].

The education level of CHD patients, the almost patients 41% were illiterates, primary education percent 21%. The result revealed that a greater number of CHD patients had illiterate, which means they have facing

 ISBN 978-9959-9703-2-9

difficulty in bringing counseling and disease management. The educated people have more chance to receive information about the causes, risk factors, treatment, and prevention of CHD, thus can apply to prevent measure through diet control and therapeutic lifestyle more than illiterate ones.

Table (2) shows whose weighing-up regularly, the most of patients 63% were significant ($p \leq 0.05$) weighing regularly compared to 37% careless patients, who were not weighing regularly. A clear majority of patients were overweight and suffered from obesity, this is due to a lack of awareness among patients who are illiterate about the risks of excess weight. Weigh monitoring is important to keep you normal and prevent obesity.

The results revealed a significant difference ($p \leq 0.05$) between the two groups, as shown in Table 3: few patients are aware of the causes of coronary heart disease, whereas more patients—63%—have no notion.

The probable reasons may be the high proportion of illiteracy perhaps patients didn't pay attention to the advice given by doctors on the first CHD attack.

In table (4) shows, who have chronic illnesses, the majority of patients have Diabetes 42% percent and Hypertension 51% percent. The result has shown the most patients with coronary heart disease had duplicated illnesses. The majority of patients had chronic illnesses more than that is 72%, there were hypertension, diabetes, and a combination of both in increasing rates [9]. Diabetes substantially increases the risk of CHD and magnifies the effect of other risk factors for CHD such as raised cholesterol levels, raised blood pressure, smoking and obesity, [11].

The performance of the physical exercise, very few patients had performed daily, were 9%, compared with who were exercise occasionally 54%, thus was shown in table (5). The highest percentage of patients had practiced a sedentary lifestyle. This result agreed to the finding estimated that over 20% of CHD in developed countries was due to physical inactivity [13]. It recommended physical activity levels are 30 minutes of moderate physical activity on five or more days per week [14].

Table (6) shows the anthropometric assessment of CHD patients during the survey in the hospitals, that frequency of normal range 22%, overweight 56%, Obese percent 22%. The result revealed that the majority of patients were overweight and obese. They were no paying attention to risks with poor lifestyle due to the lack of weight control and poor awareness about the risk of weight gain increased risk factors of CHD. Obesity is an independent risk factor for CHD. It is also a

 ISBN 978-9959-9703-2-9

risk factor for hypertension, hyperlipidemia, diabetes, and impaired glucose tolerance. Central or abdominal obesity is most significant. Those with central obesity have over twice the risk of heart attack [15].

The age groups (30–50) and (51–70) have a highly significant link with other ailments, according to Table 7. While epidemiological research has shown that diabetes, hypertension, and hyperlipidemia are independent risk factors for CHD, there is no association between elders older than 70 and other disorders [16]. it also indicates there is no correlation of age groups with family history and smoking, this find is slightly agreed with some research estimates that over 20% of CVD is due to smoking and disclosed that finding mentioned premature CHD is that before age 55 years in men and 60 years in women. [17, 18].

The blood lipid profile of CHD patients is shown in "Figure 1": 55% of them had total cholesterol above 181 mg/dl, 15% had triglycerides above 174 mg/dl, 23% had LDL above 125 mg/dl, and 42% had HDL below 40 mg/dl.

IV.CONCLUSION AND RECOMMENDATION

According to the findings of the current study, most CHD patients are between the ages of 51 and 70. They have only received a primary education, are illiterate, and are overweight and obese, which may be obvious indicators of coronary heart disease risk factors. They exercise only occasionally and live a largely sedentary lifestyle, and they are unaware of the causes or even risk factors for coronary heart disease. Age groups showed a statistically significant association ($P \leq 0.05$) in the results.

By choosing a nutritious diet, avoiding trans-fatty acids in processed foods, engaging in regular exercise, maintaining normal blood glucose levels, and maintaining their blood fat profiles as advised, patients can lower their risk factors by adopting a therapeutic lifestyle change.

The first steps in enhancing Libyans' quality of life and addressing health disparities are to (a) evaluate and comprehend their health risks; (b) raise public awareness of heart disease risk factors; (c) include them in research; and (d) motivate minority advocates and researchers to concentrate on Libyans' cardiac health. Additionally, studies on the cardiac health of the Misrata people may encourage minority health advocates to increase knowledge of the risk factors for CHD.

 ISBN 978-9959-9703-2-9

Table 1. Shows the socio-demographic of CHD patients

Variables	Groups	Percent
Age groups (year)	30 - 50	17%
	51 - 70	52%
	>70 years	31%
Gender groups	Male	55%
	Female	45%
Education level	Illiterate	41%
	primary	21%
	secondary	15%
	university	3%
	post-university	20%

Table 2. Shows who is weighing up regularly

Weighing up regular	Frequency	Percent	P-value
No	37	37%	
Yes	63	63%	0.000
Total	100	100%	

Table 3. Shows the Knowledge about causes of coronary heart disease

Known the causes of CHD	Frequency	Percent	P-value
No	63	63%	
Yes	37	37%	0.000
Total	100	100%	

Table 4. Shows who has chronic illnesses

Chronic illnesses	Frequency	Percent
Asthma	3	3%
Diabetes	52	41%
Hypertension	64	51%
Liver diseases	1	1%
Hypo/ hyperthyroidism	3	2%
Other	2	2%
Total	125	100%

Table 5. Shows the performance the physical exercise

Performance the physical exercise	Frequency	Percent
daily	9	9%

ISBN 978-9959-9703-2-9

3-4 days/week	7	7%
1-2 days/week	29	29%
occasionally	54	54%

Table 6. Shows the anthropometric Assessment

Classification BMI	Frequency	Percent
Normal range	22	%22
Overweight	56	%56
Obese	22	%22
Total	100	%100

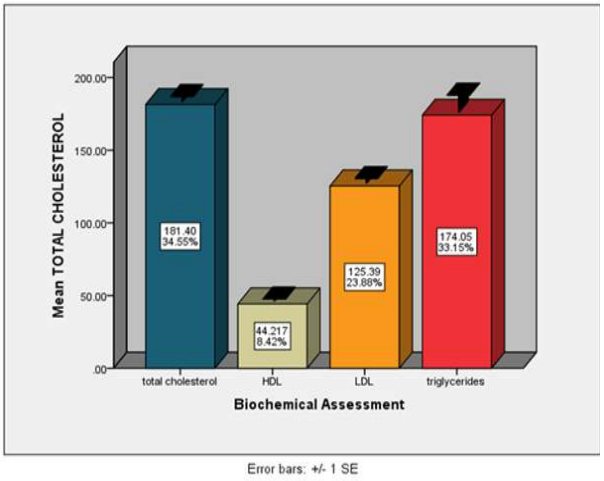

Fig.1. Blood fat profile of CHD patients during the survey

Table 7. Shows the correlation between age groups and other variables

Variables	Age Groups	(r)	P-value
Family history	30 - 50	-.075-	.774
	51 - 70	.260	.063
	>70 years	.047	.803
Other illness	30 - 50	.611**	.009
	51 - 70	-.010-	-.010-
	>70 years	.152	.415
Smoking	30 - 50	.115	.683
	51 - 70	-.068-	.653
	>70 years	-.131-	.507

r= correlation, ** P≤0.001

REFERENCES

[1] M. Dariush, Fish consumption and stroke risk in elderly individuals: the cardiovascular health study. Archives of Internal Medicine, 2005, 165.2: 200-206.

[2] A. H. A. American Heart Association, Re: Heart disease and Stroke Statistics-2010 Update. 2010, Retrieved from http://circ.ahajournals.org/cgi/reprint/121/7/e46

[3] C. D. C. Centers for Disease Control and Prevention. Re: Heart Disease and Stroke Prevention (2007).

[4] N. C. Agrinier, M. Cournot, J. Dallongeville, D. Arveiler, D. Ducimetiere, J. Ferrieres, Menopause, and modifiable coronary heart disease risk factors: A population-based study.

 ISBN 978-9959-9703-2-9

Maturitas Journal, 2010, 65, 237-243.

[5] M. Hussain M, N. Khan, M. Uddin, M. M. Nozha. Chest pain, coronary artery disease and risk factors: A global snapshot. J Dow Univ Heal Sci Karachi 2014;**8**:74–80.

[6] P. Goyal, S. C. Kale, R. Chaudhry, S. Chauhan, N. Shah, Association of common chronic infections with coronary artery disease in patients without any conventional risk factors, Indian Journal of Medical Research, 2007, 125(2), 7872-7876.

[7] Y. Cavusoglu, B. Timuralp, T. Us, Y. Akgun, G. Kudaiberdieva, B. Gorenek, N. Ata, Cigarette smoking increases plasma concentrations of vascular cell adhesion molecule-1 in patients with coronary artery disease. Angiology, 2004, 55, 397-402.

[8] Z. Mei, L. M. Strawn, A. Pietrobelli, Validity of body mass index compared with other body-composition screening indexes for the assessment of body fatness in children and adolescents. Am J Clin. Nutr. 2002; 75:978.

[9] C. K. Chow, A. C. Pell, "Walker, Families of patients with premature coronary heart disease: an obvious but neglected target for primary prevention BMJ, 2007, 8335 (7618):481-500.

[10] G. W. Mikhail, "Coronary heart disease in women, BMJ, 2005, 3331(7515):467-8.

[11] E. T. Jimenez, Prevalence risk assessment for Cardiovascular Diseases among Young Women and the impact of therapeutic lifestyle Modification", Journal of the American Dietetic Association, 2008, 108 (2): 347-356.

[12] J. J. Carrero, "Intake of fish oil, oleic acid, folic acid, and vitamins B-6 and E for 1 year decreases plasma C-reactive protein and reduces coronary heart disease risk factors in male patients in a cardiac rehabilitation program, The Journal of nutrition, 2007, 137.2: 384-390.

[13] F. W. Booth, M. V. Chakravarthy, E. E. Spangenburg, "Exercise and gene expression: physiological regulation of the human genome through physical activity, The Journal of physiology, 2002, 543(2), 399-411.

[14] N. M. Hawkins, S. Scholes, M. Bajekal, "The UK National Health Service: delivering equitable treatment across the spectrum of coronary disease. Cardiovascular Qual Outcomes, 2013, 16(2):208-16. Doi: 10.1161/CIRCOUTCOMES.111.000058. Epub .12.

[15] V. C. Kuppuswamy, S. Gupta, "Excess coronary heart disease in South Asians in the United Kingdom, BMJ, 2005, 28330 (7502):1223-4.

[16] N. Umesh, P. Monika, T. Christopher, Prevalence of conventional risk factors of CHD, JAMA, 2003, 290: 898-904.

[17] R. Gupta, P. Joshi, V. Mohan, K. S. Reddy & S. Yusuf, Epidemiology and causation of

 ISBN 978-9959-9703-2-9

coronary heart disease and stroke in India. Heart, 2008, 94 (1): 16-26.

[18] A. J. Arti-Carvajal, I. Sola, D.Lathyris, Homocysteine-lowering interventions for preventing cardiovascular.

 ISBN 978-9959-9703-2-9

المؤتمر الدولي الثاني للعلوم والهندسة
2nd International Conference on Science and Engineering
ICSE 2023
Faculty of Engineering - University of Bani Waleed
Bani Waleed, Libya

Paper Code: ICSE-030

CROSS-SECTIONAL STUDY OF CHECKING AN ANESTHETIC MACHINE PARTS AND INSTRUMENT: SURVEY STUDY OF ANAESTHETIC TECHNICIANS IN LIBYA

Sumia R Emhemed [a], Kaothar S Abuokraa[b] *, Enas K Alsseid, Hana A Albasha, Mawada M Alhudairy
[a] Department of Anaesthesia and Intensive Care, Faculty of Medical Technology, University of Zawia, Libya
[b] Department of Anaesthesia and Intensive Care, Faculty of Medical Technology, University of Zawia, Libya
* Corresponding author: K.abuokraa@zu.edu.ly

Abstract: The anaesthetic machine (AM) is one of the most essential devices used by anaesthesiologist's, and understanding its characteristics and functions is a crucial component of anaesthetic practice. The pre-use check to ensure the correct functioning of AM and equipment is essential to patient safety. The check is included in the World Health Organization Surgical Safety Checklist. **Aims of this study:** To evaluate if the technicians perform sufficient check or not. In addition, if there were, any problems reported because of insufficient check. **Methodology:** Descriptive cross-sectional study used online questionnaire. Google Forms app was the best option available because of the global pandemic covid-19. Most questions in this study were multiple choice and some were short answers. **Results:** The total responses received are 53 from 18 different hospitals, the most from Zliten Hospital with 13 responses. The majority of participants' experience years were less than five years with 60.38% (n=32). Participants Most of the answers showed a middling presence of constantly checking. The highest always-checking rate was for ventilators with 81.12% (n=43). From the total number of participants, 45.28% (n=24) experience problems related to inadequate check of AM before anaesthesia. **Conclusion**: This study's results demonstrate that the standard of checking anaesthetic equipment before use is inappropriate as a 24 of them reported problems related to poor check.

Keywords: (Anaesthesia machine, Anesthesiologists, Checklist, Instrument, patient safety and technician)

Introduction

An anaesthesia machine (AM) is a medical device used to control the patient's ventilation and oxygen delivery and to administer inhalation anaesthetics [1]. The AM is one of the most important tools used by anaesthesiologist's, and understanding its characteristics and functions is essential. AM is subject to continuous change and

 ISBN 978-9959-9703-2-9

innovation [2].

Broadly, the term AM apparatus or equipment is taken to mean the set of elements intended to provide medicinal gases and anaesthetics to a patient [3].

Components of the Anaesthetic Machine; AM has six basic subsystems: Gas supplies; including pipelines and cylinders, Gas flow measurement and control (flow meters), Vaporizers, Gas delivery presented as a breathing system and ventilator, Scavenging, and Monitoring. Functions of the Anaesthetic Machine; the machine performs four essential functions: as the following Provides oxygen (O2), accurately mixes anaesthetic gases and vapours, enables patient ventilation., and minimizes anaesthesia-related risks to patients and staff [1-3].

Checking the Anesthetic Machine; daily standard systemic before use, AM checking is an essential procedure to ensure patient safety [4]. One checklist cannot satisfactorily test the integrity and safety of all existing AM due to their complex variations in design [5]. Many anaesthetic associations, including the American Association of Anaesthesiology (ASA) and the Association of Anaesthetists of Great Britain and Ireland (AAGBI), have published checklists. The issue with Statements: The proper check is required because patient and working-related equipment safety is crucial. Due to insufficient checks, there were several cases recorded in various regions of the world, and the patients' conditions put them in danger of losing their lives. This study was designed to evaluate whether the anaesthesia technicians perform adequate checking or not. If there were, any problems reported because of insufficient checks.

Methodology

Descriptive cross sectional study used online questionnaire to evaluate the pre-anaesthesia routine check of AM and equipment in Libyan hospitals, and also if there were any complications regarding inappropriate checks have been reported.

To achieve the study goal the Google form survey was used to gather data from participants (anaesthesia technicians). Google Forms can be utilized for biomedical surveys and may help in gathering information from a large sample within a short time [6].

The survey Link was online shared via e-mails and trusted social media sites for two months from March to May 2021.

Survey design:

The survey was designed based on the other anaesthesia community checklist protocol. This survey aimed to ask the participants about the AM checking they performed before anaesthesia. All questions in the study were short answer questions and multiple-choice

 ISBN 978-9959-9703-2-9

questions, and all question's answers were required. Before starting small description was added to introduce ourselves, our work, and the general goal of our study.

Results and Discussion

Two months (March to May 2021) after sharing the survey the online survey was deactivated and ended receiving new participants. The total number of responses was 59 responses, six of the total responses were excluded because they came from unemployed technicians or the working place could not identify also one respondent was not from Libya.

Anaesthesia equipment is important for the safe conduct of anaesthesia, but equipment malfunction may also contribute to morbidity and mortality [7]. The AM has most often been involved in equipment-related morbidity [8]. Human factors were important causes of problems, and the AM was most often involved. Moreover, this has led to the extensive use of preoperative checklists [9]. As checking for AM must be performed before anaesthesia to sidestep any issues related to insufficient checking and humble preparation, this survey was created to study the checking of AM in Libyan hospitals. Google Form application was used to create the survey then, it was online shared. After two months, the survey was deactivated and responses were 59 in total. Six responses were excluded, and the results of 53 responses were used.

The survey questions analysis

1. General Section

The first section of the survey was general and asked about the experience of working as an anaesthetic technician and working place.

In the first question, the contributor's experience arranges into three groups (0-5), (5-10) and (more than 10). Most of the technicians who participated in this survey have experienced less than 5 years with 60.38%, which counts 32 of the total 53 participants. Other experience groups owned 32.08% and 7.55% respectively. As shown in

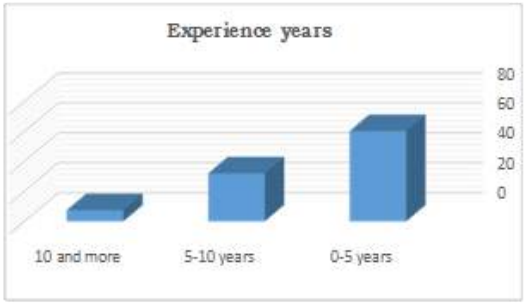

Figure (1)

Fig.1: Experience years

As the participants were from 18 various working locations, we obtained responses from several Libyan hospitals (both government and private), as shown in Table 1.

Table.1: The working place of participants and

ISBN 978-9959-9703-2-9

the count of responses from each working place.

Hospital	Count	Hospital	Count
Zliten medical center	13	Aljala Hospital Tripoli	1
Zawia Teaching Hospital	10	Surman General Hospital	2
Almarge Hospital	2	Derna Hospital	1
Alkalil Clinic	1	Ali Omer Askar Hospital	1
Musrata Medical Centre	2	Sabrath Teaching Hospital	2
Alhadba Hospital	4	Alkoms Hospital	1
Albasatin Clinic	2	Nawat Almostakbal Clinic	1
Tripoli Medical Center	2	Maslata Hospital	1
Aljala Hospital Benghazi	6	Sebha Hospital	1

In the first section, two questions were asked about the working place and experience of participants. This work does not study the relationship between the experience and the protocol of checking, those questions took place in this study to identify that all participants are anaesthesia workers.

Many cases reported have been published were related to inappropriate checking of Am and instruments, many of the cases put the patients in life-threatening situation.s

The examination rates of AM power supply were 43.4% always, 47.17% sometimes and 09.43% never check the power supply. Anaesthesia providers dependent on sophisticated electrically powered equipment such as the anaesthesia gas machine and monitors to safely care for their patients [10]. A massive power failure that adversely affects the operating room's ability to function is rare, and the available related literature is somewhat limited [11]. All anesthesiologists are supposed to always check the power supply before performing any operation because all anaesthetic depend on the power supply.

1. Checking an Anaesthetic machine section

The second section of the survey represents 13 questions about the checking of AM. As presented in Tables 2 and 3.

Table.2: indicated the result of checking an Anaesthetic machine section (Q1-11).

Result	ALWAYS		SOMETIMES		NEVER
	Per cent	Count	Per cent	Count	Per cent
1. Check the power supply	43.40%	23	47.17%	25	9.43%
2. Check the gas cylinder	77.36%	41	13.21%	7	9.43%
3. Checking Pipelines	41.51%	22	43.40%	23	15.09%
4. Checking flowmeter result	58.49%	31	32.08%	17	9.43%
5. Checking the breathing system	90.57%	48	7.55%	4	1.89%
6. Checking the vaporizers	71.70%	38	22.64%	12	5.66%
7. Checking	81.13%	43	16.98%	9	1.89%

ISBN 978-9959-9703-2-9

the Ventilator						
8. Checking the Suction machine	69.81%	37	26.42%	14	3.77%	2
9.Checking and configuration of monitor	83.02%	44	15.09%	8	1.89%	1

The result of the section questions was presented respectively as follows: The first question was about checking the power supply; the examination rates were close between (always 43.4% & sometimes 47.17%) and 09.43% of the technician was never checked. All anesthesiologists are supposed to always check the power supply before performing any operation because all anaesthetics depend on the power supply.

The second question was asked about the check the gas cylinder; the equivalent 77.36% of anaesthesia technicians always check, and this is a good percentage to avoid any risks associated with gas cylinders, 13.21% do sometimes check and never check 9.43%. One of the participating technicians informs us about the problem of a gas leak from the cylinder because of poor checking.

The third question was about the check of the pipeline; the equivalent of 41.51% of all participants always performed checks of pipelines, and, 43.40% do sometimes check and the never checking was 15.09%. Concerning the importance of routine inspection of the AM's flexible hose pipeline, a case report of a sudden beginning of persistent unusual sound in the operating room during surgery was shown to be caused by nitrous oxide leakage from the AM's flexible hose pipeline [12]. Another research revealed that gas pipelines, cylinders, Rotameters, vaporizers and ventilator disconnect alarms were rarely checked [13].

Flowmeter checking was performed as follows: 58.49% always check, so it is necessary to check it because it evaluates the rate of gas flow that passes through it. The percentage of sometimes checking is 32.08% the never was 9.43%.

The breathing system is considered one of the most important devices to be checked, so the percentage of technicians checking was always 90.57% and 7.55% sometimes checking and they never checking was so small only 1.89%. Described some problems related to the flowmeter as dirt or static electricity can cause a float to stick and misrepresents actual flow. The flowmeter must align properly in the vertical position to avoid inaccurate readings.

The breathing system is considered an important device to be checked, so our data shows 90.57% of technicians were always checking the breathing system. In one case report related to an unchecked breathing system, after the patient was anaesthetized and the resident attempted mask ventilation,

 ISBN 978-9959-9703-2-9

no ventilating pressure could be achieved in the circuit and no gas moved with the sound of gas escaping from the system was heard and the machine was quickly inspected. An opened CO2 canister was found and the top part contained no soda lime. Despite closing the circuit, no ventilation was possible [15].

There was 71.7% of anaesthetic technicians doing always check, 22.64% of them do sometimes check and the percentage of never check is 5.66%. Therefore, it is important to check it because it vaporizes anaesthetic fluids to deliver them to the patient. Regarding the vaporizer check or study, prove that there was 71.7% of anaesthetic technicians always check, 22.64% sometimes check and 5.66% never check the vaporizers. One problem mentioned by some participants was that the vaporizer was not filled as a result of an inappropriate AM check.

Research's studied vaporizers were approximately seven years old and had been maintained regularly by the Australian Datex-Ohmeda service center. As awareness has been reported because of, malfunctioning of the vaporizer attached to the AM they doubt that the fault was caused by, excessively long actuating spindles which were confirmed later by Datex-Ohmeda in four of the vaporizers.

In two of the vaporizers, the fault was in the upstream spindle. In one vaporizer, the problem involved the downstream spindle, and in the other, the spindle was unspecified [16]. It is important to check it because it vaporizes anaesthetic solutions to deliver them to the patient. Several case reports reported leak issues, with most of them having in common the inappropriate positioning of vaporizers on the AM. Others report inappropriate adjustments in the mounting system due to a missing rubber O-ring. Timely identification of this problem is facilitated by checking the anaesthetic machine with the vaporizer in the ON and OFF positions [17].

The percentage of ventilator non-examination is very low, and through the results, the examination rate was always recorded as 81.13% and sometimes 16.98%. In one case, the ventilator was inadvertently turned off during anaesthesia. This was a new anaesthetic machine, where the `power button' protruded from the cabinet, and the anaesthetists inadvertently pushed it. The ventilator stopped and the patient's pulse oximeter reading decreased to 45% before the error was detected [9]. In the same manner, one technician who participated in our study said he faced the problem of a sudden unexpected ventilator stop, and he does not explain the reason for this.

In one case report, the ventilator did not work promptly; the airway pressure was increasing

 ISBN 978-9959-9703-2-9

and the bag was empty while the ventilation with the Ambu-bag was normal. After checking, the AM anesthesiologists noticed a kinging in the hose connecting the ventilator chamber to the airway pressure release valve [18].

The sucking or suctioning device has a big role in the operation, it cleans and suctions foreign objects from the patient's mouth, for example (blood, broken teeth or vomiting), and so 69.81% of anaesthesiologist's always check. Moreover, 26.42% of them sometimes check the suction unit.

When we asked the technicians about the checking of the suction unit, 69.81% of them always check, and 26.42% of them sometimes check, As the sucking or suctioning device has a big role in the operation, the problem was mentioned by one technician is that the suction unite did not work and another device was not reachable. Because he did not test the suction, unite before starting anaesthesia.

The monitors are important in measuring all body functions. The percentage of permanent examination is 83.02%, and the percentage of examination sometimes is 15.09%. As for the never check it was very little 1.89%. The monitors are important in measuring all body functions. Our data were shown 83.02% practice permanent examination and sometimes 15.09%.one participating technician signaled the loss of CO2 concentration from the monitor screen. A similar study of AM checking practice publicized that, only one of 40 anaesthetists questioned calibrated an oxygen analyzer [19]. In one case, the non-invasive arterial pressure readings were falsely high, and the patient received a large dose of volatile anaesthetic, while the patient, in reality, was severely hypotensive. This was related to technical failure including leaks from the tubing and cuff [9], as the authors mentioned this problem involved elements of human error.

As our result showed 71.7% always checked the airway instruments, 22.64% sometimes, and the never checking rate was 5.66%. One of the participants mentioned that he had a problem with airway instruments were not fully prepared. Between cases, checks sometimes performed were by 50.94% of technicians, just 34.85% were always checked, and never check was 13.21%. In similar data checking of equipment between cases was performed by 12.5% overall 40 anaesthetizes [19]. In addition, the researcher reported the case of an open CO2 absorber after the service of the machine had been performed between the cases [14]. The anesthesiologist did not check the AM before use in the upcoming case; this caused the unable to ventilate the patient during induction.

 ISBN 978-9959-9703-2-9

Table.3: indicated the result of checking an Anaesthetic machine section (Q12-13).

Result Q 12&13	YES		NO	
	Per cent	Count	Per cent	Count
12. Availability of Checking list in working place	41.51%	22	58.49%	31
13. Technicians facing problems related to AM checking	45.28%	24	54.72%	29

The 12th question asked about the presence of an anaesthetic machine checklist; for daily in your working place, 58.59% of the anaesthesiology technicians do not have a list of the mechanism of examination of the anaesthesia device in their workplace, compared to 41.51% who have a list of the examination mechanism at their place of Working. The next question asked about the problems that anaesthesia technicians had faced during anaesthesia 45.28% of all participants experience problems related to inadequate check of AM before anaesthesia.

Our study revealed that 58.59% of the technicians do not have a checklist of the anaesthesia devices in the workplace, in compare 41.51% who have a list of the examination mechanism at their place of work. The AM check has been included in the World Health Organization's Surgical Safety Checklist. The pre-use AM check is recognized worldwide to ensure the correct functioning of anaesthetic equipment is essential to patient safety [20]. From a total number of participants, 45.28% of all experience problems related to inadequate check of AM before anaesthesia. This demonstrates that the standard of checking anaesthetic equipment before use is poor.

At the end of the survey, we asked the participants who faced problems about the problem they faced. Many problems mentioned by the participants related to inadequate checks. These problems are presented on the following list:

1 .Leak from an oxygen cylinder
2 .Anaesthesia failure
3 .Leaking of sevoflurane in surgical room
4 .Ventilator does not working suddenly
5 .Suction machine is not ready
6 .Leak in the breathing circuit
7 .There is leakage or exhaustion of gases cylinders
8 .Suction machine does not work
9 .Airway instruments were not ready
10 .Empty the sevoflurane vaporizer.
11. The CO2 saturation does not appear on the monitor.

Conclusion

This study is the first to evaluate the AM checking and used instrument, performed by

 ISBN 978-9959-9703-2-9

the anaesthesia technicians in several Libyan institutions with varying participant experience levels. The study's findings, the checking was always proceeding, although some of which stemmed from inadequate checking for AM. Developing a Libyan AM checklist is necessary to be used in all Libyan hospitals, to make the checking procedure more efficient and straightforward.

As limitations for this work, the COVID-19 world pandemic and the small number of participations responses.

Arabic section:

دراسة مقطعية لفحص أجزاء آلة التخدير: دراسة مسحية لفنيي التخدير في ليبيا

سمية امجداً، كوثر أبوكراع ب، إيناس الصيد، مودة الحضيري، هناء الباشا
أقسم التخدير والعناية الفائقة كلية التقنية الطبية / جامعة الزاوية / ليبيا
البريد الالكتروني للمراسلة: K.abuokraa@zu.edu.ly

الملخص:
الخلفية: آلة التخدير (AM) هي واحدة من أهم الأجهزة التي يستخدمها أطباء التخدير، وفهم خصائصها ووظائفها هو عنصر حاسم في ممارسة التخدير. يعد فحص الاستخدام المسبق لضمان الأداء الصحيح لـ AM والمعدات أمرًا ضروريًا لسلامة المرضى. يتم تضمين الفحص في قائمة التحقق من سلامة العمليات الجراحية لمنظمة الصحة العالمية. أهداف هذه الدراسة: لتقييم ما إذا كان الفنيين يقومون بفحص كافي لألة التخدير أم لا. بالإضافة إلى، إذا كان هناك أي مشاكل تم الإبلاغ عنها بسبب عدم كفاءة الفحص الروتيني لألة التخدير. المنهجية المتبعة في هذه الدراسة: استخدمت الدراسة المقطعية الوصفية الاستبيان عبر الإنترنت. وكان تطبيق Google Formsهو الخيار الأفضل المتاح بسبب جائحة كورونا Covid-19.كانت معظم الأسئلة في هذه الدراسة عبارة عن خيارات متعددة وبعضها كان إجابات قصيرة. النتائج: إجمالي الردود الواردة 53 من 18 مستشفى مختلفًا، وكان معظمها من مستشفى زليتن مع 13 ردًا. كانت غالبية سنوات خبرة المشاركين أقل من خمس سنوات بنسبة 60.38٪ (العدد = 32) المشاركون أظهرت معظم الإجابات حضورًا متوسطًا من التدقيق المستمر. كان أعلى معدل فحص دائم لأجهزة التنفس الصناعي بنسبة 81.12٪ (العدد = 43) من إجمالي عدد المشاركين، 45.28٪ (العدد = 24) يعانون من مشاكل تتعلق بعدم كفاية فحص AM قبل التخدير. الخلاصة: توضح نتائج هذه الدراسة أن معيار فحص معدات التخدير قبل الاستخدام غير مناسب حيث أبلغ 24 منهم عن مشاكل تتعلق بفحص ضعيف.

الكلمات المفتاحية :(آلة التخدير، الأداة، سلامة المريض، فني التخدير، قائمة المراجعة، وطبيب التخدير).

Abbreviations and Acronyms

(AM) ANESTHEISA MACHINE

(ASA) American Association of Anaesthesiology

(AAGBI) Association of Anaesthetists of Great Britain and Ireland

Acknowledgment

We would like to convey our gratitude to everyone who assisted us with this study, especially the anesthesiologists and hospital personnel who completed our questionnaire; without their involvement, this work would not have been possible.

References

[1] BUTTERWORTH J. F., MACKEY D. C., WASNICK J. D. Morgan & Mikhail's Clinical Anesthesiology. LANGE medical book,2013 , PP. 43-86.

[2]Romero-Ávilaa P., Márquez-Espinósb C., & Afonsob J. R. C. (2021) Historical development of the anaesthetic machine: from Morton to the integration of the mechanical ventilator. Brazilian Journal of

 ISBN 978-9959-9703-2-9

Anesthesiology 71; 148-161

[3] Romero-Ávila, Pablo, Carlos Márquez-Espinós, and Juan Rafael Cabrera-Afonso. "Historia de la ventilación mecánica. De la Antigüedad a Copenhague 1952." Revista médica de Chile 148.6 (2020): 822-830.

[4] Al Suhaibani M, Al Malki A, Al Dosary S, Al Barmawi H, Pogoku M. Pre-use anaesthesia machine check; certified anaesthesia technician based quality improvement audit. Anaesthesia, Essays and Researches. 2014 Sep;8(3):354.

[5] Goneppanavar U, Prabhu M. Anaesthesia machine: checklist, hazards, scavenging. Indian Journal of anaesthesia. 2013 Sep;57(5):533.

[6] Mondal H, Mondal S, Ghosal T, Mondal S. Using Google forms for medical survey: A technical note. Int J Clin Exp Physiol. 2018;5 (4):216-8.

[7] Caplan RA, Vistica MF, Posner KL, Cheney FW. Adverse anaesthetic outcomes arising from gas delivery equipment: a closed claims analysis. The Journal of the American Society of Anesthesiologists. 1997 Oct 1;87(4):741-8.

[8] Bothner U, Georgieff M, Schwilk B. The impact of minor perioperative anaesthesia-related incidents, events, and complications on postanesthesia care unit utilization. Anesthesia & Analgesia. 1999 Aug 1;89(2):506-13.

[9] Fasting S, Gisvold SE. Serious intraoperative problems--a five-year review of 83,844 anaesthetics. Canadian Journal of Anesthesia. 2002 Jun 1;49(6):545.

[10] Vetter AG. Preparing for Total Power Failure in the Operating Room. AANA journal. 2019 Aug 1;87(4).

[11] Yasny J, Soffer R. A case of a power failure in the operating room. Anesthesia Progress. 2005;52(2):65-9.

[12] Aqil M, Hussain A. Safety concerns start well before the anaesthesia machine. Anaesth Pain & Intensive Care. 2011 Oct;15(2):123-5.

[13] Mayor AH, Eaton JM. Anaesthetic machine hecking practices: a survey. Anaesthesia. 1992 Oct;47 (10):866-8.

[14] Wiener-Kronish JP, Cohen NH, Leslie K, Gropper MA, Eriksson LI, Fleisher LA, editors. Miller's anaesthesia, 2-volume set E-book. Elsevier Health Sciences; 2019 Oct 7.

[15] Ianchulev SA, Comunale ME. To do or not to do a production check-up of the anaesthesia machine. Anesthesia & Analgesia. 2005 Sep 1;101(3):774-6.

[16] Ong BC, bin Katijo J, Tan BL, Lee CC, Chan YW. Acute failure of oxygen delivery. The Journal of the American Society of Anesthesiologists. 2001 Oct 1;95(4):1038-9.

[17] JJ, Polania Gutierrez, and K. R. Rocuts. "Anesthesia Vaporizers." (2020). [online]. Available at:https://www.researchgate.net/publication/342862564

[18] Shahriari A, Rahmati J. Malfunction of an Anesthesia Machine with Decoupling Valve. Archives of Anesthesiology and Critical Care. 2020 Aug 18;6(3):146-7.

[19] Mayor AH, Eaton JM. Anaesthetic machine checking practices: a survey. Anaesthesia. 1992 Oct; 47(10):866-8.

[20] Association of Anaesthetists of Great Britain and Ireland (AAGBI), Hartle A, Anderson E, et al. Checking anaesthetic equipment 2012: association of anaesthetists of Great Britain and Ireland.

 ISBN 978-9959-9703-2-9

Anaesthesia. 2012; 67(6):660-668.
doi:10.1111/j.1365-2044.2012.07163.x

 ISBN 978-9959-9703-2-9

المؤتمر الدولي الثاني للعلوم والهندسة
2nd International Conference on Science and Engineering
ICSE 2023
Faculty of Engineering - University of Bani Waleed
Bani Waleed, Libya

Paper Code: ICSE-036

PREVALENCE OF PREMATURE LOSS OF PRIMARY TEETH AMONG SCHOOL-CHILDREN AGED (6-10 YEARS OLD) IN THE LIBYAN CITY OF BANI WALEED AND ASSESSMENT OF PARENTAL KNOWLEDGE AND AWARENESS TOWARDS SPACE MAINTAINER

Waed Alfaytouri Almaqroush[a], Buthaina Abdalsalam khamkham[b]; Alaa salah Aldin Ali[c]
Department Dental Technology, Faculty of Medical Technology, Bani Waleed University, Libya
Waed Alfaytouri Almaqroush, Dental technician, Bani Waleed, Libya.
E-mail: waed01af@gmail.com

Abstract: The premature loss of primary teeth is one of the most common dental problems affecting the growth and development of children's teeth. It is often caused by dental caries. Premature loss of the primary teeth results in a loss in the length of dental arch and leads to malocclusion. Space Maintainers play an important role in managing the spaces created by the early loss of primary teeth. The use of space maintainers depends on parent's awareness and knowledge towards space maintainers. The current study was goaled to define prevalence of premature loss of primary teeth among schoolchildren (6-10 years old) in the Libyan city of Bani Waleed, as well as, evaluating the awareness level of their parents toward space maintainers. A descriptive cross-sectional questionnaire-based study was conducted. The data were analyzed and summarized statistically using SPSS version 26.0. Chi-square test was carried out to detect correlation between variables. The results revealed that (55.1%) of the children suffered of premature loss of their teeth with no significant variation among the genders (P>0.05). The highest prevalence (16.4%) was recorded at the age of 7 years old. (70.5%) caused by dental caries. (82.40%) of parent's respondents that they don't know what is (SM) appliances and when used. This study demonstrated that, prevalence of premature loss of primary teeth among school-children was high, and the Knowledge of space maintainers among Bani Waleed parents is very less. So, dentists need to create awareness about space maintenance of primary teeth and preventive orthodontic.

Keywords: Primary teeth, Premature loss of teeth, Malocclusion, Preventive orthodontic, Space maintainer

Introduction

The primary dentition plays an important functional, morphological and psychosocial role in the dental growth and development of children. In addition to providing appropriate conditions for the establishment of normal occlusion, esthetics, mastication and speech. Furthermore, Maintenance of the integrity of the primary dental arch has a strong influence on the development and eruption of the permanent teeth, preserving the length of the

 ISBN 978-9959-9703-2-9

dental arch and conserving the space necessary for the eruption of the permanent teeth [1]. Exfoliation of primary teeth and eruption of permanent teeth is a normal physiological process [2]. Premature loss of primary teeth leads to disruption in this physiological process of exfoliation [3]. Furthermore, one of the most important goals of pediatric dentistry is maintain the primary teeth till they are naturally exfoliated [4]. Premature loss of teeth is defined as the loss of a primary tooth before the time of natural exfoliated [4- 5]. One of the most common dental problems affecting children is premature loss of primary teeth that leads to negative consequences in both dentition and malocclusion [6]. Parents are in charge of their children's oral hygiene habits and regular dental visits in the 1st year of infancy [7]. Inappropriate oral hygiene is a key behavioral risk factor for premature loss of primary teeth [4], [8]. Many parents think that losing primary teeth prematurely is unimportance. They believe that the losing of primary tooth is not significant as losing of the permanent tooth. Primary teeth work as natural space maintainer for secondary teeth [9]. Premature loss of primary teeth may occur by local or systemic factors. Local causes include dental caries (Fig. 1), which is the most common cause, dental trauma, periodontal diseases and abnormal root resorption [10- 12].

Fig. 1: Severe dental caries of the 1st and 2nd lower primary molars, intraoral arch length reduced (*International Journal of Oral Science*).

There are systemic diseases, such as leukemia, diabetes, and hyperthyroidism, can affect the oral cavity and lead to subject to exfoliation of the primary teeth. Premature loss of primary teeth leads to shifting of adjacent teeth into the space of tooth loss created making abnormal axial inclination spacing between teeth and shifting of dental midline [13], which can cause crowding along with short arch length. [3].

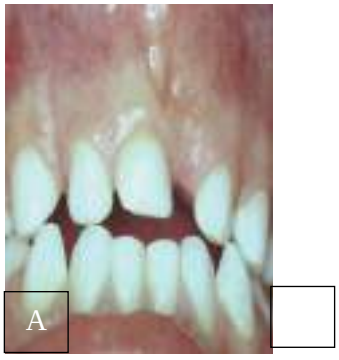

 ISBN 978-9959-9703-2-9

Fig. 2: (A). Clinical photograph and (B). Radiograph showing the migration of primary teeth into space after early loss of primary upper left central incisor [14].

This deters the normal eruption and deviation of their permanent teeth from pathways guiding to malocclusion [13]. In form of dental crowding, ectopic eruption, tooth rotation, excessive overjet, crossbite, excessive overbite, impaction of permanent teeth (Fig. 3), supra-eruption of opposing teeth and unfavourable molar relationships [3] (Fig. 4).

Fig. 3: Impaction the permanent upper central incisors after loss by dental trauma of all 4 primary upper incisors and canine [14].

Fig. 4: The migration of adjacent teeth and decrease of space required for the eruption of permanent (*Collection of the Department of Pediatric Dentistry*).

Premature teeth loss in children should be treated as soon as possible to prevent the development of malocclusion [6]. Early orthodontic treatments are often in the beginning of developing dentition help to improve favorable developmental changes [15]. Space maintainer is the safest way to maintain space after premature loss of tooth and prevent malocclusion. (SM) is a fixed or removable appliance used to maintain the length of the dental arch and the relationship between teeth after premature loss or extraction of primary teeth. [16] (Fig. 5).

 ISBN 978-9959-9703-2-9

Fig. 5: Unilateral band and loop space maintainer [17].

It will eliminate or decrease the severity of a developing malocclusion, the complexity of treatment, and overall treatment time and cost as complicated occlusions are more expensive to correct. [18- 19]. Dentists should be taken early management after premature loss of primary teeth including preventive and corrective measures to prevent malocclusion in future [20- 21]. The use of preventive orthodontics depends on parents' knowledge and awareness of space maintenance. The Parents usually obtain information about immunizations, nutrition and diet, prevention of injury and accident at the hospital during their child's regular medical visits for checkups, but in the case of oral hygiene, the position is completely different, and the dentist is visited in the later stages of caries progression and malocclusion which increases the possibility of losing teeth early. Most of the time, the parents responsible for the oral care of children believe or feel that since primary teeth will be replaced in any way, it is not worth their while to spend time/money on providing good oral health to children. Even in advanced countries, most parents still take their children to the dentist for therapeutic and not for preventive treatments [22].

This title is important in terms of determining such problem which affects dental growth and development of the child's teeth and the extent of its prevalence, spreading knowledge and awareness among parents of preventive orthodontic treatment from the consequences of early loss of primary teeth, which is “space maintainer” appliance.

AlMeedani LA. *et al.* 2020, who studied Prevalence of premature loss of primary teeth among children in Dammam city and parents’ awareness toward space maintainers. The purpose of this study was to assess the prevalence of early loss of primary teeth among children in the Saudia city of Dammam and to evaluate parent’s attitudes toward space maintainer appliance. Used to examine decay-missing-filled index and premature loss of primary teeth. Questionnaires were distributed to the parents of selected children to explore their demographic data and their knowledge toward space maintainers. The study revealed a high prevalence of premature loss of primary teeth among children in Saudi

 ISBN 978-9959-9703-2-9

Arabia. parents were unaware towards space maintainer, its used, benefits and maintenance.

According to Bamashmoos KA. *et al.* 2020, who studied Prevalence of Premature Loss of Primary Teeth at the Age of 6-10 Years in Sana'a City, Yemen. The goal of study to define the prevalence of premature loss of primary teeth among children (6-10 years) in Sana'a city, Yemen. Cross-sectional observational research involved 1091 student (6-10 years). All clinical examinations were carried out under natural light by the first author, an experienced examiner. The prevalence of premature loss in current study is comparable to that of developing nations, the rate was low at 10 years for children, but the rate increased at 6,7 and 9 years.

According to Ali A. *et al.* 2022, Assessment of Parental Knowledge towards Space Maintainer as an Essential Intervention after Premature Extraction of Primary Teeth. This study evaluated parents' knowledge towards space maintainers as preventive measures following premature loss of primary teeth. A descriptive study was conducted using a cross-sectional questionnaire. The knowledge of parents about space maintainers was (49.8%), which is deemed inadequate. It was considered essential to rise knowledge among parents about space maintainers as preventive treatment after premature loss of primary teeth.

To the knowledge of the researchers, this study is the first was conducted in the city of Bani Waleed to define extent prevalence of premature loss of primary teeth among children (6-10 years old), and assessment of parent's knowledge and awareness towards space maintainer as an essential intervention after premature loss of primary teeth in Bani Waleed as this is an important in preventive treatment planning and awareness so, necessary spread knowledge this problem between the medical society and community in general.

Question of the research: How is the level of prevalence of premature loss of primary teeth among school-children (6-10 years old) and awareness of Bani Waleed their parents towards space maintainers in Bani Waleed city?

Hypothesis: The prevalence of premature loss of primary teeth among school-children (6-10 years old) is high and the level of awareness of Bani Waleed parents toward space maintainer is low.

 ISBN 978-9959-9703-2-9

1. Material and methods

2.1. Study design: A cross-sectional questionnaire based descriptive-analytical study was carried out.

2.2. Study population: The target population included 1273 students of both genders (6 to 10) years old, as well as their parents. The students were selected from 30 elementary (private and public) schools are located in five schools' clusters in the Bani Waleed city. The sample size was determined using (Krejcie and Morgan, 1970) Table, the total number of students in the Bani Waleed city is 9000, based on the ministry of education; the sample size enters table N=9000 is 368 sample size. From the overall target population, 1273 participants were selected to provide significant results.

2.3. Sampling technique: multistage multistage sample method which the first stage using sample cluster technique, the city's schools were divided into five clusters. The second stage was to ensure that all private and public schools in each cluster were included in the study, thus we randomly picked 18 public schools and 12 private schools, representing almost (36%) of the total number of schools based on Education 2022. The third stage was to ensure that all classes of children aged from 6 to 10 years old were involved in the study in all randomly selected schools. Then, at random, we took one class from each level. Finally, we distributed by hand to each class as a whole; so that we can attain the sample size requirement. After completing the questionnaire by parents, we returned the next day to receive it from the students.

2.4. Study duration: This cross-sectional study was conducted from January 31st, 2023 to May 15th, 2023.

2.5. Details of the Questionnaire:

Table 1: Distribution of study participants

		Frequency	Percent (%)
Gender	Male	685	53.8%
	Female	588	46.2%
Age group	20-30	196	15.4%
	31–45	765	60.1%
	46 and above	312	24.5%
Education level	Intermediate	182	14.3%
	Secondary	182	14.3%
	University	909	71.4%
	Total	1273	100%

2.6. The questionnaire designed so that the questions fall into four categories. The

ISBN 978-9959-9703-2-9

first section gathered sociodemographic data of the parents: Gender, age, educational level. The second section gathered sociodemographic data of the child included: Gender, age. The three section surveyed parents' knowledge of oral health; The third section surveyed parents' knowledge and awareness toward space maintainers.

2.7. Statistical analysis: The data were analyzed and summarized statistically using SPSS version (26.0). Chi-square test was carried out to detect correlation between variables. A Significant level test was ($p<0.05$). Data from the questionnaires were analyzed using the following: Table, Frequencies, Percentages.

3. Results: A total of 1273 questionnaires were gathered in this study; (94.3%) were answered completely. The results of Demographic data show 685 (53.8%) male and 588 (46.2%) female. According to survey, the majority of the participants were in the age range of 31–45 years 765 (60.1%) and 909 (71.4%) had completed university studies as their highest education (Table1).

The result revealed that of the 1273 children consisted of 612 male (48.1%) and 661 female (51.9%) student. The majority of the students were in the age 7 years 401 (31.5%) while the minority of the students were in the age 10 years 31 (2.4%) (Table 2).

		Frequency	Percent (%)
Gender	Male	612	48.1%
	Female	661	51.9%
Age	6 years	184	14.5%
	7 years	401	31.5%
	8 years	336	26.4%
	9 years	321	25.2%
	10 years	31	2.4%
	Total	1273	100%

When the parents were asked about their oral health knowledge, high parentage of parents 691 (54.3%) believe that primary teeth are not important (Fig. 6).

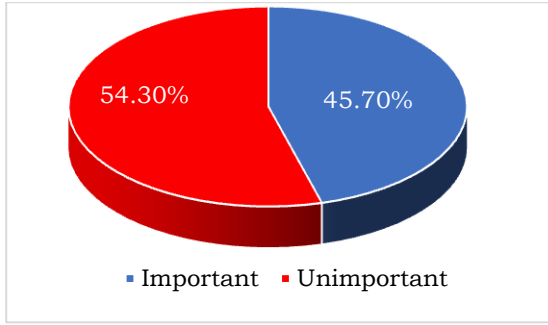

Fig. 6: Importance of primary teeth.

Through the previous values, the level of awareness of the importance of teeth is low. The parents' lack awareness of the teeth importance and maintenance until the time of natural exfoliation. It is one of the reasons that affect the health of primary teeth and increases

ISBN 978-9959-9703-2-9

Table 2: Child's data including gender and age.

the possibility of early loss, and these results are not harmony with previous studies [23].

The parents (47.2%) answered that the child should visit the dentist only child has pain,

and (62.3%) of parents indicated that their children had visited the dentist (Fig. 7.)

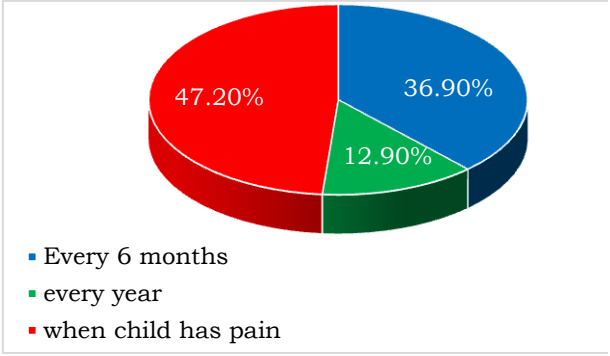

Fig. 7: Frequency of dental visit.

The parents didn't agree on the child's need of visit to the dentist in every 6 months and this depicts their level of awareness about how much importance they do give to their child's oral health. This study results are not supportive of previously published literature [24].

When asked the parents a question regarding if their children suffects premature loss of primary teeth (55.1%) answered their children had premature loss of their teeth (Table 3 and Fig. 8).

		Male	Female	Total
Yes	N	334	367	701
	%	26.2%	28.8%	55.1%
No	N	278	294	572
	%	21.8%	23.1%	44.9%
	N	612	661	1273

Table 3: Distribution of children's gender according to early loss.

The (28.8%) were female and (26.2%) were male, a significant was (p>0.05) this indicates that there is no difference between males and females in premature loss of their teeth.

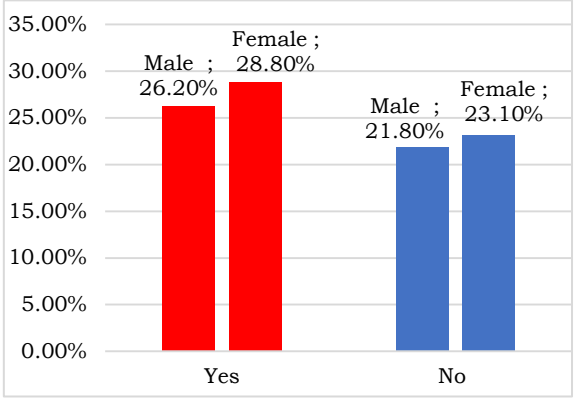

Fig. 8: Prevalence of premature loss of primary among gender.

Compared to other studies in some cities: (Dammam) Saudi Arabia, (Melmaruvathur, Tamil Nadu) India, (Sana'a) Yemen, and (Thamar) Yemen. early loss of primary teeth

ISBN 978-9959-9703-2-9

was (20%), (20.8%), (26%) and (40.54%) respectively and this study higher than these studies [6], [25- 27]. This difference may be due to the higher rate of dental caries in primary teeth. The rise in the rate of early primary teeth loss could be attributed to dentists and parents assuming that preventing and treating a primary tooth is unnecessary because the teeth will eventually be lost or extracted.

According to several socio demographic variables, there was no significant difference in early primary teeth loss between males and females.

This illustrates that premature loss is not related to the sex of the child, but can be due poor oral hygiene.

The prevalence of early loss was significantly reduced($p>0.05$) at 10 years (1.3%), but the rate increased non-significantly to (13.5%), (14.7%), and (16.4%) in the schoolchildren at aged 8, 9 and 7 years, respectively (Fig. 9).

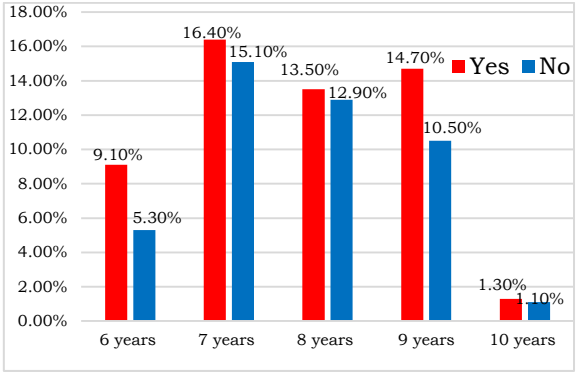

Fig. 9: The prevalence of premature loss of primary according to age.

The children had premature loss their teeth caused by (70.5%) dental caries, (12.7%) dental trauma and (16.8%) caused by any other reason (Fig. 10).

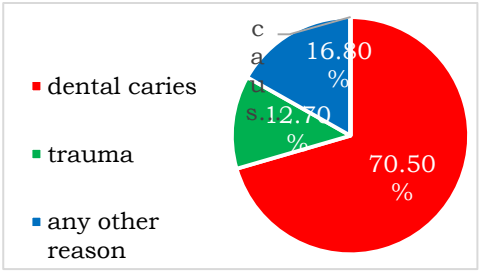

Fig. 10: The causes distributed of the premature loss of primary teeth.

The higher percentage was due to dental caries, which is the most common cause of early tooth loss, and this may be due to poor oral health. Some parents take their children to the dentist in the late stages of decay, which leads to early tooth loss. On the other hand,

ISBN 978-9959-9703-2-9

some dentists prefer tooth extraction rather than treatment.

The (36.6%) of the children lost only one tooth, (36.9%) were lost two teeth and (24.8%) lost three or more teeth (Fig. 5).

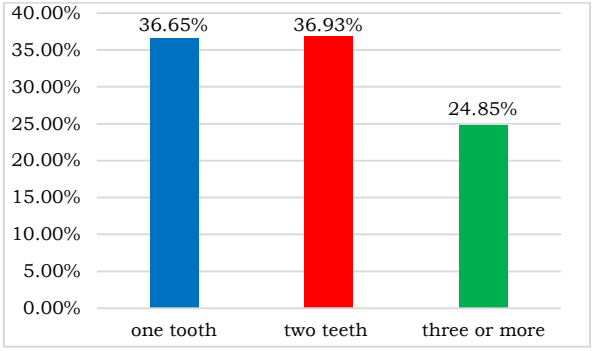

Fig. 11: Number teeth lost by premature loss.

The highest percentage (57.3%) of parents believe that premature loss of primary teeth will not harm the permanent teeth (Fig. 12).

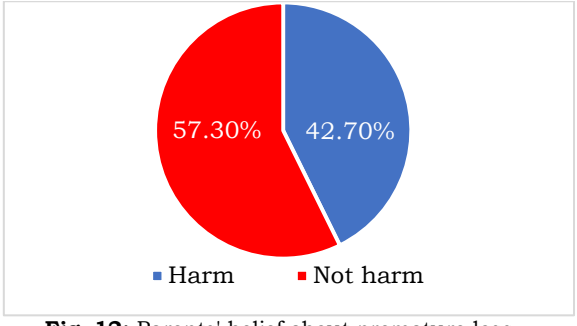

Fig. 12: Parents' belief about premature loss.

This belief indicates that the parents are not aware of the consequences of early loss and dental problems in both dentition that will occur in the future. Their awareness is limited that the primary teeth will be replaced by the permanent teeth anyway.

Regarding parents' knowledge about space maintainers appliances, (82.40%) of parent's respondents that they don't know what is (SM) appliances and when used. The majority of the male parents were don't know what is (SM) (84.1%) and the female parents (80.4%), a significant was (p=0.090) this indicates that there is no difference between males and females in knowledge about space maintainer. No difference between age group of parents in knowledge about (SM) a significant was (P=0.485), also between educational level a significant was (P=0.334). (Table 4 and Fig. 13).

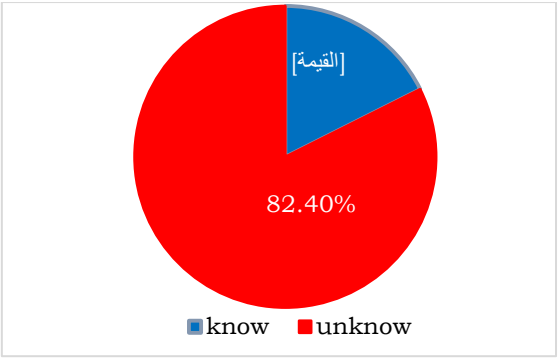

Fig. 13: Distribution of the percentage of parent's knowledge about (SM).

ISBN 978-9959-9703-2-9

Table 4: The demographic data of the parents' distribution according knowledge about

		Yes	No	Total	Chi-Square	P value
Male	N	109	576	685	2.900	0.090
	%	15.9%	84.1%	100.0%		
Female	N	115	473	588		
	%	19.6%	80.4%	100.0%		
20-30	N	37	159	196	1.448	0.485
	%	18.9%	81.1%	100.0%		
31-45	N	139	626	765		
	%	18.2%	81.8%	100.0%		
<46	N	48	264	312		
	%	15.4%	84.6%	100.0%		
Intermediat	N	28	154	182	2.192	0.334
	%	15.4%	84.6%	100.0%		
Secondary	N	27	155	182		
	%	14.8%	85.2%	100.0%		
University	N	169	740	909		
	%	18.6%	81.4%	100.0%		

Most of the parents (82.8%) were unaware of the fact that there are appliances available for their children's h as an early treatment. This is in accordance with study conducted in Al-Kharj, KSA. by Alduraihim HS *et al.* [22]. Then compared to other studies conducted in some cities: Riyadh, Saudi Arabia, Parents' awareness toward space maintainers was (49.8%) and our study lower than this study [28].

When asked parents who do they know (3.6%) of parents know space maintainer from dentist, (6%) form Family and relatives, and (8%) know appliance from social media. (95.8%) of the parents answered the dentist did not explain how it is important to use a space maintainer after premature loss of teeth. The percentage of parents who treated their children with space maintainer is (2.20%).

Note: From the previous ratios, it was found that parents' knowledge of the space maintainer is very low, as they answered the rest of the questions related to the device.

The (15.7%) of the parents replied "Yes" a child with a space maintainer need regular visits to

 ISBN 978-9959-9703-2-9

the dentist, and (1.5%) replied "No" and about (82.8%) were unaware.

When asked the parents a question regarding if they know what should you do when the permanent teeth are erupting while the child still wearing the space maintainer, 162 (12.7%) answered I will immediately go to the dentist, 39 (3.1%) answered wait for the next visit 18 (1.4%) answered I don't care and 1054 (82.8%) answered they don't know. And we asked what should you do if (SM) breaks if they know 186 (14.6%) of the parents answered they will immediately go to the dentist, 28 (2.2%) answered at any time and 1056 (83.2%) answered they don't know.

When asked the parents a question regarding if they know which type of food your child should be avoiding while wearing the space maintainer appliance, 1086 (85.3%) parents answered I don't know and 47 (3.7%) parents mentioned Vegetables and fruit, 21 (1.6%) parents answered soft drinks, 53 (4.2%) of the parents answered Candies and 66 (5.2%) mentioned all above. last question we asked the parents if they know when the space maintainer appliance should be removed and 1139 (89.50%) of them answered that they don't know and 134 (10.5%) parents answered yes.

The level of unawareness and knowledge about the space maintainers results in decreased response rates about the last few queries as the types of food that should be avoided when having space maintainers and when does the dentist remove of appliance *et al.*

4. Conclusion

The prevalence of premature loss of primary teeth was high (55.1%) in the Bani Waleed, Libya. According to age, the highest prevalence was registered at 7 (16.4%) years followed by 9 (14.7%) years and 8 (13.5%). The premature loss was more in females (28.8%) than males (26.2%). The majority of the children had two missing teeth (36.9%). Dental caries was the main reason for early loss of primary teeth (70.5%). The parents in Bani-Waleed City were not aware of primary teeth importance and maintenance. Most parents (82.8%) in Bani Waleed city were unknow space maintainer and when used. The higher educated respondents were more knowledgeable than the lower educated.

This indicates the need to raise awareness of space maintainers among the general population.

As a result, it is essential to increase oral health awareness among children and their parents in order to make them understand the important of primary teeth and maintenance of oral health. To reduce the prevalence of dental caries and the early loss of primary teeth,

 ISBN 978-9959-9703-2-9

parents must be urged to take responsibility for cleaning their children's teeth. It is strongly advised that educational lectures and workshops be established in order to promote knowledge of kids about hygiene of oral cavity amongst fathers and mothers. To pique parents' interest and drive, oral health practitioners must be taught in new effective learning methodologies. Parents should be encouraged to bring their children to the dental clinic for a dental check-up every 6 months. Parents of children with early loss of primary teeth should be advised to bring their children to the dental clinic to have space maintainers and Dentists need to explain to parents the importance of primary teeth and must raise knowledge among parents towards (SMs) and their longevity during regular dental visits in order to keep the integrity and minimize occlusal discrepancies of dental arches.

We suggest an increased awareness level of space maintainers is need in the parents of Bani Waleed city. Further replication of this study in different settings, and sample populations is also needed in the future.

References:

1. Moyers RE. (1991), Ortodontia. 4th ed. Rio de Janeiro: Guanabara Koogan.
2. Rao, AK., Sarkar, S. (1999), Changes in arch length following premature loss of deciduous molars. J Indian Soc Pedo Prev Dent. 17:29-32.
3. Brothwell, DJ. (1997), Guidelines on the use of space maintainers following premature loss of primary teeth. J Can Dent Assoc. 63:753-766.
4. Al-Shahrani N, Al-Amri A, Hegazi F, Al-Rowis K, Al-Madani A, Hassan KS. (2015), The prevalence of premature loss of primary teeth and its impact on malocclusion in the Eastern Province of Saudi Arabia. Acta odontological Scand. 73(7):544-549. https://doi.org/10.3109/00016357.2014.939709.
5. Cavalcanti AL, Alencar CRBD, Bezerra P, Granville-Garcia AF. (2008), Prevalence of early loss of primary molars in school children in Campina Grande, Brazil. Pakistan Oral Dent J., 28(1):113.
6. AlMeedani LA, Al-Ghanim HZ, Al-Sahwan NG, AlMeedani SA. (2020), Prevalence of premature loss of primary teeth among children in Dammam city and parents' awareness toward space maintainers. Saudi J Oral Sci., 7:85-9. http://dx.doi.org/10.4103/sjos.SJOralSci_9_19.
7. Nagarajappa R, Kakatkar G, Sharda AJ, Asawa K, Ramesh G, Sandesh N. (2013), Infant oral health: Knowledge, attitude and practices of parents in Udaipur, India. Dent Res J (Isfahan). 10:659-65.
8. Kumari NR, Sheela S, Sarada PN. (2006), Knowledge and attitude on infant oral

 ISBN 978-9959-9703-2-9

health among graduating medical students in Kerala. J Indian Soc Pedod Prev Dent., 24:173-6. https://doi.org/10.4103/0970-4388.28072.

9. Alshehri A, Nasim V. (2015), Infant oral health care knowledge and awareness among parents in Abha city of Aseer Region, Saudi Arabia. Saudi J Dent Res 6:98-101. https://doi.org/10.1016/j.sjdr.2015.01.001.
10. Borum MK, Andreasen JO. (1998), Sequelae of trauma to primary maxillary incisors. I. Complications in the primary dentition. Endodontics Dent Traumatol 14(1): 31–44. https://doi.org/10.1111/j.1600-9657.1998.tb00806.x.
11. Cardoso L, Zembruski C, Femandes DS, Boff IPV, Pessin V. (2005), Evaluation of prevalence of malocclusion in relation to premature loss of primary teeth. Pesq Bras Odontoped Clin Integr. 5:17-2.
12. Almedida Heilborn JC, Küchler EC, Fidalgo DS, *et al.* (2011), Early primary tooth loss: prevalence, consequence and treatment. Int J Dent 10(3):126-130.
13. Khanna P, Sunda S, Mittal S. (2015), "Keep My Space"- A Review Article. International Journal of Oral Health Dentistry, Jan-March. 1(1):11-15.
14. Gideon H, Howard L. (2014), Premature loss of primary anterior teeth due to trauma– potential short- and long-term sequelae. Dental Traumatology. 30: 100–106. https://doi.org/10.1111/edt.12081.
15. Peter Schopf. (2003), Indication for and frequency of Early Orthodontic Therapy or Interceptive Measures. Journal of Orofacial Orthopedics. 649(3):186-200. https://doi.org/10.1007/s00056-003-0234-6.
16. Green J. (2015), Mind the gap: Overview of space maintaining appliances. Dent Nurs., 11:24-7. http://dx.doi.org/10.12968/denn.2015.11.1.24.
17. Marwah, Nikhil. (2019), Textbook of Pediatric Dentistry, New Delhi | London | Panama: Jaypee Brothers Medical Publishers (P) Ltd.
18. Wo ng ML, Che Fatimah Awang, Ng LK, Norlian D,Rashidah Dato Burhanudin, Gere MJ. (2004), Role of interceptive orthodontics in early mixed dentition. Singapore Dent J., 26:10-4.
19. Keski-Nisula K, Hernesniemi R, Heiskanen M, Keski-Nisula L,Varrela J. (2008), Orthodontic intervention in the early mixed dentition: A prospective, controlled study on the effects of the eruption guidance appliance. Am J Orthod Dentofacial Orthop, 133:254-60. https://doi.org/10.1016/j.ajodo.2006.05.039.
20. Heilborn J, Kuchler E, Fidalgo T, Antunes L, Costa M. (2011), Early primary tooth loss: Prevalence, consequence, and treatment. Int J Dent., 10:10-3.
21. Linjawi AI, Alajlan SA, Bahammam HA, Alabbadi AM, Bahammam MA. (2016),

 ISBN 978-9959-9703-2-9

Space Maintainers: Knowledge and Awareness among Saudi Adult Population. J Int Oral Health. 8:733-8.

22. Alduraihim HS, Alsulami SR, Alotaibi SZ, El-Patal MA, Gowdar IM, Chandrappa PN. (2020), Assessment of Saudi parent's awareness towards space maintainers at Alkharj city: A cross-sectional study. J Family Med Prim Care. 9:1608-13. https://doi.org/10.4103%2Fjfmpc.jfmpc_1146_19.
23. Shamsaddin H, Shojaeipour R, Haghighat ST, Pouraskari Z, Sayadizadeh M. (2019), Assessing the awareness of parents and satisfaction of children with intraoral space maintainers. J Islam Dent Assoc Iran. 31:33-39.
24. Haneen A. (2019), Parents knowledge, behavior and attitude regarding their children's oral health and the consequences of premature loss of primary teeth. EC Dental Science. 18:1862-1871. https://doi.org/10.4103/jisppd.jisppd_257_18.
25. Selvabalaji A, Vasanthakumari A, Ishwarya M, Preethi Archana S, Ekambareswaran K, Swetha Rk. (2022), Prevalence of Early Primary Teeth Loss in 5-9-year-old Schoolchildren in and around Melmaruvathur: A Cross-sectional Study, J Contemp Dent Pract., 23(10):1004-1007. https://doi.org/10.5005/jp-journals-10024-3403.
26. Bamashmoosm KAO, Alhasani AH, Al-Akwa AAY, Zabara AQMQ, Al-Shamahy HA, Al-deen HMS, Al-labani MA. (2020), Prevalence of premature loss of primary teeth at the age of 6-10 years in Sana'a city, Yemen. Universal Journal of Pharmaceutical Research. 5(4):42-46. https://doi.org/10.22270/ujpr.v5i4.439.
27. Murshid S, Al-Labani M, Aldhorae K, Rodis O. (2016), Prevalence of prematurely lost primary teeth in 5-10-year-old children in Thamar city, Yemen: A cross-sectional study. J Int Soc Prev Comm Dent., 6(8):S126–S130. https://doi.org/10.4103/2231-0762.189739.
28. Amel Ali, Mamata Hebbal, Nada Aldakheel, Norah Al Ghamdi, Elzahraa Eldwakhly. (2022), Assessment of Parental Knowledge towards Space Maintainer as an Essential Intervention after Premature Extraction of Primary Teeth. Healthcare. 10, 1057. https://doi.org/10.3390/healthcare10061057.

Financial support and sponsorship

Self-sponsored.

Conflicts of interest

There are no conflicts of interest.

Acknowledgment

All thanks and appreciation to everyone who helped and supported us. Special thanks to Dr. Salah Al deen Salem Abolobeda and the statistician Mr. Hamza Ali Jaeda.

 ISBN 978-9959-9703-2-9

المؤتمر الدولي الثاني للعلوم والهندسة
2nd International Conference on Science and Engineering
ICSE 2023
Faculty of Engineering - University of Bani Waleed
Bani Waleed, Libya

Paper Code: ICSE-054

INVESTIGATION ON LEVEL OF PRACTICE AND ATTITUDE OF DENTISTS TOWARD SPACE MAINTAINERS AS AN ESSENTIAL INTERVENTION FOR PREMATURE LOSS OR EXTRACTION OF PRIMARY TEETH (A FIELD STUDY IN BANI WALEED, LIBYA)

Buthaina Abdalsalam khamkham[1], Waed Alfaytouri Almaqroush[2], Alaa SalahAldin Ali[3]
Department Of Dental Technology, Faculty of Medical Technology, Bani Waleed University, Libya
Corresponding author: Buthaina Abdalsalam Khamkham[1], Dental Technicon, Bani Waleed, Libya.
Waed Alfaytouri Almaqroush[2], Dental Technicon, Bani Waleed, Libya.
Alaa SalahAldin Ali[3], Dental Technicon, Bani Waleed, Libya
E-mail: Buthainaabdalsalam155@gmail.com[1]
waed01af@gmail.com[2]
alafoudas2001@gmail.com[3]

Abstract: Premature loss of primary teeth is one of the most frequent issues affecting children's dental growth and development. The premature loss of primary teeth causes the migration of adjacent teeth into the lost space and prevents permanent teeth from erupting. This leads to a number of dental discrepancies, including malocclusion and loss of the dental arch, that require early preventive measures. The use of space maintainers appliances through safe yet is one of the most popular preventative methods, but it requires proper knowledge and practical expertise to produce effective therapy results. Therefore, this study aimed to determine the level of practice and attitude among dentists in Bani Waleed, Libya, about the possibility of using space maintainers and their prevalence as an essential intervention for premature loss or extraction of primary teeth. A descriptive, cross-sectional, questionnaire-based study was distributed among dentists. Statistical Package for the Social Sciences (SPSS) was used to analyze the filled-out questionnaires (IBM, NY, USA, Version 26.0). The results revealed that (69.1%) did not utilize space maintainers. The majority of the sample (71%) uses Band and loop space maintainers. Cost (36.4%) was the major reason for not using space maintainers, followed by parental refusal (25.4%), (21.9%) claimed that patients aren't compliant with follow-up, and (16.3%) of them pointed to time-consuming. From this, It can be concluded that numerous dentists don't use space maintainers as an essential intervention to avoid malocclusion when there is premature loss of the primary teeth. However, Significant numbers of dentists place space maintainers one week after tooth extraction.

Keywords: Primary teeth, premature loss, preventive orthodontic, space maintainers

Introduction

 ISBN 978-9959-9703-2-9

Primary teeth play an essential role in children's growth and development in terms of speaking, chewing [1], facial appearance, preventing bad oral habits, and, of course, in the orientation and eruption of permanent teeth. The eruption of permanent teeth after the shedding of primary teeth is a normal physiological process. Primary teeth work as the ideal space maintainer for permanent dentition. However, in some cases, such as where primary teeth are lost prematurely or early extraction is inevitable due to severe decay, delayed permanent teeth eruption may cause teeth to migrate (Fig. 1), which results in loss of the arch length, which may appear as malocclusion in permanent teeth such as crowding, impaction of permanent teeth, supra erupting of opposing teeth, and others [2].

Figure. 1: Migration of adjacent teeth and reduction of space required for the eruption of 2.5 *(Collection of the Department of Pediatric Dentistry)*

Along with dental caries and gingival disease, malocclusion is one of the most frequent dental issues [3]. Both corrective and interceptive methods are used to treat malocclusion. To prevent or reduce the severity of developing malocclusion in growing children, early detection and appropriate referral of cases requiring preventive and interceptive orthodontic treatments are crucial. This reduces the complexity of treatment as well as overall treatment time and costs in the future. One of the preventive methods "space maintenance," includes using certain appliances referred to as "space maintainers", which are fixed (Fig. 2) or removable

appliances used to preserve the arch length following the premature loss or extraction of the primary tooth [4].

Figure 2: Band and loop space maintainer *(Textbook of Pediatric Dentistry)*

The loss of arch length may result in many issues, such as overbite, ectopic eruption,

crowding, and crossbite formation, as well as overjet and dental centerline discrepancies (Fig. 3) [5].

Figure. 3: Unilateral early loss of the right primary canine, showing the resultant inclinations of the incisors and loss of space and centerline discerption *(International Journal of Oral Science)*

The use of interceptive orthodontics is based on dentists' knowledge and practice of space maintainers [6, 7]. Parents often have very low awareness of space maintainers; therefore, dentists must educate them. For this, there should be sufficient practice guidelines regarding the usage of space maintainers among dentists to offer better therapy. In order to compare our study with other published research on this topic of space maintainers, it was very challenging to find studies with similar objectives to our study [8, 9]. So we conducted a field study to determine the level of practice and attitude among dentists in Bani Waleed – Libya, about the possibility of using space maintainers and their prevalence as an essential intervention to prevent malocclusion or other consequences of premature loss or extraction of primary teeth in a growing child. present similar studies has been conducted in many cities around the world Similar studies have recently been carried out in other cities throughout the world. Dr. P. S. Krithika *et al.* 2019, who studied assess the dentists' understanding of space maintainers at the graduate and postgraduate levels in Chennai. Aimed at assessing the dentists' postgraduate and graduate knowledge about space maintainers in Chennai's northwestern area. According to the survey, almost all dentists (97.5%) are conscious of the importance of space maintainers. A large number of dentists were knowledgeable about the situational selection criteria, follow-up duration, and elimination criteria. It concluded Upon reflection, it was determined that dentists had a good knowledge of space maintainers. The increasing popularity might be due to parents' improved awareness of the importance of primary teeth for sound permanent teeth. [10].

1. *Materials and Methods*

2.1. Study design:

A cross-sectional study was carried out from January 31, 2023, to June 3, 2023, among dentists.

2.2. Sample size:

The sample size was calculated using the (Krejcie and Morgan) Table [11], based on the total number of dentists in Bani-Waleed City that was taken from the Department of Health Services – Bani Waleed. It consisted of (55) dentists.

 ISBN 978-9959-9703-2-9

2.3. Development of the Questionnaire:

A questionnaire with 13 closed-ended questions was prepared. It was written in the English language, and 2 orthodontists reviewed it to identify the items that were crucial to retention based on the validity and assessment of the content.

2.4. Details of the Questionnaire:

The questionnaire had 2 sections. The first section included questions about the gender and number of years of dental experience. The second section involves questions about the use of space maintainers, reasons for none use, placement, types and follow-up treatment for the space maintainers.

Percentage	Parameter		Number
Gender	Male	31	56.4 %
	Female	24	43.6 %
Experience	< = 9 years	25	45.5 %
	10 – 19 years	11	20 %
	20 – 29 years	9	16.4 %
	More than 30 years	8	14.5 %

2.5. Statistical analysis:

Statistical Package for the Social Sciences (SPSS), version 26.0, IBM, New York, USA, was used for the analysis of descriptive statistics. Pie charts, bar charts, and percentage tables were used to present the results.

2. Results and Discussion:

In the current study, 55 dentists have been included in the sample that consisted of 31 male and 24 female dentists, with a gender split of 56.4% and 43.6%, respectively. When it comes to experience, The majority of dentists (45,5%) have been in dental practice for < = 9 years, while (20%) have been in dental practice for 10 -19 years, There were almost equal percentages of those who had 20-29 or more than 30 years' experience, (Table 1). It should be mentioned that male dentists outnumbered females in this study. Despite the reality that more than 40% of the sample had experience in dentistry for more than ten years they all still required to be reminded on the options for therapy for primary teeth.

Table 1: Dentists' sociodemographic features.

(69.1%) of the dentists did not utilize space maintainers during their years of practice. On

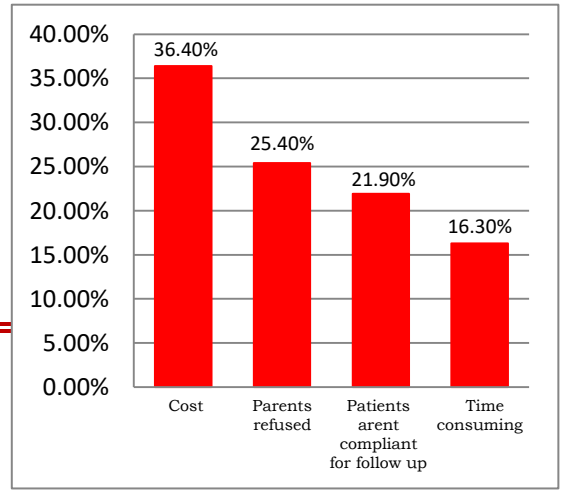

the other hand, space maintainers were used by (30.9%) of dentists (Fig. 4).

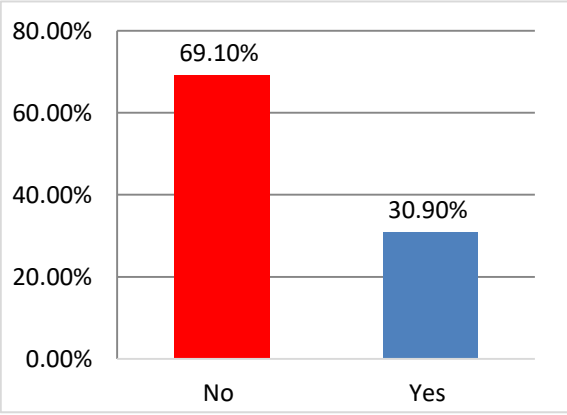

Figure. 4: Using of space maintainer.

The study showed that (51.4%) of dentists educate children and parents about the necessity of space maintainers, whereas (48.6%) of dentists don't educate them.

When these dentists were also questioned about the causes behind not utilizing space maintainers. The Significant percentage (36.4%) of dentists claim financial reasons, this may require to be addressed more by promoting dentists' usage of space maintainers and lowering space maintainer costs. followed by parental refusal (25.4%); therefore, greater emphasis should be placed on educating parents about the benefits of utilizing space maintainers for their children to prevent malocclusion. (21.9%) claimed that patients are not compliant with follow-up. (16.3%) of them pointed time-consuming, space maintainers may be an argumentative choice therapy for some dentists who do not use space maintainers and may believe that attempting to utilize this treatment for children is a waste of time and, in certain instances, harmful to the remaining dentition (Fig. 5).

Figure. 5: The reasons of not using space maintainers by dentists.

Band and loop, or crown and loop space maintainer, was the most frequently utilized type (71%). This confirms previously published

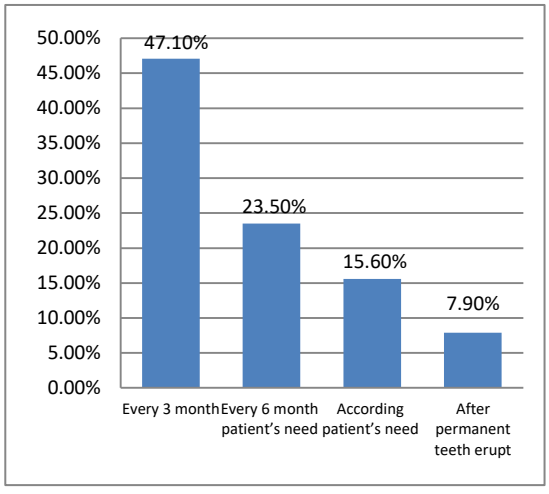

results that the band and loop space maintainer is frequently utilized and meets virtually all requirements [12]. The lingual arch came in second (16%) of the dentists. Only (9%) of dentists have utilized partial dentures.

ISBN 978-9959-9703-2-9

It is enjoyable to observe that only (4%) of dentists used the Distal Shoe, owing to the difficulties of using this kind of space maintainer and the potential danger of infection if we used it (Fig. 6). A number of new types of space maintainers have recently been introduced, including Glass fiber reinforced composite space maintainers [13, 14], fixed space maintainers combined with open-face stainless steel crowns [15], simple fixed space maintainers bonded with flow composite resin [16], and free end space maintainers [17]. These kinds of space maintainers may not be utilized in the city, although according to authors, they have shown a good chance of being used in the years to come.

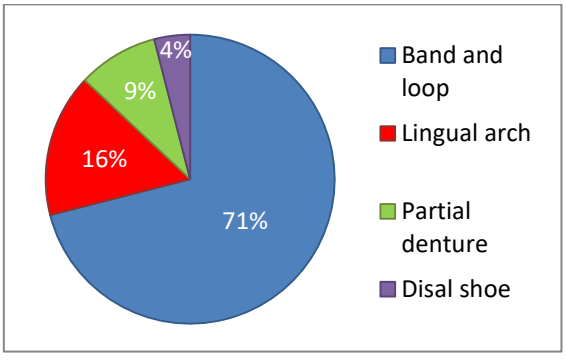

Figure. 6: Distribution of the types of space maintainer used by dentists.

The study indicates that the majority of dentists (54%) prefer placing space maintainers one week after extraction, which can prevent the development of malocclusion or minimize its severity. According to the authors [18], that pointed out how important it is to preserve space in time to prevent possible proximal drifting of adjacent teeth. In addition, opposing teeth tend to supra erupt rapidly in positions without opposing occlusion. Minority (17%) prefer immediate placement.

Most dentists (47.1%) agree that space maintainers should be followed up every 3 months. Other dentists were split between those who believe that space maintainers should be followed up every 6 months (23.5%), as needed by patients (15.6%), and after the eruption of permanent teeth (7.90%) (Fig. 7).

Figure. 8: Dentists opinions regarding how frequently space maintainers should be followed-up.

3. Conclusion

Following are the conclusions drawn from the current study's findings:

1. More than half of dentists do not utilize space maintainers as a prevention measure for premature loss of primary teeth.
2. The majority of dentists (51%) educate children and parents about the necessity of space maintainers.

ISBN 978-9959-9703-2-9

3. The most popular type of space maintainer used by dentists was a band or a crown and loop.
4. A significant percentage of dentists prefer to place space maintainers 1 week after extraction.
5. More than one-third of the dentists approved that space maintainers should be followed up every 3 months.
6. The main reasons for not using space maintainers were financial reasons and parents' refusal.

4. Acknowledgment:

We genuinely show gratitude to everyone who assisted us in carrying out this research.

5. Conflicts of interest:

The authors assert that There are no conflicts of interest.

6. Financial support and sponsorship:

Self-sponsored.

7. References:

1. Vij AA, Reddy A. Using digital impressions to fabricate space maintainers: A case report. Clin Case Rep. 2020.
2. Ramakrishnan M, Dhanalakshmi R, Subramanian EMG. Survival rate of different fixed posterior space maintainers used in Paediatric Dentistry - A systematic review. Saudi Dent J. 2019 Apr;31(2):165–72.
3. Vinothini V, Sanguida A, Selvabalaji A, Prathima GS, Kavitha M. Functional Band and Loop Space Maintainers in Children. Case Rep Dent. 2019.
4. Shulman E. Fabrication of a Band and Loop Space Maintainer [Internet]. Vol. 7, MedEdPORTAL. 2011.
5. Aditya LR, Gartika M, Primarti RS. Evaluasi kepatuhan perawatan space maintainer lepasan pada anakChildren compliance evaluation on removable space maintainer treatment [Internet]. Vol. 30, Jurnal Kedokteran Gigi Universitas Padjadjaran. 2018. p. 51.
6. Raviteja NVK, Prasad MG. Clinical Evaluation of Ghana Shyam's TEFF (Telescopically Expanding Fixed Functional) Space Maintainer Versus Conventional Band and Loop Space Maintainer [Internet]. Vol. 20, Pesquisa Brasileiraem Odontopediatria e Clínica Integrada. 2020.
7. Chunawala Y, Morawala A, Ambiye A, Jain K, Kataria S. Clinical Evaluation of the Effectiveness of Glass Fiber1reinforced Composite Space Maintainer vs Band-and-

 ISBN 978-9959-9703-2-9

loop Space Maintainer following Loss of Primary Teeth: An in vivo Study [Internet]. Vol. 1, International Journal of Clinical Dentistry and Research. 2017.

8. Qudeimat MA, Fayle SA. The longevity of space maintainers: a retrospective study. Pediatr Dent. 1998. 20; 267-272.

9. Kirzioglu Z, Erturk SO. Success of reinforced fiber material space maintainer. J Den Child-2004. 71; 158-162.

10. Dr. P. S. Krithika, Dr. Joyson Moses MDS., Dr. R. Sharanya MDS, Dr. Pallavi. C, Dr. Kalpana. H. Knowledge of Dental Practitioner on Space Maintainers as Treatment Modality for Premature Loss of Primary Teeth. Volume-8, issue-3, march-2019.

11. Krejcie, R &Morgan, D. (1970), Determining sample size for research activities. Educational and Psychological Measurement. 30, 607-610.

12. Olsen, N.H. Space maintenance. Dent Clin N Amer 1959. 59; 339-53.

13. Kargul, B, Caglar, E, Kabalay. U. Glass fiber reinforced composite resin space maintainer: case reports. J Dent Child (Clinc). 2003. 70: 258-61.

14. Kargul, B, Caglar, E, Kabalay. U. Glass fiber-reinforced composite resin as fixed space maintainers in children: 12-month clinic follow-up. J Dent Child (Clinc). 2005. 72: 109-112.

15. Yilmaz, Y, Kocogullari, M. E, Belduz, N. Fixed space maintainers combined with open-face stainless steel crowns. J ContempDent. Pract. 2006. 1: 95-103.

16. Simsek, S. Yilmaz, Y Gurbuz, T. Clinical evaluation of simple fixed space maintainers bonded with flow composite resin. . J Dent Child (Clinc). 2004. 71: 163-168.

17. Barberia, E, Lucavechi, T, Carenas, D, Maroto, M. Free-end space maintainers: design, Utilization and advantages. J Clin Pediatr Dent, 2006. 31: 5-8.

18. Lindemeyer, R.G, Glavich, G.G. Space maintainer for the loss of a permanent molar in the adolescent patient: Report of case. J Dent Child 1996. 63; 213-215.

 ISBN 978-9959-9703-2-9